

New Approaches in Coal Chemistry

Publication Date: October 26, 1981 | doi: 10.1021/bk-1981-0169.fw001

New Approaches in Coal Chemistry

**Bernard D. Blaustein,
Bradley C. Bockrath, and
Sidney Friedman, EDITORS**

*Pittsburgh Energy Technology Center
U.S. Department of Energy*

Based on a symposium
sponsored by the Pittsburgh
Section of the American Chemical
Society at the 12th Central
Regional Meeting, Pittsburgh, PA,
November 12–14, 1980.

A C S S Y M P O S I U M S E R I E S **169**

AMERICAN CHEMICAL SOCIETY
WASHINGTON, D. C. 1981



Library of Congress CIP Data

New approaches in coal chemistry.
(ACS symposium series; ISSN 0097-6156; 169)

Includes bibliographies and index.

1. Coal—Congresses.

I. Blaustein, Bernard D., 1929- . II. Bockrath,
Bradley C., 1942- . III. Friedman, Sidney, 1926- .
IV. American Chemical Society. Pittsburgh Section.
V. Series.

TP325.N5 662.6'2 81-12740
ISBN 0-8412-0659-7 AACR2 ACSMC8 169 1-443

Copyright © 1981

American Chemical Society

All Rights Reserved. The appearance of the code at the bottom of the first page of each article in this volume indicates the copyright owner's consent that reprographic copies of the article may be made for personal or internal use or for the personal or internal use of specific clients. This consent is given on the condition, however, that the copier pay the stated per copy fee through the Copyright Clearance Center, Inc. for copying beyond that permitted by Sections 107 or 108 of the U.S. Copyright Law. This consent does not extend to copying or transmission by any means—graphic or electronic—for any other purpose, such as for general distribution, for advertising or promotional purposes, for creating new collective work, for resale, or for information storage and retrieval systems.

The citation of trade names and/or names of manufacturers in this publication is not to be construed as an endorsement or as approval by ACS of the commercial products or services referenced herein; nor should the mere reference herein to any drawing, specification, chemical process, or other data be regarded as a license or as a conveyance of any right or permission, to the holder, reader, or any other person or corporation, to manufacture, reproduce, use, or sell any patented invention or copyrighted work that may in any way be related thereto.

PRINTED IN THE UNITED STATES OF AMERICA

**American Chemical
Society Library
1155 16th St. N. W.**

In New Approaches in Coal Chemistry; Blaustein, B., et al.;
ACS Symposium Series; American Chemical Society: Washington, DC, 1981.

Washington, D. C. 20036

ACS Symposium Series

M. Joan Comstock, *Series Editor*

Advisory Board

David L. Allara

Kenneth B. Bischoff

Donald D. Dollberg

Robert E. Feeney

Jack Halpern

Brian M. Harney

W. Jeffrey Howe

James D. Idol, Jr.

James P. Lodge

Marvin Margoshes

Leon Petrakis

Theodore Provder

F. Sherwood Rowland

Dennis Schuetzle

Davis L. Temple, Jr.

Gunter Zweig

FOREWORD

The ACS SYMPOSIUM SERIES was founded in 1974 to provide a medium for publishing symposia quickly in book form. The format of the Series parallels that of the continuing ADVANCES IN CHEMISTRY SERIES except that in order to save time the papers are not typeset but are reproduced as they are submitted by the authors in camera-ready form. Papers are reviewed under the supervision of the Editors with the assistance of the Series Advisory Board and are selected to maintain the integrity of the symposia; however, verbatim reproductions of previously published papers are not accepted. Both reviews and reports of research are acceptable since symposia may embrace both types of presentation.

PREFACE

In 1926, the First International Conference on Bituminous Coal (ICBC) was held in Pittsburgh, PA, at the midpoint of a three-decade-long period when coal represented a commodity of immense industrial importance and an object of intense scientific interest. At that time coal was the primary fuel of industry and the source of coke for steel manufacture and of many of the chemicals upon which a great new chemical industry rested. Gasification of coal still provided most of the town gas used for many domestic and commercial purposes. Efforts to convert coal to liquid fuels used the latest advances in high-pressure technology and led to the development of metal sulfide catalysts that are still mainstays in modern petroleum refining.

The scientific importance of coal at that time may be judged by the awarding of the Nobel Prize in Chemistry for 1931 to Friedrich Bergius for his pioneering work in using recently developed high-pressure technology for coal liquefaction. Following World War II, coal rapidly lost its position as a fuel and as a source of chemicals in favor of the cheaper, plentiful petroleum, and scientists simultaneously lost interest in the search for information about the origin of coal, its elusive structure, and its oftentimes puzzling reactivity.

The recent awareness that “the well may be running dry” has led to a renewal of our interest in coal and a resurgence of interest in its chemistry. One result of this is that in Pittsburgh, PA, on November 12–14, 1980—54 years after the first ICBC was held in this city—the 12th Central Regional Meeting of the ACS included a symposium on “New Approaches in Coal Chemistry.” The chapters in this symposium volume, with one exception, were among those presented at the meeting.

The reawakening of interest in coal research has come at a time when the sophistication of the methods available for conducting the research is orders of magnitude greater than it was in 1926. Today, such state-of-the-art measurements as Mössbauer, CP/MAS solid-state NMR, FTIR, new and advanced MS techniques (MS/MS), and EPR, among others, are used to investigate the structure and reactions of coal. Other techniques, both old and new, are using microprocessor capabilities and computer assistance to give increased resolution and to derive information from experimental results hitherto too complex to manipulate. Among these

chapters we find that these modern analytical methods are uncovering new aspects of coal's physical structure; concepts developed in polymer chemistry are providing a new framework for describing its macromolecular structure; modern chemical reagents and powerful new instrumental techniques are making further progress in solving the puzzle of its chemical structure; the chemistry of the inorganic and organometallic portions are fascinating areas vitally important to coal's proper and clean use; modern theories of chemical reactivity are helping to probe the chemical mechanisms of coal conversion, oxidation, and desulfurization; and the need for improved catalysts still beckons many researchers to explore further those fields that already have yielded many important discoveries.

As our attention to coal increases, scientists of all categories now are beginning to apply their specialities. Coal is proving again to be an endlessly fascinating and rewarding material for study. It is particularly intriguing that coal is responsive to so many approaches.

The chapters in this symposium volume represent a cross-section of current research on coal. The title of the symposium reflects the application of the aforementioned techniques to coal studies, the contents of the chapters underscore how rapidly technology is transferred from one discipline to another, and the authorship reveals the universality of interest in coal studies, including as it does, contributors from government, industrial, and, especially, academic laboratories.

This upsurge in interest by members of so many disciplines is heartening. However, it is always worthwhile to remind ourselves of one of the special problems in all coal research. That is, each coal sample already has experienced a rich natural history in geologic time and may have changed further since being exposed or removed from its original site. Thus, although we know that all coals have certain common traits, any particular sample in some ways may be unique unto itself. As no one would dare to describe a particular individual citizen of this country as "the average American," so coal chemists must refrain from assuming that their individual samples are identical in character to any other samples taken from the same deposit.

In spite of the progress which has been made in studying coal and its reactions, many experiments seem to raise more questions than they answer. The chapters in this volume solve some problems, but at the same time they pose new ones. It does seem, however, that we know considerably more about the structure of coal today than we did in 1926, and we

now understand better what happens when coal is liquefied. Unfortunately, there is much more we must learn, but hopefully by using “New Approaches in Coal Chemistry” we will continue to learn.

Bernard D. Blaustein

Bradley C. Bockrath

Sidney Friedman

Pittsburgh Energy Technology Center

U.S. Department of Energy

P.O. Box 10940

Pittsburgh, PA 15236

July 7, 1981

Small-Angle X-Ray Investigation of the Porosity in Coals

M. KALLIAT, C. Y. KWAK, and P. W. SCHMIDT

Physics Department, University of Missouri, Columbia, MO 65211

Small-angle x-ray scattering measurements are reported for 15 coal samples in the PSOC series of coals. The rank of the coal was found to be the main factor determining the form of the small-angle scattering curves. One type of scattering curve was characteristic of anthracites, while a somewhat different curve was obtained for low-volatile bituminous coals. In the scattering curves from many high-volatile bituminous and some sub-bituminous coals, a shoulder was observed. A fourth kind of curve was found to be typical of other high-volatile bituminous and sub-bituminous coals and also of lignites. Analysis of the scattering curves provides evidence for the presence of three classes of pores--(1) large pores, with dimensions of at least 300 Å, (2) intermediate sized pores, with average dimensions of the order of 100 or 200 Å, and (3) very small pores, which with dimensions no greater than about 30 Å. These three types of pores are referred to as macropores, transition pores, and micropores, respectively. The system of three kinds of pores suggested by the x-ray scattering data is in good agreement with the three-class pore structure developed by other workers' investigations employing techniques besides small-angle x-ray scattering. The specific surfaces of the coals were calculated from the scattering curves. A method was developed for estimating the fractions of the total specific surface which should be assigned to the macropores and transition pores under the assumption that the specific surface computed from the scattering curves did not include any contribution from the micropores. The specific surfaces calculated from the scattering data have been compared with the specific surfaces obtained by adsorption of nitrogen at low temperatures and by carbon dioxide at room temperature. The x-ray data are not consistent with the suggestion that many pores have dimensions of some hundreds of Angstroms but have restricted openings which exclude nitrogen at

0097-6156/81/0169-0003\$05.00/0
© 1981 American Chemical Society

low temperatures. Instead, the high values of surface area obtained by carbon dioxide adsorption must be the result of the contribution of a large number of pores with minimum pore dimensions which are not greater than about 30 Å.

Small-angle x-ray scattering is a technique which provides information about structures which, though larger than the normal interatomic distances in solids and liquids, are too small to be visible in the optical microscope. Since the interval of dimensions which can be conveniently studied by small-angle scattering thus includes those of many of the pores in coals, we have used small-angle scattering to investigate the porosity of a number of coal samples. Before presenting our results, however, we will review some techniques and concepts employed in the measurement and interpretation of the scattering data.

In our small-angle x-ray scattering studies of coals, x-rays (wavelength 1.54Å) from a copper-target diffraction tube were formed into a well-defined beam and struck the coal sample, which was in powdered form and which had a thickness of about 1 mm. Figure 1 shows a schematic diagram of the scattering apparatus.

Although most of the x-rays were either absorbed in the sample or passed through it without being affected, a small fraction of the radiation, called the scattered radiation, was emitted in directions other than that of the incoming beam. One of the quantities which determines the intensity of these scattered rays is the scattering angle θ , which is the angle between the incident and scattered rays, as shown in Fig. 1. (In many discussions of large-angle x-ray diffraction, the scattering angle is called 2θ , rather than θ). The scattered intensity also depends on the structure of the scattering sample. The object of most scattering experiments is to obtain information about the structure of the sample by analyzing measurements of the scattered intensity at a series of scattering angles.

While the general relationship between the scattered intensity and the structure is so complicated that there is no general procedure applicable for the analysis of data from all kinds of samples, relatively simple methods can be used to interpret the scattering curves from the coals.

First, a general principle from scattering theory states that most of the information about the sample which can be obtained from scattering data is contained in the measurements at scattering angles which satisfy the condition

$$0 \leq hD \leq 10 \quad (1)$$

where D is a dimension characterizing the structure producing the scattering;

$$h = 4\pi\lambda^{-1} \sin(\theta/2); \quad (2)$$

and λ is the x-ray wavelength. According to (1), there is a more-or-less inverse relationship between the size of the structure producing the scattering and the angle at which the most useful scattering is observed. By convention, "small-angle" scattering has come to mean scattering at angles θ no greater than about 5 degrees. At these angles, h is essentially proportional to θ .

X-ray scattering occurs only when there are differences in the number of electrons per unit volume in different regions of the sample. Coals thus scatter x-rays because there are inhomogeneities in their electron density. According to (1), this scattering occurs at small angles because an appreciable fraction of these inhomogeneities have maximum dimensions no greater than about 1000 Å. When hD_{\min} is large, where D_{\min} is the smallest dimension appreciably affecting the scattering in a given interval of scattering angles, the scattered intensity $I(h)$ can be approximated by the relation

$$I(h) \approx 2\pi I_e d^2 S h^{-4} \quad (3)$$

where I_e is the intensity scattered by a single electron; d is the difference in the electron densities of the two phases which the sample is considered to be composed of; and S is the value of the total surface area separating these two phases in the sample. (In the small-angle region, I_e can normally be considered to be a constant, and within each phase the electron density also can be assumed to be constant.) Equation (3) has been found to be quite well satisfied when

$$hD_{\min} \geq 3.5. \quad (4)$$

In the coal samples, usually one of the two phases is coal, and the other is pores, which are considered to contain air. Sometimes, however, the effects of the mineral matter in the coal must be considered. The system then contains three phases. Our scattering data from the coals suggest that the pores and mineral matter scatter independently of each other, so that when the contribution of the minerals to the scattering must be considered, the coals can be taken to be two independent systems--one made up of coal and air, and the other consisting of coal and mineral matter. As we will explain below in more detail, we have estimated the contribution of the mineral matter to the scattering from several of the coals and have concluded that this scattering is small and often can be completely neglected.

According to (3), when $I(h)$ is proportional to h^{-4} and thus to θ^{-4} , the magnitude of the scattered intensity is proportional to the surface area dividing the two phases. The scattering data thus provide information about the specific surface of the coal samples. It is important to note, however, that meaningful results about the specific surface can be obtained only when there is an interval of scattering angles for which the intensity is at least approximately proportional to θ^{-4} .

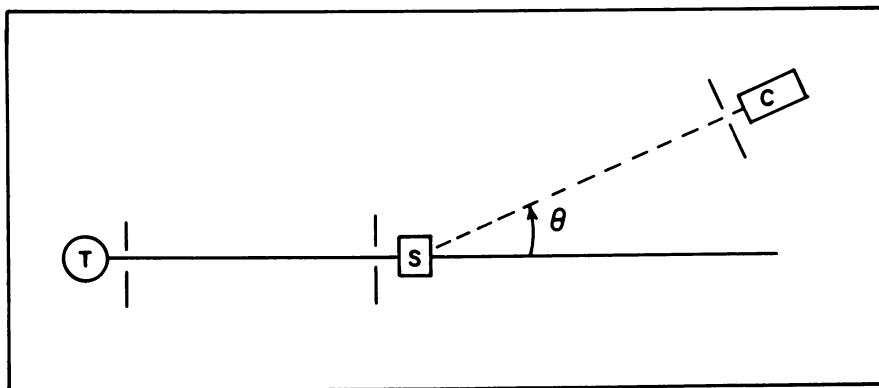


Figure 1. Schematic of a small-angle X-ray scattering system. X-rays from the tube (T) are formed into a beam by slits and strike the sample (S). The counter (C) is used to detect the intensity scattered at an angle θ .

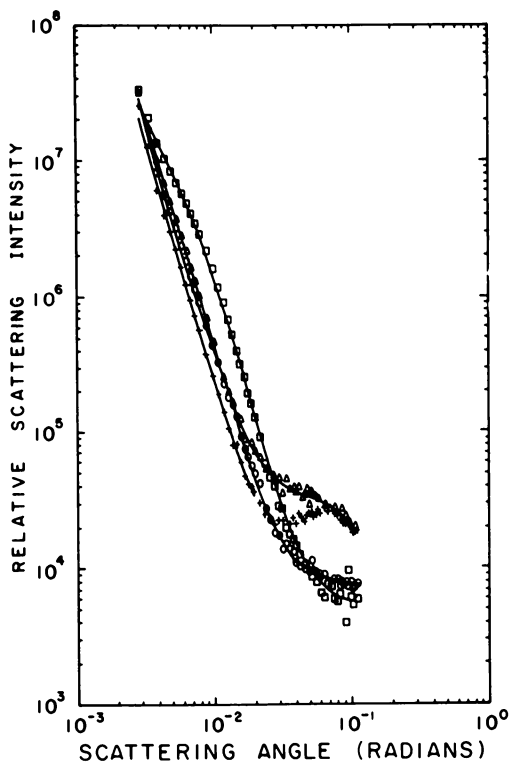


Figure 2. Typical scattering curves for the coal samples. Curves 1-4 were obtained for PSOC coals 095 (\circ), 022 (\square), 127 (+), and 081 (\triangle), respectively. The lines were determined by least-squares fits of Ref. 8.

When

$$hD_{\max} \leq 0.5, \quad (5)$$

where D_{\max} is the largest dimension characterizing the structure³,

$$I(h) \approx I_e d^2 F_0. \quad (6)$$

In (6), F_0 is a constant. The scattered intensity from relatively small inhomogeneities thus is independent of the scattering angle but is proportional to d^2 .

Results

The scattering data were recorded with a Kratky small-angle scattering system⁴ and a stationary-anode x-ray tube operated at about 30 ma average current and at a peak voltage of about 45 KV. A proportional counter was employed to detect the scattered radiation, and the x-rays scattered at the copper K- α wavelength of 1.54 Å were selected by a linear amplifier and a pulse-height analyzer. An electronic programmer was used to set the system at the desired scattering angles.

Each scattering curve was measured six times. After the results were averaged and corrected for the day-to-day fluctuations in the incident intensity, the curves were corrected for the background scattering from the scattering system and the 0.001 inch Mylar[®] plastic windows of the sample cell. Corrections were also made for the length⁵ and width⁶ of the collimating slits.

Scattering data were recorded for about 50 coal samples, most of which were obtained from the Pennsylvania State University PSOC set of coals. We will discuss the scattering from 15 of these coals. The results from the other samples were quite similar to those reported here.

We found that the form of the curve of the scattered intensity as a function of the scattering angle depends primarily on the rank of the coal. The scattering curves can be conveniently grouped into four classes. An example of each of these four types of curves is shown in Figure 2.

Curve 1 is the scattered intensity for Washington No. 4 Queen high-volatile A bituminous coal (PSOC 095). The inner part of this curve is nearly proportional to θ^{-4} , while the outer portion approaches a constant value. (In the logarithmic plot employed in Fig. 2, a straight line means that the intensity is proportional to some power of θ , and a straight line with slope -4 is obtained when $I(h)$ is proportional to θ^{-4} .) The form of this curve suggests that in this coal, there are two types of inhomogeneities, which have greatly different average dimensions. Since $I(h)$ is proportional to θ^{-4} even at the smallest scattering angles accessible with the

scattering system, in this coal there are inhomogeneities so large that inequality (4) is satisfied at all scattering angles at which data were recorded. Since the scattering was not measured at angles smaller than 0.003 radian, (4) implies that for the larger inhomogeneities $D_{\text{min}} > 300 \text{ \AA}$. Although the scattering from these large inhomogeneities predominates in the inner part of the scattering curve, the scattering from them decays rapidly as the scattering angle increases. However, the scattering from the small inhomogeneities will be considered to satisfy (5) and thus will be essentially independent of the scattering angle. Because the scattering from the large inhomogeneities decreases so rapidly with increasing scattering angle, in the outer part of the scattering curve, only the relatively weak but constant scattering from the small inhomogeneities will be observed. The scattering from PSOC 095 coal thus can be considered to be produced primarily by two types of inhomogeneities, which, as in the terminology employed by M. M. Dubinin⁷, will be referred to as macropores and micropores.

From the scattering data alone, there is no way to determine that the inhomogeneities are pores--that is, that the electron density is smaller in the inhomogeneities producing the scattering than in the rest of the coal. A similar scattering would be produced by inclusions of mineral matter with the proper dimensions. Nevertheless, the information about coals obtained by adsorption measurements and other techniques besides x-ray scattering effectively rules out the possibility that the largest part of the scattering is due to anything except pores.

We have found that scattering patterns like Curve 1 in Fig. 2 are typical of lignites and of some sub-bituminous and high-volatile bituminous coals.

For other high-volatile bituminous, medium-volatile bituminous, and sub-bituminous coals, the scattering patterns, in addition to the features of Curve 1 already discussed, have a shoulder at intermediate scattering angles. Curve 2 in Fig. 2 is an example of this type of scattering curve and was obtained for an Illinois No. 6 high-volatile bituminous coal (PSOC 022). We have interpreted the shoulder on this curve as evidence for the presence of a third type of inhomogeneity, with average dimensions between those of the macropores and micropores. To explain the scattering from these intermediate-sized inhomogeneities, which we consider to be the transition pores discussed by Dubinin⁷, we assume that these pores are so large that at the largest scattering angles at which we recorded data, (4) is fulfilled for the transition pores, and so the scattering from these pores is proportional to θ^{-4} . To produce a shoulder on the scattering curve, however, the transition pores must also be small enough that at the smallest angles at which we measured the scattering, these pores satisfy (5) and thus give an essentially constant scattering. In the inner part of the scattering curve from this coal, we consider this constant intensity to be essentially

negligible compared to the scattering from the macropores. In this region of the scattering curve, the scattering from this coal then is very nearly proportional to θ^{-4} and is caused almost entirely by the macropores. As the scattering angle becomes larger, the fraction of the scattering that is due to the macropores rapidly decreases, and so at intermediate scattering angles, most of the scattering will be produced by the transition pores, since the scattered intensity from these pores, though initially much weaker than that from the macropores, decays less rapidly with increasing scattering angle.

For there to be a shoulder on the scattering curve, the transition pores must be small enough that the intensity scattered by these pores is constant in the inner part of the scattering curve and remains essentially constant even at scattering angles large enough that the contribution from the macropores has decayed so much that it is much weaker than the scattering from the transition pores. Transition pores with these dimensions can explain the shoulder on scattering curves like Curve 2 in Fig. 2.

In this curve there are two regions of scattering angles in which the intensity is proportional to θ^{-4} . The inverse-fourth-power scattering in the innermost part of the curve can be ascribed to the macropores, and the magnitude of the scattered intensity at these angles is proportional to the surface area of these pores. The scattered intensity is also proportional to θ^{-4} in the part of the curve on the right of the shoulder--i.e., at scattering angles larger than those where the shoulder is observed. The magnitude of the scattered intensity in this interval of scattering angles is proportional to the sum of the surface areas of the macropores and transition pores. For there to be a shoulder on a scattering curve, the inverse-fourth-power scattering from the transition pores must be appreciably greater than from the macropores.

For low-volatile bituminous coals, such as Pennsylvania E. Lower Kittanning coal (PSOC 127), and Upper Freeport coal (PSOC 318) and also for the medium-volatile bituminous coals PSOC 130 and PSOC 134, a rather broad peak is found in the outer part of the scattering curve, as is illustrated by Curve 3 in Fig. 2. For this coal, (PSOC 127), the inner portion of the scattering curve, as in Curves 1 and 2, is proportional to θ^{-4} . The macropore structure can thus be considered to be quite similar to that in the lower-rank coals. The peak, which corresponds to a Bragg spacing of about 20 Å, has previously been reported by Hirsch⁸, who interpreted it as being due to interactions between the fundamental scattering units in these coals, which were made up of a few layers of planar aggregates containing aromatic rings. Because of the presence of this peak, the magnitude of the scattering from the micropores cannot be easily assessed, although the presence of micropores certainly cannot be excluded. According to the interpretation given for Curve 2 in Fig. 1, however, the contribution of the transition pores in PSOC 127 to the scattering must be quite small.

Curve 4 of Fig. 1 shows the scattered intensity for Pennsylvania Buck Mountain anthracite (PSOC 081). Quite similar scattering curves were recorded for some other anthracites.

The inner part of the scattering curves for the anthracites is very similar to the corresponding region of Curve 3 in Fig. 1. The macropore structure in anthracites thus is probably quite similar to that in low-volatile bituminous coals.

The distinguishing characteristic of the scattering curves for the anthracites is the outer part of the scattering curve, where the intensity is usually higher than for the lower-rank coals, and, though sometimes nearly constant, usually decreases smoothly.

Although there were no well-defined peaks in any of the scattering curves from the anthracites, the outer portion of the scattering pattern for these coals could be a vestige of a maximum like that in the curves for the low-volatile bituminous coals. An alternative explanation of the form of this part of the scattering curve for anthracites is that the average dimensions of the micropores in these coals are so large that inequality (5) is not satisfied, and so the scattering from the micropores is not independent of the scattering angle. Then, if the micropores scatter independently of each other, the scattering in this part of the curve can be approximated by the expression—

$$I(h) = I_0 e^{-(1/3)h^2 R^2}, \quad (7)$$

where I_0 is a constant, and R , the average radius of gyration⁹ of the inhomogeneities, is a measure of the average size of the inhomogeneity. Equation (7) is a good approximation when hR is not much larger than 1. For spheres¹⁰ with radius a , $R = (3/5)^{1/2}a$. With (7), a radius of gyration $2.4 \pm 0.2 \text{ \AA}$ was calculated for the micropores in anthracite PSOC 081.

The scattering in the outer region of the intensity curves for the anthracites could also be the result of a combination of all these effects. In other words, the scattering could be due to three kinds of structures: (1) the tail of the inverse-fourth-power scattering from the macropores and transition pores, (2) the structure which is responsible for the peak corresponding to a Bragg distance of about 20 Å, and (3) micropores for which the scattering is described by (7). In different coals, the relative magnitudes of these three effects would differ, and as a result there would be some differences in the form of the outer part of the scattering curve.

We wish to point out the outer part of the scattering curve for PSOC Coal 135, which is a medium-volatile bituminous coal, is quite similar to the corresponding curves for the anthracites. The fact that the outer portion of the scattering curves from both a medium-volatile bituminous coal and also from anthracites have the same form can be quite naturally explained if the scattering at these angles is the result of superposition of the three structures mentioned above.

Further study, however, is necessary before a detailed and quantitative explanation of the outer part of the scattering curves from these coals is possible.

Determination of Specific Surfaces

To obtain an equation describing the scattering from the pores in the coals, we assumed that

$$I(h) = I_{00} I_e A \left[\frac{S_{ma}^0}{h^4} + \frac{S_{tr}^0}{(h^2 + a^2)^2} + \frac{C_{mi}}{(1 + b^2 h^2)^2} \right], \quad (8)$$

where

$$I_{00} = \frac{2\pi d^2}{T} \frac{M}{A}. \quad (9)$$

In (8) and (9), I_e is the intensity scattered by one electron, S_{ma}^0 and S_{tr}^0 are the specific surfaces, or surface areas per unit mass of coal, of the macropores and transition pores, respectively; the constant C_{mi} is proportional to the weak but constant scattering from the micropores; b is a constant characterizing the micropore dimensions; M and A are respectively the mass of the sample and its cross-section area perpendicular to the incident beam; T is the x-ray transmission; and a is a constant inversely proportional to the average dimensions of the transition pores. The factor $1/T$ is included in (9) to take account of the absorption of x-ray in the samples, since (3) was developed under the assumption that the samples were non-absorbing. The transmission T can be expressed

$$T = \frac{I}{I_0} = \exp(-\mu \frac{M}{A}); \quad (10)$$

where I_0 is the x-ray intensity striking the sample; I is the intensity transmitted through the sample; and μ is the mass absorption coefficient.

The term proportional to S_{ma}^0 in (8) describes the scattering from the macropores and was obtained by rewriting (3), while the middle term was selected to give a reasonable and convenient approximation to the contribution from the transition pores. An intensity with this form is expected¹² from pores randomly distributed in a material with uniform electron density. This expression has the desired properties of approaching a constant value for small h and of being proportional to h^{-4} for large h .

The term

$$C_{mi}(1 + b^2 h^2)^{-2}$$

in (8) allows for the scattering from the micropores. For the

relatively small scattering angles included in our curves, this expression is essentially equivalent to (7). The form of the term was chosen for convenience in the calculations. If (7) and the expression

$$C_{mi} (1 + h^2 b^2)^{-2}$$

are to be equivalent to terms of order h^2 --that is, if to terms of order h^2

$$(1 + b^2 h^2)^{-2} \approx e^{-(1/3)h^2 R^2},$$

b must satisfy the relation

$$b = (1/6)^{1/2} R.$$

From (10)

$$\frac{M}{A} = \frac{1}{\mu} \log_e(1/T). \quad (11)$$

Thus, from (9), (11), and the measured value of the T, we could evaluate the quantity I_{00} . For this calculation we assumed that the coal consisted entirely of carbon, that $\mu = 4.60 \text{ cm}^2/\text{gm}$, and that the mass density of the coal 1.30 gm/cm^3 . This density is a compromise between the helium densities determined for coals of different rank and origin.

We made non-linear least-squares fits¹⁵ of (8) to the corrected scattering curves of each of the 15 coal samples. For all coals except PSOC 135 and PSOC 081, we assumed that b was zero, since except for these two coals, the data suggested that the scattering from the micropores did not depend on the scattering angle. For PSOC 081 and PSOC 135, from the least-squares fits we calculated that $b = 1.44 \pm 0.01 \text{ \AA}$ and $1.06 \pm 0.02 \text{ \AA}$, respectively. These values correspond to micropore radii of gyration of $3.5 \pm 0.1 \text{ \AA}$ and $2.6 \pm 0.1 \text{ \AA}$, respectively. The result $3.5 \pm 0.1 \text{ \AA}$ for PSOC 081 is in fair agreement with the radius of gyration $2.4 \pm 0.2 \text{ \AA}$ calculated for this coal by use of (7).

In the least-squares fits of (8) to the scattering curves for the coal samples, when there was a peak on the scattering curve, we made the fit only for angles smaller than those at which the maximum was observed. For all the other coals, we were able to fit the entire scattering curve.

The constants a^{-1} obtained from the fits provide an estimate of the average dimensions of the transition pores. From the fits we obtained values a^{-1} ranging from about 28 through 54 \AA . We could observe no pattern to the variation of a^{-1} from sample to sample. By the same argument which we used to relate the micropore radius of gyration to the parameter b which characterizes the dimension average dimension of the micropores, the radius of gyration of the transition pores is $6^{1/2} a^{-1}$, and if the pores can be

considered spherical, the sphere radius is $6^{1/2}(3/5)^{-1/2}a^{-1}$. Thus if the transition pores are considered to be spherical, the least-squares fits showed that the average pore radii varied from about 90 to 170 Å.

To find the product I_A , we measured the scattering from a concentrated Ludox[®] colloidal silica suspension and evaluated the integral Q in the equation¹⁶

$$Q = \int_0^{\infty} h^2 I_{\text{corr}}(h) dh = 2\pi^2 I_e (d_{\text{Si}})^2 c(1 - c) V, \quad (12)$$

where d_{Si} is the difference of the electron densities of the spherical silica particles and the water in which these particles are suspended; and c is the fraction of the volume V of the suspension that is occupied by the silica particles. In the integral Q , $I_{\text{corr}}(h)$ is the part of the corrected scattered intensity from the silica suspension which is proportional to h^{-4} in the outer part of the scattering curve. (In other words, $I_{\text{corr}}(h)$ is the corrected intensity after the slowly-varying or constant scattering from the solvent and any other relatively short-range structure has been subtracted.) Since the scattering from the suspension and the coals were measured under the same conditions, the value of I_A calculated for the suspension could be used with all of the coals.

From (12) and (11)

$$Q D_{\text{Si}} = 2\pi^2 I_e A d^2 c(1 - c) \frac{M}{A} = 2\pi^2 I_e A d^2 c(1 - c) \frac{\log_e(1/T_{\text{Si}})}{\mu_{\text{Si}}} \quad (13)$$

where D_{Si} is the mass density of the silica suspensions; A is the cross-section area of the sample; and T_{Si} and μ_{Si} are the transmission and mass absorption coefficient of the suspension. To find $I_{\text{corr}}(h)$ from the corrected scattering curve for the suspension, we made a least-squares fit of an equation like (8) to the corrected scattering curve from the suspension. We evaluated the integral Q by a technique¹⁷ previously developed in our laboratory. As given by the manufacturer and verified¹⁷ from scattering measurements, $D_{\text{Si}} = 2.28 \text{ gm/cm}^3$. We used this mass density to calculate the D_{Si} electron density and employed the measured concentration $k \text{ gm}$ of silica per gm of suspension to compute the mass absorption coefficient μ_{Si} and the volume fraction c , with the assumption that one gram of suspension consisted of $k \text{ gm}$ of SiO_2 with density D_{Si} and $(1 - k) \text{ gm}$ of water.

After we had determined I_A and calculated I_e for the coal samples, we evaluated the specific surfaces $S_{\text{ma}}^{\text{so}}$ and $S_{\text{tr}}^{\text{so}}$ for the macropores and transition pores in the 15 coals. These specific surfaces are listed in Table 1. We estimate that the uncertainty in the specific surfaces is about $\pm 40\%$.

Table 1
SPECIFIC SURFACES FOR THE COALS OBTAINED FROM THE SCATTERING CURVES AND FROM ADSORPTION DATA

PSOC-NO	RANK	STATE & SEAM NAME	SURFACE AREA (m ² /g)		X-RAY SCATTERING MACRO- PORES	X-RAY SCATTERING TRANSITION PORES
			ADSORPTION N ₂	ADSORPTION CO ₂		
PSOC-081	ANTHRACITE	PENNSYLVANIA BUCK MOUNTAIN	ND	ND	1.54	2.37
PSOC-318	LOW. VOL.	PENNSYLVANIA E. UPPER FREEPORT	<1.0	186	1.09	1.45
PSOC-127	LOW. VOL.	PENNSYLVANIA E. LOWER KITTANNING	<1.0	271	1.23	1.29
PSOC-130	MED. VOL.	W. VIRG. POCAHONTAS #3	<1.0	249	1.08	1.43
PSOC-135	MED. VOL.	ALABAMA PRATT	<1.0	227	1.33	1.09
PSOC-134	MED. VOL.	ALABAMA PRATT	<1.0	208	0.86	1.54
PSOC-095	HVA.	WASHINGTON #4 QUEEN	<1.0	220	1.6	4.08
PSOC-105	HVB.	INDIANA #1 BLOCK	16.0	105	2.06	44.5
PSOC-197	HVC.	OHIO #6 MIDDLE KITTANNING	11.0	ND	2.15	4.04
PSOC-185	HVB.	INDIANA #6	49.0	ND	0.85	7.87
PSOC-022	HVC.	ILLINOIS #6	99.0	189	18.4	17.6

Table 1 (Cont.)

SPECIFIC SURFACES FOR THE COALS OBTAINED FROM THE SCATTERING CURVES AND FROM ADSORPTION DATA

PSOC-NO	RANK	STATE & SEAM NAME	SURFACE AREA (m ² /g)			
			ADSORPTION N ₂ CO ₂	TOTAL	X-RAY SCATTERING MACRO- PORES	TRANSITION PORES
PSOC-212	HVC.	OHIO #2 QUAKERTOWN	3.7 254	9.16	1.47	7.68
PSOC-181	SUBBIT. A.	INDIANA UPPERBLOCK	49 ND	24.01	4.41	19.6
PSOC-138	SUBBIT. C.	TEXAS DARCO LIGINITE	2.5 254	7.25	2.71	4.55
PSOC-188	HVB.	ILLINOIS #2 COLCHESTER	32 ND	15.95	0.48	15.5

ND: Not determined. The specific surfaces from adsorption measurements were taken from the PSOC data bank, except for coal 105, for which these specific surfaces were recently measured by R. G. Jenkins. The x-ray specific surfaces were calculated from the least squares fits.

The Contribution of Mineral Matter to the Scattering

To estimate the scattering by the mineral matter in the coals, we prepared four ash samples by low-temperature ashing.

The scattering from these samples was assumed to be proportional to the scattering that would have been produced by the mineral matter when it was in the coals. Allowance was made for the fact that the intensity from the ash differed from that scattered by the minerals in the coals because of the fact that in the ash samples, the minerals were surrounded by air, rather than embedded in the coal. The size of the particles of the mineral matter, however, was considered to be unaffected by the ashing process.

The scattered intensity from the ash samples was proportional to h^{-4} over almost all of the interval of scattering angles at which data were recorded, although in the outer part of the curve, the intensity approached a weak but constant value. To estimate the specific surface associated with the mineral matter, the mineral densities were approximated by considering that the mineral matter was either pyrite or kaolinite--that is, that mineral matter which was not pyrite had a density and chemical composition enough like those of kaolinite that the scattering from the minerals would be essentially the same as if they were composed of kaolinite. The pyrite and total mineral matter concentrations were taken from the data in the PSOC analyses. Our estimates showed that in the inner part of the scattering curves, the mineral matter contributed from about 10% to 25% of the total surface area. In other words, the specific surface values in Table 1 which are considered to be due only to the surface of the macropores should be reduced by 10 to 25 per cent. As this change does not exceed the uncertainty in the determination of the specific surfaces, the contribution of the mineral matter can, at least in these preliminary evaluations of the specific surface, be neglected.

The effect of mineral matter is so small that it is completely negligible compared to the combined specific surface of the macropores and transition pores in coals with scattering curves which have a shoulder.

Discussion

Although the magnitude of the scattered intensity in the outer part of the scattering curve can be taken as a rough measure of the extent of the micropore structure, as yet we have found no really reliable way to obtain quantitative information from this part of the curve. Interpretation of this region of the curve is complicated by the fact that peaks like the 20 Å maximum in POSC Coal 127 can mask the scattering from the micropores and also

because in this interval of angles, the part of the "small-angle" scattering curve that gives information about the micropores may not be separable from the "small-angle tail" of the large-angle diffraction pattern. For example, the small-angle tail of the first maximum in the large-angle diffraction pattern may not be negligible in the angular region sensitive to the micropores. Further study is therefore necessary before quantitative information about the micropores can be obtained from the small-angle scattering data.

In Table 1 we list the sum of the specific surfaces of the macropores and transition pores and also the specific surfaces obtained by low temperature nitrogen adsorption and by adsorption of carbon dioxide at room temperatures. The nitrogen and carbon dioxide specific surfaces are taken from the PSOC data bank, except for coal PSOC 105. Since the specific surfaces in the data bank for this coal appeared questionable, they were remeasured by R. G. Jenkins at Pennsylvania State University.

Information about the pore structure in the coals can be obtained by comparison of the specific surfaces determined by the three techniques. Before discussing the detailed results, however, we would like to point out some general properties of the different methods of determining specific surfaces.

For a surface to be detected in adsorption measurements, the adsorbed gas must be able to penetrate the pores. Adsorption methods thus will not detect closed pores. Also, nitrogen at low temperatures may not penetrate pores as small as those which carbon dioxide can enter at room temperature.

While x-ray scattering detects both open and closed pores, only pores for which the minimum dimension satisfies (4) will contribute to the specific surface calculated from the scattering curves. The properties of the x-ray and adsorption techniques must be kept in mind during comparison of the specific surfaces obtained by these techniques.

The differences between specific surfaces determined by low-temperature nitrogen and room-temperature carbon dioxide adsorption have been ascribed¹⁸ to the fact that many of the pores in the coals are accessible only through small, constricted openings which cannot be penetrated by nitrogen molecules at liquid nitrogen temperatures, while carbon dioxide molecules at room temperature have sufficient energy to go into the pores. On the other hand, if the pore dimensions are large enough that (4) is satisfied in a given interval of scattering angles, the scattering will be proportional to h^{-4} regardless of the size of the entrances to the pores. Moreover, as we have mentioned, the scattering process will detect completely closed pores. On the other hand, unless the minimum pore dimensions are large enough to satisfy (4), the scattered intensity will not be proportional to h^{-4} , and so these pores will not be included in the surface calculated from the scattering curves.

All of the differences between the specific surfaces obtained by adsorption and small-angle scattering therefore cannot be explained by the existence of pores with restricted entrances. Instead, since the specific surfaces from adsorption of carbon dioxide at room temperature are always much greater than those obtained from the scattering data, there must be a large number of pores for which smallest pore dimensions do not satisfy (4).

As can be seen from the scattering curves in Fig. 2, the scattered intensity for coals PSOC 081 and PSOC 127 begins to deviate from a θ^{-4} dependence for scattering angles greater than 0.02 radians, while this deviation starts at about 0.03 and 0.04 radians for coals 095 and 022, respectively. Since (4) is not satisfied at larger scattering angles, the minimum dimensions of the pores which contribute to the specific surfaces calculated from the scattering data cannot be less than about 45 Å in coals 081 and 127, 30 Å in coal 095, and 22 Å in coal 022. These minimum pore dimensions are so large that both carbon dioxide at room temperature and nitrogen at low temperature can penetrate pores smaller than those contributing to the x-ray-scattering specific surface. Thus, when the specific surface calculated from the scattering curves exceeds the specific surface from low temperature nitrogen adsorption, there must be closed pores inaccessible to nitrogen at low temperature, while if the latter specific surface is greater than the former, there will be many pores penetrable by nitrogen but not detected by small-angle scattering.

Since the specific surfaces from the x-ray scattering curves thus are due to the relatively large pores, it is not surprising that the adsorption techniques, which are capable of detecting surface areas of much smaller structures, often give specific surfaces considerably larger than those calculated from the scattering curves.

For the Coals 318, 127, 130, 135, 134, and 095, all of which are of relatively high rank, the nitrogen specific surfaces are very small, while the carbon dioxide surfaces range from about 180 through 250 m^2/gm . The specific surfaces from the x-ray data vary from 2.4 through 5.7 m^2/gm . Since the nitrogen specific surfaces are smaller than those from the scattering curves, we can conclude, at least tentatively, that there are an appreciable number of pores large enough to be detectable by scattering but impenetrable to nitrogen at low temperatures. These pores, for example, could be completely sealed. On the other hand, since the carbon dioxide specific surfaces are always much larger, there must be many pores with minimum dimensions less than about 20 Å which are accessible to carbon dioxide at room temperature.

For the four of the last eight coals listed in Table 1, the carbon dioxide specific surfaces vary from 100 to 255 m^2/gm . There thus must be an appreciable number of micropores in these coals, just as in the higher-rank coals discussed previously. However, for the last 8 coals in Table 1, both the x-ray and nitrogen

specific surfaces are larger than for the first 8 coals in the table. The specific surfaces calculated from the x-ray scattering curves for these 8 coals are sometimes larger and sometimes smaller than the surfaces determined by low-temperature nitrogen adsorption. When the x-ray specific surface exceeds surface area measured by low-temperature nitrogen adsorption, there must, as we have mentioned, be an appreciable number of pores large enough to be detected by scattering but closed to nitrogen. On the other hand, when the low-temperature nitrogen specific surface is larger than that from the x-ray data, there must be a significant fraction of the pores which are too small to be included in the x-ray specific surface.

There are pronounced shoulders on the scattering curves for PSOC Coals 105, 022, and 188, while there are no shoulders on the curves for Coals 197 and 138. The shoulders in the scattering curves from Coals 185 and 181 are less evident, and a shoulder can be seen for Coal 212 only after careful inspection. These results suggest that there will be well-defined shoulders in the scattering curves only when the specific surface of the transition pores is at least ten times as great as that of the macropores.

For the first seven coals in Table 1, the surface area from the transition pores is only one to two times as great as the specific surface from the macropores. There are no inflections in the scattering curves for any of these coals, in agreement with the above criterion for the presence of an inflection in the scattering curve.

The fraction of the volume associated with a given type of pore can be described as the product of an average dimension and the specific surface for this pore class. When, as is true for many of the coals listed in Table 1, the specific surface contributions from the macropores and transition pores are roughly equal, the specific volume occupied by the macropores therefore will be, in general, considerably larger than the volume of the transition pores, for which the average dimension is much smaller than that of the macropores. Gan, Nandi, and Walker¹⁴ have combined measurements by mercury porosimetry and low-temperature nitrogen adsorption at 77 K to find the fractions of the pore volume associated with the macropores, transition pores, and micropores. Among the coals for which they calculated pore-volume distributions were PSOC Coals 127, 135, and 197, which we have examined by small-angle x-ray scattering. They also studied PSOC Coal 105A, which probably is very similar to the coal PSOC 105 which we investigated. In Coals 127 and 135, they found that the volume occupied by the transition pores was very small, and that over half the pore volume was taken up by micropores. These conclusions are quite consistent with the specific surface results in Table 1, according to which the transition pores make a relatively small contribution to the specific surface, and the specific surface from room-temperature carbon dioxide adsorption

is much larger than the surface area obtained by other techniques. Similarly, Gan, Nandi, and Walker found that the fraction of the pore volume occupied by the transition pores is about four times as great in PSOC Coal 105A as in PSOC Coal 197. This result is in at least qualitative agreement with our calculation that in PSOC Coal 105, for which the small-angle x-ray scattering curve has a pronounced inflection. Also, as can be seen in Table 1, the specific surface associated with the transition pores is much larger than in PSOC Coal 197, for which there is no inflection in the scattering curve.

The PSOC coals were especially convenient samples for our x-ray studies, because in the data bank, there is a considerable amount of information about these coals obtained by techniques other than x-ray scattering. Without these other results we would not have been able to make such a detailed interpretation of the scattering data. Moreover, since we had studied PSOC coals, we could compare our porosity studies with the work of others, such as that of Gan, Nandi, and Walker¹⁴. On the other hand, as the other small-angle x-ray scattering studies of coals¹⁹⁻²², which we are aware of did not investigate PSOC coals, we could not make a quantitative comparison of our scattering results with those previously published.

It is natural to ask whether the least-squares fits of (8) to the scattering curves for these 15 coals are merely exercises in curve fitting or whether the fact that quite good fits can be obtained, in many cases over the whole scattering curve at which data were recorded, means that the pore structure used in developing (8) really has some connection with the pore structure in the coals. This point is especially important because in principle, more than one sample can produce the same small-angle x-ray scattering pattern.

As is true for almost all small-angle scattering studies, the interpretation of the scattering data must take account of other information about the sample besides the scattering data. Since other studies of coal have suggested a pore structure which consists of three classes of pores--macropores, transition pores, and micropores, and as this structure provides a useful way of analyzing the scattering data, we feel that at least the general features of our interpretation of the scattering curves are essentially correct.

We therefore suggest that the x-ray scattering method can be useful in studies of the pore structure of coals. In particular, the scattering curves from medium-rank and low-rank coals can provide an estimate of the specific surfaces associated with the macropores and the transition pores. This information is difficult to obtain by other techniques.

ACKNOWLEDGMENTS

We would like to express our sincere gratitude and appreciation to S. R. Koirtyohann for assistance with the preparation of the ash samples by low-temperature ashing, to Robert G. Jenkins for measuring the specific surfaces of PSOC Coal 105, and to S. S. Pollack, D. W. Houseknecht, B. E. Cutter, Robert G. Jenkins, and Phillip L. Walker, Jr. for advice and assistance during parts of the investigation. Sponsored by the U.S. Department of Energy.

Literature Cited

1. Guinier, A.; Fournet, G.; Walker C. B.; Yudowitch K. L.; "Small-Angle Scattering of X-Rays"; Wiley: New York, 1955, Eq. (26), p. 17.
2. Ref. 1, pp. 3-4.
3. Ref. 1, Equations (6) and (21), Chapter 2.
4. Kratky, O.; Skala Z. Zeits. Elektrochem.-Ber. Bunsenges. phys. Chemie 1958, 62, 73-77.
5. Lin J. S.; Von Bastian, C. R.; Schmidt P. W. J. Appl. Cryst. 1974, 7, 439-442.
6. Taylor, T. R.; Schmidt P. W. Acta Phys. Austriaca 1967, 25, 293-296.
7. Dubinin, M. M. in "Chemistry and Physics of Carbon"; (Walker, P. L., Jr., ed.), Vol. II, Dekker: 1954, New York, 1956; pp. 51-59.
8. Hirsch, P. B. Proc. Roy. Soc. (London) 1954, 226A, 1954, 143-169.
9. Ref. 1, pp. 24-28.
10. Ref. 1, p. 26.
11. Guinier, A. "X-Ray Diffraction in Crystals, Imperfect Crystals, and Amorphous Bodies"; Freeman: San Francisco, 1963; pp. 3-4.
12. Debye, P.; Anderson, H. R. Jr.; Brumberger, H. J. Appl. Phys. 1957, 28, 679-683; Goodisman, J.; Brumberger, H. J. Appl. Cryst. 1971, 4, 347-351 and J. Appl. Cryst. 1979, 12, 398-399.
13. "International Tables for X-Ray Crystallography, Vol. III"; published for the International Union of Crystallography by Kynoch Press, Birmingham, England, 1962; p. 162.
14. Gan, H.; Nandi, S. P.; Walker, P. L., Jr. Fuel 1972, 51, 272-277.
15. Bevington, P. R. "Data Reduction and Error Analysis for the Physical Sciences"; McGraw-Hill: New York, 1969, Program CURFIT, pp. 237-240.
16. Reference 1, p. 157, Equation (33).
17. Patel, I. S.; Schmidt, P. W. J. Appl. Cryst. 1971, 4, 50-55.
18. Gregg, S. J.; Sing, K. S. W. "Adsorption, Surface Area, and Porosity"; Academic Press: London and New York, 1967, pp. 211-217.

19. Durif, S. J. Chim. Physique 1963, 60, 816-24.
20. Kröger, C.; Mues, G. Brennstoff-Chemie 1961, 42, 77-84.
21. Spitzer, Z.; Ulický, L. Fuel 1976, 55, 21-25.
22. Lin, J. S.; Hendricks, R.W.; Harris, L. A.; Yust, C. S. J. Appl. Cryst. 1978, 11, 621-625.

RECEIVED April 29, 1981.

Carbon-13 CP/MAS Study of Coal Macerals of Varying Rank

RONALD J. PUGMIRE—Department of Fuels Engineering, University of Utah, Salt Lake City, UT 84112

KURT W. ZILM—University of Utah Research Institute, Salt Lake City, UT 84112

DAVID M. GRANT—Department of Chemistry, University of Utah, Salt Lake City, UT 84112

STEPHEN R. LARTER and JAMES ALLEN—Union Oil Company of California, Brea, CA 92621

JOSEPH T. SENFTLE, ALAN DAVIS, and WILLIAM SPACKMAN—College of Earth and Mineral Sciences, Pennsylvania State University, University Park, PA 16802

Work in our laboratory on a number of different coals demonstrated that significant structural differences were evident in ^{13}C NMR spectra of coals of different rank. The question arises as to which components and/or properties of coal are responsible for the spectral responses observed.

It is known that the properties of coal are controlled both by rank and petrographic composition (type). Thus, to predict the chemical properties of a given coal, it is necessary to know its petrographic composition and the chemistry of each component (maceral) at the rank in question. A study of individual macerals (or maceral groups) over a range of ranks is essential to determine a) the differences between individual macerals, and b) the differences within individual macerals of varying ranks. At the present time, petrographic composition can be determined by established microscopical techniques, but detailed chemical data on individual macerals are lacking. Such chemical data is required to efficiently develop many current coal based synthetic fuels technologies. Recent work by Given and Co-workers (1-3) described the dependence of coal liquefaction behavior on coal characteristics (3). Statistical correlations were found for the following parameters; total sulfur content (organic and inorganic), total reactive macerals, and percent carbon. The statistical analysis of the data demonstrated a differentiation between subsets of the total data base consisting of eastern and interior province coals and western province coals. While the latter subset "did not give any satisfactory correlation" (with liquefaction behavior). . . "it seems that a rank parameter together with parameters representing petrographic composition are the most relevant properties of such coals" (3).

Given, et. al. (2) have reported the molecular parameter analysis of asphaltenes obtained from coals of variable petrographic compositions based on proton NMR analysis. However,

0097-6156/81/0169-0023\$05.00/0

© 1981 American Chemical Society

molecular parameter analysis of coal liquefaction products gives only indirect evidence of the initial coal structure. Non-destructive techniques have been employed to examine the fraction of aromatic carbon, f_a , for coals by the graphical densitometer method of Van Krevelen, Chermin, and Shuyer (4) and by analyses of proton second moments obtained from broadline proton NMR data (5, 6). An extensive list of maceral f_a values have been published by Dormans, Huntjens, and Van Krevelen (7) and these authors concluded that the relative aromaticity of macerals is in the order fusinite > micrinite > vitrinite > exinite at a given rank. A much more limited number of macerals have been examined by broadline proton NMR techniques (5, 6, 8) and the data on relative f_a values are consistent with those reported by Van Krevelen, et. al. (7).

The direct determination of the aromaticity in coal was first reported by VanderHardt and Retcofsky (9) using non-spinning carbon-13 NMR techniques. More refined studies using a combination of cross-polarization and magic-angle spinning (CP/MAS) has been used to examine the aromaticity in a number of different coals (10, 11).

Two recent studies have examined the ^{13}C NMR spectra of coal macerals and lithotypes respectively. Retcofsky and VanderHardt (12) reported the aromaticities of the vitrinite, exinite, micrinite, and fusinite from Hershaw hvAb coal using non-spinning cross-polarization techniques. The f_a values of 0.85, 0.66, 0.85, and 0.93 -0.96 for these macerals demonstrate clear variations between the materials at a given rank. Gerstein et. al. (13) used carbon-13 CP/MAS proton combined rotation and multiple pulse spectroscopy (CRAMPS) to examine Iowa vitrain (Star coal) and a Virginia vitrain (Pocahontas #4 coal) with aromaticities of 0.71 and 0.86 respectively.

We have employed CP/MAS techniques for characterizing two sets of coal macerals. In the first set, we examined eight maceral samples (two alginites, two sporinites, three vitrinites and one fusinite) of Carboniferous and Permo-Carboniferous age which have been previously reported (14). We now compare this work with a set of six hand picked vitrinite macerals from the Lower Kittanning seam.

Experimental

NMR. The CP/MAS spectra were obtained on a single coil, double-tuned probe similar in design to that reported earlier (15) but modified (16) for the electromagnet of the Varian XL-100-15 system. A homebuilt receiver system allows single coil operation. The probe uses a D_2O external lock and a special rotor and stator assembly design to provide MAS. The carbon-13 (25.16 MHz) and the proton (100.06 MHz) radio frequency fields are 17 G and 12 G, respectively for 90 watts of power. The ^1H spin locking pulse of 90° may be varied in terms of length and amplitude while the amplitude of the ^{13}C irradiation can be controlled to within 0.1 db to match the Hartmann-Hahn (17) condition. The isolation between the two channels is in excess of

60 db. The CP/MAS spectra were obtained using a single contact sequence (9). A contact time of 2.0 msec and a cycle time of 3.0 sec were used in these experiments and the magic-angle spinner was operated at approximately 5,000 revolutions per second.

Sample Separation and Characterization. Three vitrinite samples (Silkstone, High Hazels, and Westfield) were obtained by hand-picking of macroscopic vitrain bands in Carboniferous coals. Selected vitrain particles were crushed to pass a B. S. 100 mesh sieve (250 μ) and polished mounts were prepared. Sample purity was determined by point-counting (sample reflectivity) 500 points, giving a \pm 2% (by volume) accuracy (18).

Alginites were obtained from selected Permo-Carboniferous torbanites (i.e. algal-rich coals) which, upon petrographic analysis, were found to be rich in the required component. No concentration steps were required for samples used in this work as small blocks were selected in which the initial alginite concentrations were adequate (see Table I).

Sporinite samples were prepared from durain bands in pre-selected Carboniferous coals. Generally, sporinite in durains occurs in intimate mixtures with other macerals, mostly inertinites. To prepare concentrates, the differences in specific gravities between maceral groups were utilized (18) following a float/sink technique modified after Dormans, et. al. (7). Briefly, small blocks of durain were crushed to pass the B. S. 240 mesh sieve (104 μ), and the pulverized material was dispersed in $ZnCl_2$ solution of 1.30 specific gravity (powder:liquid; 1:5 w/v). The suspension was centrifuged at 2500 rpm for 15 minutes to give well-separated "float" and "sink" fractions. The "float" was recovered, suspended in $ZnCl_2$ solution of 1.25 specific gravity, and re-fractionated into two layers by centrifugation as above. "Floats" from this procedure were repeatedly re-processed under similar conditions until no more "sinks" were produced. The fractionation produced by each separation was monitored by microscopical analysis to observe that separation was proceeding as desired and to implement minor corrective procedures as necessary. Purities given in Table I of the final concentrates were determined by point-counting (see above). Full details of original samples, separation procedures and microscopical analyses are given by Allen (19).

The fusinite sample was hand-picked from a discrete fusain lens located within a Carboniferous coal. Microscopical examination of the sample showed that the recovered material contained fusinite, semi-fusinite and mineral matter as the major components. The concentrate was not demineralized.

Six vitrinite samples from the Lower Kittanning seam were hand-picked to represent a wide range of vitrinite reflectance. These samples exhibited a minimum of 97% vitrinite and were used without further purification. Samples were supplied by Professor Alan Davis of Pennsylvania State University.

TABLE I
Petrographic Analysis of Maceral Concentrates

Vitrinite Concentrates	Rank ^a	Vitrinite % ^b	Exinite %	Inertinite %		
Silkstone ^c	1.04	94.5	1.1 sporinite	4.2 micrinite > fusinite > semi-fusinite		
High Hazles Westfield	0.68 0.47	97.0 95.5	0.2 sporinite 0.8 sporonite	2.8 dominantly semi-fusinite 3.7 dominantly granular micrinite		
Sporinite Concentrates ^d	Rank ^a	Sporinite % ^b	Vitrinite %	Inertinite %		
Silkstone Shallow	1.04 0.56	89.7 88.1	1.0 1.4	9.3 micrinite and fusinite 10.5 semifusinite > micrinite		
Alginite Concentrates	Rank ^a	Alginite % ^b	Sporinite %	Inertinite %	Vitrinite %	Mineral Matter %
Torbane Hill (Scotland)	n.d.	90.8	0.4	4.9	3.0	0.9
New South Wales ^e	n.d.	93.0	0.4	3.1	2.1	1.5
Fusinite Concentrate						
Westfield Fusinite	0.47	(see footnote f)				

a. Rank was determined for each sample from reflectivity data measured on the associate vitrinite component.

b. These values reflect the purity of the major maceral component.

c. Pyrite counted to less than 1%.

d. Resinite was detected in trace amounts.

e. Except for this Australian sample, all others were from England and Scotland.

f. Hand picked simultaneous with the collection of the Westfield vitrinite sample. Quantitative petrographic data are not available, but qualitative examination indicated that the fusain sample contained mostly fusinite and semifusinite, with some mineral matter.

The petrographic analyses of the first set of maceral concentrates are given in Table I while the chemical analyses are given in Table II. These macerals have all been thoroughly extracted with dichloromethane prior to obtaining spectra (20). Thus the data given refer to the insoluble portion of the samples. The vitrinite samples from the Lower Kittanning seam were run as received. The chemical analysis is given in Table III.

Results

The samples examined in the first set of macerals to be discussed are described in Tables I-II, while the ^{13}C CP/MAS spectra of the alginite, sporinite, vitrinite, and fusinite samples are given in Figures 1-4. Figure 5 provides a useful summary of the chemical shift ranges of selected structural units of interest. A cursory glance at these spectra in Figures 1-4 indicates that a unique spectral pattern is exhibited for each maceral type. The differences are sufficient between maceral types within this limited sample set to enable one to distinguish between the macerals.

The alginite spectra in Figure 1 are essentially identical. This result is expected from previous botanical and chemical studies on these alginites (21-24). The spectra display a simple structure in both samples which is dominated by long chain CH_2 groups (resonance lines in 29 ppm region). The shoulder at lower field (30-55 ppm) is due to branched centers and alicyclic materials. Little structural information is evident in the 55-75 ppm range where one would observe aliphatic carbons attached to nitrogen or oxygen. This observation is consistent with the low values found for nitrogen plus oxygen content (5-6%). The unsaturates region (resonance lines below 100 ppm) is a structureless band representing 13%, (e.g. f_a , defined as the fraction of total carbon that is unsaturated) of the total observed carbon. Degradation of alginite kerogens by chemical oxidation (23, 25) and pyrolysis (19, 23, 24, 26-28) have shown that these materials are largely unbranched aliphatic hydrocarbon chain polymers with major alicyclic, heterocyclic and aromatic regions. Thus carbon resonances in the aromatic region are to be expected. In addition, there is evidence for the presence of olefinic structures in alginite kerogen (23). Therefore, the resonances in the broad unsaturated region may be due to a complex group of olefinic and aromatic carbons but such structural groups represent less than 20% of all carbons present.

The sporinite spectra (Figure 2), while exhibiting broad similarities, are found on careful examination to have subtle differences in both the aliphatic and aromatic regions. In the aliphatic portion of the spectra these differences are associated with variations in the relative amounts of CH_3 , CH_2 , and $(\text{CH}_2)_n$ structural moieties. Both spectra exhibit shoulders at 13-15 ppm (terminal methyl region), but the band at 22-24 ppm in the

TABLE II
Chemical Composition of Maceral Concentrates

	Elemental Analysis				Proximate Analysis				NMR Carbon Analysis f_a % aromatic
	C	H	S	N+O	Atomic H/C Ratio	Volatile Matter % (daf) ^a	Fixed Carbon		
<u>Vitrinite</u>									
Silkstone	86.6	5.5	1.0	6.9	0.76	47	53	66	
High Hazles	82.3	5.0	1.1	11.6	0.73	46	54	67	
Westfield	77.2	4.8	0.5	17.5	0.75	52	48	56	
<u>Sporinite</u>									
Silkstone	87.1	6.4	0.4	6.1	0.88	56	44	51	
Shallow	80.6	6.7	1.2	11.5	1.00	63	37	47	
<u>Alginite^b</u>									
Torbane Hill (Scotland)	82.8	10.8	0.4	6.0	1.57	97.8	2.2	13	
New South Wales	84.0	10.7	0.5	4.8	1.53	98.8	1.2	13	
<u>Fusinite</u>									
Westfield	n.d.				0.38		n.d.	72	

TABLE III
Ultimate and Proximate Analysis of Vitrinite Macerals

PSMC-	Ultimate Analysis					Proximate Analysis		
	C	H	S (%dmmf)	O	N	H/C	Volatile Matter (%dmmf)	Fixed Carbon
67	82.2	5.5	1.5	9.4	1.5	0.80	41.6	58.4
19	84.4	6.0	2.6	6.8	1.6	0.85	41.4	58.6
34	83.9	5.2	0.9	8.5	1.6	0.74	35.0	65.0
43	87.0	5.7	1.8	4.9	1.6	0.79	34.6	65.4
47	88.0	5.3	0.8	4.6	1.6	0.72	26.6	73.4
53	89.1	4.6	0.6	3.9	1.5	0.62	18.6	81.4

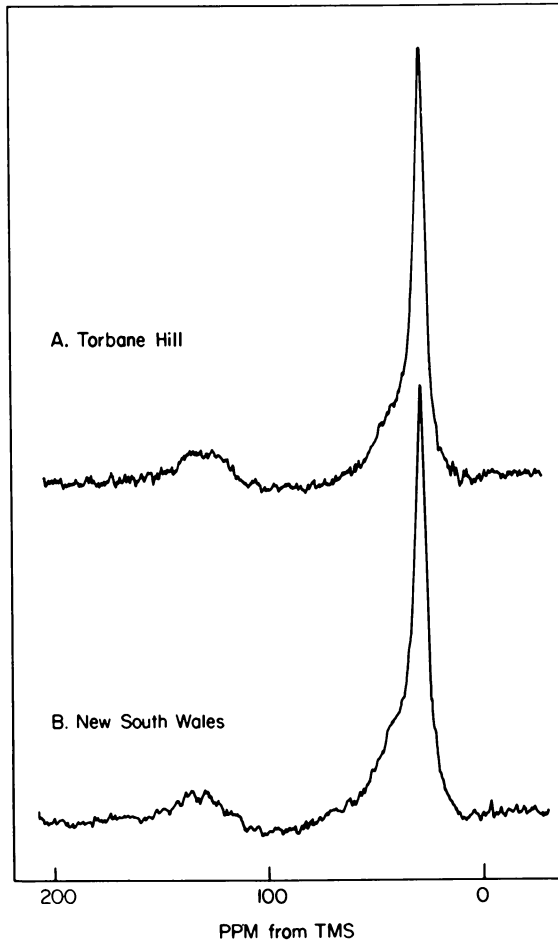


Figure 1. CP/MAS spectra of alginite concentrates from widely separated sources: Scotland (A) and Australia (B).

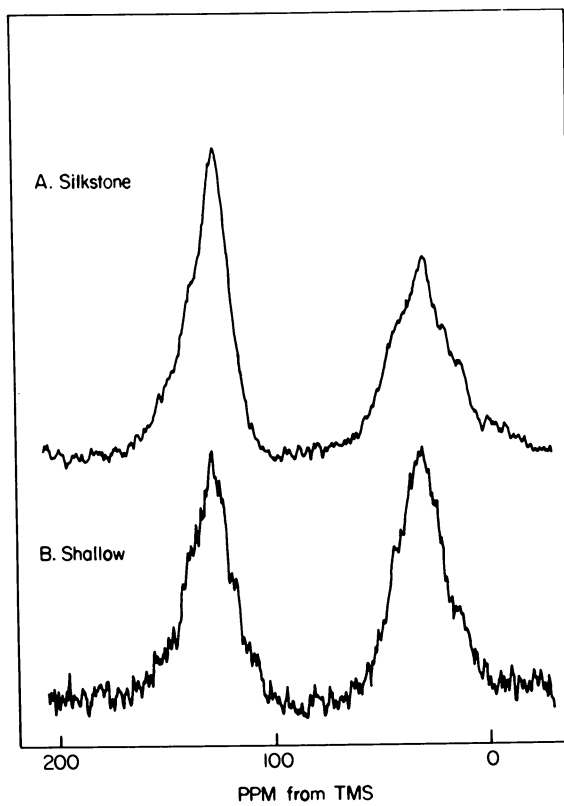


Figure 2. CP/MAS spectra of sporinite concentrates arranged in order of decreasing rank

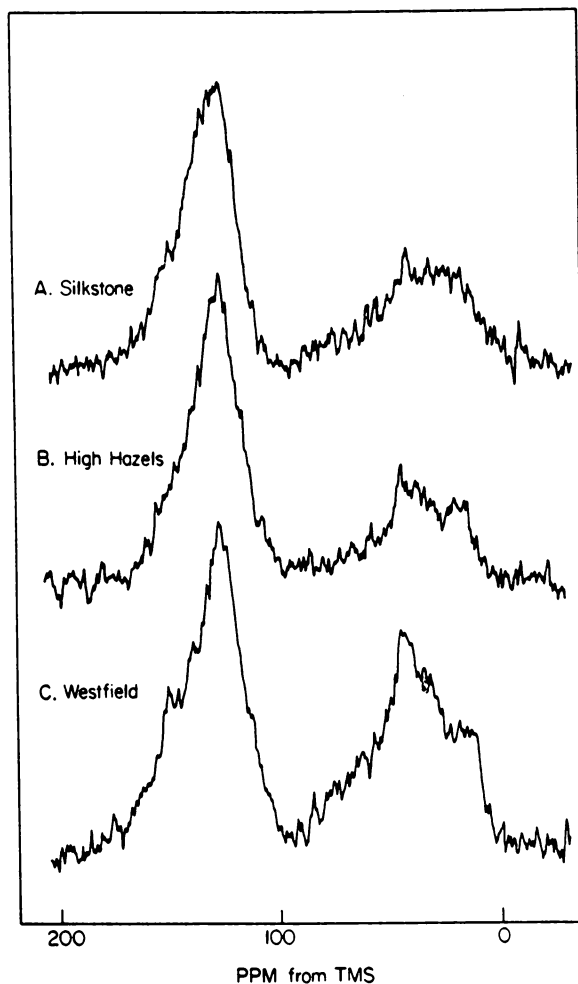


Figure 3. CP/MAS spectra of vitrinite concentrates arranged in accordance with decreasing rank from top to bottom.

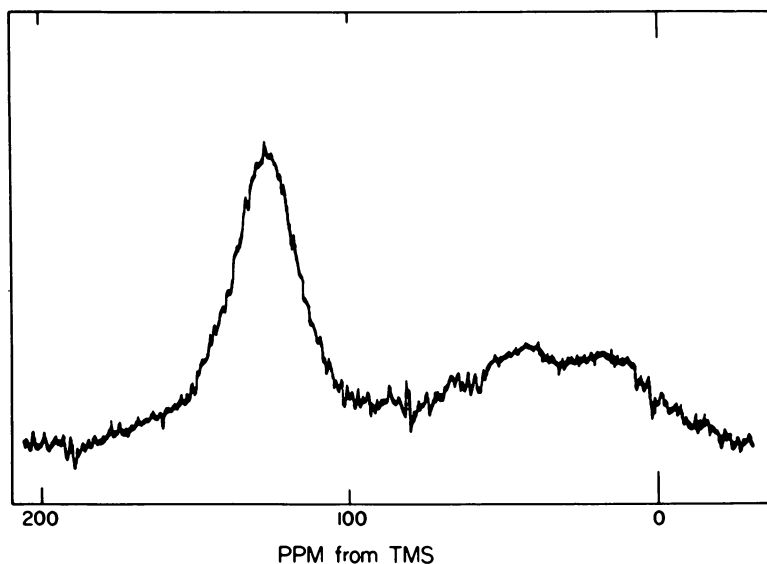


Figure 4. CP/MAS spectra of fusinite obtained from Westfield mine. The lack of any fine structure in the spectrum is most likely due to high concentrations of paramagnetics.

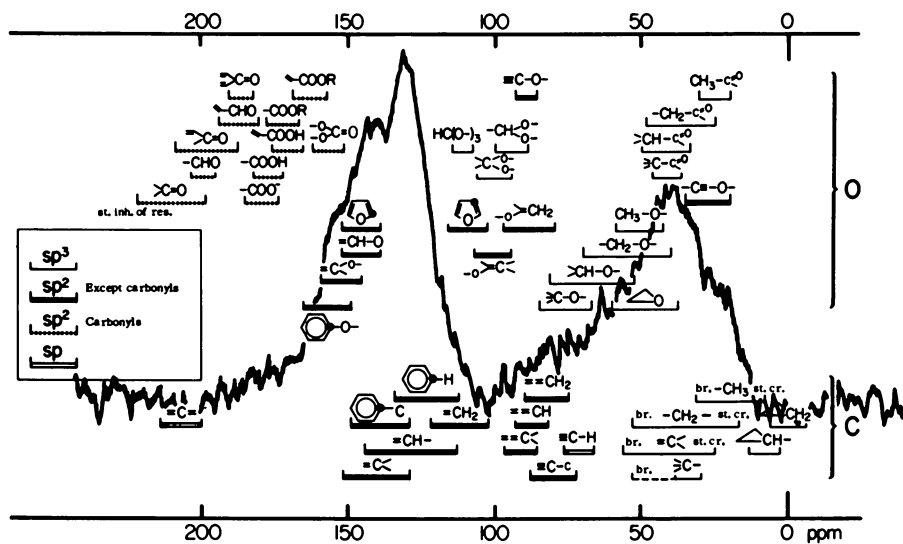


Figure 5. Composite of C-13 NMR correlation chart and PSMC-67

Silkstone sporinite is not distinguishable in the Shallow maceral sample. This spectral region is characterized by branched CH_3 groups and sterically crowded CH_2 groups. In both spectra the maximum intensity in the aliphatic region is at 30 ppm which is a region characteristic of cyclic and alicyclic CH_2 groups as well as branched CH_3 and sterically crowded CH groups. The 45-55 ppm spectral region of the aliphatic band is due to CH_2 , CH , and C carbons at or adjacent to highly branched centers.

The unsaturates region exhibits shoulders at approximately 155 and 136 ppm which can be attributed to oxygen functional groups and aromatic carbons adjacent to a nitrogen atom (150-155 ppm) and quaternary carbons in alkylated rings, bridgehead carbons, thio-ethers and aromatic carbons two bonds removed from a nitrogen atom (130-140 ppm). The Shallow sporinite exhibits two shoulders at approximately 117 and 112 ppm. These shoulders fall in the range characterized by pyrrole and furan ring structures as well as vinyl, substituted vinyl and alkylated aromatic rings. The unsaturates band in the Silkstone sporinite spans a similar spectral region but no structural component can be distinguished. The f_a values for these two samples are consistent with rank considerations; i.e., f_a for Shallow and Silkstone sporinites are 0.47 and 0.51, respectively. The vitrinite reflectance, % carbon, and % volatile matter suggest that the Silkstone sample is of higher rank than the Shallow material.

The vitrinite samples exhibit spectral patterns (Figure 3) that are clearly different from those observed in the sporinite concentrates. The spectral patterns, however, display differences that are significant between the vitrinites. The aromatic portion of the spectra display similar band shapes with shoulders at ca. 153-155 and 136-140 ppm which are due to structural features similar to those described for the sporinites (*vide supra*). On the other hand, the differences in the aliphatic portion of each spectra are worthy of comment. The region due to terminal methyl groups (13-15 ppm) decreases in intensity relative to the most intense spectral region (40-45 ppm) in the order Westfield < High Hazles < Silkstone. The 22-24 ppm region varies in intensity for the three samples studied. Interestingly, the 30 ppm region is devoid of structure suggesting that the cyclic and alicyclic CH_2 group are not a predominant structural feature. In all vitrinites the most intense aliphatic peak is in the 40-45 ppm region which is indicative of highly branched aliphatic structures. A similar spectral band was previously observed in whole coals (29) where a possible correlation with conversion properties was discussed. The Westfield sample contains a significant amount of intensity in the 60-80 ppm region. One finds branched aliphatic ethers and thio-ethers, highly branched amines, acetylenic, thio-acetylenic and allene type carbons in this region. Allene and acetylenic structures are not likely to be found in coals. Hence, the data in this region is consistent with the relatively high content of nitrogen and

oxygen (Table III) found in the Westfield vitrinite. The relative loss of heteroatoms with increasing rank as determined by ^{13}C NMR is consistent with theories concerning changes in coal undergoing progressive catagenesis (30).

The fusinite spectrum contains structureless aromatic and aliphatic bands. A good deal of difficulty was encountered in acquiring data on this sample as the signal-to-noise ratio was poor for a comparable number of transients of the other samples examined. This may reflect the higher free radical concentration found in these materials (31) compared to other macerals. The data suggests that the fusinite sample is a condensed aromatic material with little hydrogen attached to the aromatic carbons (the atomic H/C ratio is one half that found for the vitrinites). This is consistent with classical coal theory and with the p-gc and p-ms fingerprints of this particular sample (24). However, the spectrum also show the presence of 20-30% aliphatic carbon ($f_a = 0.72$) in the structure, which is a value far higher than might be expected for a pure fusinite. It is possible that the semifusinite content in this sample is sufficiently high to enhance the aliphatic content of the mixture but no data are available to compare semifusinite and fusinites in this respect. The aliphatic band spans the region of ca. 10-65 ppm and hence has a distribution of structural carbons similar to the other macerals as noted earlier. Hence, CH_3 , CH_2 , $(\text{CH}_2)_n$, CH and C groups must be present in a variety of structural patterns. The extension of the band to low field (65 ppm) also suggests the presence of oxygen, nitrogen, or sulfur functional groups.

The measured f_a values for the alginite, sporinite and vitrinite samples are plotted against percent fixed carbon in Figure 6. A linear regression analysis of the data demonstrates a high degree of correlation ($R^2=0.9897$) between f_a values and % fixed carbon, or alternatively, % volatile matter. The intercept of 0.11 indicates that a portion (ca. 10%) of the aromatic (or ethylenic) carbon is lost during the pyrolysis process used to determine volatile matter content in the coal material. Such a loss would most likely come from loss of aromatic material (including hydroaromatics) that did not extensively polymerize during the coal pyrolysis process.

We have also used CP/MAS techniques to examine a set of six vitrinite samples hand-picked from the Lower Kittanning seam. The rank of the samples ranged from low volatile to high volatile B bituminous. The ultimate and proximate analysis are given in Table III. This set of samples was selected in order to assess the nature of structural changes observed when carefully selected coal samples of varying rank from a given seam are examined using CP/MAS techniques. In each case, the samples contained greater than 97% vitrinite.

For purposes of clarity, the CP/MAS spectrum of PSMC-67 is given in Figure 5 as a composite of ^{13}C chemical shifts of structural units containing H, C and O (32). The vitrinite

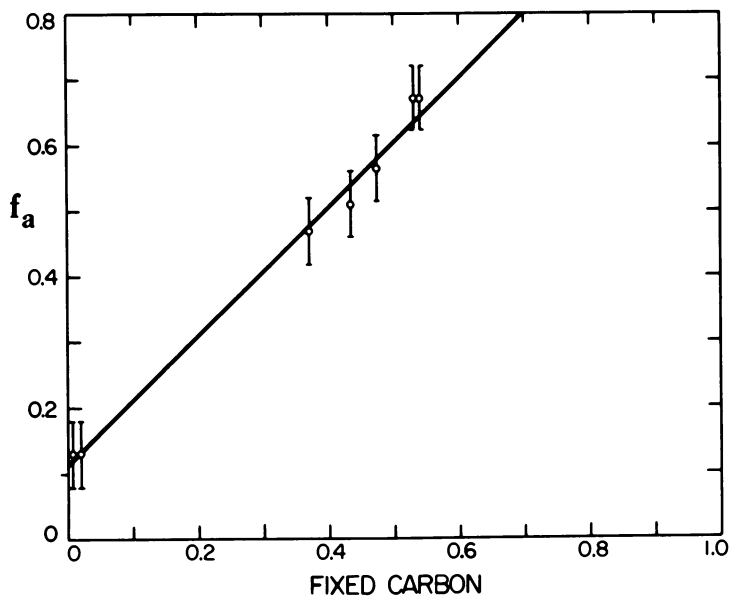


Figure 6. Plot of f_a vs. fixed carbon. The solid line is derived from the linear least-squares fit. The errors in f_a are estimated at $\pm 10\%$. Intercept, 0.11; slope, 1.00; $R^2 = 0.99$.

spectra thus displays the range of chemical structural types that give rise to resonance lines in different spectral regions. No effort was made to eliminate from the presentation chemical species (e.g. acetylenes, allenes, etc.) which are not expected to be present to any significant extent in the coal. Nitrogen and sulfur were not included in the display for simplicity of presentation and also due to the low concentration of these elements relative to oxygen. The banded structure observed in Figure 5, however, does provide enough detail to discuss major structural types present. A casual observation demonstrates that a significant amount of aliphatic oxygen is present (50-90 ppm region). Assuming allene and acetylene groups are not present, the 75-95 ppm region suggests the presence of oxygen containing structural types such as glucoside or pyranoside moieties which would be associated with cellulose, lignin, etc. containing materials. The 50-75 ppm range would contain aliphatic carbons associated with ether (either aliphatic or aromatic) and ester structural units.

Figure 7 displays the spectral changes that occur with rank progression. The spectra of PSMC-67, -53, and -43 represent the extremes and mid-point, respectively, of the rank of the samples. It is clear from an examination of the spectra that significant structural changes are occurring in the aromatic region. These observations are as follows: 1) significant decrease in the intensity in the region beyond 150 ppm; 2) significant decrease in the 135-145 ppm region; 3) a decrease in the line intensity in the 110-120 ppm region. In fact, the peak width at half height decreases in a nearly linear fashion by a factor of two as the vitrinite reflectance of the samples increase. Observations 1 and 2 are most likely due to loss of aromatic oxygen (phenols, aryl-aryl and aryl-aliphatic ethers), aromatic cyclic ethers (e.g. furans) and/or ring dealkylation. The 110-120 ppm region would represent alkene structures, β -carbons in aromatic cyclic ethers (furans), and ortho-carbons in phenols and phenolic ethers. Hence, decreasing relative intensity in these spectral regions suggests loss of aromatic oxygen structural units and possible ring dealkylation. This loss of structural features associated with oxygen is expected based on the known loss of oxygen with increasing rank (33).

The six sample series studied exhibited progression from a highly functional aromatic structure to one that displays little functionality. The aromatic band in PSMC-53 spans a chemical shift range characterized primarily by simple aromatic and condensed aromatic ring systems with significantly less functionality than observed in lower rank samples in this series.

In the aliphatic region, subtle differences are observed in the 15-40 ppm range. However, the aliphatic oxygen region of the spectrum (50-95 ppm) exhibits little perceptible difference, being characterized by a broad featureless band in each case. A careful examination of the spectrum of all six samples gives

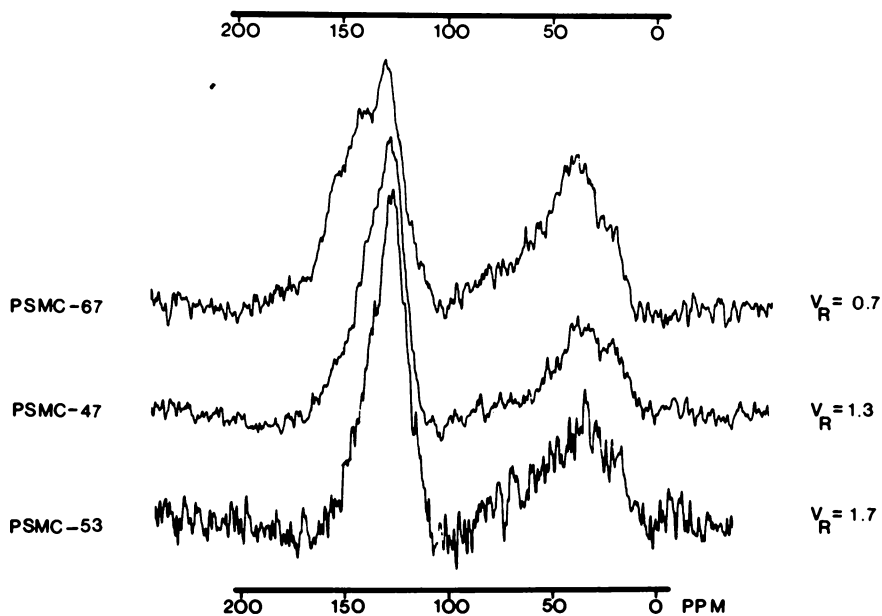


Figure 7. CP/MAS spectra of vitrinite samples from the Lower Kittanning Seam. The spectra represent changes that occur with rank progression. V_R refers to vitrinite reflectance values.

no indication of the extensive loss in oxygen functionality that is observed in the aromatic region. The rationale is not clear for the loss of aromatic oxygen with rank progression with no apparent concomitant loss in aliphatic oxygen in this sample set. Similar data from sample sets from additional coals of different rank, geological age and coal province, are needed to help interpret these observations.

Another interesting observation was made in this sample set. The f_a values did not cover the range expected. In fact, little variation in f_a values was observed (0.67 - 0.72). While most workers in the field agree that paramagnetic centers (stable free radicals and paramagnetic materials in the mineral matter) will cause sufficient line broadening to prevent observation of carbons in the vicinity of such centers, it is generally assumed that such centers are randomly distributed through the coal structure and, hence, a representative structural framework is observed (34). If random distribution of paramagnetic centers does not occur, the values obtained by the CP/MAS method would then represent lower limits if such centers were located (as is assumed) predominantly in the aromatic structure. If, on the other hand, the stable free radicals were mainly associated with aliphatic groups, the measured f_a values would be too high. Another possible source of error in measuring f_a values is non-equivalent response by all carbons present. In the case of bridgehead carbons that are far removed from protons, spectral distortions could occur which would lead to low values of f_a . If one were to progress from a highly protonated aromatic ring structure to a highly condensed ring structure, a bias in the line intensities in the aromatic region may occur. If such were the case, the measured f_a values may not increase with rank as rapidly as one might expect. This matter is presently a subject of investigation in our laboratory. The f_a values determined here for the sporinites and first set of three vitrinites are in fact low compared to some previously published data (7, 13). However, when the measured f_a values for the alginite, sporinite and three vitrinite samples are plotted against percent fixed carbon a reasonably linear relationship (see Figure 6) is obtained. Regression analysis yields a correlation constant of $R^2 = 0.99$ suggesting internal consistency within the data even though the CP/MAS technique may be estimating f_a on the low side. These tentative results require further supporting data as there are still broad ranges in which no data are yet available. It is not entirely clear why fixed carbon should be a simple function of sample aromaticity as small aromatic pyrolysis products (benzene, toluene, etc.) would be expected to appear in the volatile fraction during proximate analysis. Even so, large fused aromatic ring systems would not be expected to be volatile and would fall in the fixed carbon components. The offset of the line in Figure 6 is given by the intercept (0.11), and this is in the direction where the fraction of volatile aromatic

carbon lost is greater than the fraction of non-volatile aliphatic carbon retained in the pyrolysis process. Therefore, it may well be fortuitous that the slope (1.00) from the least squares treatment of the data in Figure 6 indicates a one to one relationship between the two different indices. When a similar analysis was made of the data on the Penn State vitrinites, no such relationship was found. This dichotomy is not at present understood.

Conclusions

The data presented in this paper provides information suggesting that the ^{13}C CP/MAS technique offers a significant approach to the investigation of the ultimate chemical structures of different macerals. While the spectral differences within a maceral group are subtle and only touched upon lightly due to the limited sample set available for study at the present time, the variation in spectral features between maceral groups is readily apparent from these results. In fact, the large differences noted between maceral types combined with the general homogeneity of chemical functionality observed within each group of macerals in the first maceral set studied suggests that macerals may be chemically more homogeneous than the parent coals. On the other hand, the rather significant variation in functionality observed in the Penn State maceral set indicates that systematic changes do in fact occur within a given coal seam that can be attributed to rank consideration. A more thorough understanding of these factors and a rationalization of the relative homogeneity of the sporinite and maceral groups from the English coals compared to the significant changes observed in the Pennsylvania vitrinite samples must await the availability of additional well characterized macerals for study.

Acknowledgments

Financial support was provided by the Department of Energy, Office of Energy Research, under Contract No. DE-AS02-78ER05006, Office of Fossil Energy under Contract No. DE FG 22-80PC30226, and Contract No. DE-AC22-80PC30013.

Literature Cited

1. Given, P. H.; Conauer, D. C.; Sparkman, W.; Lovell, H. L.; David, A.; Bisway, B.; Fuel, 1975, 54, 40.
2. Ibid, 1975, 45, 40.

3. a) Abdel-Baset, M. B.; Yarzab, R. F.; Given, P. H. Fuel, 1978, 57, 89; b) Yarzab, R. F.; Given, P. H.; Spackman, W.; Davis, A. Fuel, 1978, 59, 81.
4. Richards, R. E.; York, R. W. J. Chem. Soc. (Lond.) 1960, 2489.
5. Ladner, W. R.; Stacey, A. E. Fuel, 1963, 42, 75.
6. Tschamler, H.; de Ruiter, E. Coal Science, Advances in Chemistry Series 55 (Ed. R. F. Gould), Am. Chem. Soc., Washington, D.C., 332.
7. Dormans, H. N. M.; Huntjens, F. J.; Van Krevelen, D. W. Fuel, 1956, 36, 321.
8. Andrew, E. R.; Bradbury, A.; Eades, O. G. Nature, 1958, 182, 1695.
9. VanderHardt, D. L.; Retcofsky, H. L. Fuel, 1976, 55, 202.
10. Bartuska, V. J.; Maciel, G. E.; Schaeffer, J.; Stejeskal, E. D. Fuel, 1977, 56, 354.
11. Miknis, F. P.; Bartuska, V. J.; Maciel, G. E. American Laboratory, 1979, November, 19.
12. Retcofsky, H. L.; VanderHardt, D. L. Fuel, 1978, 57, 421.
13. Gerstein, B. C.; Ryan, L. M.; Murphy, P. D. Fuels Division Preprints, American Chemical Society, 1979, Volume 24, No. 1, 90.
14. Zilm, K. W.; Pugmire, R. J.; Larter, S. R.; Allen, J.; Grant, D. M. Fuel, 1981, 60, 0000.
15. Cross, V. R.; Hester, R. H.; Waugh, J. S. Rev. Sci. Instrum. 1978, 47, 1186.
16. Zilm, K. W.; Alderman, D. W.; Grant, D. M. J. Magn. Reson. 1978, 30, 563.
17. Hartmann, S. R.; Hahn, E. L. Phys. Rev. 1962, 128, 2042.
18. I. C. C. P. International Handbook of Coal Petrography 1963, 2nd Edition, C.N.R.S. (Paris).
19. Allen, J. Unpublished Ph.D. Thesis 1975, University of Newcastle, England.
20. Dichloromethane was employed as described in Reference 25 after which the samples were carefully and thoroughly dried.
21. Blackburn, K. B.; Temperley, B. N. Trans. Roy. Soc. Edin. 1936, 58, 841.
22. Dulhunty, J. A. Proc. Linn. Soc. New South Wales, 1944, 69, 26.
23. Allen, J.; Bjory, M.; Douglas, A. G. Advances in Organic Geochemistry 1979 (Eds. A. G. Douglas and J. R. Maxwell), Pergamon Press, in press. (A geochemical study of the exinite group maceral alginite selected from three Permo-Carboniferous torbanites).
24. Larter, S. R. Unpublished Ph.D. Thesis 1978, University of Newcastle, England.
25. Djuricic, M. V.; Vitorovic, D.; Andresen, B. D.; Hertz, H.S.; Murphy, R. G.; Preti, G.; Bieman, K. Advances in Organic Geochemistry 1971, (Eds. H. R. Bon Gaertner and H. Wehner) Pergamon (1972), 305.

26. Cane, R. F.; Albion, P. R. Geochem Cosmochem Acta. 1973, 37, 1543.
27. Larter, S. R.; Douglas, A. G. Environmental Biogeochemistry and Geomicrobiology 1978, (Eds. W. E. Krumbein) Ann Arbor, 373.
28. Larter, S. R.; Solli, H.; Douglas, A. G. J. Chromatogr. 1978, 167, 421.
29. Zilm, K. W.; Pugmire, R. J.; Grant, D. M.; Wiser, W. H.; Wood, R. E. Fuel 1979, 58, 11.
30. Van Krevelen, D. W. Coal, Elsevier Amsterdam 1961.
31. Austen, D. E. G.; Ingram, D. J. E.; Given, P. H.; Binder, C. R.; Hill, L. W. Coal Science Adv. in Chemistry Series 55 (R. F. Gould Ed.), ACS Publications, 1966, 344.
32. Wehrli, F. W.; Withlin, T. Interpretation of Carbon-13 NMR Spectra Heyden and Son Ltd., New York, 1976, 311.
33. See for instance, Berkowitz, N. An Introduction to Coal Technology Academic Press, New York, 1979, 36.
34. Retcofsky, H. L. private communication, 1980.

RECEIVED July 28, 1981.

Cross-Linked Structures in Coals: Models and Preliminary Experimental Data

LUCY M. LUCHT and NIKOLAOS A. PEPPAS

School of Chemical Engineering, Purdue University, West Lafayette, IN 47907

Treatment of the structure of bituminous coals as cross-linked macromolecular networks can provide important information on their extraction, swelling and liquefaction behavior at low and high temperatures. A modification of the Flory statistical mechanical analysis of Gaussian network chains has been applied to highly crosslinked macromolecular networks of coal for the determination of their number average molecular weight between crosslinks, \bar{M}_c , and the coal volume fraction of the swollen samples, $v_{2,s}$, at equilibrium swelling in pyridine at different temperatures. Three key factors in this analysis are discussed and clarified: the nature of crosslinks in coal, the significance of the number of repeating units between crosslinks, N , and the nature and significance of the pore structure. Values of \bar{M}_c for coal networks of fixed "aromatic cluster" size, \bar{M}_0 , obtained by numerical solution of the modified Gaussian chains model are 400-450 for bituminous coals. These values were determined experimentally from physicochemical swelling data of several American coals and compared with relevant experimental data from previously reported studies.

Important theoretical and experimental considerations of the use of macromolecular theories for the description of coal network structures have been recently analyzed (1). Relevant equations describing the equilibrium swelling behavior of networks using theories of modified Gaussian distribution of macromolecular chains have been developed by Kovac (2) and by Peppas and Lucht (3) and applied to various coal systems in an effort to model the relatively compact coal network structures (1,4). As reported before (1), Gaussian-chain macromolecular models usually employed in the description of polymer networks (such as the Flory

0097-6156/81/0169-0043\$05.00/0

© 1981 American Chemical Society

model, 5) are inapplicable for short, stiff chains. Although the modified Gaussian network equations provide an accurate description of physicochemical phenomena observed in highly crosslinked networks (within the assumptions made in their derivation), their application to actual coal macromolecular structures is a rather difficult task. Coal heterogeneities are in part responsible for this problem. Specifically, the nature of the crosslinks and the number of repeating units between crosslinks, N , appearing in the modified Gaussian model equations are not unambiguously defined because of the varying size, structure and chemical composition of the groups involved in the structure of the crosslinked chains of coal.

This contribution deals with some important aspects of coal structure evaluation using modified Gaussian models. Further clarification of the nature and functionality of the crosslinks is presented, including an analysis of refinements in the mathematical equations for the determination of \bar{M}_c . Preliminary experimental data of relevance to this analysis are also presented and discussed.

THEORETICAL CONSIDERATIONS

Equilibrium Swelling Theory

A detailed development of the modified Gaussian swelling equations is outlined elsewhere (1,2). Briefly, the procedure involves analysis of a macromolecular chain as a set of bond vectors. The distribution and partition functions are written in terms of the end-to-end vector r and the equilibrium force f to which the macromolecular chain is subjected. A specific series function is used to expand the distribution function, leading to a modified distribution, which is used to derive expressions for the end-to-end distance as a function of applied force. These expressions can be used to determine the Gibbs free energy due to elastic forces, ΔG_{el} . The Flory-Huggins theory is used for the expression of the free energy of mixing of macromolecules with swelling agent molecules, ΔG_{mix} . At equilibrium swelling, the excess chemical potential of the swelling agent in the network is zero, leading to equations relating parameters characteristic of the macromolecular network to thermodynamic properties of the system.

Equation (1) developed by Peppas and Lucht (3), is based on this analysis and it is applicable to isotropic highly crosslinked networks. It can be used to determine important structural parameters of the macromolecular network, such as the number average molecular weight between crosslinks, \bar{M}_c , and the crosslinking density of the network, ρ_x . In the following equations v and V_1 are the specific volume of the "idealized" coal network and the molar volume of the swelling agent respectively, $v_{2,s}$ is the equilibrium volume fraction of coal in the swollen macromolecular network, χ is the coal network/swelling

agent Flory thermodynamic interaction parameter at the corresponding swelling temperature and $v_{2,s}$, and N is the number of repeating units between crosslinks.

$$\frac{1}{\bar{M}_c} = \frac{\frac{\bar{v}}{v_1} [\ln(1 - v_{2,s}) + v_{2,s} + \chi_1 v_{2,s}^2] [1 - \frac{1}{N} v_{2,s}^{2/3}]^3}{[\frac{1}{2} v_{2,s} - v_{2,s}^{1/3}] [1 + \frac{1}{N} v_{2,s}^{1/3}]^2} \quad (1)$$

$$\rho_x = 1/\bar{v} \bar{M}_c \quad (2)$$

Nature of Crosslinks in Coal

Experimental observations show that bituminous coals satisfy at least one important macroscopic characteristic of a cross-linked network: they swell in numerous solvents without being dissolved by them even at high temperatures (1, 6-9), unless thermal degradation or reaction occurs. In the development of mathematical models to describe network behavior, crosslinks are assumed to be *points* (usually carbon atoms) or *short bridges* (usually of molecular weight much smaller than \bar{M}_c) whence three or more chains are initiated.

Based on recent experimental data on molecular weight distributions of depolymerized coal products (1) and the structure of functional groups in coal (4) we propose a coal crosslinked structure where the crosslinks are a bonding region, where three or more chains are joined through a single *cluster*. This cluster is probably an aromatic or heterocyclic group of molecular weight from 100-400 (10) similar to groups proposed by Wisner in his model coal network structure (11). Figure 1 presents a schematic analysis of the proposed physical structure.

Although this hypothesis reverses the usual concept of a crosslink, the network theories derived before (1,2) can still be applied as long as the molecular weight between crosslinks is considerably higher than the molecular weight of a cluster. The realization that the coal crosslinks have a finite volume implies that the calculated values of \bar{M}_c using equation (1) and related expressions will be smaller than the actual \bar{M}_c by a fraction, f , of the molecular weight of the cluster, \bar{M}_0 , where f is a constant varying between 0 and 1, taking the value of 0.5 for tetra-functional crosslinks.

$$\bar{M}_{c, \text{actual}} = \bar{M}_{c, \text{calc.}} + f \bar{M}_0 \quad (3)$$

In lignites, the probably small extent of crosslinking should eliminate the need for correction. However this correction may be important in bituminous coals and anthracites where crosslinking could be extensive. Actually, the effect of "bulky" crosslinks should be included in the non-Gaussian model analysis

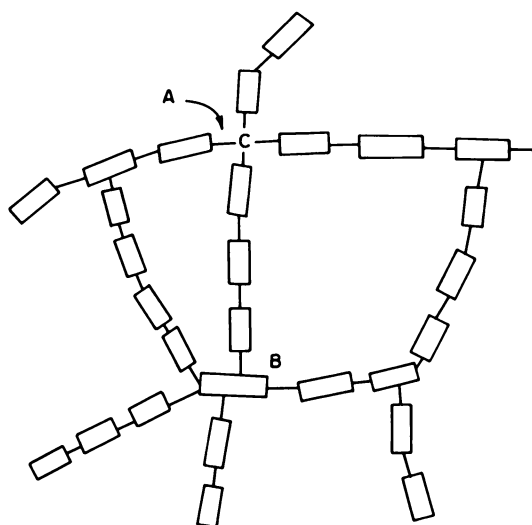


Figure 1. Proposed cross-linked structure in coals: Aromatic ring cluster (\square); connecting bond (—); tetra functional cross-link (A); multifunctional crosslink (B).

since this type of crosslink may lead to modified expressions for the end-to-end distance. Nevertheless, the approach described above can lead to reasonable determination of \bar{M}_c without additional modifications.

Repeating Unit Size

The number of repeating units between crosslinks, N , a parameter appearing in equation (1), can be simply defined as the ratio of the number average molecular weight between crosslinks, \bar{M}_c , to the average molecular weight of the clusters, \bar{M}_0 .

$$N = \bar{M}_c / \bar{M}_0 \quad (4)$$

Actually, in equation (3) it is assumed that $\bar{M}_0 = \bar{M}_r$, where \bar{M}_r is the molecular weight of a hypothetical repeating unit, which includes a cluster and a connecting bond. This is a reasonable assumption in view of the comparatively small size of the connecting bond (usually $-\text{CH}_2-$, $-\text{S}-$, or $-\text{O}-$, (1)) with respect to the cluster size and molecular weight. Simultaneous use of equations (1) and (4) can lead to the values of \bar{M}_c . For bituminous coal networks, a reasonable value of \bar{M}_0 of 150 will be used henceforth.

EXPERIMENTAL PART

To evaluate the swelling behavior and the crosslinked parameters of coal networks, swelling data were obtained for seven American coals supplied in fine particles by the Pennsylvania State University coal bank. To eliminate experimental artifacts, several separations and purifications were performed prior to swelling, according to the general experimental protocol reported in earlier communications (1,12).

The coal samples were sieved under nitrogen to 20-30 mesh size using ASTM approved sieves, and they were floated in a benzene/ CCl_4 solution of density 1.3 gr/cm^3 to remove most of the mineral matter and to isolate most of the vitrinite (see also Table I). Soxhlet extraction of the samples was performed in pyridine at its boiling point, and the insoluble coal matrices (residues) were dried under vacuum to constant weight and resieved to 20-30 mesh size. To ensure maximum solvent removal, the coal samples were dried to constant weight under nitrogen at approximately 700 mm Hg and $50-60^\circ\text{C}$. Swelling was performed at temperatures of $57 \pm 2^\circ\text{C}$. Data were also obtained for unextracted samples of 30-40 mesh size at 25°C and 50°C .

Swelling was carried out in a sealed chamber in the presence of excess pyridine vapors at atmospheric pressure and at the temperatures mentioned before. Thermodynamic equilibrium was achieved after 24 hours. Due to the porous structure of the coal samples not all the imbibed swelling agent contributed to the coal swelling. A considerable portion of this solvent

**American Chemical
Society Library**

1155 16th St. N. W.

Washington, D. C. 20036

TABLE I: Apparent Swelling Behavior of Coal Samples

P.S.U. Identification Number	ASTM Rank	Elemental Analysis (% daf)		Swelling Conditions		X-Factor (I)	Swelling v_2 , app
		C%	O%	Mesh Size	T(°C)		
418	Lignite	67.45	23.89	20-30	57	.289	.636
				30-40	50		
				30-40	25		
416	Subb	72.37	19.31	20-30	57	.346	.625
				30-40	50		
				30-40	25		
266	HVB	77.30	14.51	20-30	57	.403	.677
				30-40	50		
				30-40	25		
772	HVB	78.22	10.62	20-30	57	.413	.638
				30-40	50		
				30-40	25		
212	HVC	79.04	13.25	20-30	57	.423	.661
				30-40	50		
				30-40	25		
341	HVA	83.26	4.41	20-30	57	.472	.723
				30-40	50		
				30-40	25		
384	Anthracite	91.14	3.23	20-30	57	.563	.975
				30-40	25		

Only the 20-30 mesh coals were extracted before swelling.

remained in the pores without further contribution to coal swelling*.

An estimate of the *total* amount of swelling agent imbibed by the porous coal particles can be obtained by calculating an *apparent value* of $v_{2,app}$ by use of equation (5) which assumes additivity of volumes.

$$v_{2,app} = \frac{V_c}{V_{c,s}} = \frac{V_c}{V_c + V_s} = \frac{m_c/\rho_c}{m_c/\rho_c + m_s/\rho_s} \quad (5)$$

Here m , ρ and V denote weight, density and volume of the two components, i.e. coal and swelling agent, which are designated by the subscripts c and s respectively; then $V_{c,s}$ designates the volume of the swollen coal. An apparent volume degree of swelling, Q_{app} , can also be determined from equation (6).

$$Q_{app} = 1/v_{2,app} \quad (6)$$

Accurate determination of the coal volume fraction in the swollen coal particles can be done by calculating and excluding the pore volume, V_p , occupied by the solvent during swelling. Values of the porosity p , expressed according to equation (7) in terms of the pore volume per dry coal weight m_c , were determined from recent studies for similar coals (13). Where no values of this parameter were available, an interpolation of the porosity versus carbon content data (% C, dmmf basis) was used to determine p .

$$p = V_p/m_c \quad (7)$$

Then the weight of the solvent *effectively swelling the coal* can be calculated as,

$$m'_s = M - m_c - \rho_s V_p \quad (8)$$

where M is the total weight of the coal sample after swelling. Assuming additivity of volumes of the dry coal matrix, V_c , and the solvent that effectively swelled the coal, V'_s , it is possible to determine the true value of the coal volume fraction in the swollen coal (excluding the pores), $v_{2,s}$, by equation (9).

$$v_{2,s} = \frac{V_c}{V_c + V'_s} = \frac{m_c/\rho_c}{m_c/\rho_c + m'_s/\rho_s} \quad (9)$$

From equations (7), (8) and (9) it can be finally determined that:

$$v_{2,s} = 1 \left/ \left[1 + \frac{[M - (1 + p\rho_s)m_c]}{m_c} \left(\frac{\rho_c}{\rho_s} \right) \right] \right. \quad (10)$$

The true value of $v_{2,s}$ (equation 10) is the one to be used for the determination of \bar{M}_c since it refers to the swelling of the coal matrix, excluding the pore structure. Use of the value of $v_{2,app}$ (from equation 5) in equation (1) would lead to unacceptable values of \bar{M}_c . This is an error frequently made in previous studies.

Determination of the number average molecular weight between crosslinks, \bar{M}_c , was achieved by using equations (1), (4) and (10), using the following parameters for the coal samples and swelling agent (pyridine): $\rho_c = 1.30 \text{ gr/cm}^3$, $\rho_s = 0.982 \text{ gr/cm}^3$, $v_1 = 80.56 \text{ cm}^3/\text{mole}$, $v = 0.769 \text{ cm}^3/\text{gr}$ and $\bar{M}_0 = 150$.

The necessary values of the coal/swelling agent interaction parameter χ at 25°C were determined from equation (11), which presents a linear relationship between χ and the carbon content (on a % daf basis).

$$\chi = 0.0116 (\%C) - 0.4901 \quad (11)$$

Over the temperature range of 25–60°C the χ factor was assumed constant. The arithmetic values of χ used for this interpolation were derived by separating χ into an enthalpic and an entropic contribution. These terms were calculated from experimentally determined solubility parameters of the pure swelling agent and the non-swollen coal (1, 9). This thermodynamic treatment does not account for effects such as formation or disruption of H-bonds specific to a particular coal-solvent system. Although such models exist for simpler or more thoroughly characterized systems, models which can incorporate solvent specific effects into the determination of χ for coal systems are not available to this point. It is possible to use swelling agents which do not exhibit specific effects; however, most good swelling agents for coal may affect the tenuous bonds.

RESULTS AND DISCUSSION

"Apparent" Swelling Behavior

Table I summarizes the elemental analysis of the coal samples used (as supplied by the coal bank), the calculated values of the χ factors, the swelling conditions and the experimentally determined values of $v_{2,app}$ for these studies. Use of the "initial" elemental analysis of the coal samples (before extraction and swelling) for plotting the data is preferable here, since this elemental analysis is readily available and independent of processing conditions.

A general dependence of the apparent coal equilibrium volume

fraction $\nu_{2,app}$ on the carbon and oxygen content (on a daf % basis) is observed. Figure 2 shows this dependence of $\nu_{2,app}$ on the carbon content, obtained with extracted and unextracted coals of various sizes and at temperatures of 57°C and 50°C respectively. Based on the number of data presently available, $\nu_{2,app}$ (and the derived parameter Q_{app} , the apparent degree of swelling) do not significantly change in the range of 67% to 78% carbon content. Smooth curves can be fitted to these data for the range of carbon contents investigated. Similar behavior is observed when plotting volume fraction data for swelling at 25°C, as in Figure 3. The same figure includes experimental values of $\nu_{2,app}$ determined by Sanada and Honda (8) for a set of coal samples of similar range in carbon content. These data are included here because these authors did not make any mention of subtracting the pore volume in their calculations. Therefore, their calculated values of volume fractions may be apparent volume fractions, $\nu_{2,app}$.

The dependence of $\nu_{2,app}$ on the oxygen content of extracted and unextracted coal samples (on a daf basis) is presented in Figure 4. The same Figure includes the data of Sanada and Honda (8) and Kirov *et al* (9) for comparative reasons. The unextracted coal samples do, for the most part, show more "apparent" swelling, i.e. smaller values of $\nu_{2,app}$, than the extracted ones. This behavior may be the result of collapse of the pore structure due to extraction. This speculation is presently under investigation.

True Swelling Behavior - Effect of Porous Structure

The effect of $\nu_{2,s}$ on the determined values of M_c is shown in Figure 5, which presents data from numerical simulation of coal swelling behavior using hypothetical values of χ -factors ranging from 0.2 to 0.8. These calculations were done with the same coal and swelling agent parameters as before, for cluster size $\bar{M}_0 = 150$. Numerical calculations for cluster sizes between 100 and 300 showed that the calculated values of M_c were rather insensitive to change of \bar{M}_0 (at least in the range of "reasonable" values of molecular weights of coal clusters).

Values of the true coal volume fraction in the swollen coal particles were obtained from the experimental values of Table I for coals of size 20-30 mesh swollen in pyridine at $57 \pm 2^\circ\text{C}$. Equation (10) was used to determine these values of $\nu_{2,s}$ which are reported in Table II.

The dependence of the true $\nu_{2,s}$ on the carbon and oxygen content (on a % daf basis) is analyzed in Figure 6. The data show that within the range of 67-83% C the true coal swelling is not dependent on the elemental analysis. Above 83% C the degree of swelling decreases sharply. Table II also includes calculated values of M_c (for cluster size $\bar{M}_0 = 150$) from the corrected (true) values of $\nu_{2,s}$ and the corresponding χ -factors. This analysis shows that according to our hypothesis of "cluster-connecting

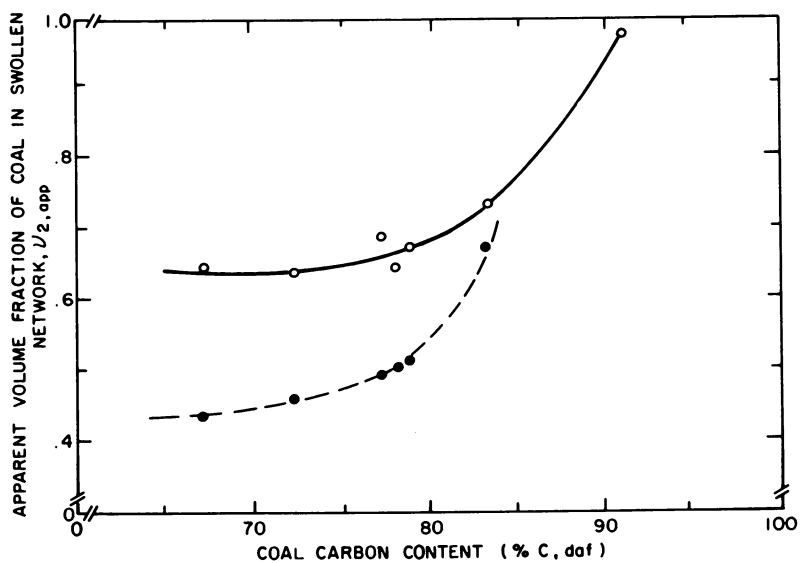


Figure 2. Dependence of apparent coal volume fraction at equilibrium swelling on the carbon content (% C, daf), for various American coals. Experimental values of $v_{2, app}$ for pyridine vapor swelling: $57 \pm 2^\circ\text{C}$, 20–30 mesh (extracted coals) (○); 50°C , 30–40 mesh (unextracted coals) (●).

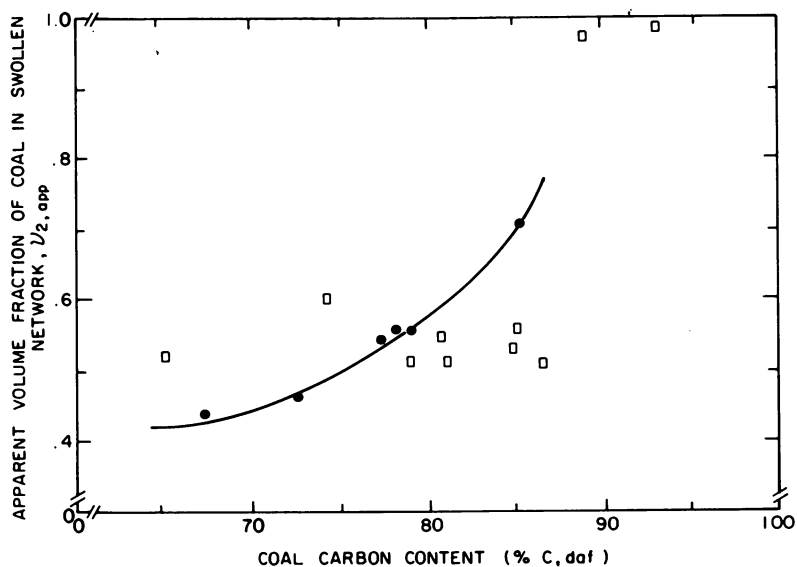


Figure 3. Dependence of apparent coal volume fraction at equilibrium swelling on the carbon content (% C, daf), for various American and Japanese coals. Curve fits the Purdue data (American coals only). Experimental values of $v_{2, app}$ for pyridine vapor swelling at 25°C: 30–40 mesh (unextracted coals) (●); Sanada and Honda (1966), 30–60 mesh (□).

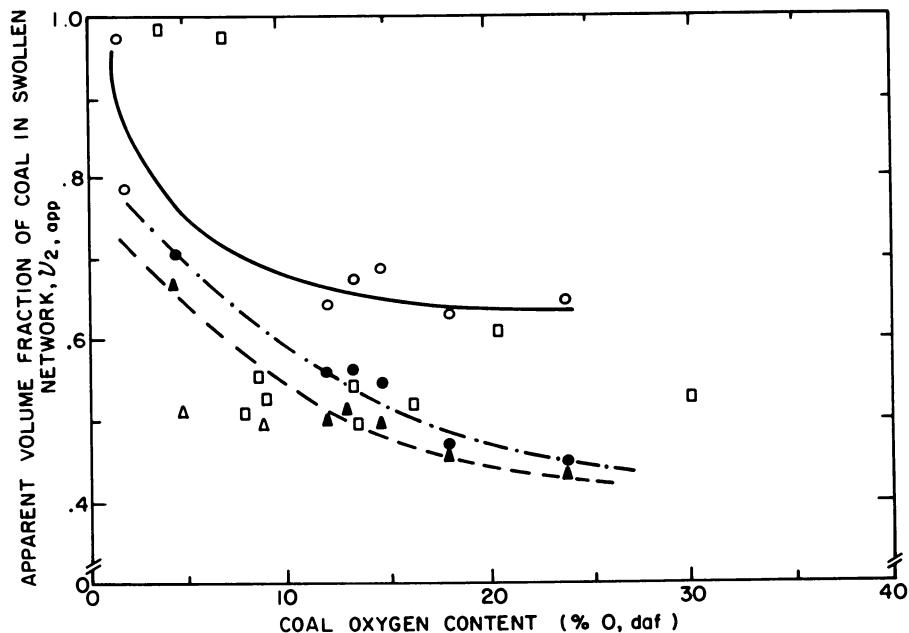


Figure 4. Dependence of apparent coal volume fraction at equilibrium swelling on the oxygen content (% O, daf) of various coals. The three curves represent best fitting of the three sets of Purdue data for American coals. Values for other coals (8, 9) are included for comparison. Experimental values of $v_{2, app}$ for pyridine vapor swelling: $57 \pm 2^\circ\text{C}$, 20–30 mesh (extracted coals) (\circ); 50°C , 30–40 mesh (unextracted coals) (\blacktriangle); 25°C , 30–40 mesh (unextracted coals) (\bullet); Sanada and Honda (1966) 25°C , 30–60 mesh (\square); Kirov et al. (1967) 25°C , 50–170 mesh (\triangle).

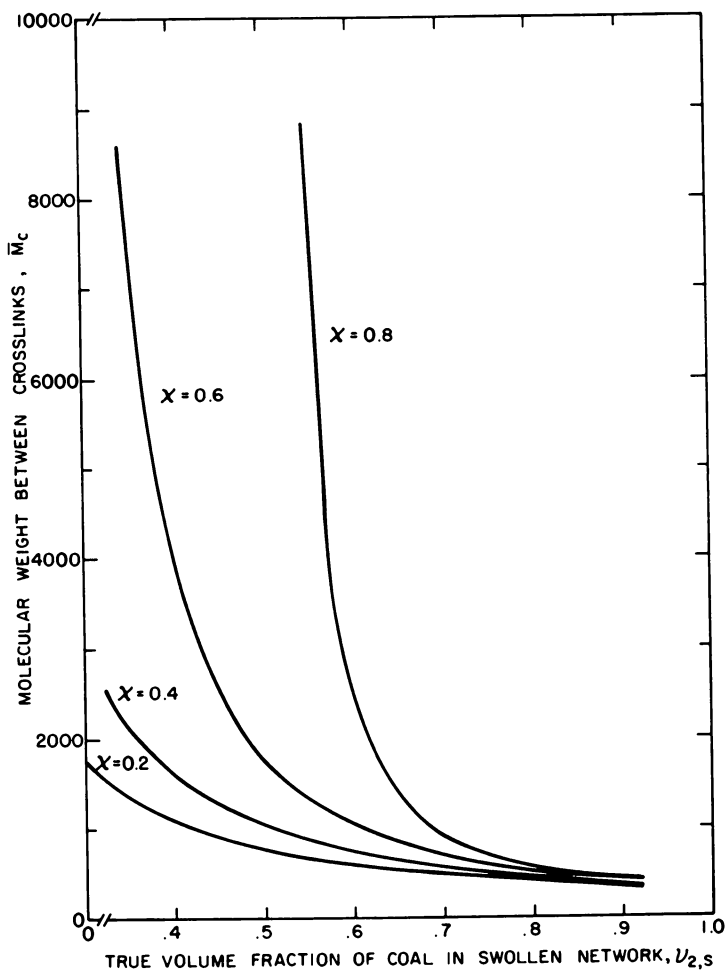


Figure 5. Numerical calculation of the \bar{M}_n between cross-links, \bar{M}_c , as a function of the thermodynamic parameter χ and the coal volume fraction $v_{2,s}$. Curves are calculated for $v = 0.769 \text{ cm}^3/\text{g}$, $\bar{V}_1 = 80.56 \text{ cm}^3/\text{mol}$ and cluster size $\bar{M}_0 = 150$.

TABLE II. True Swelling Behavior of Crosslinked Structure in Coal Samples *

P.S.U. Identification Number	ASTM Rank	Elemental Analysis (% daf)		Porosity p ($\frac{13}{3}$) ₃ (cm ³ /gr)	True $v_{2,s}$	X-factor (1)	\bar{M}_c
		c%	0%				
418	Lignite	67.45	23.89	.123	.832	.289	410
416	Subb	72.37	19.31	.159	.816	.346	445
266	HVB	77.30	14.51	.152	.862	.403	430
772	HVB	78.22	10.62	.141	.842	.413	405
212	HVC	79.04	13.25	.142	.819	.423	445
341	HVA	83.26	4.41	.072	.858	.472	400
384	Anthracite	91.14	3.29	.108	.956	.563	380

*Samples of 20-30 mesh swollen in pyridine at 57 ± 2°C.

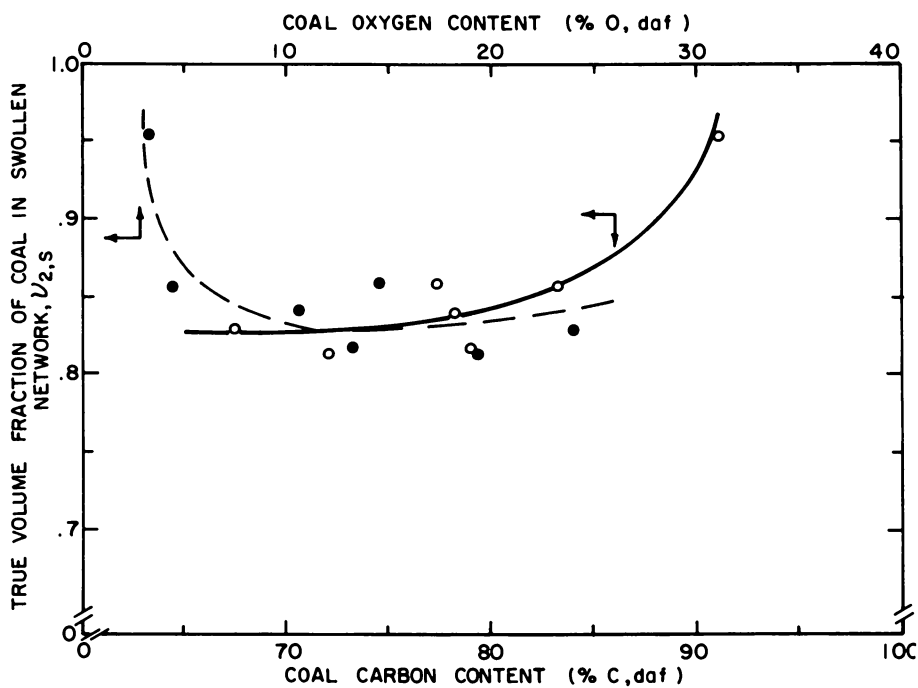


Figure 6. Dependence of true coal volume fraction at equilibrium swelling in pyridine at $57 \pm 2^\circ\text{C}$ on the (○) carbon and (●) oxygen contents (% , daf) of various American coal samples.

bonds" in crosslinked coal structures (see Figure 1), approximately three clusters may be found between two multifunctional crosslinks. Average molecular weights in the range of 400-500 were determined for cluster size of 150. The calculated values of \bar{M}_c for anthracites are not considerably different from the corresponding values for other coals. Due to the small number of anthracite samples tested no further explanation will be attempted here.

It must be noted that the present analysis of \bar{M}_c serves only as an approximate indication of the expected values of molecular weight between crosslinks. If one recalls that the values of χ -factor and porosity p used here are determined from best fitting of data by other investigators for similar coals it is evident that this analysis is subject to error. Experimental data for χ and p are being obtained for our coals in our laboratory. However, this contribution shows how experimental data can be used to improve determination of \bar{M}_c and to present, for the first time, approximate values of this important physical parameter of the crosslinked structure of coals.

Finally the present analysis (see Figure 6) does not include enough experimental data in the range of 85% carbon, namely the range where Larsen (14) claims that a maximum in \bar{M}_c is observed. Obviously more data in this range are needed. However, a similar maximum in swelling behavior at 75% carbon claimed by Nelson *et al* (13) is not apparent when the statistical mechanical model developed by Peppas and Lucht (3) is applied to determine crosslinked densities.

Acknowledgements

This work was supported by the Department of Energy, Grant #ET-78-G-01-3382. Preliminary studies were also supported with funds from the Purdue Coal Research Center. We wish to acknowledge very helpful discussions with T. Ruppel of the Pittsburgh Energy Technology Center (PETC). The coal samples were kindly provided by the Pennsylvania State University, College of Earth and Mineral Sciences.

REFERENCES

1. L.M. Lucht, and N.A. Peppas, Amer. Inst. Phys. Confer. Proceed., (in press).
2. J. Kovac, Macromol., 11, 362, (1978).
3. N.A. Peppas and L.M. Lucht, paper presented at the 87th National AIChE Meeting, Boston, August 1979.
4. J.W. Larsen and J. Kovac, in J.W. Larsen, ed., "Organic Chemistry of Coal", ACS Symposium Series, 71, 36, ACS, Washington, D.C., 1978.
5. P.J. Flory, "Statistical Mechanics of Chain Molecules", Interscience, New York, 1969.
6. D.W. van Krevelen, Fuel, 44, 229, (1965).

7. I.G.C. Dryden, *Fuel*, 30, 34, (1951).
8. Y. Sanada and H. Honda, *Fuel*, 45, 295, (1966).
9. N.Y. Kirov, J.M. O'Shea and G.D. Sergeant, *Fuel*, 46, 415, (1967).
10. D.D. Whitehurst, in J.W. Larsen, ed., "Organic Chemistry of Coal", ACS Symposium Series, 71, 1, ACS, Washington, D.C. 1978.
11. W. Wiser, *ACS Fuel Prepr.*, 20(2), 122, (1975).
12. N.A. Peppas, Annual report on DOE Grant 3382, (1979).
13. J.R. Nelson, O.P. Mahajan and P.L. Walker, Jr., *ACS Org. Coat. Plast. Prepr.*, 43(2), 337, (1980).
14. J.W. Larsen, *Amer. Inst. Phys. Confer. Proceed.*, (in press).

RECEIVED May 5, 1981.

Coal Structure and Thermal Decomposition

PETER R. SOLOMON

Advanced Fuel Research, Inc., 87 Church Street, East Hartford, CT 06108

Although coal has been in use for over six hundred years, there is still no agreed-upon model for the chemical structure of coal or how it comes apart during a chemical reaction. The increased use of complicated processing of coal to produce alternative fuels or reduce pollution has made it imperative to obtain an understanding of the fundamental chemistry.

The most widely held view of coal structure pictures coal as groups of fused aromatic and hydroaromatic ring clusters, possibly linked by relatively weak aliphatic bridges. The ring clusters contain heteroatoms (oxygen, sulfur and nitrogen) and have a variety of attached functional groups.

Several investigators have suggested coal structures based on constraints provided by available data. Much of this work was recently reviewed by Davidson (1). In the early 1960's Given (2,3) suggested a structure based on x-ray data for the cluster size and infrared measurement for the concentrations of aliphatic and aromatic hydrogens. To fit Brown's values for aromatic hydrogen, H_{ar} (4), Given made extensive use of dihydroanthracene or dihydrophenanthrene linkages. These structures make the maximum use of aliphatic carbons as substitutes for aromatic hydrogens resulting in a low value for H_{ar} . Brown's values for H_{ar} , however, appear to be too low when compared to other methods of determining H_{ar} including recent FTIR measurements (5). Wiser's model (6) uses a higher value of H_{ar} and reflects liquefaction and thermal decomposition data by including more easily broken weak aliphatic bonds such as ethylene bridges between ring clusters. A recent structure contributed by Heredy and Wender (7) is similar to Wiser's. It is based on a combination of analytical data and used a mathematical analysis to determine H_{ar} . Experiments on coal which change the hydrogen concentration by reduction or catalytic dehydrogenation agree with what would be expected for this model. Suggested structures by Whitehurst et al (8) have been based on the analysis of short contact time coal liquefaction products which are believed to reflect structure in the

0097-6156/81/0169-0061\$05.00/0
© 1981 American Chemical Society

parent coal. Other models which propose different views of the structure have been presented by Pitt,⁽⁹⁾ Chakrabarty and Berkowitz⁽¹⁰⁾ and Hill and Lyon⁽¹¹⁾.

This paper considers the implications of a number of analytical techniques and extensive thermal decomposition data (5,12-15) in defining a structure for a Pittsburgh seam coal, PSOC 170. The thermal decomposition experiments yield information on the coal fragments which are similar in composition to the parent coal and on the concentration of chemical species and their relative bond strengths. The analytical techniques applied to the coals and thermal decomposition products include: 1) Fourier Transform Infrared (FTIR) Spectroscopy for the quantitative determination of hydroxyl, aliphatic (or hydroaromatic) and aromatic hydrogen and aliphatic and aromatic carbon and qualitative determination of oxygen functional groups and the distribution of aromatic hydrogen (whether 1,2 or more adjacent hydrogens on a ring), (5,15). 2) Carbon and proton NMR for determination of the fractions of aromatic carbons and hydrogens (16). 3) Elemental analysis. 4) Gel permeation chromatography (GPC) and vapor phase osmometry (VPO) for determining the molecular weight of coal fragments (17).

The above results are summarized in a proposed molecular structure and proposed description for the origin of thermal decomposition products. The purpose of presenting molecular structures is to summarize research results in a concise form which will allow a convenient comparison to other work. For example, the proposed structure is similar to those of Wiser (6) and of Heredy and Wender (7). But these structures only represent aspects of the structure which are constrained by available data, and are not unique. They may be wrong in details for which data is missing. Care should therefore be exercised in the way such models are interpreted.

An important factor influencing the distribution of thermal decomposition products is the availability of aliphatic or hydroaromatic hydrogen. This factor is considered for several examples in which the distribution of products may be varied substantially by varying the thermal decomposition conditions.

Coal Structure and Thermal Decomposition

The hypothetical coal molecule and thermal decomposition products for PSOC 170 are presented in Figs. 1 and 2. The structure parameters for the suggested molecule, the corresponding parameters determined for PSOC 170 and the source for the data are summarized in Table I. Some of the details of the model are as follows: 1) The structure contains only one carboxyl. The carboxyl concentration is based on the yield of CO₂ which is believed to be its thermal decomposition product. No other carbonyl's are included as the carbonyl peaks

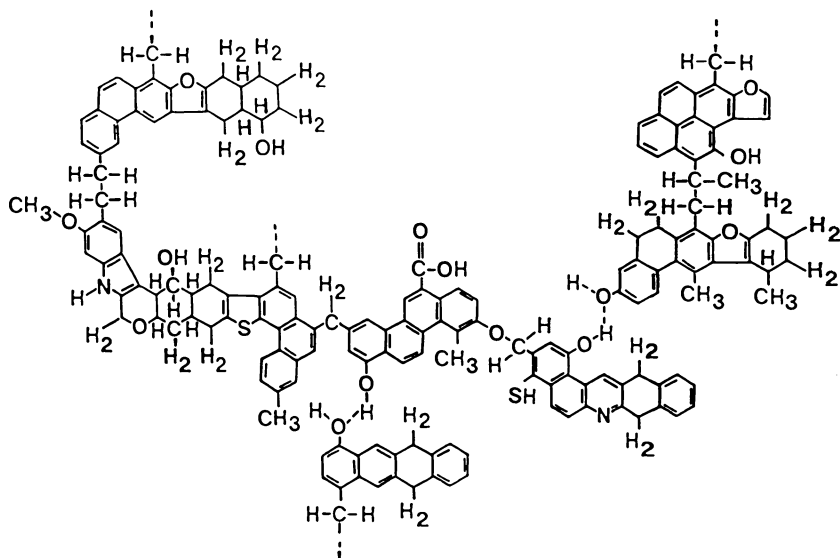


Figure 1. Summary of coal structure information in a hypothetical coal molecule

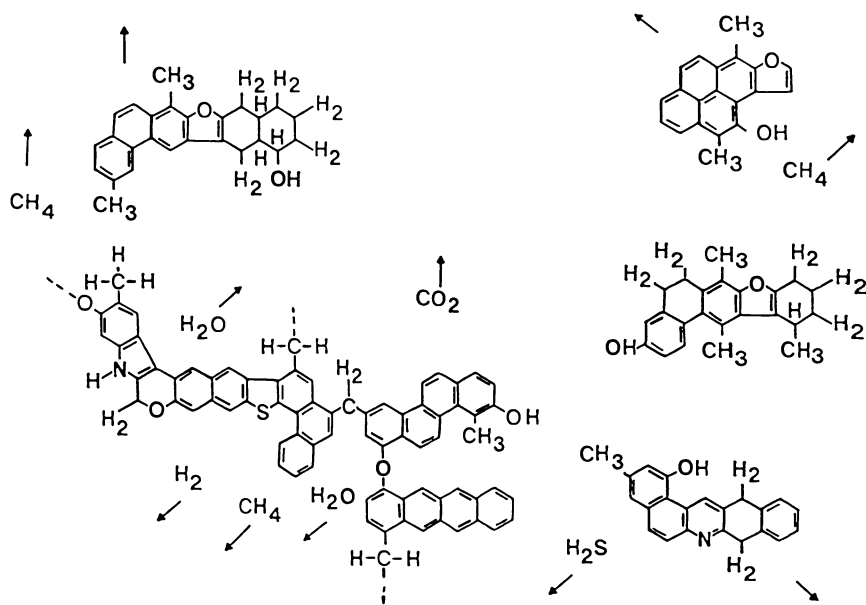


Figure 2. Cracking of hypothetical coal molecule during thermal decomposition

TABLE I

COAL STRUCTURE PARAMETERS (weight fraction DMMF)

<u>PARAMETER</u>	<u>MODEL</u>	<u>COAL</u>	<u>SOURCE</u>
C	.81	.82	CHN Analyzer ¹³
H	.055	.054	CHN Analyzer ¹³
O	.098	.094	Difference
N	.011	.014	CHN Analyzer ¹³
S(O)	.026	.019	SEMP ¹³
C _{al}	.60	.60	NMR and FTIR ^{15, 16}
C _{ar}	.20	.22	NMR and FTIR ^{15, 16}
C _{methyl}	.030	.03	Ave. Literature value ³²⁻³⁹
C _{ar/C}	.74	.73	NMR and FTIR ^{13, 16}
H _{al}	.033	.033	FTIR ¹³
H _{ar}	.018	.018	FTIR ¹³
H _{OH}	.0029	.0027	FTIR ¹³
H _{methyl}	.0074	.0075	Ave. Literature value ³²⁻³⁹
H _{ar-1 adj}	.006	.006	FTIR
H _{ar-2 adj}	.008	.007	FTIR
H _{ar-3or4 adj}	.004	.005	FTIR
O _{OH}	.046	.043	FTIR ¹⁵
O _{COOH}	.013	.009	Thermal Decomposition ¹³
O _{CO}	.039	.041	Thermal Decomposition ¹³
N _{ring}	.011	.014	Thermal Decomposition ^{14, 19}
S _{ring}	.013	.01	Thermal Decomposition ¹⁴
S _{mercaptan}	.013	.01	Thermal Decomposition ¹⁴
12H _{al} /C _{al}	1.9	1.8	Ave. Literature Value ¹⁵
Molecular Weight of Ring Cluster	350	400	GPC and VPO on TAR ¹⁷

from FTIR are very small. 2) Other than hydroxyl oxygens which are determined from FTIR, the remainder of the oxygen is shown in ether linkages, mainly oxygens linked to aromatic carbon on the basis of the position of the ether absorption in the infrared. 3) Infrared also shows the presence of strong hydrogen bonding which is indicated in Fig. 1. 4) From thermal decomposition measurements it has been observed that roughly one half of the organic sulfur, but little nitrogen can be removed at relatively low temperatures (14). For this reason, the nitrogen is shown only as part of an aromatic ring but sulfur is shown both in rings and as mercaptan side groups. 5) The structure makes use of hydroaromatic structures suggested by Given (2,3) and recently identified in oxidation studies by Deno et al. (18). 6) The structure contains ethylene bridges which break and stabilize in thermal decomposition to yield increased methyl groups in the decomposition fragments. 7) The cluster size matches the size of thermal decomposition fragments determined by VPO and GPC (17). 8) The methyl group concentration and aliphatic stoichiometry match literature values.

The thermal decomposition of the model structure is illustrated in Fig. 2. Again, it should be emphasized that the suggested model fits available data but is non unique. The model presents the situation after the weak links in the structure are ruptured. For example, the bond between aliphatic carbons or between the oxygen and an aliphatic carbon are most likely to break. The breaking of these bonds releases the ring clusters with their attached functional groups as shown in Fig. 2. These large molecules comprise the coal tar.

Simultaneous with the evolution of tar molecules is the competitive cracking of the bridge fragments, attached functional groups and ring clusters to form the light molecules of the gas (see Fig. 2). A given species, a hydroxyl group for example, may evolve as part of the tar without rupture of its local bonds or may evolve into the gas with local bond rupture.

Thermal decomposition results suggest the following relationship between the components of coal and the evolved light species (12,13,14). At low temperatures there is very little rearrangement of the aromatic ring structure. There is, however, decomposition of the substituted groups and aliphatic (or hydroaromatic) structures resulting in CO₂ release from the carboxyl, H₂O from hydroxyl, hydrocarbon gases from aliphatics, H₂S from mercaptans and some CO from weakly bound ether groups (see Fig. 2). At high temperature there is breaking and rearrangement of the aromatic rings. In this process, H₂ is released from the aromatic hydrogen, CS₂ from the thiophenes, HCN from ring nitrogen and additional CO from tightly bound ether linkages. As this process continues the char becomes more graphitic.

A striking feature of thermal decomposition which was observed for a variety of coals is that the temperature dependent evolution rate of a particular species is similar for all coals (12,13,14). This is true even though the amount of the species may vary substantially from one coal to another. These rates characterize the thermal decomposition of the various functional groups. They depend on the nature of the functional group but appear insensitive to coal rank. The differences between coals may be attributed to differences in the mix of functional groups.

The thermal decomposition experiments performed by Solomon and co-workers (5,12-15) were done in a thin bed under vacuum. Under these conditions, the tar molecules may be removed quickly from the reacting bed and undergo minimal secondary reactions. Therefore, many of the coal structural elements are preserved in tar and careful analysis of these products can supply clues to the original structure. For example, the average molecular weight of the PSOC 170 tar was determined to be about 370 by VPO and 490 and 385 by GPC (16).

The evidence that the tar consists of minimally disturbed fragments of the parent coal is the striking similarity between the two materials which has been observed in elemental composition, FTIR spectra and NMR spectra (12,13,14,19,20,21). For most bituminous coals the two materials are almost identical suggesting that the tar is a representative sampling of the coal molecular structure. The tar differs slightly from the parent coal in that it has a higher concentration of aliphatic hydrogen, especially methyl groups. This extra hydrogen is presumably abstracted from the char to stabilize the free radical sites formed when the bridges were broken. Similar arguments were given by Wiser(22) and by Wolfs et al.(23). The observation that the tar is rich in aliphatic hydrogen but not in aromatic hydrogen when compared to the parent coal has implications concerning the nature of the aliphatic linkages. The result suggests that the bonds which were broken to free the ring clusters were predominantly between two aliphatic carbons, not between an aromatic and an aliphatic. The bridges must therefore be ethylene or longer. It might be argued that the tar was simply that part of the coal which is hydrogen rich. The high methyl concentration in the tar compared to the coal can only be explained, however, by assuming that new methyl groups were formed during thermal decomposition. The increased concentration of aliphatic hydrogen should relate directly to the density of ethylene or longer bridges in the parent coal. For PSOC 170 tar, the concentration of aliphatic hydrogen is about 6.1% compared to 5.4% for the coal. This suggests an average of 2.5 extra hydrogens or 2.5 bridges per cluster of 360 molecular weight.

The relationship between the coal organic structure and the products of thermal decomposition has been incorporated into a general kinetic model. The model has proved successful in simulating the results of vacuum thermal decomposition experiments for a variety of bituminous coals and lignites (5,12,13). It has also proved to be successful in limited application to other conditions such as coal proximate analysis (15), hydropyrolysis and liquefaction (24).

The Role of Aliphatic or Hydroaromatic Hydrogen in Coal Conversion

In thermal decomposition the simultaneous evolution of tar and light gases creates a competition for hydrogen to stabilize free radical sites. This hydrogen is most likely to come from the aliphatic or hydroaromatic portion of the coal. Supporting evidence comes from the observation that tar evolution ceases when the aliphatic peak in the FTIR spectra of chars goes to zero. At this point there is still aromatic hydrogen left in the char (5). If the above argument is correct, it is reasonable to expect the tar yield to depend on H_{a1} . In Fig. 3, the tar yield in vacuum pyrolysis is plotted against H_{a1} for a number of coals (circles). Also plotted are the yields of heavy hydrocarbons, (i.e., oils and BTX) from hydropyrolysis (squares), (25). Indeed, there is a strong correlation between tar yield and H_{a1} . A similar correlation was reported by Lahiri et al. (26).

A number of results indicate that the conditions of coal conversion may significantly influence the results of the competition for hydrogen. Some conditions appear to preferentially inhibit the evolution of the large molecules allowing the light species to escape with most of the H_{a1} . An example is pyrolysis in thick beds as in the determination of "proximate analysis fixed carbon". Under thick bed conditions the tar has ample opportunity for repolymerization as it percolates through the bed. This results in substantially lower tar yields than the corresponding yield for vacuum pyrolysis in a thin bed. Since the most important mechanism for removing aromatic carbon from the coal is tar evolution, the low tar yield means that most of the aromatic carbon will be retained in the "fixed carbon". This results in the near equality between "proximate analysis fixed carbon" and "aromatic carbon" originally reported by Van Krevelen (27) and recently studied by Solomon (15). High pressures also inhibit tar evolution (28).

Some recent results from the Mobil research program (8,29) seem to show the opposite effect. Under certain mild liquefaction conditions the soluble products are very similar in composition to the parent coal and the yield shows a rank dependence which is similar to what is observed in thermal

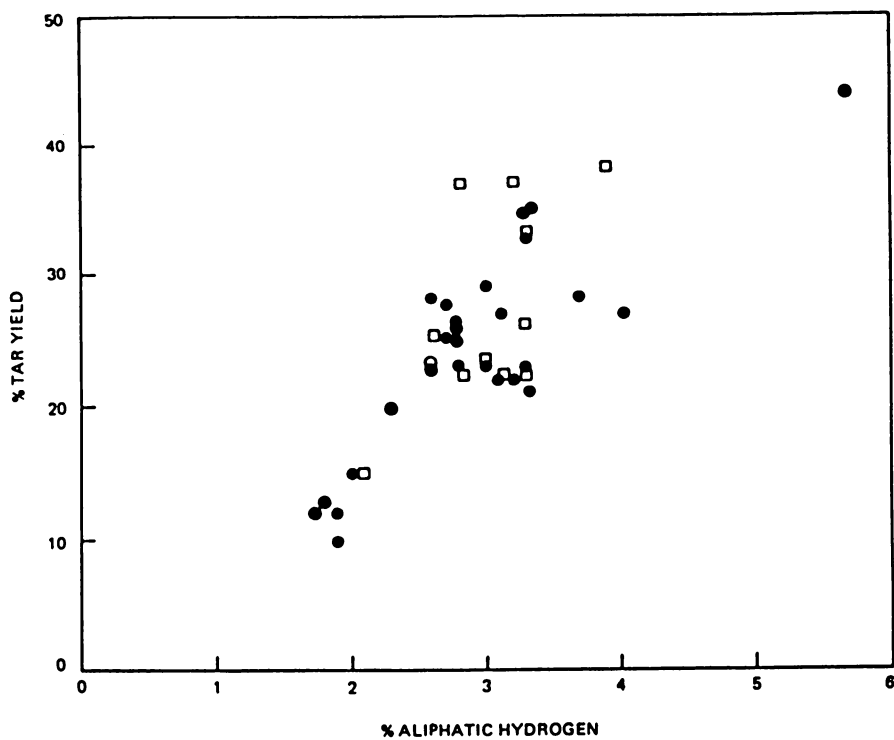


Figure 3. Correlation of tar yield with aliphatic hydrogen (24): CCNY (□); UTRC (●).

decomposition except that the yields are higher by a factor of two and a half (30). Under the conditions of these experiments, there is little or no hydrogen donated from the solvent so the hydrogen for stabilizing free radical comes from the coal. The solvent may act however, to retain and transfer H_{a1} from the coal and to remove the heavy molecules into solution. Both conditions presumably make more H_{a1} available for tar formation. If all the coal's H_{a1} is available for tar formation, (none used for light species) then for the case of PSOC 170, yields of heavy products of 80% to 90 % should be possible. This estimate is based on the use of H_{a1} for tar formation in vacuum thermal decomposition. Yields of this magnitude are in agreement with the Mobil results (8,29) on coals of similar rank.

Summary

1. The molecular structure presented in this paper is an attempt to summarize a variety of data including new measurements of H_{ar} and thermal decomposition results for a Pittsburgh seam coal. The structure is similar to those presented by Wiser (6) and Heredy and Wender (7). It differs from Wiser's in having more oxygen in rings, nitrogen only in rings, explicit hydrogen bondings, and larger cluster size. It differs from that presented by Given (2,3) in having more easily broken aliphatic linkages and a higher value of H_{ar} . The structure contains the appropriated composition to match elemental analysis, FTIR analysis and NMR analysis.

2. The expected thermal decomposition of the proposed structure is in agreement with the distribution of thermal decomposition products from the coal. The products include minimally disturbed ring cluster fragments from the molecular structure which comprise the coal "tar". Analysis of the tar gives information on the ring cluster size in the coal and on the structure of the aliphatic bridges.

3. The variation in thermal decomposition yields, which depend on bed geometry, pressure, solvents, etc, are in agreement with the suggested role of internal aliphatic or hydroaromatic hydrogen in stabilizing free radicals in the competitive evolution of light species and tar.

LITERATURE CITED

1. Davidson, R. M., "Molecular Structure of Coal, IEA Coal Research" London, 1980.
2. Given, P. H., *Fuel*, 1960 39, 147.
3. Given, P.H. *Fuel*, 1961 40, 427.
4. Brown, J. K., *J. Chem. Soc.*, 1955, 744.
5. Solomon, P. R., ACS Div. of Fuel Chemistry, Preprints, 1979, 24, #2, 184, and *Advances in Chemistry*, to be published.
6. Wiser, W. H., Reported in Division of Fuel Chemistry, Preprints, 1975, 20, 122.
7. Heredy, L. A. and Wender, I. ACS Division of Fuel Chemistry Preprints, 1980, 25, #4.
8. Whitehurst, D.D., Mitchell,, T. O., Farcasiu, M. and Dickert, J.J. Jr., "The Nature and Origin of Asphaltenes in Processed Coals", Final Report, EPRI, AF-1298, Dec., 1979.
9. Pitt, G. J., Structural analysis of coal. In: "Coal and Modern Coal Processing: an Introduction", Pitt, G. J. and Millward, G. R. (eds.) London, UK: Academic Press, 1979, 27.
10. Chakkrabartty, S.K., Berkowitz, N., *Fuel*, 1974, 53, 240.
11. Hill, G. R., and Lyon, L. B. *Ind. Eng. Chem.*, 1962, 54, 36.
12. Solomon, P. R., and Colket, M. B., 17th Symposium (International) on Combustion, The Combustion Institute, Pittsburgh, PA. 1979, p. 131.
13. Solomon, P. R., and Hamblen, D. G., "Understanding Coal Using Thermal Decomposition and Fourier Transform Infrared Spectroscopy", Presented at the Conference on the Chemistry and Physics of Coal Utilization, Morgantown, WV, June 2-4, 1980.
14. Solomon, P. R., Report NSF/RA-770422, NTIS, #PB278496/AS, "The Evolution of Pollutants During the Rapid Devolatilization of Coal", 1977.
15. Solomon, P. R., *Fuel*, 1981, 60, 3.
16. This work was performed by Bernard Gerstein and co-workers at Ames Laboratory. It is being prepared for publication.
17. The GPC work was done by Duayne Whitehurst and co-workers at Mobil and by Alberto LaCava at CCNY. The VPO measurements were made by John Larsen at the University of Tennessee.
18. Deno, N. C., Curry, K., Jones, A. D., Minard, R., Potter, T., Rakitsky, W. and Wagner, K., "Low Temperature Chemical Fragmentation of Coal", Presented at the Conference on the Chemistry and Physics of Coal Utilization, Morgantown, WV, June 2-4, 1980.
19. Solomon, P. R., and Colket, M. B., *Fuel*, 1978, 57, 749.

20. Orning, A. A., and Greifer, B., *Fuel*, 1956, 35, 381.
21. Brown, J. K., Dryden, I. G. C., Dunevein, D. H., Joy, W. K. and Pankhurst, K. S., *J. Inst. Fuels*, 1958, 31, 259.
22. Wisner, W. H., *Fuel*, 1968, 47, 475.
23. Wolfs, P. M., van Krevelen, D. W. and Waterman, H. I., *Fuel*, 1960, 39, 25.
24. Solomon, P. R., Hobbs, R. H., Hamblen, D. G., Chen, W., La Cava, A. and Graff, R. A., "Correlation of Coal Volatile Yield with Oxygen and Aliphatic Hydrogen", *Fuel*, (to be published).
25. Chen, W., La Cava, A., and Graff, R. A., *ACS Div. of Fuel Chemistry Preprints*, 1979, 24, #3, 94.
26. Lahiri, A. and Mazumdar, B. K., "Studies on Dehydrogenation of Coal and Structural Implications, Proceedings of the Symposium on the Science and Technology of Coal, Ottawa, Canada, 1967.
27. van Krevelen, D. W. and Schuyer, J., *Coal Science*, Elsevier, Amsterdam, 1957.
28. Suuberg, E. M., Peters, W. A. and Howard, J. B., 17th Symposium (International) on Combustion, The Combustion Institute, Pittsburgh, PA., 1979, p. 117.
29. Derbyshire, F. J., "Influence of Polyaromatic Solvent Components in Coal Liquefaction", EPRI, Fifth Annual Coal Liquefaction Contractor's Conference, Palo Alto, CA, May 7-8, 1980.
30. Solomon, P. R., "Quantitative FTIR Analysis of the Organic Structure of Coals and Liquefaction Products", EPRI Fifth Annual Coal Liquefaction Conference Palo Alto, CA, 1980.
31. Ladner, W. R. and Stacey, A. E., *Fuel*, 1963, 42, 75.
32. Mazumdar, B. K., *Fuel*, 1972, 51, 284.
33. Bent, R., Joy, W. K. and Ladner, W. R., *Fuel*, 1964, 43, 5.
34. Chatterjee, A. K. and Mazumdar, B. K., *Fuel*, 1968, 47, 93.
35. Dryden, I. G. C., *Fuel*, 1962, 41, 301.
36. Dryden, I. G. C., *Fuel*, 1962, 41, 55.
37. Brown, J. K. and Ladner, W. R., *Fuel*, 1960, 39, 87.
38. Oth, J. F. M. and Tschamler, H., *Fuel*, 1963, 42, 467.

RECEIVED March 9, 1981.

The Interrelationship of Graphite Intercalation Compounds, Ions of Aromatic Hydrocarbons, and Coal Conversion. II

LAWRENCE B. EBERT, JOSEPH C. SCANLON, DANIEL R. MILLS,
and LOUIS MATTY

Corporate Research—Science Laboratories, P.O. Box 45, Linden, NJ 07036

The benzenoid character of both graphite and polycyclic aromatic hydrocarbons leads to certain common features in their respective chemistries (1). In the same sense that aromatic hydrocarbons react with reductants and oxidants to form (radical) anions and cations, graphite will react to form donor or acceptor intercalation compounds. Although more complex than either aromatic hydrocarbons or graphite, coals, especially those of higher rank, also possess benzenoid character, and thus might be expected to undergo some of the same chemistry. We shall discuss the utility, and the limitations, of proposed analogies among graphite, polycyclic aromatic hydrocarbons, and selected coals. To make our talk appropriate to a symposium on modern approaches to characterization, we have chosen several specific examples of common reactions which illustrate the similarities and divergences of these systems:

1. Many metal and non-metal halides interact strongly with graphite, aromatic hydrocarbons, and coals. We have used wide line nuclear magnetic resonance to compare the graphite intercalation compound "C₁₆BF₄" with the product of the interaction of Illinois #6 coal with BF₃. Coupling our work with the known literature of complexes of aromatic hydrocarbons with BF₃, we find that BF₃ reacts differently with graphite, aromatic hydrocarbons, and various coals.
2. The reagent alkali metal/naphthalene in tetrahydrofuran reacts with graphite, polynuclear aromatics, and various coals to form chemically reduced products. In the present paper, we emphasize the use of electron paramagnetic resonance data, in the form of g values, linewidths, radical densities, and saturation characteristics, to analyze the reduced coal products and to infer certain differences between the reduced coals and the anions of graphite and simple aromatic hydrocarbons. Additionally, because the interaction of coals with alkali metal/naphthalene requires much time for completion, we have investigated internal decomposition pathways for the

0097-6156/81/0169-0073\$05.00/0
© 1981 American Chemical Society

reagent system alkali metal/naphthalene in THF, as a function of alkali metal, by the use of combined gas chromatography/mass spectroscopy (GC/MS) and high resolution nuclear magnetic resonance.

3. Potassium carbonate is a well-known catalyst for the steam gasification of carbonaceous materials. We discuss the use of in situ high temperature X-ray diffraction to demonstrate that intercalation compound-like structures are not involved as stable intermediates.

Although we shall present each topic separately in the text, we emphasize that the results of each area point to several general conclusions:

- The strongest similarity between ionic aromatic compounds and intercalation compounds of graphite is charge transfer.
- The strongest divergence between ionic aromatic hydrocarbons and intercalation compounds of graphite arises from variations in the ratio of peripheral carbons to internal carbons.
- The chemistry of aromatic clusters in various coals is modified by substituents on these clusters.

We thus infer a great similarity in the chemistry of the pi electrons of graphite and of small aromatic hydrocarbons. Apparent divergences arise for cases in which the aromatic molecules form sigma complexes, whose creation is not easily perceptible for graphite, simply because of the low ratio of peripheral carbon to internal carbon. While many coals do contain aromatic clusters, the chemistry of their pi electrons is altered by the presence of substituents which alter the electronic and steric properties of the aromatic core. Additionally, added chemical reagents may react directly not only with these substituents but also with mineral phases present in the coal to yield a product in which the pi aromatic chemistry is masked.

The Interaction Of Benzenoid Carbon With Metal And Non-Metal Halides

There are many halogen containing molecules which react not only with graphite (2) but also with polycyclic aromatic hydrocarbons (3). Recently, Beall has proposed that such molecules react with coal to form intercalation compounds (4). Any analogies here must be regarded with caution, for the interaction of halogen containing molecules with benzenoid species runs from non-existent all the way to oxidative halogenation. As an example, while zinc dichloride reacts facily with coal (5), it does not react at all with graphite (6). To examine the nature of these differences, we consider the reaction of boron trifluoride with polycyclic aromatic hydrocarbons, graphite, and Illinois #6 coal.

Aalbersberg and co-workers (7) examined the interaction of BF_3 with polycyclic aromatic hydrocarbons as anthracene, perylene, and tetracene. The interaction was weak, and could be reversed

simply by pumping on the system or adding excess water. The form of this covalent (and presumably diamagnetic) complex was considered analogous to protonated aromatics, in which the added species is bound to the edge of the aromatic molecule:



In the presence of both BF_3 and a protic acid HX , aromatic hydrocarbons give structures analogous to the following (8):



In contrast, BF_3 , which is not a good oxidant, does not react with graphite to form an intercalation compound (1). Addition of the oxidant ClF (which by itself does not react with graphite) leads to an intercalation compound containing BF_4^- , rather than BF_3 (1), with chlorine gas identified as the other reaction product (9). That graphite has been oxidized is demonstrated by the presence of a narrow ($0.12 \text{ mT} = 1.2 \text{ G}$) electron spin resonance signal in the vicinity of $g = 2.0027$, present at all temperatures between -168°C and 23°C (see Figure 1). Such a signal is directly analogous to those found in aromatic radical cations (10). While this signal is asymmetric and possesses an area independent of temperature, it is not Dysonian, as is discussed below.

The wide line fluorine nuclear magnetic resonance of the intercalation compound " $\text{C}_{16}\text{BF}_4^-$ " may be used not only to demonstrate the chemical identity of the inserted species but also to establish the translational freedom of this species. The chemical shift of the fluorine resonance is at $(70 \pm 10) \text{ ppm}$ vs. CF_3COOH , consistent (11) with BF_4^- (71 ppm) but not with BF_3 (54 ppm). (The neutral/anion complex, B_2F_7^- , is also possible (12)). The derivative extremum linewidth is narrow ($0.02 \text{ mT} = 800 \text{ Hz}$) at all temperatures between -168°C and 23°C . A simple calculation suggests that translation, and not rotation, is the cause of this narrow line. Assuming a first stage compound (as indicated by X-ray diffraction)

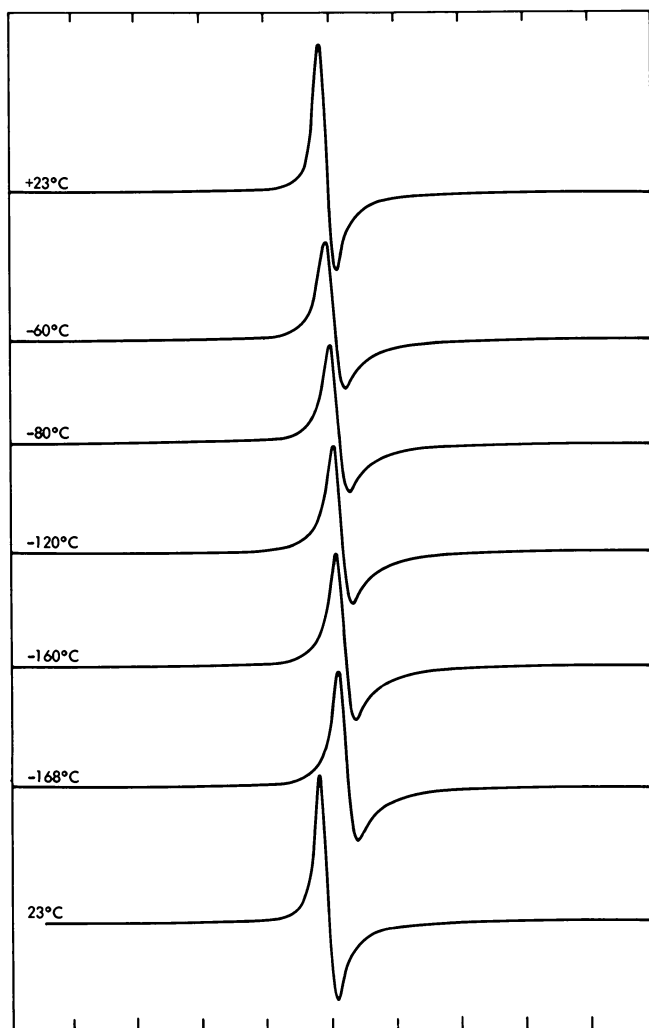


Figure 1. The derivative mode of the ESR absorption (9.11 GHz) of $C_{16}BF_4$, as a function of temperature. Total scan range is 4 mT (= 40 G) and the figures have been offset horizontally for viewing ease. Although the behavior seen here is indicative of a conduction carrier resonance, the reader should consult the text for a full discussion.

and a uniform hexagonal lattice of BF_4^- anions, there will be a distance of 568 pm between tri-coordinate BF_4^- species leading to an intermolecular second moment of 0.113 G^2 , or a Gaussian model linewidth of 0.67 G, three times larger than that observed.

The narrow fluorine resonance of " C_{16}BF_4 " is quite in contrast to the fluorine absorption found for the product of Illinois #6 coal with BF_3 . At room temperature, we observe a 0.25 mT (=2.5 G) wide, dipolar-broadened, spectrum not indicative of translation freedom. In contrast to the weakly bound complexes of BF_3 with aromatic hydrocarbons, we anticipate BF_3 to react strongly with oxygen functionality in the coal, through hydration with water, hydrolysis with acids (13), and ether complex formation (14), to give fluorine absorption lines which are in the rigid lattice condition.

The point of the preceding examples is to demonstrate that a single reagent, BF_3 , can react in completely different ways with polycyclic aromatic hydrocarbons, graphite and certain coals. The mere presence of a reaction does not demonstrate a commonality.

The Alkali Metal/Naphthalene/Tetrahydrofuran System

Although the capability of the alkali metal/naphthalene/tetrahydrofuran system to reduce graphite and polycyclic aromatic hydrocarbons has long been known (15, 16), it is the research of Sternberg and co-workers on reducing, and then alkylating, coal which has brought attention to this system (17, 18). The products of this reductive alkylation treatment have remarkable solubilities in organic solvents and thus have stimulated much interest (19, 20). While the model for this chemistry could be taken as the reduction of simple aromatic hydrocarbons, the long reaction times required (~ 100 hours) and the presence of high oxygen levels in the coals ($\sim 10\%$) suggest that other chemistries could occur.

Electron spin resonance investigation of reduced coal products demonstrates the relative absence of aromatic radical anion structures in the reduced, but not alkylated, products. If there were a one-to-one correspondence between alkali metal consumed and radical anions generated in the reduced coal (i.e., as in alkali metal naphthalenide), we would expect an intense ($\sim 10^{21}$ spins/gram ~ 0.03 spin/C atom), exchange-narrowed resonance near $g = 2.0028$. In fact, treatment of either Illinois #6 bituminous or Wyodak subbituminous coals with potassium naphthalenide produces little change in the electron spin resonance spectrum with respect to g value, linewidth, or radical density (1, 21). An additional confirmation of the absence of radical anion structures in the reduced coal may be inferred from the saturation behavior of the ESR absorption, as given in Figure 2. While coals as Illinois #6 or Wyodak, possessing 10^{18} to 10^{19} spins/gram, have T_1 's of the order of 10^{-5} to 10^{-6} sec (22), organic solids possessing high concentrations of radicals, as solid diphenyl picryl hydrazyl, have T_1 's of the order of 10^{-8} to 10^{-9} sec (10, 23). As is

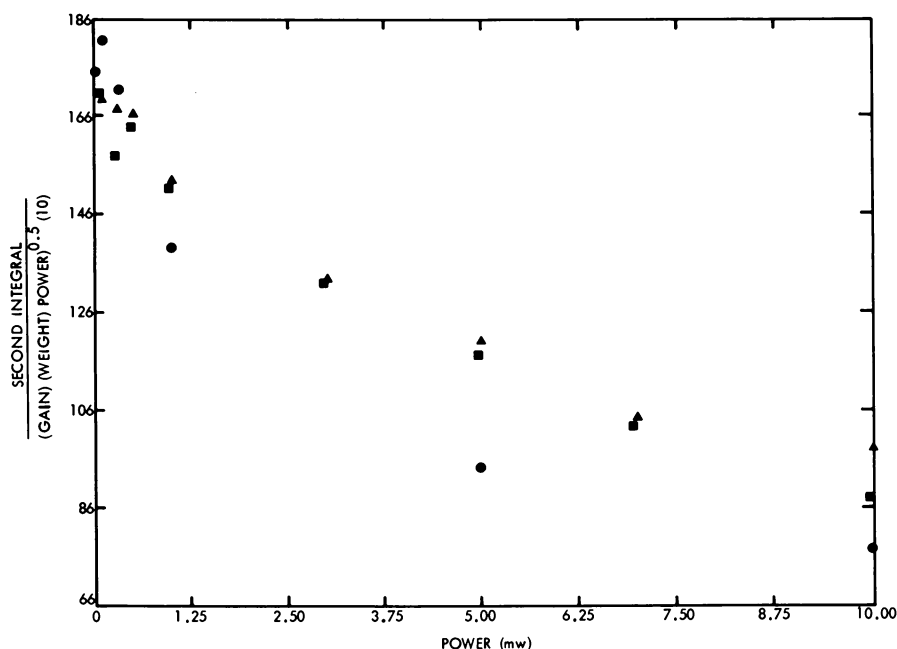


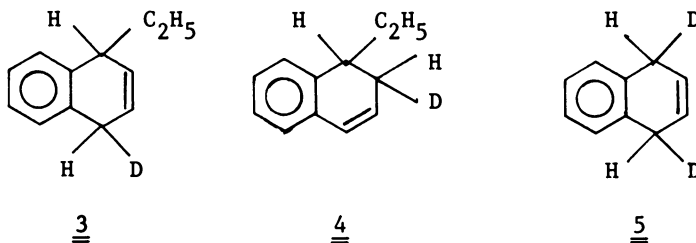
Figure 2. A plot of the apparent area of the ESR absorption against microwave power for Illinois #6 coal and two chemically treated Illinois #6 coal products.

In this display, a nonsaturating material would appear as a horizontal line. The reader should note that the initial Illinois #6 and naphthalenide-treated Illinois #6 coals have virtually the same saturation profile. Thermal treatment of the coal with potassium at 300°C actually makes T_1 longer. Dry Illinois #6 (▲); Sternberg Illinois #6 (■); K/Illinois #6 (300°C/4h) (●).

evident from the figure, the T_1 of the reduced coal is, within the limits of error, equal to the T_1 of the starting coal, and thus we see no evidence for the dominance of electron-electron interactions, as would be expected for a solid containing a high concentration of free radicals.

In this absence of evidence for increased radical density, one could postulate the presence of spin-paired, diamagnetic, dianions in the reduced coal. However, using the chemistry of polycyclic aromatic hydrocarbons as a model, we find that such dianions are neither expected to be statistically abundant (24, 25) nor, as good bases, to be inert to the reductive system on a time scale of 100 hours (26).

Of this latter point, we have utilized combined GC/MS to analyze solutions of alkali metal naphthalene in THF (90 mM metal, 40 mM naphthalene, 25 ml THF) quenched with D_2O , so that we may determine the stability of the reactant system itself on a time scale of 100 hours. The predominant product, other than naphthalene itself, for both sodium and potassium naphthalene quenches was 1-ethyl 1-protio, 4-deutero 4-protio naphthalene (3) (and/or the 1,1,2,2 isomer (4)) rather than the expected 1-deutero 1-protio, 4-deutero 4-protio naphthalene (5).



The product slate for the lithium quench was even more complex, with approximately equal amounts of four products: 1-ethyl naphthalene, 1-(4-hydroxybutyl) naphthalene, 1-ethyl 1-protio, 4-deutero 4-protio naphthalene, and 1-(4-hydroxybutyl) 1-protio, 4-deutero 4-protio naphthalene. Hydrogen gas, in the isotopic form HD, was evolved on quenching the lithium and sodium systems, but not the potassium system.

These results indicate that the naphthalene radical anion is not stable to the solvent tetrahydrofuran at room temperature on a time scale of 100 hours. Decomposition pathways are alkali metal dependent. Sodium and potassium naphthalene attack THF through a proton abstraction, cycloreversion mechanism, as previously described by Bates for the butyllithium/THF system (27). Lithium naphthalenide attacks the THF not only by the Bates mechanism but also by a nucleophilic ring opening, as is implicit in earlier high temperature work on lithium naphthalenide in THF (28) and in work on the attack of THF by tritylmagnesium bromide (29). The two smaller alkali metals, lithium and sodium, leave behind a

hydride product, while the potassium does not. High resolution ^7Li NMR of an unquenched, aged solution of lithium naphthalenide, given in Figure 3, unequivocally shows the presence of two different lithium environments, one of which is consistent with paramagnetic lithium naphthalenide (left) and one consistent with a diamagnetic lithium salt (right).

Thus, one reason for the apparent divergence between coal and graphite/aromatic hydrocarbons with respect to reductive chemistries may arise from the instability of the reducing system on the timescale required for coal reaction. The necessity of these long reaction times results in part from the presence of many substituents found on aromatic clusters in coals. For the higher rank coals (30), these are expected to be predominantly -R, -OH, and -OR groups (rather than -COOH or -CHO) which through inductive and resonance effects will destabilize anions and thus retard reduction (31). Additionally, the presence of bulky substituents on aromatic rings, as would be found for coal rather than simple aromatic hydrocarbons, also retards reduction, because of steric interference with solvation of the radical anion or dianion (31). Of course, not only the substituents but also mineral matter can react directly with potassium naphthalenide.

Steam Gasification Of Carbon Catalyzed By K_2CO_3

The reaction of various carbonaceous materials with steam to yield CO , CO_2 , and H_2 has been intensively studied. Of special interest has been the catalysis of this reaction by various alkali metal containing compounds, most notably potassium carbonate (32-37). Various mechanisms have been proposed, some including alkali metal atoms (37) or even graphite intercalation compounds (38) as intermediates.

To evaluate the possibility of such intercalation compound intermediates, we have conducted in situ X-ray diffraction investigation which would reveal intercalation compound formation both as a change in the graphite Bravais lattice and as a change in thermal expansivity. Temperature variant X-ray diffraction experiments, employing a Guinier-Simon camera, were carried out on mixtures of graphite and potassium carbonate (5-20 wt%) contained in open capillaries exposed to a water saturated (23°C) nitrogen flow. With temperature increasing from 23°C to 700°C (100°C/hour), only graphite and K_2CO_3 lattices were observed, while at 700°C the graphite Bragg peaks disappeared, unaccompanied by intercalation compound formation. The thermal expansivity of the graphite lattice was $3 \times 10^{-5} \Delta c/(^\circ\text{C})$, as for normal graphite, and in contrast to the value of $4 \times 10^{-5} \Delta c/(^\circ\text{C})$ that we have found for C_8K in the range -158°C to 23°C.

The failure to find evidence for intercalation compound intermediates in steam gasification indicates the importance of sigma, rather than pi, electrons in the reaction, and is consistent with the view of the importance of the attack by gaseous molecules on the edges of graphite planes (39).

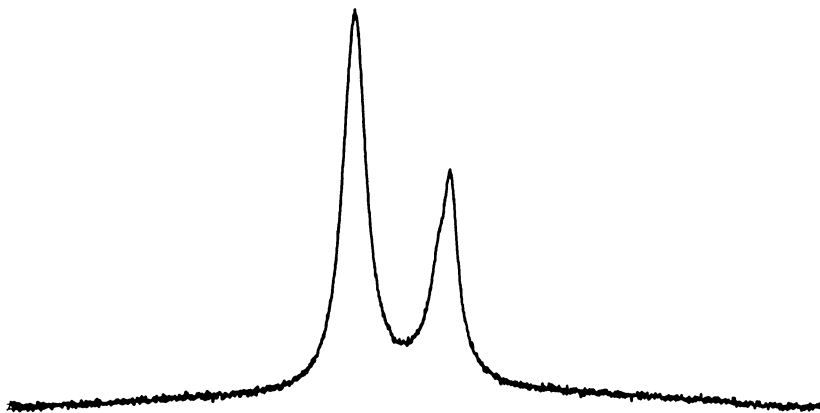


Figure 3a. The Li-7 NMR (34.8 MHz) of a two-week-old solution of Li-naphthalenide in THF.

With respect to an external standard of aqueous LiClO_4 , the larger peak is 11.95 ppm downfield, the smaller 1.6 ppm upfield, with the displayed spectrum width in the figure equal to 4000 Hz. The downfield peak arises from Li-naphthalenide, with the shift arising from the Fermi contact term (at room temperature for lithium, a shift downfield of 10 ppm corresponds to a hyperfine constant of $+ 0.005 \text{ mT} = + 0.05 \text{ G}$). At short reaction times, the downfield peak is even broader than shown here, possessing a full width at half maximum of 880 Hz.

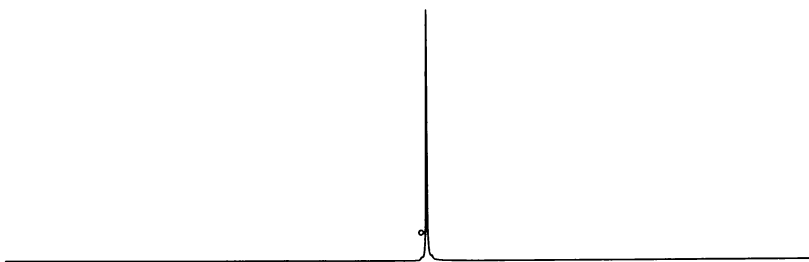


Figure 3b. The Li-7 NMR (34.8 MHz) of n-butyllithium in n-hexane. With the spectrum width equal to 4000 Hz, the single sharp peak comes at 1.6 ppm downfield from LiClO_4 (aq). In the context of this chapter, a positive value of chemical shift refers to an upfield shift.

Summary

Table 1 summarizes the results of the three specific reactions discussed in this paper. With some intuition, we can generalize these findings.

The intercalation of graphite reflects changes in the pi electron system of graphite, either through reduction (addition of electrons, as by naphthalenide) or through oxidation (removal of electrons, as by BF_3/ClF). When the pi electron system is unchanged ($\text{K}_2\text{CO}_3/\text{H}_2\text{O}$ or BF_3 alone), intercalation does not occur, although chemistry at the edges of graphite planes may occur.

The formation of aromatic radical anions or cations from polycyclic aromatic hydrocarbons is directly analogous to intercalation compound formation. Additionally, however, Lewis acids (as BF_3) can form weak charge transfer compounds by attacking the edges of the molecules; such chemistry is easily detected because of the high ratio of $C_{\text{peripheral}}/C_{\text{internal}}$ of these polycyclic aromatic molecules relative to graphite.

Bituminous coals, in possessing a large number of substituents (as -R, -OH, -OR), both can undergo chemistry at these sites (as with BF_3) and can have their bulk benzenoid chemistry modified by inductive effects of these substituents.

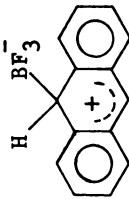
Experimental Details and Comments

Discussions of both the equipment (40) and chemical procedures (1, 21) have appeared elsewhere.

Briefly, wide-line nuclear magnetic resonance was examined with a Varian WL 112 spectrometer, with radiofrequencies supplied by a General Radio 1061 frequency synthesizer. Electron paramagnetic resonance investigation utilized a Varian E line Century Series console, an E-102 microwave bridge (9.5 GHz), and an E-231 cavity (TE₁₀₂ rectangular). A discussion of the appropriate units for reporting EPR and NMR results has been given (41). A Guinier-Simon camera, manufactured by Enraf-Nonius Delft, was used for variable temperature x-ray diffraction. The high resolution lithium-7 NMR was measured on a JEOL FX-90, and the GC/MS data was taken on a DuPont 21-491. Upfield NMR shifts are taken positive.

The details of the EPR investigation of the graphite compound " C_{16}BF_4 " merit some discussion. Because the material is an electronic conductor, we suspended the polycrystalline sample in eicosane, melted the mixture under hot water, vibrated the sample to get random orientation, and froze the mixture under cold water. Because " C_{16}BF_4 " is an anisotropic conductor (it does not have metallic conductivity orthogonal to the planes), the interpretation of the EPR results requires care. Thus, in a thick plate of an isotropic metal as lithium, one observes a Dysonian asymmetry parameter A/B which is dependent on temperature, varying between

Table I
Summary Of Reaction Results

	<u>graphite</u>	<u>aromatic molecules</u>	<u>coals</u>
Reduction of benzenoid framework by naphthalene ⁻	predominant	predominant	present, but not predominant
Reduction of benzenoid framework by K ₂ CO ₃ /H ₂ O	not observed	-----	-----
Form of complex with BF ₃	no compound found (unless ClF present)		BF ₃ hydrate, BF ₃ etherate, and similar

2.7 and 19 as the ratio of the conduction electron diffusion time to the electron T_2 varies from 10^2 to 10^{-4} (42). Additionally, one can interrelate the linewidth and g value of the EPR absorption to the electronic conductivity scattering time through the theory of Elliott (43, 44). Curiously, we see from Figure 1 of this paper that the A/B parameter, the linewidth, and the g value of the EPR absorption of " $C_{16}BF_4$ " are essentially unchanged over the temperature range -168° to $+23^\circ C$. This behavior stems directly from the anisotropy of " $C_{16}BF_4$ ", which gives this and other graphite intercalation compounds (45) much in common with the EPR behavior of other anisotropic conductors (46), magnetic impurities in metals (47), and the NMR behavior of metallic nuclei in bulk metals (48), rendering a casual interpretation of this "conduction carrier" resonance difficult (49, 50). Parenthetically, in support of our analogy between graphite acceptor compounds and aromatic radical cations, we have found the carbon-13 wide-line NMR signals (dispersive mode at 10 MHz, 12 MHz, and 15 MHz) of the compounds $C_{10}AsF_5$, $C_{13}CrO_3$, $C_{14}UF_6$, and $C_{14}PF_6$ all to fall in the range (-36 ± 20) ppm vs. external benzene, consistent with the de-shielding effects found for aromatic radical cations (51).

The stability of the alkali metal/naphthalene/tetrahydrofuran system also merits some discussion. Both our results and those of Sternberg (17) suggest that naphthalene will decompose as long as excess alkali metal is present. If one deals with stoichiometric solutions of the radical anion, there is evidence suggesting long term stability (52), and we cannot in fact prove that some unknown impurity is responsible for the decomposition observed. Our tetrahydrofuran was distilled from $LiAlH_4$ and used immediately under helium in a VAC atmosphere dry box.

Finally, we note that our inferences on the nature of the coal/ BF_3 product are consistent with recent work on products of coal with $ZnCl_2$ and $AlCl_3$ (53). Neither BF_3 , $ZnCl_2$, nor $AlCl_3$ will directly intercalate graphite (2, 6), but all are considered to form sigma complexes with aromatic molecules (7, 54).

Acknowledgements

We thank J. S. Bradley for the distilled tetrahydrofuran and K. D. Rose for the high resolution lithium nuclear magnetic resonance spectra. R. H. Schlosberg, B. G. Silbernagel, and the three referees for this paper made many useful comments.

Literature Cited

1. Part I: Ebert, L. B.; Matty, L.; Mills, D. R.; Scanlon, J. C. Mat. Res. Bull. 1980, 15, 251.
2. Selig, H.; Ebert, L. B. Adv. Inorg. Chem. Radiochem. 1980, 23 281.
3. Burkhardt, L. A.; Hammond, P. R.; Knipe, R. H.; Lake, R. R. J. Chem. Soc. A 1971, 3789.

4. Beall, H. Fuel 1979, 58, 319.
5. Wood, R. E.; Wisner, W. H. Ind. Eng. Chem./Proc. Res. Dev. 1976, 15, 144.
6. Ebert, L. B. Ann. Rev. Mat. Sci. 1976, 6, 181.
7. Aalbersberg, W. I.; Hoijtink, G. J.; Mackor, E. L.; Weijland, W. P. J. Chem. Soc. 1959, 3055
8. Perkampus, H. H.; Baumgarten, E. Angew. Chem., Int. Ed. 1964, 3, 776.
9. Leffler, A.; Selig, H.; manuscript in preparation.
10. Singer, L. S.; Kommandeur, J. J. Chem. Phys. 1961, 34, 133.
11. Emsley, J. W.; Feeney, J.; Sutcliffe, L. H.; "High Resolution Nuclear Magnetic Resonance", Vol. II; Pergamon: Oxford, 1966.
12. Brownstein, S.; Paasivirta, J. Can. J. Chem. 1965, 43, 1645.
13. Diehl, P. Helv. Phys. Acta 1958, 31, 685.
14. Gerrard, W.; Lappart, M. F. Chem. Rev. 1958, 58, 1081.
15. Novikov, Yu. N.; Vol'pin, M. Russ. Chem. Rev. 1971, 40, 733.
16. Hoijtink, G. J.; de Boer, E., van der Meij, P. H.; Weijland, W. P. Rec. Trav. Chim. 1956, 75, 487.
17. Sternberg, H. W.; Delle Donne, C. L.; Pantages, P.; Moroni, E. C.; Markby, R. E. Fuel 1971, 50, 432.
18. Sternberg, H. W.; Delle Donne, C. L. Fuel 1974, 53, 172.
19. Alemany, L. B.; King, S. R.; Stock, L. M. Fuel 1978, 57, 738.
20. Dogru, R.; Erbatur, G.; Gaines, A. F.; Yurum, Y.; Iclî, S.; Wirthlin, T. Fuel 1978, 57, 399.
21. Ebert, L. B.; Mills, D. R.; Matty, L.; Pancirov, R. J.; Ashe, T. R. Advances in Chemistry Series, #192, "Coal Structure", American Chemical Society: Washington, D.C., 1981.
22. Smidt, J.; van Krevelen, D. W. Fuel 1959, 38, 355.
23. Austen, D. E. G.; Ingram, D. J. E.; Tapley, J. G. Trans. Far. Soc. 1958, 54, 400.
24. Jensen, B. S.; Parker, V. D. J. Am. Chem. Soc. 1975, 97, 5211.
25. Jensen, B. S.; Parker V. D. Acta Chem. Scand. B 1976, 30, 749.
26. Carnahan, J. C.; Closson, W. D. J. Org. Chem. 1972, 37, 4469.
27. Bates, R. B.; Kroposki, L. M.; Potter, D. E. J. Org. Chem. 1972, 37, 560.
28. Fujita, T. Suga, K.; Watanabe, S. Synthesis 1972, 11, 630.
29. Jensen, F. R.; Bedard, R. L. J. Org. Chem. 1959, 24, 874.
30. Blom, L.; Edelhausen, L.; van Krevelen, D. W. Fuel 1957, 36, 135.
31. House, H. O.; "Modern Synthetic Reactions", 2nd ed.; Benjamin: Menlo Park, Ca., 1972; p 198.
32. Taylor, H. S.; Neville, H. A. J. Am. Chem. Soc. 1921, 43, 2055.
33. Long, F. J.; Sykes, K. W. Proc. Roy Soc. (London) 1952, A215, 100.
34. Walker, P. L.; Shel'ef, M.; Anderson, R. A. in "The Chemistry and Physics of Carbon", Vol. 4; Dekker: New York; 1968, pp 287-383.

35. Johnson, J. L. Catal. Rev.-Sci. Eng. 1976, 14, 131.
36. Rudolph, P. F. H. Energiespectrum 1977, 1, 311.
37. McKee, D. W.; Chaterjii, D. Carbon 1978, 16, 53.
38. Wen, W.-Y., Catal. Rev.-Sci. Eng. 1980, 22, 1.
39. Walker, P. L. in "Scientific Problems of Coal Utilization", ed. B. R. Cooper; U.S. Department of Energy: Washington, 1978; pp 237-247.
40. Ebert, L. B.; Mills, D. R.; Scanlon, J. C. Mat. Res. Bull. 1979, 14, 1369.
41. Crooks, J. E. J. Chem. Ed. 1979, 56, 301.
42. Feher, G.; Kip, A. F. Phys. Rev. 1955, 98, 337.
43. Elliott, R. J. Phys. Rev. 1954, 96, 266.
44. Beuneu, F.; Monod, P. Phys. Rev. B 1978, 18, 2422.
45. Ebert, L. B.; Selig, H. Mat. Sci. Eng. 1977, 31, 177.
46. Kahn, A. H. J. Appl. Phys. 1975, 46, 4965.
47. Winter, J. "Magnetic Resonance in Metals"; Clarendon: Oxford, 1971; Chapter 10.
48. Bloembergen, N. J. Appl. Phys. 1952, 23, 1379.
49. Ebert, L. B.; DeLuca, J. P.; Thompson, A. H.; Scanlon, J. C. Mat. Res. Bull. 1977, 12, 1135.
50. Khanna, S. K.; Falardeau, E. R.; Heeger, A. J.; Fischer, J. E. Sol. St. Commun. 1978, 25, 1059.
51. Forsyth, D. A.; Olah, G. A. J. Amer. Chem. Soc. 1976, 98, 4086.
52. Paul, D. E.; Lipkin, D.; Weissman, S. I. J. Amer. Chem. Soc. 1956, 78, 116.
53. Taylor, N. D.; Bell, A. T. Fuel 1980, 59, 499.
54. Morita, M.; Hiroswawa, K.; Sato, T. Bull. Chem. Soc. Jpn. 1977, 50, 1256.

RECEIVED April 27, 1981.

A Study of Coal Oxidation by Charged-Particle Activation Analysis

D. J. SCHLYER and A. P. WOLF

Department of Chemistry, Brookhaven National Laboratory, Upton, NY 11973

It has been recognized for many years that exposure of coal to air can significantly alter the processing characteristics of the coal. This effect is more pronounced in lower rank coals and in fact some brown coals will undergo spontaneous combustion at or near ambient temperatures.

Both the initial oxidation and the effect this oxidation has on the processing characteristics of the coal have been an area of interest for many years (1). In the last few years there has been a renewed interest in the oxidation of coal and several new analytical techniques have been applied to this problem (2-6). Several salient features of the process have been revealed including the chemical forms the oxygen takes when bound to the coal. It has been noted that the oxidation is not uniform throughout the particle as evidenced by the formation of a discoloration of the coal near the surface (7). This "oxidation rim" is directly related to the behavior of the coal.

The purpose of this study is to apply the unique technique of Charged Particle Activation Analysis (CPAA) to distinguish the characteristics of the oxidation process from a different point of view and define parameters which can be determined by this technique. The parameters to be determined are (1) the kinetics of the adsorption of oxygen containing species, (2) the elemental composition of the oxide layer and how deeply it extends into the particle, and (3) the number of reactive sites on or near the surface.

Experimental

Kinetic Experiments. The technique of Charged Particle Activation Analysis (CPAA) for analysis of oxygen in coal has been described previously (8). In the experiments to study the adsorption of oxygen onto the coal, a slight modification of this procedure has been used. Small lumps of coal were transferred in

0097-6156/81/0169-0087\$05.00/0
© 1981 American Chemical Society

an oxygen-free atmosphere to a spex mixer and ground so that about 80% of the particles had diameters from 45 microns (325 mesh) to 74 microns (200 mesh) with the remainder of the particles having diameters outside this range. The samples were then dried at 100°C under vacuum for 18 hours to remove moisture. Again all handling of the samples was done under an inert atmosphere. The samples were removed from the vacuum oven at room temperature and exposed to the air in flat shallow pans for a given period of time. After this exposure the samples were either sealed directly into a one mil (.025 mm) aluminum packet or returned to the vacuum oven, evacuated at 65°C for 3 hours and then sealed into the packets. The packets were then irradiated with He-3 at an energy of 10 MeV. The samples were counted and analyzed as described previously (8) to determine the oxygen to carbon ratio. A propagation of errors on this technique gives a precision of about 0.3% absolute. In actual experiments the precision has been about 1% absolute.

Oxygen Depth Profile. In order to measure the oxygen depth profile a range of particle sizes was needed. The coal sample was ground as usual. The particles were then sorted according to size by using standard sieves. In most cases this separation procedure was done in air. An exception to this was the procedure used to determine if the oxygen to carbon ratio varied in different size coal particles before exposure to air. In that case the sieving was done under an inert atmosphere and the samples immediately irradiated. After sieving the coal particles were exposed to the air for 60 days in a controlled humidity room (relative humidity 45%) and then sealed into the aluminum packets for irradiation. The nuclear reaction cross-section for production of C-11 and for F-18 change as a function of the particle energy. Since the change may be different for production of C-11 than it is for F-18, the nuclear reaction cross-section ratio must be determined as a function of energy. Standards to determine the nuclear reaction cross-section ratio for the oxygen depth profile experiments were "sandwiches" made from varying thicknesses of polyester and polyethylene films layered on top of one another. The standards consisted of a film of (1/4 mil to 2 mil) polyester of known composition followed by a polyethylene (1 mil to 5 mil) film followed by another polyester film which together represent the oxide layer, the central unoxidized coal, and another oxide layer. Layers of these "sandwiches" were sealed in the aluminum packets and irradiated and counted in a manner identical to that used for the coal samples. Comparison of the actual O/C ratio for a given "sandwich" to the experimentally determined F-18/C-11 gave the cross-section ratio as a function of particle size.

Experiments on the sorption of oxygen radiotracers were performed in the following way. A column was prepared by filling a 1/4" stainless steel tube one foot long with coal of 100-220

mesh. This column was placed in a gas chromatograph equipped with both a thermal conductivity detector and a radiodetector so that both a mass trace and an activity trace could be obtained for each experiment. The column temperature was lowered to -40°C using a liquid nitrogen cooling system while flushing with the helium carrier gas. After the gas sample was injected onto the column, the temperature was held at -40°C for two minutes at which point any unreacted oxygen had eluted. The temperature of the column was then raised linearly to a final temperature of 250°C . This temperature was held for 5 minutes. Two series of experiments were carried out using radioactive oxygen-containing molecules. A column of Pennsylvania Anthracite never exposed to air after grinding was prepared and exposed to molecular oxygen labelled with a trace of oxygen-15 prepared from the $^{16}\text{O}(\text{p},\text{pn})^{15}\text{O}$ nuclear reaction. A column of North Dakota Lignite was prepared and injected with a mixture of labelled O_2 , CO_2 and H_2O . The oxygen-15 in these molecules was prepared from the $^{15}\text{N}(\text{p},\text{n})^{15}\text{O}$ nuclear reaction and thus the mixture contained only a trace of molecular oxygen. The tracer, with or without added carrier, was placed in a 5 cc gas syringe and injected onto the coal column. After the heating cycle was completed the column temperature was gradually lowered while the column was continuously flushed with the helium carrier gas. Each of these columns were used for several runs. The repeatability of the results was very good.

Results

Kinetic experiments. The experimental curves for the uptake of oxygen-containing molecules versus time are shown in Figure 1 for three types of coal. The three types all follow the same general behavior in that they show a rapid uptake of oxygen followed by a more gradual uptake. In the case of the lower rank coal, this uptake lasts for a considerable amount of time. The lower curve in each case is the uptake of oxygen containing species after the sample had been placed in the vacuum oven at 65°C for 3 hours. In all cases a considerable amount of the oxygen can be pumped off. The anthracite shows essentially no increase in oxidation or O_2 uptake after about 15 minutes. In the lignite the irreversible uptake continues for a very long period of time. This is probably due to chemical oxidation of the coal.

Oxygen Depth Profile. When coal samples of different particle size (400 mesh to 35 mesh) which had not been exposed to air after grinding were analyzed for the oxygen to carbon ratio, it was essentially the same for all sizes. This implies that the oxygen to carbon ratio is constant throughout the particle. When the same analysis was carried out for coal exposed to air for two months, there was a definite increase in the oxygen to carbon

ratio as the particle size decreased. This indicates that an oxide layer has been produced on the outside of the coal particle upon exposure to air. In order to estimate the depth of the layer a model must be used. Three models have been explored in the attempt to estimate the depth of penetration. The first of these is a layer of constant composition which falls to the unoxidized value at a point within the sphere. The second is a linear decrease in the O/C from the outside of the particle towards the center and the third is an exponential decrease in the ratio. The predicted depth of the oxide layer is fairly insensitive to the model chosen but the oxygen to carbon ratio on the surface of the coal particle is extremely sensitive to the model. As a result it is possible to give meaningful numbers for the depth of the oxide layer but not for the oxygen content of the surface. The curves derived from the first model are given in Figure 2. The volume of the oxide layer for a given oxide layer thickness (V_o) divided by the total volume of the particle (V_p) is plotted versus the particle diameter to obtain the curve shown. These curves have been corrected for the experimentally determined nuclear cross-section ratio. Figure 3 is the data from the activation of New Mexico Sub-bituminous compared to the model curves. The values obtained for the oxide layer depths for the three types of coal oxidized for two months at 21°C are given in Table I.

Table I
Oxide layer depths
(2 months exposure at 21°C)

<u>Coal type</u>	<u>Depth in microns</u>
Anthracite	4
Sub-bituminous	7
Lignite	10

Labelled Oxygen Adsorption. When five milliliters of oxygen labelled with a trace of O-15 were injected onto the Pennsylvania anthracite, about 5% was retained on the column at low temperature. All of this oxygen was desorbed during the heating cycle. When a mixture of labelled O₂, CO₂ and H₂O labelled with O-15 in proportions of 80:15:5 in 5 cc of nitrogen was injected onto the column with no added carrier (approximately 10¹⁴ molecules of O₂ due to ppm impurities of O-16, O₂), all of the activity was retained on the column. When 1 cc of O₂ was added to the mixture only activities which corresponded to CO₂ and H₂O were retained on the column. When 1 cc of a 50:50 mixture of CO₂ and O₂ was added only about 5% of the activity was retained on the column. This activity probably corresponds to the water activity.

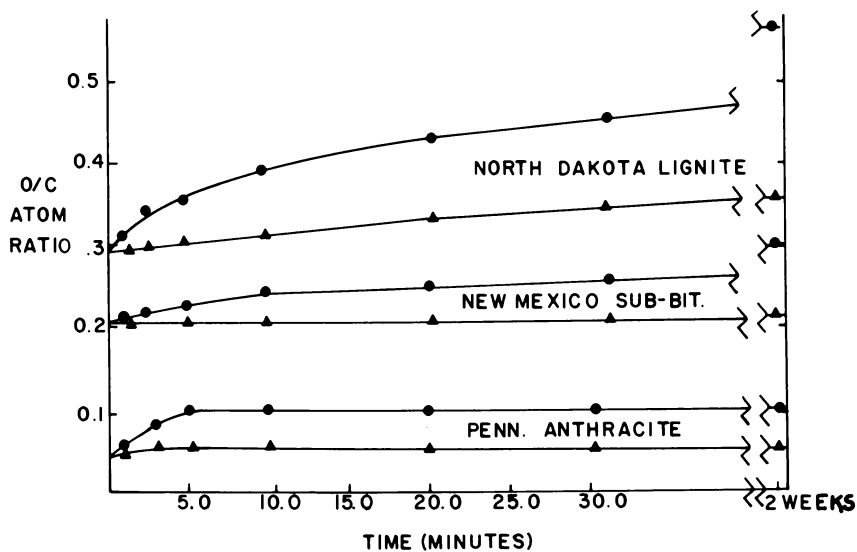


Figure 1. Uptake of oxygen by selected coals vs. time: no heat or pumping (●); heated at 65°C under vacuum (▲).

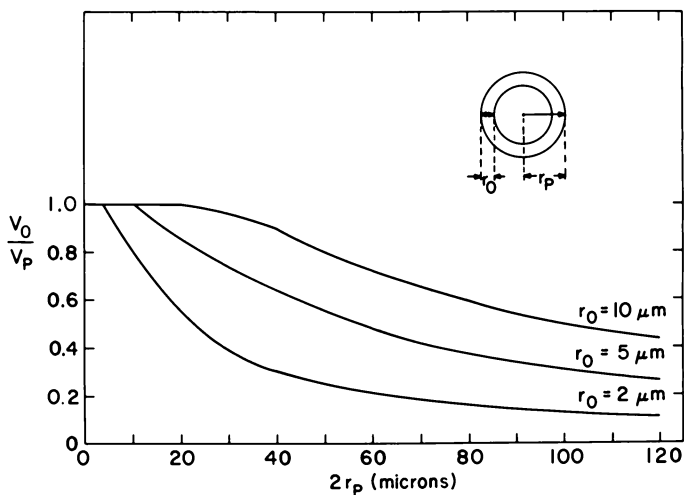


Figure 2. Volume of oxide layer divided by the total volume of the particle diameter for model

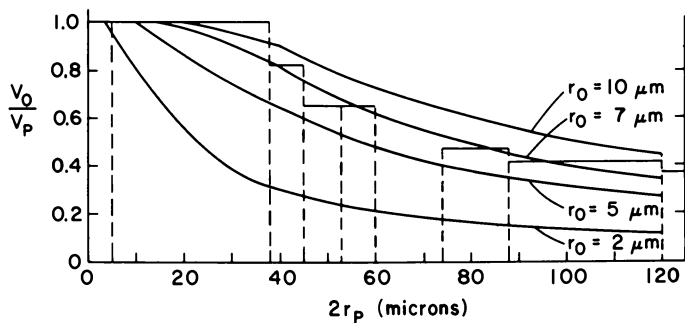


Figure 3. Comparison of experimental data for New Mexico subbituminous with model

Discussion

Several salient features have emerged from work done in other laboratories on the low temperature oxidation of coal. These are listed below:

- (1) The adsorption of oxygen onto most types of coal follow Elovich kinetics i.e. a rapid uptake followed by a much more gradual uptake (9)
- (2) The oxygen adsorbed by low rank coals can form phenolic-OH or carbonyl groups (10-12). The phenolic groups can split out H₂O to form ether linkages.
- (3) Water sorption isotherms on low rank coals have a standard type II sigmoid shape typical of porous adsorbents (4).
- (4) The heat of desorption for macroscopic amounts of water off most coals is very near that of the heat of vaporization of water (4).
- (5) The apparent activation energies for oxidation are very low.

The current studies using radiochemical techniques are in agreement with these findings. The adsorption of oxygen onto the coal follows Elovich-type kinetics. Recent modelling studies have demonstrated the equivalence of Elovich kinetics with diffusion and adsorption in microporous solids (13,14). These studies tend to support the idea of solid state diffusion with the fairly low activation associated with these processes as a rate limiting step in the coal oxidation. The depth of penetration of the oxygen seems to be directly related to the rank of the coal. In the cases studied here, the anthracite showed the least penetration while the lignite showed the deepest. This function of rank is probably a result of porosity of the coal. It has been possible to demonstrate that for the lower rank coals that there are very few (more than 10¹⁴/g but less than 10¹⁹/g) reactive sites for strong oxygen adsorption. From the data collected we wish to propose the following mechanism for low temperature oxidation.

Oxygen is adsorbed weakly onto the surface of the coal. This adsorbed oxygen can then migrate across the surface or into the interior of the coal particle to a reactive site at which point it becomes chemically bound. The form of this chemical bond is phenolic-OH, carbonyl or peroxide type moieties. As the surface layers become saturated, the oxygen will diffuse deeper into the particles through pores and crevices to react with sites within the coal particle. This is the second, slower part of the adsorption process. At some point the chemical potential against diffusion into the particle becomes great enough that the oxidation from the exterior of the particle ceases. This point will be determined by the porosity of the coal and the temperature at which the oxidation is carried out. As

temperature is increased the oxide layer will extend deeper into the coal particle.

Acknowledgment

Research carried out at Brookhaven National Laboratory under contract with the U. S. Department of Energy and supported by its Office of Basic Energy Sciences.

Literature Cited

1. See for example Dryden, I. G. C. in Chemistry of Coal Utilization, Supplementary Volume (Ed. H. H. Lowry) Wiley, New York, 1963, Ch. 6, p. 272.
2. Painter, P. C., Snyder, R. W., Pearson, D. E., Kwong, J. FUEL, 59, 282 (1980).
3. Bouwman, R. and Freriks, I. L. C. FUEL, 59, 315 (1980).
4. Bhattacharyya, K. K. FUEL, 50, 214 (1971).
5. Avison, N. L., Winters, R. M., and Perlmutter, D. D. AIChE Journal 25, 773 (1979).
6. Swann, P. D., Allardice, D. J. and Evans, D. G. FUEL, 53, 85 (1974).
7. Dugan, P. and Moran, V. J. FUEL, 49, 415 (1970).
8. Schlyer, D. J., Ruth, T. J. and Wolf, A. P. FUEL, 58, 208 (1979).
9. Newman, J. O. H., Stanley, L., Evans, P. L., Coldrick, A. J. T. and Kempton, T. J. Nature 214, 280 (1967).
10. Ignasiak, B. S., Clugston, D. M. and Montgomery, D. S. FUEL, 51, 76 (1972).
11. Swann, P. D. and Evans, D. G. FUEL, 58, 276 (1979).
12. Ignasiak, B. S., Szaldow, A. J. and Berkowitz, N. FUEL, 53, 229 (1974).
13. Harris, J. A. and Evans, D. G. FUEL, 54, 277 (1975).
14. Yang, R. T. and Wong, C. J. Phys. Chem. 84, 678 (1980).

RECEIVED March 9, 1981.

A Fundamental Chemical Kinetics Approach to Coal Conversion

STEPHEN E. STEIN

Department of Chemistry, West Virginia University, Morgantown, WV 26506

At the present time, few, if any, details of chemical reaction mechanisms in coal conversion are known with certainty. This situation is particularly distressing in the areas of coal liquefaction and pyrolysis where chemical kinetics may strongly influence process efficiency and product quality. To improve this situation, in recent years a number of research groups have been performing chemical studies of coal and "model" compound reactions.

Thermochemical kinetic methods (1) can be of great value for interpreting and generalizing results of these studies. These methods are now indispensable for mechanistic analysis of many practical chemical systems involving highly complex reactions, including oxidation, combustion, atmospheric chemistry and pyrolysis. With recent extensions of thermochemical kinetics estimation methods to coal-related molecules (2,3,4) and free radicals (5), it is now feasible to apply thermochemical kinetics analysis to a wide range of coal-related chemical systems. Thermochemical and kinetics estimation methods are particularly suited for analysis of coal systems since these methods are applicable not only to reactions of molecules but also to reactions of specific molecular structures.

This work presents the first systematic application of these methods to coal chemistry. This analysis is intended not only to suggest likely reaction mechanisms, but also to demonstrate the unique power of thermochemical kinetics methods for semi-quantitative analysis of the complex chemistry of coal conversion.

Conversion of Gas-Phase Data to the Liquid Phase

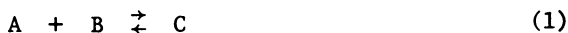
Since most predictive thermochemical and kinetics methods yield gas-phase values, it is necessary to consider the applicability of these values to the liquid phase. For equilibria involving no change in the number of moles, $\Delta n = 0$,

0097-6156/81/0169-0097\$07.50/0
© 1981 American Chemical Society

a good basis exists for assuming that, in the absence of significant differences in solvent-molecule interactions between reactants and products, equilibrium constants are nearly the same in gas and liquid phases (6). Within the framework of transition-state theory, the same conclusion applies to rate constants for unimolecular reactions not subject to "cage" effects (7a). In practice, cage effects can be significant only for bond homolysis reactions ($R_1-R_2 \rightarrow R_1\cdot + R_2\cdot$).

In contrast, when $\Delta n \neq 0$ one finds considerable disagreement in the literature concerning relative gas and liquid equilibrium (and rate) constants, even in the absence of solvation effects. Depending on the particular theoretical treatment, bimolecular reaction rate constants have been estimated to be somewhere between 2 and 100 times faster in solution than in the gas phase (6). However, the very limited experimental data available indicate that there is little, if any, systematic difference between bimolecular rate constants in the two phases (6d).

We have examined this problem as follows. For associative equilibria



relative liquid and gas-phase equilibrium constants, K_1/K_g , have been computed using vaporization data (8) and equation 2 (6d),



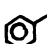
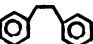


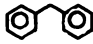



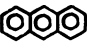
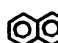


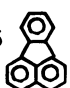
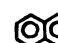
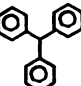
$$\frac{K_1}{K_g} = \frac{P_A^\circ P_B^\circ}{P_C^\circ} \left(\frac{V_s}{RT}\right) K_\gamma \quad (2)$$

where P_A° is the (ideal gas) vapor pressure of neat liquid A, V_s is the molar volume of the solution and K_γ is the ratio of condensed-phase activity coefficients, $\frac{\gamma_A \gamma_B}{\gamma_C}$. An analogous

formula for relative bimolecular rate constants, k_1/k_g , holds if C is regarded as the transition state. A detailed description of these calculations is in preparation, but the major conclusion is that in the absence of substantial solvation differences between reactants and products (or transition state), within a factor of ca. 2, $K_1 \sim K_g$ and $k_1 \sim k_g$. For specific equilibria of interest, $K_1 \sim K_g$ may often be directly evaluated by means of equation 2 using P° and K_γ values obtained from the literature, from estimation methods (9) or by analogy to related systems.

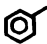
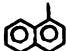
Available vapor pressure data (8) may be used to roughly examine the magnitude of solvation effects on equilibrium constants. Table I lists (K_1/K_g) values for selected equilibria involving polyaromatic molecules. Clearly, reactions leading to increased aromaticity are inherently favored in solution relative to the gas phase. Table II shows changes in vapor pressures resulting from replacement of (hydrogen-bonding)

Table I. K_1/K_g for Polyaromatic Equilibria¹

	K_1/K_g ²	T/K
2  \rightleftharpoons 	1.6	350
2  \rightleftharpoons 	0.59	350
 +  \rightleftharpoons 	0.73	350
2  \rightleftharpoons 1.2 	2.6	350
2  \rightleftharpoons 1.4 	2.3	500
2  \rightleftharpoons 1.25 	4.3	500
2  \rightleftharpoons 1.25 	1.8	500
2  \rightleftharpoons 1.05 	0.055	500

1. H_2 required to balance reactions may be assumed to be in the gas phase; K_1/K_g values are not affected by H_2 .
2. Calculated with a slightly modified form of equation 2 (6d) where $\Delta n \neq -1$ assuming $K_\gamma = 1$; solvent is assumed to be pure reactant except where noted; vapor pressures were taken from reference 8b and corrected for non-ideal behavior by methods in reference 9.
3. Solvent is assumed to be an equimolar mixture of toluene and benzene.

Table II. Effects on Vapor Pressures of Replacing Hydroxyl Groups with Methyl Groups.

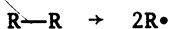
R—	$P_{\text{vap}}(\text{R-CH}_3)/P_{\text{vap}}(\text{R-OH})^*$					
	T/°C					
	50	100	150	200	250	300
n-C ₃ H ₇ —	48	18				
n-C ₆ H ₁₃ —	21	8.6	4.3			
n-C ₁₂ H ₂₅ —		4.4	3.1	2.3		
n-C ₁₈ H ₃₇ —			2.4	2.1	1.9	1.7
	28	14	8.2	5.4	3.9	2.9
			4.0	3.2	2.4	

* Note that $P_{\text{vap}}(\text{R-XR}')/P_{\text{vap}}(\text{R-CH}_2\text{R}') \sim 1$ for X = -O-, $\begin{array}{c} \text{O} \\ || \\ -\text{C}- \end{array}$, and S; P_{vap} are from reference 8.

hydroxyl groups with methyl groups. These values roughly correspond to contributions to equilibrium or rate constants arising from formation or destruction of a hydrogen bond: although K_1/K_g values will depend somewhat on the particular solvent. The negation of such effects with increasing temperature is striking. At coal conversion temperatures changes in hydrogen bonding in a reaction are not expected to change rate or equilibrium constants by more than a factor of 2-3. Other effects due to selective solvation, including polar effects and charge-transfer interactions, are also expected to be far smaller at coal conversion temperatures than at lower temperatures where such effects are most often observed. With the general assumption that equilibrium constants are nearly the same in the gas and liquid phases, a number of aspects of the thermal chemistry of coal-related molecules will now be examined.

Bond Breaking

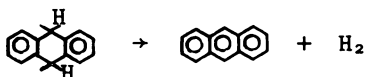
Three modes of bond breaking may be distinguished in homogeneous, non-ionic systems, namely bond homolysis,



free-radical β -bond scission



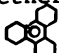
and concerted molecular decomposition,



Rate constants for specific reactions belonging to any of the above classes of reactions can often be estimated to a reasonable degree of accuracy (1). Even for cases where estimates are only accurate to an order of magnitude or worse, specific reactions may often be shown to be either far too slow to account for observed kinetics or very rapid. In addition, relative rate constants are often all that is needed to decide between competing mechanisms, and estimates of relative rate constants are often far more accurate than estimates of absolute rate constants. Each of the above three modes of bond breaking will now be individually discussed.

Bond Homolysis. A substantial number of gas-phase bond homolysis rate constants and free-radical enthalpies of formation have been determined (1,11) and a far greater number may be reliably estimated. However, two factors must be considered when applying gas-phase bond homolysis rate constants to condensed-phase systems. First, any selective solvation of product radicals will tend to increase (k_1/k_g). However, solvation effects on free radical reaction rates are generally the

exception rather than the rule, even in fairly polar media at low temperatures (i.e., <200°C) (7,12). Second, recombination of nascent free radicals formed by bond homolysis, the "cage effect", will reduce (k_1/k_g). Rates of bond homolysis have been shown to decline with increasing viscosity, although the dependence of the rate constant, k , on viscosity, η , is a rather weak one ($k \propto \eta^{-0.4 \pm 0.1}$) (7, 13). In media of unusually low fluidity, as exist in the coal matrix before dissociation, one might expect a substantial homolysis rate constant reduction, although relevant quantitative information is not yet available.

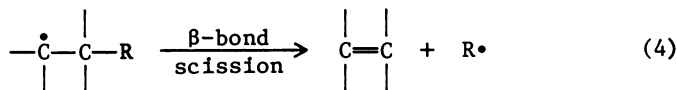
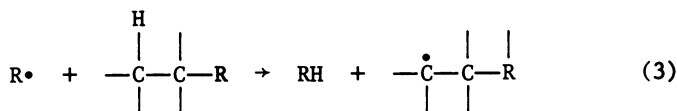
Direct studies of bond homolysis in a given molecule in both the gas and liquid phase have generally shown that homolysis rate constants are the same in the two phases within a factor of ca. 2 (6d,7). Therefore, either cage and solvation effects are both small or they largely cancel one another in the systems studied. Recent studies in our lab (14) of the dissociation of PhXCH₂Ph, X = CH₂, NH, O and S in tetralin over the range 300°C-450°C show that $k_1/k_g \sim 0.5-1.0$. Also, dissociation of bibenzyl and benzylphenylether in the relatively viscous solvent dodecahydrotriphenylene () occurs at a

rate about two-thirds of that found for dissociation in tetralin.

The above considerations imply that over a wide range of conditions gas and solution phase homolysis rate constants are, to a good level of accuracy, independent of phase or solvent.

Available rate and thermochemical data allow estimates to be made for bond homolysis rate constants for virtually all covalent bonds presumed or found to be present in coal and model compound reactions. In Table III is compiled a list of coal-related homolysis rate constants, k , and bond homolysis half lives at 400°C, $\tau_{1/2}$ ($\tau_{1/2} = \ln 2/k$ is equal to the time required to break one-half of the bonds if homolysis were the only mode of reaction). Most of these values are estimated relative to measured rate constants for bibenzyl dissociation in tetralin, and relative values are expected to be only weakly dependent on solvent. It is evident from Table III, with few exceptions, that only bonds that yield two resonance stabilized radicals upon breaking are likely to undergo significant homolysis under coal liquefaction conditions.

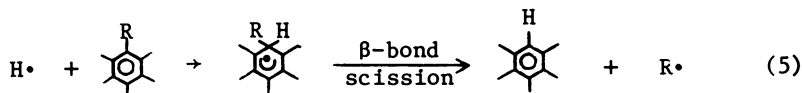
Radical β -Bond Scission. Model studies clearly show that certain bonds, such as the (-CH₂-CH₂-) bond in 1,3-diphenylpropane (15), are rapidly cleaved even though these bonds are too strong to undergo substantial bond homolysis under reaction conditions (Table III). An alternative route for bond breaking is through a chain reaction sequence involving β -bond scission, as follows:



Because of its relatively low activation energy and its involvement in a chain reaction, β -bond scission is often the dominant mode of bond breaking in the pyrolysis of large aliphatic hydrocarbons. Moreover, substitution of an oxygen atom for a methylene (CH_2) group in the above structure will often lead to an even more rapid chain reaction because of the resulting lower endothermicity of reaction 4.

The significance of β -bond scission in coal chemistry is limited by the concentration of suitable molecular structures. Rapid β -bond scission generally requires structures containing three or more consecutive, saturated, polyvalent atoms such as carbon, oxygen, nitrogen and sulfur. Examples of coal-related structures susceptible to rapid dissociation by β -bond scission are given in Figure 1. For each structure, once the C-X bond is broken by any means, the radical formed will rapidly dissociate.

It should also be noted that β -bond scission is formally involved in thermal desubstitution of aromatic rings by, say, H atoms, as follows.



The rate of this reaction is limited by the availability of H atoms, although under appropriate conditions this reaction can be an important means of bond breaking in coal systems (16).

Concerted Decomposition. Both unimolecular and bimolecular reactions involving only molecular species (no free radicals or ions) may play a role in certain aspects of coal conversion. In some types of concerted reactions, however, such as reactions involving C-C or C-O bond breaking, the significance of such reactions appears to be drastically limited by the lack of suitable molecular structures.

In the case of bibenzyl, the following pathway for decomposition has been proposed (17):

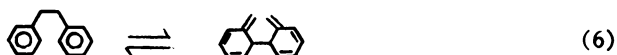


Table III. Bond Homolysis in Tetralin ($\theta = 0.00458 \text{ T/K}$)

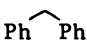
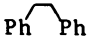
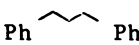
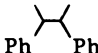
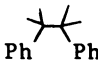
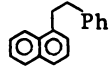
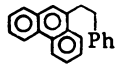
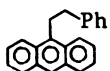
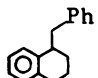
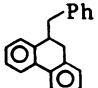
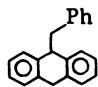
R_1-R_2	$\log[k_{\text{tet}}(R_1-R_2)/s^{-1}]$	References	$\tau_{1/2}$ (400°C)
Ph—Ph	17.9 - 117.8/ θ	a,b	10^{12} years
	16.9 - 94.1/ θ	a,b	10^6 years
	16.0 - 65.2/ θ [16.4 - 66.4/ θ]	c d	28 hours 28 hours
	17.0 - 76.2/ θ	a,b	1 year
	16.0 - 59.3/ θ	e	20 min
	16.0 - 53.1/ θ	f	12 sec
	16.0 - 62.3/ θ	g	3 hours
	16.0 - 62.7/ θ	g	4 hours
	16.0 - 57.4/ θ	g	5 min
	16.6 - 63.2/ θ	h,i	1.6 hours
	16.6 - 60.6/ θ	j	14 min
	16.6 - 60.6/ θ	j	14 min

Table III. (con't)

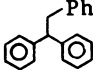
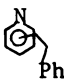
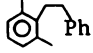
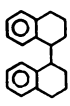
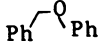
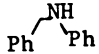
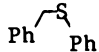
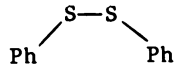
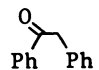
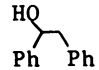
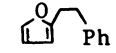
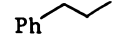
	16.0 - 60.4/θ	k	50 min
	ortho 16.0 - 66.9/θ	k	100 hours
	meta 16.0 - 65.2/θ	k	28 hours
	para 16.0 - 66.3/θ	k	60 hours
	16.0 - 62.2/θ	k	3 hours
	17.2 - 59.3/θ	h	1.3 min
	14.7 - 50.8/θ	d	40 sec
	14.8 - 56.7/θ	d	50 min
	15.8 - 54.6/θ	d	1 min
	15.8 - 60/θ	l	1 hour
	16.0 - 72/θ	m	200 days
	16.0 - 62/θ	m	3 hours
	16.0 - 63.7/θ	k	9 hours
	15.3 - 70.6/θ	n	330 days

Table III. (con't)

	15.7 - 62.4/θ	n	7 hours
	14.9 - 67.2/θ	n	70 days

^a Estimated assuming $k_{\text{tet}}(\text{R}_1\text{-R}_2)/k_{\text{tet}}(\text{Ph}-\text{Ph}) = k_{\text{gas}}(\text{R}_1\text{-R}_2)/k_{\text{gas}}(\text{Ph}-\text{Ph})$; $k_{\text{gas}}(\text{Ph}-\text{Ph})$ determined as $10^{15.1-61/\theta} \text{ s}^{-1}$ (11j).

^b $k_{\text{gas}}(\text{R}_1\text{-R}_2)$ derived from thermodynamic properties of $\text{R}_1\cdot$ and $\text{R}_2\cdot$ (1,11f) and $\text{R}_1\text{-R}_2$ properties given in reference 27 or estimated by group additivity (1), assuming $\text{R}_1\cdot/\text{R}_2\cdot$ recombination rate constant of $10^{9.5} \text{ M}^{-1} \text{ s}^{-1}$.

^c This rate constant value is used to obtain relative rate constants for bond homolysis of other bonds.

^d determined in the authors laboratory (14).

^e Assumes $k_{\text{tet}}(\text{Ph}-\text{Ph})/k_{\text{tet}}(\text{Ph}-\text{Ph}) = k_{\text{gas}}(\text{C}_2\text{H}_5)/k_{\text{gas}}(\text{C}_2\text{H}_5)$ using $k_{\text{gas}}(\text{C}_2\text{H}_5)$ described in footnote f. $k_{\text{gas}}(\text{C}_2\text{H}_5)$ obtained from $\Delta H_{\text{f},298}^\circ(\text{C}_2\text{H}_5\cdot) = 19.0 \pm 1.5 \text{ kcal/mol}$ (11b,d,e); $S_{300}^\circ(\text{C}_2\text{H}_5\cdot) = 66.7 \text{ cal/mol}\cdot\text{K}$ (1); thermodynamic properties of 1,2-dimethylbutane (28); isopropyl radical recombination rate constant = $10^{9.5} \text{ M}^{-1} \text{ s}^{-1}$ (1).

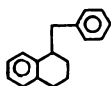
^f Assumes $k_{\text{tet}}(\text{Ph}-\text{Ph})/k_{\text{tet}}(\text{Ph}-\text{Ph}) = k_{\text{gas}}(\text{C}_2\text{H}_5)/k_{\text{gas}}(\text{C}_2\text{H}_5)$. $k_{\text{gas}}(\text{C}_2\text{H}_5)$ obtained from reference (11c), and $k_{\text{gas}}(\text{C}_2\text{H}_5)$ estimated using: $\Delta H_{\text{f},298}^\circ(\text{C}_2\text{H}_5\cdot) = 27.5 \pm 1 \text{ kcal/mol}$ (1,10b,d,e); $S_{298}^\circ(\text{C}_2\text{H}_5\cdot) = 58.0 \text{ cal/mol}\cdot\text{K}$ (1); chemical thermodynamic properties of butane (28); ethyl radical recombination rate constant = $10^{10.0} \text{ M}^{-1} \text{ s}^{-1}$ (1).

^g estimated relative to $k_{\text{tet}}(\text{Ph}-\text{Ph})$ using equation 9.

^h For each tetralyl (or hydroaromatic) radical formed, it is assumed that ΔS^\ddagger is 3 cal/mol·K greater than ΔS^\ddagger for bibenzyl homolysis. Note that $S_{\text{int}}^\circ(\text{C}_{10}\text{H}_8) - S_{\text{int}}^\circ(\text{C}_{10}\text{H}_8) \sim 3 \text{ cal/mol}\cdot\text{K}$ (2).

Table III. (con't)

ⁱ Activation energy assumed to be 2 kcal/mol lower than for Ph-Ph dissociation, since $D(C_{\text{primary}}-C_{\text{primary}}) - D(C_{\text{primary}}-C_{\text{secondary}}) \sim 2$ kcal/mol (1).

^j Estimated relative to k_{tet} () using equation 9.

^k assumes $\frac{k_{\text{tet}}(R_1-R_2)}{k_{\text{tet}}(\text{Ph}-\text{Ph})} = \frac{k_{\text{gas}}(R_1-\text{CH}_3)}{k_{\text{gas}}(\text{PhCH}_2-\text{CH}_3)}$. All k's except $k_{\text{tet}}(R_1-R_2)$ have been determined in the authors laboratory (11i,j,k,l).

^l enthalpy of formation of PhSSPh from reference (28), and of PhS• from (11k) adjusted for recent benzyl radical enthalpy of formation (11f). In the authors laboratory this molecule has been found to undergo dissociation in tetralin much more rapidly due, presumably, to a radical displacement chain reaction.

^m thermochemistry from references given in reference (11e).

ⁿ from gas-phase homolysis rate constants reported in reference (11a,m).

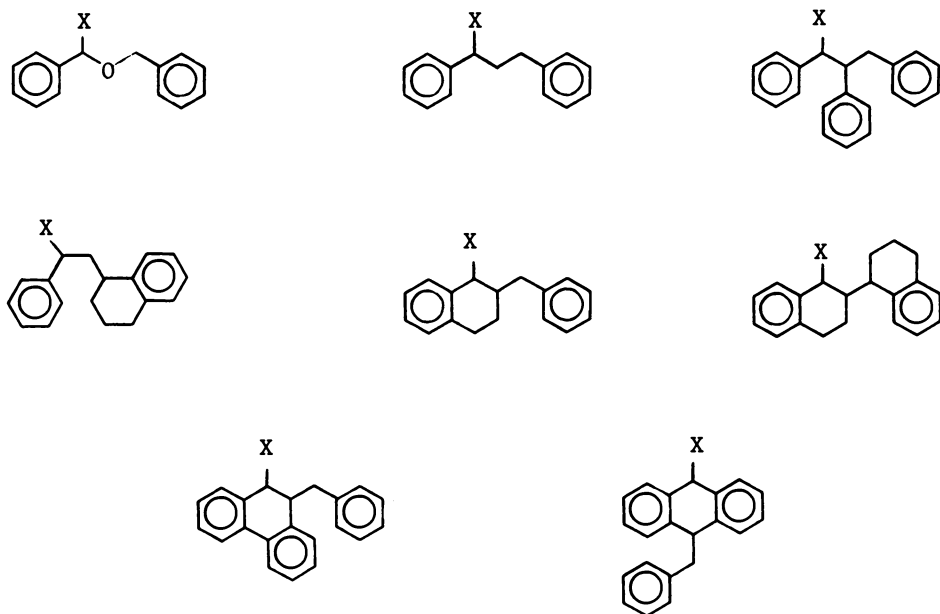
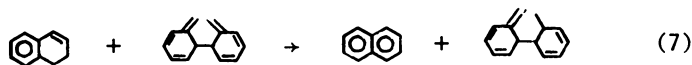
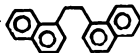


Figure 1. Coal-related structures susceptible to rapid β -bond scission (radicals formed by breaking C-X bond will decompose by β -bond scission in $\leq 10^{-2}$ s at 400°C)

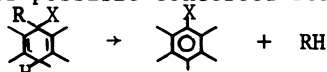


While each of these reactions is "allowed", the rate estimated for decomposition of bibenzyl by this mechanism is many orders of magnitude slower than the observed rate (18). Even if step 7 had no activation energy (a highly unlikely possibility), the rate predicted for this pathway is still orders of magnitude slower than the observed rate. Note that available thermochemical evidence strongly suggests that the intermediate polyolefinic molecule in reaction 6 does not possess substantial resonance energy. It might be argued that structures such as PhOCH_2Ph and  are more susceptible to such concerted

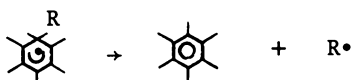
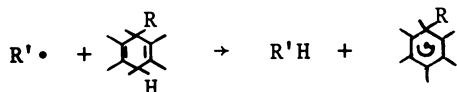
reaction paths than is bibenzyl. However, it appears to be a general rule that structures more susceptible to such concerted reactions are also more susceptible to bond homolysis. For the above two structures, and several others that we have examined, computed rates via reactions analogous to reactions 6-8 are many orders of magnitude slower than estimated (or measured) homolysis rates. For the reaction of 1,2- α -dinaphthyl ethane, for instance, the above concerted pathway is estimated to proceed at a rate $<10^{-10}$ that of bond homolysis at 300°C .

Retrograde Diels-Alder reactions are unlikely reactions in coal liquefaction chemistry due, again, to the lack of suitable molecular structures. Decomposition of cyclohexene to ethylene and 1,3-butadiene, for instance, is 40 kcal/mol endothermic and at 450°C proceeds at a rate such that the half-life of cyclohexene is 13 hours (11a). For tetralin to react by an analogous reaction, resonance stability would be lost, and the reaction would be many orders of magnitude slower than cyclohexene. Recent studies indicate that at 750°C tetralin may homogeneously decompose to benzocyclobutane and ethylene (19). Near coal liquefaction temperatures, however, this reaction would be immeasurably slow.

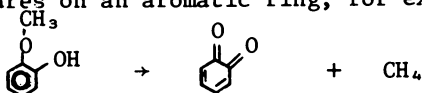
Yet another possible concerted reaction is



However, when $\text{R} = \text{CH}_3$ and $\text{X} = \text{H}$, concerted decomposition yields only H_2 (20), and when $\text{R} = \text{X} = \text{CH}_3$ this molecule reacts by free-radical pathways (21). In environments containing sufficiently high free radical concentrations the preferred mode of decomposition of such structures will be,

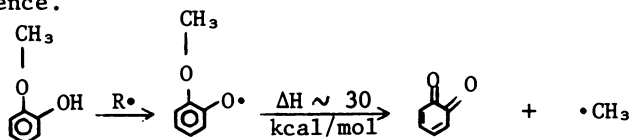


Klein and Virk (22) have pointed out that a key concerted decomposition reaction may involve adjacent (ortho) hydroxyl and ether structures on an aromatic ring, for example,



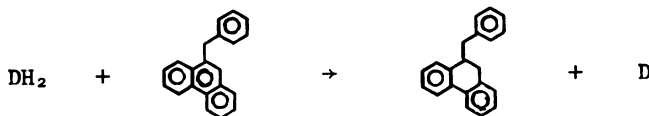
Moreover, they reported that methane formation rates from thermolysis of such molecules are significantly greater than

from thermolysis of anisole ($\text{C}_6\text{H}_5\text{OCH}_3$). However, the above structure is also prone to decomposition through a free-radical chain sequence.



Studies of *o*-hydroxyanisole pyrolysis in our lab under conditions of very-low pressure pyrolysis (23), where bimolecular reactions cannot occur, show $\cdot\text{CH}_3$ but little or no CH_4 as a product.

Concerted bimolecular reactions, such as H_2 -transfer by donor molecules (24) or direct H_2 -addition (25), are often thermochemically plausible and may play a role in bond breaking by converting thermally stable structures into structures that may decompose by free radical reactions. For example, the following H_2 -transfer leads to a structure that may readily dissociate by bond homolysis or β -bond scission.



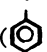
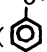
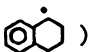
Of course, less direct, H-transfer pathways that involve free radicals are also possible and will be discussed later.

Thermochemistry of Resonance Stabilized Radicals

Based on the structural entities known to be present in

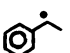
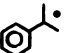
coal liquids or presumed to be present in coal, according to current models of coal structure, the predominant organic free-radicals in coal conversion are expected to possess extra stability from odd-electron delocalization. Any consideration of the reactivity of a resonance stabilized radical, $R\cdot$, requires a knowledge of its thermodynamic stability, as measured, for example, by its R-H bond strength. Therefore, before considering reactions of these radicals, the thermochemistry of two important classes of resonance stabilized radicals will be discussed.

One class of radicals are distinguished by their inability to form a new aromatic ring by loss of a single H atom.

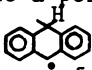
Examples are benzyl () , phenoxy () and α -tetralyl () radicals. A very simple scheme, based on Herdon's resonance theory (26), for estimation of the stability of benzylic hydrocarbon radicals has recently been proposed (5) and partly verified (11g). This scheme estimates the extra stability from odd-electron delocalization from the simple formula,

$$A \ln \left[\begin{array}{c} \text{number of different} \\ \text{resonance isomers} \\ \text{of the radical, } R\cdot \end{array} \right] - B \ln \left[\begin{array}{c} \text{number of different} \\ \text{resonance isomers} \\ \text{of RH} \end{array} \right] \quad (9)$$

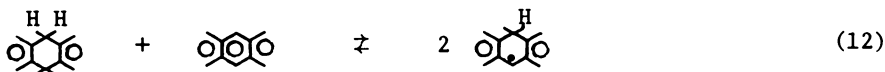
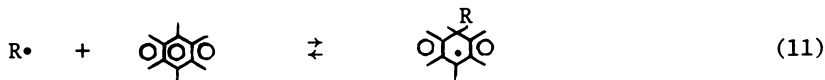
Recent thermochemical determinations suggest that $A = 14.21$ kcal/mol and $B = 17.21$ kcal/mol (11g). To obtain, for instance, benzylic C-X bond strengths, the stabilization energy calculated from equation 9 is subtracted from C-X bond strengths for corresponding saturated species. Recent studies of alkyl-benzene pyrolysis (11L) imply that within current uncertainties in relative bond strengths this formula applies to secondary and

tertiary benzylic radicals (e.g.,  and ). For complex phenoxy-type radicals less is known, although a tentative assumption is that differences in resonance stability of such radicals are the same as differences for corresponding benzylic radicals.

A second class of radicals of relevance to coal reactions are those that may form a new aromatic ring upon rupture of a single bond (or conversely these radicals may be formed by radical addition to a polyaromatic molecule). An example of

such a radical is  which may decompose to form anthracene by rupture of a C_{10} -H bond. Some modes of formation of these radicals are illustrated below:





Each of these reactions and their reverse reactions may, in fact, be involved in major reaction pathways in coal conversion. Reaction 10, for instance, is expected to be a key step in H-transfer and aromatization, reaction 11 can lead to crosslinking and polymerization while reaction -11 breaks up complex molecules, and reaction 12 should provide a steady source of free radicals in many pyrolytic systems even in the absence of weak covalent bonds (vide infra). Furthermore, these free radicals contain weak C-H bonds that may rupture to yield H atoms, which can in turn lead to breaking of C-C or C-O bonds through aromatic displacement reactions (reaction 5).

Enthalpies of H-atom addition to various sites in benzene, naphthalene, phenanthrene, anthracene and pyrene have been derived from available thermochemical data (2,27a) and formula 9, and are given in Table IV.

Differences between enthalpies of addition of $R\cdot$ and $H\cdot$ to aromatics are expected to be close to differences between $C_{\text{sec}}-R$ and $C_{\text{sec}}-H$ bond strengths (C_{sec} is a secondary carbon atom). For instance, using available thermochemistry (1,11f) addition of benzyl radicals to a given site on an aromatic ring is ca. 22 kcal/mol less exothermic than H-atom addition to the same site.


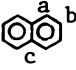
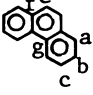
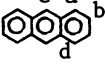
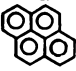
Use of the thermochemistry discussed above allows rough estimation of reaction enthalpy for a wide range of reactions involving resonance-stabilized radicals. Furthermore, reaction entropies and heat capacities may often be estimated to a good level of accuracy ($\pm 1-2$ cal/mol \cdot K) (7b). Hence, equilibrium constants may be estimated to a level of accuracy determined primarily by the uncertainty in reaction enthalpy.

Several other noteworthy features of resonance-stabilized radical thermochemistry are:

1. Aromatic substituents noticeably affect reaction thermochemistry only when such groups either directly delocalize the odd-electron or lead to a difference in strain energy between reactants and products. For example, meta- or para-alkyl groups, ether linkages, hydroxyl groups, etc. will not noticeably influence reaction thermochemistry (11l).

2. Replacement of an aromatic C-H group by an N (pyridyl) atom generally destabilizes the radical slightly. The amount of destabilization depends on the particular position of the N atom within the aromatic system (11i).

Table IV. Enthalpies of H-atom Addition to (Poly)aromatics

	$-\Delta H_{298}^1 / \text{kcal mol}^{-1}$ for H-atom addition to position						
	a	b	c	d	e	f	g
	20						
	30	38	8				
	28	26	27	27	38	16	16
	33	30	42	23			
	24						

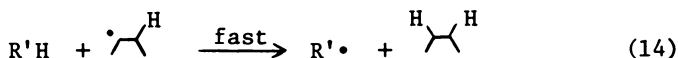
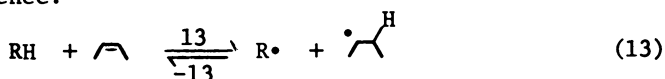
1. If ΔH pertains to reaction $\text{Ar} + \text{H}\cdot \rightarrow \text{Ar}\dot{\text{H}}$, then $\Delta H = \Delta H_{\text{r}}(\text{Ar} + \text{H}_2 \rightarrow \text{ArH}_2) + D(\text{ArH}-\text{H}) - 2\Delta H_{\text{f}}(\text{H}\cdot)$; where $D(\text{ArH}-\text{H}) / \text{kcal mol}^{-1} = 94.5 - (\text{resonance energy from formula 9})$, is the bond strength for breaking $\text{ArH}-\text{H}$ bond, ΔH_{r} is appropriate enthalpy of hydrogenation. When ArH_2 may be 1,2- or 1,4-dihydroaromatic, ΔH_{r} was chosen as the average of the two, assuming no ring strain energy for either (28). Enthalpy of hydrogenation (7c) enthalpy of formation (7a) measurements and estimates based on experimental data (2) support the idea that such strain energy is quite small.
2. $\Delta H_{\text{f}}(1,3\text{-cyclohexadienyl radical}) = 50 \text{ kcal/mol}$ from reference (1).

3. Accurate prediction of "ring strain" in hydroaromatic structures is not possible at present (28a), so available hydrogenation or other direct determinations should generally be used in preference to estimated values. This can be a very troublesome source of uncertainty.

Reactions Involving Highly-Stabilized Radicals

Using the thermochemical estimates given above, along with the considerable body of available thermochemical and kinetic data, several plausible reaction pathways in coal and model compound reactions will now be examined. This analysis is intended to discriminate between feasible and unlikely reaction mechanisms. It should be kept in mind that absolute rate constant estimates are often only very approximate, and we are testing ideas, not proving them.

Rates of Molecular Disproportionation. Simple H-atom transfer from a donor molecule to an acceptor molecule (reaction 13, molecular disproportionation) generates two free radicals and can lead to the net transfer of two H atoms by the following reaction sequence.



In tetralin, for example, this reaction leads to saturation of a double bond (or hydrogenation on an aromatic ring) and formation of two tetralyl radicals. Such a reaction sequence has, in fact, just been invoked to explain ethylene hydrogenation by cyclohexene in the gas phase (28b).

To examine the potential importance of molecular disproportionation, a means for estimating k_{13} must be found. Estimates of k_{13} will be obtained from estimates of both the rate constant for the reverse reaction (radical disproportionation, reaction -13), and the equilibrium constant, K_{13} ; i.e., $k_{13} = K_{13} k_{-13}$.

The equilibrium constant K_{13} will be obtained from estimates of reaction enthalpy, ΔH_{13} , and entropy, ΔS_{13} . The following formula provides a convenient means of estimating ΔH_{13}

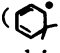
$$\Delta H_{13} = D(\text{R}\text{---}\text{H}) + D(\text{A}\text{---}\text{H}) + \Delta H_{\text{r}}(\text{A} + \text{H}_2 \rightarrow \text{A}\text{H}_2) - 2\Delta H_{\text{f}}(\text{H}\cdot) \quad (15)$$

where $D(\text{R}\text{---}\text{H})$ and $D(\text{A}\text{---}\text{H})$ are bond dissociation enthalpies of molecules in equations 13 and 14, ΔH_{r} is the enthalpy of hydrogenation of A , and $\Delta H_{\text{f}}(\text{H}\cdot)$ (= 52.1 kcal/mol at 298 K) is

the enthalpy of formation of a mole of H atoms. Reaction enthalpy can often be estimated to within + 3 kcal/mol from this formula, although errors in some cases may be even larger and are generally expected to be the major sources of uncertainty in estimates of k_{13} . Reaction entropy may be expressed as

$$\Delta S_{13} = R \ln 4 + R \ln \sigma + \Delta S_{\text{internal}} \quad (16)$$

where the first term on the right accounts for the electronic degeneracy of the two product radicals (7b), σ is, in essence, reaction path degeneracy and $\Delta S_{\text{internal}}$ is the net change in vibrational and internal rotational entropy. In all cases considered in this paper, $\Delta S_{\text{internal}} \sim 0$, although for other cases involving substantial changes in number or type of internal rotations this assumption may not be reliable, in which case more accurate estimates should be made (7b).

Now an estimate of radical disproportionation, $k_{\text{disp}} (=k_{-13})$ must be found. Since radical recombination rate constants, k_{rec} , and relative radical disproportionation/recombination rates, $k_{\text{disp}}/k_{\text{rec}}$, have been directly measured for a large number of reactions (29), k_{disp} will be estimated using the formula, $k_{\text{disp}} = k_{\text{rec}} (k_{\text{disp}}/k_{\text{rec}})$. For k_{rec} , a value of $10^{9.5} \text{ M}^{-1} \text{ s}^{-1}$ is chosen which is in the range expected for most gas-phase and liquid-phase recombination rates involving large free radicals and elevated temperatures (1,7b,c,d). The ratio $(k_{\text{disp}}/k_{\text{rec}})$, on the other hand, depends on the particular radical pair involved and should be corrected for reaction path degeneracy ($k_{\text{disp}}/k_{\text{rec}}$ values will apply to a single reaction path). For two resonance stabilized hydrocarbon radicals, $(k_{\text{disp}}/k_{\text{rec}}) \sim 0.01$ in the range 400°-500°C. This value is based on literature values for termination of benzylic radicals such as $\text{Ph}\dot{\text{C}}\text{HCH}_2\text{CH}_3$ at 118°C (30) and for the 1,3-cyclohexadienyl radical () at 100°C (31) assuming that the activation energy for recombination is 1.5 kcal/mol greater than that for disproportionation (29).

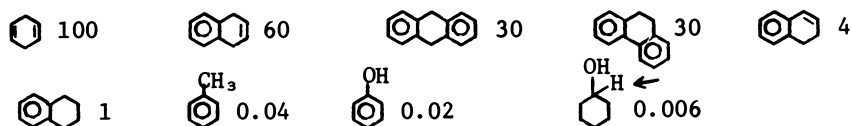
Based on the above estimates for K_{13} and k_{-13} for stabilized hydrocarbon radicals, $k_{13}/\text{M}^{-1} \text{ s}^{-1} = \sigma 10^{8.1 - \Delta H_{13}/2.3RT}$. For reactions involving one stabilized and one non-stabilized radical, $(k_{\text{disp}}/k_{\text{rec}}) \sim 0.1$ (32). For self reactions of the resonance stabilized ketyl radical, $\text{Ph}_2\dot{\text{C}}\text{OH}$, $k_{\text{disp}}/k_{\text{rec}} \sim 0.03$ (33); this value will be used for carbonyl disproportionation with hydroaromatics.

For model compound studies in excess tetralin, reaction 13 will occur with a pseudo-first-order rate constant $k/\text{s}^{-1} =$

$k_{13} [\text{tetralin}] \sim 5 k_{13}$. However, for experiments carried out at

temperatures above 446°C (the critical temperature of tetralin), concentrations of tetralin, hence k , may be somewhat smaller.

Table V presents a list of estimated enthalpies and half lives for molecular H-atom transfer (disproportionation) from tetralin to a number of unsaturated molecules. At 450°C, and even at 400°C, many structures will undergo rapid molecular disproportionation with tetralin. Approximate relative rates at 400°C for H-atom donation by molecular disproportionation for selected hydrogen donors are estimated below (sources for thermochemistry are given in footnote 1 of Table IV):






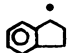

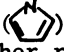

Some of these values are very approximate, especially for the dihydronaphthalenes due to ring strain uncertainties in the radical, and are meant to serve only as a rough guide until more direct evidence is available.

Estimated rates of molecular disproportionation will now be compared to observed reaction rates of unsaturated molecules in the presence of various hydrogen donors.

Collins et al. have studied a number of reactions in excess tetralin at 400°C (15). They reported 99% conversion of indene to indane after 1 hour and conversion of cyclohexene and 1-cyclohexenylbenzene to cyclohexane and cyclohexylbenzene after 18 hours. At 400°C values in Table V predict nearly complete (>90%) hydrogenation of both indene and 1-cyclohexenylbenzene after 1 hour and a conversion of cyclohexene to cyclohexane at a rate of 40% per hour. Molecular disproportionation is a feasible pathway for these reactions.

Cronauer et al. (34) reported first-order rate constants for the hydrogenation of trans-stilbene of 0.013 min^{-1} at 400°C and 0.06 min^{-1} at 450°C; predictions from Table V are 0.004 min^{-1} at 400°C and 0.04 min^{-1} at 450°C.

Rate constants for reaction of benzothiophene ()^S, indole ()^{NH} and benzofuran ()^O in tetralin at 400°C-450°C have recently been reported by Mallinson et al. (35a). To match their observed rates for these compounds, assuming that molecular disproportionation is the rate limiting step, an activation energy greater than the estimated activation energy for indene hydrogenation (38.3 kcal/mol) by 9.8, 9.2 and 5.2 kcal/mol, respectively, is required. These values are consistent with the idea that formation of radicals from heteroaromatic molecules involves loss of resonance energy in the heteroaromatic ring while relatively little stabilization energy is lost when converting indene to the α -indanyl radical

() . For example, furan () possesses less aromatic stabilization energy than either pyrrole () or thiophene () which is consistent with the observed higher reactivity of benzofuran. Predicted rates of molecular disproportionation for the series cyclopentadiene, furan and thiophene as given in Table V are in the same order as observed for the benzo-analogues. However, while pyrrole is predicted to be less reactive than thiophene, benzothiophene was found to be less reactive than indole ("benzopyrrole").

Virk and Garry (24a) have recently investigated hydrogen transfer from cyclohexanol to anthracene and phenanthrene and have reported well-behaved second-order kinetics. These workers suggest that this reaction may occur by a concerted molecular H₂-transfer. Simple second-order kinetic behavior, however, is also consistent with molecular disproportionation (and also with hydride, H⁻, transfer). However, if it is assumed that $(k_{\text{disp}}/k_{\text{rec}}) = 0.1$, predicted rates are only 1/100 of observed rates at 400°C. We therefore draw the tentative conclusion that such hydrogen transfer by alcohols is not primarily due to molecular disproportionation, although hydride transfer remains a realistic possibility. It is curious that observed relative rates of hydrogenation of anthracene and phenanthrene by cyclohexanol are virtually identical to estimated relative rates for molecular disproportionation at 350°C (estimated ratio = 30, experimental = 35).

Virk and co-workers (24b,c) and King and Stock (35b) have reported rates for H₂-transfer to anthracene and phenanthrene in solution containing 1,2- and 1,4-dihydronaphthalene and tetralin. Comparisons between reported rate constants and estimated rate constants for bimolecular disproportionation are given in Table VI. In agreement with Stock, this data does not provide evidence for a concerted H₂-transfer mechanism. Our calculations indicate that molecular disproportionation may be a major hydrogenation mechanism in these reaction systems.

Transfer of hydrogen to carbonyl groups differs from analogous transfer to unsaturated hydrocarbons primarily due to the greater likelihood for involvement of free ionic or ion-pair intermediates in the former reaction. Linstead and co-workers (36) have shown that transfer from dihydroaromatics to quinones is best explained by a rate limiting step involving hydride ion transfer. The applicability of this mechanism to other systems is presently unclear (40). For example, under appropriate conditions quinones can generate free radicals and form adducts (37). Pseudo-first order rate constants for

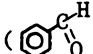
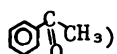
reaction of benzaldehyde () and acetophenone () have been reported by Cronauer et al. (34). Rate constants

Table V. Molecular Disproportionation with Tetralin as H-Donor

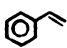
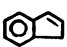
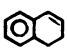
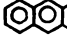
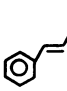

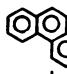
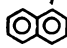


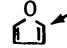

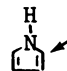
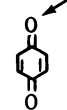
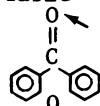
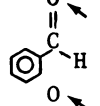
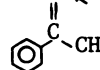
H-acceptor (A) ¹	$\frac{\Delta H^\circ_{298}}{\text{kcal mol}^{-1}}$ ²	$\tau_{1/2}$ (H-acceptor) ³	
		400°C	450°C
	34.7	3 min	32 sec
	38.3	10 min	1.7 min
	38.8 [34.5 ⁴]	8 min 43 sec	2.4 min 7.5 sec]
	41.2	54 min	6.4 min
	42.7	2.8 hrs	18 min
	44.8 ⁵	13 hrs	26 min
	45.7 ⁶	26 hrs	3.4 hrs
	53.5	200 days	12 days
	61.6	150 yrs	6 yrs
	39.1	11 min	1.5 min
	45 ⁷	1.5 hr	1.5 hr
	57 ⁷	14 yr	0.7 yr
	62 ⁷	600 yr	22 yr
	31.7 ⁸	1 sec	0.2 sec

Table V. (con't)

	41 ^{9,10}	1 min	3.8 min
	48 ¹⁰	4.0 days	8.1 hrs
	46 ^{10,11}	43 hrs	2 hrs

1. arrow denotes thermodynamically favored site of H-atom addition; ΔH and $\tau_{1/2}$ pertain to this hydrogen transfer site.
2. Derived using equation 15. When available, enthalpy of hydrogenation $A + H_2 \rightarrow AH_2$, is taken from direct measurements (27c) or differences between measured gas-phase enthalpies of formation (27a) otherwise, estimation methods (1,7b) are employed. Except where noted, bond strengths are derived from recently recommended enthalpy of formation at 298 K of benzyl radicals (47.0 kcal/mol) (11f).
3. $\equiv \ln 2/k_{1,3}$ [tetralin]; assumes [tetralin] = 5 M; $k_{1,3}$ obtained as described in text.
4. Estimated value for ΔH (1,2-dihydronaphthalene) given in reference (2).
5. Uses $D(\text{cyclohexyl-H}) = 95.5$ kcal/mol (11e).
6. Uses $\Delta H_f(9,10\text{-dihydronaphthalene}) = 36.90 \pm 0.30$ kcal/mol obtained by W. D. Good (28).
7. $\Delta H_f(AH_2)$ estimated by group additivity (1) assuming "ring strain" of 5 kcal/mol:
8. $D(\text{HO}-\text{C}_6\text{H}_4-\text{O-H})$ assumed to be equal to $D(\text{C}_6\text{H}_5-\text{O-H})$ (11h). Latter value is corrected for recent enthalpy of formation of benzyl radicals (11f).
9. Radical delocalization energy assumed to be 15 kcal/mol.
10. Assumes β -OH group lowers C-H bond strength by 4 kcal/mol (11f).
11. Enthalpy of hydrogenation is assumed to be same as for 3-pentanone (27a).

Table VI. Comparison of Empirical Rate Constants^a for H₂-Transfer from Hydroaromatics, k_{obs} , Compared to Estimated Molecular Disproportionation Values, k_{MD} .

T/°C	$\frac{k_{\text{obs}} v/k_{\text{MD}}}{k_{\text{obs}} s/k_{\text{MD}}}$	$\frac{k_{\text{obs}} v/k_{\text{MD}}}{k_{\text{obs}} s/k_{\text{MD}}}$	$\frac{k_{\text{obs}} v/k_{\text{MD}}}{k_{\text{obs}} s/k_{\text{MD}}}$	$\frac{k_{\text{obs}} v/k_{\text{MD}}}{k_{\text{obs}} s/k_{\text{MD}}}$
	1,2-Dihydronaphthalene	1,4-Dihydronaphthalene	Tetralin	
Anthracene 300	1.1	6.2	1.5 ^b	2.0 ^b
Phenanthrene 400	(1.2) ^c	(1.6) ^c	(1/21) ^c	(1/18) ^c
			4	3
			1/3	2.1

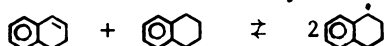
^a k_{obs}^v and k_{obs}^s are bimolecular rate constants computed from data given by Virk (24b) and Stock (35b), respectively. Donor concentrations in Virk's experiments are assumed to be 5 M, except for reactions of 1,4-dihydronaphthalene where the solvent contains 64% of this donor (3.2 M). Initial donor concentrations in experiments of King and Stock were assumed to be 2.5 M.

^bIn these cases k_{obs} is a lower limit for molecular disproportionation rate constants since during the reaction a substantial amount of the donor is converted to tetralin (35b).

^cInterpretation of k_{obs} in these cases is dubious since King and Stock (24b) demonstrated that, at 400°C, dihydronaphthalenes are converted to tetralin and naphthalene far more rapidly than they hydrogenate phenanthrene.

estimated for molecular disproportionation, k_{est} , relative to observed rate constants, k_{obs} , are: for benzaldehyde, $k_{est}/k_{obs} = 0.005$ at 400°C, 0.01 at 450°C; for acetophenone, $k_{est}/k_{obs} = 0.7$ at 400°C, 1.3 at 450°C. Therefore, while acetophenone may undergo significant molecular disproportionation with tetralin, benzaldehyde decomposes by way of other more rapid pathways.

Formation of Free Radicals by Molecular Disproportionation. A significant conclusion that may be drawn from considerations of rate and equilibrium constants for molecular disproportionation is that this path can provide appreciable concentrations of free radicals in many systems long after most weak chemical bonds have ruptured and bond homolysis has ceased to be a major source of free radicals. In "pure" tetralin, for instance, trace concentrations of 1,2-dihydronaphthalene are expected to equilibrate with tetralin and tetralyl radicals,



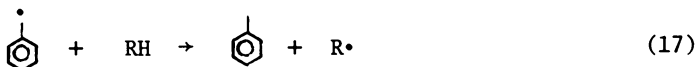
At a concentration of, say, 10^{-2} mole percent of 1,2-dihydronaphthalene, the concentration of α -tetralyl radicals at 400°C and 450°C (assuming [tetralin] = 5 M) is estimated as $10^{-7.1}$ M and $10^{-6.7}$ M, respectively. These concentrations of free radicals are in excess of that needed to carry out many chain reactions at reasonably rapid rates. For instance, using H-abstraction rate constants of benzylic radicals given in reference (38), the half-life for exchange of benzylic H-atoms in the presence of the above concentrations of radicals is ~1 hour at 400°C and ~10 min at 450°C.

Close examination of tetralin pyrolysis indicates that reactions leading to irreversible termination of tetralyl radicals are expected to be very slow due to the reversibility of tetralyl radical recombination and disproportionation reactions. This may, in effect, lead to sizable radical concentrations even when the net reaction rate of tetralin is very slow.

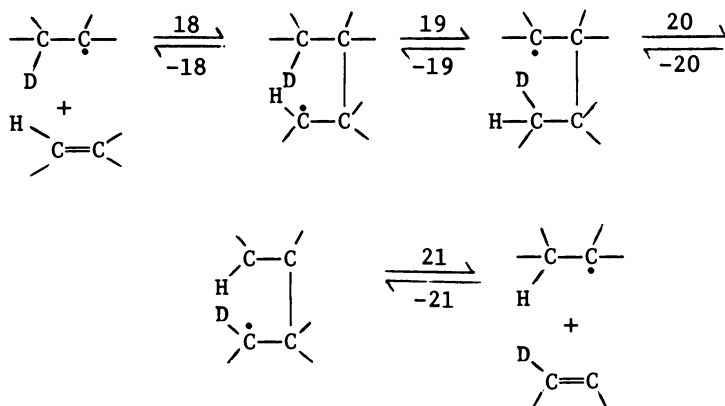
It is interesting to note that catalytic reactions tending to equilibrate tetralin, 1,2-dihydronaphthalene and naphthalene (19,39) will serve to generate free radicals since 1,2-dihydronaphthalene rapidly undergoes molecular disproportionation with tetralin. For instance, at equilibrium a 0.5% solution of naphthalene in tetralin (typical of distilled tetralin) will generate ca. 10^{-2} mol percent 1,2-dihydronaphthalene at 400°C, which will, in turn, form ca. 10^{-7} M tetralyl radicals (see above).

Free-Radical H-Atom Transfer. In competition with molecular H-atom transfer reactions, radical-induced transfer may occur,

especially in environments containing high concentrations of radicals. Benzylic and phenolic H atoms, and to some degree paraffinic H atoms, are expected to undergo exchange by simple H-atom metathesis, for instance,



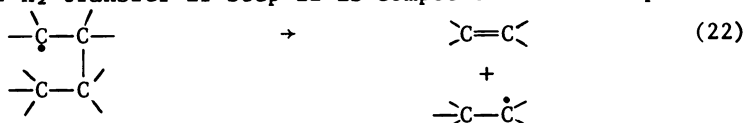
However, rapid D/H exchange of very strongly bound aromatic H atoms is known to occur both in coal systems (40) and in systems containing phenanthrene (and anthracene) and $\text{PhCD}_2\text{CD}_2\text{Ph}$ although little exchange is observed in benzene/ $\text{PhCD}_2\text{CD}_2\text{Ph}$ systems (41). Aromatic C-H bonds are ~25 kcal/mol stronger than benzylic C-H bonds; hence, rapid D/H atom randomization of aromatic H atoms cannot be explained by simple metathesis. The following mechanism may explain this randomization:



Note that steps 19 and 20 go through transition states involving relatively unstrained 5-membered rings. Related isomerizations are well known in paraffin pyrolysis.

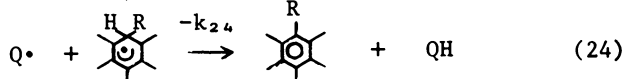
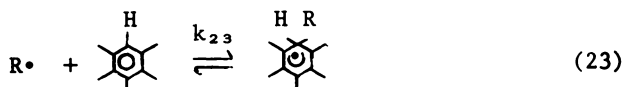
A very crude kinetic analysis of this system indicates that such reactions are plausible for reactions in which step 18 is exothermic and step 19 is not appreciable endothermic. These conditions hold for addition of PhCDCD_2Ph to all positions in anthracene and phenanthrene, especially to the 9 and 10 positions (Table IV). For benzene, however, reaction 18 is 5 kcal/mol endothermic; so randomization of H atoms on benzene is estimated to be at least 40 times slower at 400°C than H-atom randomization at any position in anthracene or phenanthrene.

The above radical addition sequence may also serve as a means of H_2 -transfer if step 22 is competitive with steps -19 & 20.



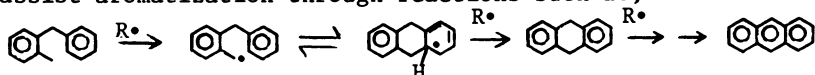
This reaction could cause homogeneous equilibration of certain hydroaromatic structures.

Free-Radical Induced Bond Formation and Aromatization. Based on current understanding of free-radical aromatic substitution reactions at low temperatures (7), a major pathway for polymerization and crosslink formation in coal systems is expected to be,



where $R\cdot$ and $Q\cdot$ are organic radicals. At coal conversion temperatures, reaction 23 is expected to be highly reversible and the rate of crosslink formation may be written, $K_{22}k_{23}[R\cdot][Q\cdot][\text{C}_6\text{H}_6]$, with $K_{23} = k_{23}/k_{-23}$. Note that the rate of such bond formation is proportional to the square of radical concentrations; hence, the very high free-radical concentrations in coal conversion would cause the reaction to proceed much faster than in typical model systems. Moreover, $Q\cdot$ may be a very stable radical because of the very weak C-H bond in the adduct radical formed in reaction 23 (typically 20-40 kcal/mol, see Table IV).

High free radical concentrations are also expected to assist aromatization through reactions such as,



Based on the above considerations, high concentrations of very highly stabilized radicals will facilitate polymerization and aromatization and in this sense can be deleterious to coal liquefaction processes.

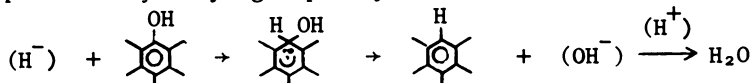
Ionic Processes and Water Formation

The potential importance of reactions involving ions or ion pairs in coal and model compound reactions has been emphasized by Ross and co-workers (42) as well as by Brower (43). For many types of reactions there exists considerable debate concerning reactive intermediates and mechanism. However, in the case of water formation, which is known to be rapid during coal liquefaction under relatively mild conditions and appears to occur in certain model compound reactions (15), it is difficult to construct plausible pathways without postulating ionic intermediates (although these intermediates may reside on solid surfaces).

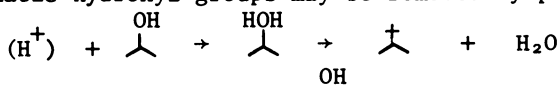
Free-radical schemes for water formation that involve $\cdot\text{OH}$ radicals are not likely since the formation of this highly

reactive free radical must involve very unfavorable thermodynamics. Concerted molecular elimination of water has never been unambiguously observed for the type of structures believed to exist in coal or to be formed during coal reactions.

Ionic reactions, on the other hand, provide a number of plausible routes for H₂O formation from organic oxygen. For instance, phenolic hydroxyl groups may be removed by hydride transfer



and aliphatic hydroxyl groups may be removed by proton transfer.



We have found that benzhydrol ($\phi\text{C}\phi$) rapidly forms diphenylmethane, benzophenone and presumably water in tetralin at 300°C (11j). We cannot construct a reasonable mechanism to account for this reaction without postulating ionic intermediates.

Test Case Pyrolysis. Liquid-Phase Pyrolysis of Bibenzyl

To begin the exploration of actual reaction pathways in complex pyrolyses of aromatic substances, we have carried out a detailed experimental and theoretical analysis of the liquid-phase pyrolysis of bibenzyl. This pyrolysis system has been studied by others (44,45,46), and the general kinetic features of this reaction system are now rather well agreed on. Complete details of this work will appear elsewhere (38a) and a few implications of this work of particular relevance to coal reactions will be discussed here.

(1) The reaction mechanism for formation of the major products of this reaction is given in Table VII. Rate parameters were obtained from both estimation procedures and separate experiments and are all within the rather narrow range expected on the basis of thermochemical kinetics considerations (1). This mechanism has been found to exactly reproduce evolution of the major products at low extents of reaction between 350°-425°C. Bibenzyl pyrolysis proceeds by conventional well-understood, free-radical reaction steps.

(2) A rather indirect mode of reaction accounts for 60% of the product trans-stilbene (reaction sequence 1, 2, 4, 5, and 6 in Table VII). The importance of this path may be traced to both the low disproportionation/recombination ratio for resonance stabilized radicals, and the high rate constant for β -bond scission of the intermediate radical recombination product, 1,2,3,4-tetraphenylbutane. Analogous decomposition routes involving formation of an adduct, followed by irreversible destruction of the adduct, may be important reaction paths in many other coal related reaction systems.

Table VII. Mechanism for Formation of Major Products in the Liquid Phase Pyrolysis of Bibenzyl (38).

	$\frac{\log k_f^a}{k_{rev}^a}$	
$\text{PhCH}_2\text{CH}_2\text{Ph} \rightleftharpoons 2\text{Ph}\dot{\text{C}}\text{H}_2$	15.9 - 65.0/ θ^b	9.8
$\text{Ph}\dot{\text{C}}\text{H}_2 + \text{PhCH}_2\text{CH}_2\text{Ph} \rightleftharpoons \text{PhCH}_3 + \text{Ph}\dot{\text{C}}\text{HCH}_2\text{Ph}$	8.62 - 16.06/ θ^c	8.5 - 19.50/ θ^c
$2\text{Ph}\dot{\text{C}}\text{HCH}_2\text{Ph} \rightleftharpoons \text{PhCH}=\text{CHPh} + \text{PhCH}_2\text{CH}_2\text{Ph}$	8.6	9.8 - 45.9/ θ^c
$2\text{Ph}\dot{\text{C}}\text{HCH}_2\text{Ph} \rightleftharpoons [\text{PhCH}_2\text{C}(\text{Ph})\text{H}]_2^+$	9.5	15.9 - 57.5/ θ
$\text{Ph}\dot{\text{C}}\text{HCH}_2\text{Ph} + [\text{PhCH}_2\text{C}(\text{Ph})\text{H}]_2^+ \rightleftharpoons \text{PhCH}_2\text{CH}_2\text{Ph} + \text{Ph}\dot{\text{C}}\text{HC}(\text{Ph})\text{HC}(\text{Ph})\text{HCH}_2\text{Ph}$	8.62 - 16.06/ θ	8.62 - 16.06/ θ^c
$\text{Ph}\dot{\text{C}}\text{HC}(\text{Ph})\text{HC}(\text{Ph})\text{HCH}_2\text{Ph} \rightleftharpoons \text{PhCH}=\text{CHPh} + \text{Ph}\dot{\text{C}}\text{HCH}_2\text{Ph}$	14.4 - 22.3/ θ^c	8.0 - 10/ θ^c
$\text{Ph}\dot{\text{C}}\text{HCH}_2\text{Ph} \rightleftharpoons \text{PhC}(\dot{\text{C}}\text{H}_2)\text{HPh}$	13 - 23.5/ θ	13 - 9/ θ
$\text{PhCH}_2\text{CH}_2\text{Ph} + \text{PhC}(\dot{\text{C}}\text{H}_2)\text{HPh} \rightleftharpoons \text{PhCHCH}_2\text{Ph} + \text{PhC}(\text{CH}_3)\text{HPh}$	8.62 - 7.9/ θ	8.62 - 22.0/ θ

a s⁻¹ or M⁻¹ s⁻¹

b $\theta = 4.576 \text{ T}/1000$

c rate constant has no influence on observed rates of product formation.

(3) Despite the fact that isomerization of bibenzyl to 1,1-diphenylethane proceeds through a rather thermodynamically unfavorable intermediate (reaction 7 in Table VII), high radical concentrations, high temperatures and high concentrations in this pyrolysis allow this isomerization to proceed at a measurable rate. This isomerization converts a thermally labile substance to one that is less thermally reactive (or at least reacts through different pathways). Related reactions may significantly hinder coal dissociation since high free radical concentrations in coal systems may cause such isomerization to compete effectively with bond breaking reactions.

(4) In highly dilute mixtures of bibenzyl in tetralin (11j), (one part bibenzyl in 200-1000 parts tetralin) 1,1-diphenylethane is formed at a rate independent of dilution and roughly one-sixth of the rate found in pure bibenzyl. This implies that free-radical concentrations are independent of the concentration of free-radical initiators in sufficiently pure tetralin.

Summary

(1) Gas-phase rate and equilibrium constants are generally not very different from solution-phase values.

(2) Bond homolysis rate constants are estimated for many covalent bonds presumed to be present in coal conversion reactions. Other modes of bond breaking are examined using thermochemical kinetic methods (1).

(3) Enthalpies of formation and entropies of resonance stabilized radicals of importance in aromatic pyrolysis are estimated to a level of accuracy suitable for order of magnitude calculations.

(4) Molecular disproportionation may constitute a major reaction pathway in coal-related systems both for transferring hydrogen and for generating free radicals. Estimated rates of this reaction are shown to often be close to observed reaction rates in model systems.

(5) A free-radical hydrogen transfer mechanism is proposed that may lead to rapid H-exchange in polyaromatic systems.

(6) Water formation is briefly examined and ionic species are suggested as the most plausible intermediates.

(7) Recent studies of bibenzyl pyrolysis are discussed in the context of coal-related chemistry.

Acknowledgement

Support for this research by DOE, Fossil Energy Division under grant EF-77-G-01-2751 is gratefully acknowledged. This work was also supported, in part, by a grant from the West Virginia Energy Research Center. The scientific origins of this work may be traced to Professor S. W. Benson and to DOE supported

research at SRI International during the years 1975-76. Discussions with David S. Ross at SRI were very helpful in the development of this research.

Literature Cited

1. Benson, S. W. "Thermochemical Kinetics", Second Edition, Wiley and Sons, New York, NY, 1976.
2. Shaw, Robert; Golden, D. M.; Benson, S. W. J. Phys. Chem. 1977, 81, 1716.
3. Stein, S. E.; Golden, D. M.; Benson, S. W. J. Phys. Chem. 1977, 81, 314.
4. Stein, S. E.; Barton, B. D. Thermochim. Acta, 1981, in press.
5. Stein, S. E.; Golden, D. M. J. Org. Chem. 1977, 42, 839.
6. For general discussions of relations between gas and liquid rate constants see,
 - a. Laidler, K. J. "Chemical Kinetics", McGraw-Hill, Inc., New York, NY, Chap. 5.
 - b. Benson, S. W. "Foundations of Chemical Kinetics", McGraw-Hill Book Co., New York, 1980, Chap. 18.
 - c. Hammes, C. G. "Principles of Chemical Kinetics", Academic Press, New York, 1978, Chap. 7.
 - d. Martin, H. Angew. Chem. Int'l. Ed. 1966, 5, 78.
 - e. Stein, S. E. submitted.
7. "Free Radicals, Vol. I and II"; Kochi, J., ed., Wiley and Sons, New York, NY 1973.
 - a. Koenig, T.; Fischer, H. Chap. 4.
 - b. O'Neal, H. E.; Benson, S. W. Chap. 17.
 - c. Ingold, K. U. Chap. 2.
 - d. Kerr, J. A., Chap. 1.
8. Sources of vapor pressures used in this analysis are:
 - a. Zwolinski, B. J.; Wilhort, R. C. "Handbook of Vapor Pressures and Heats of Vaporization of Hydrocarbons and Related Compounds", API Project 44, Thermodynamics Research Center, College Station, TX, 1971.
 - b. Boublik, T.; Fried, V.; Hala, E. "The Vapor Pressures of Pure Substances", Elsevier, New York, 1973.
 - c. "CRC Handbook of Chemistry and Physics", Chemical Rubber Co., Cleveland, OH, 1980.
 - d. Stein, S. E. J.C.S. Faraday Trans. I, 1981, in press.
9. Reid, R. C.; Prausnitz, J. M.; Sherwood, T. K. "The Properties of Gases and Liquids", Third Edition, McGraw-Hill, Inc., New York, 1977.
10. Hildebrand, J. H.; Prausnitz, J. M.; Scott, R. L. "Regular and Related Solutions", Van Nostrand Reinhold Co., New York, 1970, Chap. 7.

11. Some sources of use in the present work are:
- a. Benson, S. W.; O'Neal, H. E. "Kinetic Data on Gas Phase Unimolecular Reactions", NSRDS-NBS 21, U. S. Government Printing Office, Washington, D. C., 1970.
 - b. Tsang, W. Int. J. Chem. Kinetics 1978, 10, 821.
 - c. Walker, J. A.; Tsang, W. ibid. 1979, 11, 867.
 - d. Culshan, M. A.; Baldwin, R. R.; Evans, G. A.; Walker, R. W. JCS Faraday I, 1977, 366.
 - e. Kerr, J. A.; Trotman-Dickinson, A. F., "Bond Strengths of Polyatomic Molecules", in reference 8c.
 - f. Rossi, M.; Golden, D. M. J. Am. Chem. Soc. 1979, 101, 1230.
 - g. McMillan, D. F.; Trevor, P. L.; Golden, D. M. J. Am. Chem. Soc. in press.
 - h. Colussi, A. J.; Zabel, F.; Benson, S. W. Int. J. Chem. Kinetics 1977, 9, 161.
 - i. Barton, B. D.; Stein, S. E. JCS Faraday I, 1981, in press.
 - j. Miller, R. E.; Robaugh, D. A.; Stein, S. E., work in progress.
 - k. Robaugh, D. A.; Stein, S. E. Int. J. Chem. Kinetics, in press.
 - l. Barton, B. D.; Stein, S. E. J. Phys. Chem. 1980, 84, 2141.
 - m. Colussi, A. J.; Benson, S. W. Int. J. Chem. Kinetics, 1977, 9, 295.
12. Walling, C.; Bristol, D. J. Org. Chem. 1971, 36, 733.
13. a. Pryor, W. A.; Smith, K. J. Am. Chem. Soc. 1970, 98, 5403.
b. Walling, C.; Waits, H. P. J. Phys. Chem. 1967, 71, 2361.
14. Preliminary results are reported by Miller, R. E.; Stein, S. E. ACS Div. of Fuel Chem. Preprints, 1979, 24 (3), 271.
15. Benjamin, B. M.; Raaen, V. F.; Maupin, P. H.; Brown, L. L.; Collins, C. J. Fuel 1978, 57, 269.
16. Vernon, L. W. Fuel 1980, 59, 102.
17. Virk, P. S. Fuel 1979, 58, 149.
18. Stein, S. E. Fuel 1980, 59, 900.
19. Bergman, M. R.; Comita, P. B.; Moore, C. B.; Bergman, R. G. J. Amer. Chem. Soc. 1980, 102, 5692.
20. Frey, H. M.; Lister, D. H. J. Chem. Soc. (A) 1967, 1800.
21. Frey, H. M.; Krautz, A.; Stevens, I. D. R. J. Chem. Soc. (A) 1969, 1734.
22. Klein, M. T.; Virk, P. S. ACS Div. Fuel Chem. Preprints 1980, 25 (4), 180.
23. Golden, D. M.; Spokes, G. N.; Benson, S. W. Angew. Chemie, Int. Ed. (English) 1973, 12, 534.
24. a. Garry, M. J.; Virk, P. S. ACS Fuel Div. Preprints, 1980, 25 (4), 132.
b. Bass, D. H.; Virk, P. S. ibid., 25 (1), 17.

24. c. Virk, P. S.; Bass, D. H.; Eppig, C. P.; Ekpenyong ibid., 24 (2), 144.
25. The reverse reaction, H₂ elimination from 1,4-cyclohexadiene is well known, see reference 11a.
26. Herndon, W. C.; Ellsey, M. L. J. Amer. Chem. Soc. 1974, 96, 5331; Herndon, W. C., ibid., 1973, 95, 2404.
27. a. Cox, J. D.; Pilcher, G. "Thermochemistry of Organic and Organometallic Compounds", Academic Press, New York, 1970.
- b. Stull, D. R.; Westrum, E. F., Jr; Sinke, G. C. "The Chemical Thermodynamics of Organic Compounds", Wiley and Sons, NY, 1969.
- c. Williams, R. B. J. Amer. Chem. Soc. 1942, 64, 1395.
28. a. See footnote 25 in reference 2.
- b. Benson, S. W. Int. J. Chem. Kinetics 1980, 12, 755.
29. Gibian, M. J.; Corley, R. C. Chem. Rev. 1973, 73, 441.
30. Gibian, M. J.; Corley, R. C. J. Amer. Chem. Soc. 1972, 94, 4178.
31. James, D. G. L.; Stuart, R. D. Trans. Faraday Soc. 1968, 64, 2735.
32. Neuman, R. C.; Alhadeff, E. S. J. Org. Chem. 1970, 35, 3401.
33. Weiner, S. A. J. Amer. Chem. Soc. 1971, 93, 6978.
34. Cronauer, D. C.; Jewell, D. M.; Shaw, Y. T.; Modi, R. J. Ind. Eng. Chem. Fundam. 1979, 18, 153.
35. a. Mallinson, R. G.; Chau, K. C.; Greenkorn, R. A. ACS Fuel Div. Preprints, 1980, 25 (4), 120.
- b. King, H.-H.; Stock, L. M., submitted, 1981.
36. Braude, E. A.; Jackman, L. M.; Linstead, R. P. J. Chem. Soc. 1954, 3548; also see later papers in Linstead and co-workers listed in reference 37.
37. Becker, H-D in "The Chemistry of the Quinonoid Compounds", S. Patai, ed., Wiley and Sons, New York, 1974, Chap. 7, p. 335.
38. a. Miller, R. E.; Stein, S. E. J. Phys. Chem. in press.
- b. Abstraction rate constant derived from Jackson, R. A.; O'Neill, D. W. Chem. Commun. 1969, 1210.
39. Gangwer, T.; MacKenzie, D.; Casano, S. J. Phys. Chem. 1979, 83, 2013.
40. a. Cronauer, D. C., poster presentation at "Conference on Chemistry and Physics of Coal Utilization", Morgantown, WV, June 1980.
- b. Ratto, J. J.; Heredy, L. A.; Shawronski, ACS Fuel Div. Preprints 1979, 24 (2), 155.
41. Benjamin, B. M., unpublished results described in "Basic Coal Sciences Project Advisory Committee Report", Gas Research Institute, Chicago, IL 1980, p. 6-8.
42. Ross, D. S.; Blessing, J. E. ACS Fuel Div. Preprints, 1979, 24 (2), 125.
43. Brower, K. R. Fuel 1977, 56, 245.
44. Poutsma, M. L. Fuel 1980, 59, 337.
45. Brower, K. R. J. Org. Chem. 1980, 45, 1004.
46. Livingston, R.; Zeldes, H.; Conradi, M. S. J. Amer. Chem. Soc. 1979, 101, 4312.

Short-Contact-Time Coal Liquefaction: Effect of Coal Rank and Solvent Source on Conversions and Heptane-Insoluble Product Compositions

JAMES R. LONGANBACH

Battelle Columbus Laboratories, 505 King Avenue, Columbus, OH 43201

The SRC-I coal liquefaction process is designed to produce a clean, coal-derived solid fuel in a single, noncatalytic reaction step. (1) Design of a demonstration plant for the SRC-I process is now under way. (2) A two-step, hydrogen efficient modification of the noncatalytic SRC I technology has been proposed and studied extensively on a laboratory scale. (3-6) Two-step SRC I technology is also being tested in pilot plant scale facilities. (7, 8)

In the two-step SRC process the purpose of the first step is to dissolve the coal at short contact times. The second step, using more severe conditions, might be used to regenerate solvent quality or, if necessary, to reduce the sulfur content of the product. A single coal dissolution step might find practical application if solvent were available from a nonprocess source.

Experimental

Coals and Solvents. Wyodak (Belle Ayr) subbituminous and Monterey bituminous coals were used. Analyses are shown in Table I. The coals were received as minus 1-inch lumps and were ground after cooling with liquid nitrogen. During grinding the coal temperature did not rise above ambient and the evaporation of the liquid nitrogen provided some protection from exposure to air. The ground coals were stored in glass bottles under nitrogen. The grinding procedure results in a slight increase in the moisture content due to condensation.

Two solvents were used. Their analyses are given in Table II. Solvent -019 is a hydrogen-enriched SRC I recycle solvent. Solvent -035 is a hydrogen-depleted SRC I preheater effluent solvent. These solvents represent extremes in the process derived solvents associated with the SRC I process. Solvent -019 contains more hydrogen, has a higher hydrogen-to-carbon ratio and much more β -hydrogen which is an indication of tetralin-like materials which can act as hydrogen donors in coal liquefaction. Solvent -035 contains more aromatic hydrogen as measured by both H^1 and

0097-6156/81/0169-0131\$05.50/0
© 1981 American Chemical Society

TABLE I. COAL ANALYTICAL DATA
(Weight Percent)

	Monterey	Wyodak (Belle Ayr)
Moisture	10.57, 12.2 ^(a)	29.80, 33.8 ^(a)
Elemental Analyses, dry basis		
Carbon	66.77	68.94
Hydrogen	5.17	5.40
Nitrogen	1.23	1.14
Sulfur	4.30	0.38
Oxygen (by difference)	11.34	19.41
Ash	11.19, 11.13 ^(a)	4.73

(a) Analyses taken after grinding.

TABLE II. SOLVENT COMPOSITIONAL DATA
(400 °F to 800 °F Boiling Range)

Mobil Solvent No.	Hydrogenated SRC I Recycle (92-26-019)	Preheater Effluent Recycle (92-03-035)
<u>Elemental Analyses</u>		
C	87.73	87.51
H	9.67	8.15
O	1.48	2.88
N	0.99	1.24
S	<0.1	0.39
H/C	1.32	1.12
<u>NMR Analyses</u>		
Polyaromatics	1.7	1.5
Aromatics	17.0	37.6
α	24.4	24.6
β	38.5	22.1
γ	18.4	14.3
C ¹³ aromatics	51.6	74
Basic N (%)	0.34	0.42

C^{13} NMR. Aromatics are unreactive as hydrogen donors. The hydrogen-depleted solvent also contains more oxygen.

Summary of Experiments. Fifteen coal liquefaction experiments were done using two coals and two solvents supplied by Mobil Research and Development Corporation. Each coal-solvent combination was tried at conditions designed to give conversions to pyridine solubles of about 65 and 80 percent of MAF coal.

The time-temperature curves in the large reactor system include significant amounts of time during heatup at temperatures high enough for reaction to occur but below the desired reaction temperatures (see Figure 1). The total heatup time averaged 4.7 minutes and in some cases the desired reaction temperature was overshot. The average heatup time in Mobil Research and Development's 300 cc coal liquefaction apparatus is about 1 minute. In order to facilitate comparison of results obtained in the two reactors and to compare results of different runs made in the Battelle apparatus, a method was needed to compute a relative reaction severity, R_S .

Such a parameter has been developed at Mobil and applied to the Battelle experiments. (9)

R_S , a rate averaged severity, is defined as follows:

$$R_S = \int e^{-E/R T_r} \Delta t$$

where t = Time, minutes

T_r = Temperature, °K

E = Activation energy, 30 kcal/mole.

Table III shows the nominal reaction times, temperatures, and reaction severities designed to give the desired conversions with Wyodak (Belle Ayr) subbituminous coal.

TABLE III. RELATIONSHIP BETWEEN REACTION TIME, TEMPERATURE, REACTION SEVERITY AND CONVERSION OF WYODAK COAL TO PYRIDINE SOLUBLES

Reaction Time, min	Temp, °F (°C)	% MAF Coal Conversion to Pyridine Solubles	Reaction Severity, R_S ($\times 10^{-10}$)
6	800 (427)	65	25
6	860 (460)	80	65
2	860 (460)	65	25

The first half of the experiments were run to specified conditions of time and temperature while the second half were run to specific levels of R_g , calculated as the reaction progressed. The experimental conditions are summarized in Table IV. The shorter residence times used when R_g was calculated as the reaction progressed reflect the portion of the reaction which occurred during heatup. The desired reaction severities of 2, 25, and 65×10^{-10} were much more closely approached in the later experiments.

Apparatus Description. A schematic diagram of the apparatus used in these experiments is shown in Figure 2. One-gallon stirred autoclaves were used for the reactor and quench vessels and a 2-liter stirred autoclave was used for the preheater. A coal-solvent charge of 1500 to 1800 g was used which left an adequate head space for hydrogen in the reactor. The autoclaves were connected in series with 3/8-inch transfer lines separated by manually operated valves. Each autoclave was equipped with a vent line so the system could be purged with nitrogen before reaction and vented after reaction. Samples of the vent gases from each autoclave were taken separately. Each autoclave was also equipped with two thermocouples, one in the body of the autoclave used to control the heater and a recording thermocouple in the solution to measure the reaction temperature. AC2 was also equipped with an inlet line for hydrogen and a separately controllable internal heater to decrease the heatup time at the start of reaction. The internal heater was also used to control the temperature of the reaction during the reaction period. AC3 was equipped with a cooling coil to shorten the quench time at the end of the reaction period.

Experimental Procedure. The coal and solvent were mixed together and the moisture content of the coal was removed by distillation in glassware at atmospheric pressure. The water-free slurry was then added to AC1 with the stirrer on by applying a vacuum to the system through the vent lines. This insured that the coal did not settle out. The preheater temperature was 200 °C.

AC2 was preheated empty to 20–30 °C above the reaction temperature such that the equilibrium temperature reached when the reactants were added was 5 to 10 °C below the desired reaction temperature. The internal heater was used to make up the heat difference needed to reach the desired temperature.

After purging with nitrogen and heating the system, the slurry was transferred from the preheater to the reactor. Typical transfer times between autoclaves were 5 to 10 seconds. The reactants were stirred rapidly and the hydrogen overpressure, typically 1500 psig added hydrogen, was added quickly to AC2.

After transfer from the preheater to the reactor the temperature was followed to the minimum and then a temperature reading

Table IV. Actual Reaction Conditions for Coal Liquefaction Experiments*

	1	2	3	4	8	9	10	11
Coal	← ————— Wyodak ————— →							
Solvent	-019	-019	-019	-019	-035	-035	-035	-035
Average Temp, C	433	462	459	457	458	450	422	442
Residence Time, min	6	6	2	2	2	6	2	6
Reaction Severity, R_s ($\times 10^{-10}$)	43.6	77.7	32.4	66.1	39.2	90.1	14.8	73.7

Table IV. Continued

	Run No.						
	12	13	14	15	16	17	18
Coal	← ————— Monterey ————— →						
Solvent	-035	-035	-035	-035	-019	-019	-019
Average Temp, C	459	456	426	424	424	412	460
Residence Time, min	4.3	1.1	4.5	0.5	3.5	0.5	4.8
Reaction Severity	61.1	27.5	25.8	6.4	26.5	2.7	65.9

(a) A 3:1 solvent to dry coal ratio was used for all of the experiments.

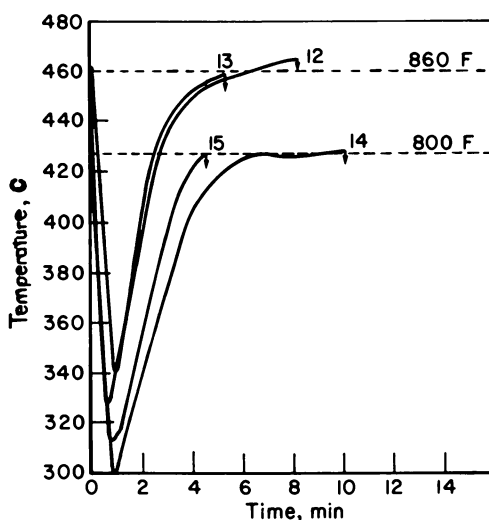


Figure 1. Typical time vs. temperature curves for Battelle coal liquefaction experiments

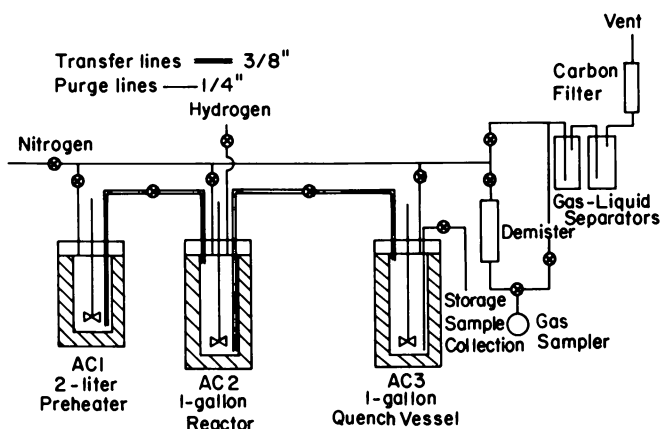


Figure 2. Schematic of coal liquefaction apparatus. AC2 is equipped with an internal heater and AC3 is equipped with an internal cooling coil. All autoclaves and the heated filter are equipped with pressure gauges, thermocouples, and temperature controllers.

was taken every 10 seconds and a hand calculator was used to determine R_S . The plot of temperature versus time was rechecked after the experiment to get a final R_S . At the conclusion of the desired reaction time the products were transferred to AC3 and quickly cooled to 200 °C using the internal cooling coil. Each autoclave was vented separately to about 20 psig. The sample was then collected from AC3 and stored in a refrigerated glass bottle under nitrogen.

Product Workup Procedures. A sample of the products was continuously extracted with THF and then with pyridine. Pyridine insolubles were analyzed for ash and conversions of MAF coal to pyridine solubles were calculated on the basis of the ash analyses and the mass recoveries. A mass recovery balance was calculated for each experiment. The mass recoveries averaged 97.8 percent. The mass and ash based conversions diverged by an average of only 2.7 percent.

The THF solubles were distilled under vacuum to obtain fractions containing THF (<70 °C), water (70 °C to 110 °C), light oil (100 °C to 204 °C), and solvent (204 °C to 427 °C). The distillation residue was SRC. This procedure may result in coking and cracking of the SRC residue and inaccurate separation at the cut point between solvent and SRC.

The workup procedure was later modified to distill only THF, water and light oil. Solvent and SRC were separated by dropping a THF solution of the slurry into boiling heptane with rapid stirring. THF distilled off and the heptane was increased to at least a 20:1 ratio of heptane-to-sample and allowed to cool overnight with stirring. After filtration and drying, heptane solubles were counted as solvent derived and heptane insolubles were considered to be SRC. The 427 °C+ distillation residue has been found to average 28 percent heptane solubles. Thus, a different SRC yield structure is obtained depending on the product workup method used.

Results and Discussion

MAF Coal Conversions to Pyridine Solubles. MAF coal conversions, based on ash analyses, are shown for each coal-solvent combination in Figure 3. Subbituminous coal is converted more slowly, resulting in lower conversions at identical reaction severities than bituminous coal. Maximum conversions are higher with bituminous coal, approaching 90 percent on an MAF basis for the Monterey coal compared to about 75 percent for Wyodak coal. As reaction severity approaches zero the Monterey coal conversion is about 70 percent and the Wyodak is about 40 percent. Liquefaction appears to occur very rapidly to these levels and then slower to the maximum conversion. The initial liquefaction may be a physical dissolution while the slower rate represents a reaction in which chemical bonds are broken, although other explanations are possible. (10)

The quality of the solvent also affects the conversion levels. With the hydrogen-enriched solvent (-019) conversions approach maximum levels at all reaction severities tried in this work and no retrograde reaction was observed to reform pyridine insolubles. A maximum conversion followed by a decline in conversion was seen with the hydrogen-depleted solvent (-035) with both coals. The maximum conversions are 5 to 10 percent lower with the hydrogen-poor solvent than the best observed conversions obtained with the hydrogen-rich solvent for each coal.

SRC Composition. The elemental analyses of the SRCs obtained by the distillation workup procedure from the liquefaction of Wyodak coal in the hydrogen-enriched solvent (-019) are shown in Figure 4 as a function of reaction severity. The use of the heptane precipitation workup procedure changes the composition of the SRC using the same coal and solvent. These elemental analyses are shown in Figure 5. The trends with increasing reaction severity are the same. The hydrogen and oxygen contents decrease, carbon content increases, and nitrogen and sulfur are not affected significantly by increasing reaction severity. Comparison of the nondistillable (SRC) product compositions obtained by the two product workup methods are shown in Figure 6. The less soluble material which remains after heptane precipitation contains less hydrogen, more nitrogen and oxygen and about the same amounts of sulfur and carbon. The heptane precipitation procedure was used to obtain the SRC fractions discussed below.

The elemental analyses of SRCs from the liquefaction of Wyodak coal in the hydrogen-depleted solvent (-035) are shown in Figure 7. These data were obtained over a wider range of reaction severities. Up to a point the trends are roughly the same as seen with the hydrogen-enriched solvent. However, at the highest reaction severity tried, the conversion decreased and at this point the oxygen content of the SRC increased, and the carbon and hydrogen contents decreased.

A comparison of the effect of the two solvents on the composition of SRCs from Wyodak subbituminous coal is shown in Figure 8. Compared to the hydrogen-enriched solvent, use of the hydrogen-depleted solvent results in a SRC with higher sulfur and oxygen contents and lower carbon and hydrogen contents.

The oxygen content of the hydrogen-depleted solvent is higher, as was noted earlier, which suggest that the oxygen content of the solvent increases during liquefaction. Oxygen in the coal reports to water, gases such as CO and CO₂, and smaller molecules which have boiling points within the solvent range as the coal is liquefied. The rates and fractions of oxygen distribution to each product type appear to be a function of the hydrogen content of the solvent and the extent of reaction.⁽¹⁰⁾

The compositions of the SRC product fraction obtained from liquefaction of Monterey bituminous coal with the hydrogen-

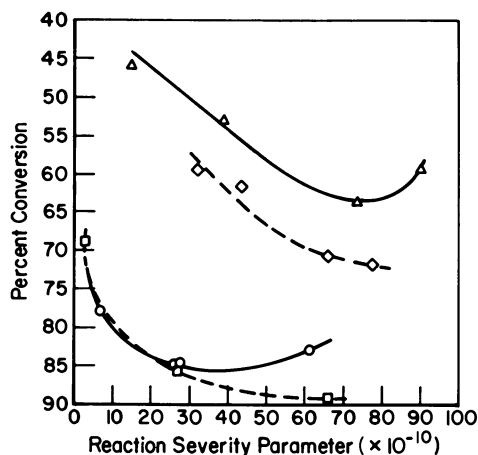


Figure 3. Comparison of conversion of MAF Wyodak (-035 solvent (Δ); -019 solvent (\diamond)) and Monterey (-035 solvent (\circ); -019 solvent (\square)) coals to pyridine solubles (based on ash analysis)

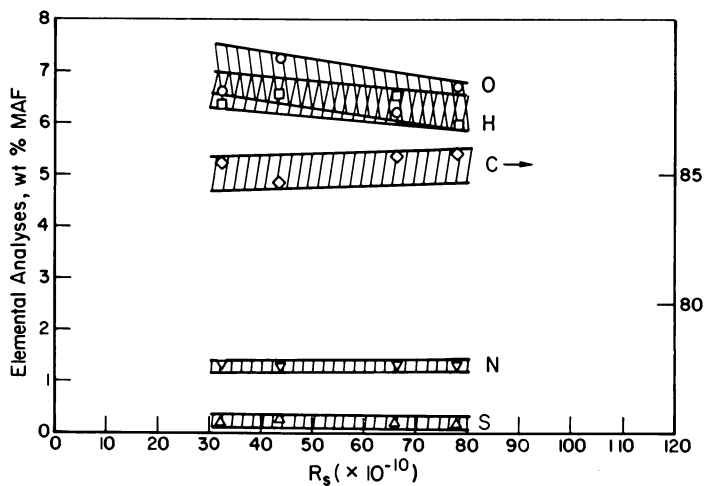


Figure 4. Elemental analyses of SRC from liquefaction of Wyodak coal in -019 solvent (prepared by distillation)

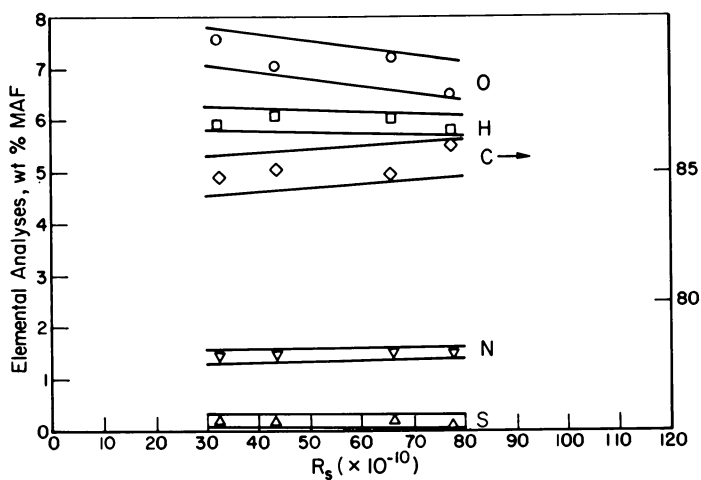


Figure 5. Elemental analyses of SRC from liquefaction of Wyodak coal in -019 solvent (prepared by heptane precipitation)

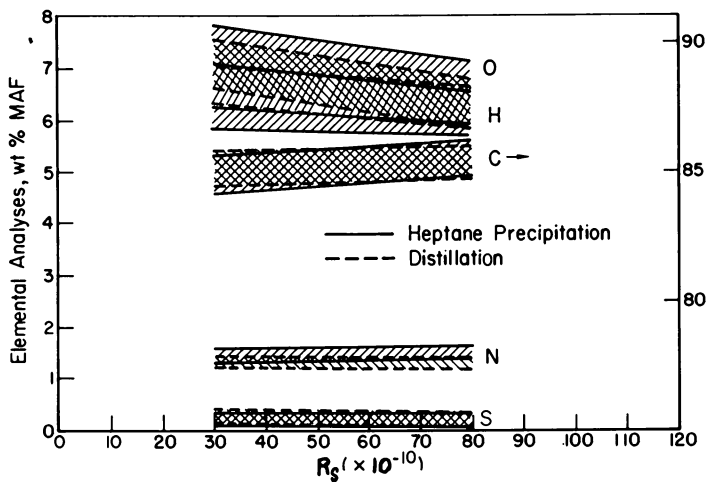


Figure 6. Comparison of elemental analyses obtained by distillation and heptane precipitation from liquefaction of Wyodak coal with -019 solvent

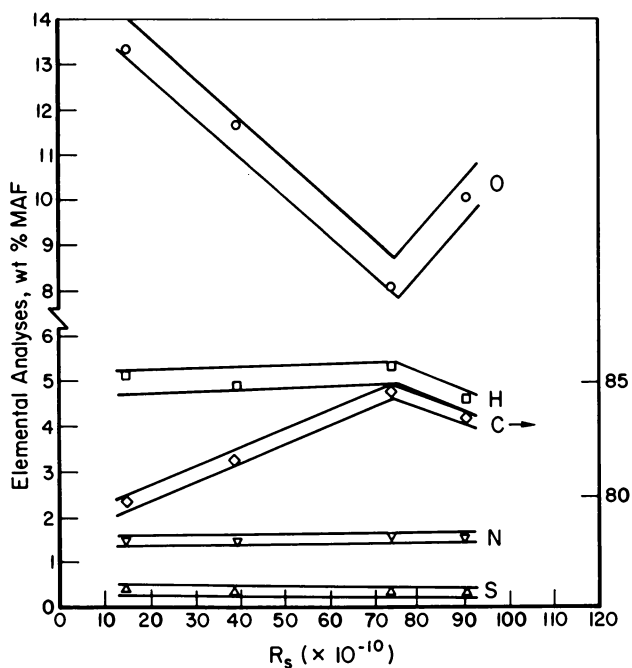


Figure 7. Elemental analyses of SRC from liquefaction of Wyodak coal in -035 solvent (prepared by heptane precipitation)

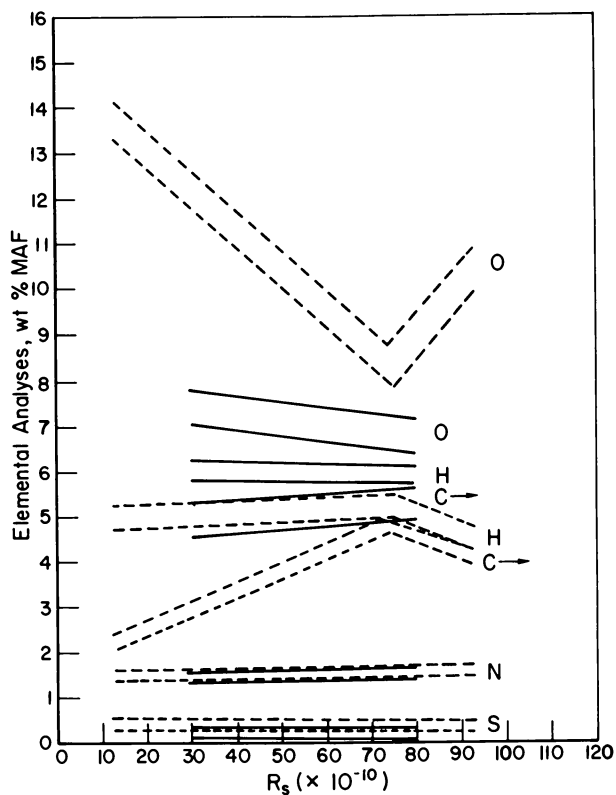


Figure 8. Comparison of elemental analyses of SRC from liquefaction of Wyodak coal in -019 (—) and -035 (---) solvents (heptane precipitation data)

enriched solvent (-019) are shown in Figure 9. The corresponding compositions are shown in Figure 10 for liquefaction in the hydrogen-depleted solvent (-035). With both solvents oxygen and sulfur contents decrease and carbon and nitrogen contents increase with increasing reaction severity. Hydrogen content is nearly unchanged with increasing reaction severity with the hydrogen-enriched solvent but decreases with increasing reaction severity with the hydrogen-depleted solvent.

The reversal of carbon, hydrogen and oxygen contents when retrograde reactions are observed at high reaction severities with Wyodak subbituminous coal (Figure 7) are not as apparent when retrograde conversion occurs with Monterey bituminous coal (Figure 10).

The rates of change of the carbon, hydrogen and oxygen concentrations with increasing reaction severity are the most obvious differences due to solvent source at the lower range of reaction severities tried with Monterey coal. These are compared in Figure 11. The changes are more rapid with hydrogen-enriched solvent since conversion is greater and more of the less soluble portion of the coal, containing less oxygen and more carbon is soluble in the solvent. Hydrogen content also increases and sulfur content decreases more rapidly, probably reflecting better hydrogen transfer from the hydrogen-enriched solvent.

The comparison in Figure 12 shows the effect of coal rank on the elemental compositions of the nondistillable products. The hydrogen, carbon and oxygen contents of the nondistillable products converge as reaction severity is increased. Nitrogen and organic sulfur contents, which are higher in the bituminous coal, are significantly different in the heptane insoluble fractions resulting from liquefaction in the hydrogen-enriched solvent. The organic sulfur content in the Wyodak subbituminous coal is unaffected by increasing reaction severity while the types of organic sulfur compounds in the Monterey bituminous coal are removable as reaction severity is increased.

Carbon, hydrogen and oxygen contents also converge as reaction severity is increased with the hydrogen-depleted solvent (-035) until retrograde reactions occur with the Wyodak coal (Figure 13). No data at equally high reaction severities are available for the Monterey coal. Trends with nitrogen and sulfur are the same as those described previously with the hydrogen-enriched solvent.

Summary

MAF conversions to pyridine solubles from short contact time coal liquefaction are dependent on the coal type, solvent source, and reaction severity. As reaction severity increases conversions approach a maximum value with a hydrogen-enriched solvent but go through a maximum and decline with a hydrogen-depleted

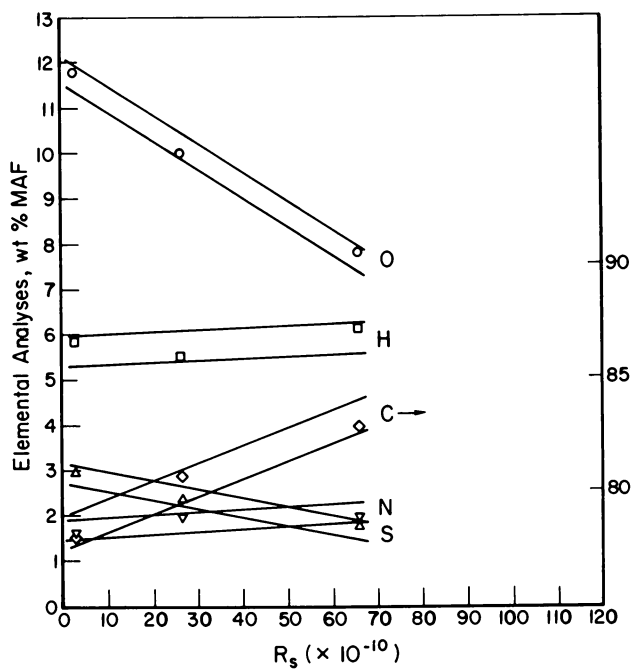


Figure 9. Elemental analyses of SRC from liquefaction of Monterey coal in -019 solvent (prepared by heptane precipitation)

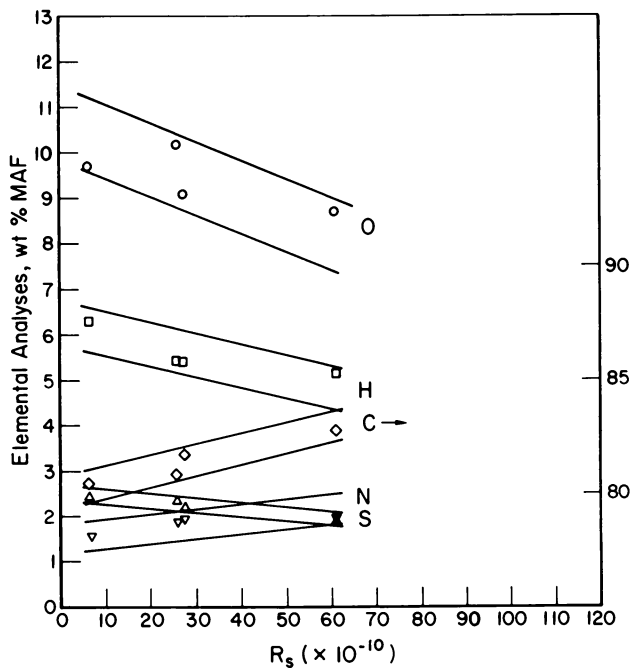


Figure 10. Elemental analyses of SRC from liquefaction of Monterey coal in -035 solvent (prepared by heptane precipitation)

**American Chemical
Society Library
1155 18th St. N. W.**

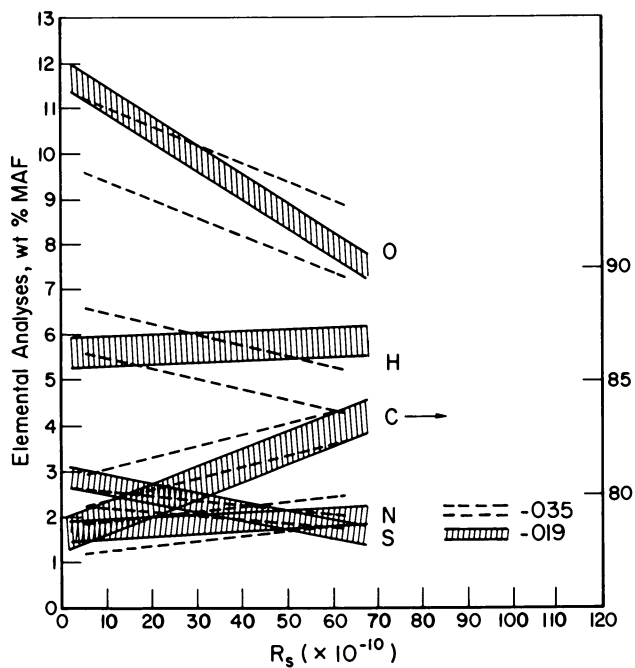


Figure 11. Comparison of changes in elemental analyses with reaction severity for liquefaction of Monterey bituminous coal in -019 and -035 solvents

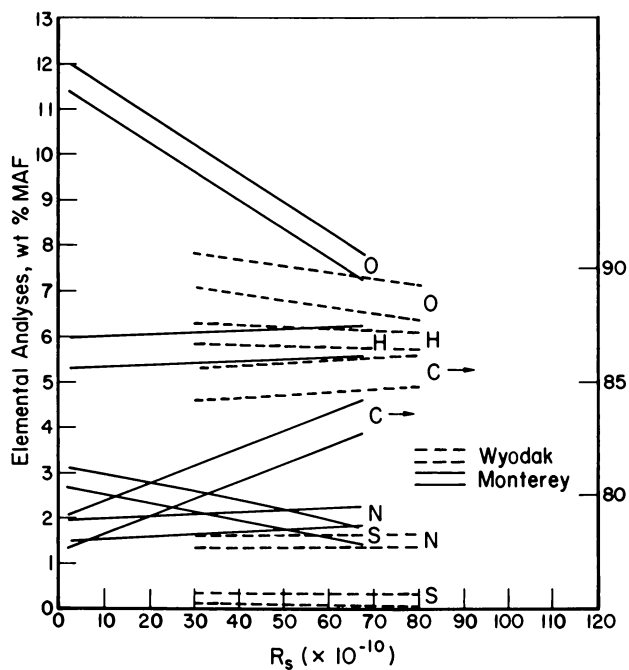


Figure 12. Comparison of elemental analyses of nondistillable products from liquefaction of Wyodak and Monterey coals in -019 solvent

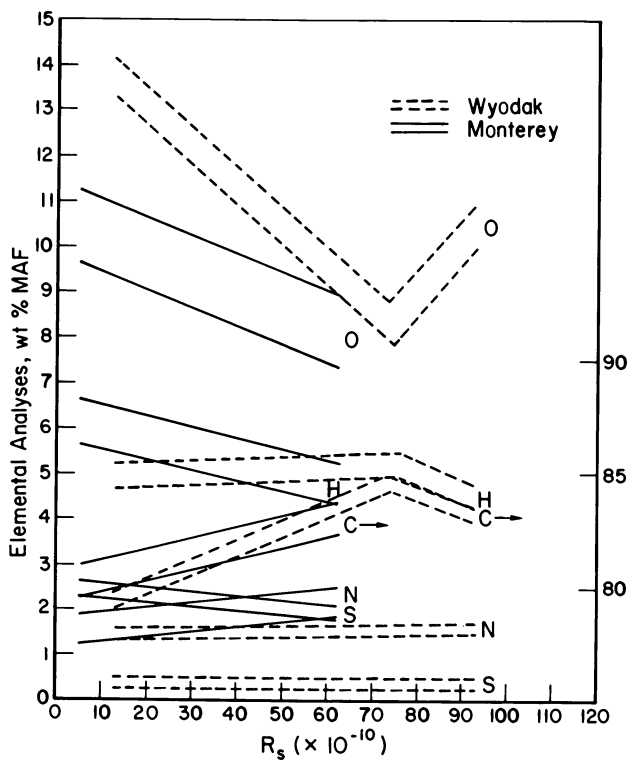


Figure 13. Comparison of elemental analyses of nondistillable products from liquefaction of Wyodak and Monterey coals in -035 solvent

solvent. Subbituminous coal liquefies more slowly and reaches a lower maximum conversion than bituminous coal. SRC type products have been isolated as an 800 °F+ distillation residue and as heptane insolubles. The heptane insoluble materials contain less hydrogen and more nitrogen and oxygen.

When Wyodak subbituminous coal is dissolved in either a hydrogen-depleted solvent or a hydrogen-enriched solvent, the concentrations of hydrogen and oxygen in the heptane insolubles decrease and carbon increases as the reaction severity is increased. When retrograde reactions occur at high reaction severities with the hydrogen-depleted solvent, the oxygen content of the heptane insolubles increases and hydrogen and carbon decrease.

Liquefaction of Monterey bituminous coals with either solvent results in increasing concentrations of carbon and nitrogen and decreasing concentrations of sulfur and oxygen in the heptane insolubles with increasing reaction severity. Hydrogen content does not change significantly with increasing reaction severity when a hydrogen-enriched solvent is used but decreases significantly when a hydrogen-depleted solvent is used. Sulfur content also decreases faster with increasing reaction severity when a hydrogen-enriched solvent is used.

Comparison of analyses of heptane insolubles from the liquefaction of Monterey bituminous and Wyodak subbituminous coals in the hydrogen-enriched solvent shows that carbon, hydrogen and oxygen concentrations converge with increasing reaction severity to form a product with similar elemental analyses. The same convergence is seen when the hydrogen-depleted solvent is used. There are significant differences in the nitrogen and organic sulfur contents related to the concentrations of these elements in the starting coals.

Acknowledgment

This work was conducted under a subcontract to Mobil on the EPRI Contract No. RP-1655, which is jointly funded by EPRI and Mobil R&D Corporation. Mrs. L. A. Atherton is the EPRI Project Manager.

The assistance of Dr. F. J. Derbyshire, Mobil R&D Corporation, Central Research Division, who is the Technical Representative for Battelle's subcontract with Mobil, is gratefully acknowledged.

Literature Cited

1. Kloepper, D. L., Rogers, T. F., Wright, C. H., and Bull, W. C., "Solvent Processing of Coal to Produce a Deashed Product"; report to Office of Coal Research, U.S. Department of the Interior by Spencer Chemical Division of Gulf Oil Corporation; OCR R&D Report No. 9, 1965.

2. Tao, J. C., Malhotra, R. K., Sukel, T. M., Foster, E. P., and Morris, S. M.; "Solvent Refined Coal (SRC I) Technology, Product Markets, and Economics"; presented at Third International Coal Utilization Exhibition and Conference: Houston, Texas, November 18-20, 1980.
3. Whitehurst, D. D., Farcasiu, M., and Mitchell, T. O.; "The Nature and Origin of Asphaltenes in Processed Coals"; report to EPRI by Mobil Research and Development Corporation; EPRI RP410-1; February, 1976.
4. Longanbach, J. R., Droege, J. W., and Chauhan, S. P.; "Short Residence Time Coal Liquefaction"; report to EPRI by Battelle's Columbus Laboratories; EPRI RP779-5; June, 1978.
5. Whitehurst, D. D., Mitchell, T. O., Farcasiu, M., and Dickert, J. J., Jr.; "The Nature and Origin of Asphaltenes in Processed Coals"; report to EPRI by Mobil Research and Development Corporation; EPRI RP410-1; 3 volumes; December, 1979.
6. Kleinpeter, J. A., Burke, F. P., Dudd, P. J., Jones, D. C.; "Process Development for Improved SRC Options: Interim Short Residence Time Studies"; report to EPRI by Conoco Coal Development Company; EPRI RP1134-1; June, 1980.
7. Potts, J. D., Chillingworth, R. S., Hastings, K. E., and Unger, H.; "Alternative Modes of Processing SRC in an Expanded Bed LC-Finer to Produce Low Nitrogen Distillates"; presented at the 86th National AIChE Meeting; Houston, Texas; April 3, 1979.
8. Moroni, E. C. and Shen, J.; "Advanced Two-Stage Liquefaction Processes"; presented at the 12th Central Regional ACS Meeting; Pittsburgh, Pennsylvania; November 12-14, 1980.
9. Varghese, P., Derbyshire, F. J., and Whitehurst, D. D.; "Control of Short Contact Time Coal Liquefaction"; EPRI Contractors Conference on Coal Liquefaction; Palo Alto, California; May 7-8, 1980.
10. Whitehurst, D. D., Mitchell, T. O., and Farcasiu, M.; "Coal Liquefaction, The Chemistry and Technology of Thermal Processes"; Academic Press, New York, 1980, 178-189.

RECEIVED March 9, 1981.

The Effect of Solvent Compositions on the Liquefaction Behavior of Western Subbituminous Coal

L. R. RUDNICK and D. D. WHITEHURST

Mobil Research and Development Corporation, P.O. Box 1025, Princeton, NJ 08817

There is considerable evidence in the literature that Western coals behave differently toward liquefaction than do coals from the East or from the Interior (1). The differences can be attributed to the geological and biological history of these regions and yielded a different skeletal structure for Western coal. Coal liquefaction studies have demonstrated that the direct liquefaction of Western coals is more problematic and requires more severe conditions than for Eastern coals.

Our earlier work has shown that short contact time coal liquefaction when coupled with catalytic upgrading can offer several advantages including economy of hydrogen usage. These previous studies of short contact time (SCT) dissolution were conducted using synthetic solvent mixtures with both Eastern and Western coals. The work presented here has examined the short contact time liquefaction of Belle Ayr coal using process derived solvents. One requirement for such a process is that it be self-sufficient in solvent and that an appropriate solvent quality can be maintained in the overall process. This may require that the solvent used in the first step be generated elsewhere.

The purpose of this paper is to describe some of our findings which examine the liquefaction behavior of Western sub-bituminous coal to determine which components of the solvent are most critical in the short contact time dissolution stage. The work will be presented from two points of view:

- The effect of solvent composition on coal liquefaction, and
- The effect of coal conversion and the reaction conditions on the composition of the solvent.

Effect of Solvent Composition on Coal Conversion

Past work by us as well as others has identified the following critical solvent components: hydrogen donors, phenols, hydrogen shuttlers, hydrogen abstractors. Our studies used low boiling model compound mixture solvents for ease of distribution

0097-6156/81/0169-0153\$05.00/0
© 1981 American Chemical Society

of solvent and coal products. High solvent to coal ratios were used to allow rapid heat-up on injection of the coal into the reactor. Thus accurate time-temperature-conversion relationships could be achieved.

In the present study we are using representative process derived solvents which could be produced and recycled at lower (commercially feasible) solvent to coal ratios. These changes created several new experimental problems which will be discussed.

The solvents which have been used to date represent two extremes (Table 1). One is a hydrogen enriched (9.67% H) SRC-1 recycle solvent (92-26-019) while the other is a hydrogen depleted (8.15% H) SRC-1 preheater effluent solvent (92-03-035). Reactions were performed in a 300 cc stainless steel batch autoclave which has been previously described in detail (1). The experimental procedure has also been described (2). Experiments in this paper were performed at 1400 psig of hydrogen at a solvent to coal ratio of three to one.

We have previously derived a parameter called Reaction Severity (R_s) which provides a measure of the extent of reaction expected from a given time-temperature sequence (3). One could attempt to average the temperature over the period of reaction by integration of the product of temperature and time increments. The average temperature could then be calculated and the total area (time \times t_{avg}) would be representative of the extent of reaction. The details of R_s derivation are provided in Reference 3.

Figure 1 shows the relationship between conversion, defined as gas + pyridine soluble liquids, and R_s derived at two different maximum temperatures. It can be seen that the conversions obtained at similar severities are the same (within experimental error). This is true even though all of these data involved rather extreme time-temperature fluctuations. Within limits a certain reaction severity can be obtained either at lower temperature (800°F) for longer time (6 min.) or at higher temperature for shorter time.

With changing reaction severity the composition of SRC product also changes systematically (Table 2). The hydrogen content and H/C mole ratio both decrease with increasing severity. The nitrogen and sulfur contents show little variation. The oxygen values may indicate that the response of conversion to soluble products and deoxygenation may have different activation energies. We have noted in past work that this Western coal did produce less polar materials initially; thus the oxygen content may indeed go through a maximum at short time. The table also shows that the aromatic carbon content of the hexane insolubles (SRC) increases with reaction severity.

The data shows that, for Belle Ayr coal, the initial SRC product, at $R_s \leq 11$, is lower in aromatic carbon and richer in aliphatic carbon than the parent coal. With increasing severity, the situation changes; at R_s of 20-25 the carbon distribution in the SRC is similar to that of the parent coal; at $R_s > 25$, the SRC product is more aromatic and less aliphatic than the coal. This

Table 1. Compositional Data of Solvents (400°–800°F boiling range)

<u>SOLVENT #</u>	SRC-1 PREHEATER EFFLUENT RECYCLE <u>92-03-35</u>	HYDROGENATED SRC-1 RECYCLE (CONOCO) <u>92-26-019</u>
<u>ELEMENTAL ANALYSES</u>		
C	87.51	87.73
H	8.15	9.67
O	2.88	1.48
N	1.24	0.99
S	0.39	< 0.1
H/C	1.12	1.32
<u>NMR ANALYSES</u>		
POLY AR	1.5	1.7
AR	37.6	17.0
α	24.6	24.4
β	22.1	38.5
γ	14.3	18.4
¹³ C AR	74.0	51.6
<u>BASIC N (%)</u>	0.42	0.34
CCR	0.07	0.10

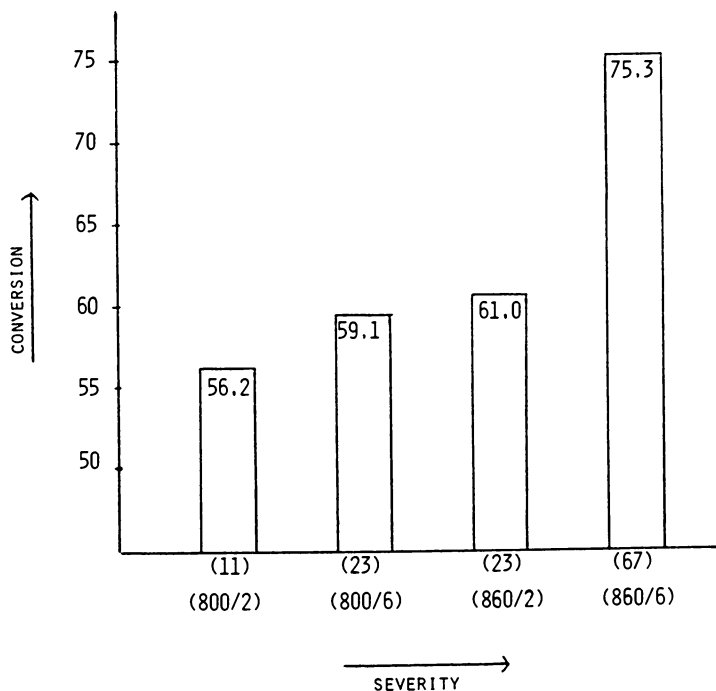


Figure 1. Relationship between conversion and severity

Table 2. Relationship Between SRC Composition and Severity

SEVERITY	11	23	23	67
T/T	800°F/2 MIN.	800°F/6 MIN.	860°F/2 MIN.	860°F/6 MIN.
C	81.87	81.76	83.17	86.09
H	7.08	5.95	6.09	5.82
O	9.45	9.98	8.76	6.12
N	1.40	1.57	1.51	1.58
S	0.21	0.24	0.22	0.21
H/C	1.04	0.87	0.88	0.81

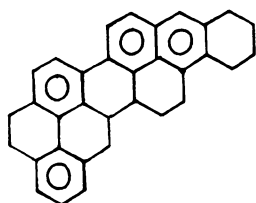
is in agreement with our earlier work which showed that the H/C atomic ratio of the low severity SRC was higher than that in the parent coal and that, with increasing severity, it decreased to a value lower than that in the coal. Similar observations were made in earlier studies where it was shown that the initial liquefaction products of Wyoming coal were also richer in hydrogen and aliphatic carbon and lower in phenolic content than both the parent coal and products from larger time reactions.

There are indications that the formation of these initial hydrogen enriched products and the rate at which the hydrogen content subsequently decreases is dependent upon the solvent donor capacity.

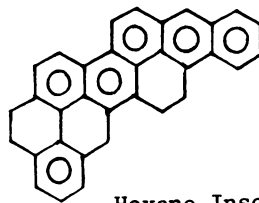
The hydrogen to carbon (H/C) atomic ratio of the SRC follows the relative changes in aromatic and aliphatic carbon distribution, being reduced with increasing aromatization.

With increasing SRC yield, concomitant with increasing conversion, the product becomes more aromatic. Three effects should be distinguished; firstly, that the progressive increase in coal conversion involves the liquefaction of an increasing proportion of elements within the coal structure which are more aromatic and richer in heteroatoms. The second aspect to be considered is that, with increasing severity, some hydrogen richer portions (e.g. aliphatic substituents) of the SRC will be reduced in molecular weight which will remove them from the SRC product range. Lastly, the effect of increasing severity will lead to dehydrogenation of hydroaromatic components in the SRC. The net result of these considerations will effect a reduction in H/C atomic ratio of the SRC, as observed.

Calculation based on previous data show that the aromatic carbon content of the SRC can only be increased to the values shown by data by dehydrogenation reactions. These calculations take into account the carbon types present in residue and in the gases. As an illustration of some of these effects, if it is assumed that the average molecular weight of the SRC is ca. 480, then the average structural unit will contain 33 carbon atoms. In the parent coal, this unit contains 22 aromatic and 11 aliphatic carbons. At $R_s = 67$, this changes to 28 aromatic carbons and 5 aliphatic carbons. This is represented in model structures below:



Belle Ayr Coal

Hexane Insoluble
After $R_s = 67$

It should be noted that these models only consider the cyclic carbon structure; no heteroatoms or side chains have been included. Though this may not be totally accurate one very important observation is that the extent of ring condensation increases dramatically. This implies that the portion of coal which becomes hexane insoluble (SRC) products is extensively dehydrogenated even when high hydrogen content process derived solvent (92-26-019) is used.

Using reaction severity it is now possible to compare the liquefaction behavior of different solvents. Solvents containing higher hydrogen donor concentration (92-26-019) are more effective than the hydrogen-depleted solvent (92-03-035) even at short times. The results also show that up to 55% conversion is essentially solvent independent.

The severity parameter also allows us to compare our results with those of others (Battelle). Figure 2 shows that the results with solvent 92-26-019 compare very well. Other synthetic and fractionated process derived solvents were used and these results also show that up to 55% conversion is independent of solvent composition.

The overall products of coal conversion can also vary when reacted with solvents of different compositions. A combination of data from our earlier studies using solvents containing $\sim 40\%$ tetralin and data from this project shows that in general all of the CO_2 production ceased by about $R_s = 50$ or in other words, the short contact time regime.

Carbon monoxide, by contrast, continued to increase with increasing severity. The results were somewhat scattered but did indicate that CO formation involved more difficult transformations.

The SRC yields at short times parallel conversion and few light liquids were formed. Figure 3 compares some of the key compositional features of SRC's produced with different solvents. It is clear that the SRC contains more hydrogen and higher H/C mole ratios when produced with solvents rich in hydrogen donors as opposed to solvents which are deficient in hydrogen donors even at the same conversion level. Sulfur contents though low in all cases are slightly lower when hydrogen rich solvents are used. Nitrogen contents were insensitive to solvent composition. The trends noted earlier of hydrogen, H/C mole ratio and oxygen are the same for both solvents used and the data are supportive of lower oxygen content SRC's when produced at higher temperatures.

In summary, we find that the application of reaction severity parameter to predict conversion appears useful. We have now coupled computer calculations of this value directly to our reactors as a means of preselecting the conversion desired by a computer controlled quench.

For Belle Ayr coal, conversion up to $\sim 55\%$ is independent of solvent composition. Beyond this point, conversion is responsive

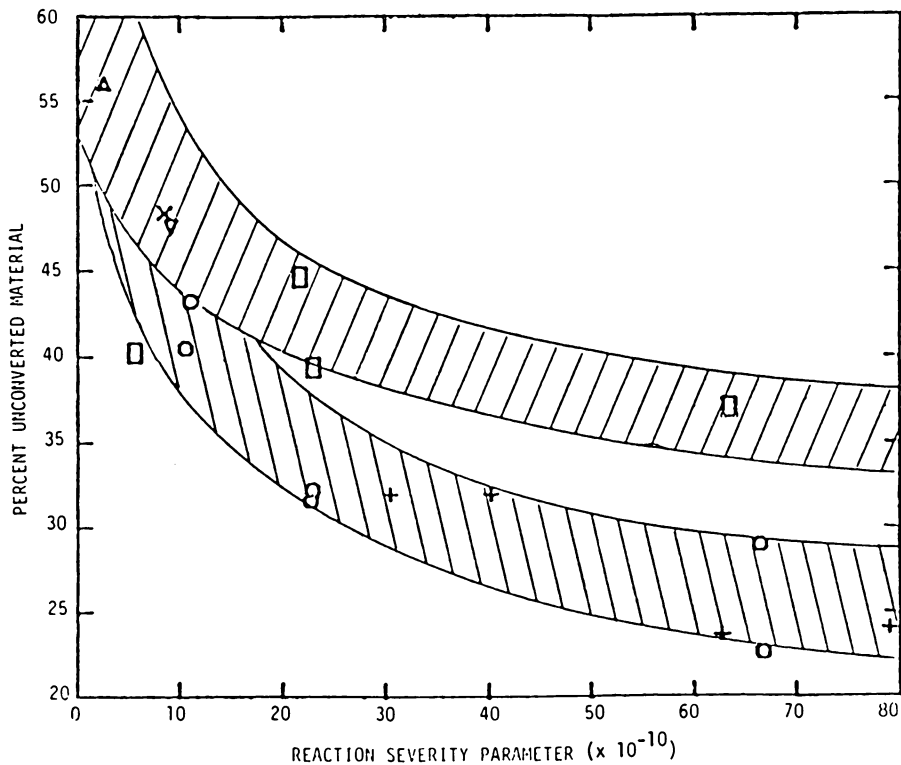


Figure 2. Conversion to pyridine solubles. Solvent: 92-26-019 (\circ); 92-03-035 (\square); SS* 43 (Δ); 92-01-050 (∇); 92-01-051 (\times); BATELLE 92-26-019 (+).

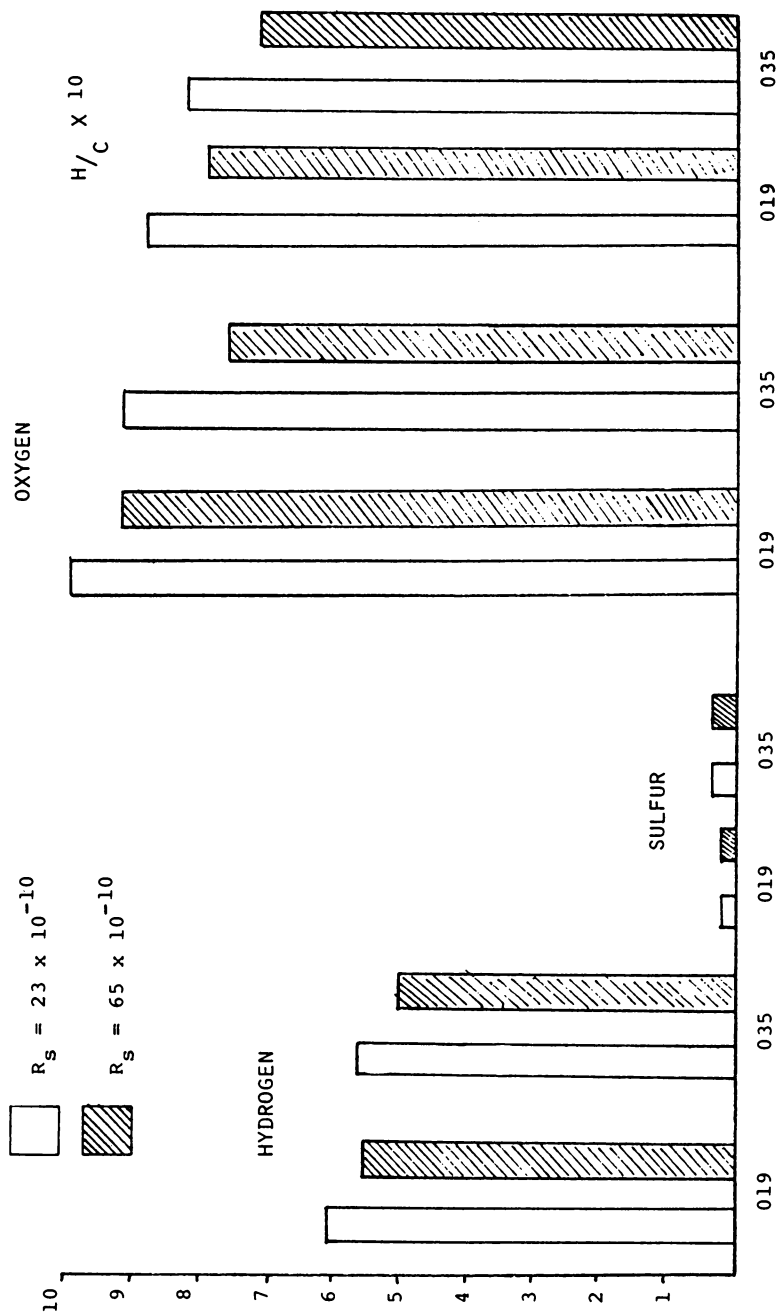


Figure 3. Elemental analyses of heptane-insoluble SRC

to solvent composition with hydrogen donor rich solvents providing higher values. This two component conversion may require the incorporation of conversion level and solvent quality into the severity parameter in order to develop a quantitative predictive equation.

The SRC composition is dependent on solvent composition at all conversion levels and high hydrogen donor solvents produce higher quality products.

SRC's produced at different temperatures have different compositions (oxygen contents) at the same reaction severity and it may be necessary to use a different assumed activation energy for compositional changes.

In order for a coal liquefaction process to be viable two requirements must be met. First, the process must be self-sufficient in solvent, in other words that the quantity of recycle solvent be greater than or equal to the initial solvent used to initiate the process, and second, the solvent quality must remain sufficiently high to perform desired conversion of the coal while keeping to a minimum solvent consuming reaction, charring, and gas formation.

Effect of Coal Conversion on Solvent Composition

Earlier work at Mobil and other laboratories (4,5) had identified several processes responsible for solvent degradation (e.g. hydrogen transfer, cracking, isomerization, alkylation and condensation). In general, each of these processes converts a molecule which is useful in the liquefaction process to one which is less useful. Each of these processes can lead to both changes in structure and the physical properties of the solvent components.

Product Isolation. The use of true process derived solvents instead of the model compound solvents used in past work (6) led to several unexpected complications which required that we modify our methods of product isolation.

The major problem area was the observation that even hydrogen enriched solvents can react with coal or other solvent components to produce products of higher boiling range and are thus difficult to separate from SRC's by distillation. When a 400-800°F solvent was employed to convert Belle Ayr coal to SRC at 800-860°F for 2-6 minutes contact time approximately 4-6% of the solvent is converted to material boiling above 800°F. These higher boiling components are soluble in paraffins and can be distilled or sublimed at higher temperature.

Our previous studies with model compound solvents indicated that higher boiling products can be produced via dimerization by coupling of aromatic methyl groups and by alkylation of the solvent by light coal fragments.

When distillation is used to isolate solvent range material the SRC yields were often higher than the calculated conversions for these runs. Our past experience with a synthetic solvent containing high hydrogen donor contents did not have this problem. Assuming that the higher SRC yields at similar conversion were due to the experimental difficulty of distilling at temperatures above 800°F, the SRC samples were sublimed at 245°C/0.5 mm. The SRC yields obtained after sublimation result in better agreement with runs employing synthetic solvents. However sublimation is experimentally tedious and difficult to perform on a large scale. A new procedure was developed which would minimize the problems encountered in distillation at temperatures above 800°F while still providing clean separation of solvent components. Extraction of the SRC's with hexane in a soxhlet apparatus provided hexane soluble and insoluble fractions. In this way we defined SRC as the portion of the THF soluble product that is insoluble in hexane. The hexane soluble portion is considered as solvent or distillable products. When SRC yield was calculated in this way and compared with older data in which the oils (obtained by liquid chromatography) were subtracted the agreement was much better (Figure 4). In order to minimize any problems due to encapsulation of soluble materials in the precipitate the reaction products are dissolved in THF (the solvent used for autoclave washing, etc.) and the soluble products are added dropwise to an excess (20 times the m.a.f. coal fed) of hot heptane (85-90°C). At this temperature the THF flashes off and the solute is efficiently partitioned into heptane soluble and insoluble products. The heptane slurry is then distilled to totally remove THF, additional heptane being added as necessary. Finally, additional heptane is added to increase the dilution to 30 times the m.a.f. coal fed. The mixture is then allowed to cool and stand overnight, with stirring, before filtering.

Changes in Solvent Composition. The compositional data for the low and high hydrogen solvents are shown in Table 1. The SRC-1 Preheater Effluent (92-03-035) represents a low hydrogen recycle solvent (8.15% H). NMR analysis indicates a high aromatic content with a correspondingly low value for β hydrogen which indicates a low concentration of hydroaromatics. The aromatic carbon content, as determined by ^{13}C NMR, is high and is consistent with a low concentration of hydroaromatics. It is interesting to note that although the absolute values for nitrogen differ in the two solvents, the ratio of basic N to total nitrogen is 0.34 in both cases.

A comparison by vpc of the high hydrogen (92-26-019) and low hydrogen (92-03-035) solvents shows differences in major components as well as in the boiling point distributions. The high hydrogen solvent having a variety of possible hydroaromatic structures for each aromatic carbon structure has fewer unique major components than the solvent of low hydrogen content.

Comparison of the low hydrogen solvent (92-03-035) with the heptane soluble fraction from a SCT liquefaction which employed the low hydrogen solvent by vpc indicates that the heptane solubles closely resemble the starting solvent.

The reaction conditions and product analyses of the hexane solubles for SCT liquefaction of Belle Ayr coal in high and low hydrogen solvents are shown in Tables 3 and 4 respectively.

Examination of the composition of recovered solvent from those runs with high hydrogen solvent (92-26-019) indicates that the hydrogen content decreases with increasing severity and approaches the hydrogen content of the recovered pre-heater effluent solvent after only 6 minutes of reaction (Figure 5). We also observed an increase in the oxygen content in the hexane solubles with increasing severity. The nitrogen content decreased slightly with increasing severity while sulfur content remained relatively constant. The nature of this oxygen has not yet been established.

Structural Changes of Solvent Components. Of the several possible reactions which solvent components can undergo we have examined three:

- cracking of solvent to form gases
- condensation of solvent molecules, and
- alkylation of solvent by coal.

Examination of gas samples taken prior to the injection of coal from our SCT runs with Monterey coal and with low hydrogen solvent indicate that as the severity of the conditions to which the solvent is exposed increases, the amount of paraffins and olefins ($C_1 - C_5$) increases (Figure 6). A gas make of 3.6% was formed in the run of highest severity.

If we then compared the solvents isolated after preheating at low and high severities we find that the solvent which has been subjected to higher severity is shifted to higher boiling point distribution by virtue of the loss of lighter boiling components.

Table 5 shows the composition of the solvents subjected to preheat, the solvent composition based on the percentage of preheated solvent in the total reaction solvent and the composition of the heptane solubles isolated from each reaction. The data shows that the preheated solvents are reduced in percent hydrogen and hydrogen to carbon ratio with increasing severity of preheat. The hydrogen to carbon ratio of the heptane solubles after reaction with coal is essentially the same as that of the solvent (92-03-035 + preheated solvent) which reacted with coal.

Condensation reactions also represent a process by which components of solvent can interact to produce materials of higher boiling point. If recycle solvent is isolated by distillation then condensation can result in loss of solvent range components.

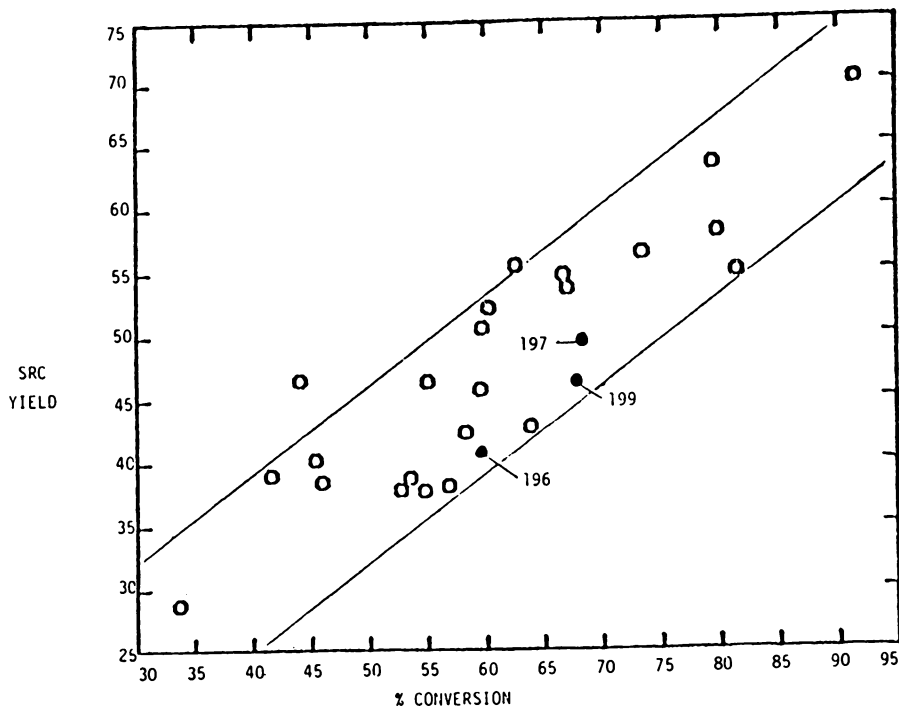


Figure 4. Wyodak SRC vs. conversion

Table 3. Reaction Conditions and Product Analyses. Hydrogenated Recycle Solvent, -019; Hexane Solubles, Belle Ayr Coal

	TEMP (°F)	TIME (MIN)	SEVERITY	H/c	c	H	O	N	S
92-26-019	-	-	-	1.32	87.73	9.67	1.48	0.99	0.1
AC-196	800	2	11	1.31	86.46	9.41	3.05	0.85	0.06
AC-199	800	6	23	1.26	84.24	8.85	5.67	0.78	0.08
AC-197	860	2	23	1.17	81.15	7.92	10.15	0.81	0.09
AC-198	860	6	67	1.11	84.90	7.87	5.98	0.72	0.07

Table 4. Reaction Conditions and Products Analyses. SRC-1 Preheater Effluent Solvent, -035; Hexane Solubles, Belle Ayr Coal

	TEMP (°F)	TIME (MIN)	SEVERITY	H/c	c	H	O	N	S
92-03-035	-	-	-	1.12	87.51	8.15	2.88	1.24	0.39
AC-201	800	2	5.68						
AC-208	860	2	21.78	1.12	87.62	8.20	3.07	0.96	0.07
AC-209	800	6	23.17	1.06	87.31	7.68	3.78	0.82	0.30
AC-210	860	6	63.58	1.07	87.02	7.77	3.60	0.87	0.41

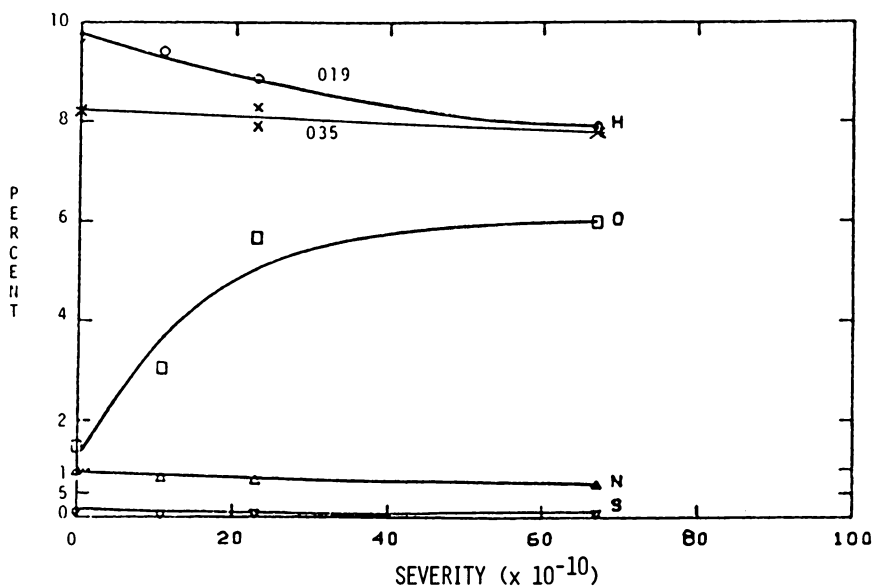


Figure 5. Hydrogen/oxygen/nitrogen/sulfur content vs. severity

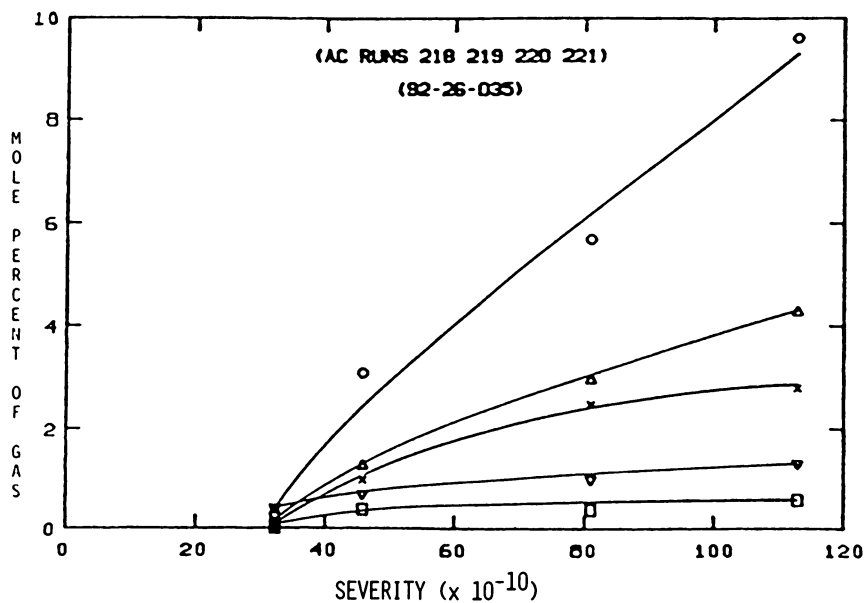


Figure 6. Light gases produced during solvent preheat: methane (○); ethane (Δ); propane (×); propene (∇); ethylene (□).

Table 5. Changes in Solvent CompositionCOMPOSITION OF SOLVENTS - AFTER PREHEAT

	<u>221</u>	<u>220</u>	<u>218</u>	<u>219</u>	<u>035</u>
C	88.45	88.61	88.72	88.54	87.51
H	8.17	7.85	7.53	7.42	8.15
N	0.66	0.58	0.58	0.66	1.24
O	2.13	2.70	2.85	2.77	2.88
S	0.38	0.29	0.36	0.42	0.39
Ash	0.07	0.13	< 0.01	0.15	-
H/C	1.11	1.06	1.02	1.01	1.12
Severity	32.6	45.9	81.06	112.9	-

COMPOSITION OF SOLVENTS - AFTER REACTION WITH COAL

	<u>218</u> <u>Heptane</u> <u>Sol.</u>	<u>221</u> <u>Heptane</u> <u>Sol.</u>	<u>220</u> <u>Heptane</u> <u>Sol.</u>	<u>219</u> <u>Heptane</u> <u>Sol.</u>
C	(87.90) * 85.83	(87.80) 88.30	(87.52) 87.55	(87.30) 86.77
H	(7.95) 7.98	(8.18) 8.24	(8.14) 8.13	(8.11) 8.02
N	(1.03) 1.09	(0.98) .53	(1.06) .58	(1.04) .57
O	(2.87) 4.53	(2.80) 2.68	(3.03) 3.47	(3.21) 4.02
S	(0.38) .43	(0.42) .46	(0.39) .39	(0.42) .48
Ash	(0.09) .14	(0.05) .14	(0.03) .13	(0.02) .07
H/C	(1.09) 1.12	(1.12) 1.12	(1.12) 1.12	(1.12) 1.11
Severity	2.65	2.71	23	65.3

* (Solvent composition based on percentage of preheated solvent in the total reaction solvent)

For example, the solvent products of a liquefaction carried out with a synthetic solvent (80% 2-methyl naphthalene, 18% p-cresol and 2% γ -picoline) were shown (by gc/ms) to have formed a variety of dimeric products. Figure 7 presents the gas chromatogram of this solvent after reaction in which the major components were identified.

It can be seen that the major product 1,2-dinaphthyl ethane results from coupling of the methyl groups of 2-methyl naphthalene. This and other 2-methyl naphthalene condensation products have boiling points above 800°F. Other high boiling products result from the condensation of p-cresol with 2-methyl naphthalene. The same condensation processes occur independently of the coal used though the absolute amounts varied. Such dimers formed preferentially in solvent mixtures in which methyl aromatics were prevalent. As the concentration of tetralin decreased there was an increase in the yield of methyl naphthalene dimers (Figure 8). This was independent of the coal and implies that the quality of the recycle stream must remain high to minimize condensation processes.

We have found in the present work that as the reaction severity is increased the average molecular weight (as measured by FIMS) of the hexane soluble components (solvent) increases for SCT liquefaction. The hexane insolubles do not significantly vary in average molecular weight although a slight decrease is observed.

Some of the chemical transformations which can be responsible for changes in the boiling point of the solvent are disproportionation, dimerization, and condensation. Isomerization, which has been studied in detail by others (4,5) has not been mentioned because although isomerization significantly affects the quality of the solvent, boiling point shifts are minimal.

Disproportionation provides the possibility for modified reactivity of alkyl chains and also produces structures capable of condensing to form heterocyclic rings.

Dimerization and condensation of alkyl aromatics and phenols produce higher boiling polycyclic aromatic hydrocarbons which may not be isolable as recycle solvent.

Alkylation of solvent represents still another pathway for changing the properties of a recycle solvent. If we consider alkylation in terms of the transfer to methyl groups from coal to solvent components, then there are several structural and physical changes that occur to the solvent. Alkylation will increase the hydrogen content of the solvent at the expense of coal since the solvent molecule will have a C-H replaced by C-CH₃. This represents an increase in the aliphatic content and conversely a decrease in the aromatic content of the solvent. Kleinpeter (7) has indicated that alkylation of condensed aromatics is a problem. High aliphatic character will decrease the ability of the solvent to act as a physical solvent for coal liquefaction products.

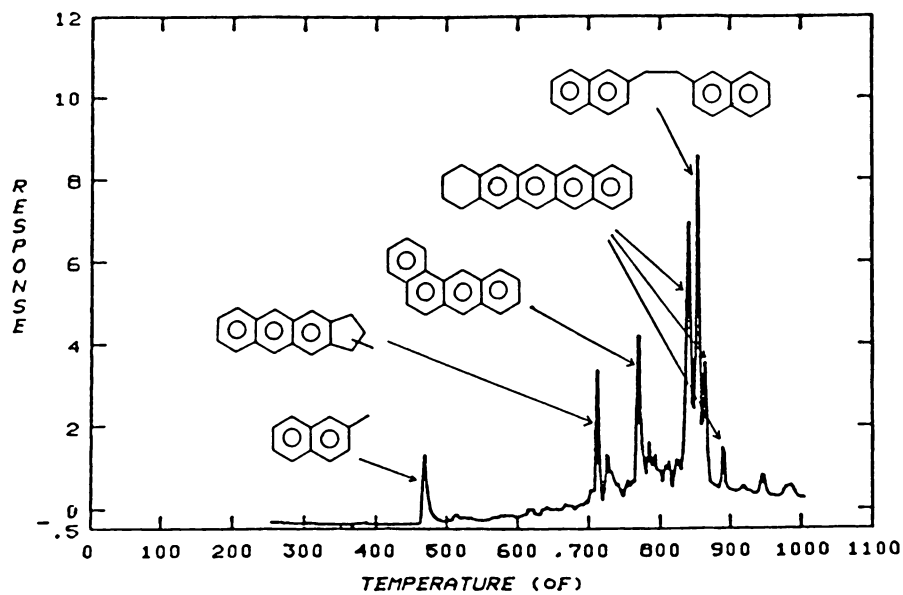


Figure 7. Temperature vs. response of solvent components

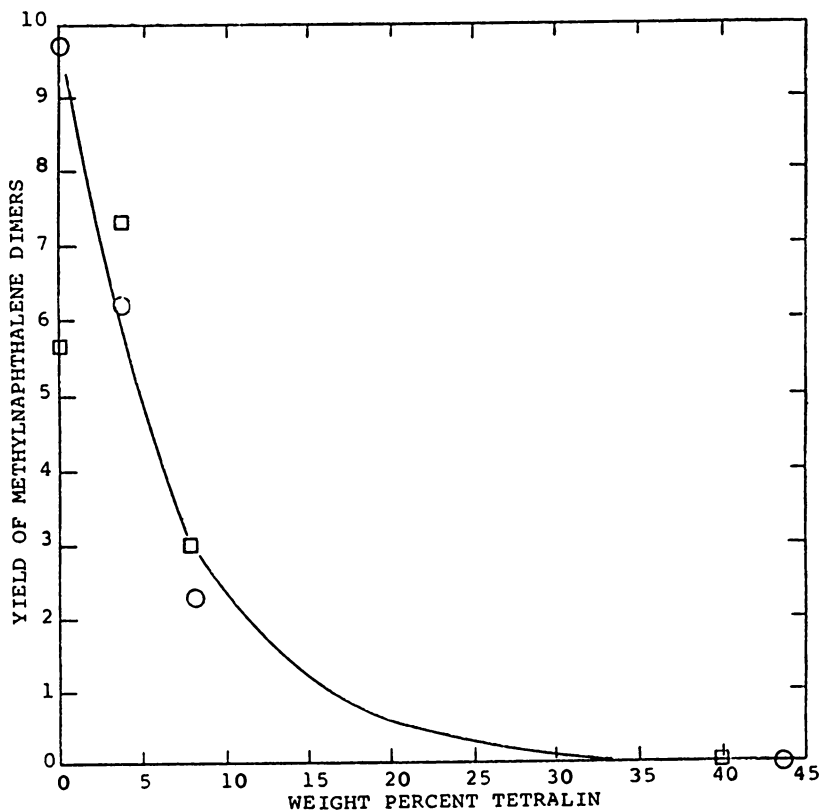


Figure 8. *H*-donors and yield of methylnaphthalene dimers: Wyodak (○); Monterey (□).

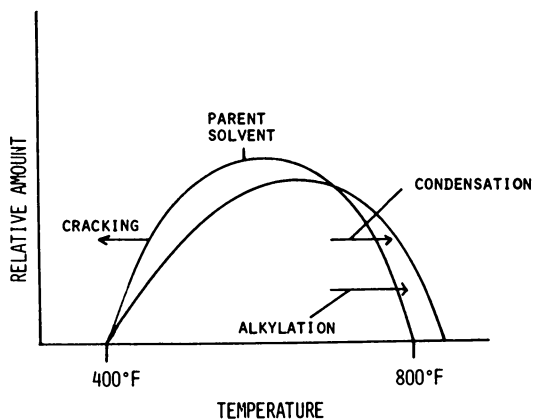


Figure 9. Solvent changes during SCT coal liquefaction

There will also be a small but real increase in the molecular weight of the alkylated aromatic solvent components which result in an increase in the boiling points of these components.

These alkyl aromatics can then further condense and dimerize to produce products of higher boiling point as discussed above. We are presently attempting to estimate the amount of solvent alkylation which occurred in the autoclave runs described above.

In summary, the effects of solvent composition on the liquefaction of Western sub-bituminous coal and the effect that the conditions of the reaction and the coal has on the solvent have been described. Use of our newly defined reaction severity parameter to predict conversion allowed us to compare various liquefaction experiments. A new product isolation procedure useful for SCT conversions, allows separation of SRC from solvent range material. Experiments have been performed in process derived solvents of low and high hydrogen content. Belle Ayr coal conversion up to $\sim 55\%$ was found to be independent of solvent composition. Beyond this point, conversion is responsive to solvent composition with hydrogen donor rich solvents providing higher values. The SRC composition is dependent on solvent composition at all conversion levels and high hydrogen donor solvents produce higher quality products (higher hydrogen content). Not only are there differences in the SRC composition but also in the solvent range material isolated from these runs. Three processes were found to be important in considering the self sufficiency of solvent in liquefaction technology; cracking of the solvent to form gases (which is $\leq 3.6\%$ of solvent used), condensation of solvent components, and alkylation of solvent by coal (Figure 9).

Acknowledgement

This work was conducted under Electric Power Research Institute (EPRI) Contract No. RP-1655 which is jointly funded by EPRI and Mobil Research and Development Corporation. Mrs. L. F. Atherton is the EPRI Project Manager.

The authors are indebted to F. J. Derbyshire, B. O. Heady, G. A. Odoerfer, and P. Varghese who provided considerable consultation and assistance in the progress of this work.

Literature Cited

1. Whitehurst, D. D., Farcasiu, M., Mitchell, T. O., and Dickert, Jr., J. J., "The Nature and Origin of Asphaltenes in Processed Coals," First Report Under EPRI Project RP-410-1, February 1976.
2. Whitehurst, D. D., Farcasiu, M., Mitchell, T. O., and Dickert, Jr., J. J., "The Nature and Origin of Asphaltenes in Processed Coals," Second Annual Report Under EPRI Project RP-410-1, July 1977, and references cited therein.

3. Varghese, P., Derbyshire, F. J. and Whitehurst, D. D., Proceedings of the 1980 Symposium on Instrumentation and Control for Fossil Energy Processes, Virginia Beach, June 1980.
4. Cronauer, D. C., Jewell, D. M., Shah, Y. T., Modi, R. J. and Seshadri, K. S., Ind. Eng. Chem. Fundam., 18, 368 (1979).
5. Ruberto, R. G., Fuel Processing Technology, 3, 7 (1980).
6. Whitehurst, D. D., Proceedings of the Electric Power Research Institute Contractor's Conference on Coal Liquefaction, May 8-10, 1979, Palo Alto, California, and references cited therein.
7. Kleinpeter, J. A. and Burke, F. P., Proceedings of the Electric Power Research Contractor's Conference on Coal Liquefaction, May 8-10, 1979, Palo Alto, California.

RECEIVED March 9, 1981.

Interaction of Naphthalene with Bituminous Coal: An EPR and NMR Study

JOSEPH J. RATTO and IRA B. GOLDBERG

Rockwell International Science Center, Thousand Oaks, CA 91360

Coal, mixtures of coal with naphthalene- d_8 , or mixtures of coal with naphthalene- h_8 were heated at 400°C for periods up to 10 h. After cooling to ambient temperature, the heated coal was investigated by EPR spectrometry, and the reacted naphthalene was investigated by NMR spectrometry. The radical concentrations in the heated coal increased slightly with time, while the radical concentrations in the coal heated with naphthalene increased more rapidly suggesting that the solvent may act as a stabilizing agent for the thermally generated radicals. The g -factors of the samples of treated coal decreased rapidly from the room temperature value of 2.00282 to a constant value in the range 2.00265 ± 0.00003 during the time period from 1 h to 10 h, suggesting that the radicals rapidly become more hydrocarbon in nature. The peak-to-peak linewidths from the coal-naphthalene- d_8 samples were slightly narrower than the linewidths from the coal-naphthalene- h_8 samples, indicating that deuterium was not preferentially incorporated close to the stable radical centers. Significant hydrogen exchange was observed between the coal and naphthalene- d_8 . The incorporation of protium into the α position of naphthalene- d_8 occurred more rapidly than in the β position, and a model was developed to account for the rate of this exchange.

One of the methods used in the production of liquid fuels from coal is to heat coal in the presence of solvents in order to dissolve and stabilize low molecular weight fragments. Many studies (1-6) have been devoted to elucidating the chemical mechanism of product formation in hydrogen donor and non-donor solvents. In most of these studies, the time dependence of the product yield was used as a measure of the rates of reaction, or the product yield was correlated with the solvent, the rank of the coal or other properties of the coal. In order to gain a better understanding of the nature of the coal-solvent interactions, we

0097-6156/81/0169-0173\$05.00/0
© 1981 American Chemical Society

monitored the time dependence of the radical production and the degree of hydrogen exchange between the coal and solvent.

A number of workers (7-15) have used isotope labeling of donor and nondonor solvents to investigate hydrogen transfer, hydrogen exchange reactions between coal and model compounds, and structural rearrangements of the solvent under liquefaction conditions. In this study, Illinois bituminous coal, and mixtures of coal and either naphthalene- d_8 or naphthalene- h_8 were heated at 400°C to examine the time dependence of the reaction between coal and naphthalene. Aromatic hydrocarbons such as naphthalene can partially dissolve coal at a temperature of 350°C. The mechanism of this solvation (6,16) has been attributed to physical break-down of the coal particles due to normal solvent activity and to chemical interaction of the solvent with the coal. This chemical activity may be the result of transfer of hydrogen via solvent from one part of the coal to thermally generated radicals in another part of the coal. Resulting radicals may then be stabilized by the solvent, may rearrange to form low molecular weight products, or may combine with large molecular groups to form chars. To determine the concentration and nature of the radicals in these reactions, the coal and coal products were examined by electron paramagnetic resonance (EPR) spectrometry. Deuterated naphthalene was used to distinguish between hydrogen (2H) originating from the solvent and hydrogen (1H) originating from the coal. Deuterium incorporated into positions in the coal close to radical centers will narrow the linewidth of an EPR absorption. Isotope labeling was also used to measure the exchange of hydrogen between the solvent and the coal. The spent solvent was analyzed by 1H and 2H nuclear magnetic resonance (NMR) spectrometry to follow the exchange process in different structural positions.

Experimental

Materials Illinois No.6 coal (74.5% C, 5.1% H, 1.3% N, 19.1% S and O, by weight, daf basis); 4.0% water and 13.1% ash by weight, -200 mesh was dried at 110°C in vacuum for 4 h prior to use. Naphthalene- d_8 , containing 98.5% 2H enrichment, naphthalene- h_8 (Aldrich Chemical Co.) and anhydrous ethyl ether (J.T. Baker Chemical Co.) were used. NMR analysis showed that the starting naphthalene- d_8 contained 1.5% 1H ; 0.9% was in the α position and 0.6% was in the β position.

Sample Preparation Multiple samples from Sets 1-4 were prepared. **Set 1:** A 30 mg sample of coal was evacuated for 18 h at < 0.2 Pa (10^{-4} torr) and sealed in a 4.4 mm o.d., 12 cm long quartz tube. **Sets 2 and 3:** Coal and naphthalene- d_8 (Set 2) or coal and naphthalene- h_8 (Set 3) were mixed in a 1:1 weight ratio. A 150 mg sample was placed in a 6.5 mm o.d., 15 cm long thick-walled pyrex tube. The tube was cooled in liquid nitrogen, evacuated at < 0.2 Pa for 15 min, closed to vacuum, then allowed to

warm to room temperature. These steps were repeated three times before sealing the sample under vacuum. Set 4: A 60 mg sample of coal and naphthalene- d_8 was degassed as described for Sets 2 and 3 and was sealed in a 4.4 mm o.d., 12 cm long quartz tube.

Experimental Procedure The four sets of samples were heated for different lengths of time, ranging from 10 to 600 min in a Marshall cylindrical furnace at 400°C. The glass tubes were attached lengthwise to a rod extending through the furnace which was tilted at an angle of 20° from the horizontal position. The tubes were rotated at 200 rpm to provide agitation. The times required for sample heat-up and cool-down between 25°C and 400°C were respectively 200 s and 80 s. After cool-down, Sets 1 and 4 were examined unopened by EPR spectrometry. Samples from Set 1 were repeatedly heated and re-examined by EPR spectrometry at room temperature. Sets 2 and 3 were opened, and the reacted naphthalene was extracted from the sample with ethyl ether at ambient temperature. Based on the initial and final weights of the coal, less than 4 mg (~ 5 wt%) of coal was extracted from the spent coal using this procedure. The remaining spent coal was evacuated at < 0.2 Pa for 18 h and sealed under vacuum in quartz tubes for analysis by EPR spectrometry. Based on the initial weight, the amount of spent naphthalene extracted from the coal ranged from 70-95 wt%. The spent naphthalene was sublimed, and the naphthalene was examined by NMR spectrometry.

NMR and EPR ^2H and ^1H NMR spectra of naphthalene samples were obtained with a JEOL FX-60-Q spectrometer at 9.18 MHz and 59.79 MHz, respectively. Spectra were accumulated in the free induction decay mode and were reconstructed by Fourier transform. A 45° pulse interval was used corresponding to 75 μs for ^2H and 14 μs for ^1H . Chloroform and acetone- d_6 or chloroform- d were used as ^1H or ^2H NMR solvents with TMS as reference for ^1H NMR spectra. Samples were contained in 10 mm o.d. quartz tubes, and the probe temperature was 30°C. Quantitative measurements were made using p -dioxane- d_8 (^2H) and p -dioxane (^1H) as internal standards. Transforms and numerical integrations were obtained using software supplied by JEOL, Inc. EPR measurements were made at 9.533 GHz using a TE₁₀₄ mode dual sample cavity. The computer-controlled spectrometer and the integration techniques have been described elsewhere (17). Data analysis was carried out with off-line BASIC programs to determine the double integral, g -factor and linewidth (ΔHpp). Less than 250 μg of diphenylpicrylhydrazyl (95%) were used to calibrate the spectrometer. The Curie temperature of the standard was assumed to be -26 K. Sample sizes were selected to ensure that the cavity was not overloaded, which would cause non-linear response of the EPR signal (18). g -Factors were measured against Mn^{2+} in CaO (19). The magnetic field at which the derivative of the absorption crossed the baseline of the spectrum was selected for the determination of the g -factor.

Results and Discussion

EPR Measurements of Heated Samples The EPR spectrum of the unheated coal (Figure 1a) is composed of a sharp and a broad spectral component. The narrow component has a larger signal amplitude than the broader one and almost obscures the high field lobe of the broader component. This sharp component has been attributed to fusains in the coal (20), while the broad component has been associated with exinite and vitrains (21). When the coal or mixtures of coal and naphthalene are heated, the intensities of the sharp component decreases relative to that of the broad component. This appears to occur: (a) because the linewidth of the broader peak decreases so that the amplitude of the derivative increases thereby masking the sharp component, and (b) because the intensity of the sharp component decreases. Both sharp and broad components were observed only for the coal in the absence of non-donor solvent. The presence of oxygen can cause considerable broadening of the linewidths; therefore, the measurements must be made after removing oxygen in order to observe details of the spectra.

Radical Concentrations The number of radicals relative to the concentration in unheated coal was determined from the susceptibility according to the Curie-Weiss law (22). The radical concentrations from Set 1 are shown in Figure 2. The repeated heating of a single coal sample is shown by the lines connecting the data points. In general, as the coal sample is heated for longer periods, more radicals are produced as shown by the upward trend of the data points between the pairs of dotted and broken lines. Samples of coal heated for a short period of time (10-15 min) show a slight reduction in the number of radicals even after cooling to room temperature. A maximum of 40% more radicals were present after heating for 120 min. Grandy and Petrakis (23) reported a seven-fold increase of the radical concentration of a Powhatan No. 5 HVb coal on heating to 450°C with 10.35 Pa of hydrogen measured at the elevated temperature in a rapid heat-up EPR cavity. Reheating our samples of coal resulted in a slight increase or virtually no change in the radical concentration. On the other hand, fresh samples heated for 25 to 120 min show a significant increase in the number of radicals produced. It is difficult to ascertain the experimental scatter of these samples. Double integrals were reproducible to ca. $\pm 2\%$; however, heating and rotation of the samples can cause a redistribution of the paramagnetic material within the sample tube during reaction. This can cause considerable scatter in the data, and we have no way to evaluate this source of error.

The number of radicals produced after heating the coal samples from Sets 2 and 3 relative to the radicals present in unheated coal are shown in Figure 3. These coal samples were separated from the solvent and sealed under vacuum before the EPR measurements were made. The broken and dotted lines indicate the general

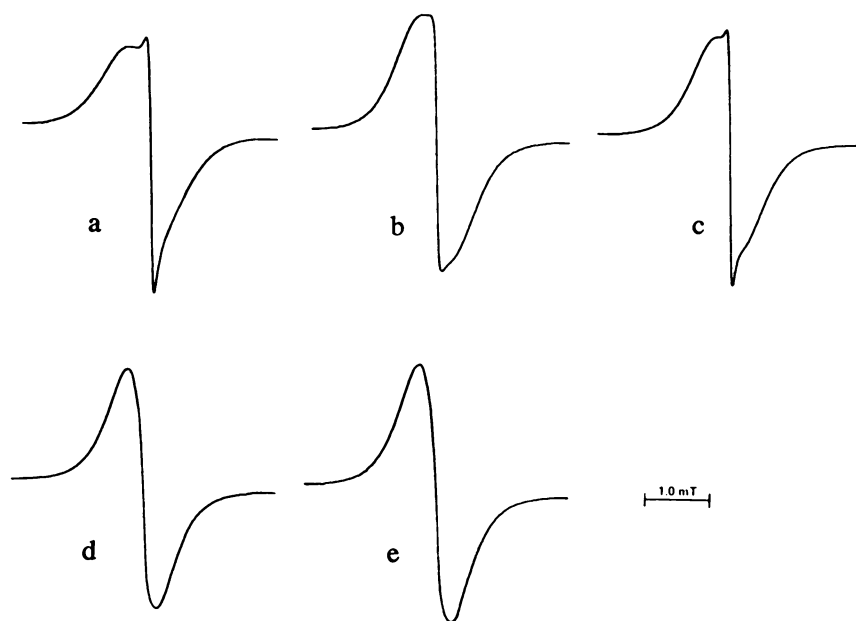


Figure 1. EPR spectra of coal, coal-naphthalene- h_8 and coal-naphthalene- d_8 heated at 400°C: a. unheated coal; b. coal heated for 30 min; c. coal heated for 10 h; d. coal heated with naphthalene- d_8 for 10 h; e. coal heated with naphthalene- h_8 for 10 h.

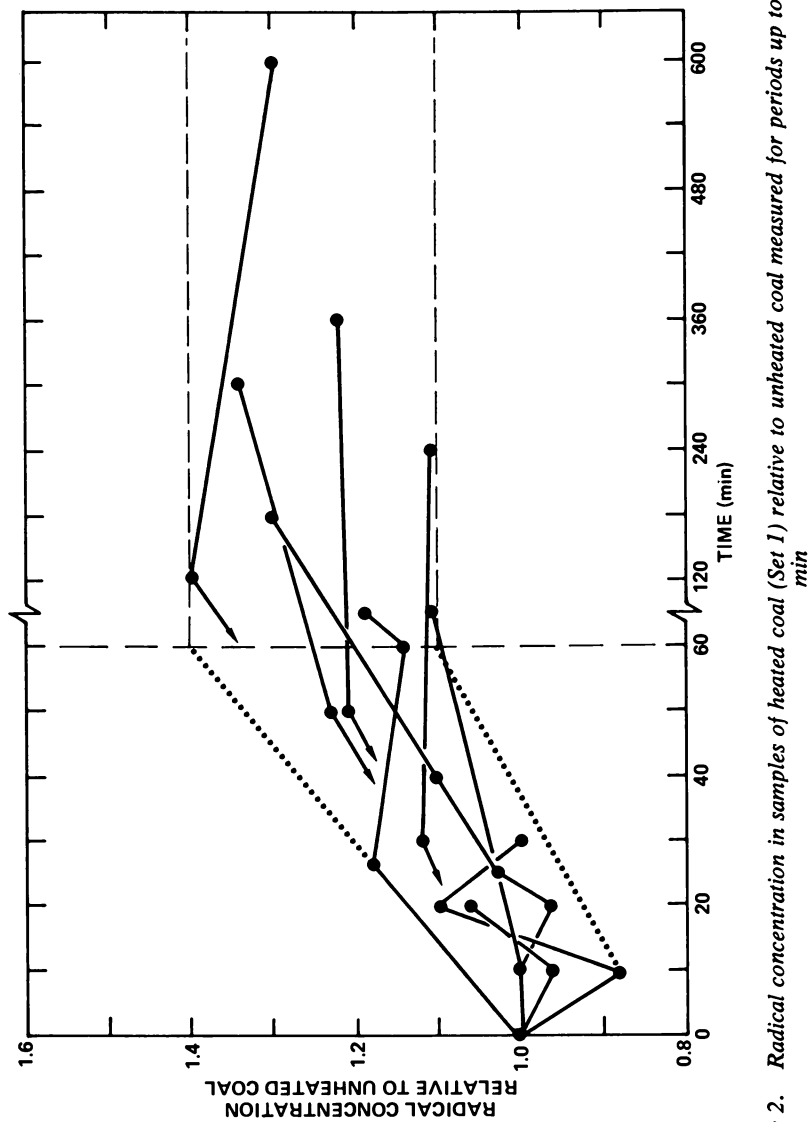


Figure 2. Radical concentration in samples of heated coal (Set 1) relative to unheated coal measured for periods up to 600 min

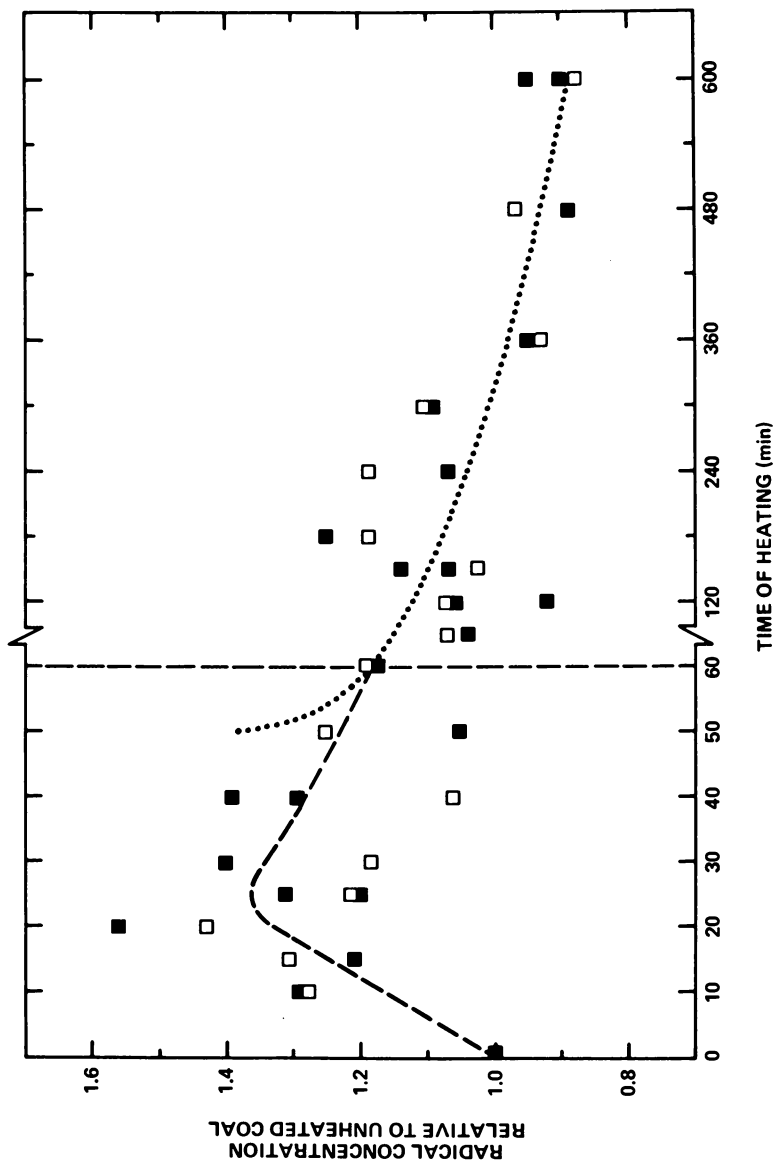


Figure 3. Radical concentration in samples of coal heated with naphthalene- d_8 (Set 2, \blacksquare) or naphthalene- h_8 (Set 3, \square) relative to unheated coal measured for periods up to 600 min

trend of the data. The greatest change of the radical concentration occurs within the first hour. The relative radical concentration increases to a maximum of approximately 1.3 to 1.4 after 25 min. The concentration then slowly decreases to ca. 1.2 after 60 min and to ca. 0.9 after 600 min. This steady decrease in the concentration of the radicals after 25 min is consistent with the hypothesis (6,16) that naphthalene acts as a hydrogen transfer agent, that is, hydrogen is transferred from one part of the coal to thermally generated radicals in another part. Resulting naphthyl radicals can either continue the chain or end it by forming other products. A discussion of the stability of the naphthyl radicals is given elsewhere (14). Some of the reduction in radical concentration may also occur by combination of dissolved radicals derived from the coal or by combination of these radicals with either heterogeneous coal or other dissolved radical species.

g-Factors The g-factors of samples from Sets 1-4 are shown in Figure 4. In general, the sets of data parallel each other with the g-factors of Set 4 \approx Set 2 $>$ Set 3 $>$ Set 1. To show the general trends, lines are drawn through the data from the heated coal-naphthalene mixtures (\blacksquare , \square , and Δ) and through the data from the heated coal (\bullet). Although no measurements were made on the coal heated between 0 and 10 min because of the finite heat-up time, there is a large difference between the room temperature value (2.00282 ± 0.00002) and the values obtained after 10 min of heating each of the four sets ($2.00263 - 2.00268$). This suggests that the concentration of heteroatom containing radicals decreases rapidly during the first few minutes of heating. Other workers (22,24,25) have described similar behavior for heated coals.

The average value of the g-factors of samples of coal heated between 1 h and 10 h is 2.00263 with a standard deviation of 0.00003. This indicates that only small structural changes, if any, occur. Studies of unsubstituted aromatic hydrocarbon radicals (26,27) have shown that either neutral radicals or radical ions of large size should exhibit g-factors of 2.00262 ± 0.00001 . σ -Radicals are expected to exhibit g-factors smaller than 2.00262. Thus, it is possible that the radicals in heated coal are π -aromatic, of neutral charge, and contain very little heteroatom character. g-Factors of coals heated with naphthalene (Sets 2 and 3) are larger (2.00266 to 2.00270) but parallel the g-factors of the heated coal (Set 1), suggesting that these radicals may have significantly larger heteroatom content; they may be stabilized by the solvent. Part of the difference between g-factors of Sets 2 and 3 (ca. 0.00003 units) may be an artifact due to the different line shapes (Figure 1); the broader line of Set 3 allows more weight to the sharper spectral component at the point at which the derivative crosses the baseline. g-Factors of the samples from Sets 2 and 3 increase after heating between 8 to 10 h as shown by the dotted line in Figure 4. A possible explanation for this increase is that radicals are formed in the coal after long

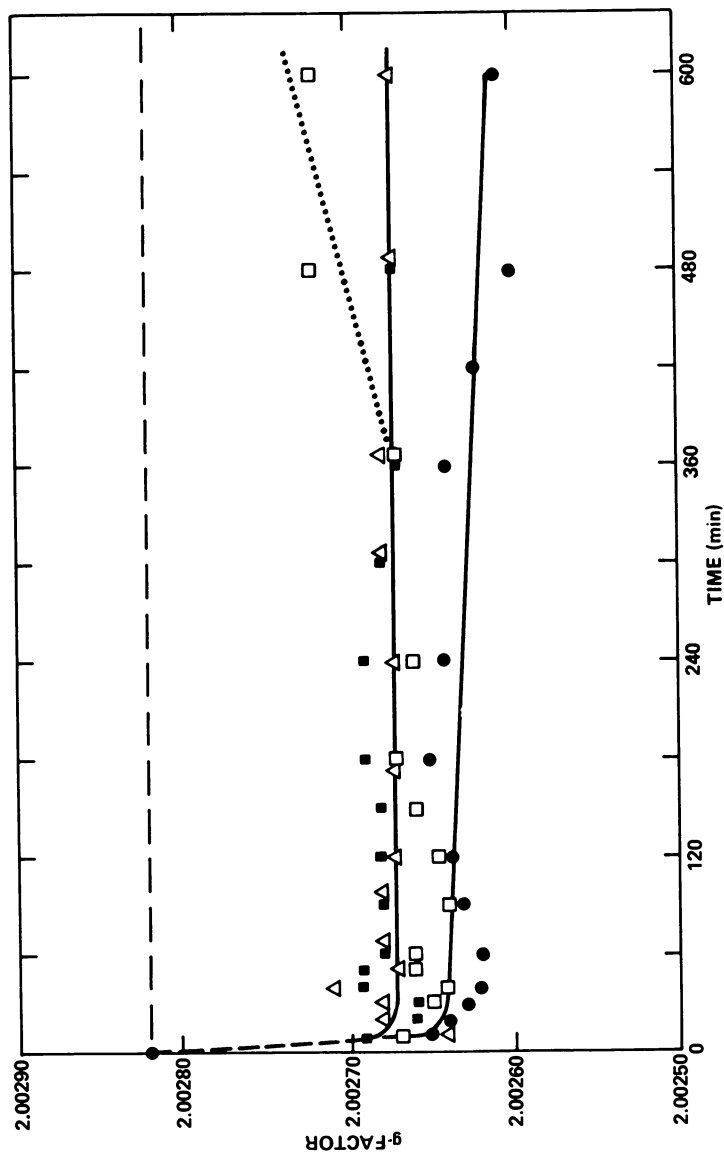


Figure 4. The g -factors of Illinois No. 6 coal heated for the same periods of time under different conditions: Set 1, ●, coal heated in sealed tubes; Set 2, ■, coal heated with naphthalene- d_8 ; Set 3, □, coal heated with naphthalene- h_8 ; Set 4, △, coal heated with naphthalene- d_8 and unopened.

heating times which react irreversibly with oxygen or the solvent on exposure at ambient temperature thus increasing the g-factors. Lewis and Singer (28) have reported the measurement of the g-factors of 25 aryloxy radicals. The g-factors varied between 2.0032 and 2.0040.

The samples from Sets 2 and 4 can be compared to examine the effect of exposure of the spent coal to air before resealing under vacuum followed by measurement of the g-factors and linewidths. The samples from Set 2 were opened, and the samples from Set 4 were unopened. As shown in Figure 4, the g-factors from Set 4 are equal to the g-factors from Set 2 within experimental uncertainty. This indicates that exposure to air and solvent at ambient temperature does not significantly affect the g-factor of the product. If oxygen does have an effect on the radicals in the sample, those radicals which are changed are not detected. This result indicates that peroxy radicals, if formed, do not influence these measurements.

Linewidths The EPR spectra of the spent coal samples from Sets 1-4 contained both sharp and broad components. Several examples are shown in Figure 1. The measured values are shown in Figure 5. The sharp component was only observable for Set 1 over the entire range of heated samples. It decreases slightly from 0.13 mT (1 mT = 10 Oe) after heating for 20 min to 0.09 mT after heating for 600 min. The sharp components of the spectra of heated coal-naphthalene mixtures (Sets 2 and 3) could be measured only for samples heated for up to 40 min before being obscured by the high field lobe of the broad component of the derivative spectrum. These values were very close to the values of the heated coal samples, Set 1.

The linewidths (ΔH_{pp}) of the broad component from Set 1 decrease rapidly during initial heating and are constant at 0.45 ± 0.02 mT for samples heated from 10 to 600 min. ΔH_{pp} of the broad component of Sets 2 and 3 are much broader initially, starting at 0.68 mT (10 min) and decreasing to 0.49 mT (180 min). ΔH_{pp} of Set 2 decreased further to 0.45 mT after 600 min of heating while that of Set 3 remained constant at 0.49 mT.

In Figure 4, the values of ΔH_{pp} from Set 4, sealed samples of heated coal-naphthalene- d_8 which have not been exposed to air, parallel the values of ΔH_{pp} from Set 2, the corresponding separated samples exposed to air, but those of Set 2 are much broader. This broadening may be due to the samples irreversibly absorbing oxygen from the air during the extraction of naphthalene. This result suggests that even prolonged evacuation does not remove all of the oxygen from the coal product. It is also possible that exposure to the solvent causes some change in the environment of the radical, although the g-factors suggest that the radicals are chemically equivalent.

Linewidths of radicals can reflect the degree of delocalization of an unpaired electron in an aromatic radical and the extent

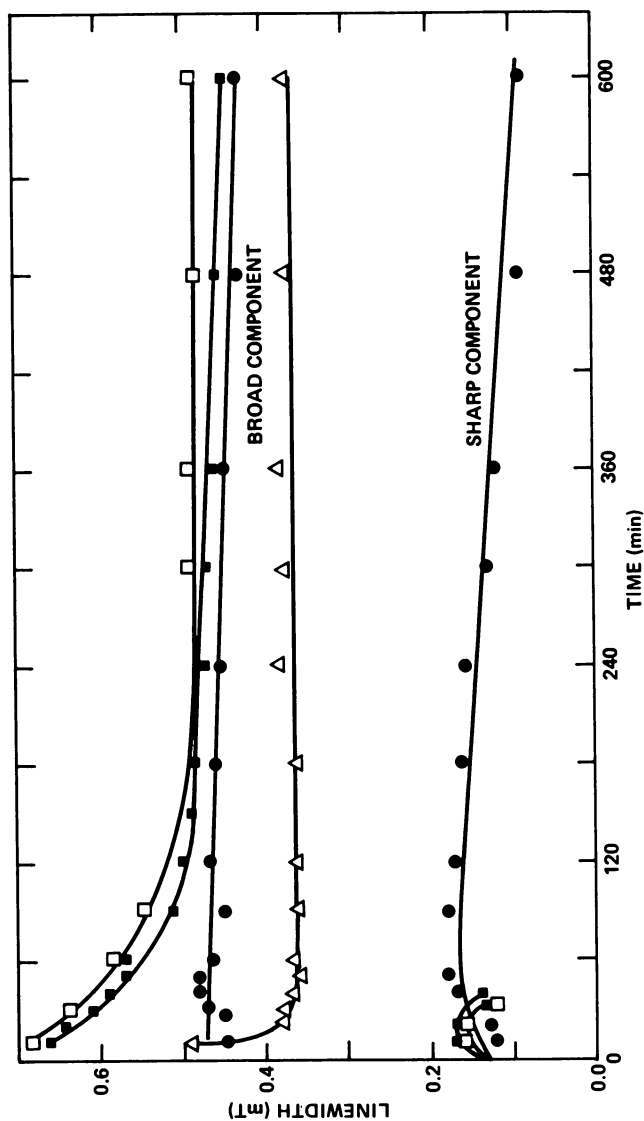


Figure 5. Peak-to-peak linewidths of coals heated for different periods of time: Set 1, ●, coal heated in sealed tubes; Set 2, ■, coal heated with naphthalene- d_8 ; Set 3, □, coal heated with naphthalene- d_8 ; Set 4, △, coal heated with naphthalene- d_8 and unopened.

of hydrogen incorporation. A hydrogen atom bonded to a carbon atom in a π -electron system exhibits a hyperfine splitting which is proportional to the fraction of electron spin density on that trigonal carbon. As the electron becomes more delocalized, the linewidth tends to narrow for two reasons: (a) The spin density on each carbon decreases so that each hyperfine splitting due to hydrogen is smaller, and the number of hydrogen atoms interacting with the electron increases, so that the spectral density increases in the region in which the total nuclear spin is near zero. (b) A consequence of increased delocalization is that the radical contains a higher proportion of tertiary (bridgehead) carbon atoms so that spin density is consumed without a corresponding increase of hyperfine interactions. A reduction in the number of β hydrogen atoms (bonded to carbon atoms α to the aromatic system) will also decrease the linewidth. This occurs because of fewer hyperfine interactions which result from the interaction of the spin on the trigonal carbon with two or three hydrogens. Applying this reasoning to coal samples of Sets 1 and 3 indicates that coal heated without solvent forms more highly conjugated systems than the coals heated with solvent. This is also supported by the lower g-factor.

Deuterium labelling permits the extent of hydrogen incorporation near the radical centers to be estimated. Sample Sets 2 and 3 were treated identically, except that in Set 2, naphthalene- d_8 was used as a solvent, while in Set 3, naphthalene- h_8 was used. If the only source of linewidth of the coal is due to inhomogeneous hyperfine broadening, as described above, and if all of the 1H in the coal is replaced by 2H , the linewidth should decrease by a factor of 3.25 (22). After heating for 10 h, 21.1% of the 2H in the naphthalene of Set 2 is replaced by 1H (see Figure 6). Based on this amount of 2H being incorporated in the coal, the linewidth of Set 2 should be about 0.03 mT [(1/3.25) (.211)(.49 mT)] smaller than that of Set 3 after heating for 10 h. The experimental difference is 0.04 mT, which is close to the predicted amount. This result suggests that exchange is not significantly preferential near the sites of the stable radical products, in contrast with results obtained for autoclave experiments (22) in which coal was heated with D_2 and Tetralin- d_{12} .

Exchange of Hydrogen Between Coal and Naphthalene Incorporation of 1H into the α and β positions of naphthalene- d_8 as measured by 1H NMR spectrometry is shown in Figure 6. Progressively more protium was found to be incorporated into the naphthalene- d_8 solvent as the reaction time was increased. During the first few minutes, the incorporation in both positions occurred more rapidly than later in the reaction. Throughout the measured duration of the reactions, the rate of incorporation of protium into the α position was more rapid than in the β position.

If we define the total hydrogen (deuterium and protium) in either the α and β positions as unity, so that f_α or f_β represent

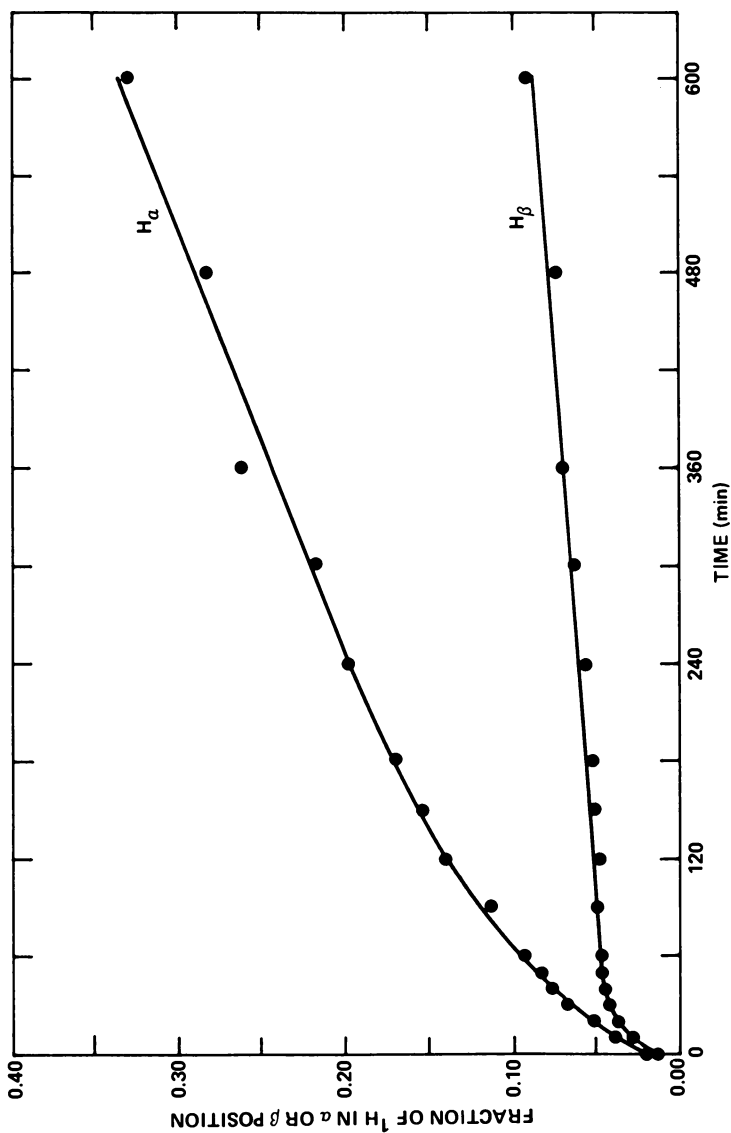
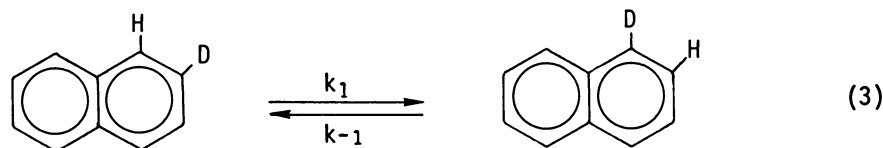
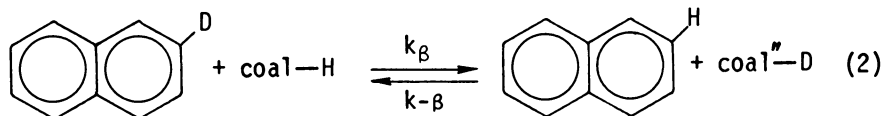
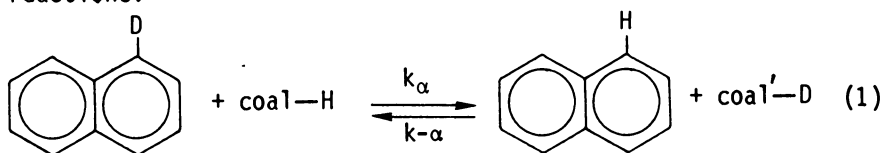


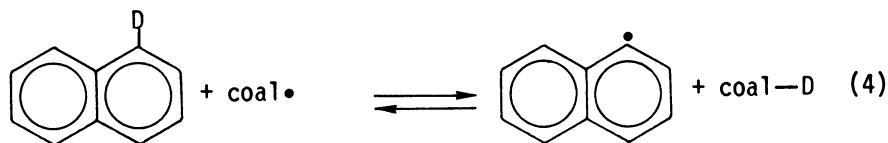
Figure 6. Fraction of protium incorporated in the α and β positions of naphthalene- d_8 as a function of reaction time. The fraction of $^1\text{H}_\alpha$ and $^1\text{H}_\beta$ is defined such that $^1\text{H}_\alpha + ^2\text{H}_\alpha = 1.0$ and $^1\text{H}_\beta + ^2\text{H}_\beta = 1.0$.

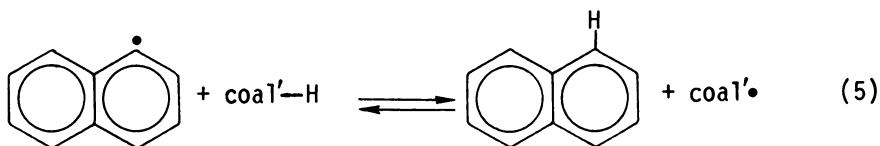
respectively the fraction of protium in the α or β positions, then the respective fractions of deuterium are given by $1 - f_\alpha$ and $1 - f_\beta$. After heating for 600 min, f_α increased from 0.018 to 0.33, while f_β increased from 0.012 to 0.092. This represents an increase from 1.5% [$100 \cdot (0.018 + 0.012)/2$] protium to 21.1% protium. Our measurement of f_α is equal to 0.138 after 60 min and is close to the value of 0.108 reported (14) for naphthalene-d₈ and HVB Loveridge Mine, Pittsburgh Seam coal heated in an autoclave reactor at conditions of 1 h and 400°C.

A simple chemical model to interpret the data in Figure 6 is based on the following chemical mechanism for the exchange reactions:



The α -hydrogen exchange, Reaction 1, and the β -hydrogen exchange, Reaction 2, are interrelated by a 1,2-hydrogen exchange as shown in Reaction 3. Each of these reactions may be more complicated than that shown above, since they probably involve solvent or coal radical intermediates. In reactions 1 and 2, for example, the coal probably abstracts $^2\text{H}^\bullet$ from the naphthalene-d₈ to form a naphthyl radical, and subsequently the naphthyl radical abstracts $^1\text{H}^\bullet$ from a different part of the coal as shown in Reactions 4 and 5:





By using the additional simplifying assumptions that the number of active coal sites remains constant during the reaction and that the forward and reverse rate coefficients are equal, $k_{\alpha} = k_{\alpha}^{-1}$, $k_{\beta} = k_{\beta}^{-1}$ and $k_1 = k_1^{-1}$, then the rate equations for the incorporation of ^2H into the α and β positions of naphthalene reactions can be written

$$\frac{df_{\alpha}}{dt} = k_{\alpha} N_{\text{C}} f_{\text{C}} - k_{\alpha} N_{\text{C}} f_{\alpha} - k_1 N_{\beta} (f_{\alpha} - f_{\beta}) \quad (6)$$

and

$$\frac{df_{\beta}}{dt} = k_{\beta} N_{\text{C}} f_{\text{C}} - k_{\beta} N_{\text{C}} f_{\beta} - k_1 N_{\alpha} (f_{\beta} - f_{\alpha}) \quad (7)$$

where the first term of Reactions 6 and 7 is the forward rate, the second term is the reverse rate, and the third term is the 1,2-hydrogen exchange rate. In these equations, f_{C} is the fraction of active sites in the coal substituted with protium, and N_{α} , N_{β} and N_{C} are the number of active sites in the naphthalene and coal respectively.

If all of the protium and deuterium remains in the reactive components, the conservation of protium can be written

$$f_{\alpha} N_{\alpha} + f_{\beta} N_{\beta} = (1 - f_{\text{C}}) N_{\text{C}} \quad (8)$$

Since $N_{\alpha} = N_{\beta}$, solving for f_{C} we obtain

$$f_{\text{C}} = 1 - (f_{\alpha} + f_{\beta}) \frac{N_{\alpha}}{N_{\text{C}}} \quad (9)$$

This can be substituted into Equations 4 and 5 to give

$$\frac{df_{\alpha}}{dt} = k_{\alpha} N_{\text{C}} \left[1 - f_{\alpha} \left(\frac{N_{\alpha}}{N_{\text{C}}} + 1 \right) - f_{\beta} \frac{N_{\alpha}}{N_{\text{C}}} \right] - k_1 N_{\alpha} (f_{\alpha} - f_{\beta}) \quad (10)$$

and

$$\frac{df_{\beta}}{dt} = k_{\beta} N_C \left[1 - f_{\beta} \left(\frac{N_{\alpha}}{N_C} + 1 \right) - f_{\alpha} \frac{N_{\alpha}}{N_C} - k_1 N_{\alpha} (f_{\beta} - f_{\alpha}) \right] \quad (11)$$

The exact solutions of Equations 10 and 11 can be obtained by Laplace transforms or the solution of simultaneous differential equations. The resulting coefficients of f_{α} and f_{β} are very complex functions of k_1 , k_{α} , k_{β} , N_{α} and N_C . However, as seen in Figure 6, the reactivity of the β position is small relative to the α position. Thus, in the limiting condition where f_{β} is close to the initial value and neglecting exchange between the α and β positions,

$$\frac{df_{\alpha}}{dt} \approx k_{\alpha} N_C \left[1 - f_{\alpha} \left(\frac{N_{\alpha}}{N_C} + 1 \right) \right] \quad (12)$$

Integrating with respect to f_{α} , gives

$$\ln \left[1 - f_{\alpha} \left(\frac{N_{\alpha}}{N_C} + 1 \right) \right] = k_{\alpha} (N_C + N_{\alpha}) t \quad (13)$$

As an upper limit of the amount of active hydrogen in the coal, we can assume that all hydrogen in coal is equally active; then N_{α}/N_C equals 0.5 under these experimental conditions. A plot of $\ln [1 - 1.5 f_{\alpha}]$ versus time showed that the general form of Equation 13 is obeyed, and $k_{\alpha} (N_C + N_{\alpha}) \approx 2.0 \times 10^{-5} \text{ s}^{-1}$ in the entire period of 10 h. Although this value is related to the rate constant k_{α} , it can not be directly compared with other rate constants involving model compounds under homogeneous conditions. As a qualitative comparison, some first order rate constants of reactions of Tetralin have been measured at 400°C: the decomposition of tetralin to form naphthalene - $4.8 \times 10^{-7} \text{ s}^{-1}$ and the rearrangement of tetralin to 1-methylindan - $9.4 \times 10^{-7} \text{ s}^{-1}$; the transfer of hydrogen from Tetralin to : benzothiophene - $4.7 \times 10^{-8} \text{ s}^{-1}$, indole at 425°C - $2.0 \times 10^{-6} \text{ s}^{-1}$, and benzofuran - $2.7 \times 10^{-6} \text{ s}^{-1}$ (29). Although the decomposition of Tetralin to form naphthalene or 1-methylindan and the hydrogen transfer reactions of tetralin with model compounds appear to be slower than the exchange of the hydrogen in naphthalene with the hydrogen in coal, these reactions are homogeneous while the coal-naphthalene reaction is heterogeneous. We are investigating the rate of transfer and exchange of hydrogen in the coal-Tetralin system in order to compare it with the coal-naphthalene system.

Structural Analysis of the Spent Solvent The spent naphthalene-h₈, extracted from the spent coal with ethyl ether, was examined for hydrogenation or dimerization of the solvent. No dihydronaphthalene or Tetralin were detected by ¹H NMR spectrometry.

Conclusions

Heating coal or mixtures of coal-naphthalene at 400°C provided useful information about changes in the thermally generated radicals. The radical concentrations, g-factors and linewidths from the samples of heated coal (baseline measurements) and the samples of heat coal-naphthalene were compared to study the effect of solvent interaction with the coal. After a few minutes of heating, the g-factor of the heated coal approached the value of 2.00263, which is close to the g-factor of a small, neutral or a large, ionic π -aromatic radical. The g-factors of the coal and naphthalene samples were on the average slightly greater than those of the coal samples. The broad linewidths of the coal samples were constant at 0.45 ± 0.02 mT, while the linewidths of the coal-naphthalene samples initially decreased to 0.37 mT, were constant from 10 min to 7 h, then increased slightly between 7 h to 10 h. The linewidths of the samples of heated coal exposed to air at room temperature were irreversibly broadened, even after evacuating the samples to < 0.2 Pa for 18 h.

The spent naphthalene- h_8 was examined by 1H NMR for structural changes in the solvent. No hydrogenation of the naphthalene was detected. The naphthalene- d_8 was examined to determine the amount of deuterium which was exchanged with protium in the coal. After 10 h, 21.1% of the deuterium in the α and β positions of naphthalene had exchanged. The α position was the most active position for exchange.

By examining the narrowing of the linewidths of the coal-naphthalene- d_8 samples compared to the coal-naphthalene- h_8 samples, it was found that deuterium was not preferentially incorporated close to stable radical centers in the coal. A model was developed to interpret the exchange process, and a rate of exchange in the α position was calculated to be $k_\alpha(N_c + N_\alpha) \cong 2.0 \times 10^{-5} s^{-1}$.

Acknowledgement

The authors gratefully acknowledge K.E. Chung for helpful discussions.

Literature Cited

1. R.C. Neavel, *Fuel* **55** 237 (1976).
2. W.H. Wiser, *Fuel* **47** 237 (1976).
3. M.B. Abdel-Beset, R.F. Yarzeb and P.H. Given, *Fuel* **57** 89 (1978).
4. S.R. Gun, J.K. Sama, P.B. Chowdhua, S.K. Mukherjee and D.K. Mukherjee, *Fuel* **58** 171, 176 (1979).
5. I. Mochida, A. Tokorabe and K. Takeshita, *Fuel* **58** 17 (1979).
6. L.A. Heredy and P. Fugassi, in "Coal Science" P.H. Given, Ed., *ACS Advances in Chemistry Series 55*, 1966; p 448.

7. J.A. Franz, *Fuel* 58(6) 405 (1979).
8. B.M. Benjamin, E.W. Hagamon, V.F. Raaen, and C.J. Collins, *Fuel* 58(5) 386 (1979).
9. C.J. Collins, V.F. Raaen, B.M. Benjamin, P.H. Maupin and W.H. Roark, *J. Amer. Chem. Soc.* 101(17) 5009 (1979).
10. D.C. Cronauer, D.M. Jewell, Y.T. Shah and R.J. Nodi, *Ind. Eng. Chem. Fundam.* 18(2) 153 (1979).
11. D.C. Cronauer, D.M. Jewell, Y.T. Shah and R.J. Nodi, *Ind. Eng. Chem. Fundam.* 18(4) 368 (1979).
12. D.C. Cronauer, D.M. Jewell, R.J. Nodi, K.S. Seshadri and Y.T. Shah, in "Coal Liquefaction Fundamentals," D.D. Whitehurst, Ed., *ACS Symposium Series* 139, 1980; p 371.
13. H.-H. King and L.M. Stock, *Fuel* 59(6) 447 (1980).
14. J.J. Ratto, L.A. Heredy and R.P. Skowronski, in "Coal Liquefaction Fundamentals," D.D. Whitehurst, Ed., *ACS Symposium Series* 139, 1980; p 347.
15. R.P. Skowronski, J.J. Ratto, and L.A. Heredy, "Proceedings of Atomic and Nuclear Methods in Fossil Energy Research," Conference held Dec. 1-4, 1980, Mayagvez, Puerto Rico, to be published.
16. D.D. Whitehurst, M. Farcasiu, T.O. Mitchell, and J.J. Dickert, Jr., "The Nature and Origin of Asphaltenes in Processed Coals," Annual Report, 1977, Mobil Research and Development Corp., Princeton, New Jersey, Report EPRI AF-480.
17. I.B. Goldberg, H.R. Crowe, and R.S. Carpenter, II, *J. Magn. Res.* 18 84 (1975).
18. I.B. Goldberg and H.R. Crowe, *Anal. Chem.* 49 1353 (1977).
19. J. Rubio, E. Munoz, J. Boldu O., Y. Chen, and M.M. Abraham, *J. Chem. Phys.* 70 633 (1979).
20. D.E.G. Austen, D.J.E. Ingram, P.H. Given, C.R. Binder and L.W. Hill, in "Coal Science," P. H. Given, Ed., *Adv. Chem. Series* 55 1966; p 344.
21. H.L. Retcofsky, J.M. Stark and R.A. Friedel, *Anal. Chem.* 40 1699 (1966).
22. I.B. Goldberg, H.R. Crowe, J.J. Ratto, R.P. Skowronski and L.A. Heredy, *Fuel* 59 133 (1980).
23. D.W. Grandy and L. Petrakis, *J. Magn. Res.* 41(3) 367 (1980).
24. L. Petrakis and D.W. Grandy, *Anal. Chem.* 50 303 (1978) and *Fuel* 59 227 (1980).
25. H.L. Retcofsky, private communication.
26. B.G. Segal, M. Kaplan, and G.K. Fraenkel, *J. Chem. Phys.* 43 4191 (1965); R.D. Allendoerfer, *J. Chem. Phys.* 55 3615 (1971).
27. K. Mobius, *Ber. Bunsenges, Phys. Chem. A* 20 1102 (1965).
28. I.C. Lewis and L.S. Singer, Abstracts of 22nd Rocky Mt. Conference on Analytical Chemistry, Denver, CO, Aug 10-14, 1980.
29. R.G. Mallinson, K.C. Chao, and R.A. Greenkorn, *ACS Fuel Div. Preprints* 25(4) 120 (1980).

RECEIVED May 27, 1981.

Coal Mineral Matter Catalysis in Liquefaction

BRADLEY C. BOCKRATH and KARL T. SCHROEDER

U.S. Department of Energy, Pittsburgh Energy Technology Center,
P.O. Box 10940, Pittsburgh, PA 15236

It is generally appreciated that the mineral matter associated with some coals may act as a catalyst for liquefaction. A common observation is that among bituminous coals from the eastern United States, those with a relatively high mineral matter content also provide relatively high liquefaction yields. Also, addition of coal-derived mineral matter increases the liquefaction yields from those coals with low mineral matter content. The involvement of pyrite in these effects has been fairly well established. The importance of clay and/or other minerals is less well defined.

The catalytic properties of coal-derived mineral matter are of fundamental importance to the practical operation of coal liquefaction processes. However, little is known about the basic chemical reactions by which the mineral matter acts or how these reactions are related to the liquefaction of coal. Such knowledge might assist us in reaching the full potential in the use of these catalysts. Especially attractive goals include increasing the activity of the catalyst, manipulating its selectivity to provide maximum distillate yields at minimum hydrogen consumption, and determining the optimum operating conditions under which these catalysts may be employed.

Inferences may be drawn from reports on liquefaction studies regarding the types of chemical reactions that might be catalyzed by mineral matter. For example, hydrogenation activity has been indicated by an increased rate of hydrogen uptake by creosote oil in the presence of pyrite (1) and the accelerated disappearance of major aromatic compounds such as naphthalene (2). The viscosity of liquid products from coal has been observed to decrease with addition of pyrite (3,4), which implies removal of polar functional groups and/or reduction in molecular weight. After hydrogenation with pyrite present, the sulfur content of creosote oil was found to be somewhat lower than when hydrogenated without pyrite (1). Confirmation that pyrite is indeed connected with catalytic activity has been made by studies with model compounds. Hydro-

This chapter not subject to U.S. copyright.

Published 1981 American Chemical Society

desulfurization of thiophene (5) and benzothiophene (6) has been reported, but the pyrite catalysts were found to be much less active than commercial CoMo catalysts. In one case (6), pyrite was found to promote hydrogenation of benzothiophene but was ineffective at actual extraction of sulfur from the hydrogenated product, dihydrobenzothiophene. The low temperature ash of mineral matter from Western Kentucky coal was reported to isomerize 1-butene to trans-2-butene (5). Pyrites from mineral deposits have been shown to catalyze the dehydrogenation of tetralin* (7). Residues from coal liquefaction processes and crystalline pyrite mineral were shown to catalyze the conversion of isopropanol to acetone and propene (8).

Although mineral matter may provide a catalytic surface for various reactions during the liquefaction of coal, it is also possible that a large number of free radical reactions are initiated by thermolysis of the organic components in coal. Any study of catalytic activity must separate effects caused by the former from those caused by the latter. A sizeable portion of the work described below is devoted to establishing that separation.

Experimental

Materials. Tetralin, purchased commercially, was passed over activated alumina and stored under argon before use. In order to correctly identify the isomer of methylindan found in the product mixtures, authentic 1- and 2-methylindans were prepared from the corresponding indanones by reaction with methylmagnesium iodide, dehydration, and subsequent hydrogenation over Pd on asbestos.

Mineral matter was a Deister table concentrate from Robena mine coal. It contained 68% pyrite and less than 4% organic material. The remainder was largely clay. In one case, a hand-picked sample taken from a pyrite nodule found in a Pittsburgh seam coal was used. The microcrystals were crushed and sieved to 325 x 400 mesh. X-ray diffraction analysis indicated the only major component was pyrite, with a trace of marcasite also present. After heating in tetralin at 450°C for 15 min., the X-ray diffraction patterns of the recovered microcrystals indicated conversion was complete to pyrrhotite 1C. The coal was hvB, Homestead Mine, Kentucky, ground to pass 200 mesh. Ash and pyrite contents were 16.8% and 4.9%, respectively. The asphaltene was a homogenized mixture of samples isolated from liquid products derived from Pittsburgh seam, hvA coal. Its ash content was <0.1%(9).

Methods. Reactions were run in stainless steel micro-autoclaves of 30 mL. capacity. Reactors were charged with 20 g. tetralin plus the appropriate additive, flushed with *Tetralin is a registered trademark of E.I. DuPont de Nemours & Co.

nitrogen and sealed. Five such autoclaves were attached to a module designed to fit a reactor apparatus equipped with both heating and cooling fluidized sandbaths. Heating was accomplished by immersion of the entire module in the hot bath which had been preheated to 500-510°C. Heat-up time to final temperature of 450⁺⁵°C was 6⁺¹ minutes. Each autoclave was equipped with an individual thermocouple. Autoclaves at both ends of the module were always used as controls and were charged with just tetralin. The entire module was shaken pneumatically at 55-60 cycles/minute, with the autoclaves in a horizontal position. Cool-down to under 200°C in less than 3 minutes was accomplished by immersion in the second sandbath held at room temperature. Gasses formed were vented at room temperature, the reactors were weighed, and the products were poured into centrifuge tubes. After centrifugation at 2000 rpm for 60 minutes, the liquid was decanted and analyzed by VPC. The internal standard method was used to make a quantitative determination of the products. Five standard solutions were prepared with concentrations bracketing the expected range of the unknowns. Relative correction factors used in this study had coefficients of determination >0.98. Most of the analyses were done with 10' x 1/8" stainless steel columns packed with Carbowax 20M on Chromosorb-WAW. Some were done with a 50M fused silica capillary column coated with SP-2100. A Hewlett-Packard 5840* gas chromatograph equipped with autosampler was used to provide replicate analyses. Relatively short times for full chromatographic analyses were achieved with the capillary column. When it was used in conjunction with the autosampler and computerized data reduction, analysis of each unknown and standard solution could be replicated at least 3 and usually 4-6 times within a reasonable length of time. Use of many standard solutions and many replicate analyses allows a fairly high degree of precision to be obtained. We estimate typical precision of the determination of an unknown to be + 2% of its value.

Results and Discussion

The reactions of tetralin in the presence of coal were investigated to determine the extent of conversion along various pathways in the absence of further added catalysts. As may be seen from Figure 1, the yield of products generated under typical liquefaction conditions (450°C, 30 minutes) increases with the amount of coal added. Three products arise from tetralin: naphthalene, n-butylbenzene, and 1-methylindan. Positive identification of the latter isomer was made by comparison of gas chromatographic retention times with those of authentic samples of 1- and 2-methylindan prepared by independent synthesis.

The decalins* recovered in the product were present in the tetralin before reaction as minor impurities. The cis- and trans-isomers were fully resolved in our chromatograms and positively identified by spiking experiments with authentic samples. Material balance calculations indicate that the total amount of decalins was essentially unchanged over the course of the reaction. Hooper et al. (10) have also reported that the amount of decalin in tetralin did not change when it was heated to 450°C with coal. However, we do observe that the ratio of the trans- to cis-isomer is greatly changed and seems to approach an equilibrium value after reaction at the highest coal concentration.

All of these reactions presumably arise through free radical mechanisms. The abstraction of hydrogen from tetralin by coal to produce naphthalene is of course expected. What sets this reaction apart from the rest is the linear dependence of naphthalene yield on coal concentration. From the slope of the yield curve, we calculate that hydrogen was removed from tetralin in the amount of 2.5 wt. percent of the added coal. This is a reasonable amount of hydrogen to be transferred to coal under liquefaction conditions. However, we note a recent report on the decomposition of 1,2-diphenylethane in tetralin in which Benjamin states that over twice the amount of naphthalene required in the formation of toluene was produced (11). Presumably, the excess appears as molecular hydrogen. In the present case, we cannot rule out the possibility that some fraction of the naphthalene was produced by a similar mechanism.

The rearrangement of tetralin to 1-methylindan is the most prominent reaction at coal concentrations less than about 14 wt. percent coal. As may be seen by the intercept, a significant amount of rearrangement took place even in the absence of coal. There is now good evidence that rearrangement arises primarily and perhaps exclusively from the 2-tetralyl radical (12,13). It has been demonstrated that this rearrangement is to some extent reversible (12) and that degradation of 1-methylindan to lower molecular weight products also occurs. These reactions may account for the non-linear form of the yield curve in Figure 1. In contrast, it has been shown (12,15) that under liquefaction conditions similar to those used here, tetralin is not formed from naphthalene, the only one of these products with a linear yield curve.

The yield of n-butylbenzene also increases with coal concentration, although the relative amounts are much smaller than the yields of either naphthalene or 1-methylindan. The relative amount of the cracking of aliphatic groups from tetralin and 1-methylindan has been observed to increase in the presence of vitrinite (12). It has been suggested that the opening of the aliphatic ring of tetralin may be accounted for by the intervention of hydrogen atoms (10,16). Although the

*Decalin is a registered trademark of E.I. DuPont de Nemours & Co.

autoclaves were not pressured with hydrogen gas in our experiments, hydrogen atoms might still arise from the interaction of free radicals with minor amounts of hydrogen gas generated during the course of the reactions or by β -scission of hydrogen atoms from suitable radicals. Vernon (17) has demonstrated that such a mechanism can account for the cracking of otherwise thermally stable compounds.

The isomerization of the decalins is most easily explained as a free radical reaction initiated by hydrogen abstraction at one of the tertiary carbons. Inversion at the free radical center followed by hydrogen abstraction would yield the other isomer of decalin. Sufficient repetition of the process would bring about equilibrium between the *cis* and *trans* forms.

Figures 2 and 3 contain yield curves for naphthalene and 1-methylindan as a function of reaction time for tetralin and tetralin plus coal, pyrite, or asphaltene. The asphaltene was a homogenized mixture of several samples isolated from coal liquefaction products during other work in our laboratory (9). This asphaltene sample contained essentially a negligible ash content (<0.1%). Therefore, it contains many organic structures similar to those found in coal, but unlike coal, its reactions will be free of any complicating factors due to mineral matter. The yields of naphthalene and 1-methylindan are greater in the presence of asphaltene than in its absence, although not quite as high as in the presence of coal. This is additional evidence that these two products arise mainly from reactions associated with the presence of the organic portion of coaly matter. These reactions are quite likely free radical in nature.

Pyrite vs. Pyrrhotite. Figures 2 and 3 also contain yields of naphthalene and 1-methylindan found in the presence of mineral matter isolated from Robena mine coal on a Deister table. The major component of this sample was pyrite (68%). X-ray diffraction analysis of the residue recovered after reaction confirmed that the reduction of pyrite to pyrrhotite was complete within the shortest reaction times (15 min.). The stoichiometric amount of naphthalene expected from the corresponding oxidation of tetralin may be calculated. In Figure 2, the dotted line is the sum of this calculated value and the "thermal" yield found in the absence of additives. As may be seen, the naphthalene yield always exceeds this calculated sum, and the amount of the excess increases with time. Thus, as required if pyrrhotite is acting as a (de)hydrogenation catalyst, naphthalene is produced beyond, in both time and amount, that required by the reduction of pyrite. However, we note that the addition of pyrite is even more effective than asphaltene in promoting the formation of 1-methylindan (Figure 3). Although not shown in the figures, we have also found that equilibration of *cis*- and *trans*-decalin and the ring opening of

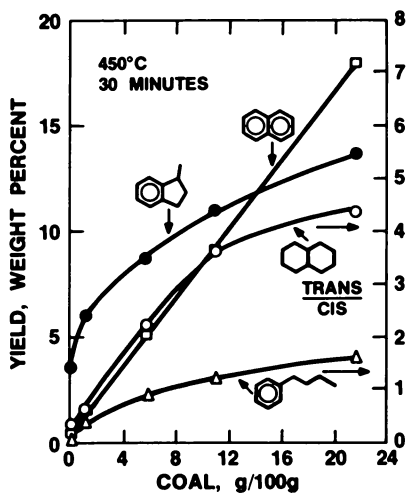


Figure 1. Yields of products from Tetralin and the ratio of trans/cis Decalin as a function of added Western Kentucky, Homestead mine coal

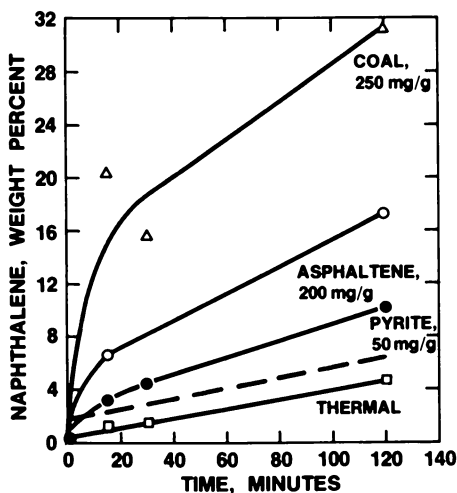


Figure 2. Naphthalene yield as a function of time in the presence of various additives. The dotted line is the sum of the thermal yield curve and the calculated amount of naphthalene obtained by the full reduction of 50 mg of pyrite

tetralin to *n*-butylbenzene is promoted by addition of pyrite, just as in the cases of coal or asphaltene. Since all of these products have been shown to arise from non-catalytic reactions, we cannot establish on the basis of this data whether catalytic or simply free radical processes dominate.

The results described above illustrate the problem of separating effects due to catalysis provided by pyrrhotite from those due to the chemistry of the reduction of pyrite. It must also be borne in mind that reduction of pyrite produces a nearly equivalent amount of H_2S , which remains available to enter subsequent reactions by mechanisms now only poorly understood. In order to remove these complications, pyrrhotite was prepared by the reduction of pyrite with tetralin, isolated from the reaction residue, and then heated with fresh tetralin. Figures 4 and 5 contain the yields of naphthalene and 1-methylindan, and the ratios of *trans*- to *cis*-decalin as a function of concentration. In this case, the pyrite was a hand-picked sample of micro-crystals taken from a coal nodule. As may be seen, the yields of naphthalene and 1-methylindan, and the ratio of *trans*- to *cis*-decalin all increase with pyrite concentration. The slope of the line for naphthalene yield is 0.91. A slope of 0.53 is calculated for stoichiometric reduction of FeS_2 to FeS by tetralin to yield naphthalene. Thus, roughly half of the naphthalene produced can be accounted for by the demand for hydrogen in the reduction of pyrite.

The yield curves found in the presence of the recovered pyrrhotite shown in Figure 5 are quite different from those for pyrite. Production of 1-methylindan and *trans*-decalin was negligible. The increment in naphthalene yield is about 0.6 g/g pyrrhotite. On a molar basis, this is equivalent to about 0.45 g/g pyrite. This value is in good agreement with the amount of excess naphthalene produced during the reduction of pyrite. From this comparison, pyrrhotite by itself appears to catalyze the dehydrogenation of tetralin but is unable to initiate the free radical reactions which lead to 1-methylindan or *trans*-decalin by abstraction of secondary or tertiary hydrogens, respectively. With this limited set of data, it cannot be established whether the lack of radical reactions is due to the absence of radical initiators or lack of a good chain carrier such as H_2S , both of which are normally generated when pyrrhotite is formed *in situ* by the reduction of pyrite.

These studies have shown that a variety of reactions are promoted when either organic matter from coal or mineral matter from coal, principally pyrite, is heated to liquefaction temperature with tetralin. However, when just pyrrhotite is heated with tetralin, only dehydrogenation is catalyzed. Thus, in order to evaluate the effects of iron sulfides, it is of critical importance to separate their actions as reactants from their actions that are truly catalytic in nature.

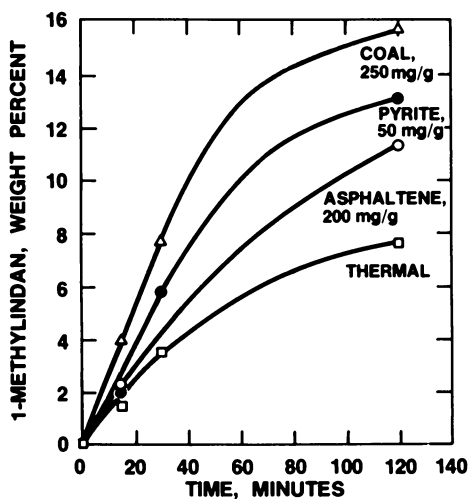


Figure 3. 1-Methylindan yield as a function of time in the presence of the same additives shown in Figure 2

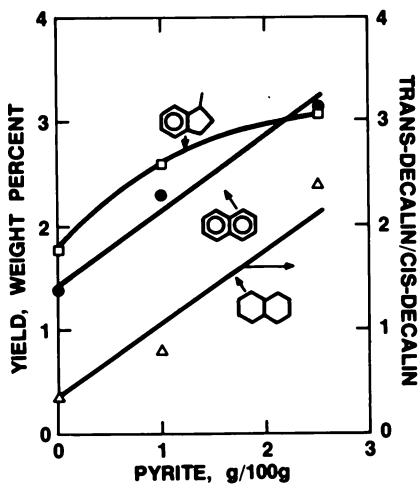


Figure 4. Yields of 1-methylindan and naphthalene and the ratio of trans/cis-Decalin as a function of pyrite concentration after reaction with Tetralin at 450°C for 15 min

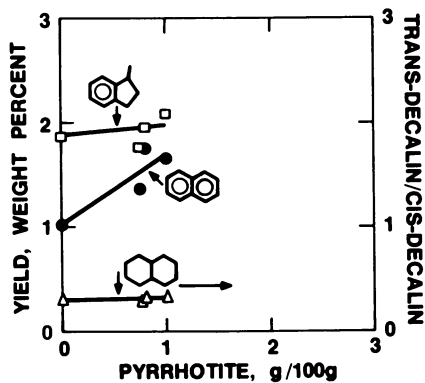


Figure 5. Product distribution after reaction of fresh Tetralin with pyrrhotite recovered after reduction of pyrite illustrated in Figure 4. Reaction conditions were 450°C for 15 min.

Acknowledgment

We gratefully acknowledge the assistance of our colleagues at the Pittsburgh Energy Technology Center. Dr. Sidney Pollack and Christine Spitler provided the X-ray analyses of pyrites and pyrrhotites. Visiting Prof. Al Giardini of the University of Georgia picked several pyrite samples. We are also indebted to Dr. Sidney Friedman for many helpful suggestions.

Reference to a brand or company name is made to facilitate understanding and does not imply endorsement by the U.S. Department of Energy.

Literature Cited

1. Tarrer, A. R.; Guin, J. A.; Pitts, W. S.; Henley, J. P.; Prather, J. W.; and Styles, G. A. Am. Chem. Soc. Fuel Div. Preprints 1976, 21(5), 59.
2. Prather, J. W.; Tarrer, A. R.; Guin, J. A.; Johnson, D. R.; Neely, W. C. Am. Chem. Soc. Fuel Div. Preprints, 1976, 21(5), 144.
3. Appell, H. R.; Miller, R. D.; Illig, E. G.; Moroni, E. C.; Steffgen, F. W. "Coal Liquefaction with Synthesis Gas"; PETC/TR-79/1; Technical Information Center, United States Department of Energy: Oak Ridge, TN, 1979.
4. Granoff, B.; Thomas, M. G. Am. Chem. Soc. Div. Fuel Preprints, 1977, 22(6), 183.
5. Hamrin, C. E.; Morooka, S. Fuel 1978, 57, 776.
6. Guin, J. A.; Lee, J. M.; Fan, C. W.; Curtis, C. W.; Lloyd, J. L.; Tarrer, A. R. Ind. Eng. Chem., Process Des. Dev. 1980, 19, 440.
7. Gangwer, T. E.; Prasad, H. Fuel 1979, 58, 577.
8. Joly, J. P.; Ollis, D. Journal of Catalysis 1979, 60, 216.
9. Steffgen, F. W.; Schroeder, K. T.; Bockrath, B. C. Anal. Chem. 1979, 51, 1164.
10. Hooper, R. J.; Battaerd, H. A. J.; Evans, D. G. Fuel 1979, 58, 132.
11. Benjamin, B. M. Fuel 1978, 57, 378.
12. Benjamin, B. M.; Haamon, E. W.; Raaen, V. F.; Collins, C. J. Fuel 1979, 58, 386.
13. Franz, J. A.; Camaioni, D. M. Fuel 1980, 59, 803.
14. Franz, J. A.; Camaioni, D. M. J. Org. Chem. 1980, 45, 5247.
15. Franz, J. A. Fuel 1980, 58, 405.
16. Penninger, J. M. L.; Slotboom, H. W. Rec. Trav. Chim. Pays-Bas 1973, 92, 513.
17. Vernon, L. W. Fuel 1980, 59, 102.

RECEIVED March 9, 1981.

The Kinetics of Flash Hydrogenation of Lignite and Subbituminous Coal

B.L. BHATT¹, P. T. FALLON, and M. STEINBERG

Process Sciences Division, Department of Energy and Environment,
Brookhaven National Laboratory, Upton, NY 11973

A reaction model, based on a single coal particle surrounded by H₂ gas, is developed for the hydrogenation of lignite and subbituminous coal. Conversion data from experiments conducted at various pressures, temperatures, particles residence times and gas residence times are correlated to calculate activation energies and to obtain one set of kinetic parameters. A single object function formulated from the weighted errors for the four dependent process variables, CH₄, C₂H₆, BTX, and Oil yields, was minimized using a program containing three independent iterative techniques. The results of the nonlinear regression analysis for lignite show that a first-order chemical reaction model with respect to carbon conversion, satisfactorily describes the dilute phase hydrogenation. Data obtained from experiments using subbituminous coal are correlated using similar techniques. Results from data analysis of the two types of coals are compared. The mechanisms, rate expressions, and design curves developed can satisfactorily predict conversions to various products at different conditions and hence can be used for scale-up and reactor design.

Flash hydrogenation is a short residence time (1 to 10 sec) gas-phase, non-catalytic process in which pulverized coal is rapidly heated (20,000-30,000° C/sec) in hydrogen to obtain liquid and gaseous hydrocarbons directly. Experiments were conducted in a 2 lb/hr, 1" ID x 8 ft long downflow tubular reactor in the range of 500° to 900°C and 500 to 3000 psi H₂ pressure for North Dakota Lignite and New Mexico subbituminous coal (1). The ultimate analyses of these coals are given in

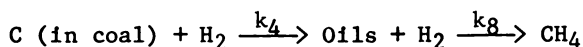
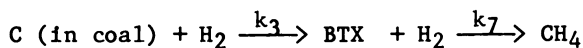
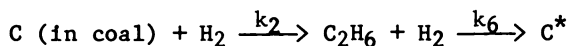
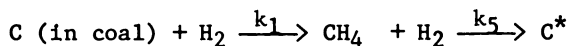
¹ Current address: Air Products and Chemicals, Inc., P.O. Box 427, Marcus Hook, PA 19061.

0097-6156/81/0169-0201\$05.00/0

© 1981 American Chemical Society

Table I. An on-line process gas chromatograph analyzed the gas stream for 10 components every 8 minutes from sample taps located at intervals of 2 feet along the length of the reactor (2). The heavier hydrocarbon products (> C₉), collected in liquid product condensers, were measured at the end of each experiment.

Modelling. The flash hydrogenation is assumed to take place via the following reaction steps:



C* designates the non-reactive elemental carbon contained in the char product. The chemical reaction is assumed to be the rate controlling step. This assumption is justified in the Discussion of Results. The reactions are considered to be first order with respect to fraction of carbon remaining in coal as well as converted to hydrocarbons and mth order with respect to H₂ partial pressure. The details of the development of the model is reported elsewhere (3). The experimental data correlated was obtained from dilute phase operation in an excess of hydrogen atmosphere, so the partial pressure of hydrogen was considered to be approximately equal to the total system pressure and was assumed constant along the length of the reactor.

For isothermal conditions, differential equations set up from material balances of each component can be solved analytically to obtain the relationships in Table II.

Arrhenius behavior of the rate constant with temperature was assumed as follows:

$$k_i = k_{i0} e^{-E_i/RT} \quad \text{for all } i$$

Regression Technique. A minimization program 'MINUIT' (4) was used on CDC 7600 to fit the equations to the data and find the unknown parameters. Three different minimization algorithms, Monte Carlo, Simplex, and Variable Metric, available in MINUIT, were used for the correlation.

A single object function was formulated for the four

TABLE I
ULTIMATE ANALYSIS (WT PCT DRY) OF LIGNITE
AND SUBBITUMINOUS COALS

	North Dakota ⁽¹⁾ Lignite	New Mexico ⁽²⁾ Subbituminous
Carbon	59.0	59.3
Hydrogen	4.0	4.2
Oxygen*	25.5	16.8
Nitrogen	0.9	1.2
Sulfur	0.6	0.8
Ash	10.0	17.7
	<u>100.0</u>	<u>100.0</u>

*By difference

- 1) From Baukal Noonan Inc. Mines, P.O. Box 879, Minot, N. Dakota 58701
- 2) From Western Coal Co. Mines, P.O. Box 509, Farmington, N. Mexico 87401

TABLE II

$$\begin{aligned}
 [\text{CH}_4] &= \frac{k_1}{u_{gs} k_{1234} - k_5} \left[e^{-k_5 P_{H_2}^m} \frac{t_s}{u_{gs}} - e^{-k_{1234} P_{H_2}^m} t_s \right] \\
 [\text{C}_2\text{H}_6] &= \frac{k_2}{u_{gs} k_{1234} - k_6} \left[e^{-k_6 P_{H_2}^m} \frac{t_s}{u_{gs}} - e^{-k_{1234} P_{H_2}^m} t_s \right] \\
 [\text{BTX}] &= \frac{k_3}{u_{gs} k_{1234} - k_7} \left[e^{-k_7 P_{H_2}^m} \frac{t_s}{u_{gs}} - e^{-k_{1234} P_{H_2}^m} t_s \right] \\
 [\text{Oils}] &= \frac{k_4}{u_{gs} k_{1234} - k_8} \left[e^{-k_8 P_{H_2}^m} \frac{t_s}{u_{gs}} - e^{-k_{1234} P_{H_2}^m} t_s \right]
 \end{aligned}$$

Weighting factors inversely proportional to the variance of each dependent variable were used (5). To take into account the variable number of data points available for each dependent variable, weighting factors were taken proportional to the number of data points and can then be represented as follows:

$$W_i = \frac{N_i}{\sum (Y_i - \bar{Y}_i)^2} \quad \text{for } i = 1, 2, 3, 4.$$

Results of Regression Analysis. For simplification, it was assumed that all activation energies for initial formation of hydrocarbons from coal are the same, i.e. $E_1 = E_2 = E_3 = E_4$. A rationale for this is that during decomposition, coal is in equilibrium with the same transition complex regardless of the final products.

Data from 83 experimental runs, with H_2 /coal weight ratio of about 1, using North Dakota Lignite, were correlated. Details of the correlation for the lignite are reported elsewhere (3). For New Mexico subbituminous coal, data from 47 experimental runs, also with H_2 /coal weight ratio of about 1, were correlated. For these runs, 166 data points, corresponding to different locations in the reactor, were available for CH_4 , C_2H_6 and BTX concentrations. Oil data, obtained from the total amount of oil collected in the condensers, were available for 17 runs.

Estimated values of various parameters for subbituminous coal are tabulated in Table III, along with those found for lignite. The order of magnitude of the parameters is the same for both coals. Correlation coefficients and standard errors for the subbituminous coal are tabulated in Table IV. The standard error of 8% carbon conversion for CH_4 seems to be high, but because of higher amounts and variation in the CH_4 data, a correlation coefficient of 0.92 is obtained, indicating excellent correlation. The correlation of the oil data is better compared to those of C_2H_6 and BTX data.

Using Student's *t* statistics, hypothesis: $\rho=0$ was tested (6). It was found that the hypothesis $\rho=0$ can be rejected at the 0.005 significance level. It therefore appears almost certain that the % carbon conversions to CH_4 , C_2H_6 , BTX and Oils can be related to reaction temperature, H_2 partial pressure, particle residence time, and gas residence time by the correlations.

Using Fisher's *Z* transformation (6), 95% confidence limits for the overall correlation coefficient for the subbituminous coal were $0.70 < r < 0.84$.

A sensitivity analysis was performed on the correlation. The kinetic parameters and correlation coefficients were estimated for $N = 166, 156, 146,$ and 136 with $N_4 = 17, 16, 15,$

TABLE III
ESTIMATED VALUES OF VARIOUS PARAMETERS

	North Dakota Lignite	New Mexico Subbituminous
k ₁₀ , sec ⁻¹	5.0 x 10 ⁵	5.5 x 10 ⁶
k ₂₀ , sec ⁻¹	7.5 x 10 ⁶	6.7 x 10 ⁶
k ₃₀ , sec ⁻¹	4.4 x 10 ⁶	6.3 x 10 ⁶
k ₄₀ , sec ⁻¹	4.6 x 10 ⁶	4.0 x 10 ⁶
k ₅₀ , sec ⁻¹	5.2 x 10 ¹	4.8 x 10 ¹
k ₆₀ , sec ⁻¹	1.7 x 10 ¹⁰	1.7 x 10 ¹⁰
k ₇₀ , sec ⁻¹	1.6 x 10 ⁹	1.5 x 10 ⁹
k ₈₀ , sec ⁻¹	4.6 x 10 ¹⁶	6.9 x 10 ¹⁶
E (E ₁ thru E ₄), cal/g mole	42,700	43,200
E ₅ , cal/g mole	20,100	20,900
E ₆ , cal/g mole	54,200	55,000
E ₇ , cal/g mole	50,300	51,100
E ₈ , cal/g mole	84,200	84,700
m (power of P _{H₂})	0.14	0.15

and 14 respectively. The correlation coefficients obtained are tabulated in Table V. The correlation coefficients do not show any significant change (< 5% variation) indicating that the correlation is good.

Design curves were developed in the range of the experimental data from the kinetic parameters and rate expression, using a Tektronix interactive graphic terminal connected with CDC 6600. Figures 1, 2 and 3 show percent carbon conversion to CH_4 vs. reactor length, gas residence time, and particle residence time, at various temperatures and pressures. For pressures of 1500 psi and 2500 psi, maxima in CH_4 yields are found within the range of the experiments. CH_4 yield increases and occurs at lesser residence times as the temperature increases. Figures 4, 5, and 6 show percent carbon conversion to C_2H_6 , BTX and Oils, respectively vs. reactor length for various temperatures at 1500 psi. The maximum yields of these products decrease and occur at lesser residence times as the temperature increases.

Maximum yields of various products and necessary operating conditions are tabulated in Table VI. Maximum yields from subbituminous coal are found at 2500 psi, which is the highest pressure used in experiments for that coal. For comparison purposes, lignite yields are also tabulated for 2500 psi, though some experiments were conducted at 3000 psi with the lignite, obtaining higher yields. For both coals, the CH_4 maximum is found at higher temperature and occurs at shorter residence times, compared to C_2H_6 , BTX and Oils. Higher maximum yields of CH_4 and BTX and slightly lower maximum yields of C_2H_6 and Oils were obtained for the subbituminous coal compared to the lignite. Maximum % carbon conversion to CH_4 vs. pressure is plotted in Figure 7. The maximum CH_4 conversion shows a linear increase with increase in pressure for both coals. At all pressures, the maxima are found at 900°C and the subbituminous coal maximum yields to CH_4 are higher than those from the lignite.

Discussion of Results and Conclusions. The results of regression analysis show that a chemical reaction model, first order with respect to fractional carbon conversion, with a production and a decomposition step for each of CH_4 , C_2H_6 , BTX and Oils, satisfactorily describes the dilute phase flash hydrogenation of both lignite and subbituminous coal.

The activation energy estimates of > 20,000 cal/gmole justify the assumption that chemical reaction is the rate controlling step. The activation energy for the initial formation of hydrocarbons was 42,700 cal/gmole for lignite and 43,200 cal/gmole for subbituminous coal, with estimated errors of only 50-80 cal/gmole. This indicates that the error involved

TABLE IV
CORRELATION COEFFICIENTS AND STANDARD ERRORS
FOR THE SUBBITUMINOUS COAL RESULTS

	Correlation Coefficient	Standard Error, %C Conversion
CH ₄	0.92	8.0
C ₂ H ₆	0.66	3.2
BTX	0.72	2.9
Oils	0.81	0.7
Overall	0.78	

TABLE V
RESULTS OF THE SENSITIVITY ANALYSIS FOR THE SUBBITUMINOUS COAL
CORRELATION COEFFICIENT

N	N ₄	CH ₄	C ₂ H ₆	BTX	Oils	Overall
166	17	0.92	0.66	0.72	0.81	0.78
156	16	0.92	0.65	0.71	0.84	0.77
146	15	0.92	0.64	0.69	0.81	0.76
136	14	0.92	0.66	0.69	0.80	0.77

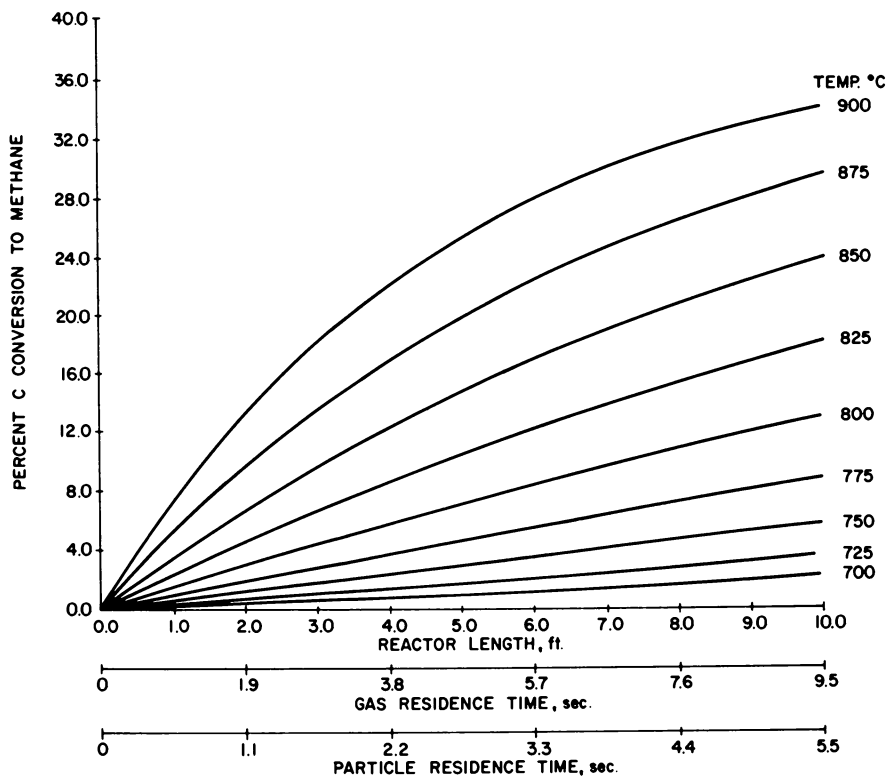


Figure 1. Flash hydrogenation of subbituminous coal: pressure = 500 psi; H_2 flow rate ≈ 1 lb/h; coal feed rate ≈ 1 lb/h.

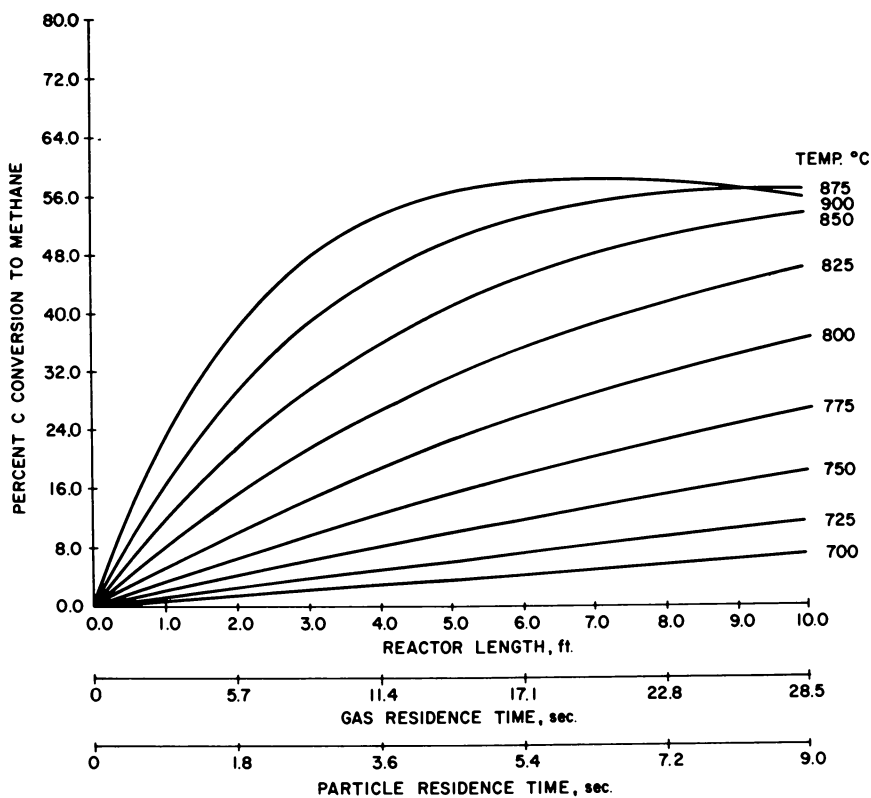


Figure 2. Flash hydrogenation of subbituminous coal: pressure = 1500 psi; H_2 flow rate ≈ 1 lb/h; coal feed rate ≈ 1 lb/h.

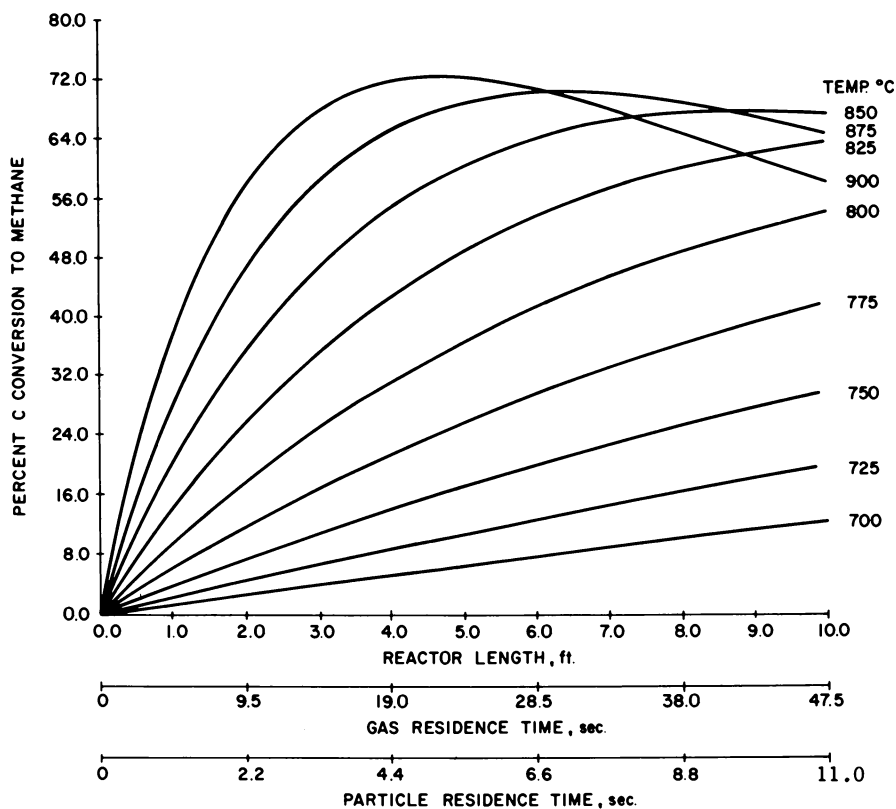


Figure 3. Flash hydrogenation of subbituminous coal: pressure = 2500 psi; H_2 flow rate ≈ 1 lb/h; coal feed rate ≈ 1 lb/h.

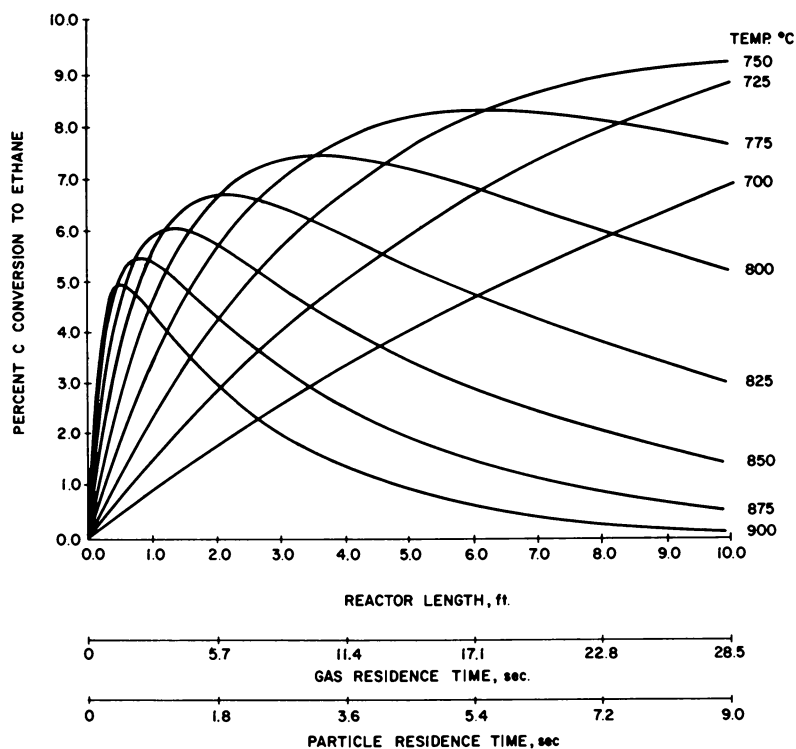


Figure 4. Flash hydrogenation of subbituminous coal: pressure = 1500 psi; H_2 flow rate ≈ 1 lb/h; coal feed rate ≈ 1 lb/h.

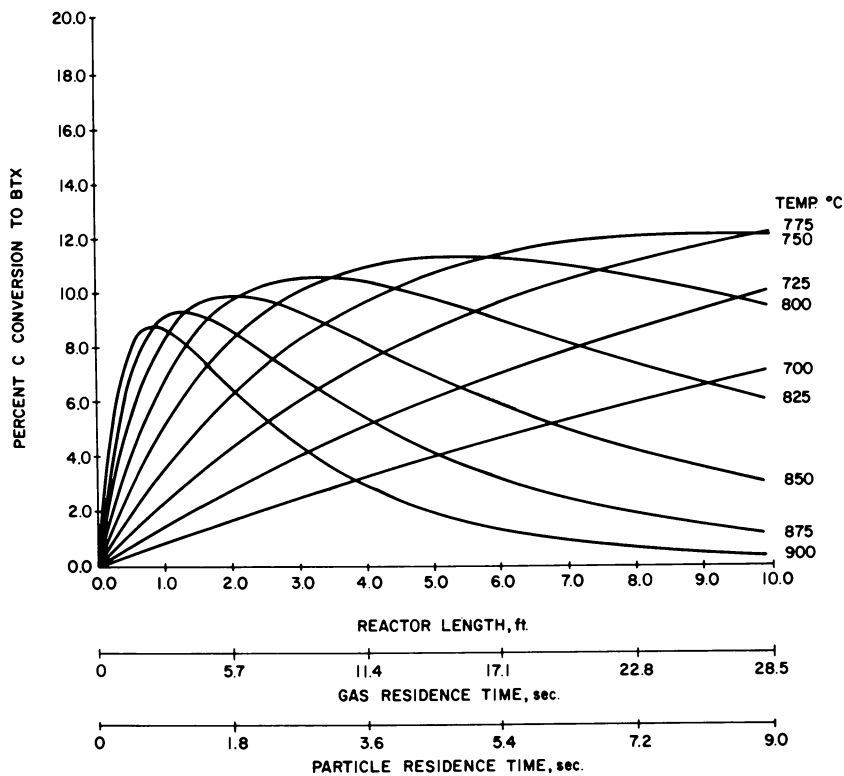


Figure 5. Flash hydrogenation of subbituminous coal: pressure = 1500 psi; H_2 flow rate ≈ 1 lb/h; coal feed rate ≈ 1 lb/h.

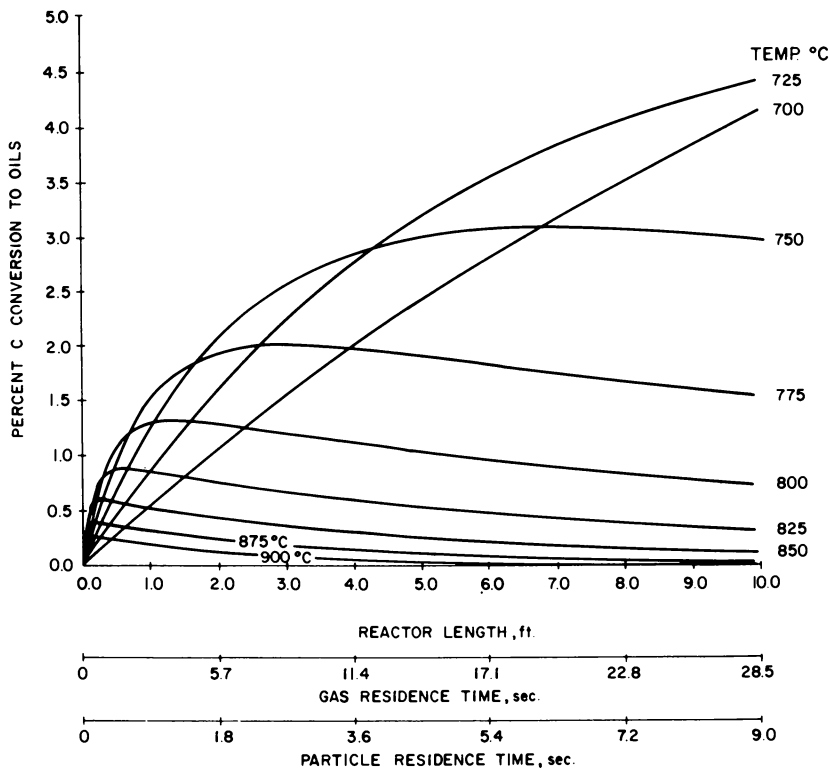


Figure 6. Flash hydrogenation of subbituminous coal: pressure = 1500 psi; H_2 flow rate ≈ 1 lb/h; coal feed rate ≈ 1 lb/h.

TABLE VI
 MAXIMUM CARBON CONVERSIONS TO VARIOUS PRODUCTS AT 2500 PSI

% C Conv. to	Max. CH ₄		Max. C ₂ H ₆		Max. BTX		Max. Oils	
	Lignite Subbit.	Subbit.	Lignite Subbit.	Subbit.	Lignite Subbit.	Subbit.	Lignite Subbit.	Subbit.
CH ₄	67	73	26	25	18	25	11	9
C ₂ H ₆	2	2	10	9	9	9	7	5
BTX	1	1	8	14	9	14	7	10
Oils	0	0	5	3	8	3	8	6
Total	70	76	49	51	44	51	33	30
Operating Conditions								
Pressure, psi	2500	2500	2500	2500	2500	2500	2500	2500
Temp., °C	900	900	750	750	725	750	700	700
Reactor Length, ft	3.5	4.5	8	8	8	8	8	8
Solid res. time, sec	3.9	5.0	8.8	8.8	8.8	8.8	8.8	8.8
Gas res. time, sec	16.6	21.4	38.0	38.0	38.0	38.0	38.0	38.0

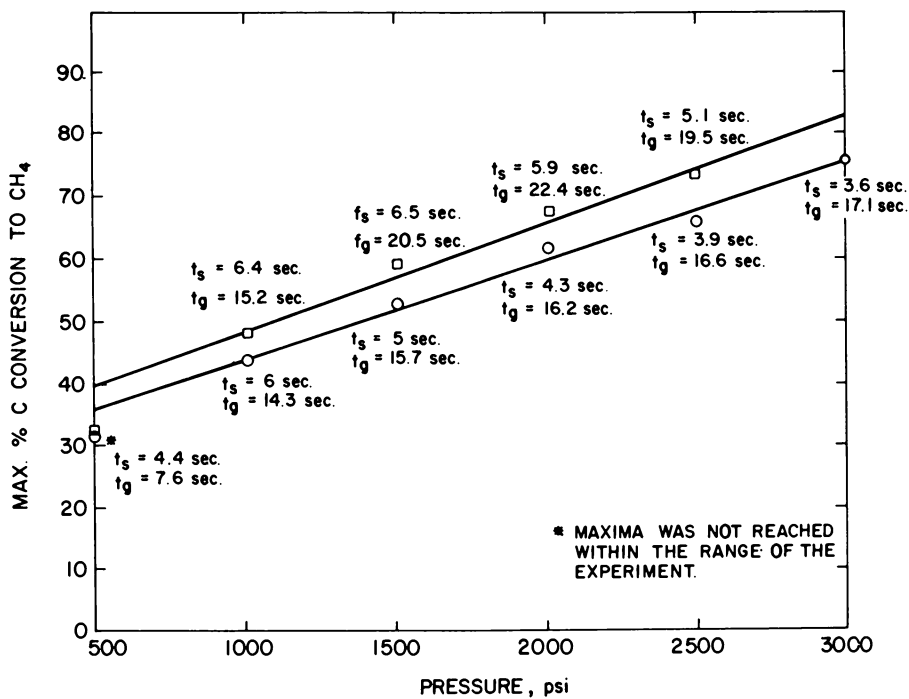


Figure 7. Flash hydrogasification of coal: maximum percentage of carbon conversion to CH_4 vs. pressure (at $900^\circ C$). Solid residence time (t_s); gas residence time (t_g); North Dakota lignite (\circ); New Mexico subbituminous (\square).

in the assumption, that all the activation energies for initial formation of hydrocarbons from coal are the same ($E_1 = E_2 = E_3 = E_4$) is probably small. The values of these activation energies estimated are comparable to the mean activation energy of 48,700 cal/gmole found by Anthony (7) for devolatilization of Montana Lignite and the activation energy of 48,900 cal/gmole found by Bhatt (5) for hydrolysis of North Dakota Lignite. The kinetic parameters (k_{50} , k_{60} , k_{70} , E_5 , E_6 , E_7) corresponding to the decomposition steps for CH_4 , C_2H_6 and BTX are found to be almost the same for both lignite and subbituminous coal, as expected. The pre-exponential factors for oils are different for the two coals, probably due to some difference in nature of the oils produced. The pre-exponential factors (k_{10} , k_{20} , k_{30} , k_{40}) for initial decomposition of subbituminous coal are found to be different than those for lignite. At optimum conditions, subbituminous coal produces more CH_4 and BTX and slightly less C_2H_6 and Oils than lignite. The power of the hydrogen partial pressure, m , was about +0.14 to +0.15. This indicates a small increase in % carbon conversion to hydrocarbons with increase in hydrogen partial pressure.

The correlation for subbituminous coal with overall correlation coefficient 0.78, having 95% confidence limits of 0.70 and 0.84, is considered good.

The mechanism, rate expressions, and the design curves developed satisfactorily represent the experimental data and hence can be used for scale-up and reactor design.

The model developed might be applicable to other types of coal while the regression technique used is applicable to any experimental data for correlation.

The model was developed from experiments conducted in a downflow reactor, where gas residence times are greater than solid residence times. The model may not be able to predict residence time effect in a fluid bed or upflow reactor where solid residence times are greater than gas residence times. But it does give useful information for pressure and temperature effects in these reactors.

Literature Cited

1. Fallon, P.T., Bhatt, B., and Steinberg, M. "The Flash Hydrolysis of Lignite and Subbituminous Coals to both Liquids and Gaseous Hydrocarbon Products"; Brookhaven National Laboratory; BNL 26210; presented at the 178th National Meeting of the American Chemical Society; Washington, D.C., 1979.
2. Steinberg, M., Fallon, P., Dang, V., Bhatt, B., Ziegler, E., and Lee, Q. "Reaction and Process Engineering for the Flash Hydrolysis (FHP) of Coal"; Brookhaven National Laboratory; BNL 25232; presented at 71st Annual Meeting of the American Institute of Chemical Engineers; Miami Beach, Florida, 1978.

3. Bhatt, B., Fallon, P.T., and Steinberg, M. "Reaction Modelling and Correlation for Flash Hydropyrolysis of Lignite"; Brookhaven National Laboratory; BNL 27574; presented at the 15th Intersociety Energy Conversion Engineering Conference: Seattle, Washington, BNL 27574R, 1980.
4. James, F., and Roos, M. "MINUIT - A System for Function Minimization and Analysis of the Parameter, Errors and Correlations"; Computer Physics Communications, 10, 1975, p 343-367.
5. Bhatt, B. "Kinetics of Coal Devolatilization and Hydropyrolysis"; Ph.D thesis; Polytechnic Institute of New York, 1980.
6. Spiegel, M.R. "Theory and Problems of Statistics"; Schaum's Outline Series; McGraw-Hill Book Company, 1961; p 344.
7. Anthony, D.B. "Rapid Devolatilization and Hydrogasification of Pulverized Coal"; Sc. D. Thesis; Dept of Chemical Engineering; Mass Institute of Tech., Cambridge, 1974.

Nomenclature

[BTX]	fraction of carbon converted to benzene, toluene and xylene.
$\overline{[BTX]}_{\text{exp}}$	mean of [BTX] _{exp}
[CH ₄]	fraction of carbon converted to methane.
$\overline{[CH_4]}_{\text{exp}}$	mean of [CH ₄] _{exp}
[C ₂ H ₆]	fraction of carbon converted to ethane.
$\overline{[C_2H_6]}_{\text{exp}}$	mean of [C ₂ H ₆] _{exp}
E, E _i	activation energy, cal/gmole
F	object function
k _i	rate constant, sec ⁻¹
k _{i0}	pre-exponential factor, sec ⁻¹
k ₁₂₃₄	sum k ₁ +k ₂ +k ₃ +k ₄ , sec ⁻¹
m	order of reaction with respect to H ₂ gas
N, N _i	number of data points
[Oils]	fraction of carbon converted to Oils

$\overline{[Oils]}_{exp}$	mean of $[Oils]_{exp}$
P_{H_2}	partial pressure of hydrogen, psi
r	sample correlation coefficient
R	gas constant, cal/gmole °K
t_s	solid residence time, sec
T	temperature (absolute), °K
u_g	gas velocity, ft/sec
u_s	solid velocity, ft/sec
u_{gs}	ratio u_g/u_s
W_i	weighting factors
Y, Y_i, Y_{ij}	dependent variable
\bar{Y}, \bar{Y}_i	mean of Y
<u>Greek letter</u>	
ρ	theoretical population coefficient of correlation
<u>Subscripts</u>	
cal	calculated value
exp	experimental value
g	gas
i	i th component
s	solid

RECEIVED June 16, 1981.

Characteristics of Coal-Derived Liquids from Different Processes: Relationships to Coal Structure

LARRY L. ANDERSON, KWANG E. CHUNG¹,
RONALD J. PUGMIRE, and JOSEPH SHABTAI

Department of Mining and Fuels Engineering, William C. Browning Building,
University of Utah, Salt Lake City, UT 84112

The structural description of coals at molecular level has not heretofore been possible for several reasons. Included among these are the heterogeneous nature of coals, as well as the difficulties in direct examination of a solid material which cannot be easily converted to simpler degradation products by mild, predictable chemical reactions. As solid materials, coals can be examined by relatively few methods which give precise chemical structural information. Methods which have been used include X-ray diffraction and fluorescence, ultraviolet, infrared and visible light absorption, reflectance and refractive index, proton and C¹³ nuclear magnetic resonance, magnetic susceptibility and density. Results from such measurements have been used for clarification of some general structural features of coals. Liquids derived from coals are more amenable to studies which yield molecular level information. However, the method of converting solid coals to liquids must be well defined and controlled in order to provide data which can be useful for elucidation of structural features in the original coals.

In the past, derived liquids have been prepared from coals by extraction, chemical reaction (reduction, hydrogenolysis, alkylation, etc.) and destructive distillation (pyrolysis). Depending on the conditions of liquefaction, the chemical changes have varied considerably in depth. These preparation processes are very complex and some assumptions are always necessary in describing the chemistry involved.

In order to formulate a chemical picture of coals, many types of conversion have been studied along with descriptions of the chemical changes involved (1-5). The results reported by different investigators do not always agree since different coals were used and sample preparations were not uniform. However, from the work cited and other results, the following general description seems appropriate for bituminous coals.

¹ Rockwell International Science Center, 1049 Camino Dos Rios, Thousand Oaks, CA 91360.

Coals are chemically heterogeneous and no one representation or model appears adequate for descriptive purposes. Based on microscopic, X-ray and other spectral analyses no regular or repeating structure, as in simple polymers, seems appropriate. Rather, coals are apparently composed of a variety of condensed aromatic-hydroaromatic ring structures having substituents, e.g. short chain aliphatic groups as well as O-, S- and N-containing groups, some of which serve as linking units between the ring structures (1-5). The structural components range from highly stable, e.g. aromatic rings, to reactive functional groups, e.g. OH and SH. It has been concluded that ring clusters contain from 1 to 6 aromatic rings, with an average of about 3, condensed with 1 to 2 hydroaromatic rings. These clusters are linked together by means of carbon-carbon, etheric, thioetheric, and other bonds, which are more susceptible to attack than the clusters themselves. Products of coal pyrolysis, hydrogenation and extraction could provide structural information on the clusters if it is assumed that the latter are preserved in most of these reactions, except at temperatures high enough to cause cracking of aromatic ring systems, e.g. >600°C. There is evidence that aromatic rings remain unchanged even under drastic hydrolytic conditions (500-600°C; hydrogen pressure, 2500-3000 psi; absence of catalyst) (6).

The objective of this communication is to report structural information on a bituminous coal from a thorough characterization of its extracts. The characterization was carried out according to a scheme devised on the basis of our current understanding of coal chemistry. The scheme consists of considerations in preparation, fractionation, and analysis of coal-derived liquids (CDL) to obtain molecular-level information on the CDL per se as well as on the parent coal. The information obtained relates mostly to the structure of component clusters.

Experimental

A high volatile (Clear Creek, Utah) bituminous coal (Table I) was ground to -40+100 mesh and subjected to liquefaction by two methods: (A) hydrogenation as a dry powder in a short-residence-time hydrogenation unit, using ZnCl₂ as catalyst (7,8), and (B) solubilization with NaOH-ethanol at two different temperatures. Process descriptions of these liquefaction procedures follows:

TABLE I

Proximate and Ultimate Analyses of Clear Creek Coal (-40 +100 mesh)			
Proximate Analysis (wt %)			
Moisture	6.0	Ash	10.0
Volatile Matter	39.4	Fixed Carbon	45.6

TABLE 1 (Cont'd.)

Ultimate Analysis (wt %, MAF basis)			
Carbon	79.3	Hydrogen	5.5
Nitrogen	1.7	Oxygen (difference)	13.4
Atomic Ratio H/C		0.83	

Procedure A. Coal derived liquids (CDL) were obtained by hydrogenating dry powdered coal in a coiled-tube reactor (9). The reactor temperature was 500°C and the hydrogen pressure applied was 1800 psig. The residence time of coal and/or products was 10–20 seconds. The pulverized coal had been previously impregnated with 5% by weight of zinc chloride. Products of the hydrogenation treatment included 10% gases, 5% light liquids (b.p. <250°C), 55% heavy liquids, 15% char and 15% water (per cents by weight of dry mineral matter free coal). Conversion was 85% assuming char as unreacted coal. C^{13} nuclear magnetic-resonance analysis of the feed coal and heavy liquids indicated that about 80% of the carbons in the product were in a similar chemical environment as in the solid coal (10). It was expected that particularly the heavy fraction (b.p. >250°C) would retain some of the features of the feed coal. This fraction was therefore selected for characterization. The work-up included washing with distilled, deionized water to remove catalyst, stripping water and light products, distilling under vacuum and extracting with solvents. It was found that paraffinic material made up part of the heavy liquid product (HVL) and these were removed by extraction with ethanol and acetone at ambient and -5–0°C, respectively. With the paraffinic materials removed, the remaining liquid was designated as HVL-P.

Procedure B. Solubilization with NaOH-ethanol was done following the procedures developed by Ouchi et al (11,12). In each experiment 24 grams of coal was reacted with 120 grams of ethanol and 40 grams of sodium hydroxide. Reactions were conducted in a stirred autoclave at 300°C and at 320°C, using a processing time of 100 minutes after the reaction temperature was reached. At the completion of the reaction, the reactor was cooled to room temperature. Distilled, deionized water was introduced inside the reactor, and the product was collected in two forms:

- i. Water slurry--the fraction of the product dissolved or floated as small particles upon stirring.
- ii. Solid product--the rest of the product attached to the reactor wall.

SP-300 and SP-320 were the designations given to the solubilization products obtained at 300 and 320°C, respectively.

Fractionation of CDL

In preliminary experiments, distillation and solvent extraction were compared to each other as separation means. HVL (or

HVL-P) was extracted with two solvents: once with ethanol, and once with cyclohexane at room temperature and a solvent/sample ratio of 10. HVL-P, the ethanol-soluble fraction (ES) of HVL, and cyclohexane-soluble fraction (CyS) of HVL-P were distilled at temperatures ranging from 250° to 365°C under a variable vacuum down to 2 torr. Distillable fractions were designated "light", "middle" and "heavy" with the undistilled part termed "resid". The "light" fraction was yellowish and fluid up to -5°C; the "middle" fraction was reddish and fluid at room temperature but solidified at lower temperatures, while the "heavy" fraction was red, and the "resid" fraction was black.

The water slurry of SP-300 was acidified to pH 2 with 10% HCL to obtain two forms of precipitates: one was lumpy and the other was powder-like. After separation from the solution, each form of precipitate was dried. The former was designated as fraction I and the latter, fraction J. The solid product from SP-300 was acidified, separated from the solution and dried. Then the product was extracted with pyridine at room temperature with a solvent/sample ratio of 10. The soluble portion was called fraction K. Thus SP-300 was divided into four fractions: fractions I, J, K, and Pyridine-Insoluble. Likewise, SP-320 was divided into four fractions: fractions I', J', K', and Pyridine-Insoluble. Figure 1 summarizes the procedures used in the preparation of all CDL products. Elemental compositions, molecular weight, nuclear magnetic resonance and infrared spectra were obtained for each major fraction. Details of the preparation of specific fractions of HVL-P and solubilization products and analyses can be found elsewhere (13,14).

Analyses

Fractions separated as described above were analyzed for elemental composition, molecular weight, and ash content. Nuclear magnetic resonance and infrared spectra were obtained for most fractions. No complete analytical data were obtained for certain fractions, where insolubility or insignificant yield prevented some of the determinations.

A Perkin-Elmer Model-240 Analyzer was used for determination of carbon, hydrogen, nitrogen and oxygen contents. Molecular weights were determined by vapor phase osmometry using a Corona Model 117 Apparatus (Wescan Instruments, Inc.). Procedure and concentrations were carefully selected in order to ensure good accuracy. Determinations were performed using approximately 0.5 and 1.0 milligrams of sample per ml. of solvent (14). Chloroform was used as the solvent for HVL-P and its fractions, and pyridine was used for SP-320 and SP-300 fractions. Some molecular ion values and distributions were also obtained by Plasma Desorption Mass Spectroscopy (15).

Proton magnetic resonance (PMR) spectra were obtained using a Varian EM-390 spectrometer at 90 MHz. Deuterated chloroform

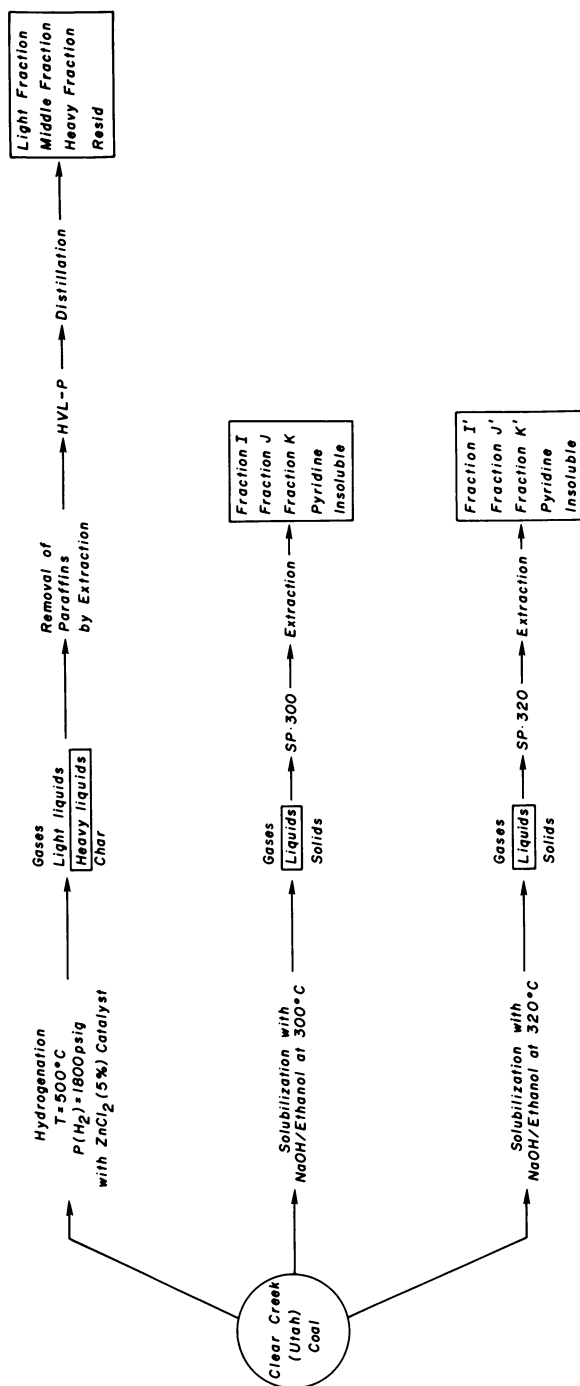


Figure 1. Preparation and fractionation of coal-derived products

was used as solvent for HVL-P and its fractions and pyridine-D₅ for SP-320 and SP-300 fractions. Tetramethylsilane was used as the reference for assignment of chemical shifts. Residual protons in a solvent were determined by means of an internal standard, p-dioxane.

Infrared spectra were obtained using a Perkin-Elmer Model 283 Spectrometer. Spectra of liquid samples were obtained from smear coating on KBr cells and KBr pellets were used for solid samples.

Structural parameters were obtained for the fractions of HVL-P using elemental composition, molecular weight and PMR data.

Definitions and formulae of the molecular parameters (16,17,18,19) obtained are as follows:

NUMBER OF AROMATIC CARBONS

$$C_A = C - \frac{1}{2} (H_{2\alpha} + H_\beta) - \frac{1}{3} (H_{3\alpha} + H_\beta) \quad (1)$$

FRACTION OF AROMATIC CARBONS (=AROMATICITY)

$$f_A = \frac{C_A}{C} \quad (2)$$

TOTAL NUMBER OF RINGS

$$R_T = \frac{2C - H + 2}{2} - \frac{1}{2} C_A \quad (3)$$

NUMBER OF AROMATIC CLUSTERS

$$C_{AP} = H_A + \frac{1}{2} H_{2\alpha} + \frac{1}{3} H_{3\alpha} \quad (4)$$

$$\#c1 = \frac{1}{3} (C_{AP} - \frac{1}{2} C_A) \quad (5)$$

NUMBER OF AROMATIC RINGS

$$R_A = \frac{C_A - 2 \#c1}{4} \quad (6)$$

NUMBER OF NAPHTHENIC AND SATURATED RINGS

$$R_N = R_T - R_A \quad (7)$$

MOLECULAR WEIGHT = MW (8)

In addition to the molecular parameters defined above, the following cluster parameters were also calculated:

$$\text{CLUSTER SIZE} = R_A / \#c1 \quad (9)$$

$$\text{CLUSTER WEIGHT} = MW / \#c1 \quad (10)$$

In the formulae, C and H are the numbers of carbon atoms and hydrogen atoms, respectively, in the empirical formula of a sample. The formula was obtained from elemental composition and molecular weight. Regarding the elemental compositions of SP-300 and SP-320 fractions, substantial amounts, ~ 10%, of an unknown component were revealed by the analysis. In the calculation of empirical formulae, the unknown was assumed to be Na or Cl incorporated into the fractions during the solubilization, since more than 85% of original ash in coal was recovered in the pyridine insolubles of SP-300 and SP-320. The incorporation means that the molecular weight of each fraction includes the contribution of Na or Cl in the fraction. In the empirical formula, Na or Cl was not included because the contribution of either one was minor. The number of hydrogen, H, was divided into those of five types, H_{AP} , $H_{2\alpha}$, $H_{3\alpha}$, H_{β} and H_{γ} based on the assignments of NMR spectrum. This division was done in HVL-P fractions. In SP-300 and SP-320 fractions, however, $H_{3\alpha}$ and H_{γ} were included in $H_{2\alpha}$ and H_{β} , respectively, because their spectra showed that (1) $H_{3\alpha}$ and H_{γ} were much smaller than $H_{2\alpha}$ and H_{β} , respectively, and (2) the resolution was poor.

Parameters, R_A , R_N , R_T , MW and #cl are for the average molecule of a sample: they will be called molecular parameters. Parameters, $R_A/\#cl$ and $MW/\#cl$, are for the average cluster; these will be called cluster parameters. Carbon aromaticity, f_A , is for either the average molecule or the average cluster; (\bar{f}_A , of the molecule is assumed to be the same as that of the cluster).

Results and Discussion

The CDL products prepared in this study were characterized with the purpose of determining structural similarities and differences. Since the products from the two alternative types of conversion (hydrogenation or solubilization) were from the same coal, it was expected that some relationships to structures present in that coal would be possible.

A proper method of fractionation is indispensable in the study of the composition of coal-derived liquids (CDL). Data in Table II show large differences between solvent extraction and distillation as fractionation methods. Two fractions, ES and EI-AS, from ethanol extraction exhibited little differences from each other, while two fractions from distillation of ES revealed marked differences in molecular weight, H/C ratio, hydroxyl group content and physical appearance.

The data in Table III likewise show a major difference between solvent extraction and distillation. Cyclohexane soluble material, CyS, had a wide spread in molecular weight as did HVL-P itself. Cyclohexane dissolved all of the Light and Middle fractions, and about 50% of the Heavy fraction and Resid in HVL-P. Thus, cyclohexane extraction is not as effective as distillation

TABLE II

Yields and Analytical Data on Ethanol-Extraction Products
from HVL-P and Distillation Products from the Ethanol
Soluble Fraction

Separation Process	Solvent Extraction of CDL ^a		Distillation of ES	
	ES ^d	EI-AS	ES-dist. ^e	ES-resid
Products				
Yield				
Wt %	60.3	25.4	56.0	44.0
Mole %	--	--	71.7	28.3
Average Molecular Formula				
C	17.9	19.3	12.9	27.7
H	20.2	21.7	16.7	27.6
N	0.2	0.2	0.1	0.3
O	1.2	1.1	1.1	1.1
Molecular Wt	257	273	192	383
Atomic H/C	1.13	1.13	1.29	1.00
Total O (% W/W) ^b	7.38	6.17	9.41	4.69
Phenolic O (% of Total oxygen) ^c	58.2	52.7	70.0	26.4
Physical Appearance at room temperature	Black Liquids, Very viscous.		Yellowish- Brown liq, Much Less Viscous Than ES.	Black Solid, Brittle and Shiny.

^aThe third fraction (EI-AI) is mostly paraffinic material.

^bDetermined by difference from C-H-N analysis.

^cDetermined from NMR spectra, elemental composition and molecular weight.

^dES=ethanol soluble fraction, EI-AS=ethanol insoluble-acetone soluble fraction.

^eYields (weight % and mole %) for ES-distillate and ES-resid are based only on the total quantity of ES.

TABLE III

Comparison of Distillation Products from HVL-P
and its Cyclohexane Soluble Fraction

Sample	Operation	Product	Molecular Weight	Yield	
				Weight %	Mole %
HVL-P	---	---	258	100	(100) ^a
	Distillation	Light	183	19.2	30.4
		Middle	210	15.7	21.6
		Heavy	272	17.6	18.7
		Resid	390	40.0	29.2
		Loss	--	7.5	--
HVL-P	Cyclohexane	CyS		72.1	--
		CyP		29.7	--
CyS	---	---	267(254)	72.1(100) ^a	(100) ^a
	Distillation	Light	181	19.6(27.2)	40.4
		Middle	229	16.7(23.2)	27.2
		Heavy	290	7.9(11.0)	10.2
		Resid	401	23.8(33.0)	22.2
		Loss	---	4.1(5.6)	--

^aValues in parentheses are weight % of total CyS. Mole % values are for HVL-P or CyS.

in fractionating HVL-P according to molecular size. The advantage of fractionation by distillation to the understanding of the nature of HVL-P will become clear as we examine other data.

Structural parameters were obtained for the fractions of HVL-P using elemental analysis, molecular weight determinations and PMR data. Structural parameters for HVL-P and its fractions are given in Table IV. The values are experimental, except those in parentheses which are calculated for the total liquid product from the weighted values of the four fractions. Experimental values of HVL-P agree well with the calculated ones, indicating good consistency. Along with the differences in molecular weight and yield, the structural parameters, except for #cl, change considerably from one fraction to another. These large variations nearly coincide with the change in the number of aromatic rings, R_A .

The number of aromatic clusters, #cl, revealed that molecules in Light, Middle and Heavy fractions consisted of one aromatic cluster, while about 30% of the molecules in the Resid have, on the average, two clusters. Overall, molecules in HVL-P have one aromatic cluster, i.e., HVL-P is apparently a product of almost complete depolymerization of the coal.

If one assumes that aromatic bonds are not broken during the production of HVL-P, then large (4- to 6-ring) arene molecules like those in Heavy and Resid would not be converted to smaller (1- to 3-ring) arene molecules like those in Light and Middle fractions. This non-convertibility suggests that the HVL-P fractions were derived from a very limited number of different arene structural groups in the feed coal. There are supporting views on the stability of aromatic clusters (12,20,21,22), and there is experimental evidence indicating considerable similarity in the fundamental arene structures of the coal and of the coal-derived liquid (10). The following examination of solubilization products provides more quantitative data on the origin of the aromatic clusters.

Since the values of molecular weight are number averages, it is possible that the molecules comprising a particular fraction vary greatly in size and structure. To determine the molecular weight distribution in HVL-P, the latter was investigated by plasma desorption mass spectroscopy (PDMS). This method of analysis, described by MacFarlane et al (15), is less destructive than electron impact ionization. While the exact relation to actual molecular weight values for coal derived materials has not been determined, the spectra should give a qualitative picture of the molecular size distribution. Figure 2 shows the result for HVL-P, depicting this CDL as a complex mixture with maximum molecular size of less than 1000 but with major portions having molecular weights between 180 to 370 and 370 to 750. The number average molecular weight 258 (268) from Table IV seems, therefore, reasonable. This HVL-P product was fractionated by vacuum distillation, as previously described, to obtain the HVL-P fractions.

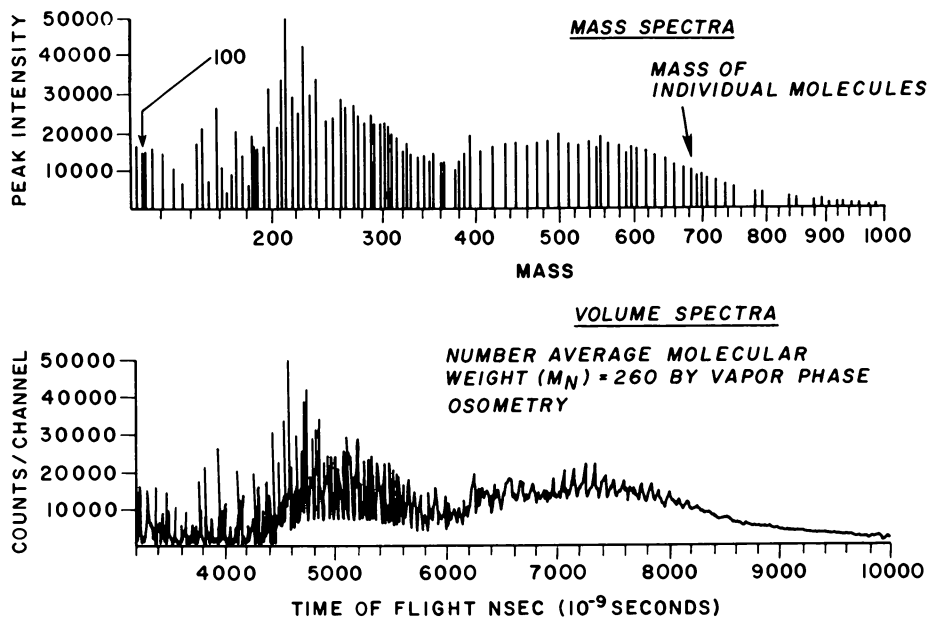


Figure 2. PDMS for heavy coal-derived liquid produced from Clear Creek (Utah) high-volatile bituminous coal. The liquid was produced by hydrogenation at 10–20 s in a catalytic process. The test was based on University of Utah heavy CDL (HCG) No. 267–22 positive ion 4 ns/CH 20000 s.

TABLE IV
Structural Parameters of HVL-P and Its Fractions

	HVL-P	Light	Middle	Heavy	Resid
Weight %	100 (92.5)*	19.2	15.7	17.6	40.0
Mole %	--- (100)	30.4	21.6	18.7	29.2
Mol. Wt.	258 (268)	183	210	272	396
f_A	0.63 (0.60)	0.55	0.58	0.59	0.68
R	3.2 (3.4)	1.8	2.3	3.7	5.6
R_A	2.4 (2.4)	1.2	1.6	2.4	4.4
R_N	0.8 (0.9)	0.6	0.7	1.3	1.2
#c1	1.1 (1.1)	1.0	1.1	1.0	1.3

*Values in parentheses for the total liquid (HVL-P) were calculated from the data of the four fractions. For example:

$$(MW)_{\text{HVL-P}} = MW_L \times Wt_L + MW_M \times Wt_M + MW_H \times Wt_H + MW_R \times Wt_R$$

where: L, M, H and R = Light, Middle, Heavy and Resid fractions, respectively
 MW = molecular weight
 Wt = weight fraction for the individual fractions

Table V shows yields and structural parameters of SP-300 fractions. These fractions were black solid materials like the feed coal, as compared to dark-brown viscous liquids of the HVL-P fractions. The overall average molecular weight of SP-300 was more than three times that of HVL-P. SP-300 fractions have much larger R_A , R_N and #cl than HVL-P fractions. The #cl values disclosed that there were, on the average, 2.8 aromatic clusters per molecule in SP-300, as compared to 1.1 aromatic clusters per molecule in HVL-P. Thus SP-300 fractions are high molecular weight materials, in which the degree of depolymerization is relatively low. This in turn suggests that SP-300 has retained more of the original structures of the parent coal than has HVL-P.

In spite of the above differences, SP-300 had a similar cluster size, $R_A/\text{\#cl}$, to that of HVL-P. This result is very important and needs to be carefully evaluated.

HVL-P represents about 70% of condensed-phase product (CPP) (viz. liquid and solid products) which includes light liquid, heavy liquid, and char. An estimate showed that the average aromatic cluster size of CPP is 2.2, which is practically the same as that of HVL-P. This indicates that HVL-P has the average chemical characteristics of CPP. This estimate was made by assuming that the light liquid and the char were similar to Light and Resid of HVL-P, respectively, in molecular weight and cluster size. If we assume that CPP retains any stable structural features of the feed coal then HVL-P would reveal such structural features.

It seems significant that the average cluster size for HVL-P and SP-300 are identical (*vide infra*). This would seem to indicate that although SP-300 has considerably more linking units intact, as evidenced by the number of clusters per molecule (#cl), the actual clusters have essentially the same size ($R_A/\text{\#cl}$). This reinforces the notion that the aromatic clusters are stable even under the relatively drastic conditions by which HVL-P was produced.

Examination of SP-320 gives additional insight on the stability of the aromatic clusters. SP-320 fractions were black solid materials like SP-300 fractions or the parent coal. Table VI, however, shows that SP-320 fractions are lower in molecular weight, R_A , R_N and #cl than SP-300, which could be expected from the higher reaction temperature. In addition, yields were changed.

Since only the reaction temperature was different, it is reasonable to treat SP-300 as an intermediate in the production of SP-320. Then the comparison of the yields of SP-300 and SP-320 fractions discloses, for example, that a substantial portion of fraction K (in SP-300) was converted to fraction J' (in SP-320). Further, although molecular weight, R_A , R_N and #cl are much smaller, yield and $R_A/\text{\#cl}$ of fraction I' are practically

TABLE V

STRUCTURAL PARAMETERS OF SP-300 AND ITS FRACTIONS								
Yield*	MW	R _A	R _N	#c1	f _A	R _A /#c1	MW/#c1	
SP-300**	81.0	908	6.4	4.2	2.8	0.53	2.3	327
Fraction I	23.6	794	5.3	4.2	2.8	0.52	1.9	287
Fraction J	8.3	655	3.6	2.3	2.6	0.54	1.4	250
Fraction K	49.1	1050	7.9	4.7	2.8	0.53	2.8	373

TABLE VI

STRUCTURAL PARAMETERS OF SP-320 AND ITS FRACTIONS								
Yield*	MW	R _A	R _N	#c1	f _A	R _A /#c1	MW/#c1	
SP-320**	74.6	540	3.4	2.4	2.2	0.53	1.5	246
Fraction I'	25.4	496	3.4	2.3	1.8	0.56	1.9	274
Fraction J'	21.0	443	2.3	2.0	1.9	0.50	1.2	236
Fraction K'	28.2	713	4.8	2.9	3.2	0.53	1.5	223

*Weight % of coal (MAF)

**The parameters were calculated from the three fractions

the same as those of fraction I. This means that aromatic clusters were not altered during the conversion of fraction I to I'. During the conversion, linkages between aromatic clusters were broken to produce smaller molecules without cleavage of the clusters. The average cluster in fraction I and I' contained 1.9 aromatic rings.

The product yields of fractions J' and K' in SP-320 are considerably different than J and K in SP-300, indicating that some linking units have been broken as a result of this relatively small (20°C) temperature increase. There are several types of reactions, including hydrogenation, which could account for not only the change in yields but also the different number of aromatic rings per cluster ($R_A/\#cl$).

Thus, for example, when anthracene is converted to 9,10-dihydroanthracene, the number of clusters increases from 1 to 2 while $R_A/\#cl$ decreases from 3 to 1. The same trend is shown by fractions K and K'. Ross and Blessing (21) have obtained data on model compounds which support this interpretation. According to Makabe and coworkers (11,12), some Japanese coals were slightly hydrogenated in the same solubilization process as in this investigation. They did not fractionate their products. Since our results reveal that small aromatic clusters were not changed, then the large clusters of K must have undergone partial ring hydrogenation.

Infrared absorption spectra provide information about the functionality of the fractions but also give some indications about the makeup of the aromatic clusters. Infrared absorption maxima of the CDL fractions in the 690-900 cm^{-1} range (CH out-of-plane bending in substituted benzene rings) were examined in order to obtain information on the type of substitution in the aromatic rings included in the cluster systems. Strong bands observed near 800 cm^{-1} indicate that aromatic rings with two or three adjacent hydrogens, e.g. 1,4-disubstituted, 1,2,3-trisubstituted, and 1,2,3,4-tetrasubstituted rings (any condensed ring being at least disubstituted), are among the preferred ring substitution types. The presence of other substitution types is presently under investigation (23).

In order to determine whether any direct structural information about coal can be obtained from the liquids used in this study, structural parameter data are compared in Table VII. Some general observations include the following:

1. Aromaticity values (f_A) for all solubilization fractions were essentially identical (~ 0.52); f_A values were higher (0.60) for the hydrogenation product (HVL-P)
2. Molecular weights were highest for SP-300 fractions (which were prepared under the mildest conditions), lower for SP-320 and lowest for HVL-P and its fractions.
3. The number of clusters per molecule in SP-300 was highest (2.6), lower for SP-320 (2.1) and lowest for HVL-P (essentially 1), indicating the relative degree

TABLE VII

	Yield, Wt%*	Mol. Wt.	R _A	R _N	#Cl	f _A	R _A /#Cl
<u>Analytical Data on HVL-P and Its Fractions</u>							
HVL-P	100 (92.5)**	258 (268)**	2.4 (2.4)**	0.8 (0.9)**	1.1 (1.1)**	0.63 (0.60)	2.2
Light	19.2	183	1.2	0.6	1.0	0.55	1.2
Middle	15.7	210	1.6	0.7	1.1	0.58	1.5
Heavy	17.6	272	2.4	1.3	1.0	0.59	2.4
Resid	40.0	396	4.4	1.2	1.3	0.68	
<u>Structural Parameters of the Solubilization Products</u>							
SP-300	85.7	843	5.6	3.9	2.6	0.52	2.2
Fraction I	23.9	777	5.0	3.3	2.7	0.52	1.9
J	9.1	643	3.4	3.4	2.5	0.53	1.4
K	52.7	930	6.6	4.4	2.6	0.51	2.5
SP-320**	76.5	520	3.2	2.4	2.1	0.52	1.5
Fraction I'	26.6	478	3.2	2.3	1.7	0.55	1.9
J'	23.8	444	2.4	2.0	1.8	0.50	1.3
K'	26.1	690	4.4	3.1	3.1	0.52	1.4

*Weight % of coal.

**The parameters were calculated from the three fractions.

of depolymerization, *viz.* the degree of cleavage between clusters.

4. The number of naphthenic rings was lowest for HVL-P fractions (0.8), higher (2.4) for SP-320 and highest (3.9) for SP-300.

The molecular weights per cluster (Table VII) are in the same range of values as found by others for products prepared by other methods (24,25) and also by Makabe and Ouchi using NaOH ethanol on Japanese coals (11,12).

Structural parameters and IR spectra confirm the presence of oxygen-containing functional groups in the liquid products. The types and relative stability of phenolic, etheric and carbonyl functional groups have been studied by Kang (24) and it was indicated that some of these could serve as linking groups between the clusters. Recent IR studies of high volatile bituminous coal extracts, obtained under very mild conditions, clearly indicate the presence of a variety of carbonyl groups, e.g. ester and keto groups, which in addition to etheric and alkylene (e.g., methylene) groups could serve as intercluster linkages in the original coal (23).

Taking into account the results reported here on the various fractions, Figure 3 shows structures consistent with the data. Molecular formulae were determined from the elemental analyses of the fractions. Other functionalities and linking units could also satisfy the data; however, those shown were considered most likely based on the results and steric and stability considerations. The structures in Figure 3 contain only major features such as the nature of the aromatic clusters, as well as the approximate numbers of aromatic and naphthenic rings per cluster. Functional groups and side chains are indicated only in a qualitative manner.

Conclusions

Results obtained in this investigation indicate that a large portion of the bituminous coal used is composed of "super-clusters" of aromatic rings that are not significantly altered by different liquefaction procedures, e.g., hydrogenation or solubilization. Increasing the severity of the treatment appears only to break more linkages between these "super-clusters" and to cleave hydroaromatic rings condensed to them. In the HVL-P hydrogenation product essentially all of the linking units between clusters were broken, resulting in one cluster per molecule. Solubilization with NaOH-ethanol gave products which were less "depolymerized".

The implications of the results obtained include the possibility that the types and molecular weight distribution of liquid products obtainable from a particular coal are controlled to a large extent by the size and the structure of the clusters in the original coal. Therefore, the depth of the

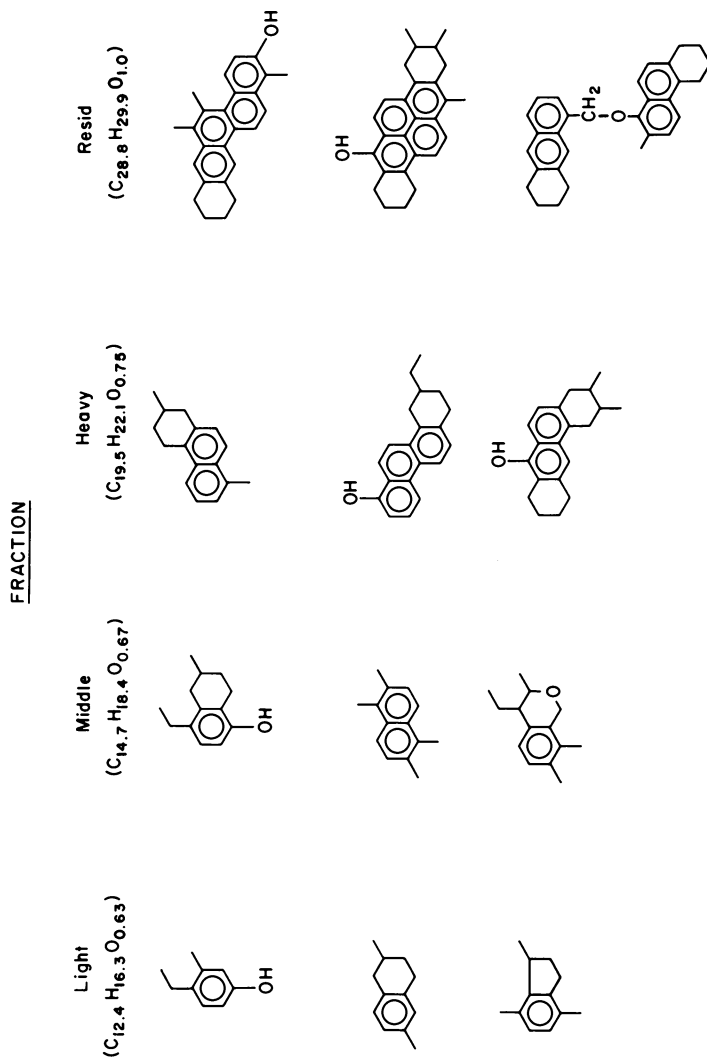


Figure 3. Possible structural units in the HVL-P fractions consistent with structural parameter data (values in parentheses represent average molecular formulae for the indicated fractions)

depolymerization of coal is apparently limited, and the limit could only be approached by elimination of all intercluster linking groups. Any further decomposition of the aromatic clusters could be achieved by upgrading reactions, e.g., ring hydrogenation followed by cracking, which do not usually occur to a significant extent in primary liquefaction processes. Further work on other coals should be done to determine the validity of this conclusion.

Literature Cited

1. Radd, F. J., Carel, B., and Hamming, M. C., Fuel, 1976, 55, 323.
2. Martin, T. G. and Snape, C. E., Amer. Chem. Soc. Fuel Chem. Div. Preprints, 1980, 25, 4, 79
3. Whitehurst, D. D., "Organic Chemistry of Coal," Amer. Chem. Soc. Symposium Series no. 71, 1978, pp. 1-35.
4. Bartle, K. D., Ladner, W. R., Martin, T. G., Snape, C. E., Williams, D. F. Fuel, 1979, 58, 418.
5. Makabe, M. and Ouchi, K., Fuel, 1979, 58, 43.
6. Ramakrishnan, R., "Hydropyrolysis of Coal Derived Liquids and Related Model Compounds," Ph.D. Thesis, University of Utah, Dec. 1978, and references therein.
7. Anderson, L. L., Wood, R. E. and Wisner, W. H., Society of Mining Engrs., A.I.M.E., Transactions, 1976, 260, 318.
8. Wood, R. E., Wisner, W. H., Anderson, L. L., Oblad, A. G., U. S. Patent 4,134,822, Jan. 1979.
9. Wood, R. E. and Wisner, W. H., Ind.Eng.Chem., 1976, 15, 1.
10. Zilm, K. W., Pugmire, R. J., Grant, D. M., Wood, R. E. and Wisner, W. H., Fuel, 1979, 58, 43.
11. Makabe, M., Hirano, Y. and Ouchi, K., Fuel, 1978, 57, 289.
12. Makabe, M. and Ouchi, K., Fuel, 1979, 58, 43.
13. Chung, K. E., "Characterization of Coal-Derived Liquids-- Relationships to Chemical Structures in Coal," Ph.D. Thesis, University of Utah, June 1980.
14. Chung, K. E., Anderson, L. L. and Wisner, W. H., Fuel, 1979, 58, 847.
15. MacFarlane, R. D. and Torgensen, D. F., Science, 1976, 191, 920.
16. VanKrevelen, D. W., Coal, Elsevier Publishing Inc., New York, 1961, Chapter 22, 433.
17. Clutter, D. R., Petrakis, L., Stenger, R. L. and Jensen, R. K., Anal. Chem., 1972, 44, 1395.
18. Kanda, N., Itoh, H., Yokoyama, S. and Ouchi, K., Fuel, 1978, 57, 676.
19. Brown, J. K., Ladner, W. R. and Shepard, N., Fuel, 1960, 39, 79.
20. Wender, I., "Catalytic Synthesis of Chemicals from Coal," Catal. Rev.-Sci. Eng., 1976, 14, 1, 97.

21. Ross, D. S. and Blessing, J. E., "Alcohols as H-Donor Media in Coal Conversion. 1. Base-Promoted H-Donation to Coal by Methyl Alcohol," Fuel, 1979, 58, 438.
22. Wiser, W. H., "Proceedings of the Conference - Scientific Problems Relevant to Coal Utilization," DOE Sym. Ser., West Virginia University, Morgantown, WV., 1977.
23. Shabtai, J., Katayama, Y., Oblad, H. B., and Anderson, L. L., unpublished data.
24. Kang, D., Anderson, L. L., Wiser, W. H., Technical Report, U. S. Dept. of Energy E(49-18)2006, University of Utah, 1979.
25. Hombach, H. P., private communication.

RECEIVED May 5, 1981.

Dialytic Extraction of Coal and Its Application to the Study of Metals Speciation

DENNIS H. FINSETH, BERNARD J. PORZUCEK, and RICHARD G. LETT

U.S. Department of Energy, Pittsburgh Energy Technology Center,
P.O. Box 10940, Pittsburgh, PA 15236

A question of considerable interest in coal hydroliquefaction chemistry is the amount and nature of "organically bound metals" in the coal. One reason for this interest is the observation that when supported metal direct conversion catalysts are used in liquefaction reactors, a primary mode of deactivation is metals deposition (1, 2). In particular, recent work at the Pittsburgh Energy Technology Center (PETC) (4,5) and elsewhere (3) has indicated very high levels of titanium deposition on supported CoMo catalysts used in the fixed bed continuous reactor system. It has been suggested that the culprits in such deposition are "soluble metal species" (6-9). The analyses of a Western Kentucky (Homestead) hvBb feed coal and of material deposited between the catalyst pellets in the fixed bed reactor at PETC (4) are shown in Table I.

Table I. Metals Analysis of Reactor Deposit and Feed Coal From Run FB-61

	Metals Analysis		
	<u>Fe</u>	<u>Si</u>	<u>Ti</u>
Reactor Deposit	11%	10%	12%
Feed Coal	3.6%	3.3%	0.1%
Enrichment Ratio (Deposit/Coal)	3	3	120

The high enrichment ratio observed for titanium in the deposit is difficult to explain if all the metal in the coal is present in the mineral state. The data can be interpreted as an indirect indication of the presence in the feed slurry of an unstable titanium species which, upon contact with the catalyst surface, codeposits with carbon, boron, and other metals. A plausible explanation for this observation would be that organotitanium compounds exist in the coal and that they thermally or catalytically decompose to yield a stable inorganic species. Some recent model compound studies by Treblow and coworkers have indicated that

This chapter not subject to U.S. copyright.
Published 1981 American Chemical Society

indeed titanium organometallics will be quantitatively converted to TiO_2 (anatase) under reactor conditions (5).

The goal of this work was to design an experiment which would allow one to establish the level of "soluble" titanium compounds in a coal. The determination of the level of these materials in coal is made extremely difficult not only by the insoluble nature of the coal but also by the difficulty in discriminating between truly soluble material and finely divided particulate matter which slips through the filters and thimbles used in classical extraction procedures, remaining suspended in the extract solution.

A number of workers have investigated the size distribution of mineral particles in coal, and it seems that irrespective of the technique used, the particle size distribution extends beyond the lower limit of the technique (10, 11). In particular, a recent transmission electron microscopy study (11) found the mineral size distribution to extend down to $\sim 50 \text{ \AA}$. This result indicates that the problem in characterizing the nature of "soluble" metal is one of discriminating between soluble molecular species and 50 \AA particulates.

Organometallics have been identified in coals via very tedious separation procedures similar to those used for their isolation from petroleum samples (12). The difficulties associated with such schemes for the characterization of organometallics in coal are far greater than those associated with similar studies of petroleum crudes. This increase in difficulty is primarily due to the insolubility of the sample. Unfortunately most methods for increasing the solubility of coal are chemically of such severity that they would simultaneously decompose any organometallic that was originally present.

Accepting the limitation that organometals can only be studied in the soluble portion of the coal, it would be very useful to have a method which would allow discrimination between "soluble" and microparticulate metals. With such a method, one could at least determine an upper limit for the soluble metal concentration.

Experimental

The procedure arrived at in this work is a modification of a previously reported dialysis method for separation of petroleum (13) and coal hydrogenation products (14). The method involves transport of soluble material through a latex rubber membrane in an appropriately chosen solvent. The only material which can be transported through the membrane is that which is truly soluble in the solvent/membrane system; therefore the technique discriminates soluble material from colloidal or suspended matter.

The apparatus used is described in Fig 1. The application of this apparatus depends on the use of a solvent which swells the latex membrane and is also a good solvent for the sample to be dialyzed. Benzene, chloroform, or methylene chloride can be used when the method is applied to coal-derived liquids. However, these solvents are not particularly effective for the dissolution of coal. On the other hand,

pyridine -- a good coal solvent -- is not as effective as CH_2Cl_2 for swelling the membrane; furthermore, a much higher pot temperature is required to use it in the reflux loop. To permit the use of pyridine as the coal solvent and CH_2Cl_2 as the reflux solvent, the apparatus was operated with CH_2Cl_2 inside the membrane and pyridine outside the membrane in the sample compartment. This is not an ideal situation because it precludes the unattended long term operation of the unit. The reason for this limitation is that the permeability of the membrane, the key to the utility of the technique, allows the CH_2Cl_2 to pass freely into the sample compartment, diluting the pyridine and thus reducing coal solubility. Simultaneously the pyridine accumulates in the dialyzer receiver, raising the boiling point and thus terminating reflux.

To perform a dialytic extraction, the apparatus is assembled and preextracted for 48 hours using pyridine and methylene chloride outside and inside the membrane, respectively. The coal (~ 100 g) is then slurried in a 2-3 fold excess of pyridine (ACS reagent grade) and placed in the sample compartment, where it is constantly stirred. The methylene chloride reflux is begun at this point, and the extract collects in the receiver. When the buildup of pyridine in the receiver results in stoppage of the reflux cycle, the contents of the receiver are collected, and it is refilled with clean methylene chloride. The overflow from the sample compartment was evaporated under a flow of dry nitrogen, redissolved in pyridine, and replaced in the sample compartment daily. The dialytic extraction is slower than the soxhlet procedure, and the yield is substantially less. For example, the yield of a four day dialytic extraction of Powhatan Coal was 6%, while a two day pyridine soxhlet on the same coal yields 12-15% extract.

After allowing it to stand overnight, the dialytic extract is isolated from the pyridine-methylene chloride solution in the receiver by filtration, three consecutive water washes, and rotary evaporation. Residual solvent was removed by freeze drying from benzene. The filtration and water washes are necessary to remove $((\text{C}_5\text{H}_5\text{N})_2\text{CH}_2\text{Cl})_2$, which unfortunately forms on mixing pyridine and methylene chloride.

Results

The comparison of a number of dialytic extracts with the parent coals is given in Table II. These results indicate that the elemental composition of the dialytic extract closely mirrors that of the organic fraction of the coal. Similar conclusions were reached when coal liquids were separated via the dialytic method. The conclusion that dialysis does not concentrate any particular compound type deserves further investigation, since obtaining a representative sample is crucial to the utility of the method. In Table II, it is particularly interesting to note that in each case the "organic sulfur" from the classical coal analysis is almost identical to the sulfur content directly determined on the dialytic extract.

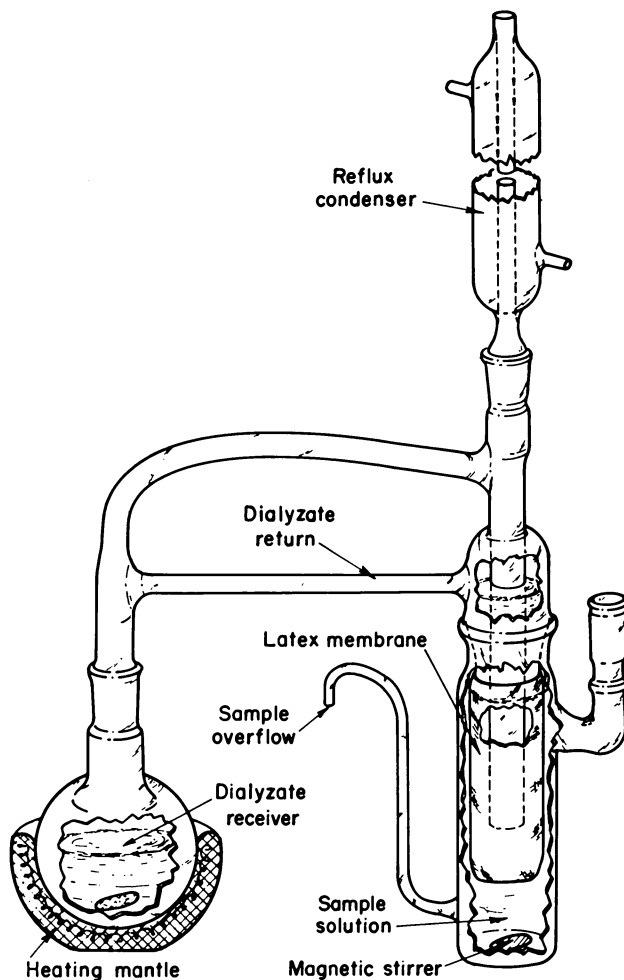


Figure 1. Continuous dialysis apparatus

Table II. Analysis of Coals and Extracts

SAMPLE	COAL ANALYSIS ^(a)					EXTRACT ANALYSIS					
	C	H	N	O	S	C	H	N	O	S	MW ^(b)
POWHATAN	808	5.6	14	82	21	825	6.6	14	65	19	450
	SOXHLET →					789	5.6	28	88	2.0	2000
BURNING STAR	783	5.2	16	11.3	23	82.4	7.4	12	6.7	2.4	380
SHANG SHI	783	5.5	11	4.7	78	81.4	6.6	9	3.0	7.9	400

^a Elemental Analysis on MAF basis

^b MW determined by VPO in pyridine

Several of these extracts have been analyzed for iron and titanium via the X-ray fluorescence technique. The results for West Virginia (Ireland Mine) hvAb coal, one which has been found to deposit titanium on fixed bed catalysts, are presented in Table III.

Table III. Metals Analysis of Ireland Mine Coal and Its Extracts

	Metals Analysis	
	Fe	Ti
Coal	4%	400 ppm
Dialytic Extract ^(a)	10 ppm	2 ppm
Soxhlet Extract	600 ppm	90 ppm

(a) The metal levels in this sample are very near background, resulting in large uncertainties (+ 100%).

These metal analyses indicate a marked reduction of both titanium and iron in the dialytic extract relative to both the coal and the soxhlet extract. The question remaining is, how much of this metal is background? It should be noted here that attainment of good trace element analyses in the low ppm range requires very careful experimental precautions and replicate analyses. This particular experiment is, by its nature, difficult to conduct in a scrupulous "trace element clean" manner. However, if it is assumed that contamination from any source (solvents, glassware, utensils, etc.) will usually add to the concentration of metal, we can use the metal content determined in the dialyze as an upper limit for soluble metals content. The higher iron and titanium concentrations in the soxhlet extract indicate that these metals may be associated with material which is not truly soluble, such as microparticulate mineral matter.

Discussion

The results of this investigation indicate that the level of transition metals in the soluble portion of Ireland Mine coal is <20 ppm. Consequently if one desires to study them in more detail, the techniques used must be sensitive to this level. The utility of this method in drawing conclusions about the absolute concentration of soluble metals depends very strongly on further work to establish the background level for metals in the experiment. If organometallics are not found to any significant extent in the soluble portion of coal, the organometallic decomposition model for catalyst deposition/deactivation may require modification. The data presented in this work suggests that if this mechanism for deactivation is operable, the organometallics are associated with the insoluble portion of the coal.

A further complicating possibility which must also be considered is that the metals are indeed present in soluble form but are bound in

**American Chemical
Society Library**

1155 16th St. N. W.

In New Approaches in Coal Chemistry; Blaustein, B., et al.;
ACS Symposium Series 20036; American Chemical Society: Washington, DC, 1981.

very high molecular weight complexes which have difficulty traversing the membrane. In work on liquefaction products, a small selectivity for lower molecular weight (size) components has been observed. (15)

Conclusion

In conclusion, it appears that the dialytic method, although somewhat more cumbersome than traditional soxhlet techniques, provides a coal extract which is representative of the soluble organic material in the coal and is free of particulates. Preliminary results indicate that this dialytic extract may be very useful in studies of the existence and/or nature of soluble metals in coal. Although further work is indicated, the very low metal content of the dialyzate casts some doubt on the model for titanium deposition on catalysts, which involves decomposition of a soluble organically associated metal species on the catalyst surface.

Acknowledgement

The authors gratefully acknowledge the aid of Mr. Edward L. Wetzel in obtaining the X-ray fluorescence metal analyses.

Literature Cited

1. Given, P. H.; Miller, R. N.; Suhr, N.; Spackman, W. In "Trace Elements In Fuel", Advances In Chemistry Series 141; Babu, S. P., Ed.; American Chemical Society: Washington, D. C., 1975; Chapter 14.
2. Stanulonis, J. J.; Gates, B. C.; Olsen, J. H. AICHE J. 1976, 22(3), 576-581.
3. Kovach, S. M.; Castle, L. J.; Bennett, J. V.; Schrodt, J. T. Ind. Eng. Chem. Prod. Res. Dev. 1978, 17(1), 62-67.
4. Makovsky, L. E.; Pollack, S. S.; Brown, F. R. Nature 1980, 228(13), 154-155.
5. Treblow, M.; Spitler, C.; Brown, F. R., presented at the Materials Research Society Annual Meeting, Cambridge, MA, Nov 1979.
6. Zubovic, P. In "Coal Science", Advances In Chemistry Series 55; Gould, R., Ed.; American Chemical Society: Washington, D. C., 1966; Chapter 13.
7. Gluskoter, H. J.; Ruch, R. R.; Miller, W. G.; Cahill, R. A.; Dreher, G. B.; Kuhn, J. K. "Trace Elements In Coal: Occurrence And Distribution", Circular 499; Illinois State Geological Survey: Urbana, IL, 1977; pp. 109-125.
8. Horton, L.; Aubrey, K. V. Chem. Ind. (London) 1950, 69(1), 541-548.
9. Filby, R. H.; Shah, K. R.; Hunt, M. L.; Khalil, S. R.; Sautter, C. A. "Solvent Refined Coal (SRC) Process: Trace Elements"; Washington State University, Nuclear Radiation Center, Pullman, WA, Mar 1978, DOE Report FE/496-T17.

10. Lin, J. S.; Hendricks, R. W.; Harris, L. A.; Yust, C. S. J. Appl. Crystallogr. 1978, 11, 621-625.
11. Strehlow, R. A.; Harris, L. A.; Yust, C. S. Fuel 1978, 57, 185-186.
12. Bonnett, R.; Caechowski, F. Nature 1980, 283, 465-467.
13. Hill, M. W.; Mansell, M. W. ACS Div. Fuel Chem. Preprints 1960, 5(3), 115.
14. Finseth, D. "Proceedings of the 14th Intersociety Energy Conversion And Engineering Conference", Boston, MA, Nov 1979, p 826.
15. Finseth, D.; Porzucek, B.; Queiser, J. A. Unpublished work.

RECEIVED May 5, 1981.

Characterization of Coal-Derived Materials by Matrix Isolation Spectroscopy

E. L. WEHRY and GLEB MAMANTOV

Department of Chemistry, University of Tennessee, Knoxville, TN 37916

The identification and quantitative determination of specific organic compounds in very complex samples is an area of intense current research activity in analytical chemistry. Optical spectroscopy (particularly UV-visible and infrared absorption and molecular fluorescence and phosphorescence techniques) has been used widely in organic analysis. Any optical spectroscopic technique to be used for characterization of a very complex sample, such as a coal-derived material, should exhibit very high sensitivity (so that trace constituents can be determined) and extremely great selectivity (so that fractionation and separation steps prior to the actual analysis can be held to the minimum number and complexity). To achieve high analytical selectivity, an analytical spectroscopic technique should produce highly structured and specific spectra useful for "fingerprinting purposes," as well as to minimize the extent of overlap of spectral bands due to different constituents of complex samples. In addition, the spectral behavior of any particular sample constituent (both the positions and intensities of the various bands) should be unaffected by the other constituents of the sample, irrespective of their identities and concentrations. Most "conventional" sampling techniques utilized in spectroscopic analysis fail to satisfy these admittedly stringent criteria. In order to maximize the selectivity of spectroscopic analysis without undue sacrifice of sensitivity, we have turned to the sampling technique of matrix isolation for the spectroscopic characterization of very complex samples.

In the technique of matrix isolation (hereafter denoted "MI"), samples which are liquid or solid at room temperature are vaporized under vacuum, and then mixed with a large excess of a diluent gas (termed the "matrix gas") which in effect, is the "solvent" in the spectroscopic analysis. This gaseous mixture is then deposited on a cold surface for spectroscopic analysis as a solid. For most purposes, temperatures of 15 K (which can be obtained by use of commercial closed-cycle refrigerators) are satisfactory; for some specialized fluorescence experiments,

0097-6156/81/0169-0251\$05.00/0

© 1981 American Chemical Society

temperatures as low as 4 K (which require use of liquid cryogenes) are occasionally needed. The purpose of the matrix isolation procedure is to produce a solid sample in which the solute molecules are distributed in an essentially random manner in the solid matrix, thus eliminating aggregation of solute molecules. In the ideal MI experiment, solute-solute interactions will be absent and solute-solvent interactions will be weak. Under these conditions, highly structured and reproducible molecular spectra are obtained, and interferences by one compound in the determination of another are minimized. The techniques and objectives of analytical MI spectroscopy are reviewed thoroughly (1), and the reader is referred to that review for additional detail.

MI Molecular Fluorescence Spectrometry

Molecular fluorescence spectrometry has long been regarded as a useful technique for the determination of polycyclic aromatic hydrocarbons (PAHs) and related materials, due to the very high sensitivities which can be achieved. However, molecular fluorescence spectra measured in liquid solution usually are broad and relatively featureless; hence, spectral interferences are common in the liquid-solution fluorometric analysis of multicomponent samples. Moreover, the fluorescence of a particular component of a complex sample may be partially quenched by other sample constituents; if quenching occurs to a significant extent, the fluorescence signal observed for a particular compound present at a particular concentration will also depend upon the identities and concentrations of other substances present in the sample. Under these conditions, it is virtually impossible to obtain accurate quantitative results. Therefore, it is generally observed that molecular fluorescence spectrometry in liquid solution media is useful for quantitative determination of individual components in complex samples only if the fluorescence measurement is preceded by extensive separation steps (ideally to produce individual pure compounds or, at worst, simple two- or three-component mixtures).

It has long been recognized that both the diffuse spectra and quenching problems can be alleviated by performing the fluorescence measurement in a low-temperature solid matrix, rather than in a fluid solution. The most common low-temperature matrices used in molecular fluorometric analysis are frozen liquid solutions; the analytical characteristics of frozen-solution luminescence spectrometry have been discussed extensively in the literature (2-10). Obviously, MI represents an alternative technique to use of frozen liquid solutions for low-temperature fluorometric analysis. There are two principal advantages of MI over frozen-solution fluorometry. First, in MI, any material which has an appreciable vapor pressure at room temperature can be used as a matrix; one is not limited by the

solubility characteristics of the sample constituents. Second, the formation of a frozen solution may be accompanied by aggregation of solute species (the solubilities of which decrease with decreasing temperature). In that event, spectral broadening and quenching may occur, and the purposes of the low-temperature measurement technique may therefore be negated. In matrix isolation, such effects cannot arise if a sufficiently large mole ratio of matrix gas to sample is employed and if the solid deposit is prepared properly (e.g., by ensuring that the surface upon which the deposit is formed has a high coefficient of thermal conductivity). The major disadvantage of MI is its restriction to samples which can be vaporized without accompanying decomposition; frozen-solution techniques of course are not subject to that restriction.

The characteristics of MI fluorescence spectra of PAHs and their derivatives have been discussed in a series of publications from this laboratory (1, 11-19); the following characteristics of MI fluorescence spectrometry are especially relevant to PAH analyses in coal-derived materials. First, highly resolved spectra are obtained, sufficient for distinguishing between isomeric PAHs, such as the six isomeric methylchrysenes (12). Especially high spectral resolution is achieved if a laser is used as the excitation source (17-19); when laser-induced fluorescence techniques are employed in conjunction with matrix isolation, it has been shown possible to excite fluorescence spectra for individual constituents of complex samples which are indistinguishable from the spectra of the pure compounds in question (17). Second, the quantitative calibration curves for MI fluorometric analyses are linear from the detection limit [which may be less than 1 pg in optimal cases (17)] to an amount of an individual PAH exceeding 1 μ g (11). Therefore, the linear quantitative working range is typically at least four, and occasionally as many as seven, orders of magnitude in solute concentration. Third, the temporal (as well as spectral) characteristics of molecular fluorescence can be used to distinguish between different fluorescent sample constituents by the technique of time-resolved fluorescence spectrometry (16); time-resolution experiments are facilitated by tendencies for fluorescence decay times for PAHs in low-temperature matrices to be somewhat longer than those observed in fluid media. Finally, as will be discussed in more detail below, the fact that MI requires vaporization of the sample means that it is amenable to direct interfacing with gas chromatographic separations.

The principal analytical disadvantage of MI fluorescence spectrometry is the obvious one that fluorescence is not a universal analytical technique. Many organic compounds of interest fluoresce weakly and can not be determined by any form of fluorescence spectrometry at realistic concentration levels. Accordingly, it is often necessary to use MI fluorometry in conjunction with other techniques which, though less sensitive

for some compounds, are responsive to substances which can not be detected by fluorescence. For this purpose, we have employed matrix isolation Fourier transform infrared (FTIR) spectrometry.

MI Fourier Transform Infrared Spectrometry

While virtually all molecules exhibit an infrared spectrum (which is a highly characteristic "fingerprint"), infrared spectrometry has received little use in the characterization of coal-derived materials. The principal reason for this situation is the relatively insensitive response of infrared absorption (which is conventionally regarded as a useful analytical technique only for major constituents of complex samples). The development and commercialization of Fourier transform infrared spectrometers has greatly enhanced the analytical sensitivity of infrared spectroscopy (20), so that it is now feasible in favorable cases to detect organic compounds in submicrogram quantities by FTIR. However, the sampling procedures conventionally employed in infrared spectroscopy (KBr discs, liquid solutions, mulls) exhibit shortcomings which are revealed in particularly dramatic fashion when high-performance FTIR instrumentation is used. As in the case of fluorescence spectroscopy, we believe the analytical capabilities of FTIR analysis can be significantly enhanced by the use of matrix isolation as the sampling technique.

MI offers several rather obvious advantages over more conventional infrared sampling procedures. First, provided that the proper matrix (e.g., argon or nitrogen) is used, the matrix material is transparent throughout the entire near- and mid-IR region, thus utilizing effectively the multiplex and throughput advantages of FTIR instrumentation. In contrast, virtually all liquid solvents, media for mull preparation, and solids for pellet preparation exhibit absorption in parts of the infrared region which are of potential analytical interest. A second important advantage of MI as an IR sampling technique is that spectral bands are usually narrower than in other media, and spectra frequently are simpler than those obtained for the same molecule in other condensed-phase sampling media or in the gas phase. Third, in an MI experiment, intermolecular (solute-solute) interactions should be suppressed, thus leading to adherence to Beer's law over wider ranges of analyte concentration than is normally observed in more conventional IR sampling media. Fourth, the size of a deposit in an MI experiment can be controlled and can be made to be very small; hence, MI has some very attractive features as a technique for microsampling in IR spectroscopy. Finally, if the proper apparatus is used, samples for FTIR analysis can be prepared rapidly by MI; many of the conventional IR sampling techniques (particularly mulls and KBr pellets) are time-consuming to prepare. The principal disadvantage of MI as an IR sampling technique is the fact, as noted above, that the sample must undergo vaporization without decomposition for the technique to be applicable.

We have described elsewhere the nature of the MI FTIR spectra of PAHs and their derivatives (1, 12, 13, 15, 18, 21-24); the following points are especially significant. First, FTIR spectra devoid of rotational structure and having individual bandwidths on the order of $2-7 \text{ cm}^{-1}$ are obtained both for PAHs and for polar derivatives thereof (such as nitrogen heterocycles). These spectra are sufficiently characteristic to enable identification of individual isomers to be made in mixtures [e.g., the six methylchrysenes (12) and the various mono- and dimethyl naphthalenes and biphenyls (24)]. Second, detection limits for individual PAHs can be as low as 50 ng, if special "microsampling" deposition apparatus is used (23). Third, Beer's law plots typically are linear over 1.5-2 decades in PAH concentration; by the complementary use of two different deposition cells, linearity over 3 decades in PAH concentration for Beer's law plots can be approached (23). Finally, for both MI FTIR and MI fluorescence spectrometry, analytical precision of ca. 3-7 % relative standard deviation can be achieved.

MI Spectrometric Characterization of Real Samples

In some cases, MI spectrometry can be used for the direct identification of PAH constituents without prior separation. For example, Figure 1 shows the fluorescence spectra, in a vapor-deposited n-heptane matrix excited by a dye laser, of a Solvent Refined Coal sample (SRC 1) at two different excitation wavelengths and with the use of time resolution to reduce the level of background fluorescence from the sample. Previous studies have shown that very sharp fluorescence spectra (frequently having bandwidths of 5 cm^{-1} or less) are obtained by laser excitation of fluorescence of PAH mixtures in organic matrices; often, selective excitation of fluorescence from a single PAH is possible even in mixtures containing more than 20 PAHs (including isomer sets) (17). In this particular example, the fluorescence spectrum of benzo[a]pyrene (BaP) is selectively excited at 383.0 nm if a time delay of 35 ns between excitation and measurement of fluorescence is used to allow the fluorescence of a possible interferent (perylene) to decay. [The use of time resolution in MI fluorometry to distinguish between compounds having similar fluorescence spectra is discussed in detail elsewhere (16)]. If the excitation wavelength is changed to 405.0 nm, perylene is now selectively excited, and time resolution is not needed to effect additional selectivity because, at that particular wavelength, only perylene fluorescence is excited. For the direct excitation of fluorescence from low-temperature samples of coal-derived materials, without prior separation steps, use of a laser as the source appears absolutely essential (2, 17).

In other cases, it may be prudent or necessary to subject the sample to some degree of separation prior to spectroscopic

analysis. In such samples, the objective of the separation is not to produce individual pure compounds, but rather to generate fractions (which themselves may still be very complex) which can be dealt with by high-resolution spectroscopy. For example, Figure 2 shows the fluorescence spectrum in a nitrogen matrix of a wastewater sample from a steel mill coking plant which had been subjected to a preliminary class separation by column chromatography (the fraction whose MI fluorescence spectrum is shown was the PAH fraction). The spectrum shown in Figure 2 is complex, but a number of PAHs can readily be identified. The selective laser excitation technique discussed in the preceding paragraph produces spectra of much greater specificity (17). For example, Figure 3 compares the MI fluorescence spectra, excited by a dye laser in a heptane matrix at 15 K, of pure benzo[a]pyrene and of the coking plant water chromatographic fraction. Although the chromatographic fraction in question contains at least 20 different PAHs including several isomers of BaP, the fluorescence spectrum clearly demonstrates that only BaP fluorescence is excited at the particular wavelength used. It must be stressed that the location of the "optimum" wavelength for excitation of fluorescence from a particular PAH requires considerable trial-and-error, but this can be accomplished with a pure sample of the PAH in question and does not vary from one sample to another. In addition, for both MI fluorescence and FTIR spectroscopy, it is necessary to assemble a file of reference spectra of pure compounds (because spectra of these compounds in low-temperature matrices are not generally available for comparison purposes in the literature). The nature of the spectrum for a particular PAH is very sensitive to the nature of the matrix used (17, 19); thus, one "file spectrum" must be obtained for each PAH of interest in each matrix to be used. For MI fluorescence, we have found that n-alkanes and nitrogen are the optimum matrices for PAHs, and argon or perfluorinated alkanes are the most satisfactory matrices for MI fluometry of polar derivatives of PAHs, such as phenols and heterocycles (17, 19). The situation is somewhat simpler in MI FTIR spectrometry, wherein only two matrix materials (nitrogen and argon) are required to deal with both nonpolar and polar aromatic compounds.

MI spectrometry can be used to identify PAHs in coal liquid samples subjected to preliminary fractionation by high performance liquid chromatography [HPLC] (15). For example, Figure 4 shows the liquid chromatogram of "Synthoil" obtained using cross-linked poly(vinyl pyrrolidone) as the stationary phase (25). Even when individual fractions of the eluant are collected and then passed back through the column, resolution of individual compounds is not achieved. However, it is known (from studies on model mixtures of pure PAHs) that PAHs elute from this stationary phase in order of increasing number of aromatic rings. Consequently, it was possible to collect seven fractions from the original coal liquid sample and then examine each one of them by MI FTIR and

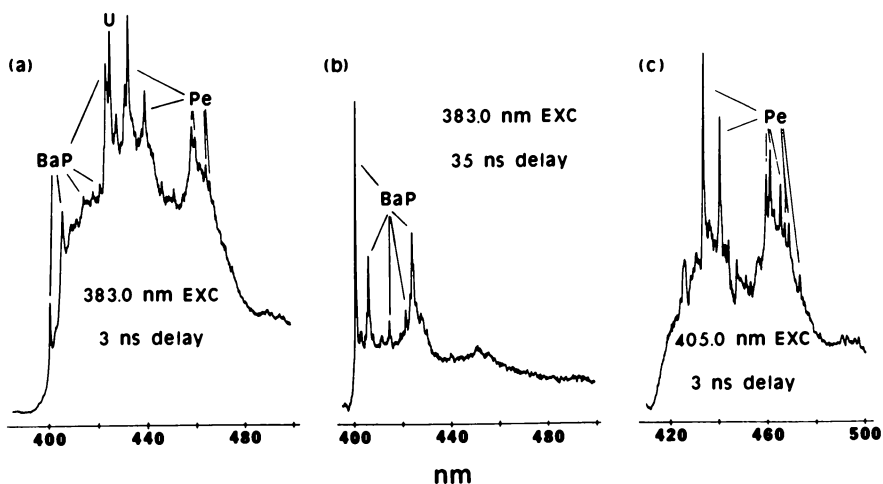
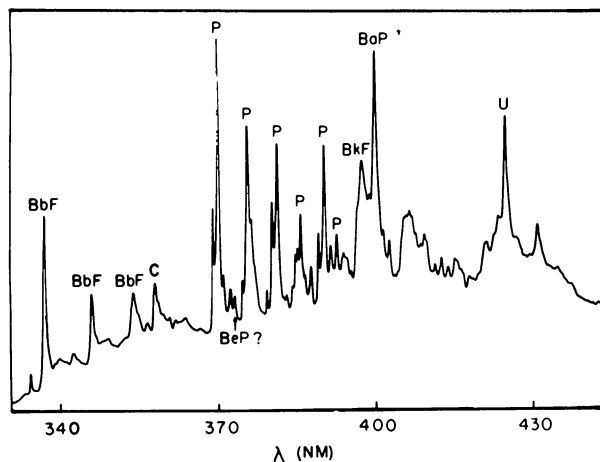
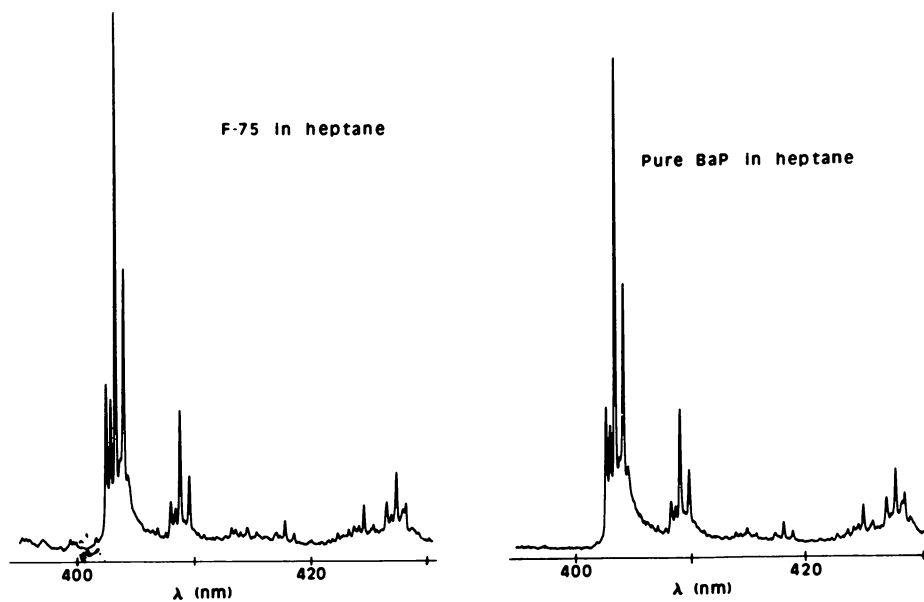


Figure 1. Dye-laser-induced fluorescence spectra of SRC-1 in an *n*-heptane matrix at 15 K. In each case, a delay was imposed between the arrival of a laser pulse at the sample and measurement of the actual fluorescence; note the difference between the 3-ns and 35-ns spectra at an excitation wavelength of 383.0 nm. Identified compounds: BaP, benzo[a]pyrene; Pe, perylene. U denotes a compound that cannot be identified because its spectrum is not included in our file of pure-compound MI fluorescence spectra.



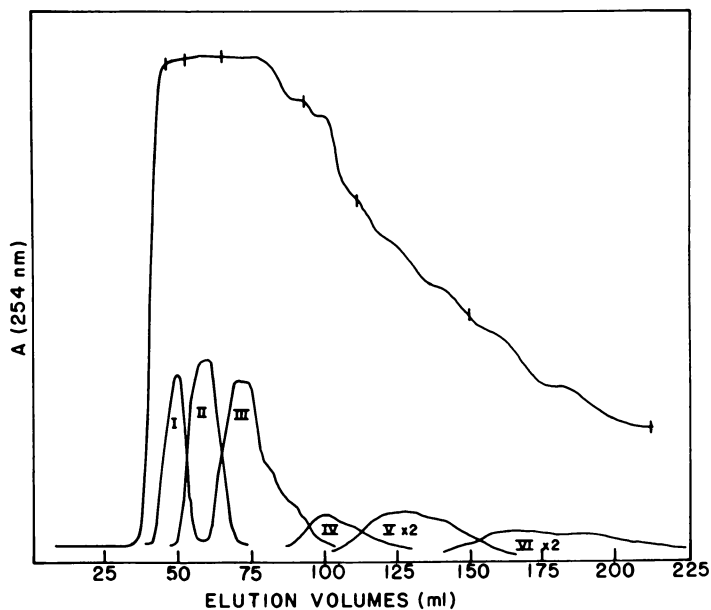
Analytical Chemistry

Figure 2. Fluorescence spectrum in a nitrogen matrix at 15 K (excited by a 2.5-kW mercury-xenon lamp) of an adsorption chromatography fraction from a coking plant water sample. Compounds: BbF, benzo[b]fluorene; C, chrysene; BeP, benzo[e]pyrene; P, pyrene; BkF, benzo[k]fluoranthene; BaP, benzo[a]pyrene; U, unknown (1).



Analytical Chemistry

Figure 3. Fluorescence spectra excited by a dye laser at 389.2 nm in an n-heptane matrix at 15 K of an adsorption chromatography fraction from a coking plant water sample (left) and of pure benzo[a]pyrene (right). Note that the two spectra are virtually superimposable (17).



American Chemical Society

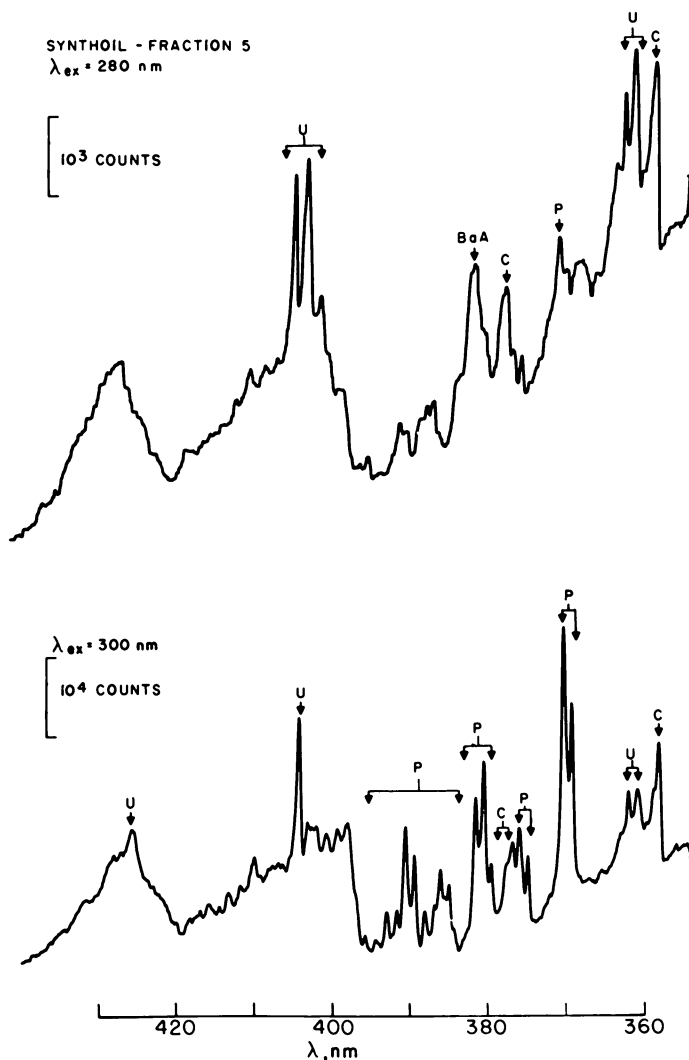
Figure 4. Upper curve: liquid chromatogram (UV detector; 254 nm) of a Synthoil sample in isopropyl alcohol; the ticks denote fractions that were rechromatographed. Bottom curves: chromatograms of each of the individual fractions after being passed through the same column (15).

fluorescence spectroscopy. For example, Figure 5 shows the fluorescence spectrum of "Fraction 5" obtained by this HPLC procedure for "Synthoil", obtained in a nitrogen matrix; the four-ring PAHs pyrene, chrysene, and benz[a]anthracene are clearly identified.

An even more efficient approach to the use of MI spectrometry in the characterization of complex samples would be direct coupling of a separation method to MI analysis. Gas chromatography (GC) is an obvious candidate for such a procedure. The fact that preparation of a sample by MI requires prior vaporization means that any compound which can be made to pass through a GC column without decomposing in the process can be detected by MI spectroscopy. Accordingly, we have constructed interfaces of both MI FTIR spectroscopy and MI fluorescence spectroscopy to gas chromatography (18). The basic idea is not to operate the GC column under conditions such that separation of complex samples into individual pure-compound chromatographic peaks occurs (which is often an unrealistic objective for very complex samples in any case), but rather to use the GC separation for essentially the same purpose as the HPLC procedures mentioned in the preceding paragraph. That is, we desire that the GC separation produce fractions which themselves are mixtures but which contain sufficiently few constituents to be amenable to MI spectroscopic analysis.

An instrumental system for performance of GC with MI FTIR (or molecular fluorescence) detection has been constructed in this laboratory. This system is similar in concept, but different in detail, from a GC/MI FTIR interface described previously by Reedy, Bourne, and Cunningham (26, 27). In such an experiment, the GC carrier gas serves as the matrix gas; a vacuum system is included to add additional matrix gas if necessary after solutes elute from the GC (in case the vapor-phase concentrations of solutes eluting from the column are too high to achieve satisfactory matrix isolation). The column effluent then passes into a cryostat head, the cold end of which is equipped with a multi-sided, movable, deposition surface. (The present arrangement employs a twelve-sided surface, fabricated from gold-plated copper.) Each GC "fraction" is deposited on one facet of the surface, following which the gold-plated copper substrate is turned by a computer-controlled stepping motor to reveal a fresh area for deposition of the next fraction. An auxiliary flame ionization detector-splitter arrangement is used to provide a "conventional" gas chromatogram of the sample and to indicate when the MI deposition surface should be turned. The optical interface to the FTIR spectrometer is a pair of KRS-5 rods used in conjunction with a mirror-type beam condenser fitted inside the cell compartment of the FTIR spectrometer. The mechanical details of this system are described in greater detail elsewhere (23, 28, 29).

Figure 6 shows an example of the MI FTIR spectra which can be



American Chemical Society

Figure 5. Fluorescence spectra in a nitrogen matrix at 15 K (excited by a mercury-xenon lamp) at two excitation wavelengths of the fifth fraction from the HPLC separation of Synthoil. Compounds: BaA, benz[a]anthracene; C, chrysene; P, pyrene; U, unknown (15).

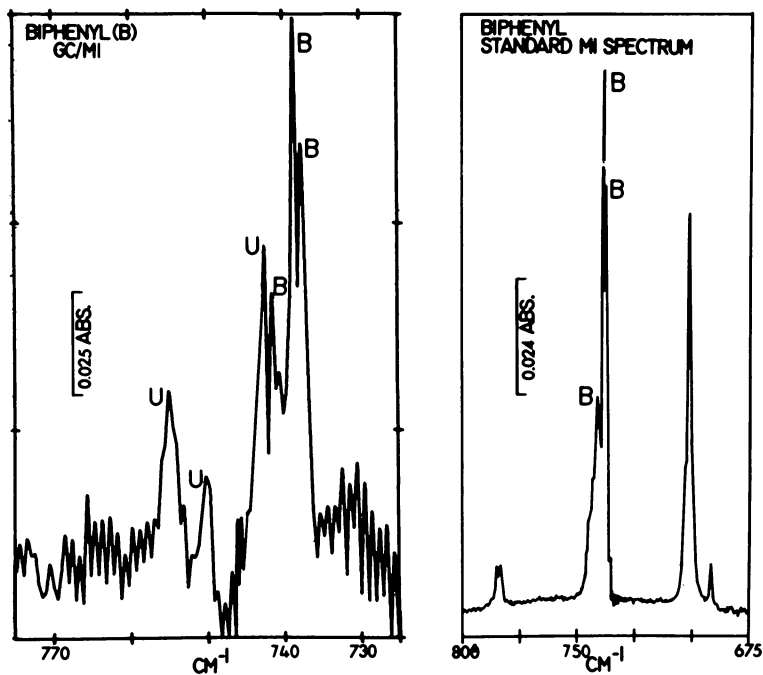


Figure 6. Left: MI-FTIR spectrum (in nitrogen at 15 K) of one chromatographic peak system from the aromatic extract of SRC-1 that had been subjected to a steam distillation clean-up step. Right: MI-FTIR spectrum of pure biphenyl (B). The comparison clearly indicates biphenyl to be one constituent of the SRC-1 sample; the other bands (U) have not been identified (28).

obtained in the gas chromatographic separation of a real sample. The sample in this case was SRC 1 which, prior to GC on an SE-30 SCOT glass column, was subjected to benzene extraction followed by steam distillation. The chromatogram of this sample contained eleven well-defined peak systems, most of which consisted of several overlapping chromatographic bands. Figure 6 shows the MI FTIR spectrum of one of the chromatographic band systems, together with a library FTIR spectrum of pure biphenyl in a nitrogen matrix. It is obvious from the spectral comparison that one of the components in the chromatographic zone is biphenyl; the other constituent(s) can not now be identified because they do not match any of the MI FTIR spectra of polycyclic compounds in our spectral library. The GC MI FTIR analysis of this, and other, coal-derived materials is discussed in greater detail elsewhere (29).

The interfacing of GC with MI fluorescence spectrometry also has been accomplished; for fluorometric examination of GC effluents, the conventional photomultiplier tube detector is replaced by a SIT vidicon to facilitate rapid acquisition of MI fluorescence spectra of individual GC fractions (30).

It should be emphasized that the objective of combining high-resolution spectroscopic detection with chromatographic separations is to minimize the chromatographic resolution required to achieve identification and quantitation of individual components in complex samples. The advantage of optical over mass spectrometry for this purpose lies in the ability of optical spectroscopy techniques to distinguish readily between isomeric compounds. The combination of separation with spectroscopic analytical techniques, termed "hyphenated methods" by Hirschfeld (31), is a field of intense activity at the present time; it is our belief that matrix isolation sampling adds an extra analytical dimension to the already powerful techniques achieved in this manner.

Summary

The technique of matrix isolation has been shown to produce highly characteristic spectra of individual components of complex samples; combination of MI spectroscopy with separation techniques promises to increase further the analytical capabilities of the technique. While our research to date has emphasized FTIR and molecular fluorescence spectrometry, MI as a sampling procedure is not limited to these two forms of spectrometry. For example, some interesting preliminary analytical results by MI Raman spectrometry recently have been described (32). It should also be stressed that the cryogenic procedures required for the vast majority of MI spectral studies are neither difficult nor unduly expensive; except in very special cases, closed-cycle cryostats requiring no cryogenic liquids (and no prior experience in low-temperature techniques) are entirely satisfactory for MI

experiments. These devices are available commercially from several manufacturers. We therefore believe that the use of MI spectrometry in the characterization of coal-derived materials and other very complex organic samples has a very intriguing future.

Acknowledgement

Financial support for our studies of MI FTIR and fluorescence spectrometric analysis was derived from a contract with the Electric Power Research Institute. Our studies in laser-induced MI fluorometric analysis have been supported by a grant from the National Science Foundation.

Literature Cited

1. Wehry, Earl L.; Mamantov, Gleb. Anal. Chem., 1979, 51, 643A.
2. Yang, Y.; D'Silva, A. P.; Fassel, V. A.; Iles, M. Anal. Chem., 1980, 52, 1350.
3. D'Silva, A. P.; Oestreich, G. J.; Fassel, V. A. Anal. Chem., 1976, 48, 915.
4. Kirkbright, G. F.; De Lima, C. G. Analyst, 1974, 99, 338.
5. Drake, J. A. G.; Jones, D. W.; Causey, B. S.; Kirkbright, G. F. Fuel, 1978, 57, 663.
6. Passwater, R. A. Fluorescence News, 1971, 5 (5), 4.
7. Shpol'skii, E. V.; Bolotnikova, T. N. Pure Appl. Chem., 1974, 37, 183.
8. Colmsjö, A.; Stenberg, U. Anal. Chem., 1979, 51, 145.
9. Brown, J. C.; Edelson, M. C.; Small, G. J. Anal. Chem., 1978, 50, 1394.
10. Lukasiewicz, R. J.; Winefordner, J. D. Talanta, 1972, 19, 381.
11. Stroupe, R. C.; Tokousbalides, P.; Dickinson, R. B., Jr.; Wehry, E. L.; Mamantov, G. Anal. Chem., 1977, 49, 701.
12. Tokousbalides, P.; Hinton, E. R., Jr.; Dickinson, R. B., Jr.; Bilotta, P. V.; Wehry, E. L.; Mamantov, G. Anal. Chem., 1978, 50, 1189.
13. Wehry, E. L.; Mamantov, G.; Kemmerer, R. R.; Stroupe, R. C.; Tokousbalides, P. T.; Hinton, E. R.; Hembree, D. M.; Dickinson, R. B., Jr.; Garrison, A. A.; Bilotta, P. V.; Gore, R. R. In "Polycyclic Aromatic Hydrocarbons," Jones, P. W.; Freudenthal, R. I. Ed; Raven Press: New York; 1978, Vol. 3, p 193.
14. Tokousbalides, P.; Wehry, E. L.; Mamantov, G. J. Phys. Chem., 1977, 81, 1796.
15. Mamantov, G.; Wehry, E. L.; Kemmerer, R. R.; Stroupe, R. C.; Hinton, E. R.; Goldstein, G. Adv. Chem. Ser., 1978, 99, 170.
16. Dickinson, R. B.; Wehry, E. L. Anal. Chem., 1979, 51, 778.

17. Maple, J. R.; Wehry, E. L.; Mamantov, G. Anal. Chem., 1980, 52, 920.
18. Wehry, E. L.; Mamantov, G.; Hembree, D. M.; Maple, J. R. In "Polynuclear Aromatic Hydrocarbons: Chemistry and Biological Effects"; Bjørseth, A.; Dennis, A. J. Ed.; Battelle Press: Columbus, Ohio; 1980, p 1005.
19. Maple, J. R.; Wehry, E. L. Anal. Chem., in press.
20. Griffiths, P. R. "Chemical Infrared Fourier Transform Spectroscopy"; John Wiley: New York; 1975.
21. Mamantov, G.; Wehry, E. L.; Kemmerer, R. R.; Hinton, E. R. Anal. Chem., 1977, 49, 86.
22. Wehry, E. L.; Mamantov, G.; Kemmerer, R. R.; Brotherton, H. O.; Stroupe, R. C. In "Polynuclear Aromatic Hydrocarbons: Chemistry, Metabolism, and Carcinogenesis"; Freudenthal, R. I.; Jones, P. W. Ed.; Raven Press: New York; 1976, p 299.
23. Hembree, D. M.; Hinton, E. R., Jr.; Kemmerer, R. R.; Mamantov, G.; Wehry, E. L. Appl. Spectrosc., 1979, 33, 477.
24. Hinton, E. R., Jr.; Mamantov, G.; Wehry, E. L. Anal. Lett., 1979, 12, 1347.
25. Goldstein, G. J. Chromatogr., 1976, 129, 61.
26. Reedy, G. T.; Bourne, S.; Cunningham, P. T. Anal. Chem., 1979, 51, 1535.
27. Bourne, S.; Reedy, G. T.; Cunningham, P. T. J. Chromatogr. Sci., 1979, 17, 460.
28. Hembree, D. M. Ph.D. Dissertation, University of Tennessee; 1980.
29. Hembree, D. M.; Mamantov, G.; Wehry, E. L. Anal. Chem., submitted for publication.
30. Wehry, E. L.; Gore, R. R.; Dickinson, R. B., Jr. In "Lasers in Chemical Analysis"; Hieftje, G. M.; Lytle, F. E.; Travis, J. C., Ed.; Humana Press: Clifton, New Jersey; 1981.
31. Hirschfeld, T. Anal. Chem., 1980, 52, 297A.
32. King, D. S.; Stephenson, J. C. Opt. Laser Technol., 1980, 12, 97.

RECEIVED March 9, 1981.

Analysis of Synfuels by MS/MS

D. ZAKETT and R. G. COOKS

Department of Chemistry, Purdue University, West Lafayette, IN 47907

The chemical and instrumental basis for mass spectrometry/mass spectrometry is reviewed. Synfuels can be monitored for particular constituents or for groups of functionally related compounds, using this two stage technique of mass analysis. These identifications and associated quantitative determinations are made on the intact sample without derivatization. Amino-polynuclear aromatics can be distinguished from the isobaric azapoly-nuclear aromatics. Aromatic hydrocarbons are readily identified and quantitated by subjecting their anions to dissociative charge inversion, a reaction with high structural specificity.

Mass spectrometry/mass spectrometry (abbreviated ms/ms) is, in its simplest form, a technique whereby a component of a complex mixture is separated in one stage of mass analysis, and subsequently, identified by a second stage of analysis, after it has undergone some type of ion/molecule interaction (1-5). This operation is sometimes referred to as taking a mass spectrum of an ion in a mass spectrum. From this simplified explanation, ms/ms is seen to be analogous to gas chromatography/mass spectrometry (gc/ms). The ion selected in the first stage of analysis by ms/ms, the precursor ion, is analogous to the component in a gas chromatographic peak. The ions that result from reactions of the precursor ion, in a reaction region, are analyzed by the second stage of ms/ms and are analogous to the ions in the gc/ms mass spectrum.

The ms/ms methodology derives from studies on metastable ions and on high energy collisions occurring within the mass spectrometer. As an analytical tool it relies on one key concept - that mixtures can be analyzed by separating components after ionization according to their masses. The sequence employed in gc/ms is separation, then ionization; the latter is reversed in ms/ms. This approach provides the unique separatory speed of the technique given the fact that ion transit times, as well as random mass

0097-6156/81/0169-0267\$05.50/0
© 1981 American Chemical Society

access (cycle) times, are negligibly small in mass spectrometers (order of 10^{-5} and 10^{-2} s, respectively). This reversal of the ionization/separation sequence also places unique requirements on the ionization methodology. In effect, one identifies ion structures in ms/ms; if these are to have meaning in terms of the structures of their neutral molecule precursors, the ionization method used must preserve structural integrity. It is partly for this reason that chemical ionization has so frequently been used in ms/ms. Simple protonation generally yields an ion $(M+H)^+$ which is structurally analogous to the molecule and can be processed as its surrogate. This processing, illustrated in Figure 1, consists of mass-analysis (ie. separation from other constituents) followed by collision-induced dissociation and mass-analysis of the resulting fragments. The latter two steps constitute the identification phase of the separation/identification sequence. Other ion/molecule reactions (Table I) can also be used to characterize molecular structure.

TABLE I.

REACTIONS OBSERVED IN MS/MS FRAGMENTATION PROCESSES

1.	$m_1^{**} \longrightarrow m_2^+ + m_3$	METASTABLE
2.	$m_1^+ \xrightarrow{N} m_2^+ + m_3$	CID
3.	$m_1^+ \xrightarrow{N} (m_1 N)^+ \longrightarrow m_2^+ + m_3$	ASSOCIATION
4.	$m_1^+ \xrightarrow{N} m_1^{2+} + e^-$	STRIPPING
5.	$m_1^- \xrightarrow{N} m_1^+ + 2e^-$	INVERSION

In addition to preserving structure, a soft ionization technique such as chemical ionization (CI) has a further advantage in ms/ms. By minimizing the number of ions generated from each molecular species the complexity of the (ionic) mixture which has to be separated is minimized. It is for this reason that electron impact ionization is seldom a good choice for ms/ms, although for compounds such as the polyaromatic hydrocarbons which give predominantly one ion in their electron impact spectra this complication is minimized.

It is intrinsic in ms/ms that the entire sample is ionized simultaneously. This means that access can be had to any component of the mixture at any time during the analysis, as contrasted with only those points in a chromatographic sequence when a compound is being eluted. It also means that competitive ionization of the various sample constituents can yield ionization efficiencies which are matrix dependent. This effect can be minimized by appropriate choice of ionizing agent or it may in fact be a desirable part of the analytical scheme. For example, use of ammonia as the reagent gas in chemical ionization will selectively protonate basic compounds and so simplify the ion mixture to be separated and identified. On the other hand, if acidic components are of special interest, one can employ OH^- reagent ion (N_2O /isobutane reagent gas) to form conjugate bases.

Quantitation in ms/ms is comparable to quantitation in gc/ms or lc/ms. In each of these techniques a variety of factors, including those just mentioned in connection with ionization efficiency, make standard addition or internal standards desirable. Internal standards are commonly isotopically labeled analogs of the analyte. Several runs must be made to quantitate and ms/ms again has an advantage in speed over the slower chromatographic techniques. Precision and accuracy of quantitation has not been sufficiently compared but at this early stage in its development, ms/ms lags in these respects.

Another basis for comparison with gc/ms is detection limits. This also allows one to inquire a little more closely into the nature of ms/ms. In this experiment as opposed to conventional ms, the attenuation in signal associated with fragmentation efficiency and the transmissivity of the second mass analyzer decreases the total observable signal by up to three orders of magnitude depending upon the particular instrumentation being used. On the other hand, for complex mixtures ms detection limits are controlled by signal to noise ratios and substantial contributions to the noise can arise from the matrix. In other words, the limiting factor in practical determinations can be chemical noise (instrumental background) not electronic noise. As shown in Figure 2, the detection limits in ms/ms can greatly exceed those attainable in ms alone. It is for this reason that detection limits in gc/ms and ms/ms are comparable, with picogram detection (of compound present in a massive matrix) being observed in ms/ms.

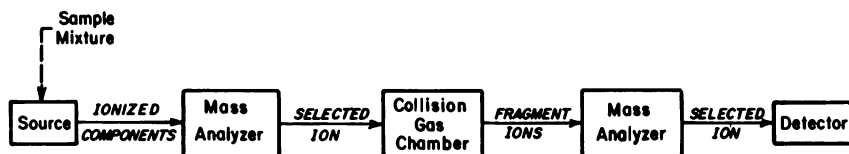
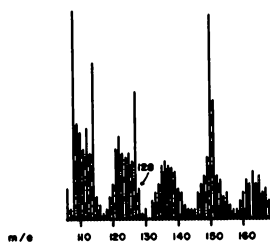
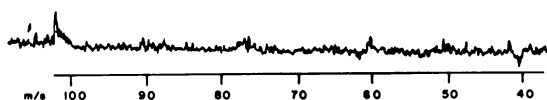


Figure 1. Schematic of the MS/MS analysis scheme

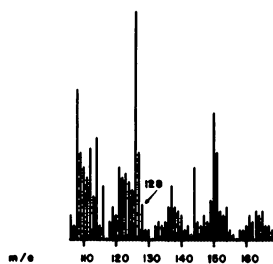
Background Mass Spectrum



Background MS/MS Spectrum
(m/e 128)



Sample Mass Spectrum



Sample MS/MS Spectrum
(m/e 128)

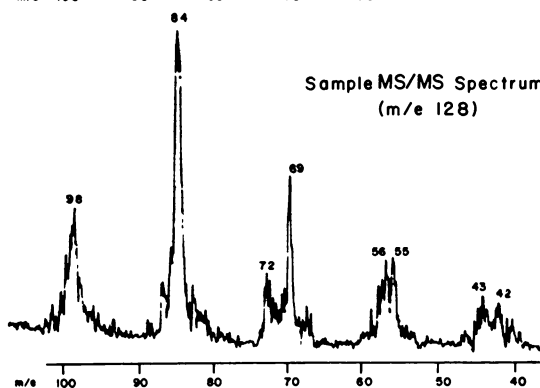


Figure 2. Chemical noise in MS (left-hand side) obscures signal (128*) due to analyte, while in MS/MS (right-hand side) chemical noise is more efficiently filtered out by the extra stage of mass separation.

In any introductory consideration of ms/ms it is appropriate to recognize that numerous options exist at every stage of the analytical protocol. These include choices of whether to use prior sample clean-up, to employ chromatography in conjunction with ms/ms or to rely exclusively on this one method. There are choices of ionization technique and ion polarity, choices of mass analyzing devices and, most particularly, of the reaction(s) which will be used to characterize the separated ions. Some of these reactions are given in Table I; the most widely used being collision-induced dissociation. Having made this selection, the problem may call for a complete spectrum of daughter ions to be obtained (a ms/ms spectrum, for maximum specificity in identification) or it may be sufficient to screen for the compound in question by monitoring a single fragmentation in its ms/ms spectrum (single reaction monitoring, SRM) and in so doing to trade specificity for sensitivity.

The flexibility of ms/ms instrumentation is such that instead of selecting with the first mass-analyzer and scanning the second, one may choose to scan both analyzers simultaneously. Under appropriate conditions this can provide a molecular weight profile of all those ions in the original mixture which fragment via loss of a particular neutral fragment (6, 7). These scans can therefore detect the presence of all compounds in the mixture bearing a particular functional group and are termed neutral loss scans. For example, aromatic carboxylic acids can be sought en masse using negative chemical ionization (NCI) to generate carboxylate anions and then scanning for the decarboxylation reaction (Figure 3). Any ion observed in the resulting neutral loss spectrum fulfills this necessary but not sufficient criterion for carboxylic acids, and can be identified by setting the first analyzer to mass-select the appropriate carboxylate and then scanning the second analyzer so as to obtain its complete ms/ms spectrum. Compound identification then proceeds by direct interpretation or by matching with the spectrum of the authentic. Unfortunately libraries of ms/ms spectra are only just beginning to be assembled. Lack of compiled reference spectra is a major problem when trying to identify the components of an entirely unknown mixture.

A final point regarding the specificity of ms/ms identifications. We have just shown how, through single reaction monitoring, they can be minimally so; alternatively, using exotic (chiral) ionizing agents it is possible to distinguish even optical isomers (8). In many cases, simple ms/ms spectra taken on protonated molecules or molecular ions do not distinguish positional isomers, a characteristic mirrored in the conventional electron impact and chemical ionization mass spectra of these compounds.

The types of mass analyzers used for ms/ms and their

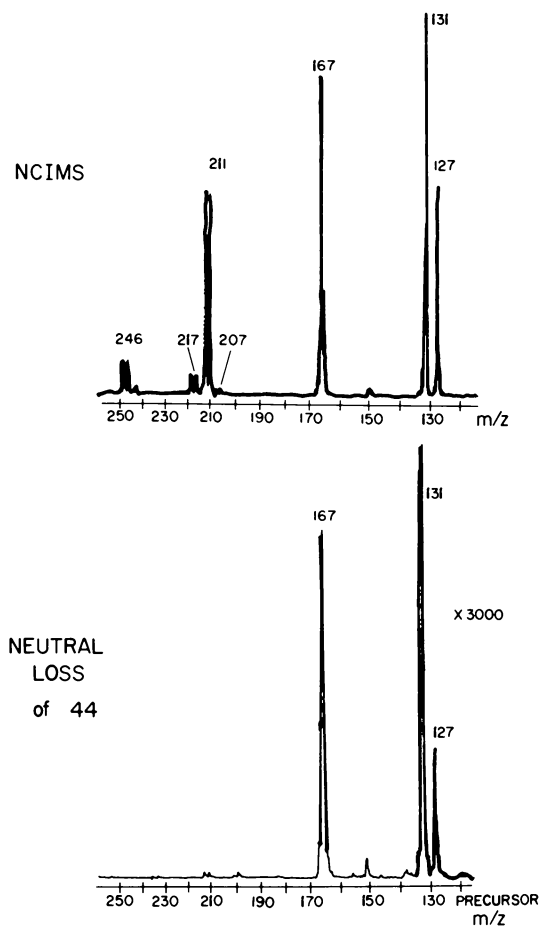


Figure 3. Neutral loss scan detection of carboxylic acids in a mixture using NCI MS/MS. Upper scan is the normal NCI MS of the mixture. The lower, neutral loss scan shows significant responses only for carboxylic acids.

arrangements are varied. In our laboratory alone we employ combinations of magnetic sectors (B) electric sectors (E) and quadrupole mass filters (Q) arranged as BE, BQ, QQ, EB, and BQQ. It should not be imagined that these configurations differ merely in resolving power or transmission and give otherwise similar results. In fact, they cover different ranges of ion translational energy (and hence change the reactions available for ion characterization), they measure different properties (mass, momentum, translational energy), they offer different scanning speeds and adaptabilities to computer control. The profound control over ms/ms spectra which can be exerted by just one factor, the translational energy of the selected ion, is illustrated in Figure 4 for 5-indanol, a coal liquid constituent. Reproducibility of ms/ms spectra from laboratory to laboratory is good, provided however, that translational energies are fixed. The basic principles behind ms/ms have been reviewed several times along with descriptions of the more common instrumental configurations (1-5,9,10).

Instrumentation

Since most of the spectra shown here were recorded using a BE spectrometer (also known as a mass-analyzed ion kinetic energy spectrometer, MIKES) (11) a brief description is in order. This type of instrument, a reversed geometry double focusing mass spectrometer, operates at high energies (3-10keV). Ions, typically $(M+H)^+$, $(M-H)^-$, M^+ or M^- , are generated by chemical ionization from samples introduced via a direct insertion probe. Magnetic mass separation is followed by high energy collisions with a target gas (chemical nature not important) at a pressure of ~1 mtorr held in a cell located at the focal point between the two analyzers. The products of collision include fast neutrals, multiply charged ions and fragment ions. The fragments are analyzed on the basis of mass to charge ratio (more specifically, kinetic energy to charge ratio) and displayed as a ms/ms spectrum. The relatively poor resolution seen in these spectra is inherent in the methodology and is due to the fragments being formed with a range of velocities. Instruments such as QQ or QQQ mass spectrometers (12,13) display unit mass resolution but since they operate at low ion kinetic energy, as now used they do not permit charge stripping and charge inversion reactions (Table 1). These reactions (14, 15) are useful in many situations.

The data acquisition and processing operations on the MIKES instrument are under computer control and we are beginning to accumulate a library of reference spectra. A computer based library search routine has not yet been implemented on the MIKES instrument but existing gc/ms software can readily be adapted to the ms/ms data base. The construction of a ms/ms data base is underway in several laboratories.

There are several mass spectrometer manufacturers which have begun to offer commercial, fully computerized ms/ms instruments (16). These instruments are capable of generating and searching

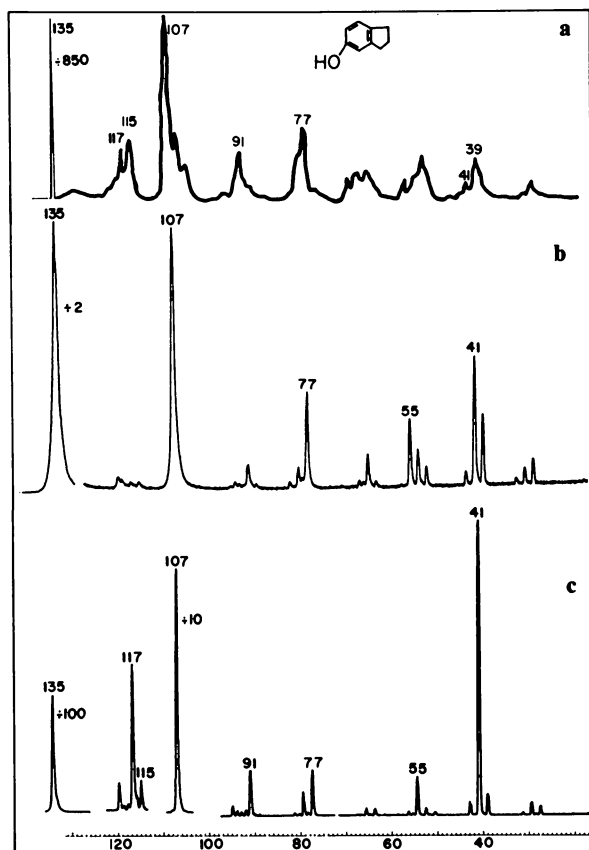


Figure 4. Effects of ion kinetic energy on the MS/MS of 5-indanol: (a) MS/MS obtained on MIKES instrument with 7000 eV translational energy; (b) spectrum obtained on hybrid BQ (magnet followed by quadrupole) mass spectrometer 95 eV; (c) spectrum obtained with QQ (tandem quadrupole) mass spectrometer at 35 eV axial energy.

ms/ms libraries and of performing many of the sophisticated scan functions in routine operation. The availability of these second generation instruments will greatly accelerate the progress made in mixture analysis by ms/ms.

Applications of MS/MS to Synfuel Characterization

The following discussion will be concerned primarily with applications of the ms/ms technique in the synfuel area. Attempts will be made to illustrate the unique capabilities of the ms/ms analysis with examples taken from our work on coal liquefaction products. Figure 5 shows the positive ion chemical ionization (PCI) mass spectrum of the coal liquid in question (SRC II mid heavy distillate, total bottoms). This spectrum is actually the normalized sum of approximately 500 individual mass spectra taken while the SRC II was thermally vaporized from a solids probe into the source of a mass spectrometer, and represents the molecular weight profile of this distillate fraction. Since isobutane CI gives to a first approximation only protonated molecular ions (and no fragment ions), the peaks represent the individual components in the SRC II arranged incrementally by molecular weight.

A compound(s) present at a given mass can be identified by selecting that mass with the first mass analyzer and obtaining the ms/ms spectrum by scanning the second mass analyzer. The identification of methylindole in SRC II (positional isomer not determined) at m/z 132 is shown in Figure 6. Notice the excellent agreement with the 3-methylindole ms/ms spectrum. The sharp peaks at masses 66-64 represent products of the charge stripping processes in which the parent ion (m/z 132⁺) has undergone a collision, converting it from a singly charged ion to a doubly charged ion (ie. $M^+ \rightarrow M^{++} + e^-$). These peaks have been observed to be sensitive to ion structure (17) and can, in some cases, be used to discriminate between positional isomers which give otherwise identical spectra. The charge stripping region, recorded at a slower scan rate, is shown for 2-methylindole and 3-methylindole in Figure 7 and can be used to differentiate between these two compounds. A slow scan of this region for the SRC II component at m/z 132 was similarly acquired (not shown) and found to differ significantly from that of both the above compounds. This component is therefore identified as a methylindole isomer by its overall ms/ms spectrum, but it is not the pure 2- or 3-isomer on the basis of charge stripping data.

In addition to identification of unknown constituents, ms/ms is eminently suited to monitoring the presence (and quantity) of selected compounds in a mixture. The absence of a time consuming chromatographic separation allows the analyst to terminate the run immediately after the required data is obtained. If one is interested, for example, in determining the levels of benzothiophene in SRC II, mass 135 can be selected with the first analyzer and the second mass analyzer set to monitor a characteristic fragment such as m/z 91 from protonated benzothiophene (Figure 8c). This analysis mode, single reaction monitoring, is

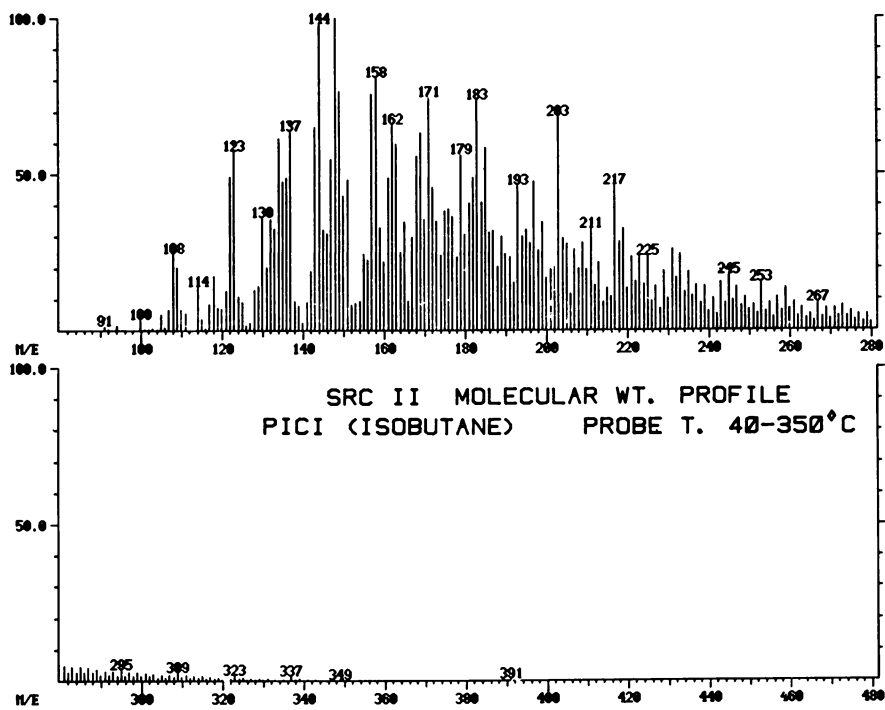


Figure 5. Integrated molecular-weight distribution of SRC-II obtained by total sample vaporization from solids probe

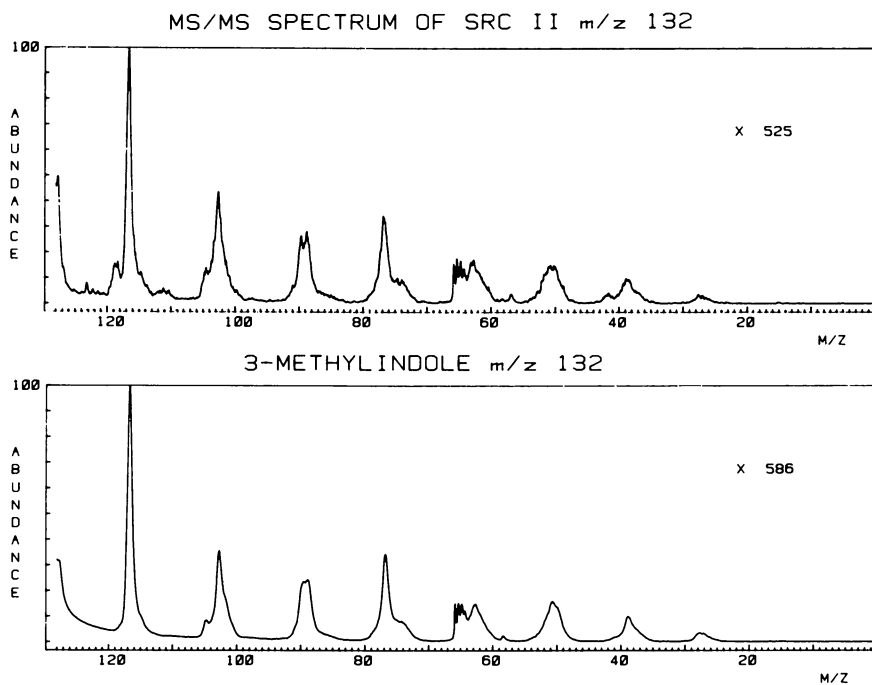


Figure 6. Comparison of SRC-II mass 132 MS/MS (upper) with the reference spectrum of 3-methylindole (lower)



Figure 7. Slow scan of the charge-stripping region in the MS/MS spectrum of 3-methylindole (upper) and 2-methylindole (lower)

extremely sensitive but not highly structure specific and is analogous to single ion detection in gc/ms. Any chosen number of different compounds (masses) could be sequentially monitored (and quantitated) by this method. To increase the specificity of detection of a particular constituent, several fragment ions may be sequentially monitored (analogous to multiple ion detection - MID - in gc/ms). Finally, a full spectrum can be recorded as shown in Figure 8, for m/z 135 in SRC II. In comparing the synfuel spectrum with the two reference spectra, one observes a good match with indanol and the absence of the characteristic benzothiophene peak at mass 69. Clearly, this particular sample contains minimal quantities of benzothiophene and a more suitable reaction to use for its quantitative determination would be the formation of m/z 69 since this ion, although not as intense as m/z 91, is not present in the indanol spectrum.

In a similar fashion one can monitor all compounds bearing particular functional groups using the neutral loss scan mode described above for carboxylic acids. This can be illustrated by an example in which a functional group, incorporated from a derivatizing agent, is identified. In a particular experiment, a small volume of SRC II was treated with acetyl chloride, which will acylate alcohols (phenols) and many amines. Acylated compounds show strong peaks in their ms/ms spectra corresponding to loss of ketene as a neutral molecule. Hence a neutral loss scan can be performed which will detect the loss of 42 mass units (ketene) and indicate the presence and molecular weights of any compound which has undergone derivatization. The derivatization procedure involved addition of 1 ml acetyl chloride to 1 ml SRC II and direct analysis of the reaction mixture after 15 minutes reaction time. Figure 9 shows the results of such an analysis. The upper scan is a normal PCI mass spectrum of the derivatized coal liquid sample. The lower scan is the neutral loss scan for the same sample. The presence of a peak in the lower scan indicates the molecular weight (after derivatization) of compounds bearing hydroxyl or amine groups. For example, the peak at mass 165 includes the mass added to a compound with molecular weight 122 by the acetyl group (42 mass units) and the ionizing proton (1 mass unit) and indicates that the compound of M.W. 122 contains a hydroxyl or amine functionality. The lower set of masses in the neutral loss scan (eg 123,135,137 ...) indicates the protonated molecular weights of the compounds which gave a positive response. In fact, two homologous series are present; the series 123,137, 151,165 ... has been identified as one comprised of alkyl substituted phenols, while the series 135,149,163 ... is consistent with alkyl indanol structures. The 135 ion, indanol itself, has been positively identified by comparison with the reference spectrum of the authentic compound (Figure 8). A small amount of isomeric methylidihydrobenzofuran may also be present at m/z 135 but the major component is either 4 or 5-indanol. Minor peaks in the neutral loss scan indicate the possible

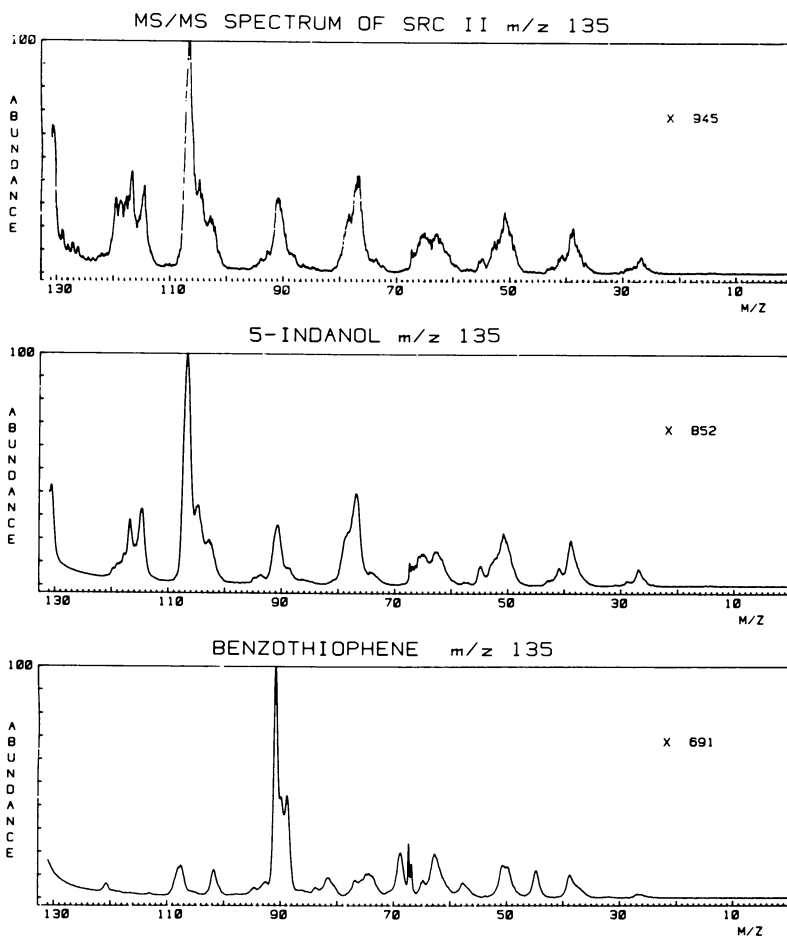


Figure 8. Comparison of SRC-II 135' MS/MS (top) with reference spectra of 5-indanol (center) and benzothiophene (lower) using isobutane PCI

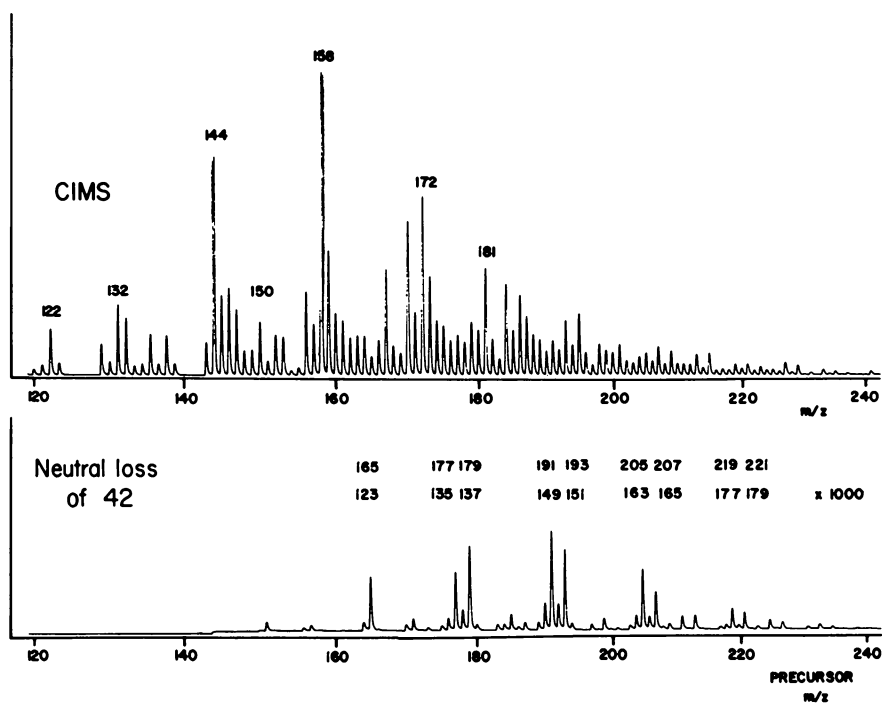


Figure 9. PCI MS of acylated SRC-II (top) compared with the neutral loss scan (lower) for the same sample

presence of two more homologous series which have not been investigated to date. Neutral loss scans can provide a rapid screening method for compounds which either show characteristic fragmentations related to particular functional groups or which can be chemically modified (derivatized) to induce such processes.

We are currently investigating the utility of these types of scans for the selective detection of the primary amine substituted polynuclear aromatic compounds (PNA) in the presence of their aza polynuclear aromatic analogs. This analysis is of significance due to the toxicity of the amino PNAs. Preliminary evidence indicates that these two types of compounds, which have the same molecular weights, and are difficult to determine by gc/ms (18), show substantially different ms/ms spectra. As demonstrated in Figure 10, naphthylamine displays an intense peak for loss of 17 (NH_3) in its PCI ms/ms spectrum. Methylquinoline on the other hand shows only minor amounts of 17 loss. Figure 10 also indicates that the component in SRC II responsible for mass 144 is a methylquinoline isomer and not a naphthylamine. If the above types of reactions also occur in 3, 4, and 5 ring amino-PNA and methyl-azaPNA compounds, a neutral loss scan, monitoring loss of 17 mass units should prove useful for determining the levels of aromatic amines in SRC materials.

Most of the ms/ms work on SRC samples has employed positive ion chemical ionization; recently however, we have begun to explore the usefulness of negative ion chemical ionization (NCI). NCI is a very selective ionization mode (19); only those compounds which can attach electrons, such as PNAs or which have acidic functionalities (eg. phenols) are ionized and contribute to the mass spectrum observed. It has been found that saturated hydrocarbons are not ionized by NCI and fuel materials give simple NCI mass spectra which accentuate the aromatic compounds present (20). Figure 11 shows the NCI mass spectrum recorded for an SRC sample (not SRC II) which has previously been investigated by PCI ms/ms (21). Many of the masses observed in the spectrum correspond to the molecular weights of PNA compounds. In attempting to identify these compounds we have found the negative ion ms/ms spectra of PNA reference compounds to be devoid of fragment ion peaks and thus of no use for structure determination. Fortunately, it is possible to observe the charge inversion process (Table 1) on the MIKES instrument. By monitoring the positive fragments from the negative mass-selected PNA ion, one obtains a spectrum with excellent signal to noise characteristics. Figure 12 (a and b) compares negative ion ms/ms with negative ion charge inversion ms/ms for 202^- generated from fluoranthene ($\text{C}_{16}\text{H}_{10}$, MW 202), a typical PNA in coal liquids. The spectrum obtained (Figure 12c) when the coal liquid is sampled and the 202^- ion selected, agrees in every detail with that of authentic fluoranthene. The total absence of any extraneous peaks in the spectrum of the coal liquid, in spite of the complexity of this material, is due to the high selectivity of ionization in the

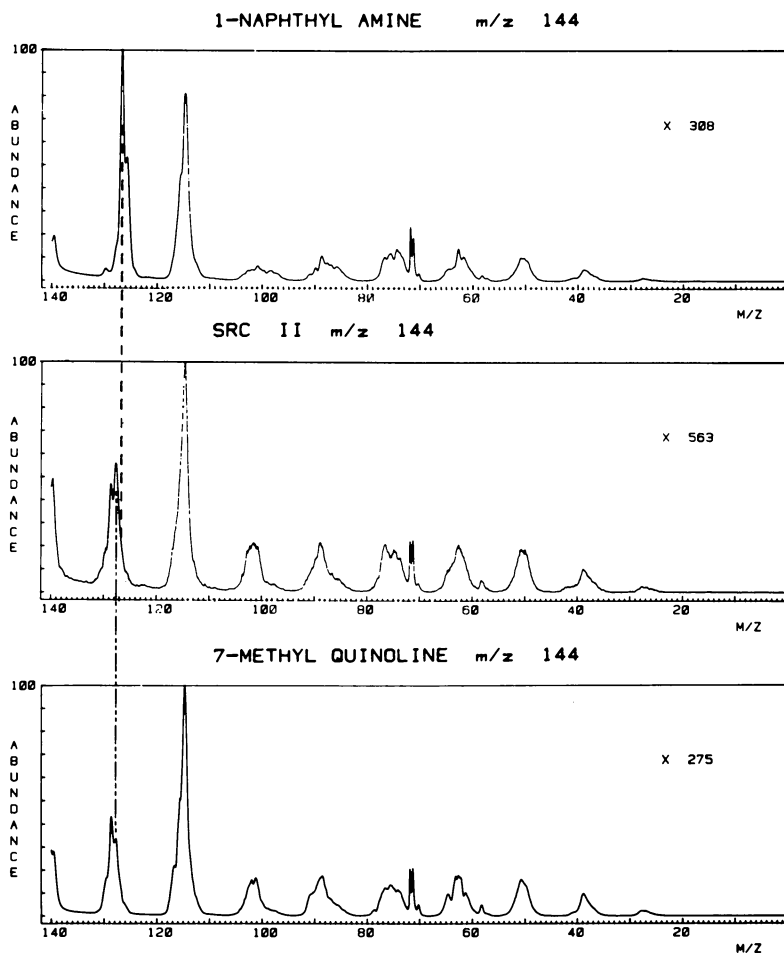


Figure 10. Demonstration of the ability to distinguish between primary amines and isobaric methyl aza aromatics using MS/MS

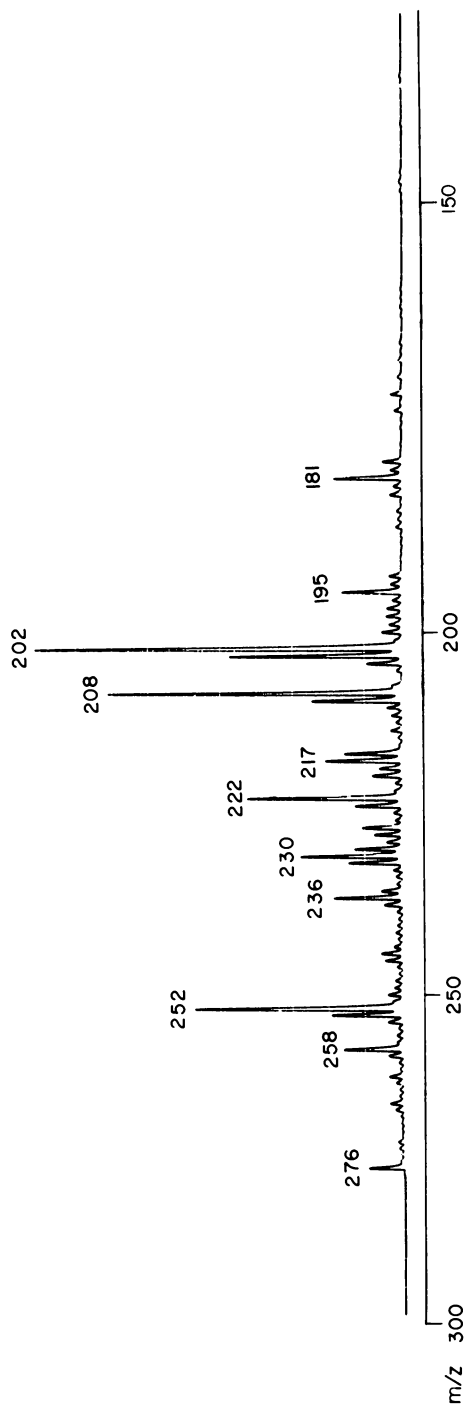


Figure 11. NCI MS of SRC: CH₄; probe temperature, 130°C.

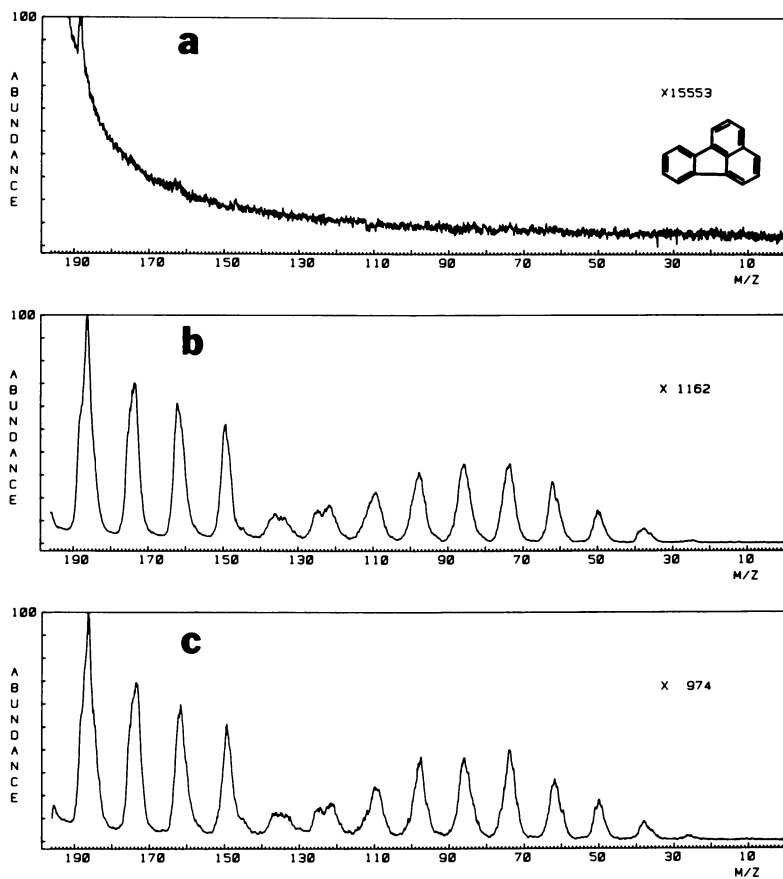


Figure 12. Comparison of fluoranthene MS/MS: (a) negative ion MS/MS ($- \rightarrow -$); (b) negative ion charge inversion MS/MS ($- \rightarrow +$); (c) negative ion charge inversion MS/MS ($- \rightarrow +$) of SRC m/z 202⁺.

NCI mode. The conclusion here is that fluoranthene and/or an isomer contributes all the signal at mass 202 in the NCI spectrum of the coal liquid. In fact, pyrene, the most probably congener of fluoranthene, does not contribute to this spectrum. This conclusion comes from measuring its ionization efficiency which is less than 1% of that of fluoranthene and its charge inversion ms/ms spectrum which shows a significant difference to that of fluoranthene, viz. the ratio of the C₂ to C₃ loss peaks is 1.8 in pyrene and 1.2 in fluoranthene. This difference represents a basis for distinguishing these two isomers using their otherwise similar charge inversion spectra. The advantage of this conceptually, but not instrumentally, more complicated mode of analysis is the elimination of saturated hydrocarbon interferences at mass 202 which would have an adverse affect upon detection limits.

The identification just described was made in minutes. (Spectral accumulation time two minutes, sample cycling time five minutes). Quantitation which was similarly straight-forward, was carried out by preparing several coal liquid samples to which had been added known aliquots of fluoranthene. For convenience the SRC sample was diluted by a factor of ten with benzene before quantification, the relatively high concentrations of fluoranthene facilitating its determination. Results are shown in Figure 13 and they establish the calibration curve and yield a value of 3 weight % fluoranthene present in the original SRC. On the basis of the S/N (Figure 12) in these and other quantification experiments we estimate the detection limits for these compounds at the parts per million level. We are currently evaluating the detection limits and optimum ms/ms method (NCI vs. PCI) for a series of PNAs commonly found in SRC II at ppm levels.

Summary

Coal liquids have been the subject of careful analytical study (22-30) and much is known about the SRC materials. In particular, gc and gc/ms have proven invaluable in these investigations. The chemical complexity, biological effects and industrial importance of these materials justifies attempts to develop alternative analytical methodologies. As shown above, ms/ms exhibits considerable promise for the qualitative and quantitative analysis of synfuels. It is apparent that there are a variety of types of ms/ms data and that the options for characterizing particular compounds can be adjusted to select for sensitivity or specificity or to minimize the deleterious effects of particular matrices. The speed of analysis and the lack of any need for sample preparation suggest a distinct advantage in programs aimed at monitoring particular sets of compounds. In addition, techniques exist for screening for functionally related compounds and obtaining approximate molecular weight distributions for functional groups. Ms/ms may have unique applicability in dynamic, real time process monitoring for virtually any set of specified constituents in samples encountered in the synthetic fuels industry.

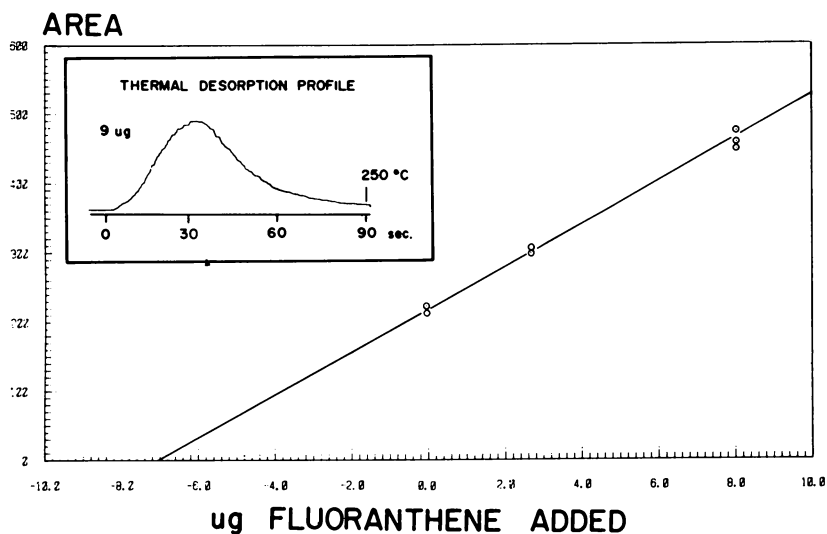


Figure 13. Quantitation of fluoranthene in SRC using standard addition method by monitoring the fragmentation process $202^+ \rightarrow 187^+$ while sample was desorbed from the solids probe. Inset is a typical SRC desorption profile (containing 9 μg fluoranthene).

Acknowledgment

Support by the Department of Energy, ET-78-9-01-3377 is gratefully acknowledged.

Literature Cited

1. Kruger, T. L.; Litton, J. F.; Kondrat, R. W.; Cooks, R. G. Anal. Chem. 1976, **48**, 2113A.
2. Cooks, R. G. Amer. Lab. 1978, **7**, 11.
3. Cooks, R. G. "Trace Organic Analysis"; H. S. Hertz and S. W. Chester, Eds., National Bureau of Standards, Washington, D.C., 1979.
4. Kondrat, R. W.; Cooks, R. G. Anal. Chem. 1978, **50**, 81A.
5. Maquestiau, A.; Van Haverbeke, Y.; de Meyer, C.; Duthoit, C.; Meyrant, P.; Flammang, R. Nouv. J. Chim. 1978, **3**, 517.
6. Zakett, D.; Schoen, A. E.; Kondrat, R. W.; Cooks, R. G. J. Amer. Chem. Soc. 1979, **101**, 6781.
7. Lacey, M. J.; MacDonald, C. G. Anal. Chem. 1979, **51**, 691.
8. Sigsby, M. L. Ph.D. Thesis Purdue University, 1980.
9. Russell, D. H.; McBay, E. H.; Mueller, T. R. Amer. Lab. 1980, **9**, 50.
10. Yost, R. A.; Enke, C. G. Anal. Chem. 1979, **51**, 1251A.
11. Beynon, J. H.; Cooks, R. G.; Amy, J. W.; Baitinger, W. E.; Ridley, T. Y. Anal. Chem. 1973, **45**, 1023A.
12. Zakett, D.; Cooks, R.G.; Fies, W. J. Anal. Chim. Acta in press.
13. Yost, R. A.; Enke, C. G. J. Amer. Chem. Soc. 1978, **100**, 2274.
14. Bowie, J. H.; Blumenthal, T. J. Amer. Chem. Soc. 1975, **97**, 2959.
15. McClusky, G. A.; Kondrat, R. W.; Cooks, R. G. J. Amer. Chem. Soc. 1978, **100**, 6045.
16. Maugh, T. H. Science 1980, **209**, 675.
17. Kemp, D. L.; Beynon, J. H.; Cooks, R. G. Org. Mass Spectrom. 1976, **11**, 857.
18. Wilson, B. W. presented at the Second Symposium on Environmental Analytical Chemistry, Provo 1980.
19. Smit, A. L. C.; Field, F. H. J. Amer. Chem. Soc. 1977, **99**, 6471.
20. Sieck, L. W.; Jennings, K. R.; Burke, P. D. Anal. Chem. 1979, **51**, 2232.
21. Zakett, D.; Shaddock, V. M.; Cooks, R. G. Anal. Chem. 1979, **51**, 1849.
22. Schultz, R.; Jorgensen, J.; Maskarinec, M.; Novotony, M.; Todd, L. Fuel 1979, **58**, 783.
23. Borowitzky, H.; Schomburg, G. J. Chromatogr. 1979, **170**, 99.
24. Lee, M. L.; Vassilaros, D. L.; White, C. M.; Novotony, M. Anal. Chem. 1979, **51**, 768.
25. Lee, M. L.; Novotony, M.; Bartle, K. D. Anal. Chem. 1976, **48**, 1566.
26. Yang, Y.; D'Silva, A. P.; Fassel, V. A.; Iles, M.; Anal. Chem. 1980, **52**, 1351.

27. Woo, C. S.; D'Silva, A. P.; Fassel, V. A. Anal. Chem. 1980, 52, 159.
28. Brown, J.; Duncanson, J.; Small, G. Anal. Chem. 1980, 52, 1711.
29. Whitehurst, D. D.; Mitchell, T. O.; Farcasiu, M. "Coal Liquefaction," Academic Press, New York, 1980, pp. 30-60.
30. Dooley, J. E.; Thompson, C. J. "Liquid Fuels From Coal," Ellington, R. T. (Ed.), Academic Press, New York, 1977, pp. 221-232.

RECEIVED May 27, 1981.

600-MHz Proton Magnetic Resonance Study of Coal-Derived Liquids

T. HARA and N. C. LI

Duquesne University, Pittsburgh, PA 15219

K. C. TEWARI and F. K. SCHWEIGHARDT

Air Products and Chemicals, Inc., Allentown, PA 18105

The newly developed 600 MHz ^1H NMR Spectrometer is used to characterize coal-derived liquids and their chromatographically separated fractions. The distinct and well resolved proton resonance lines in both aromatic and aliphatic regions and IR analysis have been used to identify the major compounds and compound types. Double resonance technique has been applied for the chemical shift identification of donor protons ($\alpha\text{-CH}_2$, $\beta\text{-CH}_2$) of partially hydrogenated polynuclear aromatic compounds. An NMR difference technique is applied to determine specific compositional changes in upgraded liquids derived under identical process conditions, but from different coal sources.

High resolution proton nuclear magnetic resonance (^1H NMR) spectrometry has been used as one of the major spectroscopic tools for chemical characterization of coal-derived materials, since Friedel (1) and Brown et al. (2) reported ^1H NMR spectra of coal-derived asphaltenes and low-temperature vacuum carbonization products. Based on the quantitative proton distribution data, structural information for complex mixtures of coal-derived materials has been obtained using the Brown and Ladner equations (3) as well as the modified equations reported elsewhere (4, 5, 6). A higher-field NMR spectrometer (220 MHz) was applied to tar component by Bartle et al. (7). The proton resonance signals of coal-derived materials were divided into eleven ranges of chemical shift values and the signals in each range were assigned to various types of hydrogen by the addition of pure compounds. Schweighardt et al. used a 250 MHz NMR spectrometer for characterization and to quantify hydroxyl groups in coal-liquefaction oils and asphaltenes (8). Hydroxyl groups in coal-derived materials were converted into trimethylsilyl ethers and proton signals in methyl groups attached to silicon were measured. The well-resolved NMR spectra enabled them to characterize the nature of the original hydroxyl groups in coal-derived materials.

0097-6156/81/0169-0289\$07.50/0

© 1981 American Chemical Society

In the present study, a 600 MHz ^1H NMR spectrometer operating at 140.9 Kgauss is used for the characterization of solvent-refined coal liquid products (SRC-II) and their chromatographically separated subfractions. The assignment of well-resolved resonance lines becomes simpler by use of the highest magnetic field possible today to identify major compounds and compound types found in coal-liquids. A double resonance technique has been used for chemical shift identification of $\alpha\text{-CH}_2$ and $\beta\text{-CH}_2$ protons attached to aromatic ring structures. An NMR difference spectroscopic technique is used on a pair of coal-liquid samples to determine compositional change between them. Such quick and direct characterization without fractionation may help to assess the slight variation of process parameters in coal-liquefaction processes.

Experimental

A liquid solvent-refined coal product (SRC-II) was made from Western Kentucky bituminous coal at the Fort Lewis SRC pilot plant, having an initial boiling point of 453 K and an end boiling point of 665 K. The coal-liquid product was fractionated using ion-exchange and silica-gel chromatography (9, 10, 11). Amberlite IRA-904 and Amberlyst A-15 were used as anion and cation-exchange resins, respectively. Activation of the resins and silica-gel was performed by the method described by Jewell et al. (9). The ratios of the coal-liquid to the ion-exchange resins and silica-gel were 1:5 and 1:150 by weight, respectively. The SRC-II middle distillates, boiling point range of 450-565 K, used were from three different coals (Illinois No. 6, Western Kentucky 9/14 and Pittsburgh Seam) derived under the same process conditions, namely hydrogen pressure 13.8 MPa, reactor temperature 730 K, and a residence time of 1 hr.

The 600 MHz ^1H NMR spectrometer which operates at a magnetic field 140.9 kgauss has been developed by Bothner-By and Dadok at Carnegie-Mellon University (12). The resolution determined by half-height width of ethanol triplet was 0.41 Hz, and signal to noise ratio for a single scan was better than 500:1. Tetramethylsilane was used as a lock signal as well as for an internal standard. Each spectrum recorded was the result of 10-100 time-average scans in CDCl_3 solutions. The difference spectrum between the two SRC-II middle distillates was obtained from the individual proton spectrum recorded under the same concentration (38.2 g/l in CDCl_3) and operational conditions.

Infrared spectra were recorded in carbon tetrachloride in 5 mm KBr liquid cells or as a thin film between NaCl plates on a Beckman IR-20 infrared spectrometer. The number-average molecular weights were determined by vapor pressure osmometry in methylene chloride solutions (3-8 g/l) (13).

Results and Discussion

The SRC-II liquid, boiling range of 453-665 K, was fractionated by solvent extraction based on its solubility in *n*-pentane. The pentane-soluble oil fraction (A) 99.3% of SRC-II, was further fractionated by sequential treatment with anion-exchange resin, cation-exchange resin and silica-gel column, as illustrated in Figure 1. Weight percent yields of the fractions, relative to A are included in Figure 1.

After treatment of Fraction A with anion-exchange resin, the non-reactive portion, acid-free fraction (B), did not exhibit absorptions characteristic of either phenolic OH or acidic NH stretching approximately at 3,600 and 3,480 cm^{-1} , respectively. This indicates that compounds containing not only phenolic OH group but also acidic NH group can be removed by the reaction with anion-exchange resin, as has been suggested by Scheppele et al. (10). 600 MHz NMR spectra of the Fractions A and B are shown in Figure 2. Removal of the acidic fraction from A results in a complete disappearance of aromatic proton signals in the range 6.42-6.77 ppm. It is known that aromatic protons show upfield shift when electron-donating groups such as hydroxy group are attached to the same ring structure. It is interesting to note that aliphatic protons in the range of 2.20-2.40 ppm assigned to $-\text{CH}_2$ protons directly attached to mono-aromatic ring structure (14), also decreased drastically after the removal of acidic fractions.

Acidic and basic fractions adsorbed on the resins were recovered by sequential elution with different solvent systems, as shown in Figure 1. Elemental analysis, molecular-weight, and empirical formula of Fraction A and four major fractions (C, D, E and G), are summarized in Table 1. The results indicate that acidic fractions, particularly Acid-II (D), have lower molecular weights and neutral fraction (E) contains no significant amount of heteroatoms per molecule. On an average, Acid-II has one oxygen atom and no nitrogen per molecule. Base-II (G) has one nitrogen atom and negligible amount of oxygen in an average molecule. It should be noted that Acid-I (C) contains oxygen and nitrogen functionalities and that total number of oxygen and nitrogen atoms in an average molecule is close to one. The results may suggest that acidic fraction (C) is a mixture of oxygen-containing and nitrogen-containing compounds. The results on the heteroatom functionalities in Table 1 are well supported by solution infrared spectra of the fractions shown in Figure 3. Table 2 lists the percent distribution of heteroatoms among the fractions, calculated from the data in Table 1. We find 80% of the total oxygen located in two acidic fractions (C and D), and 49% of the total nitrogen are in Base-II (G) in spite of its low content (6.6%). Sulfur is distributed more evenly among the fractions, but higher in neutral fraction (E) and lower in acidic Fractions C and D.

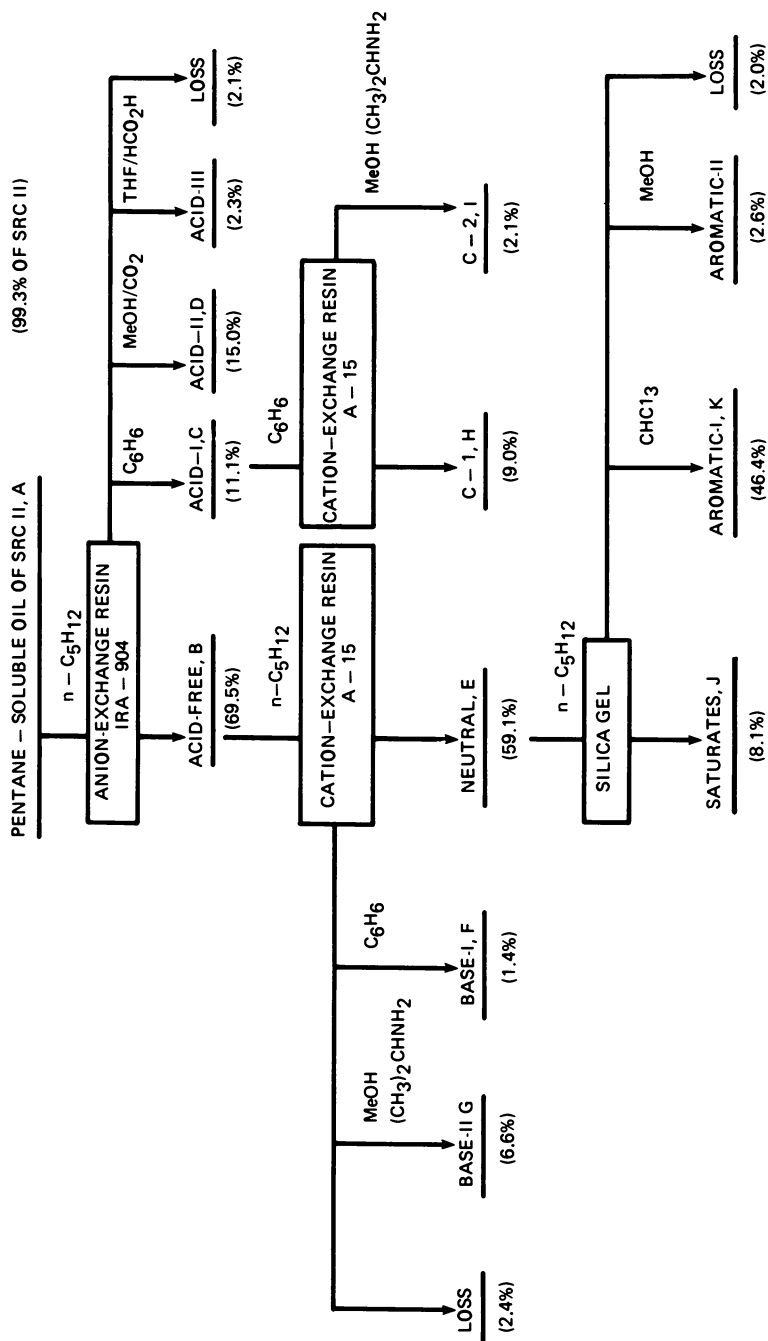


Figure 1. Chromatographic fractionation of SRC-II

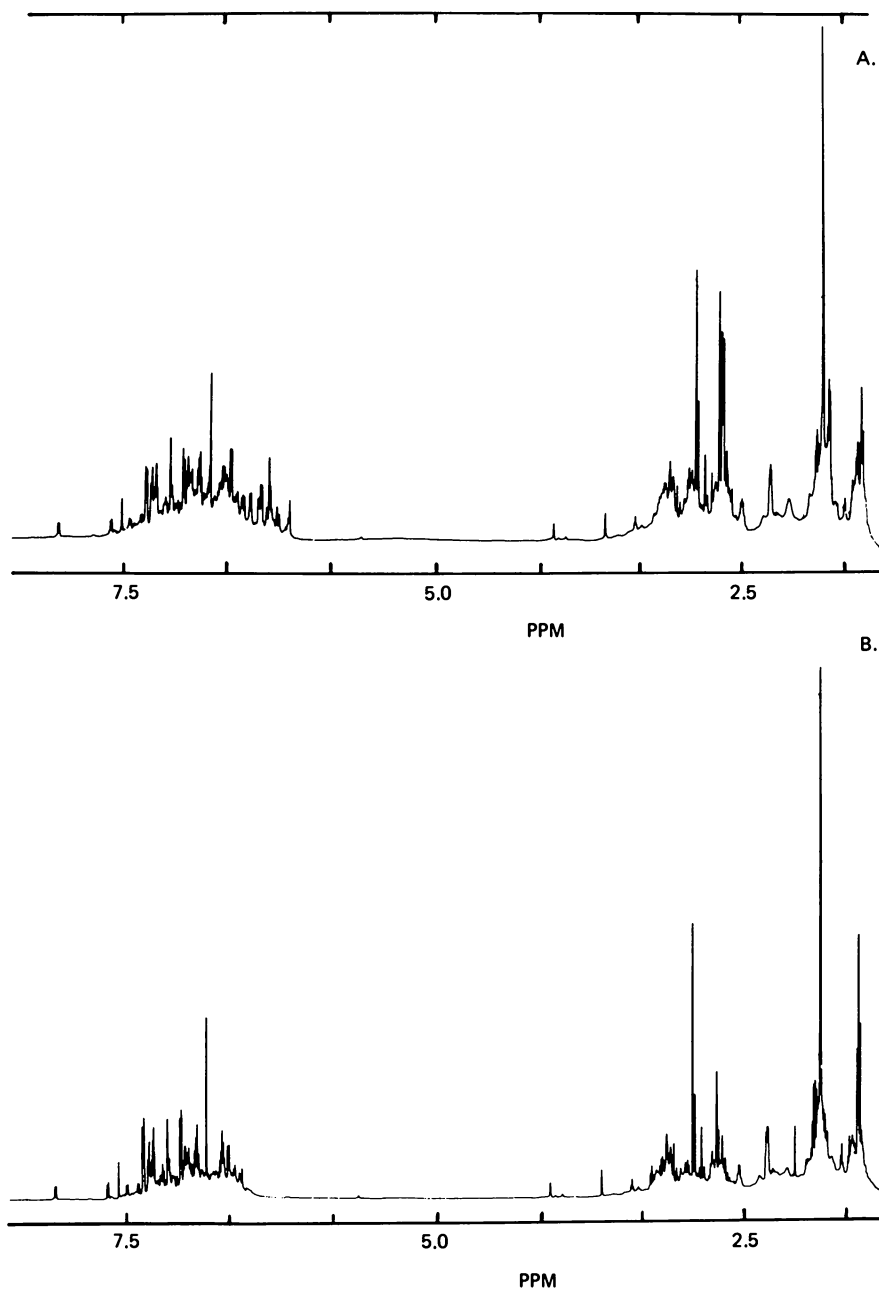


Figure 2. 600-MHz NMR spectra of Fractions A and B

Table 1
 Elemental Analysis, Molecular Weight, Empirical
 Formula of the Major Fractions of SRC-II

Fraction	A	E	C	D	G
Mol. Wt.*	161	Neutral 180	Acid-I 156	Acid-II 128	Base-II 182
Elemental Analysis:					
C	86.09	89.96	80.57	77.32	81.50
H	8.48	8.95	8.25	7.60	8.29
O**	3.99	0.61	8.91	14.66	1.39
N	1.15	0.10	2.17	0.32	8.53
S	0.29	0.38	0.10	<0.10	0.29
Empirical Formula					
(No. of atoms per molecule)					
C	11.6	13.5	10.5	8.2	12.4
H	13.5	16.0	12.8	9.7	15.0
O	0.40	0.07	0.87	1.17	0.16
N	0.13	0.01	0.24	0.03	1.11
S	0.01	0.02	0.00	0.00	0.02

* $\bar{\eta}$ Mol. Wt., using VPO in CH_2Cl_2 solutions (3-8 g/l) at 27°C.

** Oxygen was determined directly.

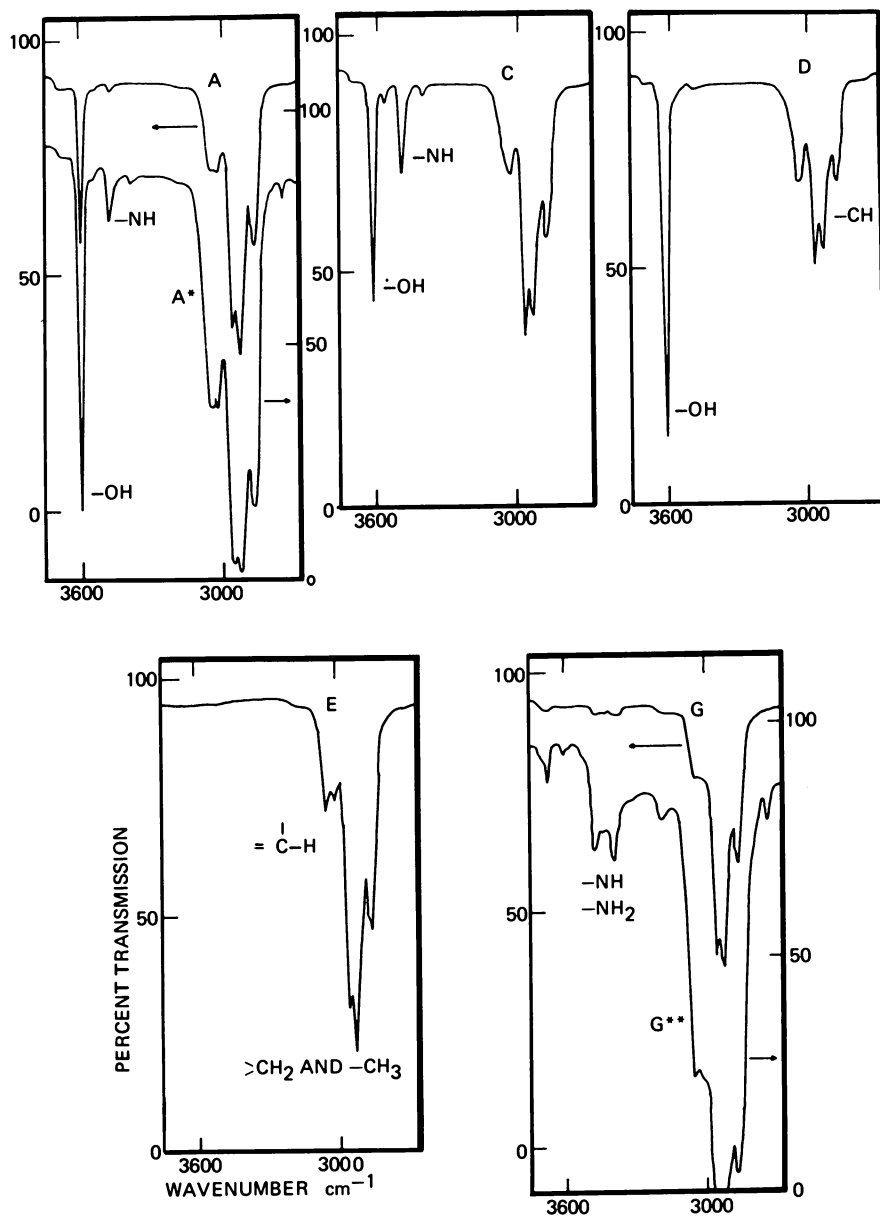


Figure 3. IR spectra in CCl_4 solutions at 1.09 g/L (*3.84 g/L, **8.05 g/L)

Figure 4 shows the boiling-point distribution, simulated by gas chromatography (ASTM D2887) for the major Fractions E, C, D, and G. Fractions C, E and G give almost the same distribution curves, although G contains larger amount of higher boiling-point compounds than C. On the other hand, Fraction D consists of lower boiling-point compounds which are concentrated in a more narrow range of boiling-point, i.e., 75% of D boils in the range of 461 to 516 K (370-470 F).

Neutral fraction (E) was further separated into saturate and aromatic fractions (Figure 1). Figure 5 shows neat infrared spectra of saturate Fraction J and aromatic Fraction K. The characteristic absorptions of the main absorptions₁ can be assigned. For example, the absorption of 1380 cm⁻¹ in Fraction J can be assigned as symmetrical bending vibration of methyl group. Judging from the shape of the absorption, we can conclude that isopropyl or t-butyl groups are not the main functionalities with regard to methyl groups in this fraction. As for the aromatic fraction (K), several modes of carbon-carbon skeleton vibration can be found in the range of 1610-1450 cm⁻¹, being partly overlapped₁ with bending vibrations of CH₃ and CH₂ groups at about 1460 cm⁻¹ (15).

The 600 MHz NMR spectrum of saturate Fraction J (Figure 6) shows a triplet at 0.89 ppm (J = 6.5 Hz) and a relatively sharp singlet at 1.26 ppm. The signal at 7.27 ppm is due to solvent impurity, chloroform. The result combined with the infrared spectrum shows that J is substantially composed of n-alkanes of high carbon numbers (16). Figure 7 shows an NMR spectrum of Fraction K in the region of aliphatic protons. Methyl protons directly attached to aromatic ring structure appear as singlets in the region of 2.2-3.4 ppm. In the case of mono-aromatic compounds, methyl protons generally appear at higher magnetic field than 2.4 ppm (14). In the case of two or more condensed aromatic ring structures, methyl protons appear at lower magnetic field than 2.4 ppm. Chemical shifts of some methyl protons attached to two and three condensed rings are listed in Table 3. The chemical shift values were determined from 600 MHz PMR spectra in CDCl₃ solution. Signals in the spectrum of Fraction K which increased in their intensities by the small addition of these model compounds are marked in Figure 7. Methyl protons of 1-methylnaphthalene appear at very low magnetic field of 2.67 ppm.

Methylene protons at β position to aromatic ring in partially hydrogenated polynuclear compounds appear in the region of 1.7-2.1 ppm. The multi-coupled signals centered at 1.77 ppm can be assigned as β -CH₂ protons in tetralin and its derivatives. Pentuplet signals at 2.05 ppm can be assigned as β -CH₂ protons in indan and its derivatives. These conclusions were made by observing the decoupling effects on the multiplet structure of α -CH₂ protons after irradiating at the center of β -CH₂ proton signals in tetralin, indan and their alkyl derivatives.

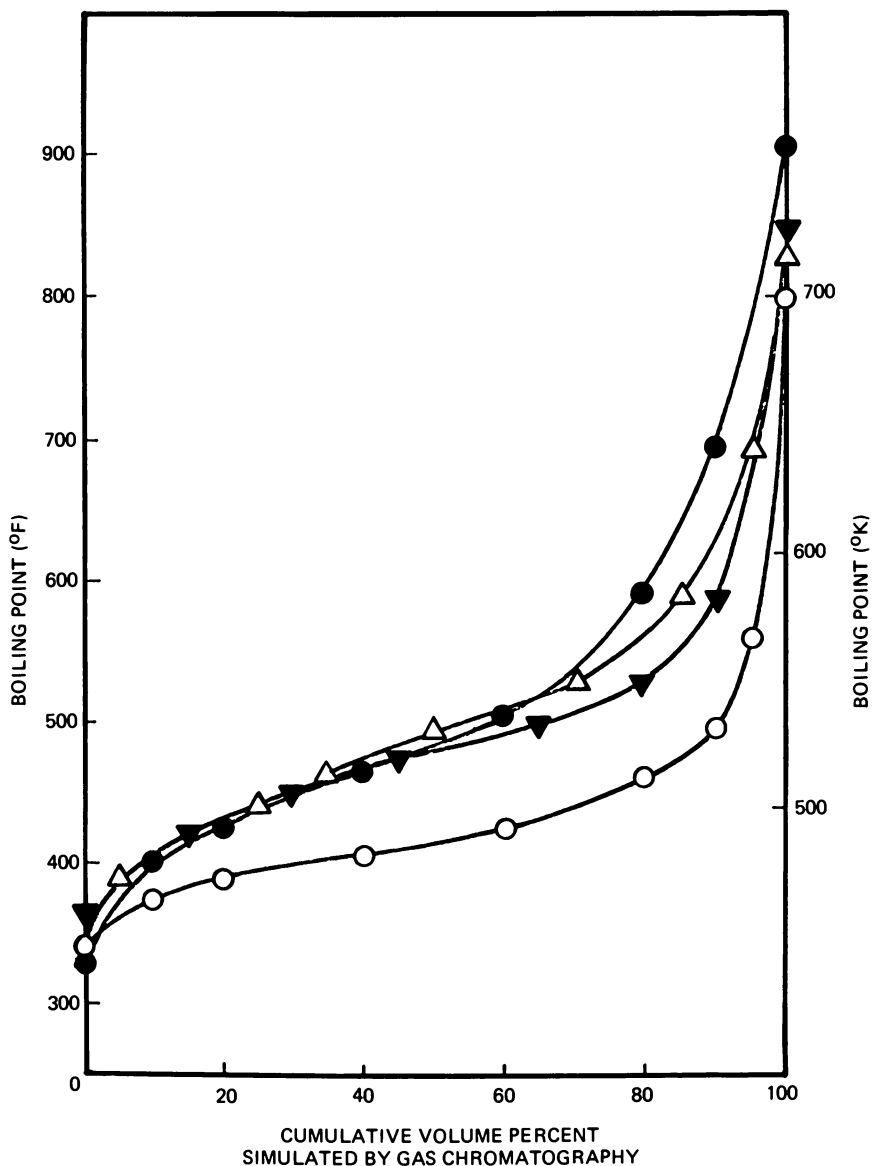


Figure 4. Boiling-point distribution of: neutrals, E, Δ ; Acid-I, C, \blacktriangledown ; Acid-II, D, \circ ; Base-II, G, \bullet .

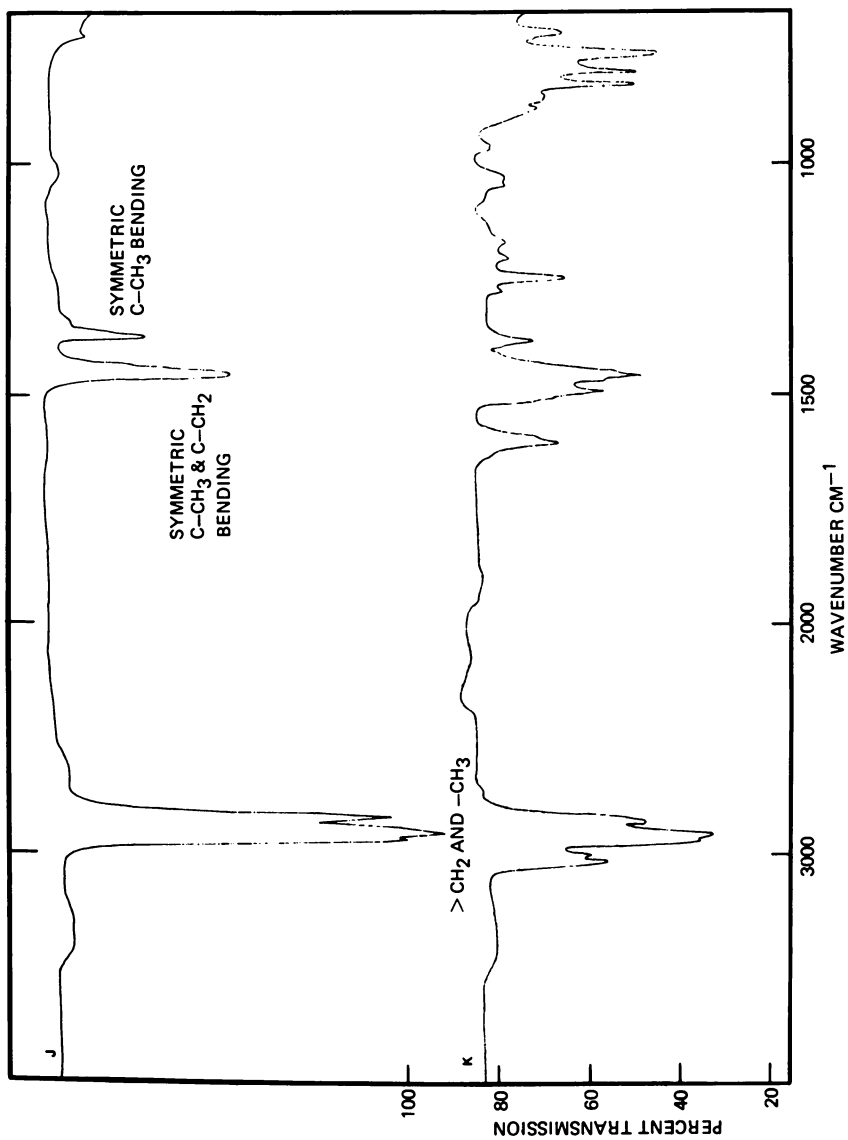


Figure 5. IR spectra of saturates J and Aromatic-I K

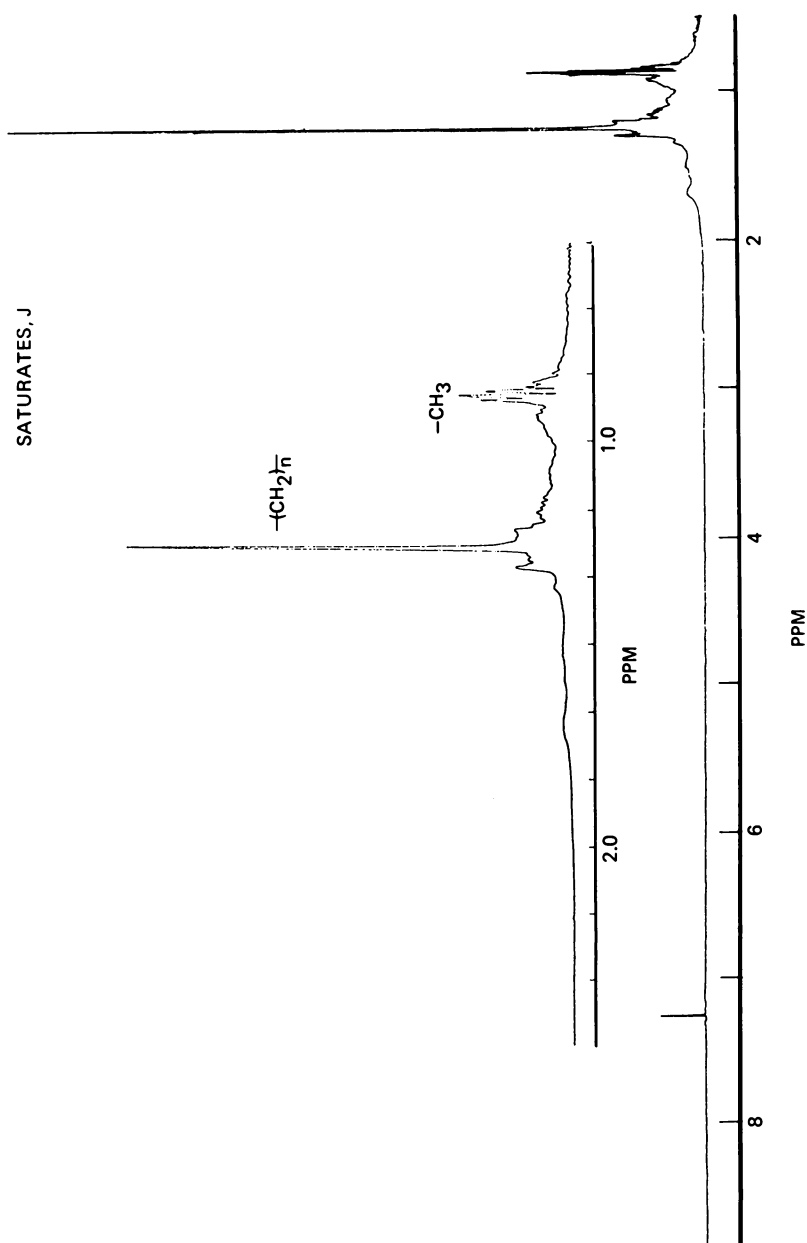


Figure 6. 600-MHz NMR spectrum of saturate fraction J

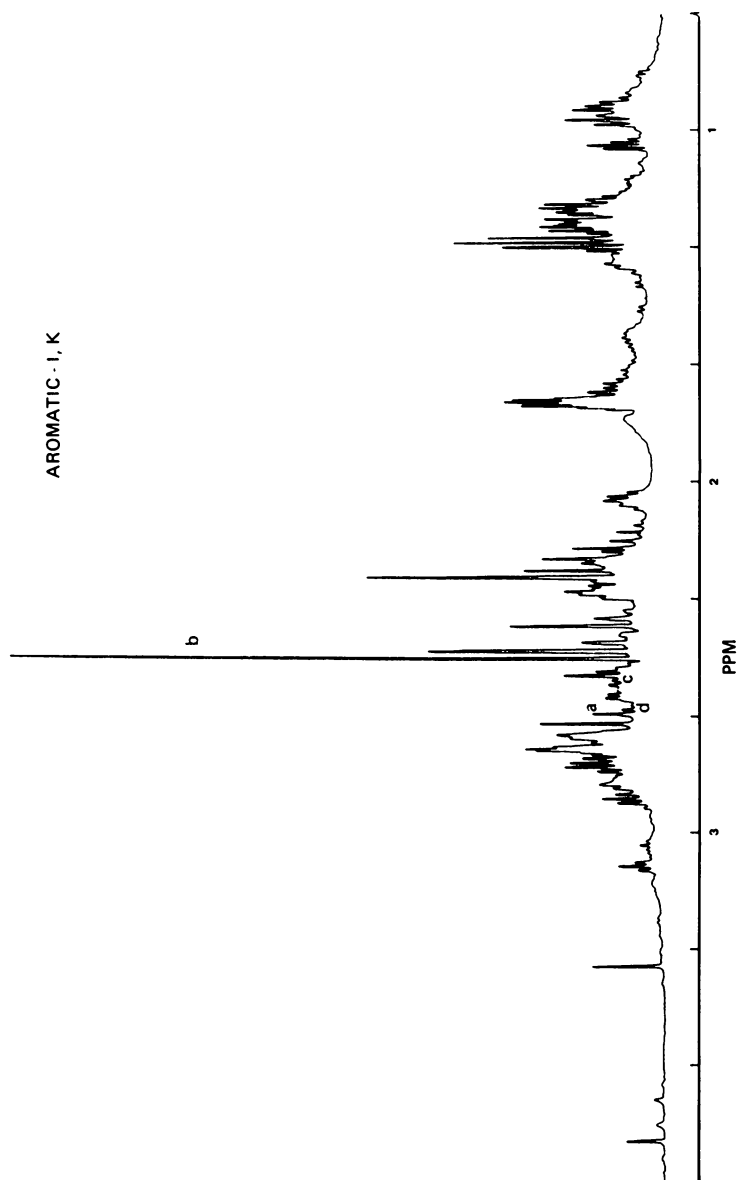


Figure 7. 600-MHz NMR spectrum of Aromatic-1 Fraction K, from 0 to 4 ppm. Specific signal intensity increased by adding: (a) 1-methylnaphthalene; (b) 2-methylnaphthalene; (c) 2-methylphenanthrene; (d) 3-methylphenanthrene.

Table 2
Percent Distribution of Heteroatoms

<u>Fraction</u>	<u>Yield, Wt.% (Relative to A)</u>				
	E	C	D	G	Others
	Neutral	Acid-I	Acid-II	Base-II	
	59.1	11.1	15.0	6.6	8.2

<u>Heteroatom</u>	<u>Distribution of Heteroatoms (wt.%)</u>				
O	9	25	55	2	9
N	5	21	4	49	21
S	78-80	3-4	<3	7	9

Table 3
Chemical Shifts (ppm) of CH₃ and CH₂ Protons
 In Various Aromatic Compounds*

CH ₃ protons α to condensed aromatic rings	
(a) 1-methylnaphthalene	2.67
(b) 2-methylnaphthalene	2.49
(c) 2-methylphenanthrene	2.57
(d) 3-methylphenanthrene	2.63
Ring-joining CH ₂ protons:	
(e) fluorene	3.88
(f) acenaphthene	3.36
(g) 9,10-dihydrophenanthrene	2.86

* Determined in CDCl₃ solutions of about 20 g/l relative to TMS.

Figure 8-(a) and (b) show the decoupled signals of α -CH₂ protons in tetralins and indans, respectively. The decoupled signals at 2.76 ppm in (a) and at 2.90 ppm in (b) correspond to α -CH₂ protons of unsubstituted tetralin and indan, respectively. The result of decoupling of Figure 8 indicates the existence of several types of α -CH₂ protons which probably are located in substituted tetralin and indan. For example, the triplet at 3.10 ppm was decoupled completely by the irradiation on the pentuplet signals at 2.05 ppm.

A methylene group resonance which joins two ring structures (bridgehead) appears at lower magnetic field, Table 3. The singlets at 3.36 and 3.88 ppm in Fraction K can be assigned to acenaphthene and fluorene, respectively.

Figure 9 shows the aromatic proton signals of Fraction K. Since more than half of the aromatic protons of Fraction K appear downfield from the benzene signal (7.37 ppm), this fraction contains a large amount of two and three condensed aromatic ring compounds. Two doublet signals (8.69 and 7.88 ppm) can be assigned to the 4,5 and 1,8 protons of phenanthrene, respectively (17). The small signals in the region of 8.47-8.63 ppm are also assigned to protons at the positions of 4 and 5 in methylphenanthrenes. This could be seen from 600 MHz ¹H spectra of 2- and 3-methylphenanthrene shown in Figure 10.

The assignment of ¹H signals of coal-liquid fractions in this study is based either on the comparison of chemical shift values of pure compounds or on the change of spectral intensities caused by the addition of such compounds. For example, 600 MHz NMR spectra of 2- and 3-methylphenanthrene are shown in Figure 10. The assignment of each proton becomes much simpler by use of the higher-field spectrometer, because the chemical shift of each proton is extended compared with coupling constants, resulting in clear separation of each proton.

Figure 11 shows the aromatic proton signals of Fraction K, C, D and G. Acidic Fractions C and D, have more proton signals at higher magnetic field, because of the strong electron-donating property of phenolic OH groups. Acid-I (C) fraction contains condensed-ring aromatic compounds such as naphthols, while Acid-II (D) has no proton signal which appears downfield from the benzene signal. This shows that Acid-II is substantially composed of mono-aromatic phenols. The spectrum in the region of aliphatic protons in Acid-II is shown in Figure 12. The intense singlets in the region of 2.20-2.40 ppm are assigned to CH₃ protons attached to mono-aromatic ring. The acidic fractions are characteristic by having high content of such CH₃ groups. The results are consistent with substantial decrease of signals between 2.2-2.4 ppm after the removal of acidic fractions from Fraction A, as shown in Figure 2. Two triplets at 1.20 and 0.92 ppm may be assigned to CH₃ protons in ethyl and n-propyl groups attached to aromatic rings, respectively. In conclusion,

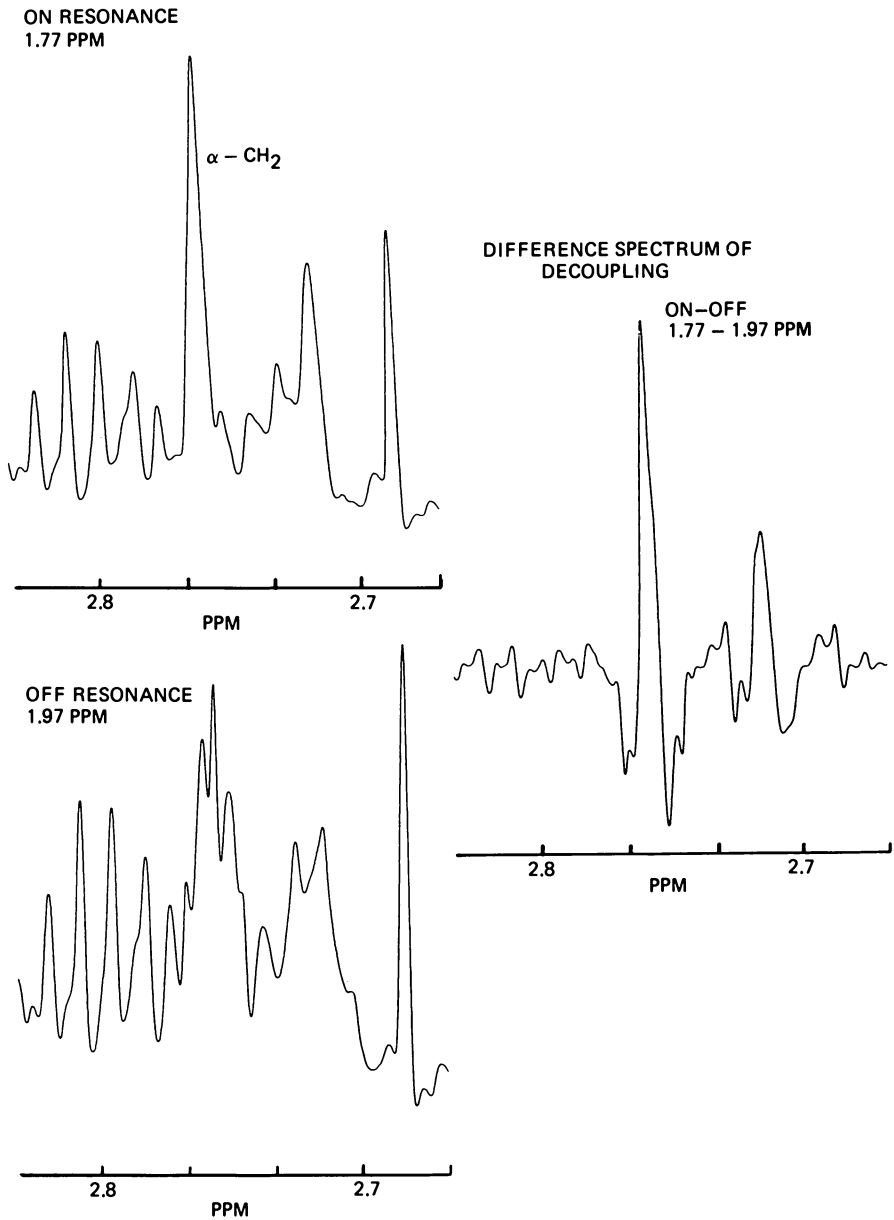


Figure 8a. Decoupling effect on $\alpha\text{-CH}_2$ proton signals in Tetralin and its derivatives. Irradiation at 1.77 ppm.

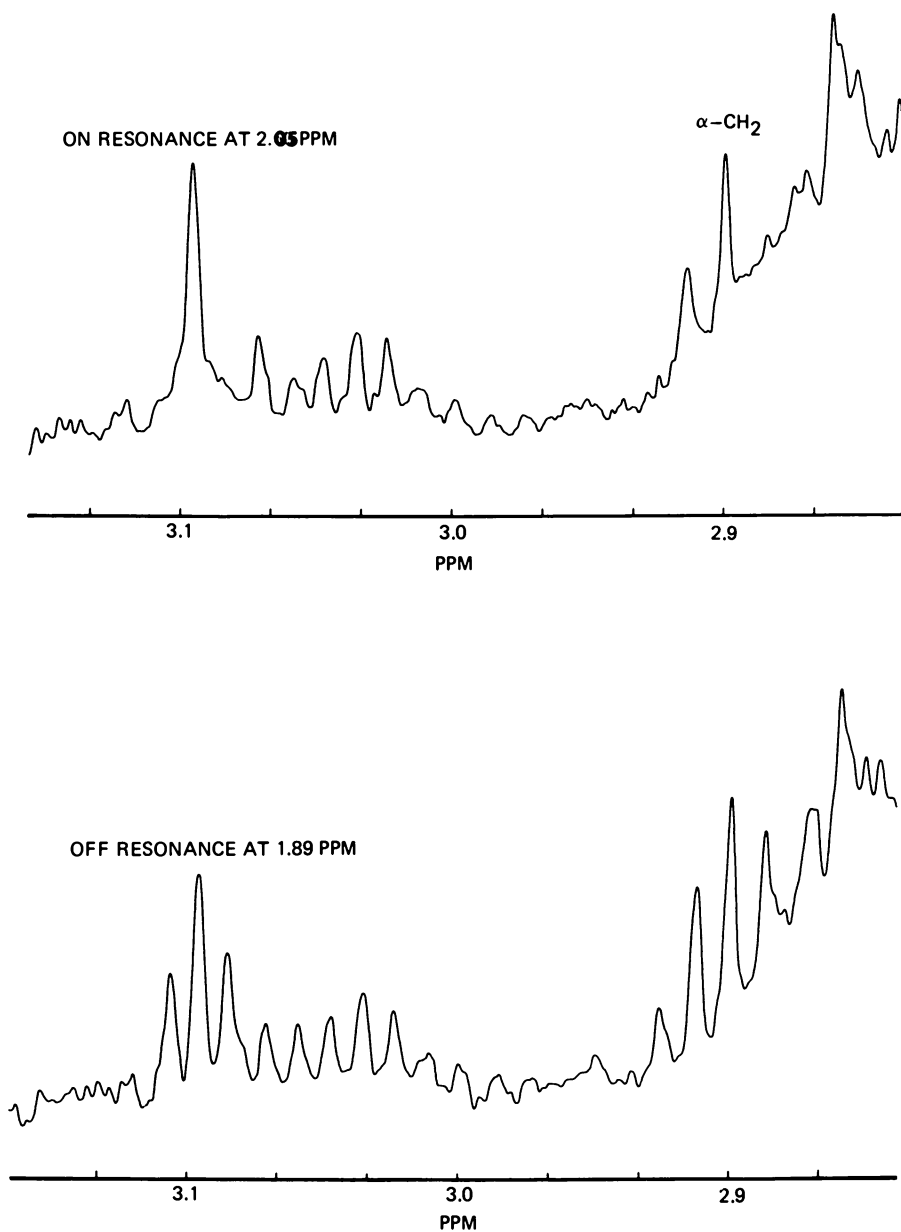


Figure 8b. Decoupling effect on α -CH₂ proton signals of indane and its derivatives. Irradiation at 2.05 ppm.

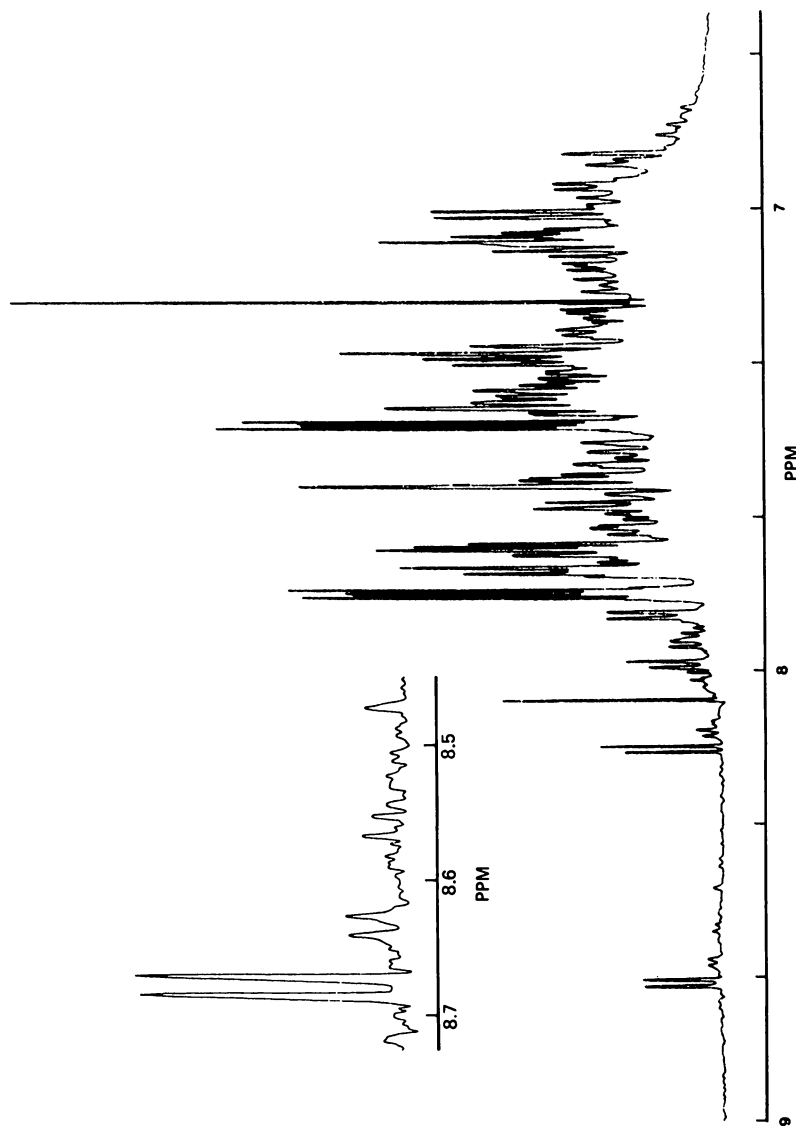


Figure 9. 600-MHz spectrum of Aromatic-I Fraction K from 6 to 9 ppm

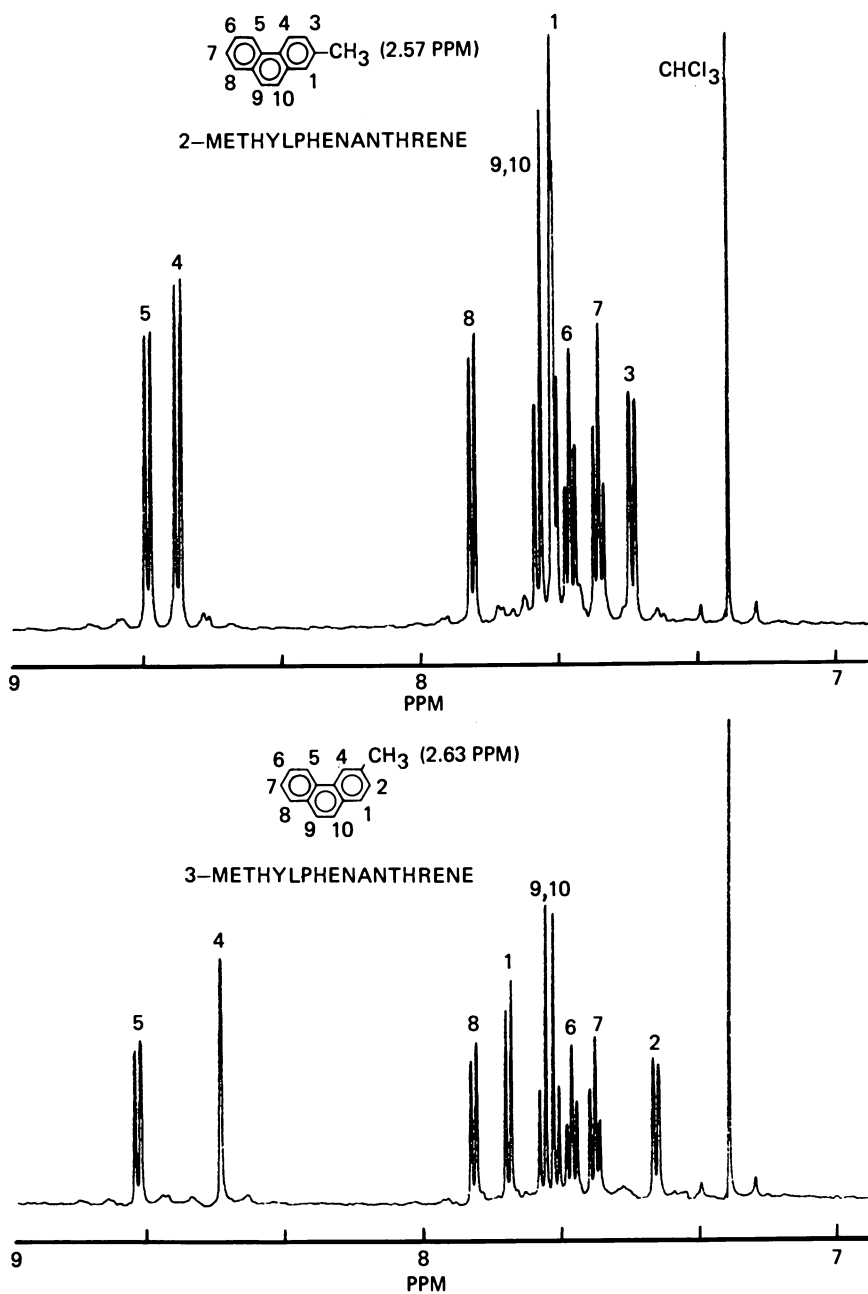


Figure 10. 600-MHz NMR spectra of methylphenanthrenes in $CDCl_3$ (20 g/L)

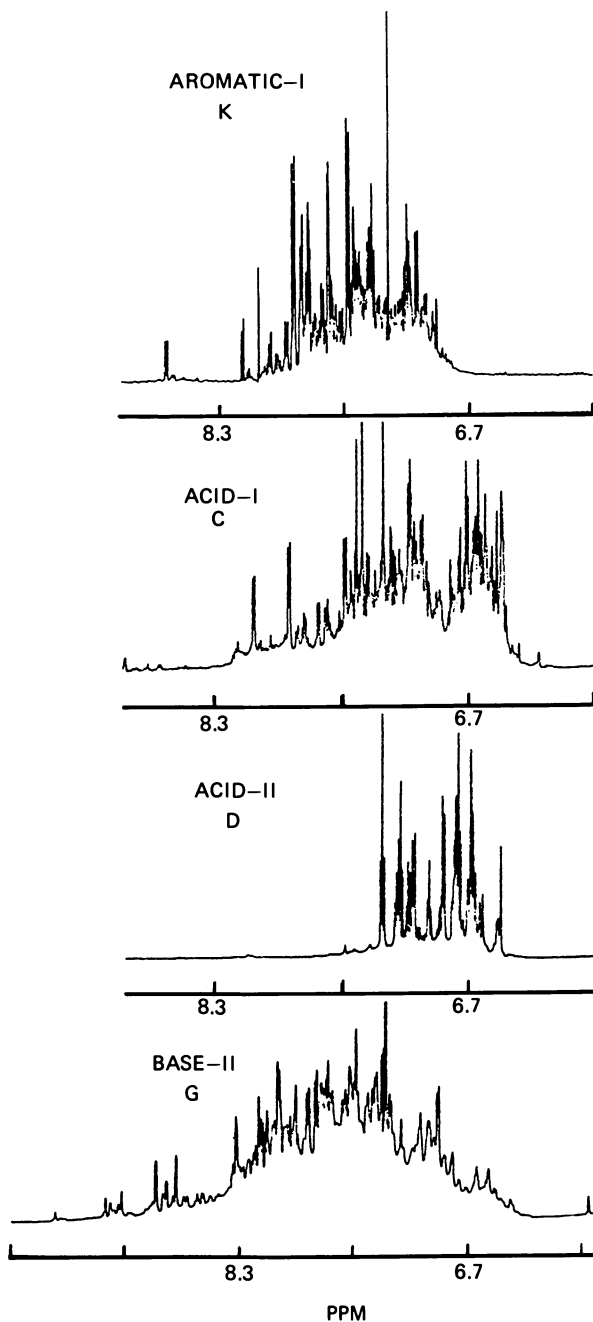


Figure 11. 600-MHz NMR spectra of Fractions K, C, D, and G from 6 to 9 ppm

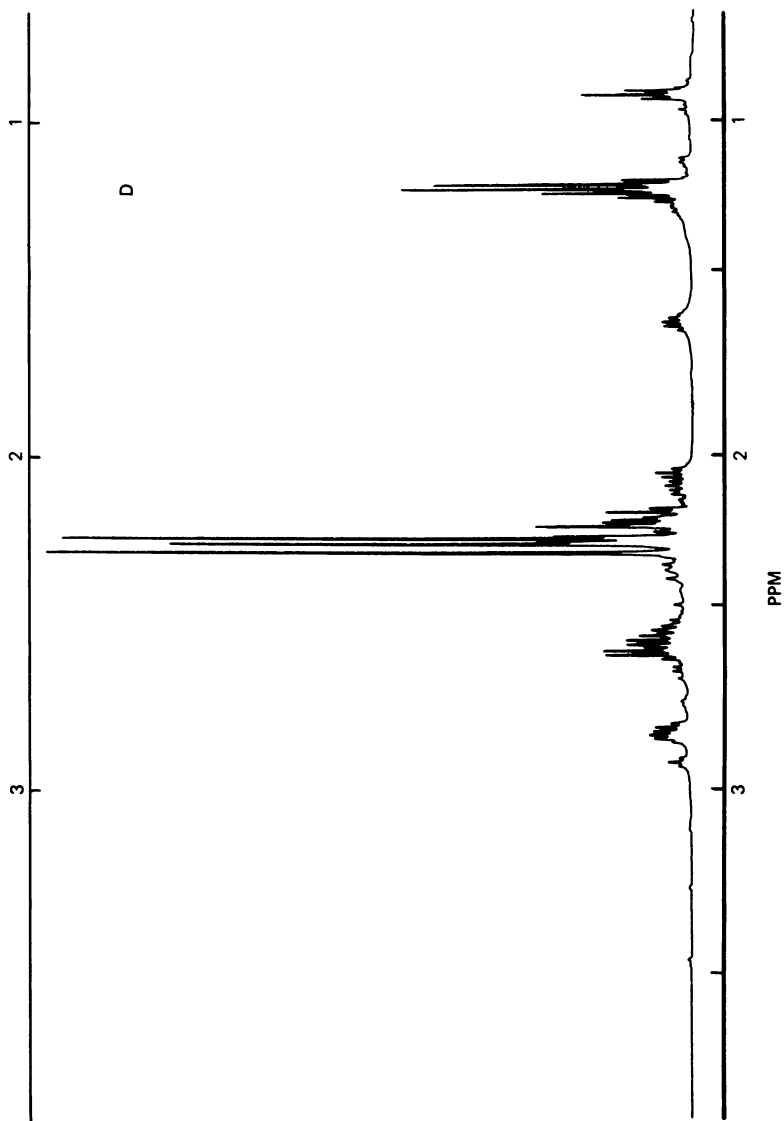


Figure 12. 600-MHz NMR spectrum of Acid-II Fraction D from 0 to 3 ppm

Acid-II fraction is mainly composed of alkyl substituted mono-aromatic phenols. As for Base-II (G) fraction, proton signals are much more widely spread than that of Fraction K particularly at lower magnetic field, as shown in Figure 11. This may suggest that the fraction is composed of heteroaromatic compounds involving nitrogen atom in the ring structure (18).

Infrared spectra in dilute solution, Figure 3, indicate that compounds which contain acidic NH group such as indoles or carbazoles are substantially concentrated in Acid-I (C) fraction. Acid-I was further treated with cation-exchange resin to be separated into Fractions H and I (Figure 1). Solution infrared spectra of H and I, Figure 13, show that all phenolic species passed through the cation-exchange resin, whereas acidic nitrogen species were almost equally distributed into two fractions. It is interesting to note the NH species, possibly amides or amines whose stretching frequency appears at 3390 cm^{-1} (19), were substantially concentrated in Fraction I. It is therefore concluded that Fraction I (19% of Acid-I) contains negligible amount of phenolic compounds but two types of NH species and that it may be reactive with both anion and cation-exchange resins. Infrared spectra, Figures 3 and 13, were used to estimate contents of functional groups relative to Fraction A. The results are listed in Table 4. The contents of phenolic OH and acidic NH groups decrease in the following order:

Phenolic OH	D > H > C > A >> I, G, E \approx 0
Acidic NH	I > C > H >> A > G > D, E \approx 0

The absorbance ratio of C-H stretching of CH_3 group to that of CH_2 group (20) increase in the following order:

$A_{\text{CH}_3} / A_{\text{CH}_2}$	H, C, D > I \approx 1.0 > G > A > E
-------------------------------------	---------------------------------------

The NMR structural parameters of major fractions, Table 5, were calculated using modified Brown and Ladner equations (5, 6). The results indicate that Acid-II is largely composed of mono-aromatics, whereas Acid-I contains di-aromatics. Although Neutral and Base-II have almost the same molecular weights and aromaticity, the former is rich in condensed aromatic structure and the latter in saturated ring structure.

The NMR difference spectroscopic technique was used to examine major compositional changes among the SRC-II distillates obtained under the same process conditions but different feed coals. Elemental analysis, specific gravity and number average molecular weight of the three distillates are listed in Table 6. The data show no distinctive difference among them. Figure 14(a) shows the difference spectrum between two SRC-II middle distillates derived from Illinois No. 6 and from Pittsburgh Seam. The proton signals above the center line represent the types of compounds present in Illinois No. 6 distillate in addition or

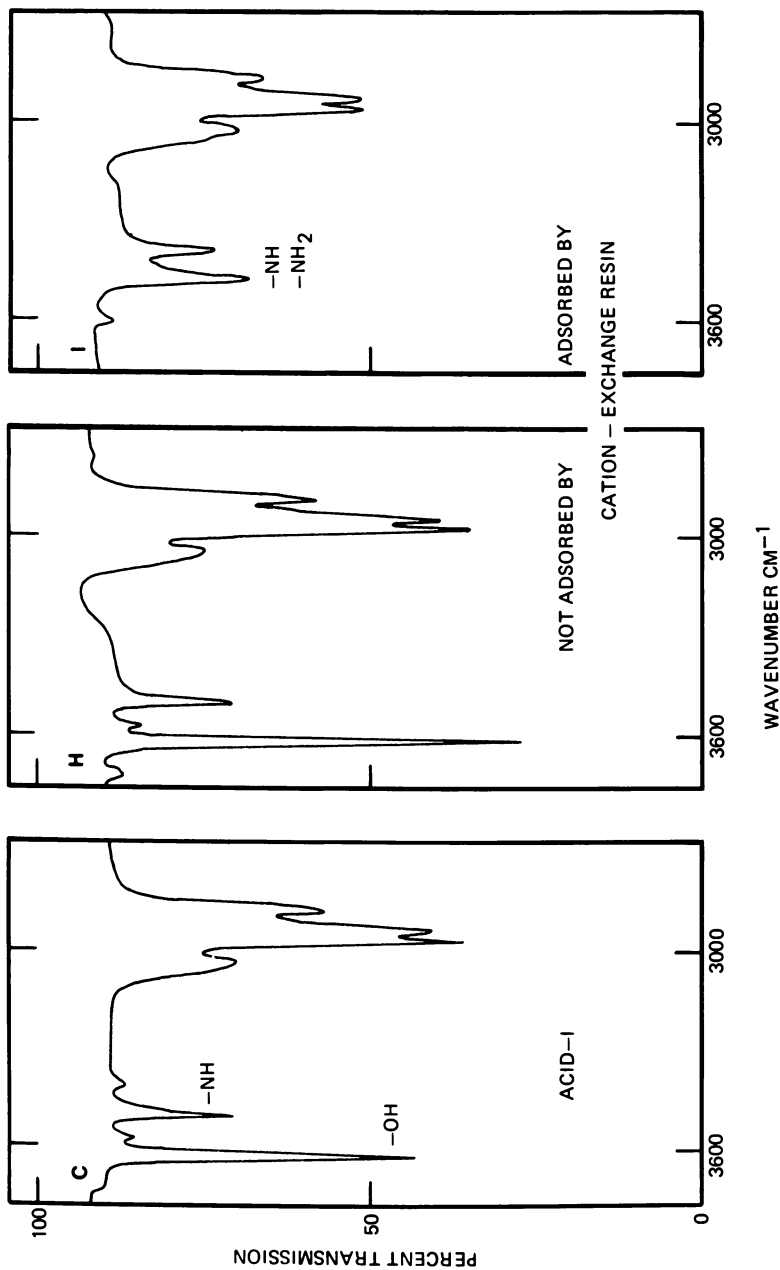


Figure 13. IR spectra in CCl₄ solutions at 1.09 g/L

Table 4
Analysis of Functional Groups in
 Chromatographically Separated Fractions

Fraction	A_{OH}^b	Absorbance of absorbance ratio ^a			
		Relative ^c A_{OH}	A_{NH}^d	Relative ^c A_{NH}	$A_{CH_3}/A_{CH_2}^e$
A	0.197	1.0	0.061 ^f	1.0	0.82
C	0.309	1.6	0.100	5.8	1.14
H	0.515	2.6	0.096	5.5	1.14
I	0.015	0.1	0.125	7.2	1.00
D	0.815	4.1	0	0	1.11
E	0	0	0	0	0.75
G	0.009 ^g	0.0	0.117 ^g	0.9	0.91

a Measured in CCl_4 solutions, 1.09 g/l, 5 mm KBr liquid cell.

b Absorbance measured at 3600 cm^{-1} .

c Relative to absorbance of Fraction A after normalization at concentration of 1.09 g/l.

d Absorbance measured at 3480 cm^{-1} .

e Ratio of the absorbance at 2960 cm^{-1} (symmetrical stretching in CH_3 group) to the absorbance at 2925 cm^{-1} (symmetrical stretching in CH_2 group).

f CCl_4 solution of 3.84 g/l.

g CCl_4 solution of 8.05 g/l.

Table 5
Structural Parameters for Major Fractions of SRC-II

Fractions		A	E	C	D	G
			Neutral	Acid-I	Acid-II	Base-II
^a Number of carbon atoms in a molecule	C [']	11.55	13.49	10.47	8.25	12.36
	Ca [']	7.51	7.99	6.74	6.21	7.14
	Ca ['] CH ₃	0.45	0.32	0.58	0.70	0.41
	Ca ['] CH ₂	1.46	1.65	1.37	0.73	2.32
	C ['] _{other}	2.13	3.53	1.78	0.61	2.49
^b Structural parameters	f _a [']	0.65	0.59	0.64	0.75	0.58
	H _{au} /ca [']	0.90	0.78	0.93	1.00	0.94
	R _T	2.03	2.51	1.72	1.32	2.32
	R _A	1.38	1.63	1.20	1.03	1.26
	R _N	0.65	0.88	0.52	0.29	1.06

^a C['] total carbon, Ca['] aromatic, Ca[']CH₃ benzylic methyl, Ca[']CH₂ benzylic methylene, C[']_{other} other than Ca['], Ca[']CH₃ and Ca[']CH₂.

^b f_a['] aromaticity, H_{au}/Ca['] ratio of substitutable aromatic edge atoms to total aromatic atoms, number of total (R_T), aromatic (R_A) and naphthenic (R_N) rings in a molecule.

Table 6
Properties of SRC-II
Middle Distillates from Different Coals

	<u>Illinois #6</u>	<u>Pittsburgh</u>	<u>Western Kentucky 9/14</u>
Elemental			
Analysis C	85.55	86.03	85.37
(wt.%) H	9.12	8.93	9.19
O	4.29	3.83	4.15
N	0.85	1.04	1.09
S	0.19	0.17	0.20
Specific			
Gravity (289 K)	0.973	0.974	0.975
Molecular			
Weight	172	185	186

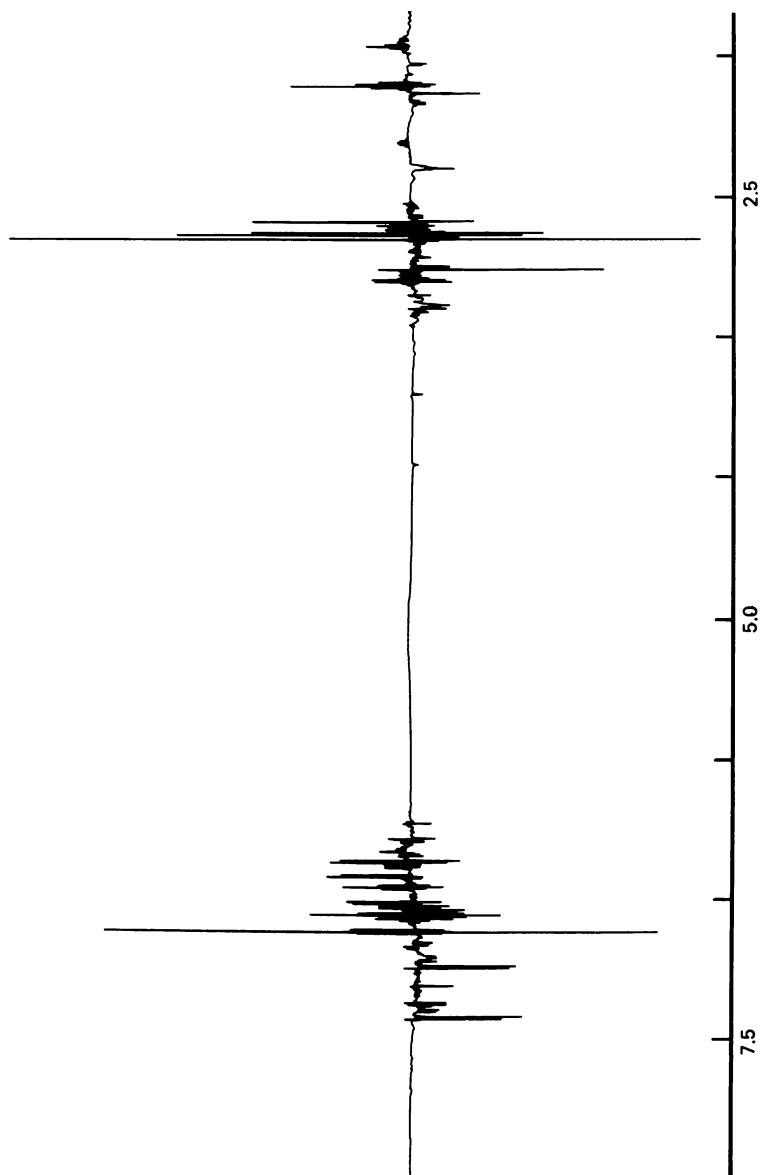


Figure 14a. Difference NMR spectrum between SRC-II middle distillates from Illinois No. 6 and from Pittsburgh Seam coal as CDCl_3 solutions at 38.2 g/L

Publication Date: October 26, 1981 | doi: 10.1021/bk-1981-0169.ch017

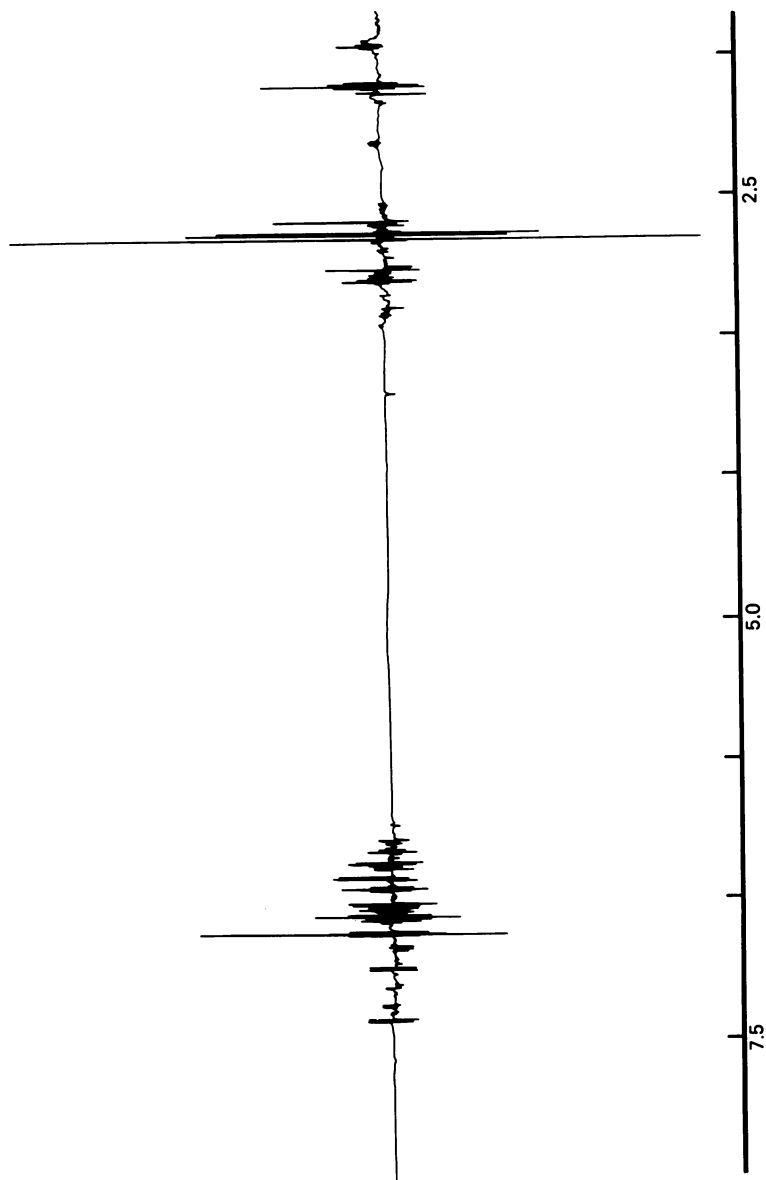


Figure 14b. Difference NMR spectrum between SRC-II middle distillates from Illinois No. 6 and from Western Kentucky 9/14 coal as CDCl_3 solutions at 38.2 g/L

in excess to compounds present in Pittsburgh Seam liquid. The product from Pittsburgh Seam Coal contains an excess amount of compounds whose resonance signals are displayed below the center line. The appearance of distinct resonance lines above the center line upfield to benzene and several intense singlets in the region of 2.20-2.40 ppm resemble the spectrum of Acid-II fraction. It may be that the product from Illinois No. 6 contains larger amount of alkyl substituted mono-aromatic phenols. On the other hand, the product from Pittsburgh Seam contains larger amount of naphthalenes and tetralins.

The difference spectrum between products from Illinois No. 6 and Western Kentucky is shown in Figure 14(b). In this case almost symmetrical signals can be found in both sides except for few signals. Slight changes in chemical shift of each signal may be brought about either by slight changes in structure of similar compounds in both coal-liquids, or by the presence of different compounds which affects the chemical shift of signals by intermolecular interaction. In conclusion, the chemical composition of these two coal-liquids is quite similar except for the fact that the product from Illinois No. 6 contains larger amount of saturate fraction or long chain substituents.

Conclusion

A coal-derived liquid (SRC-II) and its fractions are characterized by 600 MHz ^1H NMR spectrometer. Saturate fraction, being 8.1% by weight of unfractionated coal-liquid, is mainly composed of n-alkanes of high carbon numbers and the content of cycloalkanes is negligible. Aromatic fraction (49.0%) contains a considerable amount of partially hydrogenated polynuclear compounds. Double resonance techniques have been used for chemical shift identification of $\beta\text{-CH}_2$ and $\alpha\text{-CH}_2$ protons attached to aromatic ring structures. The decoupled signals may be used for quantitative analysis of donor hydrogens, which are known to be effective in hydrogen-transfer phenomenon in coal-liquefaction processes. The aromatic fraction contains larger amounts of CH_3 group attached to condensed aromatic ring structures which appear as singlets in the region of 2.4-2.7 ppm, whereas in acidic fractions almost all benzylic CH_3 groups are attached to mono-aromatic ring structure (chemical-shift range of 2.2-2.4 ppm). The relatively strong acidic fraction, Acid-II (15.0%), can be recovered from anion-exchange resin by the elution with CO_2 saturated methanol after the elution with benzene. Acid-II is substantially composed of alkyl substituted mono-aromatic phenols and 75% of the fraction boil in the narrow boiling-point range of 461-516 K (370-470 F).

The new NMR difference spectroscopic technique is applied to coal-derived liquids obtained from the same process conditions but from different coals. The slight compositional changes among the distillates are shown by the difference spectra. Such quick and direct characterization with minimal fractionation may help to assess the slight variation of process parameters in coal-liquefaction.

Acknowledgements

We acknowledge support of the U.S. Department of Energy to Duquesne University under Contract No. DE-AC22-80 PC 30252. The 600 MHz spectrometer at Carnegie-Mellon University, supported by PHS Grant No. RR-00292, was used, and we thank K. S. Lee and J. Dadok for expert advice in carrying out the NMR measurements.

Literature Cited

1. Friedel, R. A., J. Chem. Phys., 1959, 31, 280.
2. Brown, J. K., Ladner, W. R., and Sheppard, N., Fuel, 1959, 39, 79.
3. Brown, J. K. and Ladner, W. R., Fuel, 1959, 39, 87.
4. Schwager, I., Farmanian, P. A., and Yen, T. F., "Analytical Chemistry of Liquid Fuel Sources Tar Sands, Oil Shale, Coal, and Petroleum", Advanced in Chemistry Series 170, Am. Chem. Soc., 1978; p. 66-77.
5. Ouchi, K., Iwata, K., Makabe, M., and Itoh, H., Preprint, Div. Fuel Chem., Am. Chem. Soc., 1979, 24(1), 185.
6. Chung, K. E., Anderson, L. L., and Wisler, W. H., Preprint, Div. Fuel Chem., Am. Chem. Soc., 1979, 24(3), 243.
7. Bartle, K. D. and Jones, D. W., Fuel, 1969, 48, 21.
8. Schweighardt, F. K., Retcofsky, H. L., Friedman, S., and Hough, M., Anal. Chem., 1978, 50, 368.
9. Jewell, D. M., Weber, J. H., Bunger, J. W., Plancher, H., and Latham, D. R., Anal. Chem., 1972, 44, 1391.
10. Scheppele, S. E., Benson, P. A., Greenwood, G. J., Grindstaff, Q., Aczel, T., and Bieber, B., Preprint, Div. Petroleum Chem., Am. Chem. Soc., 1979, 24(4), 963.
11. Boduszynski, M. M., Preprint, Div. Petroleum Chem., Am. Chem. Soc., 1979, 24(4), 935.
12. Bothner-By, A. A. and Dadok, J., Paper presented at Symposium on "The Utility of 600 MHz NMR Spectroscopy in Biochemical and Organic Structure Determination", Pittsburgh, December 1979.
13. Tewari, K. C., Wang, J. T., Li, N. C. and Yeh, H. J. C., Fuel, 1979, 58, 371.
14. High Resolution NMR Spectra Catalog, Varian, Palo Alto, California, 1962.
15. Cannon, C. G. and Sutherland, G. B. B. M., Spectrochim. Acta 1951, 4, 373.

16. "Selected NMR Spectral Data (100 MHz)", Vol. I, Serial Numbers 51c, 69c, 89c, 98c, American Petroleum Institute Research Project 44, Thermodynamic Research Center, Texas A and M University, December 1972.
17. Jonathane, N., Gordon, S., and Dailey, B. P., J. Chem. Phys., 1962, 36, 2443.
18. Schafer, T. and Schneider, W. G., Can. J. Chem., 1963, 41, 966.
19. Schwager, I. and Yen, T. F., Anal. Chem., 1979, 51, 569.
20. Hathaway, C. D., Curtis, C. W., Meng, S., Tarrer, A. R., and Guin, J. A., Preprint, Div. Fuel Chem., Am. Chem. Soc., 1978 23(1), 275.

RECEIVED June 18, 1981.

Coal Liquid Upgrading Using Metallophthalocyanine Catalysts: Hydrogenation of the Model Compound Quinoline

L. J. BOUCHER and N. L. HOLY

Department of Chemistry, Western Kentucky University, Bowling Green, KY 42101

B. H. DAVIS

Institute for Mining and Minerals Research, Kentucky Center for Energy Research,
Lexington, KY 40583

To utilize the products from coal liquefaction (coal liquids) as a source for transportation fuels or as a chemical feed stock, the products must be upgraded. The coal liquids must be treated so as to reduce the S, N, O content, increase the hydrogen content, and decrease the viscosity and average molecular weight.(1) The application of heterogeneous catalysis to heteroatom removal received major impetus from the coal liquefaction research carried out in Germany.(2) The present-day catalyst, resulting from years of extensive research, is a combination of Co-Mo, or Ni-Mo (sulfided) usually on a high area support.(3) The early work of Givens(4) demonstrated that hydrodesulfurization, HDS, could be viewed as an extrusion of sulfur; i.e., the reaction required the addition of hydrogen at the C-S bonds being broken. The situation for nitrogen and oxygen removal appears to be different than with sulfur. For example, the heteroatom containing ring must be completely hydrogenated prior to C-N bond breaking. Stern(5) found that with indole, the first step involved hydrogenation of the five membered ring; this was followed by C-N bond hydrogenolysis to form o-ethylaniline. This C-N bond rupture is followed by hydrogenolysis to form ammonia and a hydrocarbon. Rollmann(6) found that, with mixtures of N-, S- and O-compounds, saturation of the N- and O-heteroatom ring was necessary prior to hydrodenitrogenation, HDN, but that this was not the case for S-compounds. This work suggests that the reaction network obtained for a model nitrogen compound will be the one that would occur in complex mixtures such as coal liquids.(7)

HDN of Quinoline. Satterfield *et al.*(8) proposed that there are two pathways for the HDN of the coal liquid model compound quinoline using a Ni-Mo catalyst. One pathway involves the successive formation from quinoline of 1,2,3,4-tetrahydroquinoline, o-propylaniline and then ammonia plus n-propylbenzene. A second pathway involves the successive formation of 5,6,7,8-tetrahydroquinoline, decahydroquinoline, propylcyclohexylamine

0097-6156/81/0169-0319\$05.00/0

© 1981 American Chemical Society

and then ammonia plus propylcyclohexane. An important conclusion reached is that quinoline and 1,2,3,4-tetrahydroquinoline are in thermodynamic equilibrium under essentially all reaction conditions of interest.

Katzer *et al.* (9) concluded that quinoline HDN is a complex reaction. They found that hydrogenation on Ni-Mo/Al₂O₃ occurred on both rings to form 1,2,3,4- and 5,6,7,8-tetrahydroquinoline and decahydroquinoline as reaction intermediates. In agreement with Satterfield they found the hydrogenation of quinoline to 1,2,3,4-tetrahydroquinoline reached equilibrium; the remaining hydrogenation reactions were kinetically controlled. Nitrogen removal took place through hydrogenolysis of 1,2,3,4-tetrahydroquinoline and decahydroquinoline. Kinetically, the primary nitrogen removal occurred through the quinoline, 5,6,7,8-tetrahydroquinoline, decahydroquinoline route. They found the hydrogenation and hydrogenolysis reactions were first order with respect to the nitrogen-containing substance. Hydrogenation reactions were second order in hydrogen, but hydrogenolysis reactions were of a lower dependency on hydrogen. Steric hindrance is important for several reaction steps. Hydrogenation is retarded by an adjacent puckered, cyclohexane ring or piperidine ring. It appeared that the overall reaction required a bifunctional catalyst.

HDN with Metallophthalocyanines. The above considerations clearly show that the catalytic site geometry is important in HDN. It is difficult to control, or even to identify, the catalyst site in conventional catalysts such as the commercial Co-Mo-alumina catalyst. On the other hand, homogeneous catalysts with transition metal complexes provide a well-defined catalytic site. Unfortunately, most homogeneous catalysts are not sufficiently stable to be used at the temperatures required for the hydrogenation of hetero compounds. A class of catalysts that are thermally stable are the metallophthalocyanines, [M(PC)]. (10) For example, [M(PC)] have been used as homogeneous catalysts for the hydrotreating of black oils (vacuum bottom). (11) The addition of [M(PC)], M = Co, Fe, V, Ni, Cu, and Pt, increases the amount of distillables when the oil is subjected to hydrogenation at 260-425°C and 1500-3500 psi H₂ pressure. Hydroconversion of heavy oils is also accomplished with catalysts of powdered Fe metal and [M(PC)] where M = Co, V, Ni, Cr, Mo, Pt at 420-482°C and 1000-3000 psi H₂ pressure. (12) Although [M(PC)] have never been used as HDN catalysts per se, the oils have an appreciable concentration of heteroatom-containing molecules which appear to be hydrogenated.

Hydrogenation Activity of Metallophthalocyanines. Solid [M(PC)] are effective catalysts in the hydrogenation of NO, (13, 14) hydrotropic aldehydes (15) and allyl alcohol. (16) The reactions are run in the temperature region, 100-400°C,

where the catalysts appear to be stable. A related catalyst with enhanced hydrogenation activity is obtained by reacting $[M(PC)]$ with an alkali metal-reducing agent M' . The reduced complexes, $M'_n[M(PC)]$, can contain the mono, di, tri or tetra anion ($n=1-4$) with the electrons situated in the lowest π^* orbitals of the PC ring. These catalysts are effective in the hydrogenation of olefins even at ambient temperature and also the hydrogenation of CO (17) and N_2 (18) at more elevated temperatures.

When $[M(PC)]$ are active as hydrogenation catalysts it is assumed that the $[M(PC)]$ activate both the hydrogen and the substrate. Calvin was first to show that solid $[Cu(PC)]$ activated hydrogen gas at 250–350°C. (18) $[Ni(PC)]$ is an effective heterogeneous catalyst in the gas phase reduction of allyl alcohol. In the temperature range 100–160°C n-propanol is formed. At higher temperature there is a dehydrogenation of the alcohol to form propionaldehyde, and a reduction to form propane at 300°C. (16) $[Ni(PC)]$ is also active in the hydrogenation of p-substituted hydrotropic aldehydes, e.g. 2-(p-tolyl)propionaldehyde, in the temperature range 120–300°C. (15) As a side reaction the aldehyde is dehydroformylated to yield styrene which is subsequently hydrogenated to yield ethyl benzene. The mechanism proposed for the hydrogenation involves the axial binding of the substrate to the metal. Hydrogen is activated by binding to the phthalocyanine macrocycle. The site of binding is suggested to be the central nitrogen atoms. Subsequent hydride transfer to the substrate is facilitated stereochemically and electronically by the metal. A more detailed mechanistic description of the hydrogenation activity of $[M(PC)]$ awaits future work.

We report here some results of an exploratory project on the HDN activity of $[M(PC)]$ where M represents a variety of metals. We have chosen first to study the model compound quinoline. The $[M(PC)]$ catalyst were supported on high surface area inorganic oxides to produce heterogenized catalysts. The solid catalysts are convenient to study because of the ease of separation and process adaptability. Further, due to the low solubility of $[M(PC)]$ in almost all solvents, the high surface area supported catalysts are expected to have a considerably higher effective concentration of $[M(PC)]$ than the small portion of $[M(PC)]$ that is in homogeneous solution or the low surface area solid $[M(PC)]$.

Experimental Section

Materials. Metallophthalocyanines were purchased from commercial sources and used without further purification. $[Sn(PC)]$ and $[Sn(PC)Cl_2]$ were prepared by the method of Kroenke and Kenney. (20) Hexadecane (certified) and quinoline were distilled prior to use. Inorganic oxide supports were from commercial sources and have the following properties: Al_2O_3 ,

Alon (nonporous) surface area 100 m²/g; SiO₂, Cab-o-Sil (nonporous) surface area 200 m²/g; SiO₂·Al₂O₃, W. R. Grace grade 160 % Al₂O₃ = 13, surface area 425 m²/g. The oxide was either used directly as supplied or activated by heating in vacuo to 400°C for 4 hours.

Preparation of Supported Catalysts. Catalysts were prepared with different [M(PC)] and oxide supports. The metal content was in the range 0.2-0.4 wt. %. The oxide, 5.00 g, was placed in a 500-ml round bottom flask with 100 ml pyridine. The flask was then fitted with a Soxhlet extraction apparatus which contains 0.125 g of the [M(PC)] in the cup. The extraction was carried out until all of the solid had been dissolved (typically 2-8 days). The pyridine of the resulting slurry of the supported catalyst was removed in vacuo and the solid catalyst dried in vacuo at 110°C for 4 hours. The yield was approximately 5 g. of a solid whose color ranges from green to blue, depending on the metal. To make higher loading level catalysts, a proportionate amount more of [M(PC)] was placed in the extraction thimble. In those cases where the solubility of [M(PC)] is quite limited in pyridine, an alternate procedure was used. For example, with [Sn(PC)], [Mo(PC)], [Ni(PC)], the [M(PC)] was dissolved in 9 M H₂SO₄ and the solution added to the oxide support. After 10 minutes stirring of the slurry, a tenfold volume of distilled water was added and the mixture filtered. The solid was washed with water and methanol and dried in vacuo at 110°C for 4 hours. Metal content of the catalysts was determined by atomic absorption spectroscopy.

Hydrogenation Procedure. Two 300 ml high pressure reactors, one with agitation by stirring (Parr mini-reactor) and one with agitation by rocking (Aminco), were used. Typically, the stainless steel vessel was charged with quinoline, 50 ml hexadecane and the catalyst. The sealed reaction vessel was then purged three times with H₂ and finally pressurized so that the desired pressure was achieved at operating temperature. Reactor heat-up time from room temperature was less than 15 minutes for the Parr reactor and 3 hours for the Aminco, and cool-down time was 4 hours for both reactors. At the end of the run, the pressure was released, the reaction mixture was filtered to recover the catalyst. The filtrate was subjected to G.C. analysis. In general, the conversions quoted are reproducible to ± 2% (absolute).

Results and Discussion

Catalyst Screening. In order to determine the broad pattern of catalytic activity with respect to metal and oxide surface, a series of supported catalysts, prepared in a similar way, were evaluated. For these experiments the catalyst loading level is

approximately 4×10^{-5} mole $[M(PC)]/g$ inorganic oxide. Using a value of 160 \AA^2 for the area of the planar $[M(PC)]$ and assuming that the molecules lay flat on the surface of the oxide, the $[M(PC)]$ covers 19% of the available surface area for the SiO_2 used, 40% of the surface for Al_2O_3 , and 11% of the surface area for $\text{SiO}_2 \cdot \text{Al}_2\text{O}_3$. Therefore, there is appreciable free surface area available for interaction with the reactants and the supported materials can be considered as bifunctional catalysts. If the $[M(PC)]$ molecule lies flat on the surface, one of its axial coordination positions should be involved in the interaction with the surface. Thus one axial metal position is available for binding to the substrates. Since quinoline is a basic molecule with good Lewis base donor abilities and adducts of this type of molecule are known for $[M(PC)]$ (10), it is reasonable to assume that the quinoline is binding to the central metal during the hydrogenation reaction. Whether the hydrogen is binding (and activated) to other sites on the PC or oxide surface or to the metal site in competition with the quinoline is to be determined.

The hydrogenation reactions were run under standard conditions; 24 hours duration, 1000 psi hydrogen pressure and 5.0 g (39 mM) quinoline, hexadecane as a solvent with 1.0 g catalyst. The catalytic runs at 200–300°C were carried out with the Parr reactor. The runs at 290°C–430°C were carried out with the Aminco reactor.

Table I. Hydrogenation of Quinoline to 1,2,3,4-Tetrahydroquinoline with $[M(PC)]$ supported on SiO_2 at several temperatures.

[M(PC)]	% Conversion		
	T=200°C	290°C	385°C
Mg	4		50
Mn			54
Fe	3	7	42
Co	5	7	67
Ni	9	8	90
Cu	4		48
Zn	0	2	59
Mo	5	14	91
Sn	5	10	40
Pb	1	6	40

Table I gives the results from the experiments with $[M(PC)]$ supported on SiO_2 . The conversion of quinoline is almost exclusively to 1,2,3,4-tetrahydroquinoline with only traces of other products (<1%). No propylaniline, propylbenzene, propylcyclohexane, 5,6,7,8-tetrahydroquinoline or decahydroquinoline were noted. No change is noted in the conversions when the SiO_2 is activated in vacuo at 400°C prior to supporting the complex. When the hydrogenations are run at 200°C only low conversions are

obtained. As expected, higher conversions are noted at 385°C which are dependent on the metal: Mo>Ni>Co>Zn>Mn>Mg>Cu>Fe>Sn>Pb. Under the conditions of the experiments the equilibrium conversion can be estimated to be 91%. (9) It is seen that only Mo and Ni have reached equilibrium in 24 hours. Thus, the activity of the two catalysts must be evaluated at shorter time periods in order to distinguish between the two.

Table II. Hydrogenation of Quinoline to 1,2,3,4-Tetrahydroquinoline with [M(PC)] supported on Al₂O₃ and SiO₂·Al₂O₃ at 290°C.

<u>[M(PC)]</u>	<u>Support</u>	<u>% Conversion</u>
Co	Al ₂ O ₃	9
Co	SiO ₂ ·Al ₂ O ₃	8
Fe	Al ₂ O ₃	6
Fe	SiO ₂ ·Al ₂ O ₃	10
Mo	Al ₂ O ₃	10
Mo	SiO ₂ ·Al ₂ O ₃	13
Ni	Al ₂ O ₃	7
Ni	SiO ₂ ·Al ₂ O ₃	10
Sn	Al ₂ O ₃	10
Sn	SiO ₂ ·Al ₂ O ₃	9

Table II gives the results for tests run with a variety of [M(PC)] supported on Al₂O₃ and SiO₂·Al₂O₃ using the Aminco reactor. Again, no significant difference is noted if the supports were activated in vacuo at 400°C or used as received. In general, when the data is compared to that in Table I, the activity is seen to be independent of the support material, being equal for SiO₂, Al₂O₃ and SiO₂, Al₂O₃ within experimental error. In all the hydrogenations using [M(PC)] the use of high temperature, 385°C, or acidic support does not appear to lead to appreciable hydrogenolysis of the product, 1,2,3,4-tetrahydroquinoline. Even at 430°C with Co(PC)/SiO₂ there is 83% conversion to 1,2,3,4-tetrahydroquinoline with little hydrogenolysis noted. The catalyst however, can be recovered and recycled with maintenance of activity at 430°C. This demonstrates the robust nature of the [M(PC)] catalysts.

The catalysts are not sensitive to sulfur-containing heterocycles. Thus, the presence of equimolar amounts of thiophene or thianaphthene does not affect the activity for hydrogenation of quinoline. In fact, the [M(PC)] are poor HDS catalysts showing little or no activity for HDS of thiophene and dibenzothiophene at 385°C and 1000 psi pressure. Some HDS activity is noted with benzothiophene but the conversions are almost an order of magnitude less than for the hydrogenation of quinoline. In general this agrees with the metal binding capabilities of the [M(PC)] since nitrogen donors, like quinoline, are preferred to sulfur donors. (10) The observation that

hydrogenation activity is greater than HDS activity support the idea that the quinoline substrate is binding to the metal via the axial coordination position during the catalytic cycle.

Homogeneous Catalysis. In order to learn if the supported catalysts behave similarly to the homogeneous catalysts, a number of [M(PC)] were evaluated for activity under the standard condition. Forty milligrams of [M(PC)] were used so that the catalyst could be more easily recovered after the run. Table III gives the conversions for the hydrogenation of quinoline in homogeneous solution at 300°C using the Parr mini-reactor. The order of activity for metal is: Sn>Mo>Co>Fe>Ni. Although lower, there is a comparable activity at 290°C when the [M(PC)] are supported on SiO₂. Since the catalyst concentration for the homogeneous solutions are approximately 75% higher (on a [M(PC)] basis) than for the heterogeneous reaction, it would be expected that a higher conversion would result in the former runs. [Sn(PC)Cl₂] is soluble in hot quinoline while [Sn(PC)] is not. Similarly, while [Co(PC)] and [Fe(PC)] are soluble in hot quinoline [Ni(PC)], [Mo(PC)] and Na₄[Co(TSPC)] (tetrasulfo derivative) are less soluble. This raises the question as to whether the catalysts are in homogeneous solution, are partially in solution or are only present as insoluble solids. The answer to this question, of course, will have a bearing on the activity order since the homogeneous catalysts should be more active because of the concentration advantage it has. With a low surface area solid like [M(PC)], 3-4 m²/g (21) there should be a lower effective concentration of catalytic species than for the homogeneous solution. However, this may not be an important factor since the most active materials appear to be among the least soluble.

Table III. Hydrogenation of Quinoline to 1,2,3,4-Tetrahydroquinoline in homogeneous solution at 300°C

<u>Catalyst</u>	<u>Co-Catalyst</u>	<u>% Conversion</u>
[Fe(PC)]		5
[Co(PC)]		16
Na ₄ [Co(TSPC)]		25
[Ni(PC)]		8
[Sn(PC)Cl ₂]		66
[Sn(PC)]		52
[Sn(PC)]	ZnCl ₂	71
[Mo(PC)]		31
[Mo(PC)]		42

The addition of the Lewis Acid (22, 23) ZnCl₂, in the ratio 1:1 with [M(PC)] increases the hydrogenation activity by about 1/3. Addition of more ZnCl₂ in a 2:1 or 4:1 ratio does not, however, increase the conversion further. The presence of the

SO_3^- group in the $\text{Na}_4[\text{Co}(\text{TSPC})]$ also enhances the conversion and in this case there is also an enhanced production of low boiling products (approximately 2%). The mild hydrogenolysis activity of the $[\text{Co}(\text{TSPC})]^{4-}$ may be due to the presence of the basic SO_3^- group which could catalyze the rupture of N containing ring via a Hoffman type degradation of the coordinated tetrahydroquinoline. (24) On the other hand, while ZnCl_2 did enhance the hydrogenation activity, by some as yet undescribed interaction with the substrate or $[\text{M}(\text{PC})]$, an expected increase in hydrogenolysis activity was not noted.

The I.R. spectra of the recovered catalysts indicated that the $[\text{M}(\text{PC})]$ were not altered. An exception to this was observed with the Sn(II) and Sn(IV) catalysts where the $[\text{M}(\text{PC})]$ could not be recovered. In fact the $[\text{Sn}(\text{PC})]$ appeared to be irreversibly converted to a colorless material, presumably via hydrogenation of the PC aromatic ring system. It is interesting to note that for $[\text{Sn}(\text{PC})]$ the activity of the homogeneous catalyst is some five-fold higher than for the supported catalyst. In general, for the other $[\text{M}(\text{PC})]$ the increase is two-fold or less as expected. The enhancement of the activity for the homogeneous $[\text{Sn}(\text{PC})]$ may be related to the irreversible destruction under reaction conditions.

Supported Cobalt Catalysts. Experiments were conducted with $[\text{Co}(\text{PC})]/\text{SiO}_2$ at 340°C to determine the important variables for the catalysis of a typical $[\text{M}(\text{PC})]$. Table IV gives the results for runs which were conducted for varying periods of time. It is seen that even at 100 hr. the conversion only reached 36%. The equilibrium conversion at 342°C can be estimated to be 97%. (9) Thus, the reaction is quite far from equilibrium even at long times. This may be taken as evidence for product inhibition of the catalysis. This might be expected since tetrahydroquinoline is a stronger Lewis base than quinoline. Thus, the product could bind to the metal center and prevent activation of the substrate and/or hydrogen. One important conclusion is that the reaction is not over in 24 hours and it can be assumed that the difference in conversions noted in Table I with different $[\text{M}(\text{PC})]$ are due to differences in inherent activity of the $[\text{M}(\text{PC})]$.

Table IV. Hydrogenation of Quinoline to 1,2,3,4-Tetrahydroquinoline with $[\text{Co}(\text{PC})]/\text{SiO}_2$ (%Co=0.79) at 340°C .

<u>Duration of Run</u>	<u>% Conversion</u>
12 hrs.	5
24 hrs.	16
36 hrs.	22
48 hrs.	29
64 hrs.	28
100 hrs.	36

The dependence of conversion on hydrogen pressure is shown in Table V. It is seen that the conversion is directly proportioned to the H₂ pressure and that the reaction is first order in H₂. On the other hand, Table VI shows the effect of increasing the concentration of the substrate on the extent of conversion. Increasing the quinoline concentration decreases the conversion. This observation is consistent with the postulate that quinoline and hydrogen are competing for the same site on the catalyst and that at high quinoline concentrations hydrogen activation is inhibited with a resultant lowering of the conversion. Since the quinoline, by nature of its Lewis base properties, is very likely binding to the metal atom, the inhibition implies that the hydrogen is also binding to the same site.

Table V. Hydrogenation of Quinoline to 1,2,3,4-Tetrahydroquinoline with [Co(PC)]/SiO₂ (%Co=0.16) at Several Pressures and 340°C.

<u>p(psi H₂)</u>	<u>% Conversion</u>
1000	10
1700	17
2300	24
2800	28

Table VI. Hydrogenation of Various Amounts of Quinoline with [Co(PC)]/SiO₂ at 340°C

<u>g., Quinoline</u>	<u>% Conversion</u>
1.0 ^a	65
2.0 ^b	66
3.0 ^a	51
5.0 ^a	15
5.0 ^b	17
6.0 ^b	13
8.0 ^b	11
10.0 ^b	13

^a 1 g. catalyst, %Co = 0.40

^b 1 g. catalyst, %Co = 0.79

Supported catalysts were prepared with different loading levels by impregnation of SiO₂ with pyridine solutions of the appropriate amount of [Co(PC)]. Catalysts with wt.% Co in the range 0.16 to 2.52% were obtained. Table VII gives the conversions at various loading levels. The conversion increases with loading level up to approximately 1 wt.% Co. Beyond this there is no increase in conversion with increasing Cobalt content. If it is assumed that the planar [Co(PC)] molecules pack like discs on the surface of the SiO₂ then the catalyst will have a

monolayer of [Co(PC)] at approximately 1% Co. Above this level the [Co(PC)] added will form a second layer on top of the first. The maximum number of cobalt centers is achieved at monolayer coverage and the number of centers remains at this level even with increasing Cobalt content. The observation that the highest conversion first occurs at complete monolayer coverage supports the idea that the [Co(PC)] are adsorbed on the SiO₂ surface as individual planar molecules and not crystallites.

Table VII. Hydrogenation of Quinoline to 1,2,3,4-Tetrahydroquinoline with [Co(PC)]/SiO₂ of Various Loading Levels at 340°C.

<u>Wt. % Co</u>	<u>% Conversion</u>
0.16	10
0.40	14
0.67	18
0.79	21
1.08	25
2.52	25
0.35 ^a	17



The extent of conversion is, as expected, dependent on the catalyst concentration. For example with % Co = 0.79% increasing the amount of catalyst from 0.5 g to 1.0 g increases the conversion from 10 to 21%. Finally on the basis of Cobalt content the catalyst Na₄[Co(TSPC)]/SiO₂ shows a slightly greater activity than [Co(PC)]. This effect was also noted for the homogeneous catalysts.

Catalytic Activity. It is perhaps surprising that the differences in activity for a wide range of [M(PC)] studied here are so small (approximately two-fold difference). It must be assumed that the catalytic activity is much more dependent on the phthalocyanine macrocycle than on the particular metal present.

The order of hydrogenation activity with [M(PC)] may be related to the relative strength of axial binding of quinoline and hydrogen. For those metals that show strong axial binding to the Lewis base, activation of hydrogen is inhibited and the catalytic activity reduced. Unfortunately, no equilibrium binding data is available for all the metals examined. Another consideration is the extent of binding of H₂ which should also be metal dependent. Again, no equilibrium data is available. A third consideration is the ability of the [M(PC)] to activate the H₂ molecule once it is bound. The most reasonable mode of activation would be a partial electron transfer from the [M(PC)] to the H₂, [M(PC)]^{δ+} ···H₂^{δ-}. The increased hydridic character of the hydrogen should give rise to enhanced activity. The

transferred electron density could come from either the metal centered orbitals or the highest filled PC π orbital or both. Thus, the activation of hydrogen should be related to the ease of oxidation of the catalyst, assuming that both metal and PC centers are equally effective in H₂ activation. The order of ease of oxidation for [M(PC)] is: Mn>Co>Fe>Mg>Zn>Cu>Ni. (10) There is little similarity of this order to that of the catalytic activity. It is obvious that much more work must be done to understand the catalytic activity of [M(PC)].

Conclusion

The [M(PC)] catalyst are active in the hydrogenation of quinoline to 1,2,3,4-tetrahydroquinoline in the temperature range 300-400°C and 1000-3000 psi H₂ pressure. The reaction is quite selective, with little or no hydrogenolysis of the first product noted. Thus, [M(PC)] of themselves are not HDN catalysts. They, however, may still prove useful in coal liquid upgrading since the selective hydrogenation of heteroaromatic substrates will enhance their basicity with a minimum hydrogen consumption. The increased basicity of the nitrogen-containing molecules can be exploited by utilizing simple adsorption or extraction procedures to remove them from coal liquids. This procedure might prove to be an attractive alternative to removal by HDN.

Acknowledgements

The authors wish to express their thanks to the Institute for Mining and Minerals Research for financial support of this research. Special thanks for technical assistance is given to: Laura Cannon, Eric Dadey, and Bobby Cobb.

Literature Cited

1. Cusumano, J. A.; Dalla Betta, R. A.; Levy, R. B. "Catalysis in Coal Conversion"; Academic Press: N.Y., 1978; pp. 155-220.
2. Weisser, O; Landa, S. "Sulphide Catalysts; their Properties and Applications"; Pergamon Press: Oxford, N.Y.; 1973.
3. Houalla, M; Broderick, D. H.; Sapre, A. V.; Nag, N. K.; DeBeer, V.H.J.; Gates, B. C.; Kwart, H. J. Catal. 1980, 61, 523.
4. Givens, E. N.; Venuto, P. B. Am. Chem. Soc. Preprints Div.; Petrol. Chem. 1970, 15, (4), A183.
5. Stern, E. W. J. Catal. 1979, 57, 390.
6. Rollmann, L. D. J. Catal. 1977, 46, 243.
7. Flinn, R. A.; Larson, O. A.; Beuther, H. Hydrocarbon Process. Pet. Refiner 1963, 42, 129.
8. Satterfield, C. N.; Modell, M.; Hites, R. A.; Declerck, C. J. Ind. Eng. Chem. 1978, 17, 141.

9. Shih, S. S.; Katzer, J. R.; Kwart, H.; Stiles, A. B. Am. Chem. Soc., Petroleum Preprints 1977, 22, 919.
10. Boucher, L. J. "Metal Complexes of Phthalocyanines"; in Coordination Chemistry of Macrocyclic Compounds; G. A. Melson, Ed; Plenum Press: N.Y., 1979; p. 499.
11. Stolfa, F. Catalytic Hydrogenation of Black Oils, U.S. Patent, U.S. 3,502,571; 1970.
12. Bearden, R.; Aldridge, C. L. Hydroconversion Process, U.S. Patent, U.S. 4,067,799; 1978.
13. Mochida, I.; Takeyoshi, K.; Fujitsu, H. Takeshita, K. Chemistry Letters 1976, 327; J. Mol. Catal. 1977/78, 3, 417.
14. Steinbach, F; Joswig, H-J. J. Catal. 1978, 55, 272.
15. Kropf, H; Witt, D. J. Z. Phys. Chemie. N.F. 1971, 76, 331.
16. Kropf, H; Muller, D. J. Liebigs. Ann. Chem. 1976, 1236.
17. Ichikawa, M.; Sudo, M.; Soma, M.; Onishi, T.; Tamaru, K. J. Amer. Chem. Soc. 1969, 91, 1538.
18. Sudo, M; Ichikawa, M; Soma, M.; Onishi, T.; Tamaru, K. J. Phys. Chem. 1968, 72, 1174.
19. Calvin, M.; Cockbain, E. G.; Polanyi, M. Trans. Far. Soc. 1936, 32, 1436.
20. Kroenke, W. J.; Kenney, M. E. Inorg. Chem. 1964, 3, 251.
21. Ichikawa, M.; Soma, M.; Onishi, T.; Tamaru, K. Trans. Faraday Soc. 1967, 64, 1215.
22. Mobley, D. P.; Bell, A. T. Fuel 1980, 59, 507.
23. Taylor, N. D.; Bell, A. T. Fuel 1980, 59, 499.
24. Nelson, N.; Levy, R. B. J. Catal. 1979, 58, 485.

RECEIVED March 9, 1981.

Research in the Electrochemistry of Coal-Derived Liquids

JAMES B. PIERCE¹

Department of Energy, Pittsburgh Energy Technology Center,
Box 10940, Pittsburgh, PA 15236

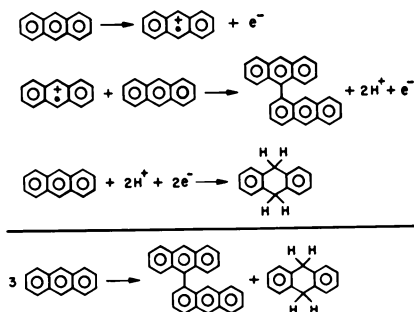
This preliminary investigation into the feasibility of using electrochemical techniques to characterize coal-derived liquids revealed that solutions of these complex materials exhibit relatively simple voltammograms, having characteristic, reproducible features. The results broach the possibility of using electrochemical measurements to study the organic redox reactions that occur during coal conversion processes. The literature of organic electrochemistry supports this by repeatedly describing electrode reactions that in all apparent respects are identical to redox reactions that occur in bulk organic systems (1-4). Among compounds related to coal chemistry polycyclic aromatic structures are quite sensitive to the application of electrical stimuli. Many studies relate half-wave potentials, $E_{1/2}$, to such properties as charge transfer absorption frequencies (5,6), molecular orbital energies (7,8,9,11), molecular ionization potentials (13), spectral quantities (10), and Hammett linear free energy relationships (12,13). All of these properties depend upon the energies of pi molecular orbitals at their valance boundaries.

Electrons transfer at electrodes on the basis of one electron per functional site for each reaction step, i.e. each electron-transfer step is an elementary reaction. From a kinetic view this is a powerful advantage.

Coal and many coal-derived liquids contain polycyclic aromatic structures, whose molecular equivalents form radical cations at anodes and radical anions at cathodes. ESR-electrolysis experiments support this (14). Chemically, radical cations form by action of H_2SO_4 (15,19), acidic media containing oxidizing agents (15,20,21,22), Lewis acid media (18,23-35) halogens (36), iodine and $AgClO_4$ (37,38), and metal salts (39,40). They also form by photoionization (41,42,43) and on such solid catalytic surfaces as gamma-alumina (44), silica-alumina (45), and zeolites (46). Radical anions form in the presence of active metals (76).

¹ Current address: Department of Chemistry, University of Lowell, Lowell, MA 01854.

In molten SbCl_3 anthracene forms radical cations which cause oxidative coupling and furnish protons and electrons to form 9,10-dihydroanthracene. The reaction is shown.



All electron and proton transfer occurs internally (34,35).

Electron transfer in organic redox systems is well documented (1-4); and although proton transfer among polycyclic aromatic structures may seem to be improbable, there is evidence that proton transfers become quite labile when such structures are excited above their ground states. This is illustrated by the behaviors of fluorene, $\text{C}_{13}\text{H}_{10}$, and protonated naphthalene, for which data is available. Fluorene, in its ground state has $\text{pK}_a=20.5$, but in its first excited singlet state $\text{pK}_a=-8.5$, i.e. $\Delta \text{pK}_a=-29.0$ (33,36,49). Thus activation enhances proton release. In the ground state protonated naphthalene has $\text{pK}_a=-4.0$, but in the first excited singlet state $\text{pK}_a=11.0$. In this case proton acceptance is enhanced (33,36,49).

To a limited extent electrochemical methods have been used to study coal extracts and coal-derived materials. Two examples are cited (50,51).

Experimental

In all experiments the electrolyte was the highest quality tetra-n-butyl ammonium tetrafluoroborate furnished by Eastman and J.T. Baker, the working electrode was glassy carbon (area = 0.31 cm^2) polished before each scan, except in film formation studies. The reference electrode was saturated calomel, and the auxillary electrode was platinum wire. Electrodes and cells were purchased from Princeton Applied Research (PAR). The instrument was a PAR Model 170 Electrochemistry System, Serial No. 6109.

Solvents used were acetonitrile (AN) and tetrahydrofuran (THF). AN was spectroquality from Matheson, Coleman, and Bell; THF, furnished by Fisher Scientific Co., was used in two grades, (a) Fisher Certified containing butylated hydroxytoluene as inhibitor and (b) HPLC grade with no inhibitor. No difference in voltammograms was observed as a result of changing the grade of

THF. Solvents, electrolyte, and coal liquids were used as received.

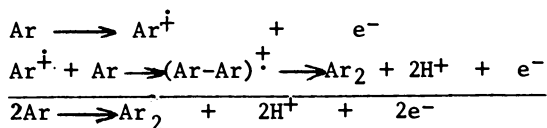
Discussion

The voltammogram of "Panasol oil", comprised chiefly of mixed methylnaphthalenes (solid line, Figure 1), shows two significant reduction peaks but no important oxidation features. However, hydrogenated "panasol oil" (dashed line, Figure 1) oxidized with a sharp peak at -1.9 volts. Such behavior indicates that electrochemical oxidation may be useful in evaluating chemical reducing properties of some coal liquids.

In Figure 2 a relatively low boiling fraction of coal-derived liquids shows a strong oxidation between +2 and +3 volts. Solvent-electrolyte background is cross-hatched. SRC II fuel oil A has similar properties (Figure 3).

At anodic potentials Anthracene oil, i.e. cresote, formed insoluble, insulating films on current-carrying electrodes (Figure 4). Figure 4a. shows oxidation traces from three successive cyclicvoltammograms with switching potential, $\lambda = +2.000$ volts. When $\lambda = +1.000$ volt (Figure 4b), the effect diminished; and at $\lambda = -0.700$ volt no electrode film formed, and the steady state traces coincided with the initial trace (Figure 4c).

Film formation at anodic potentials probably proceeds by oxidative coupling through radical cation intermediates, e.g.



Oxidative coupling has been observed for benzene (52), methyl substituted benzenes (53), triphenylethylene (54), triphenylamines (55-59), anilines (57), carbazoles (60,61), iminobibenzyls (62), and heterocyclic phenols (71,72). Intramolecular anodic coupling reactions are used for synthesizing specific ring structures (63-68). Both dimer and octamer of dibenzothiophene have been detected (69,70)

Oxidative coupling of component structures in coal-derived liquids may be assumed to increase the π -electron conjugation and lower the molecular ionization potential. Hence, a progressive increase in molecular weight increases the ease of formation of radical cations and favors oxidative coupling of the larger molecular species. This causes an exponential increase in molecular weight with time and is suggested as the mechanism by which char and coke form in coal-conversion processes.

Product oils from direct liquefaction of Blacksville Number 2 coal in the 1000 pound per day pilot plant at Pittsburgh Energy Technology Center (PETC) were examined by cyclicvoltammetry.

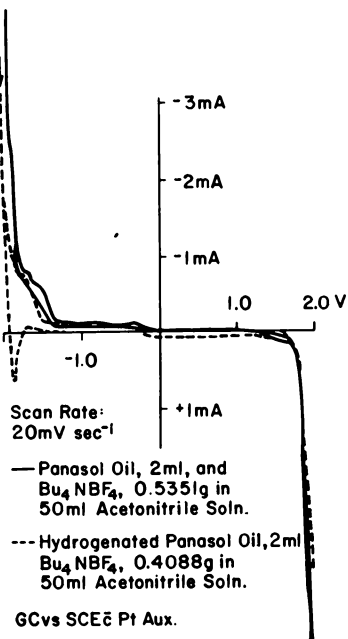


Figure 1. Cyclicvoltammograms of Panasol oil and hydrogenated Panasol oil

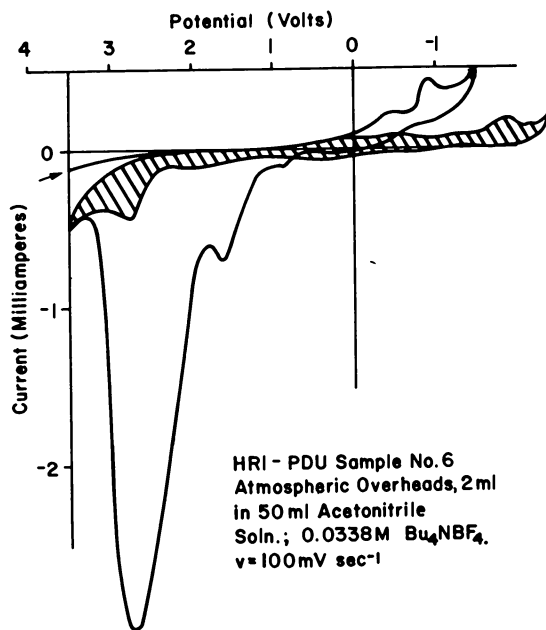


Figure 2. Cyclicvoltammogram of atmospheric overhead distillate

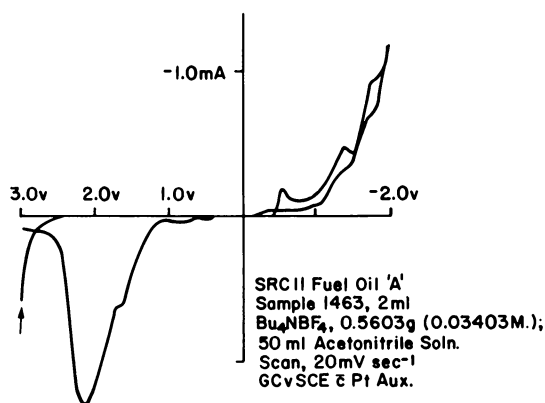


Figure 3. Cyclicvoltammogram of SRC-II fuel oil A

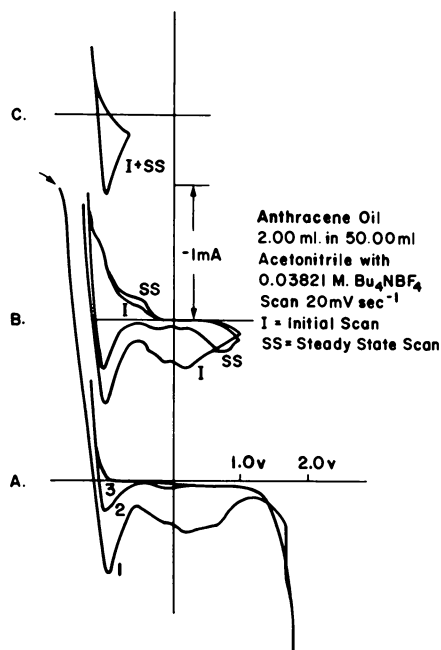


Figure 4. Effect of electrode film formation on the voltammetric traces

Tetrahydrofuran (THF), which dissolved or peptized approximately 90% of the centrifuged product oil was used as solvent. A typical voltammogram with background is shown in Figure 5.

Reduction peak currents, i_p , depend strongly upon the initial anodic potential, E_i , and the time increment between imposing the potential and starting the scan. Again, anodic potentials cause electrode film formation. The concentrations of oxidized species that built up at the anode during a series of delay times are reflected in the reduction peaks shown in Figure 6. For all subsequent measurements a standard delay time of 60 seconds was used.

The variation of peak current with concentration is linear (Figure 7). Thus, peak currents may be used to estimate concentrations of product oil.

A plot of peak potential, E_p , versus \log (scan rate), i.e. $\log v$, exhibits zero slope for reversible processes, i.e. k/v is large, and positive slope for irreversible processes, i.e. k/v is small. (k =kinetic rate constant).

Such a plot is shown (Figure 8) and displays both reversible and irreversible behavior. The critical scan rate is $v_c = 10.5$ millivolts sec^{-1} . At v_c equations for both reversible and irreversible behavior apply.

In Figure 8 the positive slope is approximately ten times steeper than a normal irreversible system should exhibit. This excessive effect is probably caused by capacitance and resistance effects. Excessive capacitance currents (Figure 9) are indicated by linear variations of E_p vs v when IR compensation was not used and E_p vs $v^{1/2}$ when IR compensation was used.

In Figure 8 the positive slope for irreversible behavior should be given by:

$$dE/d \log v = b/2$$

$$\text{Where } b = 2.3 |E_p - E_{p/2}| / 1.857.$$

This more representative slope is shown as the dashed line (Figure 8). The half-wave potential for the second reduction peak (Figure 8) is $E_{1/2} = 0.59$ volt, calculated from:

$$E_{1/2} = E_p + 1.1 RT/nF.$$

While this value may be approximate, it positions in the expected region on the potential axis. Also, irreversible reactions give $E_{1/2}$ values moderately close to those for reversible reactions (74, 75).

By equating the peak current equations for reversible and irreversible behavior at v_c the stoichiometric electron number may be found from peak potential characteristics. Thus, at 298°K:

$$n_{app} = 0.0584 / |E_p - E_{p/2}| .$$

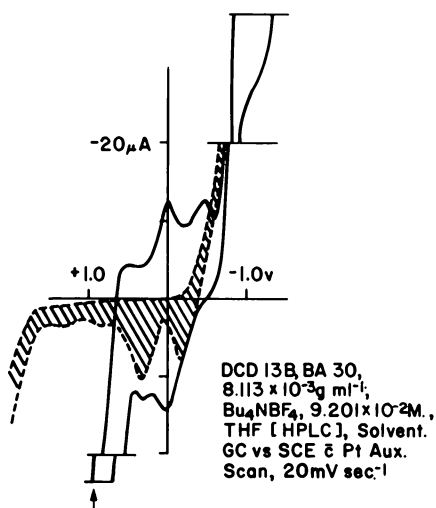


Figure 5. Typical voltammogram of product oil from the 1000-lb/d pilot plant at PETC

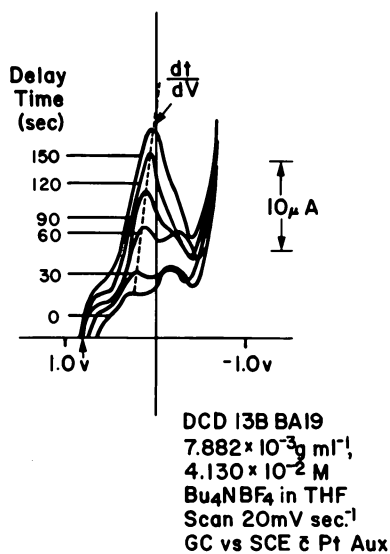


Figure 6. Effect of initial delay time on peak height and form

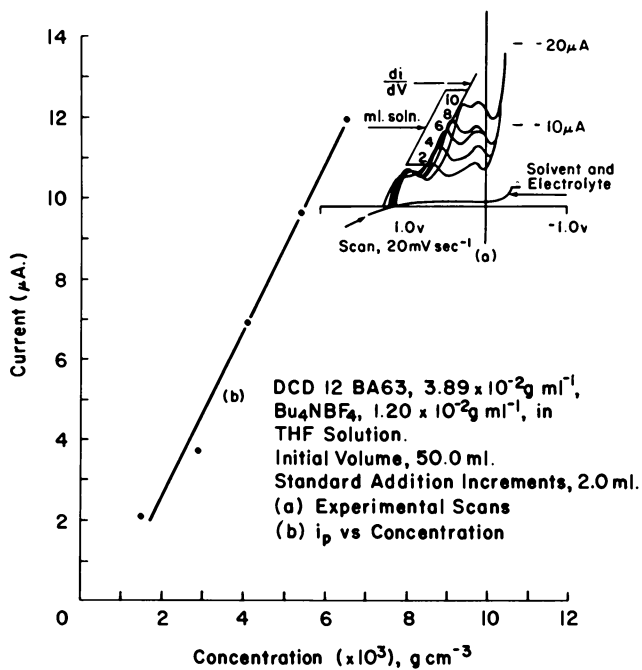


Figure 7. Variation of peak current with concentration

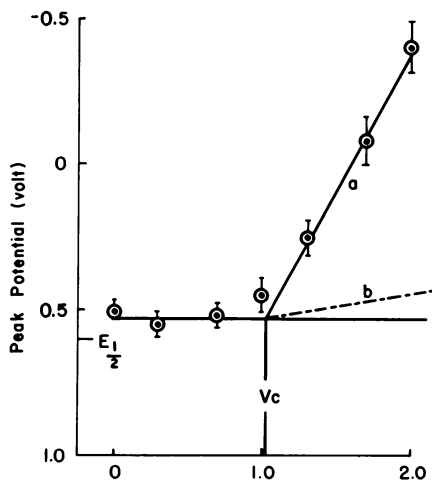


Figure 8. Irreversible and reversible behavior of product oil DCD 13 B: (a) experimental; (b) calculated from $|E_p - E_{p/2}|$.

For the second reduction peak in Figure 5, $n_{app}=0.5$. Competing reactions are indicated by a fractional value of n_{app} .

Figure 6 shows that the amount of reduction taking place depends upon the amount of oxidation that occurred initially at $E_1 = 1.000$ volt. To help evaluate electron transfer, double potential step chronoamperometry was employed (Figure 10). In each instance the potential was stepped from E_1 to $E_2 = +1.000$ volt at the instant the cell was engaged. Initial oxidation proceeded for 25 seconds after which the potential stepped back to the starting potential E_1 . In the short time of the experiment it was assumed that diffusion effects were minimal and the reduction at E_1 acted on the oxidized product formed at E_2 until it was consumed.

The working equation is:

$$it^{1/2} = nFA(D^{1/2}/M)(m/V) \pi^{-1/2},$$

Thus, at constant concentration $(it^{1/2})$ is constant. If $(it^{1/2})_c$ represents the cathodic process at E_1 and $(it^{1/2})_a$ the anodic process at $E_2 = +1.000$ volt, then the ratio,

$$(it^{1/2})_c / (it^{1/2})_a = n_c / n_a = n_R$$

represents cathodic charge consumed relative to anodic charge generated. Values of n_R for the second reduction peak are listed in Table I and illustrated in Figure 11.

Table I

$(E_p)_c$ (volt)	0.700	0.600	0.500	0.400	0.300	0.000	-0.300
n_R	0.44	0.51	0.61	0.62	0.71	1.1	1.6

The oxidation linear sweep (Figure 5) has one major, broad peak which depends on the switching potential λ . If $\lambda = -1.0$ volt, the peak is large; if $\lambda = -0.3$, it is absent. Thus, the structures oxidized to form that peak are generated at rather cathodic potentials.

Exhaustive constant potential electrolysis of product oil solutions at mercury pool electrodes produced large background currents caused by interaction between Hg and the solvent-electrolyte system. The data are misleading.

Oxidation at $E_2 = +1.000$ volt yields the product, $(it^{1/2})_a = 30 \times 10^{-6}$ amp sec^{1/2}, from which the value $D^{1/2}/M = 2.1 \times 10^{-7}$ (cm mole)/(gram sec^{1/2}), may be calculated. Neither the apparent molecular weight M nor the diffusion coefficient D are known, but D will have an approximate maximum value of 10^{-5} cm²/sec and an estimated minimum value of 10^{-8} cm²/sec.

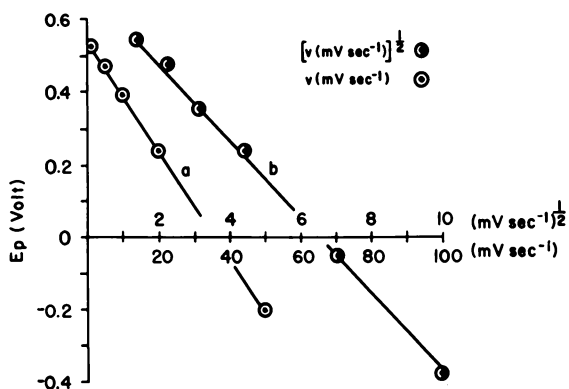


Figure 9. Effect of capacitance current: (a) DCD 13 B, IR compensation off; (b) DCD 12, IR compensation used.

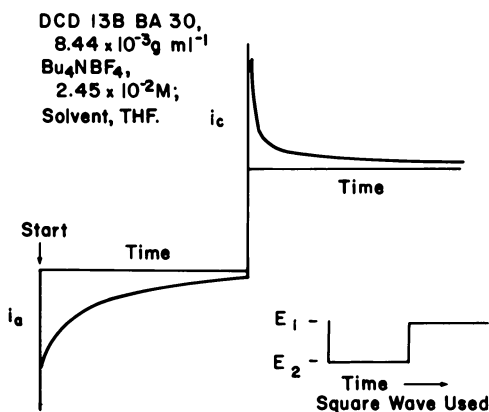


Figure 10. Double-potential-step-chronoamperometry

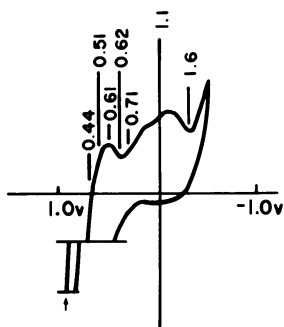


Figure 11. The n_R related to voltammogram

If $(E_p - E_{1/2})$ is eliminated between the equations expressing peak potentials for reversible and irreversible processes (73), one finds:

$$k_s/M = 5.6 \times 10^{-6} \text{ (cm mole/g sec).}$$

Again neither the electrochemical rate constant k_s nor M are known. However, a range of related values is presented in Table II.

Table II
Variations of D , M , and k_s

$D(\text{cm}^2/\text{sec})$	$M(\text{g/mole})$	$k_s(\text{cm/sec})$
1.0×10^{-5}	1.5×10^4	8.4×10^{-2}
5.0×10^{-7}	3.0×10^3	1.7×10^{-2}
1.0×10^{-8}	5.0×10^2	2.8×10^{-3}
<u>x (High)</u>		
<u>x (Low)</u>		
1.0×10^3	30	30

For a range of diffusion coefficients Table II shows values that may be expected for heterogeneous standard rate constants and apparent molecular weights. These numbers are presented as an illustration of their relative magnitudes and the manner in which they interrelate. It must be observed that the apparent molecular weight is a reaction parameter and does not, necessarily, express the molecular size.

Summary

A number of coal-derived liquids were examined by cyclic-voltammetry and other electrochemical techniques and found to show some activity. At anodic potentials films form on glassy carbon electrodes. It is suggested that this film formation is caused by oxidative coupling of radical cationic species with neutral ring structures through a mechanism similar to that which causes charring and coking in coal conversion processes.

Electrochemical measurements can characterize reactivity of coal-derived liquids.

Acknowledgements

This work was supported by the Department of Energy at Pittsburgh Energy Technology Center, Oak Ridge Associated Universities, and the University of Lowell, during a year of Sabbatical leave from the latter university. A special note of

gratitude is extended to the many people at Pittsburgh Energy Technology Center who helped to enrich this experience, and to Dr. William L. Bowden, Duracel International Corp., for many helpful suggestions.

Literature Cited

1. Bard, A.J., Ledwith, A., and Shine, H.J., "Advances in Physical Organic Chemistry", Vol. 13, Ed. by V. Gold and D. Bethell, Academic Press, 1976, pp. 156-278.
2. Allen, M.J., "Organic Electrode Processes", Chapman & Hall, Ltd., London, 1958.
3. Fry, A.J., "Synthetic Organic Electrochemistry", Harper & Row, New York, 1972.
4. Ebersson, L., and Nyberg, K., "Advances in Physical Organic Chemistry", Vol. 12, Academic Press, Ed. by V. Gold and D. Bethell, New York, 1976.
5. Bergman, I., Trans. Faraday Soc. 1954, 50, 829.
6. Peover, M.E., Electrochimica Acta, 1968, 13, 1083.
7. Pointeau, R., Ann. Chim. 1962 7, 69.
8. Koutecky, J., Zeit. Physik. Chem. (Neue Folge 1967 52, 8.
9. Gleicher, G.J., and Gleicher, M.K., J. Phys. Chem. 1967 71.
10. Vlcek, A.A., Electrochimica Acta, 1968 13, 1063.
11. Koutecky, J., Electrochimica Acta, 1968 13, 1079.
12. Brodsky, A.E., Gordienko, L.L., and Degtiarev, L.S., Electrochimica Acta 1968 13, 1095.
13. Miller, L.L., Nordblom, G.D., and Mayeda, E.A., J. Org. Chem. 1972 37, 916.
14. Sprecher, R.F., and Pierce, J.B., Unpublished work.
15. Hoijsink, G.J., and Weijland, W.P., Rec. Trav. Chim, 1957 76, 836.
16. Kon, H., and Glois, M.S., J. Chem. Phys. 1958 28, 743.
17. Aalbersberg, W.I., Hoijsink, G.J. Mackor, E.L., Weijland, W.P. J. Chem. Soc. 1959, 3049.
18. Weissman, S.I., de Boer, E., and Conradi, J.J., J. Chem. Phys. 1957 26, 963.
19. Carrington, A., Dravnieks, F., and Symons, M.C.R., J. Chem. Soc. 1961, 905.
20. MacLean, C., and Van der Waals, J.H., J. Chem. Phys. 1957 27, 287.
21. Aalbersberg, W.I., Gaaf, J., and Mackor, E.L. J. Chem. Soc. 1961, 905
22. Dallinga, G., Mackor, E.L., and Verrijn Stuart, A.A., Mol. Phys., 1958 1, 123.
23. Lewis, I.C., and Singer, L.S., J. Chem. Phys., 1965 43, 2712.
24. Lewis, I.C., and Singer, L.S., J. Chem. Phys., 1966 44, 2082.
25. Forbes, W.F. and Sullivan, P.D., J. Am. Chem. Soc., 1966 88, 2862.
26. Shine, H.J., and Sullivan, P.D., J. Phys. Chem., 1968 72, 1390.

27. Sullivan, P.D., *J. Am. Chem. Soc.*, 1968 90, 3628.
28. Buck, H.M., Bloemhoff, W., and Oosterhoff, L.J., *Tetrahedron Lett.* 1960, 5.
29. Rooney, J.J., and Pink, R.C., *Proc. Chem. Soc.*, 1961, 142.
30. Sato, H., and Aoyama, Y., *Bull. Chem. Soc. Japan*, 1973, 46, 631.
31. Forbes, W.F., and Sullivan, P.D., *J. Am. Chem. Soc.*, 1966 88, 2862.
32. Bell, F.A., Ledwith, A., and Sherrington, D.C., *J. Chem. Soc. (B)*, 1969, 2719.
33. Aalbersberg, W.I., Hoijtink, G.J. Mackor, E.L., Weijland, W.P., *J. Chem. Soc.* 1959, 3055.
34. Dworkin, A.S., Poutsma, M.L., Brynstad, J. Brown, L.L., Gilpatrick, L.O., and Smith, G.P., *J. Am. Chem. Soc.* 1979, 101, 5299.
35. Buchanan, III, A.C., Dworkin, A.S., Brynstad, J., Gilpatrick, L.O., and Smith, G.P., *J. Am. Chem. Soc.*, 1979 101, 5430.
36. Fitzgerald, Jr., E.A., Wuefling, Jr., P., and Richtol, H.H., *J. Phys. Chem.*, 1971 75, 2737.
37. Sata, Y., Kinoshita, M., Sano, M., and Akamatu, H., *Bull. Chem. Soc. Japan* 42, 1969 548, 3051.
38. Ristagno, C.V., and Shine, H.J., *J. Org. Chem.* 1971, 36, 4050.
39. Heiba, E.I., Dessau, R.M., and Koehl, Jr., W.J., *J. Am. Chem. Soc.* 1969, 91, 6830.
40. Dessau, R.M., Shih, S., and Heiba, E.I., *J. Am. Chem. Soc.* 1970, 92, 412.
41. Lewis, G.N., and Lipkin, D., *J. Am. Chem. Soc.* 1942, 64, 2801.
42. Lewis, G.N., and Bigeleisen, J., *J. Am. Chem. Soc.* 1943, 65, 2419.
43. Land, E.J., and Porter, G., *Trans. Faraday Soc.* 1963, 59, 2016, 2027.
44. Flockhart, B.D., Scott, J.A.N., and Pink, R.C., *Trans. Faraday Soc.* 1966, 62, 730.
45. Rooney, J.J., and Pink, R.C., *Trans. Faraday Soc.* 1962, 58, 1632.
46. Kurita, Y., Sonoda, T., and Sata, M., *J. Catalysis* 1970, 19, 82.
47. Vander Donckt, E., Nasielski, J., and Thiry, P., *Chem. Comm.* 1969, 1249.
48. Vander Donckt, E., Lietaer, D., and Nasielski, J. *Bull. Soc. Chim. Belges* 1970, 79, 283.
49. Ireland, J.F., and Wyatt, P.A.H., "Advances in Physical Organic Chemistry", Vol. 12, Ed., by V. Gold and D. Bethell, Academic Press, 1976, pp. 131, 221.
50. Given, P.H., and Peover, M.E., *J. Chem. Soc.* 1960, 394.
51. Darlage, L.J., Finkbone, H.N., King, S.J., Ghosal, J., Bailey M.E., *FUEL*, 1978, 57, 479.
52. Osa, T., Uildiz, A., Kuwana, T., *J. Am. Chem. Soc.* 1969, 91, 3994.
53. Nyberg, K., *Acta Chemica Scandinavica*, 1970, 24, 1609.

54. Stuart, J.D., and Ohnesorge, W.E., *J. Am. Chem. Soc.* 1971, 93, 1971.
55. Nelson, R.F., Fritsch, J.M., Marcoux, L.S., and Adams, R.N., *J. Am. Chem. Soc.* 1966, 88, 3498.
56. Nelson, R.F., Adams, R.N., *J. Am. Chem. Soc.* 1968, 90, 3925.
57. Bacon, J., and Adams, R.N., *J. Am. Chem. Soc.* 1968, 90, 6596.
58. Nelson, R.F., and Feldberg, S.W., *J. Phys. Chem.* 1969, 73, 2623.
59. Marcoux, L.S., Adams, R.N., and Feldberg, S.W., *J. Phys. Chem.* 1969, 73, 2611.
60. Ambrose, J.F., and Nelson, R.F., *J. Electrochem. Soc.* 1968, 115, 1159.
61. Ambrose, J.F., Carpenter, L.L., and Nelson, R.F., *J. Electrochem. Soc.* 1975, 122, 876.
62. Frank, S.N., Bard, A.J., Ledwith, A., *J. Electrochem. Soc.* 1975, 122, 898.
63. Falck, J.R., Miller, L.L., and Stermitz, F.R., *J. Am. Chem. Soc.* 1974, 96, 2981.
64. Ronlan, A., Hammerich, O., and Parker, V.D., *J. Am. Chem. Soc.* 1973, 95, 7132.
65. Ronlan, A., and Parker, V.D., *J. Org. Chem.* 1974, 39, 1014.
66. Parker, V.D., and Ronlan, A., *J. Am. Chem. Soc.* 1975, 97, 4714.
67. Bechgaard, K., and Parker, V.D., *J. Am. Chem. Soc.* 1972, 94, 4749.
68. Miller, L.L., Stermitz, F.R., and Falck, J.R., *J. Am. Chem. Soc.* 1973, 95, 2651.
69. Bontempelli, G., Magno, F., Mazzocchin, G.A., and Zecchin, S., *J. Electroanalyt. Chem. Interfacial Electrochem.* 1973, 43, 377.
70. Jordan, J., and Robat, A., Private Communication.
71. Bobbitt, J.M., Yagi, H., Shibuya, S., and Stock, J.T., *J. Org. Chem.* 1971, 36, 3006.
72. Bobbitt, J.M., Weisgraber, K.H., Steinfeld, A.S., and Weiss, S.G., *J. Org. Chem.* 1970, 35, 2884.
73. Gileadi, E., Kirowa-Eisner, E., and Penciner, J., "Interfacial Electrochemistry", Addison-Wesley Pub. Co., Reading, MA, 1975, p. 374.
74. Adams, R.N., "Electrochemistry at Solid Electrodes", Marcel Dekker, Inc., New York, 1969, p. 327.
75. Delahay, P., "New Instrumental Methods in Electrochemistry", Interscience, New York, 1954, p. 128.
76. Reggel, L., Friedel, R.A., and Wender, I., *J. Org. Chem. Soc.* 1957, 22, 891.

Legend of Symbols

$E_{1/2}$	Half-wave potentials
E_p	Peak potentials
$E_{p/2}$	Half-peak potentials

E_i	Initial potential in voltammetry
λ	Switching potential in voltammetry
E_1	Reduction potential in chronoamperometry
E_2	Oxidation potential in chronoamperometry
v	Scan rate
v_c	Critical scan rate
k	Reaction rate constant
k_s	Standard electrochemical reaction rate constant (cm sec^{-1})
b	Tafel slope
R	Gas constant
T	Temperature, $^{\circ}\text{K}$
n	Stoichiometric electron number
n_{app}	Apparent stoichiometric electron number
F	96,500 coulombs per mole of electrons
i	Current
t	Time
A	Area of electrode
D	Diffusion coefficient
M	Gram molecular mass
m	Mass of solute
V	Volume of solution

RECEIVED May 5, 1981.

The Fe-S-O-H System under Coal Liquefaction Conditions

W. D. RICHEY

Chatham College, Pittsburgh, PA 15232

The strategies used in studies of high temperature reactions of metals have been brought to bear on some of the problems associated with the direct liquefaction of coal. Many coals contain sulfur, combined in both organic and inorganic forms, in excess of amounts allowable under current combustion standards. In some coals much of the sulfur is in the form of pyrite, FeS_2 , which may, paradoxically, serve as a catalyst or the precursor of a catalyst for the liquefaction process. The information available for the Fe-S-O-H system has been assembled in an attempt to provide a framework for interpreting experimental results, and to facilitate the planning of further experiments.

The direct liquefaction of coal in a suitable liquid medium at a given temperature and pressure of reactive gas is a complex and only partially understood process. Iron and iron compounds have been known to facilitate the process since the early German work on coal liquefaction (1). Current efforts to develop low-cost, disposable catalysts for liquefaction have included studies of iron-containing materials. It has been observed that pyrite-containing coals liquefy more readily than "clean" (non-pyritic or low pyrite) coals. Since the effects of these iron materials, whether intrinsic or added, are relatively short-lived, it seems useful to develop an understanding of the possibilities for reactions under coal liquefaction conditions, concentrating first on the chemistry of iron-containing compounds in combination with oxygen, sulfur and hydrogen.

This paper draws on the substantial literature concerning the metal sulfides (2,3), particularly that which concerns the relative stabilities of the various iron-sulfur and iron-oxygen forms. The intention is to build a framework within which to organize the current stock of observations concerning liquefaction residues from coal liquefaction experiments at the Pittsburgh Energy Technology Center. The presentation will display the experimental results, provide a framework for their interpretation and deal with the

0097-6156/81/0169-0349\$07.00/0

© 1981 American Chemical Society

question of the relationship of autoclave and continuous reactor experiments.

First, it should be noted that pyrite, FeS_2 , if finely divided, is usually completely converted to pyrrhotite at temperatures above 350°C in an atmosphere of hydrogen and steam or of synthesis gas within reaction times of less than thirty minutes. The reaction products are a very finely divided pyrrhotite, with a stoichiometry of approximately FeS , and hydrogen sulfide.

The measure used to designate the pyrrhotites observed in coal liquefaction residues is commonly the atom percent iron. Pollack and Spittler (4) have described the adaptation of the well-established x-ray diffraction method of determining atom percent iron in natural pyrrhotites to coal liquefaction residues. The atom percent iron was estimated by this technique to 0.1 atom percent. The atom percent iron values observed in liquefaction residues, and in natural pyrrhotites, range from about 46 to 50. The latter would be the essentially stoichiometric FeS , troilite (high pyrrhotite). Experimentally, substances with all compositions from 43 to 50 atom percent iron have been prepared (2). The pyrrhotites found in nature manifest atom percent iron values clustered around 46.67 (Fe_7S_8 , monoclinic pyrrhotite) and the range 47.37-47.83 (Fe_9S_{10} - $\text{Fe}_{11}\text{S}_{12}$, the "intermediate" or "nonintegral" pyrrhotites)(5). Troilite, FeS , which occurs in certain types of meteorites and lunar rocks and is rarely found in earth rocks, has been identified in liquefaction residue vacuum bottoms.

The whole number stoichiometries Fe_7S_8 through $\text{Fe}_{11}\text{S}_{12}$ were useful in making the calculations underlying this work and in organizing the resulting phase diagrams, but the full range of intermediate atom percent iron compositions was observed experimentally.

Theoretical Background

Two related graphical representations are detailed below. Both are variants of Pourbaix diagrams, which systematize and display the relationship between thermodynamic variables for multicomponent systems. General discussions of such diagrams have been published, by Pourbaix (6), by Garrels and Christ (7), and, in the second form used here, by Gulbransen and Jansson (8). This paper deals with the conclusions that may be drawn based on only the known and inferable thermodynamics of the Fe-S-O-H system, and does not depend on the details of the structures of pyrite or the pyrrhotites, nor on the mechanism of the conversion of pyrite to pyrrhotite.

Pyrite-Pyrrhotite Stability Field. The first graphical representation (Figure 1) is of a pyrite-pyrrhotite stability field, in the form \log fugacity of sulfur ($\log f_{\text{S}_2}$) vs. temperature, T . This diagram derives from the experimentally-based diagram of Toulmin and Barton (9),

but has been redrafted for the lower portion of their temperature range as a function of $T^{\circ}\text{C}$ rather than $1/T$, in $^{\circ}\text{K}$. The major line roughly bisecting the diagram is the equilibrium line for pyrite and pyrrhotite. The solid contours (isopleths) shown correspond to integral-step values for Fe and S (e.g., $\text{Fe}_{11}\text{S}_{12}$). Also shown are atom percent iron for each of the nominal substances. A related approach to predicting the conditions necessary for producing a given pyrrhotite from pyrite has been proposed by Lambert, Simkovich and Walker (10).

$\log f_{\text{S}_2}$ is related to this work through equilibrium expressions of types



and



The first equilibrium type (see Table I) permits estimation of ΔG_f° values for the pyrrhotites from experimental f_{S_2} data, and the second equilibrium type (see Table II) permits auxiliary scales to be established. Thus for the scale $\log f_{\text{S}_2}$, a temperature-dependent scale, $\log f_{\text{H}_2\text{S}}/f_{\text{H}_2}$ could be substituted. Such a scale is shown as a set of dashed lines in Figure 1.

Phase Diagrams. The phase diagrams shown in Figures 2A-2E display the stability regions of iron, the iron oxides, pyrite and the pyrrhotites, and will assist in interpreting the significance of the form of pyrrhotite observed in coal liquefaction experiments.

The calculations which lead to the diagrams were carried out with a computer program developed by Rosof (11), using internally consistent, tabular thermodynamic data for S_2 , Fe, FeO, FeO (wüstite), Fe_2O_3 , Fe_3O_4 , FeS (troilite), FeS_2 (pyrite) and FeS_2 (marcasite) generated by Robie, Hemingway and Fisher (12). Values for the iron sulfates or their hydrates were not included in the analysis. Values for ΔG_f° for the "integral" pyrrhotites were calculated from the data in Toulmin and Barton (9). The pyrrhotite values should be considered less reliable than the Robie, Hemingway and Fisher values and the lines defining intersections (equilibria) between pyrrhotites or a pyrrhotite and pyrite, an oxide or iron might better be represented as bands. Further, the intersections of lines involving pyrrhotites should be interpreted as a narrow range of values rather than points.

In Figures 2A-2E, $\log f_{\text{S}_2}$ is shown as the horizontal axis for values from -20 to 0, and $\log f_{\text{O}_2}$ is shown as the vertical axis, for values from -10 to -40. These diagrams emphasize the forms of iron,

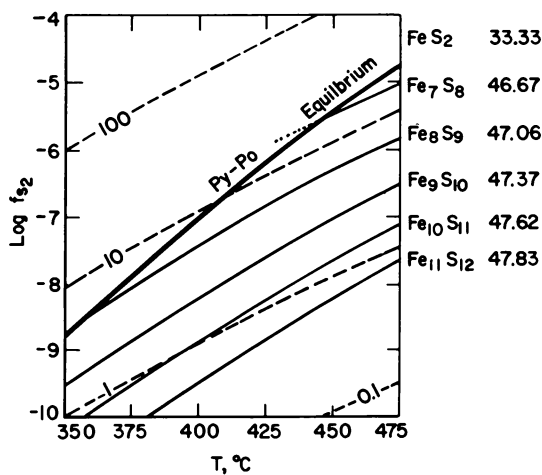


Figure 1. Pyrite-pyrrhotite stability field: Py = pyrite and Po = pyrrhotite.

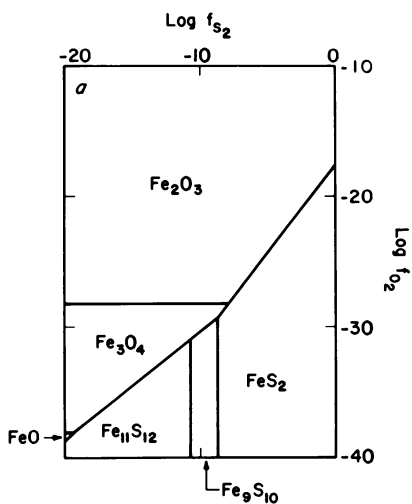


Figure 2A. Fe-S-O-H system (327°C)

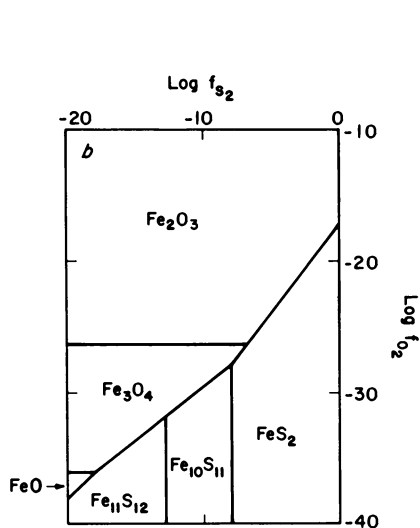


Figure 2B. *Fe-S-O-H system (350°C)*

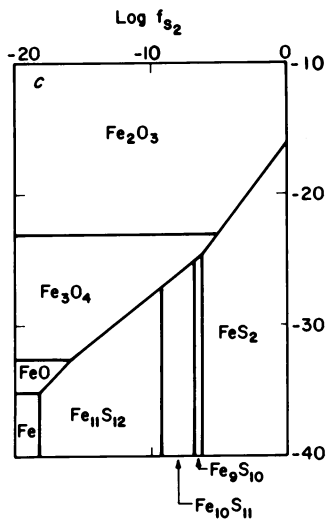


Figure 2C. *Fe-S-O-H system (400°C)*

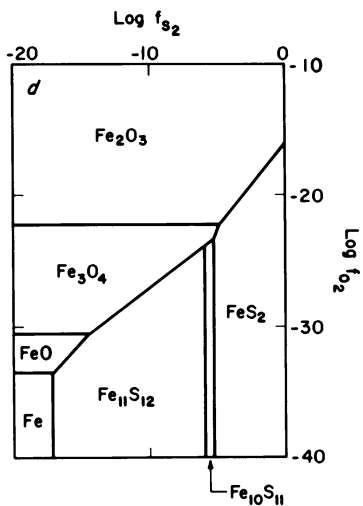


Figure 2D. *Fe-S-O-H system (427°C)*

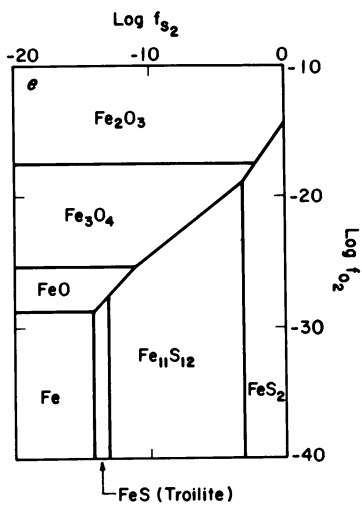


Figure 2E. *Fe-S-O-H system (527°C)*

TABLE I

The equilibrium constant for the equilibrium



may be written as

$$K_1 = 1/(f_{\text{S}_2})^{1/2} \quad 2')$$

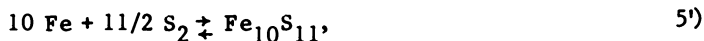
From this it follows that

$$\log K_1 = -1/2 (\log f_{\text{S}_2}) \quad 3')$$

or

$$\log f_{\text{S}_2} = -2 \log K_1. \quad 4')$$

Similarly, for the equilibrium,



the equilibrium constant would be

$$K_5 = 1/(f_{\text{S}_2})^{11/2} \quad 6')$$

and

$$\log K_5 = -11/2 (\log f_{\text{S}_2}) \quad 7')$$

Thus, from the experimentally determined f_{S_2} data, the equilibrium constants and ΔG_f° values for the pyrrhotites can be deduced.

TABLE II

The equilibrium constant for the equilibrium



may be written as

$$K_2 = \frac{f_{\text{H}_2\text{S}}}{f_{\text{H}_2}(f_{\text{S}_2})^{1/2}} \quad 8)$$

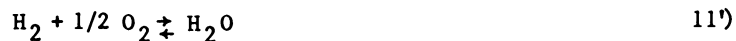
From this it follows that

$$\log K_2 = \log \frac{f_{\text{H}_2\text{S}}}{f_{\text{H}_2}(f_{\text{S}_2})^{1/2}} \quad 9)$$

and, on rearrangement

$$\log f_{\text{S}_2} = 2(\log \frac{f_{\text{H}_2\text{S}}}{f_{\text{H}_2}} - \log K_2) \quad 10)$$

Similarly, for the equilibrium



it follows that

$$\log f_{\text{O}_2} = 2(\log \frac{f_{\text{H}_2\text{O}}}{f_{\text{H}_2}} - \log K_{11}') \quad 12')$$

as elemental iron, an oxide or a sulfur form. At lower temperatures and higher values of $\log f_{S_2}$, elemental sulfur could be present but is not represented on these diagrams. In direct parallel to the $\log f_{S_2}$ and $\log f_{H_2S}/f_{H_2}$ relationship, the $\log f_{O_2}$ scale can be translated into a $\log f_{H_2O}/f_{H_2}$ scale using the equilibrium constants. All vapor phase compositions involving H, S, or O may be represented on such a diagram (H_2 , O_2 , H_2O , H_2S , SO_2 , ...).

Based on intercomparison of ΔG_f° data, regions of preferential stability are displayed. On such phase diagrams an area (a bracket of $\log f_{S_2}$ and $\log f_{O_2}$ values) is a region in which a substance identified with the area is stable relative to all other substances considered in making up the diagram. For example, marcasite, another form of FeS_2 , does not appear in any of the diagrams since it has a slightly higher ΔG_f° than pyrite over the entire temperature range. (This does not suggest that marcasite, formed under conditions which were kinetically favorable for its formation, could not persist in the presence of pyrite in the absence of an accessible kinetic pathway for the conversion.) On such a diagram a line represents defined sets of conditions (pairs of $\log f_{S_2}$ and $\log f_{O_2}$) under which two substances or phases can be in equilibrium. The point of intersection of two lines represents an equilibrium between three related substances, a triple point, an assemblage for which there would be fixed values for $\log f_{S_2}$ and $\log f_{O_2}$. Such assemblages or "points" may be thought of as buffers which would maintain a defined pair of $\log f_{S_2}$ and $\log f_{O_2}$ values until one or more of the components were consumed (13).

Diagrams have been constructed for temperature values of 327, 350, 400, 427 and 527°C, which bracket operating conditions, and make maximum use of the tabular data of Robie, et al. at 500, 600, and 700°C. Input values at 350 and 400°C were chosen by graphical interpolation. Diagrams for 450, 475, and 500°C have not yet been constructed, because the consequences of the sharp breaks in the ΔG_f° values with the phase change of sulfur at 444°C have not been worked out in detail for the graphical interpolation. Similar sets of diagrams were produced by Holland (14), but with no attempt to distinguish the pyrrhotite forms and at broader temperature intervals.

Consider now the set of diagrams:
 327°C (Figure 2A) Pyrite appears in the lower right, Fe_2O_3 , hematite, dominates the field to the top and left, Fe_3O_4 ,

magnetite, appears in the lower left and two pyrrhotites, $\text{Fe}_{11}\text{S}_{12}$ and Fe_9S_{10} , are sandwiched in between Fe_3O_4 and FeS_2 . A small FeO field appears at the lower left. It has been pointed out to me that FeO is not observed experimentally in the temperature range of this study, 250–500°C. The FeO field may be an artifact of the computational procedure.

350°C (Figure 2B) The pyrite field has moved to the right and up. The Fe_3O_4 field has increased in relative area at the expense of Fe_2O_3 . There are again two pyrrhotites, $\text{Fe}_{11}\text{S}_{12}$ and $\text{Fe}_{10}\text{S}_{11}$, with a somewhat larger combined area of stability.

400°C (Figure 2C) The trends observed for pyrite, Fe_2O_3 , Fe_3O_4 and FeO continue. A field of iron stability appears at the lower left. The pyrrhotite stability region is larger, and consists of three pyrrhotites, $\text{Fe}_{11}\text{S}_{12}$, $\text{Fe}_{10}\text{S}_{11}$ and Fe_9S_{10} . The pyrrhotites are very similar in composition and in estimated Gibbs free energy of formation. The ones which are predicted may be an artifact of the composition and free energy estimates but the more sulfur-rich forms would always occur to the right, nearest pyrite, and the less sulfur-rich to the left nearest iron, and the "missing" forms would be "sandwiched in" (have a small relative stability field) between the predicted forms.

427°C (Figure 2D) The trends observed continue, pyrite withdraws to the right and moves up, the Fe_3O_4 and FeO fields increase at the expense of Fe_2O_3 , the iron field enlarges and the pyrrhotite field enlarges, consisting of two fields, a large $\text{Fe}_{11}\text{S}_{12}$ and a smaller $\text{Fe}_{10}\text{S}_{11}$ field.

527°C (Figure 2E) The trends observed have continued, pyrite now occupies a relatively restricted field to the right but with increased stability with respect to $\log f_{\text{O}_2}$. Iron, FeO , and

Fe_3O_4 have continued to enlarge at the expense of Fe_2O_3 . A large $\text{Fe}_{11}\text{S}_{12}$ field is present and a new field, FeS (troilite), has appeared.

Reactor Zone. Recall now the introduction of (or superposition on) the pyrite-pyrrhotite stability field (Figure 1) of contours representing the $\log f_{\text{H}_2\text{S}}/f_{\text{H}_2}$, and the implication on first introducing the $\log f_{\text{S}_2}$ versus $\log f_{\text{O}_2}$ diagram that a similar relationship linked the $\log f_{\text{O}_2}$ scale with $\log f_{\text{H}_2\text{O}}/f_{\text{H}_2}$. Such scales

could be superimposed on the individual diagram, but instead a "reactor zone" has been defined and shown (See Figures 3-5). This zone could be redefined if it seems appropriate, but has initially been chosen to extend, for $\log f_{S_2}$, from relatively pure recycled hydrogen (1ppth H_2S in H_2 , $\log f_{H_2S}/f_{H_2} = -3$) to 1:1 H_2S and H_2 ($\log f_{H_2S}/f_{H_2} = 0$), a first estimate of the conditions at the reactive interface between pyrite and hydrogen. This would produce a six log-unit wide band ($\log f_{S_2}$ scale, $\log f_{S_2} = 2(\log f_{H_2S}/f_{H_2} - K_2)$) down a diagram. For $\log f_{O_2}$, the zone has been initially chosen to extend from relatively dry hydrogen (1 ppth H_2O in H_2 , $\log f_{H_2O}/f_{O_2} = -3$) to "wet" hydrogen 1:1 H_2O and H_2 ($\log f_{H_2O}/f_{O_2} = 0$), with the water assumed to arise from steam, water from the coal or from the (in the sense of this paper) auxiliary reactions of hydrogen and coal. This again would produce a six log-unit wide band ($\log f_{O_2}$ scale, $\log f_{O_2} = 2(\log f_{H_2O}/f_{O_2} - K_{11})$) across a diagram. The six log-unit square intersection of the two bands defines, for purposes of discussion, the reactor zone.

Presumably the hydrogen entering a reactor or charged into an autoclave could be relatively clean and dry, represented by a point in the lower lefthand corner of the reactor zone (or if accompanied by steam, somewhere on the left side of the square). As the reaction proceeded, the reactor gas would become relatively wet (from the balance of the coal reactions or from water in the coal) and loaded with H_2S as the H_2 was consumed, and would be represented by points near the upper righthand corner of the reactor zone. The area of the reactor zone would stay the same (6x6 log units) but the position of the reactor zone will shift with temperature since the two equilibrium constants are functions of temperature. Note that at 527°C (Figure 3), the reactor zone is almost entirely in the pyrrhotite ($Fe_{11}S_{12}$) zone. Note that at 427°C (Figure 4) the reactor zone is entirely in the $Fe_{11}S_{12}$ zone. At 327°C (Figure 5) the reactor zone is in the pyrrhotite zone ($Fe_{11}S_{12}$, Fe_9S_{10}) but in terms of the area of display, has "gone through floor."

The nature of the missing diagrams at 450°C and 500°C (missing because of uncertainty about the best thermodynamic values in the immediate vicinity of the sulfur phase change) can be inferred from those given. One can work with a set of such diagrams, several at a time, and draw some conclusions about the effects of change of temperature. There is some utility for a large set in creating three-dimensional diagrams, in this case $\log f_{S_2}$ vs $\log f_{O_2}$

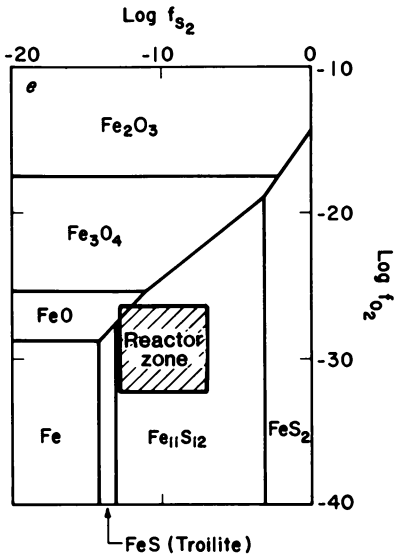


Figure 3. Reactor zone for Fe-S-O-H system (527°C)

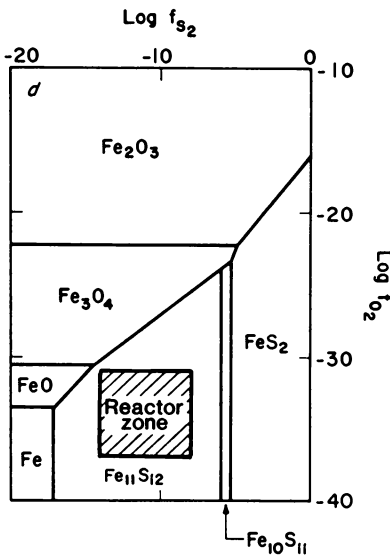


Figure 4. Reactor zone for Fe-S-O-H system (427°C)

vs T. Several of these are now presented, the first (Figure 6) a relatively conventional perspective, T increasing on the vertical axis with $\log f_{S_2}$ and $\log f_{O_2}$ decreasing from the forward corner. Note

that the iron oxides are represented on the left face and the pyrrhotites and pyrite on the right face. The iron region has been removed so that the pyrrhotite region may be seen. An "exploded" view (Figure 7) follows. Note that the pyrrhotite volume is, in a sense, "inside" the rectangular solid and is not of a simple form. Note that a volume now represents a stability zone for a substance, a surface represents a two-substance equilibrium and a line a three-substance equilibrium condition.

Coal Liquefaction Applications

If the reactor zones were superimposed on Figure 6 or 7, and the corners were to be linked up through the diagram, it seems relatively clear that one or another of the pyrrhotites would be the principal iron-containing reaction product of pyrite throughout the coal liquefaction range of temperatures and reaction conditions.

Considering Figure 1, at a constant temperature, the pyrite-pyrrhotite isopleth indicates the $\log f_{S_2}$ (or $\log f_{H_2S}/f_{H_2}$) at which

pyrite and a pyrrhotite would be in equilibrium, and further, indicates the composition of the pyrrhotite. If the vapor or fluid phase composition could be manipulated to reduce $\log f_{S_2}$ (lower the \log

f_{H_2S}/f_{H_2} (flowing H_2 or excess H_2)), the reaction would proceed

until the pyrite was consumed, and from that point (again, at constant temperature) the composition of the pyrrhotite would change becoming less sulfur rich or moving to a higher atom percent iron. Conversely, in an H_2S rich fluid, a more sulfur-rich pyrrhotite could be formed, above the equilibrium pyrite-pyrrhotite line. The contour for Fe_7S_8 is shown (dotted) crossing the pyrite-pyrrhotite equilibrium line to emphasize that metastable (at a given temperature) pyrrhotites can be found and do persist in sulfur-rich atmospheres. In natural systems, such pyrrhotites equilibrate over long time periods to stable pyrrhotites and exsolved pyrite. Stated another way, once a pyrrhotite has been formed, an increase in H_2S pressure will not result in the reformation of pyrite, but will probably yield a more sulfur-rich pyrrhotite.

In the course of an experiment, at any time, at a given temperature, a measurable or deducible $\log f_{S_2}$ and $\log f_{O_2}$ will

exist, defining a point which will lie in an area or field, or on a line. Whatever the iron-based material present at the start of an experiment, if it is not the substance represented by the area or field in which the point lies, there will be a tendency for the material

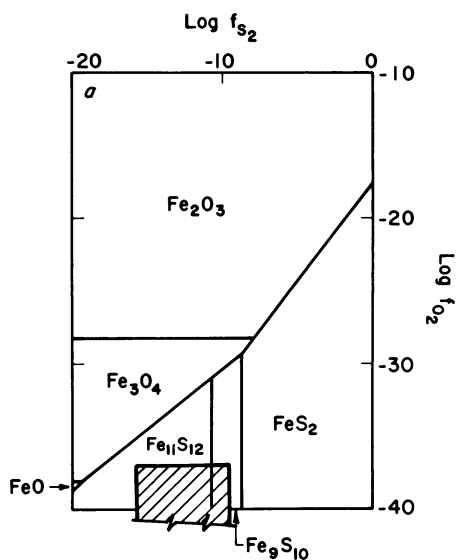


Figure 5. Reactor zone for Fe-S-O-H system (327°C)

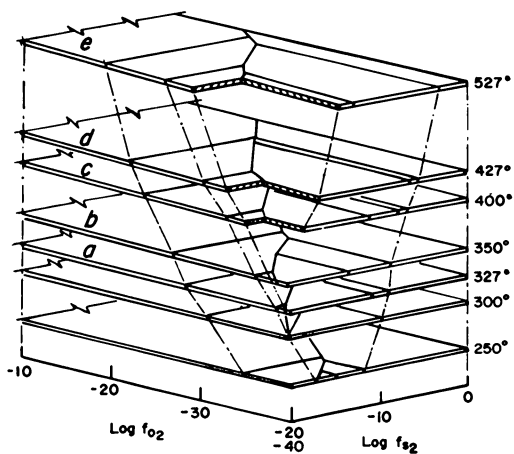


Figure 6. The $\log f_{S_2}$ vs. $\log f_{O_2}$ vs. T diagram

present to be converted to the more stable form (that of the area or field). The length of time and the mechanism for the conversion can not, of course, be predicted from the diagram. Conversely, the presence of a substance or assembly of substances, given a period of time at the temperature and a fluid phase, may be used to infer a pair or range of values of $\log f_{S_2}$ and $\log f_{O_2}$. However, the presence

of a given pyrrhotite (an area) defining a range of conditions (values of $\log f_{S_2}$ and $\log f_{O_2}$) cannot in general be used alone to deduce the nature of the starting materials.

This approach thus suggests that, based on Figure 1, the pyrrhotite first formed in equilibrium with pyrite would be Fe_7S_8 at $450^\circ C$, and between Fe_7S_8 and Fe_8S_9 at $425^\circ C$, $400^\circ C$, and $375^\circ C$, with a shift toward Fe_8S_9 as the temperature decreases. Further, for a H_2 -rich atmosphere, Figure 1 suggests that the pyrrhotite initially formed would give way to a less sulfur-rich pyrrhotite, trending toward $Fe_{11}S_{12}$. Figures 2B, 2C, 2D, and 2E, and the reactor zone Figures 3, 4 and 5, suggest that if the system were to come to equilibrium at 375 , 400 , 425 or $450^\circ C$, the pyrrhotite predicted would be $Fe_{11}S_{12}$ and, if it were not at equilibrium, the pyrrhotite would be between pyrite and $Fe_{11}S_{12}$, one of the more sulfur-rich forms, $Fe_{10}S_{11}$ or Fe_9S_{10} . Additions of one of the other iron-forms, Fe_2O_3 or Fe_3O_4 , would create a buffer system, one of the intersections on the phase diagrams, which would maintain a pyrrhotite form until the pyrite or oxide form was consumed and then maintain a two-component equilibrium relationship until the second component was consumed.

Experimental Observations: Data From Pittsburgh Energy Technology Center Studies (4,15-18).

The pyrrhotites discussed below were characterized by x-ray diffraction techniques. The composition were reported in terms of the atom percent iron in the pyrrhotite. Thus, the observed quantities were atom percent iron and temperature and the fugacities of sulfur and the related ratio of fugacity of H_2S to fugacity of H_2 were inferred.

Continuous Reactors. Consider the experimental data available for the pyrrhotites formed during coal liquefaction in continuous reactors (Table III), about a dozen observations for the ten pound per day bench scale continuous liquefaction unit at four temperatures (375 , 400 , 425 and $450^\circ C$)(15) and about the same number of observations for the 400 pound per day reactor at $450^\circ C$ ($450^\circ-460^\circ C$)(4),

TABLE III. PYRRHOTITE OBSERVED IN REACTOR RUNS (4, 15)

TEN POUND PER DAY REACTOR		ATOM PERCENT IRON
375°C	Western Kentucky Coal 1 lb/hr Flow	47.3, 47.5, 47.6
400°C	Western Kentucky Coal 1 lb/hr Flow	46.7, 47.6
	2 lb/hr Flow	47.8
425°C	Western Kentucky Coal 1 lb/hr Flow	47.6, 47.6, 47.7
	2 lb/hr Flow	47.6
450°C	Western Kentucky Coal 1 lb/hr Flow	47.6, 47.6, 47.8
	2 lb/hr Flow	47.7
FOUR HUNDRED POUND PER DAY REACTOR (4)		
450°C		
Ireland Mine; 4000, 3000, 2000 psi, 12 samples		47.6-47.9
Blacksville	2000 psi, 2 samples	48.1
450°C		
Kentucky #11	2000 psi	47.8
Kentucky #11, Cleaned, 2000 psi		47.6
Kentucky #11, Cleaned, with added pyrite, 2000 psi		47.8-47.8
460°C		
Blacksville	2000 psi	47.8

displayed in Figure 8. With one exception at 400°C, these observations fall in a band between 47.37–47.83 atom percent iron (Fe_9S_{10} – $\text{Fe}_{11}\text{S}_{12}$) or at a slightly higher atom percent iron (one of the 400 pound per day results at 460°C). This band lies at higher fugacity of S_2 and, thus, at a higher ratio of $f_{\text{H}_2\text{S}}$ to f_{H_2} (about one)

than would be intuitively expected, based only on the feed gas (0.001 $\text{H}_2\text{S}/\text{H}_2$), which would be below the base of the diagram as presented. Note that the equilibrium line for pyrite and pyrrhotite falls across the $f_{\text{H}_2\text{S}}/f_{\text{H}_2} = 10$ region, consistent with essentially complete

consumption of hydrogen at an interface. As additional hydrogen flows through the system, with the eventual consumption of the pyrite, the pyrrhotite formed (presumed to be the form on the equilibrium line) would lose sulfur, as hydrogen sulfide, becoming more iron-rich.

The 400°C point at 46.7 atom percent iron represents a sulfur-rich pyrrhotite, that is, one which represents a $\text{H}_2\text{S}/\text{H}_2$ fugacity ratio higher than 10. However, this datum is from an early run, at a low flow rate, and is suspect (15).

Consider now the continuous reactor results in terms of the phase diagrams. From Table III, grouping the three observations at 375°C and the three observations at 400°C on the 400°C phase diagram (in the absence of a 375°C diagram), we observe that we have one in the $\text{Fe}_{11}\text{S}_{12}$ range, three in the $\text{Fe}_{10}\text{S}_{11}$ range, one in the Fe_9S_{10} range, and one at Fe_7S_8 (and no evidence in X-ray analyses for pyrite, iron or the oxides).

There are four observations at 425°C, clustered at 47.6–47.7 atom percent iron, which would correspond to $\text{Fe}_{10}\text{S}_{11}$. Grouped with those are the observations at 450°C and also the 450–460°C observations for the four hundred pound per day continuous reactor, twelve at 450°C between 47.6 and 47.9 atom percent iron, two at 47.7 and 47.8 at 455°C and one at 47.8 at 460°C. They span the range $\text{Fe}_{10}\text{S}_{11}$ to $\text{Fe}_{11}\text{S}_{12}$. All of the observations thus fall in the pyrrhotite region from the pyrite region into the reactor zone and, in general, represent a more iron-rich pyrrhotite.

Autoclaves. The experimental data for the autoclave experiments at 400 and 425°C (16, 17) and for the miniautoclave experiments at 450°C (18) are in Table IV, which presents the coal, the additive (if any), the reactive gas (hydrogen or (1:1 H_2/CO) synthesis gas), the pressure, the time, one half hour or one hour, the vehicle, and the atom percent iron in the pyrrhotite observed.

Coal Only. The autoclave data of Illig and the miniautoclave data of Anderson for coal are displayed in Figure 9. The vehicle is usually SRC II distillate or anthracene oil except for those noted as

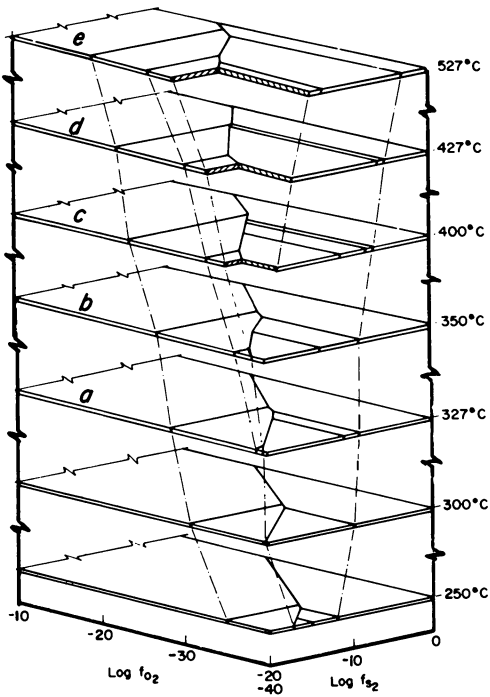


Figure 7. The $\log f_{S_2}$ vs. $\log f_{O_2}$ vs. T exploded diagram

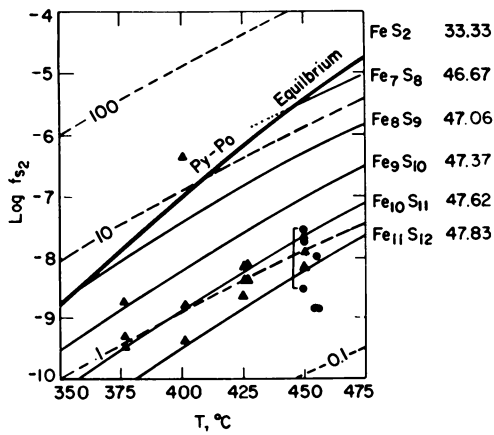


Figure 8. Pyrrhotites from reactors: 10 lb/d reactor (\blacktriangle) and 400 lb/d reactor (\bullet).

Table IV - Pyrrhotite Observed In Autoclave Runs (16, 17, 18)

Coal	Additive	Gas	Pressure	Time at 400°C	Vehicle	Atom	
						Percent	Iron
B	—	H ₂	2000	1/2	SRCII	46.9	46.9
B	—	SYN	3000	1/2	SRCII	47.4	47.4
B	—	H ₂	2000	1/2	RCL	46.5	46.5
B	H ₂ S	H ₂	2000	1/2	SRCII	46.5	46.5
B	PYK11	H ₂	2000	1/2	SRCII	47.2	47.2
B	PYK11	H ₂	2000	1/2	RCL	47.2	47.2
B	LR	H ₂	2000	1/2	SRCII	47.2	47.2
B	PYR	SYN	3000	1/2	SRCII	47.7	47.7
B	LR	SYN	3000	1/2	SRCII	47.4	47.4
B	LR ASH	SYN	3000	1/2	SRCII	47.3	47.3
B	LR ASH+S	SYN	3000	1/2	SRCII	46.9	46.9
B	S	SYN	3000	1/2	SRCII	46.9	46.9
B	MT	SYN	3000	1/2	SRCII	47.1	47.1
B	MT+S	SYN	3000	1/2	SRCII	47.1	47.1
B	MT+S	SYN	3000	1/2	SRCII	47.4	47.4

Table IV, (Cont.)

Coal	Additive	Gas	Pressure	Time at 425°C	Vehicle	Atom Percent Iron
B	PY+MT	SYN	3000	1/2	SRCII	47.0
B	—	H ₂	2000	1/2 hr.	SRCII	46.8
CKYC	—	H ₂	3000	1 hr.	A0	47.2
CKYC	PYVS	H ₂	3000	1 hr.	A0	47.4
B	H ₂ S	H ₂	2000	1/2 hr.	SRCII	46.4
B	—	SYN	3000	1 hr.	SRCII	47.1
KY9-14	—	SYN	3000	1 hr.	SRCII	47.4
KY11	—	SYN	4000	1 hr.	A0	47.7
ILL6	—	SYN	3000	1 hr.	SRCII	46.9
CKYC	—	SYN	3000	1 hr.	A0	46.8
CKYC	CS ₂	SYN	3000	1 hr.	A0	46.7
CKYC	Thiophene	SYN	3000	1 hr.	A0	46.8
CKYC	S	SYN	3000	1 hr.	A0	46.9
CKYC	PYVS	SYN	3000	1 hr.,	A0	47.3
KY11	LR	SYN	4000	1 hr.	A0	47.7

Table IV, (Cont.)

Coal	Additive	Gas	Pressure	Time at 450° C	Vehicle	Atom Percent Iron
B	—	H ₂	2000	1/2	SRCII	47.0
B	—	H ₂	2000	1/2	SRCII	46.7
B	—	H ₂	2000	1/2	SRCII	47.0
B	PYR	H ₂	2000	1/2	SRCII	46.5
B	PYR	H ₂	2000	1/2	SRCII	46.8
B	PYR	H ₂	2000	1/2	SRCII	46.9
B	PYR	H ₂	2000	1/2	SRCII	46.9
B	PYVS	H ₂	2000	1/2	SRCII	46.7

B	=	Blacksville Coal	PYK11	=	Pyrite from Western Kentucky 11 Coal
KY9-14	=	Western Kentucky 9 and 14 Coals	PYR	=	Pyrite from Robena Mine Coal
KY11	=	Western Kentucky 11 Coal	PYVS	=	Pyrite from Vesta Shannopin Coal
ILLC	=	Illinois 6 Coal	LR	=	Liquefaction Residues
CKYC	=	Clean Western Kentucky Coal	LRASH	=	Ash from Liquefaction Residues
			MT	=	Magnetite
			S	=	Sulfur

"second cycle", that is, with the recovered coal liquid-SRC II distillate mixture from a "first cycle". Note that there are a set of values for Blacksville coal with hydrogen at 400°C, 425°C (Illig), and 450°C (Anderson) and at 425°C for Blacksville coal with synthesis gas, as well as a "second cycle" value for Blacksville coal with hydrogen. There are some points for the Blacksville coal with hydrogen, at the three temperatures, which lie on or near the pyrite-pyrrhotite equilibrium line at approximately the same ratio of $f_{\text{H}_2\text{S}}/f_{\text{H}_2}$ (i.e., 10). (This is not the same as saying that the pyrrhotites are the same (i.e. have the same atom percent iron) or are in equilibrium with the same f_{S_2}). This value is well above what

one would intuitively predict, using only the composition of gas charged into the autoclave, but may represent the composition of the fluid at the interface. There are also two points for Blacksville coal from the miniautoclave that fall well below (f_{S_2} , at higher atom percent iron) the others. The "second cycle" Blacksville value indicates a higher f_{S_2} (and a high $f_{\text{H}_2\text{S}}/f_{\text{H}_2}$) which may indicate a greater solubility of H_2S in the "second cycle" solvent and a resultant sulfiding of the pyrrhotite to a value above the pyrite-pyrrhotite equilibrium line.

Values for a series of coals with synthesis gas are displayed at 425°C, the only temperature at which such pyrrhotite values are available, and are, in order of increasing atom percent iron in the reaction product pyrrhotite, Blacksville #2, Illinois #6, Blacksville #2 with synthesis gas, a cleaned Kentucky 11 coal, Kentucky 9/14, and Kentucky 11. Note that only the point for Kentucky 11 falls into the same range of values as the reactor runs.

In the next figure (Figure 10) are again displayed the Blacksville #2 values at 400 and 425°C, as well as two points representing related runs with H_2S added to the autoclave gas. The Blacksville #2 "second cycle" run falls at the same point as the 400°C run with added H_2S . The pyrrhotites above the pyrite-pyrrhotite line have a lower atom percent iron (46.5, 46.4) and, thus, a higher atom percent sulfur. These, then, represent a sulfiding of the equilibrium-line pyrrhotite in the presence of a higher $f_{\text{H}_2\text{S}}/f_{\text{H}_2}$ (about 50:1 rather than the equilibrium value of about 10:1). Note that the pyrrhotites at 400 and 425°C have a different atom percent iron, are different, but represent, at their respective temperatures, the same $f_{\text{H}_2\text{S}}/f_{\text{H}_2}$.

Coal and Coal with Added Pyrite. In Figure 11 are again presented values for Blacksville coal with additional points representing the pyrrhotites resulting when pyrite has been added to the coal in an autoclave at 400°C and in a miniautoclave at 450°C. The pyrites used are obtained from the Robena Mine, from the Vesta

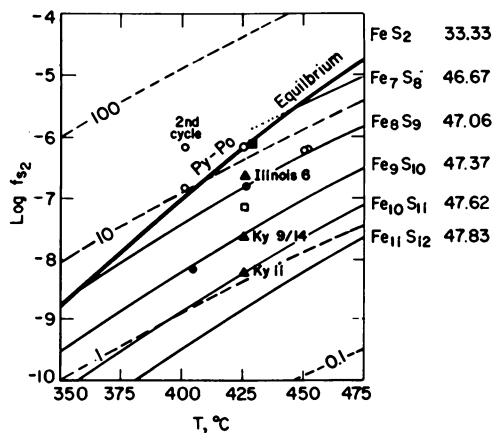


Figure 9. Pyrrhotites from autoclaves (coal only): Blacksville coal with H_2 (\circ); Blacksville coal with synthesis gas (\bullet); Clean Kentucky coal with H_2 (\square); Clean Kentucky coal with synthesis gas (\blacksquare); designated coal with synthesis gas (\blacktriangle).

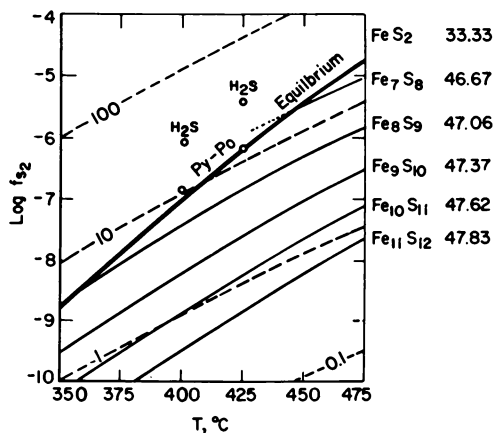


Figure 10. Pyrrhotites from autoclaves (coal plus H_2S): Blacksville coal with H_2 (\circ).

Shannopin Mine, and from Kentucky 11 coal. A value for the pyrrhotite obtained from the Kentucky 11 coal (at 425°C) has been added for comparison. Too few values are available to allow firm conclusions, but the data suggest that the miniautoclave results are in some way different than those from the larger autoclaves, and that addition of pyrite to a coal results in a pyrrhotite that resembles that which has been observed in reactor experiments. In Figure 12 are presented autoclave values at 425°C and reactor values at 450°C for (a) a Kentucky coal which has had most of the mineral matter removed by float-sink procedures, resulting in a coal with only a small fraction of the initial pyrite (and some magnetite from the cleaning procedure) ("clean Kentucky coal") and (b) clean Kentucky coal to which pyrite has been added. Note that, in both cases, the coal with added pyrite yields a pyrrhotite with a higher atom percent iron, and that the difference is about the same for the autoclave and the reactor. Recall that the reactor values at 425°C would be expected to lie on or between the two isopleths for which the 450°C values are observed, based on Figure 9. That is, again it appears that autoclave and reactor data are related, but different. The autoclave conditions are different from those shown in earlier figures in that the residence time in the autoclave was one hour rather than one-half hour.

Coal and Coal with Iron-Containing Materials. In Figure 13 are presented values for Blacksville coal and Blacksville coal with additives, mostly of iron-containing materials, but in several cases including sulfur or sulfur-containing materials. The reaction gas in this case was (1:1 H₂/CO) synthesis gas. Several previously shown points for Blacksville coal with hydrogen are included for comparison. The ash was formed from a liquefaction residue and was a high iron-content material. The liquefaction residues would have contained a pyrrhotite. There are two different pyrrhotites observed with added magnetite and sulfur in combination, 47.1 and at 47.4 atom percent iron. The two experiments differed in amount of water added to the autoclave, the lower water content producing the lower atom percent iron (47.1). The materials, in combination with elemental sulfur, produce a more sulfur-rich pyrrhotite. Without elemental sulfur the resulting pyrrhotites have a higher atom percent iron, even though the added materials may have been sulfur-containing materials, pyrite or the liquefaction residue.

Clean Kentucky Coal and Clean Kentucky Coal with Sulfur-Containing Additives. In Figure 14 are presented values for the clean Kentucky coal with synthesis gas, and clean Kentucky coal with additives containing sulfur. The additives were present in amounts calculated to contain the same relative amount of sulfur. All of the autoclave times were one hour. The point for clean Kentucky coal (which still contains some pyrite and some magnetite (as an artifact of the cleaning process) in about a 2:1 mole ratio) and the point for thiophene lie on the pyrite-pyrrhotite equilibrium line. The

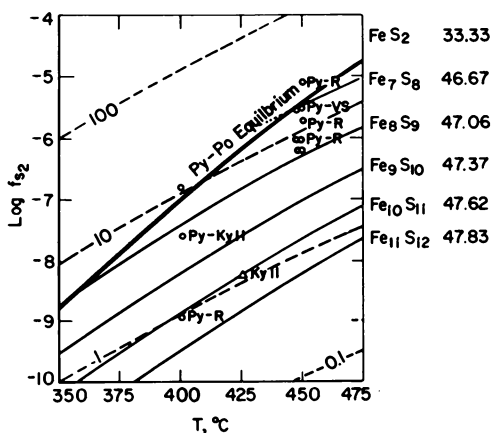


Figure 11. Pyrrhotites from autoclaves (coal plus pyrite): Blacksville coal with H_2 (\circ); designated coal with H_2 (\triangle); pyrite from Kentucky 11 coal (PY-KY11); pyrite from Robena mine (Py-R); pyrite from Vesta Shannopin mine (Py-VS).

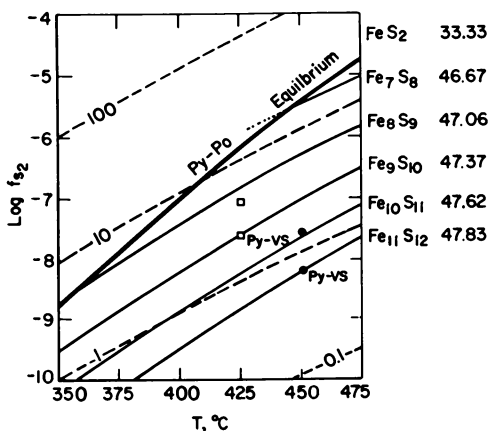


Figure 12. Pyrrhotites from autoclaves and reactors: Clean Kentucky coal in autoclave (\square); Clean Kentucky coal in 400 lb/d reactor (\bullet); Vesta Shannopin pyrite as an additive (Py-VS).

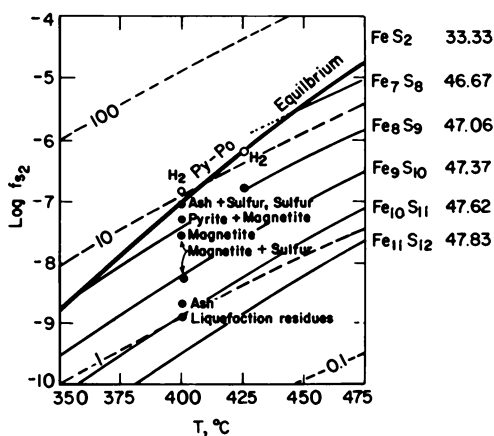


Figure 13. Pyrrhotites from autoclaves (coal plus iron-containing material): Blacksville coal with H_2 (○); Blacksville coal with synthesis gas, with additive noted (●).

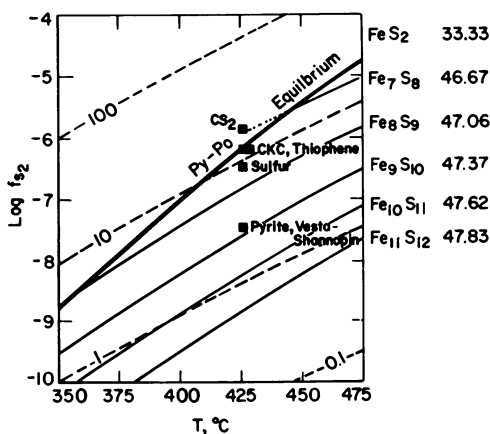


Figure 14. Pyrrhotites from autoclaves (Clean Kentucky coal plus sulfur-containing additives): Clean Kentucky coal with synthesis gas, with additive noted (■).

pyrrhotite from the run with carbon disulfide lies above the equilibrium line, at about the fugacity of sulfur that would be in equilibrium with carbon disulfide at 425°C. The point representing the addition of sulfur lies below the equilibrium line, and the point representing the addition of pyrite lies well below the equilibrium line.

The autoclave results are primarily at 400°C and 425°C with a few minireactor results at 450°C. Displayed on the phase diagrams, the pyrrhotites reported for most runs fall to the right of the reactor zone in the more sulfur rich regions (Fe_8S_9 , Fe_7S_8). The points for "second - cycle" solvent and added H_2S runs fall above the Toulmin-Barton equilibrium line, or fall on the pyrite-pyrrhotite line of the phase diagrams. The coals with higher intrinsic pyrite content or those to which pyrite or iron-containing materials were added have pyrrhotites which fall nearer the reactor zone.

Conclusions

The pyrrhotites observed are characteristic of a higher H_2S to H_2 ratio than would be intuitively expected, based on the nominally hydrogen-rich reactor and autoclave operating conditions. On the basis of the experiments for which the pyrrhotites have been characterized, the results from reactor runs are quantitatively different from autoclave runs. The mini-autoclave run results are probably different than the autoclave runs. All forms of added iron-containing materials seem to be converted to pyrrhotites and the result of adding iron is a less sulfur-rich pyrrhotite, unless a sulfur-containing material is also added. While no claim is made that the systems have achieved equilibrium, the pyrrhotites from most of the reactor runs are on the right hand side of the reactor zone of the diagram and the pyrrhotites from autoclave runs are of a composition between pyrite and the form predicted to be in the reactor zone. The autoclave runs with added iron were most like the runs in the reactors.

The systems with added iron-containing materials would amount to mineral buffer systems which should define the fugacities of oxygen and sulfur until one or more of the components of the buffer has been consumed. In general, all of the experiments have been made on thermodynamically undetermined systems, that is, not enough information has been obtained to define the systems.

While the pyrrhotite composition has been established for a very small fraction of the many coal liquefaction experiments, it does seem apparent that all of the iron forms added are converted to pyrrhotites rather quickly and that the pyrrhotites interconvert, responding to the total iron content of the system and the composition of the fluid phase.

If the search for a suitable catalyst for the liquefaction process is considered in terms of these diagrams and the current

experimental results, it would appear that under conventional operating conditions, pyrite, iron, and all the oxide forms would be converted to a pyrrhotite in the presence of sulfur. Conditions necessary to maintain one of the oxide forms would not appear to be achievable. If an initially-formed pyrrhotite (Fe_7S_8 at 450°C , for example) were to be considered the substance active in catalyzing the liquefaction of coal, the reactor would have to be run H_2S -rich to maintain the material, and diagrams of this sort suggest the range of conditions necessary.

An expanded version of this paper, including a discussion of the thermodynamic information available for the pyrrhotites, the computer programs used, and the details of the calculations, will appear in a Pittsburgh Energy Technology Center Technical Report now in preparation.

Acknowledgements

R. Hamilton provided expert professional counsel during the development of the Figures. F. Brown, B. D. Blaustein and G. A. Gibbon were consistently supportive throughout the development of this approach. S. S. Pollack, E. Ilig and D. Cillo supplied helpful suggestions and technical insights into coal liquefaction procedures.

The author is an Oak Ridge Associated Universities Faculty Research Participant, Pittsburgh Energy Technology Center, United States Department of Energy.

LITERATURE CITED

1. Wu, W. R. K.; Storch, H. H. "Hydrogenation of Coal and Tar"; U. S. Bureau of Mines Bulletin 633: Washington, D.C., second printing, 1977.
2. Vaughn, David J.; Craig, James R. "Mineral Chemistry of Metal Sulfides"; Cambridge University Press: Cambridge, 1978.
3. Sharma, R. C. and Chang, Y. A. Met. Trans. B 1979, 10B, 103-108.
4. Pollack, S. S., Spitler, C. A. A.m. Mineral. submitted for publication.
5. Arnold, R. G. Can. Mineral. 1967, 9, 31-50.
6. Pourbaix, Marcel. "Lectures on Electrochemical Corrosion"; Plenum Press, New York, 1973.
7. Garrels, R. M.; Christ, C. L. "Solutions, Minerals and Equilibria"; Harper and Row: New York, 1965.
8. Gulbransen, Earl A.; Jansson, Sven A. Chapter 4, "Thermochemistry of Gas-Metal Reactions", in "Oxidation of Metals and Alloys"; American Society for Metals, Metals Park: Ohio, 1971.
9. Toulmin, P.; Barton, P. B. Geochim. Cosmochim. Acta 1964, 28, 641-671.
10. Lambert, J. M., Jr.; Simkovich, G.; Walker, P. L., Jr. Fuel 1980, 59 687-690.

11. Rosof, Barry H. in "Applications of Phase Diagrams in Metallurgy and Ceramics/Proceedings of a Workshop held at NBS, Gaithersburg, MD, January 10-12, 1977"; National Bureau of Standards SP-496, pp. 1090-1092.
12. Robie, Richard A.; Hemingway, Bruce S.; Fisher, James R. "Thermodynamic Properties of Minerals and Related Substances at 298.15K and 1 Bar (10^5 Pascals) Pressure and at Higher Temperatures"; Geological Survey Bulletin 1452, United States Government Printing Office: Washington, D.C., 1979.
13. Crerar, David A., Susak, N. J., Borcsik, M., Schwartz, S. Geochim. Cosmochim. Acta 1978, 42, 1427-1437.
14. Holland, H. D. Econ. Geol., 1959, 54, 184-233.
15. Cillo, D., Private communication.
16. Bockrath, B. C.; Illig, E.; Schroeder, K. T.; Miller, R. D. Presented at AIME National Meeting, Chicago, February 1981; submitted for Symposium Proceedings, "Process Mineralogy in Extractive Metallurgy."
17. Illig, E., Private communication.
18. Anderson, R., Private communication.

RECEIVED May 5, 1981.

Mössbauer Study of the Transformation of Iron Minerals During Coal Conversion

P. A. MONTANO, V. SHAH, S. REDDY, and A. S. BOMMANAVAR

Department of Physics, West Virginia University, Morgantown, WV 26506

Coal is a sedimentary organic rock, highly hydrogen deficient. Its importance has grown in recent years due to diminishing production of domestic oil and increasing prices of foreign oil. The acceptance of a coal for a particular process depends on both the organic and inorganic components, and to obtain a full characterization of a coal a careful identification of the mineral matter is necessary. The presence of iron in many of the mineral components of coal makes the Moessbauer effect a useful and to a certain degree unique analytical tool. Iron-sulfur compounds, although making up a relatively small portion of coal, are significant in that they may affect all phases of the coal processing. The major group of iron-sulfur compounds in coal is the disulfide group consisting of pyrite and marcasite. Of the two, pyrite is the most abundant and is usually dominant. Pyrite and marcasite can be readily identified by x-ray diffraction. The two dimorphs are usually simply considered as pyrite, which is probably the most deleterious of the iron bearing minerals in coal: It is the source of acid mine drainage (1), and the major source of SO₂ pollution in the combustion process. Recently, however, there has been mounting evidence suggesting a possible catalytic role for pyrite (or pyrrhotite) in coal liquefaction (2), where a direct correlation has been observed between significant increases in conversion with increasing pyrite content (3). Moreover, a recent study demonstrated that the presence of pyrite in a coal tends to enhance the production of liquids of lower viscosity (4). These observations indicate that a thorough study of the transformation of pyrite during coal liquefaction is necessary. Detailed knowledge about the decomposition of pyrite, the effect of H₂ and H₂S partial pressures and the type of solvent used is necessary to understand all the factors controlling the rate of decomposition and the type of pyrrhotite formed during coal conversion.

In recent years the Moessbauer effect has been used to study the mineral matter in coal (5-9). These investigations were essentially concerned with the identification of the minerals as

0097-6156/81/0169-0377\$05.00/0

© 1981 American Chemical Society

well as the possible use of the Moessbauer effect to measure the amount of pyritic sulfur. Some researchers have also used the Moessbauer effect to study liquefaction residues and products of the oxidation of coal. More recently, this technique has been applied to characterize the type of pyrrhotite present in coal residues (10). In this paper we report the first results of the in situ study of the transformations of pyrite in coal during liquefaction.

Experimental techniques

Data acquisition and least square fitting of the Moessbauer spectrum were done in a microprocessor based computer (Promeda). The source used was a 220 mCi $^{57}\text{Co}:\text{Rh}$. All the isomer shifts in this paper are given relative to $\alpha\text{-Fe}$ at room temperature. The coal used in the study was IL6 (pyritic sulfur = 2.0 and organic sulfur = 2.0 %) and the solvent was a SRC-II heavy distillate 850⁺. A specially designed reactor for Moessbauer measurements was used. The temperature stability was $\pm 1\%$. The stoichiometries of the pyrrhotites were determined by Moessbauer and x-ray diffraction methods (10). All the samples were also measured at low temperatures (13 K) for better resolution of all the components, using a closed-cycle helium refrigerator.

Iron bearing minerals in coal: characterization using Moessbauer spectroscopy

The major minerals in coal are clays. Kaolinite is usually present in coal, but its identification by Moessbauer spectroscopy is very difficult due to the small amount of iron present and to surface contamination of the clay grains with iron oxides, mainly goethite. The other clay minerals present in coal are illite, chlorite and mixed clays. Their identification is not always easy. We have used a simple method, carrying out Moessbauer measurements at low temperatures and applying an external magnetic field to resolve the spectra and distinguish, for example, between illite and chlorite (11).

The presence of iron sulfates such as szomolnokite $\text{FeSO}_4 \cdot \text{H}_2\text{O}$ hindered the identification of the clays at room temperature. The ferric sulfates can be detected either by treating the sample with dilute HCl or by carrying out Moessbauer measurements at low temperatures. This is of particular importance for the identification of jarosites. Other minerals like siderite can be identified with relative ease. An extensive review of this area can be found in ref [11].

Transformations of pyrite

Under liquefaction conditions FeS_2 is transformed into a non-stoichiometric iron sulfide, Fe_{1-x}S . A number of different pyrrho-

tites can be formed, depending on the reaction temperature and H_2S partial pressure. Several studies have been made of the decomposition of pyrite at high temperatures (12,13) and there is overall agreement that the rate of decomposition below $400^\circ C$ is slow. Furthermore, it has been observed that this rate of decomposition is enhanced in the presence of H_2 (13). An activation energy of about 126 kJ/mole in the temperature range of $420-550^\circ C$ was reported by Schwab and Philinis (12). Attar (13) suggested that the decomposition of FeS_2 in any environment is controlled by the availability of S_2^{2-} anions on the surface and by the rate of diffusion from the bulk. Within this model the role of the hydrogen will be that of removing the sulfur from the surface. In all the above studies the assumption has been made that pyrite decomposes thermally to



and in the presence of hydrogen to



We think that these simple models do not represent reality because pure stoichiometric FeS is not the only product formed during the decomposition of FeS_2 . In our studies with synthetic mineral pyrite and coal pyrite we have always observed the presence of non-stoichiometric pyrrhotites, in some cases more than one phase (FeS is also present under certain reaction conditions). There has been a general tendency to oversimplify the analysis of the thermal decomposition of FeS_2 . It is known that films of FeS_2 can be prepared from vacuum deposition (14). Consequently, there are doubts concerning the analysis of thermogravimetric measurements on FeS_2 . We have observed that the presence of solvents changes the rate of decomposition of pyrite as well as the stoichiometry of the resulting pyrrhotite.

The most important factor controlling the stoichiometry of the pyrrhotite obtained from the decomposition of pyrite is the partial pressure of H_2S . We have observed that the atomic percentage of iron in pyrrhotite is reduced when the partial pressure of H_2S increases. This effect was apparent in runs in our laboratory as well as in liquefaction residues from runs carried out by E. Illig at the Pittsburgh Energy Technology Center. In Illig's work, a West Virginia Blacksville coal was used: In the presence of H_2 alone (2000 psi) a stoichiometry of 47.4 at.% Fe in pyrrhotite was observed at $400^\circ C$; when H_2S was added (as sulfur), the atomic % Fe was reduced to 46.85. This result is also in good agreement with earlier observations on variations in the stoichiometry of iron pyrrhotites as a function of the type of coal (IL6, WV Blacksville and KY 9/14) (10). In that study (a) the amount of total sulfur was larger for the IL6 coal and (b) the pyrrhotite formed was more iron deficient (10). It seems that the total sul-

fur in coal controls the stoichiometry of the iron sulfide formed during coal liquefaction. The combination sulfur plus pyrrhotite may be the most important element in any catalytic process associated with the mineral matter present in coal.

High temperature transformations of FeS and Fe₇S₈

We have studied the transformations of two typical iron sulfides (troilite FeS and monoclinic pyrrhotite Fe₇S₈) at high temperatures. They represent the two extremes of the compounds of the type Fe_{1-x}S. The purpose of this work was to determine the effect of temperature on the pyrrhotites, in the temperature range of interest in coal liquefaction (350–420° C).

The high temperature transformations of FeS have been studied by several authors (15). The structure of troilite below 140° C (α -transition) corresponds to a hexagonal superstructure known as 2C, where 2C implies cell edge along the C-axis twice that of the NiAs structure. Above 140° C the structure of FeS is that of NiAs, 1C phase. In Figure 1 we show the spectra of FeS at various temperatures. The magnetic transition temperature is ca. 307° C. The measurements were carried out in a vacuum furnace. The Moessbauer spectrum at room temperature gives a typical 6-line pattern with a magnetic hyperfine field of 313 ± 2 kOe, in good agreement with values reported in the literature (16). At 412° C, a temperature commonly used in direct liquefaction, the spectrum shows a single line with isomer shift (IS) of 0.51 ± 0.03 mm/sec and linewidth of 0.76 mm/sec. The large linewidth at high temperatures is attributed to diffusional broadening due to vacancy motion in the lattice. When the sample is returned to room temperature and exposed to air, partial oxidation occurs with the appearance of iron oxides. This indicates a high reactivity of the iron sulfides surfaces.

Natural crystals of monoclinic pyrrhotite, Fe₇S₈, were used for our Moessbauer measurements. The crystals were identified by x-ray diffraction and Moessbauer spectroscopy (17). Moessbauer spectra of Fe₇S₈ above the magnetic transition temperature ($T_C \approx 325^\circ$ C) are shown in Figure 2. The spectrum at 430° C shows a single very broad line (linewidth ≈ 1.13 mm/sec) with an IS = 0.50 ± 0.03 mm/sec, identical to that of FeS at high temperatures but with a much larger linewidth. We understand this to indicate a higher mobility for the vacancies at high temperatures for Fe₇S₈ than for FeS. By contrast, the spectrum at 355° C gives a partially resolved doublet. It is to be noted that these high temperature pyrrhotites are not necessarily equal to the starting phase, that considerable transformations take place in the sulfides at high temperatures. The spectrum at room temperature of the newly formed pyrrhotite is shown in Figure 3. The atomic % iron in this pyrrhotite is 47.5, the new form of pyrrhotite is hexagonal and not monoclinic as determined by x-ray diffraction.

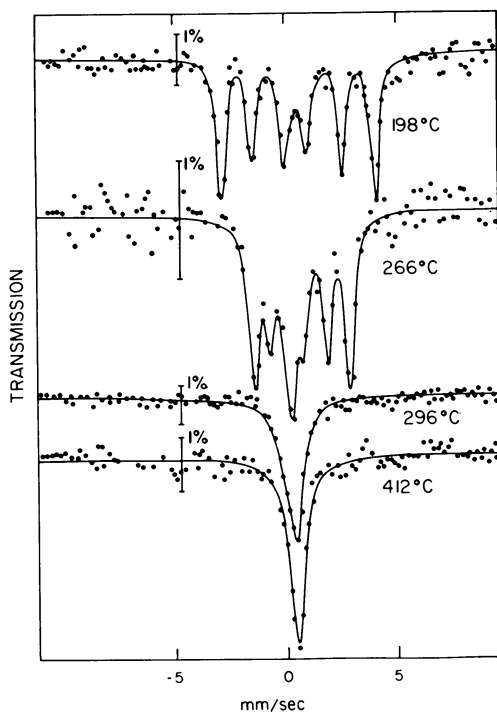


Figure 1. Mössbauer spectra of FeS at various temperatures. Continuous line is the least-square fit to the spectra.

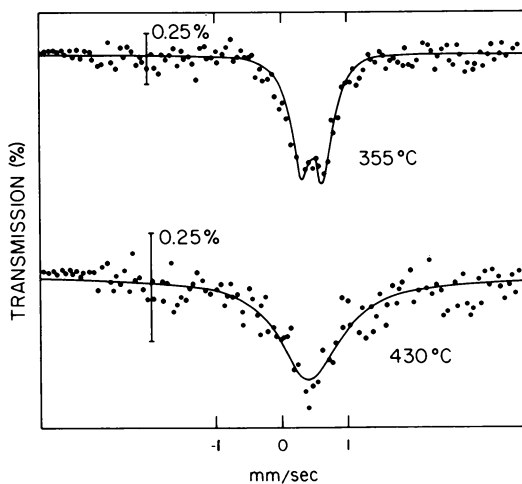


Figure 2. Mössbauer spectra of Fe_7S_8 above the magnetic transition temperature. Continuous line is the least-square fit to the spectra.

In situ study of the transformation of the iron sulfides in an IL6 coal

The transformations taking place in the FeS_2 present in a coal were studied *in situ* using a specially designed reactor for high pressures and temperatures. The coal used was an IL6 (18); its Moessbauer spectrum is shown in Figure 4. In this coal FeS_2 and $\text{FeSO}_4 \cdot \text{H}_2\text{O}$ (szomolnokite) are present, the latter formed as a result of partial oxidation of the coal during storage. SRC-II heavy distillate 850^+ was used as a solvent.

Our objective was to measure the changes in the Moessbauer parameters as a function of temperature, solvent, H_2 pressure and time. The first run consisted of a sample of about 300 mg/cm^2 coal inside the reactor under 2 psi of N_2 and no solvent. It was run between room temperature and 420°C , and maintained at 420°C for 10 minutes, long enough to obtain a Moessbauer spectrum. No evidence of transformation of FeS_2 to pyrrhotite was detectable by Moessbauer spectroscopy. After rapidly returning the sample to room temperature a Moessbauer spectrum was taken, from which it was observed that the characteristic spectrum of FeS_2 was retained with a very small amount of conversion to pyrrhotite. (The rate of decomposition is very slow in the absence of solvent and/or hydrogen.) The linewidth of FeS_2 at 420°C was $0.37 \pm 0.03 \text{ mm/sec}$ and the IS = $0.10 \pm 0.02 \text{ mm/sec}$. In a second run the same amount of coal was used, but this time with H_2 . Running time was as above and we observed that full transformation of FeS_2 to pyrrhotite took place; this transformation is evident above 300°C . The stoichiometry of the pyrrhotite obtained gave an at.% Fe of 47.9. The experiment was repeated using only the solvent (SRC-II) and N_2 , and under the same running conditions we observed full transformation of FeS_2 to pyrrhotite. The pyrrhotite formed has 48.0 at.% Fe. The spectrum of the residue of this run is shown in Figure 5.

We repeated the experiment once more with the same amount of solvent (solvent to coal ratio 2:1), coal and H_2 , running each temperature for 15 minutes. The spectra for the different temperatures are shown in Figure 6. At 410°C the linewidth of the spectrum is around 1 mm/sec , the IS = $0.37 \pm 0.05 \text{ mm/sec}$, significantly less than for FeS or Fe_7S_8 . The broad line is attributed to diffusional broadening, due both to the motion of vacancies and the presence of coal liquids in the system. The liquefaction residue of this run gives a pyrrhotite with 47.85 at.% iron. Because of the change in IS as well as the broad lines observed at high temperatures, we decided to carry out measurements with variable time: We observed that the IS tends to become more negative and the lines much broader. We interpret this as a result of the interaction of the pyrrhotites with coal. We are expanding this study to different coals and various solvents. It is to be noted that Tetralin (a better hydrogen donor than SRC-II) does not seem to be more efficient in transforming FeS_2 to Fe_{1-x}S ,

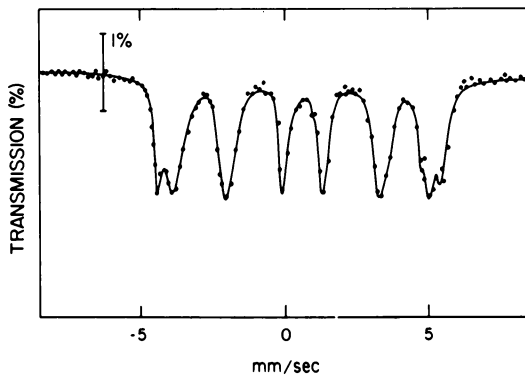


Figure 3. Mössbauer spectrum of the iron sulfide obtained from the high-temperature transformation of Fe_7S_8 . Continuous line is the least-square fit to the spectrum.

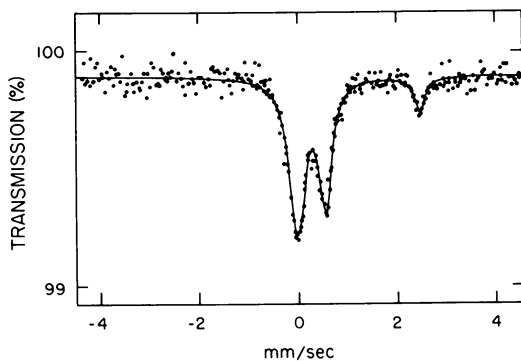


Figure 4. Mössbauer spectrum of Illinois No. 6 coal used in this study. Continuous line is the least-square fit to the spectrum.

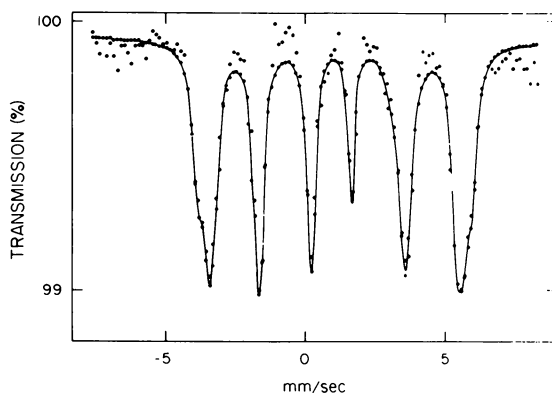


Figure 5. Mössbauer spectrum of the Illinois No. 6 liquefaction residue obtained from a run with SRC-II + N₂. Continuous line is the least-square fit to the spectrum.

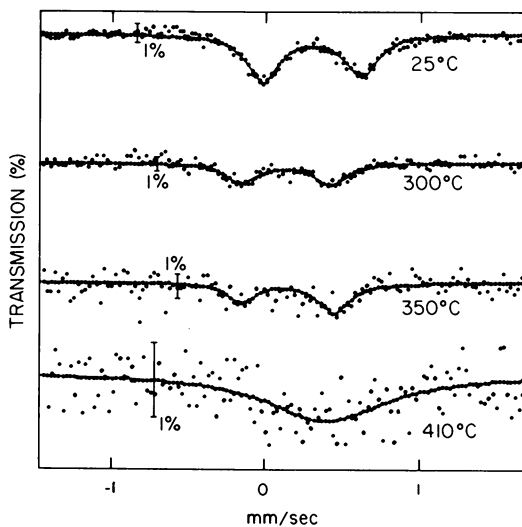


Figure 6. Mössbauer spectra (in situ) at various temperatures for the coal sample plus SRC-II and H₂. Continuous lines are the least-square fits to the spectra.

than SRC-II heavy distillates. The question of the interaction solvent-FeS₂ remains open.

For the last experiment reported here, we added 5% pyrite to the IL6 coal, the sample was well mixed and solvent was added (2:1) and mixed with the coal; the runs were carried out in the presence of H₂ (250 psi). We observed in this case that full conversion to pyrrhotite takes place in five minutes at 420° C. Similar effects as before were observed in the IS and linewidth. The atomic % Fe in the pyrrhotite formed in this experiment was 46.8, indicating a strong change in the stoichiometry of the pyrrhotite. In Figure 7 the Moessbauer spectrum of this residue is shown. It is clear to the eye that the spectra in Figures 7 and 8 are significantly different.

The above experiment was repeated to test its reproducibility and the same effect in the reduction of iron percentage in Fe_{1-x}S was observed. We attribute this to an increase in the partial pressure of H₂S due to the FeS₂ added.

The following observations summarize our experimental results:

- (1) In short periods of time (10 minutes or less) and at 420° C under vacuum or nitrogen, FeS₂ is not significantly converted to pyrrhotite.
- (2) In the presence of SRC-II heavy distillates and/or H₂, the FeS₂ in coal is converted to pyrrhotite at 420° C in a short time (less than 20 minutes).
- (3) The pyrrhotites formed at high temperatures in coal liquefaction show considerable line broadening and smaller IS than regular pyrrhotites. This is strongly suggestive of an interaction between the iron sulfides and the coal.
- (4) During longer periods of time the interaction between the iron sulfides and coal liquids becomes stronger, as suggested by the IS variation.
- (5) Adding FeS₂ to the IL6 coal produces a more iron deficient pyrrhotite in the liquefaction residue. This suggests that the stoichiometry of the pyrrhotite formed during liquefaction is controlled by the partial pressure of H₂S. The atomic percentage of iron in pyrrhotites appearing in the liquefaction residues apparently decreases when the partial pressure of H₂S in the reactor is increased.

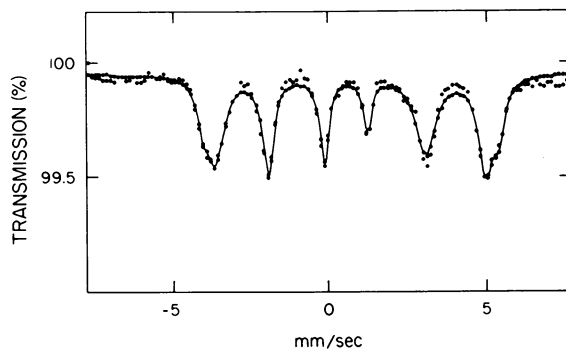


Figure 7. Mössbauer spectrum at room temperature of the liquefaction residue of the Illinois No. 6 coal run with SRC-II and H_2 . Continuous line is the least-square fit to the spectrum.

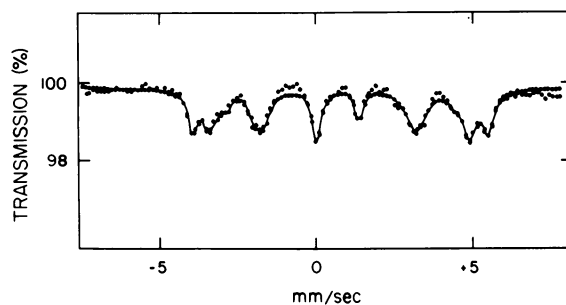


Figure 8. Mössbauer spectrum at room temperature of the liquefaction residue of the Illinois No. 6 coal + 5% FeS_2 (SRC-II and H_2 present) run. Continuous line is the least-square fit to the spectrum.

Acknowledgments

The authors acknowledge the financial support of the U.S. Department of Energy and the helpful discussions with Drs. Sidney Pollack and E. Illig of the Pittsburgh Energy Technology Center and Dr. B. Granoff of Sandia National Laboratories.

Literature Cited

1. Lau, C.M.; Shumate, K.S.; Smith, E.E. Third Symposium of Coal Mining Drainage Research, Mellon Inst., 1970; p 114.
2. Given, P.H. "Catalysis of Liquefaction by Iron Sulfides from Coals"; U.S. DOE Project Review Meeting on Disposable Catalysts in Coal Liquefaction: Albuquerque, NM, June 5-6, 1979.
3. Granoff, B.; Thomas, M.G. Preprints Div. Fuel Chem., Amer. Chem. Soc. 1977, 22 (6) 183.
4. Illig, E. "Disposable Catalysts in Coal Liquefaction"; DOE: Albuquerque, NM, 1978.
5. Lefelhocz, J.F.; Friedel, R.A.; Kohman, T.P. Geochim. cosmochim. Acta 1967, 31, 2261.
6. Montano, P.A. Fuel 1977, 56, 397.
7. Levinson, L.M.; Jacobs, I.S. Fuel 1977 56, 453.
8. Huffman, G.P.; Huggins, F.E. Fuel 1978 57, 592.
9. Jacobs, I.S.; Levinson, L.M.; Hart, H.R., Jr. J. Appl. Phys. 1978 49, 3, 1775;
Keisch, B.; Gibbon, G.A.; Akhtar, S. Fuel preprints, Amer. Chem. Soc. 1978, 263.
Huggins, F.E.; Huffman, G.P. in "Analytical Methods for Coal and Coal Products, Vol. III" ; Academic Press, 1980.
10. Montano, P.A.; Granoff, B. Fuel 1980, 59, 214.
11. Montano, P.A. "Characterization of Iron Bearing Minerals in Coal" in Coal Structure," edited by M. Gorbaty (Advances in Chemistry series); ACS, 1980;
Montano, P.A. in "Recent Chemical Applications of the Moessbauer Effect," edited by J.G. Stevens; G.K. Shenoy (Advances in Chemistry series); ACS: Washington, D.C., in press.
12. Schwab, G.M.; Philinis, J. J. Am. Chem. Soc. 1947, 69, 2588.
13. Attar, A. Fuel 1978, 57, 201 and references therein.
14. Seehra, S.S.; Montano, P.A.; Seehra, M.S.; Sen, S.K. J. Mat. Sci. 1979, 14, 2761.
15. Power, L.F.; Fine, H.A. Min. Sci. Engng. 1976, 8, N2, 106 [a good review of iron-sulfur compounds].
16. Hafner, S.; Kalvius, M. Z. Kristallog. 1966, 123, 443.
17. Levinson, L.; Treves, D. J. Phys. Chem. Solids 1968, 29, 2227.
18. IL #6 coal, ISGS 020280, coal selected for interlaboratory comparison of mineral matter in coal (R. Finkelman, Allerton House Meeting, Urbana, IL, 1979).

RECEIVED May 5, 1981.

A New Method for Analysis of Pyrite in Coal and Lignite

M. HYMAN and M. W. ROWE

Department of Chemistry, Texas A&M University, College Station, TX 77843

Measurement of the pyrite in coal and lignite by a new method is presented. The method combines the techniques of thermo-gravimetry and magnetometry and utilizes oxidizing and reducing gases. The feasibility of thermo-magnetometry has been established by measuring the magnetite contents of carbonaceous chondrites. We have found that a precision of $\sim 2-5\%$ in the magnetite measurements was typical, so that the method appears promising. Coals often contain sizeable amounts of FeSO_4 (from air oxidation of FeS_2); these would be recorded as FeS_2 by our technique. Our method thus gives an estimate of the FeS_2 prior to oxidation. No additional error is introduced due to the air oxidation of FeS_2 to FeSO_4 . Soluble iron species, predominantly FeCO_3 , could be removed prior to the reduction of the FeS_2 to metallic iron by H_2 at elevated temperatures ($\sim 400^\circ$) in the balance, with the measurements being conducted part of the time in a strong magnetic field. The formation of metallic iron is thus easily detectable through observation of the saturation magnetization which is proportional to the amount of iron formed. Our measurements of the pyrite in samples of coal and lignite from the Coal Research Section of The Pennsylvania State University are compared with previous measurements on the same samples. Reasonable agreement is observed.

We present here the preliminary results of our attempt to develop a new method for the analysis of pyrite in coal and lignite. It is well known that sulfur in coal is present in different forms. In particular, although the iron sulfide in coal is generally pyrite (1), other iron sulfides are frequently present. For example, iron disulfide occurs as marcasite, a rhombic crystalline form, as well as pyrite, a cubic crystalline form. Perhaps the term 'disulfide sulfur' should be used to replace the 'pyritic sulfur' more commonly quoted, as recently suggested by Youh (2). Since the chemical reactivity of these two disulfides of iron is similar, our method will record them equally well. Nonetheless, we will continue to refer to the pyrite determinations here, although we are really talking about the chemical species FeS_2 rather than a particular crystalline structure.

0097-6156/81/0169-0389\$05.00/0

© 1981 American Chemical Society

The results obtained so far indicate that the method is feasible, with the limited studies we have made agreeing in general with previously determined results. The primary advantages of our procedure are: (1) The method is straightforward. With about 10 minutes instruction, six different graduate students in chemistry at Texas A&M University were able to measure the FeS_2 in a coal sample, arriving at a value which agreed within the estimated precision ($\pm 1\sigma$) with the average value that we had previously determined. Under routine operation a technician with minimal qualifications could be trained easily to conduct the analyses. (2) The apparatus employed is commonly found in larger chemistry departments, where it is called a Faraday balance, in geology departments called a Curie balance, and in engineering departments, as well as industrial laboratories. (3) Automation, if desired, could be implemented readily. The principal disadvantage is the time required for an analysis. Each measurement of the pyrite content takes about 2 hours, although since the system records continuously, the operator can attend to other duties with only intermittent alterations being necessary during the two-hour reaction period, or the entire procedure can be easily programmed with micro processors.

Experimental Procedure

The system which we utilized for making the thermogravimetry - magnetometry measurements is illustrated schematically in Figure 1. Richardson (3) used a similar system to study the magnetic properties of coal char. Our system consists of a Cahn electrobalance with a non-inductively-wound heater capable of long-term operation at $\sim 800^\circ\text{C}$. A temperature controller maintains the temperature at $\pm 5-10^\circ\text{C}$ which is adequate for our technique. The system incorporates the possibility for changing the gas environment in order to control the oxidation-reduction conditions within. Finally a permanent magnet (4600 Oe) with poles shaped for Faraday analysis is used and can be moved into place to act upon the sample or be moved away at will. This system was designed for studies on meteorites (4) and a system with larger capacity for samples would be more suitable for coal studies. Our present system constrains the size of coal samples to ~ 50 mg. Larger samples would certainly be preferable for pyrite analysis in coal.

To understand the technique we are proposing here, it is necessary to realize the combined effect of temperature and a strong magnetic field on the apparent weight of a ferromagnetic material suspended from a spring or balance beam. Figure 2 shows that the apparent weight (the saturation magnetization) of a ferromagnetic material is many times its actual weight in the presence of a strong magnetic field. Note that this large increase in apparent weight, the saturation magnetization, slowly

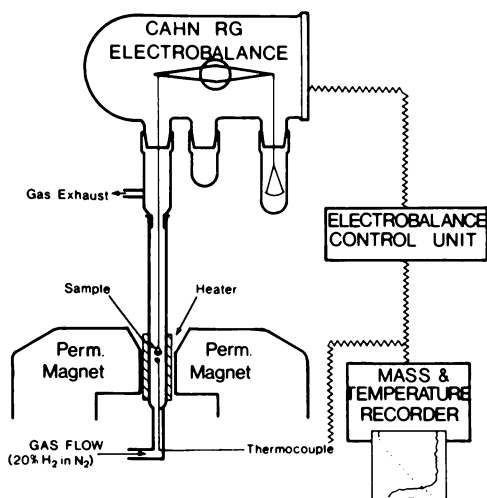


Figure 1. Schematic of the Cahn electrobalance used for measuring coal and lignite

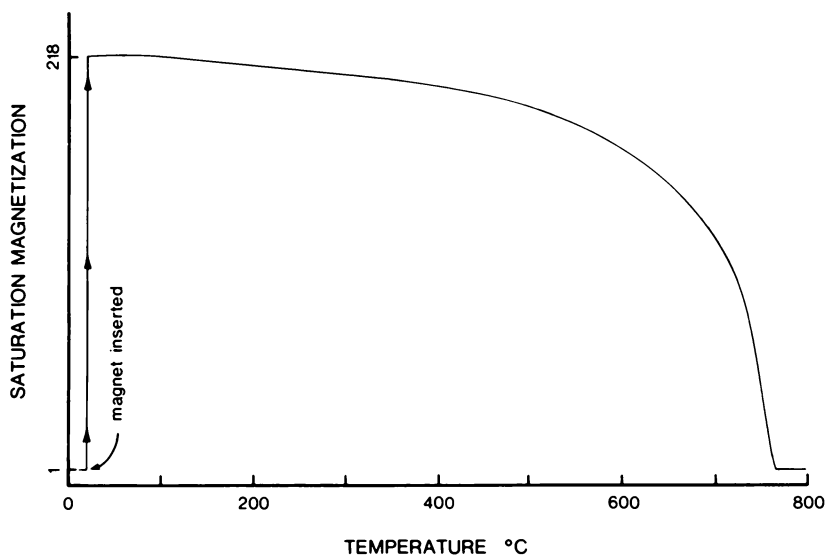


Figure 2. Variation of the saturation magnetization of 1 mg iron metal with temperature as recorded by a Faraday balance. Note that the apparent weight (saturation magnetization) of iron is much greater than its actual weight.

decreases as the temperature is increased until the apparent weight finally becomes nearly equal to the actual weight of the iron at $\sim 770^{\circ}\text{C}$, the Curie point of the iron. The Curie point (also called Curie temperature) is distinctive for the particular ferromagnetic material under question. For example, it is 390°C for Ni, 595°C for Fe_3O_4 (magnetite), 770°C for metallic iron, etc.

The method for determination of pyrite is perhaps best demonstrated by examination of Figure 3 which is a schematic representation of the data-tracing of an analysis of a hypothetical sample of coal or lignite. A run is started by weighing out a sample (region A of Figure 3) with the gas inlet open to air. The presence of initial Fe_2O_3 can be checked by inserting the magnet (B). Normally only a very slight change in weight is seen at B. An exception, noted with PSOC-625, will be discussed later. The heater is then set to $90\pm 10^{\circ}\text{C}$ which drives off the water and a weight reduction is observed (C). We now use 105°C , the value recommended by ASTM but have not found any significant difference in water content. In fact all the operating conditions have now been changed to conform with those used in ASTM procedures. After the water has been removed, the weight becomes constant (D) and this weight is the dry weight of the coal. At that point, the temperature is raised slowly to 400°C . This is sufficient to oxidize the organic material in the coal which again results in a rather extreme loss in weight (E) as the gaseous reaction products (CO , CO_2 , H_2O , etc.) and other volatiles are driven off. We have found 400°C is sufficient to oxidize all the organic material. Nonetheless we now use 700°C as noted later in our mention of proximate analysis. When the oxidation is complete, the weight is once again observed to level off (F) and the pyrite has been oxidized to Fe_2O_3 . At this point, the furnace is turned off and 20% H_2 , diluted from 100% by N_2 carrier for increased safety, is fed into the system at a rate of 65 ml/minute. Ten minutes has been found to be adequate to flush the sample area with H_2 . The magnet is re-inserted which results in an apparent weight increase due to the saturation magnetization of the Fe_2O_3 (G). For convenience in presentation of Figure 3, we have shown a scale expansion to accommodate the large increase in saturation magnetization which will result as metallic iron is formed from the reduction of Fe_2O_3 (G). The temperature is then turned to 400°C with the H_2 flowing and the Fe_2O_3 begins to be reduced to metallic Fe, measured as a large increase in apparent weight (H). When all the Fe_2O_3 is reduced to Fe, the saturation magnetization due to the iron becomes constant indicating the reaction is complete (I) and the furnace is turned off. An increase in apparent weight is noticed as the sample cools due to the increase of saturation magnetization of the iron with decreasing temperature (Figure 2) as exhibited by region J in Figure 3. Once again the apparent weight will become constant as the temperature approaches room temperature (K). The magnet is then removed and the final weight of the residue is recorded (L). For purposes of determining the pyrite content, only three regions

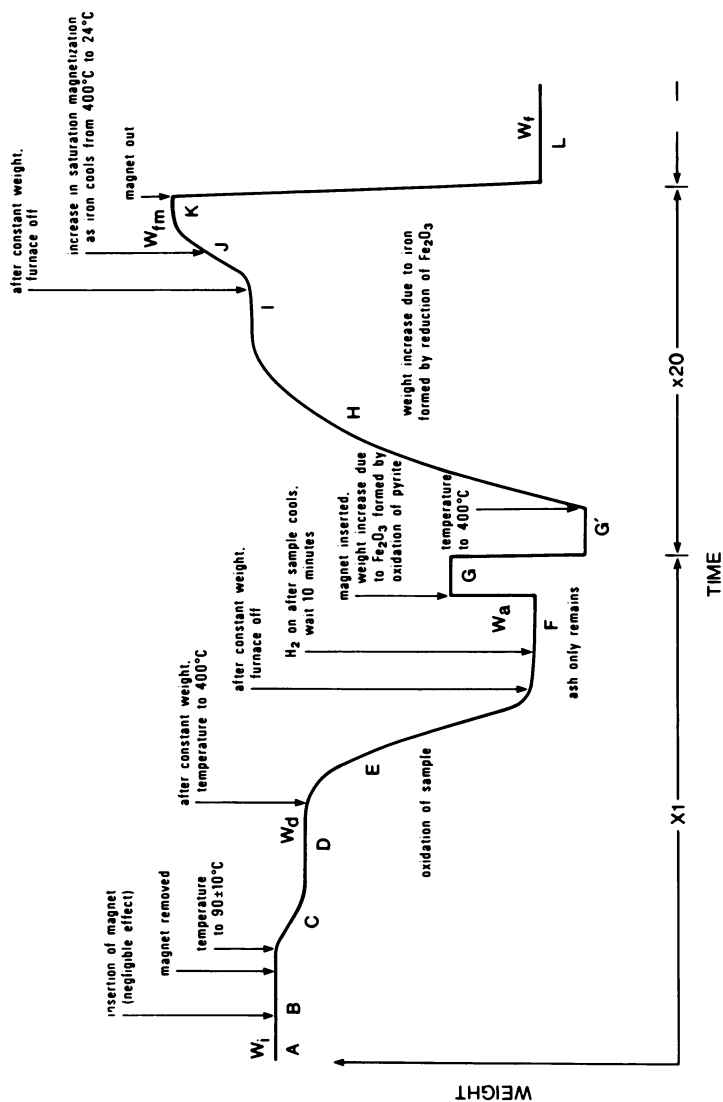


Figure 3. Schematic of weight change observed continuously as pyrite in coal or lignite is analyzed. The change in the weight-scale factor from X1 to X20 is due to the large increase in apparent weight (saturation magnetization) as the Fe_2O_3 present at G is reduced to ferromagnetic iron.

of Figure 3 are of critical importance. They are: (1) either the initial weight, W_i , of region A, or the dry weight, W_d of region D, (2) the final apparent weight with the magnet in place, W_{fm} , of region K, and (3) the final weight, W_f , of region L. The pyrite content is then calculated using stoichiometry and the saturation magnetization of the iron:

$$\%FeS_2 = \frac{W_{fm} - W_f}{218} \times \frac{M.Wt. FeS_2}{M.Wt. Fe} \times \frac{100}{W_{i,d}}$$

Where

W_{fm} = final weight with magnet in place (saturation magnetization of iron)

W_f = final weight without magnet

M.Wt. FeS_2 = molecular weight of FeS_2

M.Wt. Fe = molecular weight of Fe

$W_{i,d}$ = initial weight or dry weight, depending upon whether the per cent initial or, the per cent dry weight were desired and the factor of 218 is the room-temperature saturation-magnetization of iron.

It is also possible to obtain the per cent moisture and per cent of ash in the coal or lignite samples with this technique. The moisture and ash contents are, of course, easily obtainable from Figure 3. The moisture is simply given by

$$\% \text{ moisture} = \frac{W_i - W_d}{W_i} \times 100$$

and the ash is given by

$$\% \text{ ash} = \frac{W_a}{W_{i,d}} \times 100$$

depending on whether % ash in the original sample or for dry weight, respectively, is desired.

It would be a simple matter to obtain the proximate analysis of the coal by means of very slight alterations in the procedure (5). If nitrogen were introduced initially and the procedure followed as in Figure 3 but increasing the temperature to 700°C instead of 400°C at point (D), then the percentage of volatile matter could be obtained directly. The difference in the weight, W_d , and the constant weight observed at 700°C under nitrogen yields the weight of the volatile matter. After observation of the constant weight observed at 700°C under nitrogen, oxygen is introduced which results in the production of ash only. Then the difference in the constant weight at 700°C under N_2 and the final ash weight, W_a , yields the weight of fixed carbon. The rest of the procedure described earlier is followed unchanged. We intend to examine this proposed method of proximate analysis in detail.

Since each of the above equations involves a ratio of weights, it is the relative changes which are of importance and it is not necessary to know the actual weight in order to calculate the % pyrite, % ash, % fixed carbon, % volatiles or % moisture in the coal or lignite samples.

As stated above, the entire procedure takes ~ 2 hours maximum.

Results and Discussion

We received from Dr. P. Dolsen, Coal Research Division of the Pennsylvania State University, five samples of coal and lignite (4 of coal and 1 of lignite). These were sent to us in physical forms ranging from finely powdered material to chunks ~ 1 mm in diameter containing various proportions of water, pyrite, ash and volatile material. Thus these samples provided us with adequate variety with which to attempt standardization of our method. The description of those samples is shown in Table I from information provided to us by Penn State.

Utilizing the procedure set forth earlier, we have measured the pyrite contents of the five coal and lignite samples supplied by Pennsylvania State University. A comparison of our results with those obtained at Penn State are shown in Table II. We also obtained the per cent moisture and per cent ash on the Penn State coal and lignite samples, which we show for comparison. It should be pointed out that our % moisture and % ash were not done under conditions usually used to obtain those figures. The % moisture was calculated after heating to 90°C until constant weight was observed. The % ash was calculated after heating at only 400°C until constant weight was observed. Nevertheless, the agreement is good. Agreement between our pyrite determinations and those of the Penn State laboratory are also encouraging, though certainly not perfect. We can easily rationalize the cases in which our values are slightly larger than those of the Penn State group. Other ferrous compounds, which are initially present other than the sulfides, and which are easily oxidizable and reducible, will be recorded by our technique as pyrite. However, it is not easy to imagine why our results should be lower than those obtained at Penn State. The most likely explanation is sample inhomogeneity. Since our method, which was originally designed for an entirely different project, will handle only 50 mg samples, sample inhomogeneity could certainly be suspected. However, since we have conducted multiple determinations, our standard deviations should be taking that into account, at least partially, on the scale of samples (\sim one pound) that we received. Both PSOC-593 and PSOC-639 which are slightly lower by our technique were fairly uniform with standard deviation of $\pm 16.5\%$ and $\pm 23.4\%$, respectively, as was PSOC-625 with a standard deviation of $\pm 10\%$. The standard deviation should include not only sample inhomogeneity but the indeterminate uncertainty of our method as well. If the Penn State val-

Table I. Brief Description of the Five Coal and Lignite Samples Received from the Coal Research Laboratory of the Pennsylvania State University.

Sample Designation	Seam Name	Apparent Rank	Sample Type	Sample Location
PSOC - 593	Illinois #5	HVC	Channel-Lithotype Bright Coal	Fulton Co. Illinois
PSOC - 625	Darco Lignite	Lignite	Channel-Lithotype	Harrison Co. Texas
PSOC - 639	Wildcat	Subbit C	Channel-Lithotype	Milam Co. Texas
PSOC - 707	Pittsburgh	HVC	Channel-Subsection	Braxton Co. W. Virginia
PSOC - 725	Upper Kittanning	Med Vol	Channel-Subsection	Preston Co. W. Virginia

Table II. Comparison of Our Results with Those Provided by the Division of Coal Research, Pennsylvania State University.

Sample Designation	% Pyrite	
	Our Results	Penn. St.
PSOC-593	2.48±0.15*	2.75
PSOC-625	1.00±0.05**	0.95
PSOC-639	1.41±0.10	1.80
PSOC-707	3.4±0.4 † 3.00±0.14 †	2.75
PSOC-725	3.1±0.4 † 3.02±0.16 †	2.88

	% Moisture		% Ash	
	Our Results 90°C	Penn. St. 105°C	Our Results 400°C	Penn. St. 700°C
PSOC-593	12.7±0.2	15.9	12.2±0.5	10.3
PSOC-625	33.2±0.3	33.7	13.4±0.3	21.4
PSOC-639	24.7±0.3	25.5	23.0±0.7	29.0
PSOC-707	---	2.3	6.5±0.5	5.2
PSOC-725	1.1±0.2	2.4	8.7±0.5	8.3

*Uncertainty is standard error = σ/\sqrt{N} **Corrected ~16% downward to account for initial Fe_2O_3 . See text.

† These samples were re-run after powdering to 100 mesh.

ues reflect a single measurement, then their values and ours agree within the uncertainty of the data. Unfortunately, we presently have no information regarding the uncertainty of the Penn State data.

Two of the samples, PSOC-707 and PSOC-725, were apparently more inhomogeneous than the other three. To examine this possibility, we re-ran the samples PSOC-707 and PSOC-725 after powdering to 100 mesh. The new data, shown in Table II, on these two samples after grinding to 100 mesh indicates that our original measurements were influenced by sample inhomogeneity. The standard deviation of the initial measurements indicated a sample inhomogeneity on the order of $\pm 35\%$, whereas after powdering, a much tighter grouping of about 10% was observed. As was pointed out to us at this Symposium (6), coal samples with particle size much greater than 100 mesh are unlikely to give self-consistent results. Not only was the standard deviation of these samples reduced, but the agreement with the Penn State values was also improved, although the initial values also agreed within the estimated standard error of our measurements.

In our discussion of the technique, we stated that normally only a very slight change in weight is noted with the initial insertion of the magnet at point (B) in Figure 3. We did observe one exception to that. For PSOC-625, an increase in weight with the insertion of the magnet at (B) was $\sim 1/6$ that observed at (G). We interpreted that as the presence of some Fe_2O_3 in the PSOC-625 sample. With that assumption, we corrected the final value with a reduction equal to the ratio of the increase in weight at (B) to that observed at (G) in Figure 3. Thus the uncorrected value for the FeS_2 in PSOC-625 was 1.20%, compared to the corrected value of 1.00%. The latter is in much better agreement with the Penn State value of 0.95% FeS_2 .

In our method, other forms of iron sulfide, e.g. pyrrhotite (Fe_{1-x}S), would be calculated stoichiometrically from the iron as FeS_2 , so that if significant amounts of pyrrhotite were present, an error in our method would occur in the direction that we would report a too-high pyrite content. Other sources of error would be easily reducible compounds of iron. For example, siderite is expected to be reduced to iron in the course of our technique. If so, each atom of iron would be assumed to originate from FeS_2 which would result in our estimate of the FeS_2 content being higher than the actual value. We intend to check experimentally the extent to which siderite interferes with our procedure. Our studies to date indicate that iron silicates do not interfere with our technique, but further experiments are planned.

Coals often contain sizeable amounts of FeSO_4 due to air oxidation of FeS_2 . This factor does not lead to any complication with our method. One molecule of FeS_2 oxidizes to produce one molecule of FeSO_4 , and since our method records the FeS_2 and the FeSO_4 through their iron, our technique will measure the sum of FeS_2 and FeSO_4 molecules and convert all of them to % FeS_2 . Thus

this technique measures the FeS_2 initially present in the sample with no loss in accuracy, irrespective of the degree of oxidation of FeS_2 to FeSO_4 . If the initial pyrite content is the quantity desired, this would constitute an advantage for our method, since other techniques require an independent determination of the FeSO_4 .

The above procedure requires no pretreatment of the coal samples. However, it is possible to use a pre-dissolution step for the non-sulfide, HCl soluble iron-bearing species, before utilizing the thermogravimetric-magnetic measurements. We intend to attempt such studies in the future. This would presumably correct for the possible errors introduced by non-sulfide iron species.

Conclusion

These preliminary studies lead us to feel optimistic that this new technique for the measurement of iron disulfides in coal and lignite is a viable alternative to the present methods of pyrite analysis. In addition the method readily yields the proximate analysis as well. The principal advantages are: (1) the ease of analysis, and hence of training operators, (2) fairly widespread availability of the apparatus, (3) the cost effectiveness due to use of unskilled technicians, and (4) the fact that automation of the process should be rather easily accomplished. An accuracy approximately comparable to the ASTM method is probably feasible. This method may be superior for coal samples in which a substantial fraction of the pyrite is totally surrounded by organic matter.

Acknowledgements

The work was supported in part by the Center for Energy and Mineral Resources of Texas A&M University. We are grateful to Dr. P. Dolsen, Coal Research Division of the Pennsylvania State University, for supplying us with samples for study. We benefitted from the comments of the three reviewers: two were anonymous, the other was Dr. O.K. Manuel.

Literature Cited

1. Whelan, P.F. Finely disseminated sulfur compounds in British coals, *J. Inst. Fuel* 1954, 27, 455-458, 464.
2. Youh, C-C. Chemical reaction between hot ferric sulphate solution and iron disulfide in Miocene coals of Taiwan, *Fuel* 1977, 56, 226.
3. Richardson, J.T. Thermo-magnetic studies of iron compounds in coal char, *Fuel* 1972, 51, 150-152.
4. Hyman, M.; Rowe, M.W.; Herndon, J.M. Magnetite heterogeneity

among C1 chondrites, Geochem. J. 1979, 13, 37-39, and unpublished data.

5. Perkin-Elmer Computer-Aided Chemistry Seminar and Exhibition, January 8 and 9, 1981, and personal communication with G. Williams, Perkin-Elmer Sales Engineer; Hyman, M.; Rowe, M.W. Determination of the Calorific Value of Coal by Thermogravimetric Proximate Analysis, J. Chem. Edn., submitted 1981.
6. Personal communication, Dr. Bruce M. LaRue, National Steel Corporation.

RECEIVED March 9, 1981.

Evaluation of the Removal of Organic Sulfur from Coal

R. MARKUSZEWSKI, L. J. MILLER, and W. E. STRASZHEIM—Ames Laboratory, Iowa State University, Ames, IA 50011

C. W. FAN and T. D. WHEELOCK—Department of Chemical Engineering and Ames Laboratory, Iowa State University, Ames, IA 50011

R. T. GREER—Department of Engineering Science and Mechanics, Iowa State University, Ames, IA 50011

As the removal of sulfur from coal prior to combustion acquires more importance in order to meet evermore stringent antipollution regulations, research on the development of methods for the cleaning of coal continues to expand. Reviews are available which describe the various methods for desulfurizing coal (1, 2, 3). The sulfur content in coal is usually a few per cent, but it can range from less than 0.5 per cent to as much as 8 per cent or more. Much of the sulfur is inorganic in nature, occurring in discrete mineral phases; the inorganic sulfur is mostly pyrite with small amounts of sulfates such as gypsum. Part of the sulfur in coal is termed organic sulfur, being intimately bound to the organic coal matrix. The chemical nature of this organic sulfur is not well established. During the desulfurization of coal, some of the coarse inorganic sulfur components can be removed by strictly physical or mechanical means, but chemical methods are required to remove the finely disseminated pyrite and the organic sulfur.

A promising chemical desulfurization method being developed at the Ames Laboratory, Iowa State University, is based on leaching finely powdered coal with a hot solution of dilute sodium carbonate containing dissolved oxygen under moderate pressure (4, 5). The method has been shown to be effective in the rapid removal of most of the inorganic sulfur and a substantial portion of the organic sulfur under relatively mild conditions. However, the removal of organic sulfur varies from coal to coal (6). Even for the same coal, the reduction in organic sulfur may be variable because of sample heterogeneity, changes in process conditions, and sometimes quite unknown factors.

It appears that adding to all these difficulties is the lack of a satisfactory method for the direct determination of organic sulfur in coal that could be routinely applied to all coals under all conditions. The commonly used ASTM procedure (7) for organic sulfur is an indirect method, based on the difference between the total sulfur and the total inorganic

0097-6156/81/0169-0401\$05.00/0

© 1981 American Chemical Society

(pyritic plus sulfate) sulfur. The sulfate is determined in the liquid extracts of coal boiled with hydrochloric acid. The assumption is that only sulfate sulfur is extracted, pyritic sulfur is untouched, and all iron forms other than pyritic iron are extracted. The residue is then extracted with nitric acid to dissolve the pyrite, and the iron content in the liquid is taken as a measure of the pyrite, since all non-pyritic iron has been previously extracted by the hydrochloric acid. This measurement technique also avoids any contamination from the possible decomposition of organic sulfur compounds by the nitric acid.

This ASTM procedure is basically sound and many tests confirm its utility on raw coals (8, 9, 10). However, there may be problems in its routine application to chemically processed coals (11, 12). The chemical treatment may alter the mineral components, resulting in sulfur- and iron-bearing minerals with different solubilities in hydrochloric or nitric acid. Such changes may account for discrepancies observed between the determination of total inorganic sulfur and the sum of pyritic and sulfate sulfur (13). In addition, the organic structure of coal itself may be changed so that leaching of pyrite by nitric acid is not as effective.

The problems in the determination of organic sulfur in coal underline the need for new methods. Several approaches have been investigated (14-17), but more work is necessary for full development.

In our work, the removal of organic sulfur from coal was followed by the ASTM procedure. In addition, the fate of iron and sulfur was assessed by a series of extraction experiments with analysis of the solid residues and the liquid extracts by conventional chemical methods. Finally, an instrumental method based on electron microprobe X-ray analysis was used for the direct determination of organic sulfur in the organic coal matrix (18, 19). The analytical results from the different techniques were used to evaluate the removal of organic sulfur from three coals by the Ames oxydesulfurization process.

Experimental

Coals. The three coals chosen for the desulfurization experiments were high-volatile C bituminous coals. Lovilia/ROM was a run-of-mine coal from Monroe County, Iowa, and was probably oxidized during prolonged storage (as shown by the high sulfate content). Lovilia/ISU was a freshly mined coal that was subsequently precleaned at the Iowa State University coal preparation plant by a heavy-media (magnetite) process at 1.3 specific gravity. The Illinois No. 6 coal came from the Elm mine near Trivoli, Illinois. The Lovilia/ISU and Illinois No. 6 coals were stored under nitrogen after pulverizing and screening to -200 mesh.

Desulfurization. The coals were treated in a 1-liter autoclave under conditions of the Ames oxydesulfurization process by leaching 100 g of coal with 400 ml of 0.3 M sodium carbonate for 1 hr. at 150 C under 200 psia oxygen partial pressure. The apparatus and detailed procedure for the leaching experiments were described elsewhere (4, 5).

Acid Extraction. The raw and treated coals were extracted by acids under conditions analogous to those recommended in the ASTM method (7) for the determination of various forms of sulfur:

- Extraction A - 25 g of coal was extracted for 30 min. by 250 ml boiling 2:3 hydrochloric acid.
- Extraction B - 10 g of the washed and dried residue from extraction A was extracted an additional 30 min. by 500 ml boiling 1:7 nitric acid.
- Extraction C - 10 g of coal was extracted directly (without the hydrochloric acid pre-extraction) by 500 ml boiling 1:7 nitric acid.
- Extraction D - same as Extraction C except at room temperature, with stirring, for 12 hr.

The residues from the extractions were filtered, washed, and dried for 4 hr. at 100 C. The wash water was combined with the acidic filtrate for analysis.

Analysis. The heating value, ash content, and sulfur distribution of the raw and treated coals were determined according to ASTM procedures (7). Iron in the extracts of the raw and treated coals was determined by titration with a cerium (IV) solution. Iron in the residues from the acid extractions of the raw and treated coals was determined spectrophotometrically using ferrozine (20). The liquid extracts were analyzed for total sulfur (as sulfate) by ion chromatography after separation of the sulfate from nitrate on an alumina column (21). Nitrogen was determined in the raw and treated coal and in their nitric acid-extracted residues by a modified Kjeldahl method.

A Tracor Northern quantitative energy-dispersive X-ray analysis system with solid-state detectors was used for the electron microprobe measurements. The method is based on electron microbeam point analyses on a maceral level (18, 19). The emitted characteristic X-ray fluorescence radiation is used to quantify sulfur. Other elements of interest, such as iron and calcium, are monitored simultaneously to ensure that only the organic sulfur component is characterized. The measured values were corrected for atomic number, absorbance, and

fluorescence effects (ZAF corrections). The data points were treated statistically for the purpose of comparison. Analysis of variance was used to determine the variation within and among particles, and then a *t*-test was applied to set up confidence intervals centered around the sample means for single samples and for comparison between samples.

Calculations. The heating value (H.V.) recovery was calculated by:

$$\% \text{ H.V. Recovery} = \frac{(\text{wt. coal final} \times \text{H.V. final}) \times 100}{(\text{wt. coal started} \times \text{H.V. started})}$$

The sulfur content was converted from per cent to pounds per million Btu. by:

$$\text{lbs. S}/10^6 \text{ Btu.} = (\% \text{ S} \times 10^6) / [100 \times \text{H.V. (in Btu./lb.)}]$$

The values on a dry, mineral matter-free basis (dmmf) were obtained by using the modified Parr formula to calculate the mineral matter (m.m.) content:

$$\% \text{ m.m.} = 1.13 \times (\% \text{ Ash}) + 0.47 \times (\% \text{ pyritic})$$

The total sulfur (determined as sulfate) in the filtrates from the acid extractions was converted to per cent sulfur in the original dry coal by:

$$\% \text{ S coal} = \left[\text{SO}_4^{2-} \text{ (in g/l)} \times \text{Vol. (in l)} \times 32/96 \right] \times 100/\text{g coal}$$

The iron content in the filtrates was converted similarly to the coal basis.

Results and Discussion

The coals were desulfurized by leaching with a hot solution of sodium carbonate containing oxygen under pressure. The results of treating the coals under these oxydesulfurization conditions are presented in Table I. Substantial amounts of total sulfur were removed. The pyritic sulfur content was reduced greatly, and sulfate sulfur was almost completely removed. At first sight, organic sulfur was also removed, although to a lesser extent. There was also a small decrease in the heating value and a slight increase in the ash content. Because of these additional changes, the organic sulfur content was also calculated on a dry, ash-free (daf) and on a dry, mineral matter-free (dmmf) basis. The organic sulfur content, when compared on these bases, was still noticeably reduced by the oxydesulfurization treatment. The reduction in organic sulfur content amounted to about 15%, 75%, and 25% for the Lovilia/ISU, Lovilia/ROM, and Illinois No. 6 coals, respectively.

The iron content did not seem to be affected to any large extent.

To take into account the changes in heating value, the sulfur content was also calculated in terms of pounds per million Btu. The results are presented in Table II. The removal of total sulfur was still substantial, but the reduction in organic sulfur was much less, except in the case of Lovilia/ROM coal, for which it remained at about 74%.

The raw and the treated (desulfurized) coals were subjected to several extraction procedures, and the residues were analyzed for ash and total sulfur while the liquid extracts were analyzed for iron and total sulfur (as sulfate). These results, together with the weight of the samples before and after extraction, are presented in Table III. Extraction A (boiling with 2:3 HCl for 30 min.) is identical to the ASTM procedure for extracting sulfate sulfur and non-pyritic iron into the acid. The total sulfur in the residue should be related to the sum of pyritic and organic sulfur. The residue from extraction A was subjected to extraction B with boiling 1:7 HNO₃ for 30 min. The iron content in the liquid should correspond to the iron (pyritic) content determined by the ASTM procedure. The sulfur in the liquid should equal the pyritic sulfur plus any organic sulfur which may have been decomposed by the nitric acid treatment. The total sulfur in the residue should be only the remaining organic sulfur. Extraction C is a one-step extraction of the original coal with boiling 1:7 HNO₃, and the residue should be comparable to extraction B. The iron and sulfur content of the liquid from extract C should be related to the sum of the iron and sulfur content in the liquids from extractions A and B. Finally, since the ASTM procedure permits overnight extraction at room temperature to replace the 30-min. extraction at boiling temperature, extraction D was performed as a check. In this extraction, the original coal sample was stirred with 1:7 HNO₃ for 12 hr. at room temperature.

Several observations can be made about the data in Table III. Generally, the sulfur contents in the liquids from extraction A agree well with the sulfate content obtained by the ASTM analysis (see Table I). There is also fair agreement between the iron and sulfur contents of liquid C and the sum of the iron and sulfur content in liquids A and B. This implies that the hot one-step extraction with nitric acid is equivalent to the two consecutive extractions with hydrochloric and then nitric acid. The total sulfur content of residues C and of residues B are in excellent agreement and seem to confirm this.

The total sulfur values in residues C are comparable for the raw and for the desulfurized (treated) samples in the case of Lovilia/ISU and Illinois No. 6 coals. But for the Lovilia/ROM coal, this total sulfur content is significantly less for the desulfurized than for the raw coal, seemingly in agreement with data in Table II, indicating that organic sulfur is removed from this coal. However, the total sulfur content in residues B and C

Table I. Analysis of Different Coals Before and After Oxydesulfurization.^a

No.	Coal	H. V., Btu./lb.	Ash, %	Fe, %	Sulfur, %				Org. S, %(daf ^b)	Org. S, %(dmmf ^c)
					Tot.	Pyr.	Sulf.	Org.		
1	Lovilia/ISU raw	12,514	9.12	1.84	2.58	1.51	0.26	0.81	0.89	0.91
2	Lovilia/ISU treated	10,953	12.03	1.60	1.07	0.36	0.05	0.66	0.75	0.77
3	Lovilia/ROM raw	9,689	25.11	3.66	4.14	2.26	0.93	0.95	1.27	1.35
4	Lovilia/ROM treated	8,857	27.78	3.81	1.04	0.71	0.10	0.23	0.32	0.34
5	Illinois #6 raw	13,404	9.50	1.76	3.68	1.22	0.53	1.93	2.13	2.18
6	Illinois #6 treated	10,753	12.66	1.53	1.67	0.21	0.06	1.40	1.60	1.68

^aResults are averages of duplicate determinations by ASTM procedures.

^bdaf = dry, ash-free basis.

^cdmmf = dry, mineral matter-free basis.

Table II. Removal of Various Forms of Sulfur From Different Coals (Based on Heating Value).

No.	Coal	% H.V. ^a Recov.	Sulfur, lb./10 ⁶ Btu.				% S Removal		
			Tot.	Pyr.	Sulf.	Org.	Tot.	Pyr.	Org.
1	Lovilia/ISU raw	--	2.06	1.21	0.20	0.65	--	--	--
2	Lovilia/ISU treated	85.9	0.98	0.33	0.05	0.60	52.4	72.7	7.7
3	Lovilia/ROM raw	--	4.27	2.33	0.96	0.98	--	--	--
4	Lovilia/ROM treated	85.7	1.17	0.80	0.11	0.26	72.6	66.5	73.5
5	Illinois #6 raw	--	2.75	1.22	0.40	1.44	--	--	--
6	Illinois #6 treated	80.2	1.55	0.19	0.06	1.30	43.6	84.4	9.7

^a% H.V. Recovery = (wt. coal recovered x final H.V. x 100)/(wt. coal started x orig. H.V.).

Table III. Extraction of Raw and Treated Coals with 2:3 Hydrochloric Acid and/or 1:7 Nitric Acid

Acid Extraction of Coal ^a	Weight, g.		Dry Residue Analysis, %			Liq. Ext. Analysis ^b , %	
	Start	Resid.	Ash	Tot.S.	Tot.S (daf)	Tot. S	Fe
<u>1. Lovilia/ISU raw coal^c</u>			9.12	2.58	2.84	--	--
A	24.70	23.90	5.33	2.26	2.39	0.21	0.33
B	10.00	10.56	2.76	0.76	0.78	1.39	1.27
C	9.88	10.24	2.62	0.76	0.78	1.89	1.65
D	9.88	10.42	3.35	0.95	0.98	1.76	1.66
<u>2. Lovilia/ISU treated coal^c</u>			12.03	1.07	1.22	--	--
A	25.00	22.70	3.95	1.10	1.15	0.05	1.24
B	10.00	10.45	3.20	0.77	0.80	0.28	0.23
C	10.00	9.56	3.50	0.77	0.80	0.33	1.42
D	10.00	9.73	5.26	1.01	1.07	0.06	0.29
<u>3. Lovilia/ROM raw coal^c</u>			25.11	4.14	5.53	--	--
A	23.01	20.51	19.02	3.32	4.10	0.94	1.28
B	10.00	10.33	13.01	0.87	1.00	2.71	2.33
C	9.20	8.57	12.76	0.84	0.96	3.51	3.42
D	9.20	8.64	15.70	1.13	1.34	3.29	3.09
<u>4. Lovilia/ROM treated coal^c</u>			27.78	1.04	1.44	--	--
A	25.00	22.30	17.01	1.08	1.30	0.13	3.08
B	10.00	10.31	15.08	0.63	0.74	0.43	0.48
C	10.00	9.04	16.08	0.62	0.74	0.54	3.38
D	10.00	9.34	20.11	0.98	1.22	0.09	0.80
<u>5. Ill. #6 raw coal^c</u>			9.50	3.68	4.07	--	--
A	23.59	22.57	7.61	3.03	3.28	0.48	0.47
B	10.00	10.89	4.39	1.53	1.60	1.37	0.94
C	9.43	10.08	4.84	1.53	1.61	1.85	1.46
D	9.43	9.80	5.82	1.84	1.95	1.55	1.39
<u>6. Ill. #6 treated coal^c</u>			12.66	1.67	1.91	--	--
A	25.00	23.36	6.48	1.71	1.83	0.05	1.29
B	10.00	10.46	5.46	1.46	1.54	0.23	0.12
C	10.00	9.67	6.06	1.48	1.58	0.24	1.20
D	10.00	9.87	7.51	1.64	1.77	0.06	0.22

^aA = Extraction with boiling HCl; B = extraction of residue from A with boiling HNO₃; C = extraction with boiling HNO₃ only; D = extraction with HNO₃ only, but at room temperature.

^bExpressed in percent based on original dry coal.

^cSelected data of original, unextracted coal.

may not be a true measure of the organic sulfur content in the original coal. First of all, some labile organic sulfur compounds may be lost because of decomposition by the hot nitric acid. Then, the changes in the content and the properties of the ash caused by the acid make comparisons relating to the original ash difficult. Finally, the organic matrix itself may be changed significantly by the nitric acid treatment.

Extractions with only cold nitric acid produced generally different results. The total sulfur content of the residues D was higher than for extractions with boiling nitric acid. This may be caused by incomplete extraction of the inorganic sulfur or by less decomposition, if any, of the organic sulfur. The ash values were also generally higher for the cold than for the hot extractions. The iron and sulfur content of the liquids from the cold nitric acid extraction were substantially lower for the treated coals than for the raw coals. This significant difference may point to considerable changes in the mineral phases during the chemical desulfurization treatment. If any of the iron- and sulfur-containing minerals (or clays) were changed, they would apparently respond differently to extraction by acids. If the cold extraction procedure is used in the ASTM analysis, some of the pyritic iron may not be extracted from the treated (desulfurized) coals, but all of the pyritic iron would still be extracted from the raw coals. In such a case the organic sulfur content of the treated coal would be reported higher than the actual value.

Table IV presents the changes in the content of nitrogen and of iron in raw and in treated coals brought about by extraction with boiling nitric acid. In the original coal samples, the nitrogen content seemed to be unaffected and the iron content only slightly affected by the chemical desulfurization treatment. However, extraction of the raw coals with boiling nitric acid increased the nitrogen content by 3-4 fold. The increase was slightly less for the treated coals. This substantial take up of nitrogen may account for the increased weight of the residues (see Table III), even though the ash content was greatly reduced. At the present time, it is not known in what form the nitrogen is incorporated, but the presence of nitro groups ($-\text{NO}_2$) seems plausible.

The iron content of acid-extracted residues was generally 0.10% or less. The one notable exception, Lovilia/ROM coal treated and then extracted, had a higher content of iron. This may be related to the somewhat higher pyritic sulfur content of this sample (Table I), as determined by the ASTM procedure, resulting in an apparent lower organic sulfur content.

The data presented in Table V were obtained by energy-dispersive X-ray analysis using an electron microprobe. The method is based on monitoring the sulfur content of an organic maceral (in this case, vitrinite), which is not associated with any cations, as an index of the organic sulfur

Table IV. Nitrogen and Iron Content in Raw and in Treated Coals Before and After Extraction with Nitric Acid.

Coal	Extraction ^a	Ash, %	N, % ^b	Fe, % ^c
Lovilia/ISU raw	no	9.12	1.31	1.84
Lovilia/ISU treated	no	12.03	1.43	1.60
Lovilia/ISU raw	yes	2.62	4.63	0.10
Lovilia/ISU treated	yes	3.50	3.73	0.10

Lovilia/ROM raw	no	25.11	1.15	3.66
Lovilia/ROM treated	no	27.78	1.17	3.81
Lovilia/ROM raw	yes	12.76	3.74	0.02
Lovilia/ROM treated	yes	16.08	3.43	0.45

Illinois #6 raw	no	9.50	0.82	1.76
Illinois #6 treated	no	12.66	0.93	1.53
Illinois #6 raw	yes	4.84	4.26	0.03
Illinois #6 treated	yes	6.06	3.66	0.10

^aExtraction with boiling 1:7 HNO₃ for 30 min.

^bDetermined by Kjeldahl method.

^cIn unextracted coals, iron was determined by titration. In acid-extracted residues, iron was determined spectrophotometrically.

Table V. Electron Microprobe Analysis on Organic Maceral (Vitrinite) Level of Raw and Leached Coals and of Residues After Extraction by HCl and HNO₃.^a

No.	Coal or Residue After Acid Extn.	ASTM Sulfur, %			Probe S ^c , wt. %		Probe Fe, ^c wt. %	Probe Ca, ^c wt. %
		Tot. (dry)	Org. (dry)	Org. (dmmf ^b)	Dry	dmmf ^b		
1	Lovilia/ISU raw	2.58	0.81	0.91	0.74	0.83±0.34	0.13±0.10	0.09±0.07
2	Lovilia/ISU treated	1.07	0.66	0.79	0.59	0.68±0.17	0.11±0.06	0.94±0.45
3	Lovilia/ROM raw	4.14	0.95	1.35	0.68	0.96±0.24	0.14±0.06	0.08±0.05
4	Lovilia/ROM treated	1.04	0.23	0.34	0.51	0.74±0.35	0.16±0.10	1.81±0.96
5	Ill. #6 raw	3.68	1.93	2.18	1.79	2.01±0.36	0.10±0.06	0.05±0.06
6	Ill. #6 treated	1.66	1.44	1.68	1.29	1.51±0.42	0.11±0.06	0.20±0.09
7	Residue of #1	0.78	0.78 ^d	0.79	0.80	0.82±0.30	0.11±0.04	0.24±0.35
8	Residue of #2	0.76	0.76 ^d	0.79	0.68	0.70±0.41	0.45±0.55	0.49±0.63
9	Residue of #3	0.82	0.82 ^d	0.97	0.62	0.73±0.41	0.61±0.52	1.12±0.91
10	Residue of #4	0.63	0.63 ^d	0.76	0.54	0.65±0.26	0.30±0.18	0.59±0.93
11	Residue of #5	1.49	1.49 ^d	1.56	1.33	1.40±0.23	0.12±0.07	0.11±0.20
12	Residue of #6	1.45	1.45 ^d	1.55	1.55	1.65±0.47	0.34±0.13	0.05±0.06

^a Acid extraction by boiling 30 min. with 2:3 HCl followed by boiling 30 min. with 1:7 HNO₃.

^b dmmf = dry, mineral matter-free basis.

^c Probe values are statistical averages of 24 data points (except for samples, 9, 10, and 11 where n = 23, 20, and 23, respectively.)

^d Assumes that Total S in acid extracted residue equals Organic S.

content of the total coal (18). In addition, the iron and calcium contents were simultaneously measured. In most cases, two point analyses were obtained on 12 particles, and the data from the 24 measurements were compared with standards, corrected, and statistically reduced to the averages in Table V.

Because of the statistical nature of the data, the conclusions that can be drawn are expressed at the 95% confidence level. For the desulfurization experiments, the organic sulfur contents expressed as percent Probe S (dmmf) are compared. The percent sulfur content is between 0.04 and 0.34 lower for sample 2 than for sample 1 and between 0.28 and 0.72 lower for sample 6 than for sample 5. Thus desulfurization of organic sulfur is corroborated for the Lovilia/ISU and the Illinois No. 6 coals with average reductions in the percent sulfur content of 0.19 and 0.50, respectively. The difference in the percent organic sulfur content between samples 3 and 4, however, is not significant at the 95% confidence level. Thus, demonstration of organic sulfur removal from Lovilia/ROM is not possible by this method. These conclusions are quite different from the ones that can be drawn from Tables I and II, in which Lovilia/ROM coal seems to lose the most organic sulfur.

The sulfur data on the residues from acid extractions reflect considerable scatter, and no significant correlations can be made between the samples on this basis.

The calcium data on the residues from acid extractions also do not provide any significant correlation. However, the calcium data on the raw and treated coals point to an unusual correlation. Coals which have been oxydesulfurized by leaching with sodium carbonate solution tend to pick up calcium which is associated with the organic matrix. For example, at the 95% confidence level, the percent calcium content is higher by an average 0.85, 1.73, and 0.15 for samples 2, 4, and 6, respectively, than for samples 1, 3, and 5, respectively. It is not known how the calcium is associated with the organic matrix, although presumably it could be an ion exchange phenomenon in which Ca^{++} ions are chelated by carboxylic, phenolic, or other groups.

The electron microprobe data for iron on the organic maceral level are also quite variable. In general, however, there appears to be no significant difference in the iron content between samples 1 and 2, 3 and 4, and 5 and 6. This is reasonable since the desulfurization procedure converts insoluble iron pyrite to insoluble hematite (22, 23). The iron content of the residues from the acid extractions, on the other hand, may be slightly higher than for the corresponding coal samples. The iron may be present in finely dispersed microcrystalline phases (24). Although the scatter of the data is substantial, there is a suggestion, at least for the Lovilia/ISU and the Illinois No. 6 coals, that more iron may be present in the acid extraction residues of the desulfurized (treated) coals than those of the

raw coals. This implies that the organic sulfur levels of these treated coals may be actually lower than the values obtained by the ASTM procedures.

Conclusions

The treatment of three different coals by leaching with a hot solution of sodium carbonate containing dissolved oxygen under pressure (the Ames process) resulted in significant reduction of total sulfur. While the removal of the inorganic (pyritic plus sulfate) sulfur was obvious, the amount of the organic sulfur removed was subjected to more rigorous analysis.

The removal of organic sulfur could be given quite different values, depending on the method chosen for comparison of the organic sulfur levels in the raw and in the treated coals. In addition, the degree of removal of organic sulfur can be subject to influences arising from the analytical methodology, especially for the processed coals.

Thus, on the basis of ASTM analyses, significant reductions in organic sulfur were achieved for Lovilia/ISU and Illinois No. 6 coals and a very large reduction for Lovilia/ROM coal. These observations on the reductions apply regardless of the manner (dry, dry ash-free, or dry mineral matter-free) of expression for the organic sulfur content. When the comparison is based on the weight of sulfur per unit heating value, the removal of organic sulfur becomes modest for the Lovilia/ISU and Illinois No. 6 coals but remains still large for the Lovilia/ROM coal.

This decrease in the organic sulfur content of the Lovilia/ROM coal was corroborated by a series of extraction experiments employing ASTM procedures and other analyses for sulfur and iron. The removal of organic sulfur from the other two coals could not be confirmed by this method. However, the different extraction procedures pointed to possible changes in the mineral components and in the organic matrix itself of the coals after the chemical desulfurization treatment. Such changes can affect the analytical values obtained by ASTM procedures.

Another method of assessing the organic sulfur content was provided by the electron microprobe data. A significant reduction in the organic sulfur content was demonstrated, at the 95% confidence level, for the Lovilia/ISU and Illinois No. 6 coals but not for the Lovilia/ROM coal. These results are in contrast to the conclusions drawn on the basis of the wet chemical experiments described above.

In addition, the electron microprobe data indicated an unusual but noticeable build up of calcium associated with the organic matter of the desulfurized coal. This increase in calcium may have implications for subsequent control of sulfur emission during the combustion of the desulfurized coal. It was also shown that extractions with cold nitric acid can be affected by changes in the mineral matter content caused by the chemical

desulfurization treatment. Furthermore, coal samples extracted with nitric acid have a significantly larger nitrogen content.

Thus the difficulties in evaluating the removal of organic sulfur from coal are not only due to differences in characteristics from coal to coal, sample heterogeneity, or fluctuations in the treatment. The variations in the organic sulfur content may also stem from analytical problems which are especially likely with coals that have been altered during the chemical desulfurization treatment. This points to a need for a method of determination of organic sulfur that is direct, applicable to raw as well as chemically treated coals, and employable on a routine basis.

Acknowledgement

Ames Laboratory is operated for the U. S. Department of Energy by Iowa State University under Contract No. W-7405-Eng-82. This work was supported by the Assistant Secretary for Fossil Energy, Office of Mining, WPAS-AA-75-05-05 and WPAS-AA-75-05-15.

Literature Cited

1. Wheelock, T. D., ed.; "Coal Desulfurization: Chemical and Physical Methods," (ACS Symp. Series No. 64); American Chemical Society: Washington, D. C., 1977.
2. Meyers, R. A. "Coal Desulfurization"; Marcel Dekker, Inc.: New York, 1977.
3. Wheelock, T. D.; Markuszewski, R. In "Chemistry and Physics of Coal Utilization - 1980," (AIP Conf. Proc. Series No. 70); Cooper, B. R.; Petrakis, L., eds.; American Institute of Physics: New York, 1981, pp. 357-387.
4. Markuszewski, R.; Chuang, K.-C.; Wheelock, T. D., "Proceedings of Symposium on Coal Cleaning to Achieve Energy and Environmental Goals (Sept. 1978, Hollywood, FL)," Vol. II; EPA-600/7-79-098b; April 1979, pp. 1039-63.
5. Wheelock, T. D.; Greer, R. T.; Markuszewski, R.; Fisher, R.W. "Advanced Development of Fine Coal Desulfurization and Recovery Technology," (Annual Technical Progress Report, Oct. 1977-Sept. 1978); IS-4688; Iowa State University: Ames, IA, April 1979.
6. Wheelock, T. D.; Markuszewski, R. "Fossil Energy Quarterly Report, Oct. 9, 1979 - Dec. 31, 1979," IS-4730; Iowa State University: Ames, IA, Feb. 1980, pp. 1-56.
7. American Society for Testing and Materials, "Annual Book of ASTM Standards," Part 26; Method D2492; Philadelphia, PA, 1975.
8. Given, P. H.; Miller, R. N. *Fuel* 1978, 57, 380-1.
9. Hamersma, J. W.; Kraft, M. L. "Coal Sulfur Measurements," (Interagency Energy/Environment R & D Program Report); EPA-600/7-79-150; July 1979

10. Kuhn, J. K. In "Coal Desulfurization: Chemical and Physical Methods," (ACS Symp. Series No. 64); Wheelock, T. D., ed.; American Chemical Society: Washington, D. C., 1977, pp. 16-21.
11. Gladfelter, W. L.; Dickerhoof, D. W. Fuel 1976, 55, 355-9.
12. Chakrabarti, J. N. In "Analytical Methods for Coal and Coal Products," Vol. I; Karr, C., ed.; Academic Press: New York, 1978, pp. 280-322.
13. Markuszewski, R.; Wheelock, T. D. Presented at 2nd Chemical Congress of North American Continent: Las Vegas, NV, Aug. 24-9, 1980.
14. Raymond, R.; Gooley, R. In "Scanning Electron Microscopy/1980," Vol. I; Johari, O. ed.; (SEM Inc.: Chicago, IL, 1978, pp. 93-107.
15. Solomon, P. R.; Manzione, A. V. Fuel 1977, 56, 393-6.
16. Attar, A. In "Analytical Methods for Coal and Coal Products," Vol. III; Karr, D., ed.; Academic Press: New York, 1979, pp. 585-624.
17. Paris, B. In "Coal Desulfurization: Chemical and Physical Methods," (ACS Symp. Series No. 64); Wheelock, T. D., ed.; American Chemical Society: Washington, D. C., 1977, pp. 22-31.
18. Greer, R. T. "Fossil Energy Annual Report, Oct. 1, 1978 - Sept. 30, 1979," IS-4714; Iowa State University: Ames, IA, Jan. 1980, pp. C1-C60.
19. Greer, R. T. In "Scanning Electron Microscopy/1979," Vol. I; Johari, O., ed.; SEM Inc.: Chicago, IL, 1979, pp. 477-85.
20. Stookey, L. L. Anal. Chem. 1970, 42, 779.
21. Fritz, J. S.; Yamamura, S. S.; Richard M. J. Anal. Chem. 1957, 29, 158-61.
22. Greer, R. T.; Markuszewski, R.; Wheelock, T. D. In "Scanning Electron Microscopy/1980," Vol. I; Johari, O., ed.; SEM Inc.: Chicago, IL, 1980, pp. 541-50.
23. Chuang, K.-C.; Chen, M.-C.; Greer, R. T.; Markuszewski, R.; Sun, Y.; Wheelock, T. D. Chem. Eng. Commun. 1980, 7, (1-3), pp. 79-94.
24. Greer, R. T. In "Scanning Electron Microscopy/1978," Vol. I; Johari, O., ed.; SEM Inc.: Chicago, IL, 1978, pp. 621-6 and p. 610.

RECEIVED May 27, 1981.

Thermal Oxidative Degradation of Coal as a Route to Sulfur Functionality: An Initial Study

ROBERT B. LACOUNT, DOUGLAS K. GAPEN, WINSON P. KING,
DAVID A. DELL, FRED W. SIMPSON, and CHARLES A. HELMS

Chemistry and Physics Department, Waynesburg College, Waynesburg, PA 15370

Chemical coal desulfurization research has flourished during the past ten years. Numerous precombustion chemical beneficiation routes have been pursued that remove the inorganic sulfur (pyritic and sulfate) and some of the organic sulfur in coal. Recently Wheelock (1) reported on the status of chemical coal cleaning processes and Warzinski (2) summarized the Pittsburgh Energy Technology Center's (PETC) air-water oxydesulfurization work and referenced numerous other coal beneficiation methods.

Chemical coal desulfurization methods remove most of the inorganic sulfur and a portion of the organic sulfur. Obviously, a method to distinguish among the organic sulfur functional groups or some "type" classification of the organic sulfur present in untreated and/or treated coals would be an asset to those involved in coal desulfurization research. The predictive value of such a method should also be useful to those involved in selecting coals that will be most improved by beneficiation methods.

The present work was prompted by our observation of partial removal of organic sulfur in the PETC oxydesulfurization method (3). For a number of coals most of the inorganic sulfur and up to 40 percent of the organic sulfur was removed; however, the remaining organic sulfur is not as easily removed as the initial 20 to 40 percent. In an effort to understand better the susceptibility of organic sulfur to oxydesulfurization, we began thermal oxidative degradation of sulfur (TODS) in coal experiments. This report presents a description of this experimental method and our initial results for several coals. Diluted coal samples subjected simultaneously to an oxygen treatment and a linear increase in temperature evolve sulfur dioxide intermittantly as a function of temperature. Distinctive sulfur dioxide evolution patterns are observed among coals of different rank and between raw and treated coals. These results are discussed relative to an eventual classification of the organic sulfur forms present in the original coal.

0097-6156/81/0169-0415\$05.00/0
© 1981 American Chemical Society

Juntgen and VanHeek (4) recently summarized much of the German work on non-isothermal kinetics of gas formation in coal pyrolysis. Yergey et al. (5) applied non-isothermal kinetic methods to the hydrodesulfurization of coal. By monitoring the hydrogen sulfide evolved with a linearly increasing temperature, they described five different types of hydrogen-induced sulfur release. Attar (6,7) recently reviewed the literature for both the analysis of sulfur in coal and the distribution of organic sulfur functional groups in coal. Additionally, Attar (7,8) described a non-isothermal kinetic method for estimation of the organic sulfur containing functional groups in coal under reducing conditions. Each different sulfur functional group appears to reduce and evolve hydrogen sulfide over a specific temperature range. The method has enabled Attar to distinguish between thiolic, thiophenolic, aliphatic sulfide, aryl sulfide, and thiophenic sulfur in a number of coals.

Numerous thermal oxidation studies have been performed in an effort to understand better the coal-oxygen reaction and as a route to coal desulfurization. Sinha and Walker (9,10) studied the desulfurization of coals by air oxidation at several different temperatures. Merrill (11) studied the coal-oxygen reaction near the ignition temperature and Chamberlain et al. (12) studied the gases evolved in low-temperature oxidation of coal. Huang and Pulsifer (13) studied coal desulfurization during treatment with a variety of gases including an oxygen-nitrogen mixture. Paris (14) utilized a low-temperature reaction of ionized oxygen species for a direct determination of organic sulfur in raw coal; the sulfur was oxidized to SO_x which was collected and analyzed at the end of the reaction. Dryden (15) summarized much of the earlier coal oxidation work.

Experimental

A diagram of the thermal oxidative degradation apparatus used in this study is shown in Figure 1. Oxygen, at flow rates ranging from 5 to 50 ml/min (normally 8 ml/min) was passed through -200 mesh coal samples (undiluted or thoroughly mixed with a diluent) placed on ceramic wool near the center of a 0.8 cm (i.d.) x 35 cm vertical Vycor combustion tube. A two centimeter column of granular anhydrous magnesium perchlorate was positioned on ceramic wool one centimeter above the bottom of the combustion tube. This was sufficient to remove water of combustion from the gas stream.

A modified Coleman Model 33 Carbon-Hydrogen Analyzer was used to control the oxygen flow rate, to pretreat the oxygen (anhydrous magnesium perchlorate and anhydrous lithium hydroxide) and to hold the combustion tube in position. The analyzers' furnace was controlled by a Fisher Model 360 Linear Temperature Programmer. The rate of temperature increase was variable from 0.5 to 25 °C per minute. Normally, the temperature programmer

was used to increase the reaction temperature from 20 to $>990^{\circ}\text{C}$ at a rate of 5°C per minute. The temperature measurements reported were normally taken with a thermocouple external to the combustion tube. These observed temperatures can be related to the internal temperatures through a calibration curve constructed for each program rate using an internal thermocouple.

The exit gas stream flowed through one-eighth inch teflon tubing to a flowcell (0.8 cm (i.d.) x 7.8 cm) contained in a Beckman Instruments Microspec infrared spectrophotometer. The spectrophotometer was used to continuously monitor and record the sulfur dioxide absorption at 1350 cm^{-1} . Occasionally the instrument was used to continuously monitor the carbon dioxide absorption at 2320 cm^{-1} . The use of a single wavelength as a basis for identification of a specific substance can be misleading. Accordingly, gas samples were collected periodically from the flowcell exit port for a complete infrared spectrum and for mass spectral analysis. The dead volume between furnace and flowcell is responsible for a short time delay in analysis of the gas stream at any given rate of flow. A time correction was applied to compensate for this effect.

The diluents used in these reactions must be carefully tested to assure that they do not absorb and/or evolve sulfur dioxide over the temperature range used. All potential diluents were placed in the combustion tube and subjected to a flow of 0.52 percent sulfur dioxide in air over the entire temperature range utilized (20 to $>990^{\circ}\text{C}$) in the TODS procedure. The exit gas stream was continuously monitored for sulfur dioxide by infrared spectroscopy. The concentration of sulfur dioxide was adjusted to obtain a 50 percent transmittance reading on the infrared spectrometer. Only those materials showing little or no deviation from 50 percent transmittance over the entire temperature range were considered as diluents. Tungsten trioxide, zirconium dioxide, celite, and several silica preparations showed only very slight absorption of sulfur dioxide, and then only at temperatures greater than 650°C . While this absorption may cause some problem in future quantitative work, it should not be a factor in the present qualitative study.

Mass spectral analysis of the samples at several different temperatures show the exit gas stream to contain in addition to oxygen: carbon dioxide, carbon monoxide, sulfur dioxide, and some carbonyl sulfide. The primary sulfur containing gas in the stream is sulfur dioxide (~1%); however, a small amount of carbonyl sulfide (~0.1%) appears to be present. For any quantitative work it will be necessary to monitor the carbonyl sulfide or to optimize reaction conditions and/or add a secondary oxidation stage to decrease its concentration to a negligible level. It should be noted that mass spectral analysis of the exit gas during the sulfur dioxide peaks gave no evidence for the presence of gaseous hydrocarbons or sulfur trioxide.

A typical experiment consists of thoroughly mixing 200 mg of

-200 mesh coal with 1.0 g of tungsten trioxide (WO_3) and positioning this sample on ceramic wool in the combustion tube at thermocouple level. A 2 cm column of magnesium perchlorate is positioned on ceramic wool 1 cm from the bottom of the combustion tube (cold zone). An oxygen flow of 8 ml/min is established and the temperature is programmed from 20 to $>990^\circ C$ at a rate of $5^\circ C$ per minute.

Results and Discussion

Under the experimental conditions noted above sulfur dioxide is evolved, intermittently, as a function of temperature and distinctive patterns of evolution arise when one compares a given coal before and after chemical desulfurization treatment or when one compares raw coals of different ranks.

Figure 2 provides a record of the infrared intensity at 1350 cm^{-1} of sulfur dioxide with increasing temperature for Indiana coal with and without a diluent. A low flow rate of oxygen was necessary to avoid direct combustion (flashing) of the undiluted coal sample. This sample shows intense sulfur dioxide evolution over a rather short range (exotherm) followed by rather weak evolution at higher temperatures. In contrast, coal samples diluted with tungsten trioxide or other diluents to reduce the exothermic behavior show a more complex sulfur dioxide evolution curve.

Figures 3, 4, and 5 show the results of experiments on untreated and oxydesulfurized samples of a bituminous coal, a subbituminous coal, and a lignite. If one compares each untreated and oxydesulfurized case, distinct differences are readily apparent. Figure 3 shows strong sulfur dioxide evolution in the oxydesulfurized case and reference to Table I verifies that although the pyritic and sulfate sulfur have been removed from the starting coal, the organic sulfur remains intact. Oxydesulfurization of the Montana subbituminous coal (Figure 4) removed nearly all of the sulfate and over 75 percent of the pyritic sulfur but none of the organic sulfur. The strong evolution of sulfur dioxide present in the untreated coal from $330\text{--}380^\circ C$, but absent in the oxydesulfurized coal, should correspond to the pyritic sulfur removed. Similarly, the analysis of oxydesulfurized lignite (Table I) shows the sulfur remaining in the coal to be mainly organic and pyritic. These sulfur dioxide evolutions must be overlapping in the $225\text{--}340^\circ C$ range.

For several coals, the carbon dioxide evolved during a TODS treatment has been continuously monitored by infrared spectroscopy. Under these conditions, strong carbon dioxide evolution begins at about $200^\circ C$ and continues intermittently until $650^\circ C$. Thus, the sulfur dioxide evolution at temperatures greater than $650^\circ C$ in Figures 3, 4, and 5 we attribute to the decomposition of inorganic sulfates. When coal pyrite is

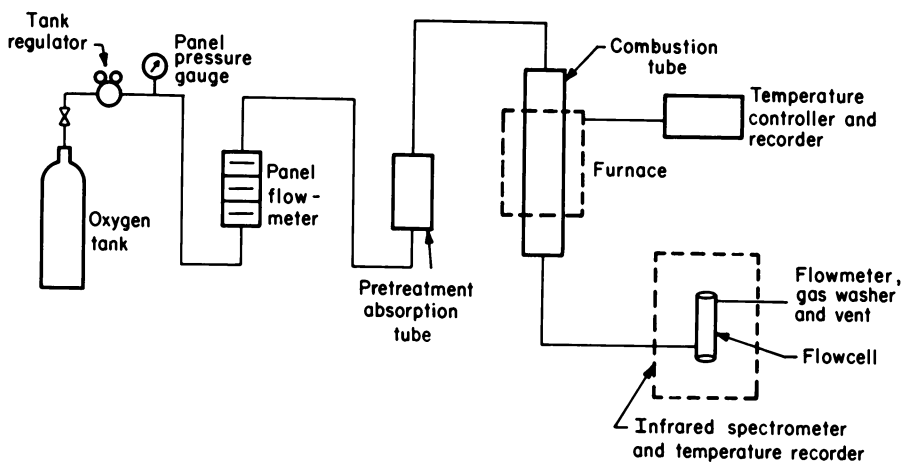


Figure 1. Thermal oxidative degradation apparatus

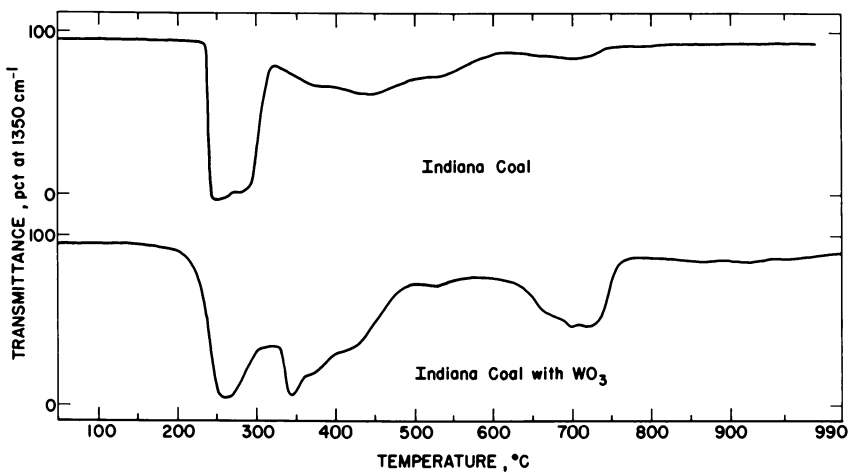


Figure 2. Thermal oxidative degradation of untreated Indiana Minshall Seam (HvCb) coal with and without a diluent

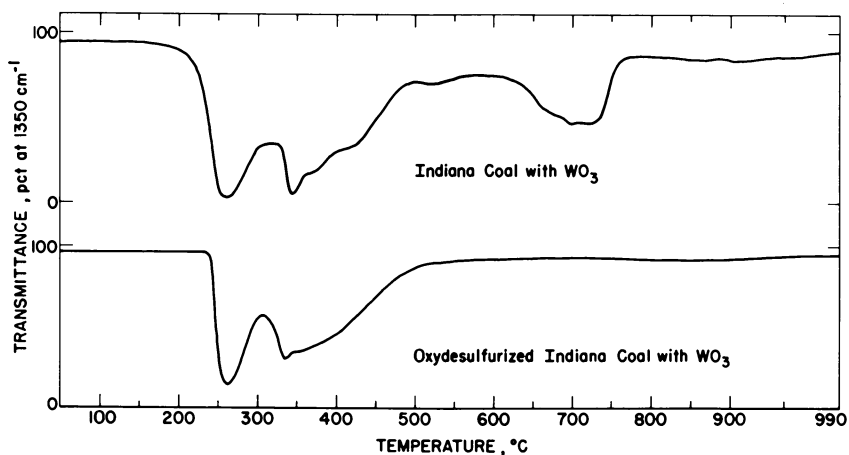


Figure 3. Thermal oxidative degradation of untreated and oxydesulfurized Indiana Minshall Seam (HvCb) coal with diluent

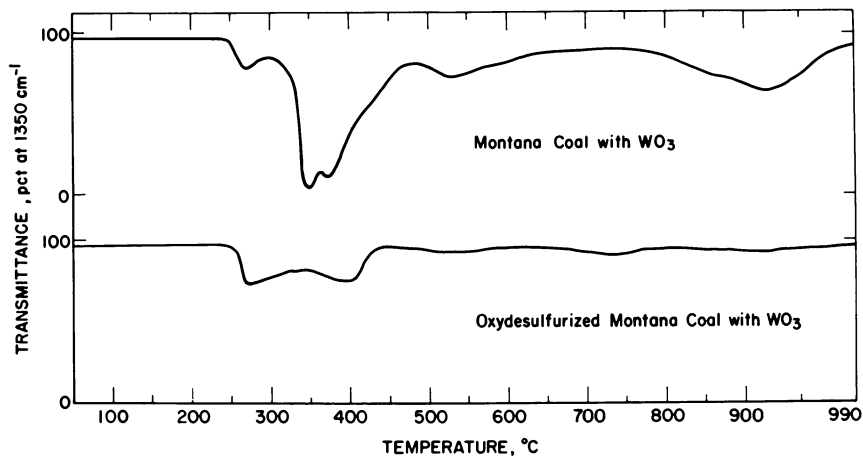


Figure 4. Thermal oxidative degradation of untreated and oxydesulfurized Montana Rosebud Seam (Sub B) coal with diluent

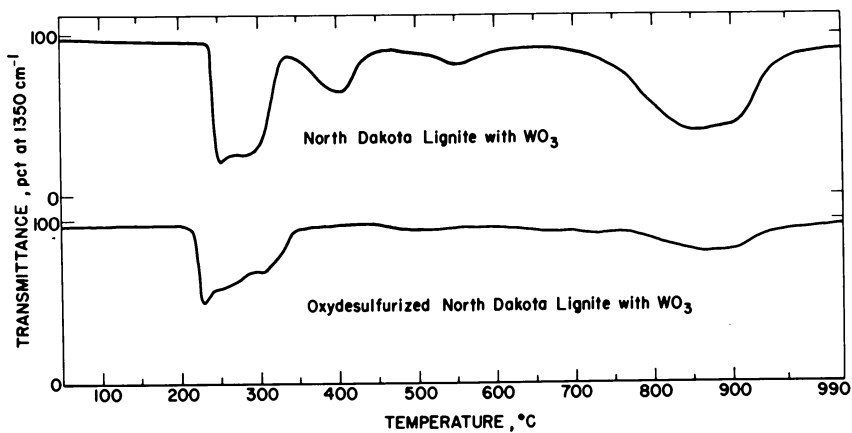


Figure 5. Thermal oxidative degradation of untreated and oxydesulfurized North Dakota lignite with diluent

Table I. Coals Subjected to Thermal Oxidative Degradation of Sulfur

Coal Seam	State	ASTM Rank	Moisture Free Weight Percent							
			Total Sulfur		Sulfate		Pyritic		Organic	
			Untr. ¹	Tr. ²	Untr.	Tr.	Untr.	Tr.	Untr.	Tr.
Minshall	IN	HvCb	6.3	2.5	2.6	0.0	1.7	0.2	2.0	2.3
Rosebud	MT	SbB	3.1	1.1	0.3	0.0	2.3	0.5	0.5	0.6
Beulah	ND	SbB ³	2.8	1.1	0.8	0.1	1.1	0.3	0.9	0.7
Pittsburgh	OH	HvAb	3.6	1.0	0.5	0.2	2.1	0.2	1.0	0.6
Upper Freeport	PA	MvB	1.6	0.6	0.2	0.0	0.8	0.1	0.6	0.5

1. Untreated

2. Treated (Oxydesulfurized coals that showed little or no change in organic sulfur were selected.)

3. This lignite has a calorific value consistent with ASTM subbituminous B coal.

L-81124

subjected to a treatment, sulfur dioxide evolution maxima at 515° C and at 640° C are observed. However, if this same pyrite is mixed with oxydesulfurized Montana Rosebud seam coal, the evolution from 250-380° C is simply enhanced. Thus, extreme care must be taken in any "assignment" of peaks to a particular type or amount of sulfur. It is quite possible that mineral matter or the carbon matrix of the coals could cause changes in (1) peak intensities by absorption of sulfur dioxide and (2) peak positions by exerting a catalytic effect.

With these uncertainties clearly in mind, one may draw a few tentative conclusions from the sulfur dioxide evolution temperatures (Table II) of the organic and inorganic substances that have been subjected to TODS experiments. Rubber, (1), known to contain alkyl sulfide and disulfide bonds exhibits a sulfur dioxide evolution maximum at 230° C. Aryl sulfides (2,3) and a condensed thiophenic system (4) show sulfur dioxide evolution maxima at 455-460° C. The inorganic sulfates (6,7,8,9, and 10) show evolution beyond 600° C. We tentatively believe that, (1) a portion of the sulfur dioxide in the 225-300° C range is due to alkyl sulfides, (2) aryl sulfides and thiophenic compounds undergo oxidative degradation in the 450° C range, (3) most of the sulfur dioxide evolution above 650° C arises from decomposition of inorganic sulfates, or other sulfur containing structures present in the mineral matter, and (4) sulfur dioxide evolution due to pyrite decomposition may give definite peaks, or broaden and enhance other sulfur dioxide absorption in the 250-380° C range. It may become necessary to remove pyritic sulfur before any attempt to distinguish among organic sulfur types. Obviously much additional work utilizing high molecular weight model systems containing sulfur of known functionality is needed before any sulfur in coal classification is attempted.

We recognized at least two potential difficulties with this oxidative degradation procedure: (1) Mass transfer can serve to broaden the observed sulfur dioxide evolution as compared with the undiluted coal. (2) At the low flow rates utilized, variation in the exit flow rate as the degradation proceeds could cause a broad sulfur dioxide evolution to appear as peaks. Results of the two experiments described below indicate to our satisfaction that these potential problems, if present, do not interfere with our interpretation.

To assure that we in fact are noting discrete peaks due to enhanced sulfur dioxide evolution and not simply flow changes superimposed on a broad sulfur dioxide evolution, the temperature of a TODS experiment was programmed (5° C/min) to 250° C and then held constant as the first sulfur dioxide peak emerged. After isothermal operation at 250° C for over two hours during which the sulfur dioxide evolution ceased, the system was cooled to room temperature and reprogrammed (5° C/min) up to 990° C. The result of this experiment on the oxydesulfurized Minshall seam coal is shown in Figure 6. The first peak (250° C) was complete

Table II. Thermal Oxidative Degradation of Organic and Inorganic Systems

Number	Substance	Temperature of Absorption Maximum (°C)
1	Rubber	230
2	Poly (phenylenesulfide)	455
3	3,3'-Thiobis - (7H-benz[de]anthracen-7-one)	460
4	Diacenaphtho [1,2-b:1',2'-d] thiophene	460
5	Coal Pyrite	515 strong 640 weak
6	Coal Pyrite (with Montana Rosebud Oxydesulfurized Coal)	250-380
7	FeSO ₄	600-730
8	Fe ₂ (SO ₄) ₃	600-730
9	Al ₂ (SO ₄) ₃	710-890
10	CaSO ₄	790-990
11	Na ₂ SO ₄	770-940

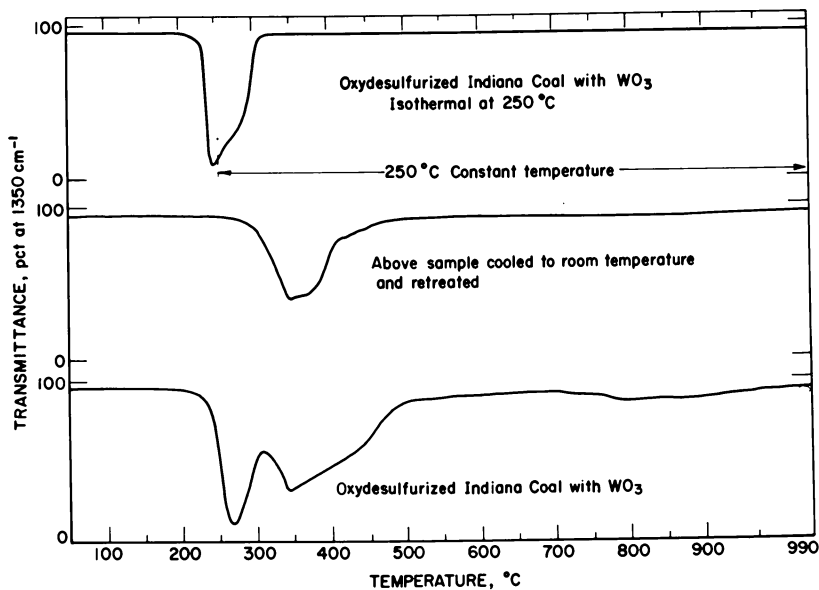


Figure 6. Comparison of a normal thermal oxidative degradation with an alternate programmed-isothermal treatment for oxydesulfurized Indiana Minshall Seam (HvCb) coal

after fifteen minutes. The shoulder on this peak is due to an observed decrease in the exit gas stream flow rate probably because oxygen is being absorbed by the carbon matrix. Another sulfur dioxide evolution maximum occurred at a temperature of 360° C as the system was programmed to 990° C. This experiment indicates to us that at least two types of organic sulfur appear to be present in this coal. No further isothermal operation was attempted with this coal, although alternate programmed-isothermal operation is planned in an attempt to improve the resolution of the observed peaks.

A second experiment involved the use of air at a flow rate of 30 ml/min compared to the typical 8 ml/min of pure oxygen. Experiments utilizing pure oxygen were restricted to low flow rates, usually 8ml/min. At a flow rate of 30 ml/min oxygen, oxidation is rapid (exotherm) and no further carbon dioxide or sulfur dioxide is observed after a programmed temperature of 275° C. To minimize variation in the exit gas flow rate and to maintain a gradual oxidation, air has been utilized at a flow rate of 30 ml/min. At this flow rate the exit gas stream showed little variation in flow and the peaks, although less intense, exhibited shape, position, and resolution comparable to those obtained by using oxygen. This experiment indicates to us that the observed peaks are not artifacts due to change in flow rate of the exit gas stream. Figure 7 compares oxygen (8 ml/min) and air (30 ml/min) TODS experiments for the oxydesulfurized Indiana Minshall seam coal. In future work, the complete range of oxygen-inert gas compositions will be explored.

Conclusions

At this time, the thermal oxidative degradation of coal appears to hold promise as an oxidation route for at least some broad distinctions among the organic sulfur forms in coal. Additionally, application of the method for a direct determination of organic sulfur in coal is under investigation. Although we remain very skeptical of this and other approaches as a meaningful quantitative route to sulfur functionality in coal, reproducible differences among coals of different rank and between raw and treated coals are present. We are continuing work to complete: (1) optimization of experimental parameters for best peak resolution; (2) quantization of results followed by particle size studies; (3) synthesis of additional model organic systems, each incorporating a different sulfur functionality and; (4) further screening of diluents and/or catalysts. This work is now continuing on a full time basis through a temporary appointment for one of the authors at the Pittsburgh Energy Technology Center.

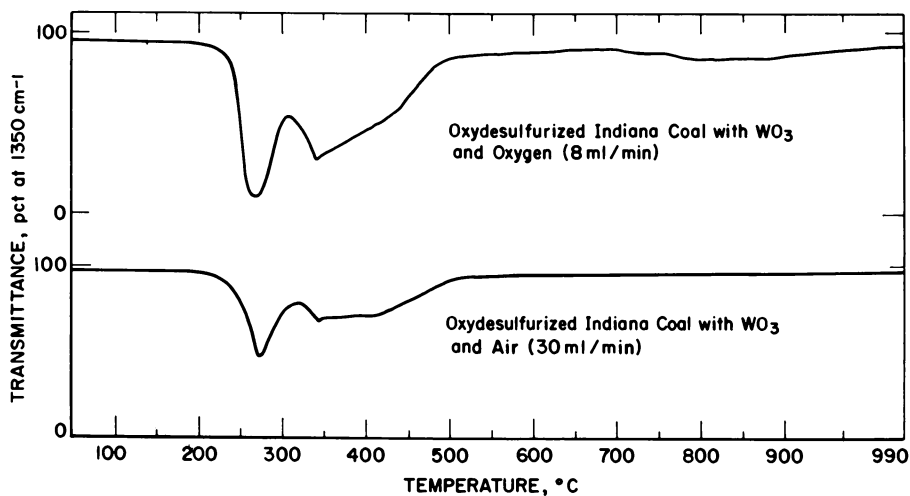


Figure 7. Comparison of the thermal oxidative degradation of oxydesulfurized Indiana Minshall Seam (HvCb) coal in oxygen and air

Acknowledgements

The authors express appreciation to Sidney Friedman and Robert Warzinski of the Pittsburgh Energy Technology Center's Process Sciences Division for samples of raw and oxydesulfurized coals and for discussions during the course of the work. The authors gratefully acknowledge the help of Charles Schmidt and Anthony Logar of the Pittsburgh Energy Technology Center's Analytical Chemistry Division for mass spectral analyses. The authors wish to thank Waynesburg College for support of this work through a Faculty Research Grant.

Literature Cited

1. Wheelock, T.D., "Status of Chemical Coal Cleaning Processes, " Fifth International Coal Research Conference, Dusseldorf, Germany., Sept. 1-5, 1980.
2. Warzinski, R.P., Friedman, S., Ruether, J.A., LaCount, R.B., "Air/Water Oxydesulfurization of Coal-Laboratory Investigation," DOE/PETC/ TR-80/6, Aug., 1980, 113 pages.
3. Friedman, S., LaCount, R.B., Warzinski, R.P., "Oxidative Desulfurization of Coal," Coal Desulfurization-Chemical and Physical Methods, ACS Symp. Series, 64, (1977) 164-172.
4. Juntgen, H., VanHeek, K.H., Fuel Processing Technology, (1979) 2, 261-293.
5. Yergy, A.L., Lampe, F.W., Vestal, M.L., Day, A.G., Fergusson, G.L., Johnston, W.H., Snyderman, J.S., Essenhigh, R.H. Hudson, J.E., IEC Proc. Res. Dev. (1974) 13, 233-240.
6. Attar, A., Corcoran, W.H., IEC Prod. Res. Dev., (1977) 16, 2, 168-170.
7. Attar, A., "Sulfur Groups in Coal and Their Transformations" Analytical Methods for Coal and Coal Products, Vol. 3 (1979) 585-625.
8. Attar, A., Dupuis, F. (1978a) Prepr. Div. Fuel Chem., Am. Chem. Soc. 23(1) 214-227.
9. Sinha, R.K., Walker, P.L., Jr., Fuel (1972) 51, 125-129.
10. Sinha, R.K., Walker, P.L., Jr., Fuel (1972) 51, 329-331.
11. Merrill, L.S., Jr., Fuel (1973) 52, 61-65.
12. Chamberlin, E.A.C., Barrass, G., Thirlaway, J.T., Fuel (1976) 55, 217-223.
13. Huang, E.T.K., Pulsifer, A.H., "Coal Desulfurization during Gaseous Treatment" Coal Desulfurization-Chemical and Physical Methods, ACS Symp. Series, 64, (1977) 290-303.
14. Paris, B., "Direct Determination of Organic Sulfur in Raw Coals," Coal Desulfurization-Chemical and Physical Methods, ACS Symp. Series, 64, (1977) 22-31.
15. Dryden, I.G.C., "Chemical Constitution and Reactions of Coal," Chem. Coal Util. Suppl. Vol. (1963) 272-289.

RECEIVED May 5, 1981.

Resource Development in the Analytical Chemistry of Sulfur Compounds for the New Coal Conversion Technologies

JOSEPH JORDAN, S. J. ANKABRANDT, A. ROBBAT¹,
and J. D. STUTTS

Department of Chemistry, 152 Davey Laboratory, The Pennsylvania State
University, University Park, PA 16802

A new comprehensive approach has been developed for the instrumental analysis of sulfur contaminants in coal gasification or liquefaction products and process streams. This is an ongoing effort. Predictive algorithms are described for computing stability domains of various sulfur moieties as function of pH, redox potential and temperature. Account was taken of the fact that certain reactions were "blocked" by sluggish kinetics, while others attained thermodynamic equilibrium. The relative abundance of all significant sulfur compounds was successfully estimated in this manner within 15% of the total sulfur present in a given process stream. Based on judicious fundamental considerations, electrochemical and thermochemical methods have been developed for the more accurate determination of important sulfur compounds, including inorganic moieties, such as H_2S , HS^- , $\text{S}^=$ (and corresponding polysulfide species), SO_2 , HSO_3^- , SO_3^- , S_2O_3^- and organosulfur heterocycles such as benzothiophene and dibenzothiophene. In this context, specific applications of differential pulse voltammetry and of "enthalpimetric analysis" are discussed. The latter involves monitoring heats of reaction by adiabatic calorimetry in dilute solutions.

Control of sulfur contamination has been recognized as crucially important in the future coal based energy technologies (1). Classical methods of chemical analysis are available for the determination of total sulfur, sulfate, sulfite, thiosulfate and sulfide. The development of a comprehensive and dependable capability for monitoring sulfur compounds by modern instrumental methods is overdue. The inorganic chemistry of sulfur is remarkably diverse (2) because of the numerous oxidation states of the element ranging from -2 (e.g., in sulfide) to +7 (persulfate). Furthermore, in a given oxidation state sulfur is capable of coexisting in the form of conjugate Bronsted acids and bases, such as SO_2 , bisulfite and sulfite. Chances are that many of the various known sulfur moieties may occur in some of the coal

¹ Current address: Department of Chemistry, Tufts University, Medford, MA 02155.

0097-6156/81/0169-0427\$05.00/0
© 1981 American Chemical Society

conversion (gasification and liquefaction) processes that are currently being developed (and/or will be developed in the future). In view of this situation, we have embarked on a systematic program, which has a two-pronged objective:

- (a) to predict from thermodynamic and kinetic considerations which inorganic sulfur moieties are likely to be present;
- (b) to develop selective and accurate instrumental methods of quantitative analysis for the determination of significant sulfur contaminants.

Results are presented and discussed in this paper outlining procedures for estimating mole fractional abundances of specified sulfur compounds from two readily feasible measurements, viz., pH and redox potential. Voltammetric and/or enthalpimetric (calorimetric) methods are described for the determination of several important inorganic sulfur compounds, as well as for the quantitation of the sulfur heterocycle dibenzothiophene in coal liquefaction products. These new approaches transcend classical capabilities (3-6), are based on quantitative theoretical correlations and are amenable to in-plant process control.

Thermodynamic Predictions, Pourbaix Diagrams and Algorithms

Quite generally, equilibrium concentrations of sulfur moieties in aqueous solution can be computed from thermodynamic data, provided the total sulfur concentration is known. Eighteen years ago (7), Marcel Pourbaix published a classical Atlas of Electrochemical Equilibria. It contained numerous so-called "Pourbaix Diagrams," outlining--in a plane of Cartesian coordinates of redox potential versus pH--boundary lines corresponding to equimolefractional distributions between compounds of a given element, which were related to each other by Bronsted acid-base and/or oxidation-reduction equilibria. In Table I, we have listed thirty-one such sulfur moieties for which appropriate thermodynamic data are available (8,9) for computing relative molefractional abundances. Figure 1 is a corresponding tridimensional representation of log (sulfur molefraction) versus redox potential and pH. It is apparent that appropriate horizontal cross-sections of such tridimensional generalized Pourbaix Diagrams can yield the conventional two-dimensional Pourbaix Diagrams. However, it is obviously desirable to take into account a fourth important variable, viz., temperature. To accomplish this, we have developed algorithms and computer programs (8-12) which have the capability of evaluating for each and every sulfur moiety an appropriate molar distribution coefficient (MDC) of sulfur, defined by Equation 1:

$$(\text{MDC})_i \equiv \frac{q_i C_i}{\sum_k q_k \cdot C_k} \quad (1)$$

Table I

Sulfur Moieties for Which Thermodynamic Data (8,9) Are Available
 ΔH_f° , ΔG_f° , S° at 25°, C_p

		<u>Formal Oxidation # of S</u>	
H ₂ S(aq)	HS ⁻	S ⁼	-2
(H ₂ S ₂)	(HS ₂ ⁻)	S ₂ ⁼	-1
(H ₂ S ₃)	(HS ₃ ⁻)	S ₃ ⁼	-2/3
(H ₂ S ₄)	(HS ₄ ⁻)	S ₄ ⁼	-1/2
(H ₂ S ₅)	(HS ₅ ⁻)	S ₅ ⁼	-2/5
		S	0
(H ₂ S ₂ O ₃)	(HS ₂ O ₃ ⁻)	S ₂ O ₃ ⁼	+2
		S ₄ O ₆ ⁼	+2.5
(H ₂ S ₂ O ₄)	(HS ₂ O ₄ ⁻)	S ₂ O ₄ ⁼ ; (SO ₂ ⁻)	+3
SO ₂ (aq)	HSO ₃ ⁻	SO ₃ ⁼ ; (S ₂ O ₅ ⁼)	+4
	HSO ₄ ⁻	SO ₄ ⁼	+6
		S ₂ O ₈ ⁼	+7

Predictive capabilities for species in parenthesis available only at 25°C (C_p not known).

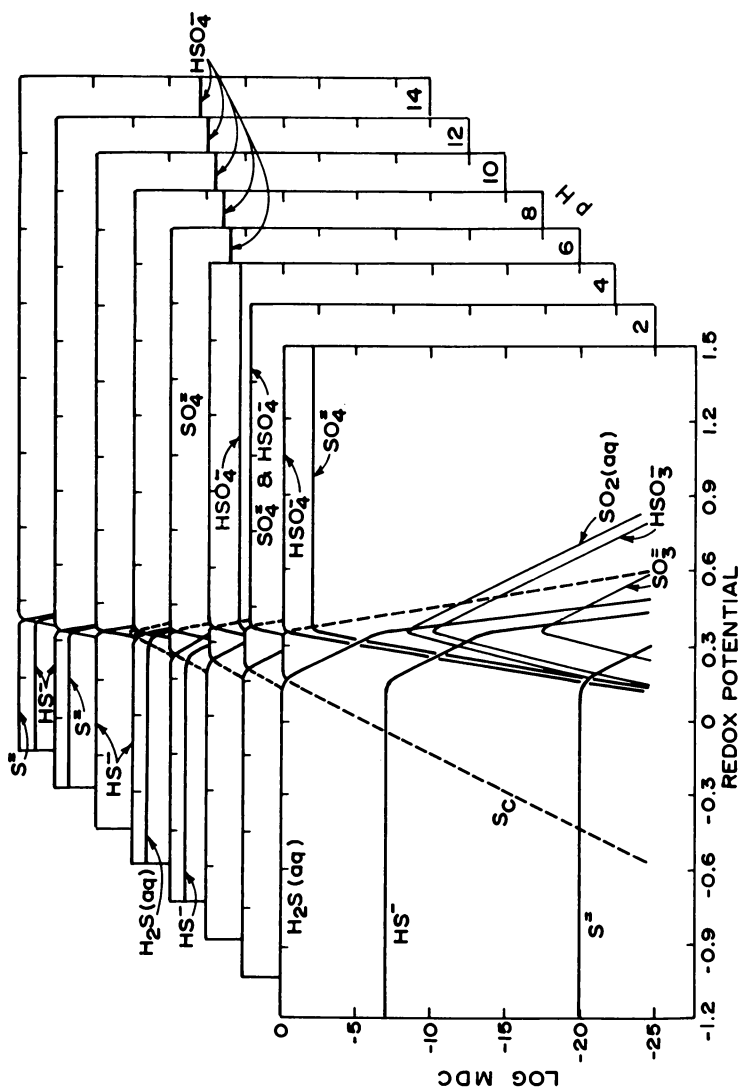


Figure 1. Tridimensional Pourbaix diagram. XYZ plot of redox potentials, MDC of sulfur and pH. Aqueous solutions at 25°C. X = redox potential, volt vs. NHE; Y = log (MDC), defined by Equation 1; i — moieties identified on curves (S_0 , insoluble orthorhombic elemental sulfur); Z = pH.

where C denotes conventional molarities of the sulfur moieties identified by the subscript and q is the corresponding number of sulfur atoms in the moiety. The denominator in Equation 1 is the experimentally accessible quantity conventionally known as "total sulfur." The following inputs are required for the computerized estimation of $(MDC)_i$'s.

1. Free energies of formation and activity coefficients of the relevant sulfur moieties at the prevailing temperature; or--alternatively--formal potentials of the corresponding redox couples.
2. The prevailing (measured) redox potential.
3. The prevailing (measured) pH.
4. The measured "total sulfur" concentration.

The actual C_i 's can--in turn--be evaluated from Equation 1.

In all coal conversion process streams analyzed in this work certain reactions were found "blocked" by sluggish kinetics, while the remainder of the system attained equilibrium. This situation is illustrated in Table II. It is apparent that if complete equilibrium had been attained, virtually all sulfur would have been converted to sulfate at the prevailing pH and redox potential (Table II, Column 2). In actual fact, sulfate was conspicuous by its absence and the most abundant sulfur species were HS^- (65% of the total sulfur) and thiosulfate (34% of the total sulfur). These experimental findings (Table II, Column 4) differ by less than 15% (of total sulfur present) from the predictions computed assuming that the oxidation states of S(VI) and higher were totally blocked by slow rates, while equilibration occurred rapidly up to and including sulfite. This suggests a convenient approach for an approximate method of sulfur speciation in coal conversion plants. It requires three readily feasible measurements, viz., pH, redox potential and total sulfur. From these data, it may be possible to estimate concentrations of various sulfur moieties (including HS^- , $S^=$, $S_4O_6^{=}$, $S_2O_3^{=}$, $HSO_3^{=}$ and $SO_3^{=}$) to within 20%, using the appropriate algorithms, computer programs, thermodynamic data base and making the proper adjustment for kinetic blocking of oxidation states $>S(IV)$. While this procedure has attractive features of simplicity and convenience, it is not a substitute for accurate quantitative speciation (v.i). Rather, it should be used for the following purposes:

1. To monitor process streams on line. Erratic fluctuations of pH and redox potential might serve as "alert signals" for anomalous sulfur speciation.
2. To pinpoint the sulfur moieties which require accurate determination.

The quasi-thermodynamic approach outlined above will obviously remain applicable to future coal conversion technologies as well, because the underlying thermodynamic principles are universal and invariant. Figure 2 is illuminating in this context: it shows that by-product waters of liquefaction processes can be differentiated from their gasification counterparts by their redox potential and pH characteristics (13).

Table II

"Kinetic Blocking" of Specified Equilibria

Specimen: Scrubber water from experimental liquefaction light oil (PETC, DCD 11, 1979).
 Pittsburgh Seam, Blacksville #2 coal. pH = 9.1; redox potential = -0.29 volt vs N.H.E.

(1) <u>Moiety</u>	<u>Mole Fraction of Sulfur in Moiety Listed in Column 1</u>			(4) <u>Found Experimentally</u>
	(2) <u>Complete Equilibration</u>	<u>Predicted (a) Assuming</u>	(3) <u>Oxidation States > S(VI) Blocked (b)</u>	
HS ⁻	Trace		0.51	0.65
S ⁼ _x	"		0.02	
S ₄ O ₆ ⁼	"	Trace		
S ₂ O ₃ ⁼	"	0.47		0.34
HSO ₃ ⁻	"	Trace		
SO ₃ ⁼	"	"		0.01
SO ₄ ⁼	1.00	---		

(a) Assignments calculated from thermodynamic data and the measured pH and redox potential.

(b) All equilibria involving sulfate (and higher oxidation states of sulfur) were ignored, while complete equilibration was assumed between sulfite and all the lower oxidation states of sulfur.

Voltammetric Methods

Differential pulse voltammetry at Levich's rotated disk electrode (14) combines remarkable advantages of selectivity and sensitivity. This is documented in Figure 3, which is a differential pulse voltammogram recorded at a glassy carbon indicator anode in a solution containing 0.00012 molar dibenzothiophene (DBT) plus 0.00012 molar benzo₂thiophene (BT). Two well-resolved "peaks" were obtained (A and B in the figure) which were proportional to the concentration of DBT and BT respectively (8,10,11 15-20). This is accounted for by the electrode reactions which are formulated in Figure 4, occurring with 100% current efficiency (i.e., without any interfering side reactions). The excellent separation between the two peaks reflects a comparable difference between the relevant standard potentials. Actual peak signals (Δi_{\max}) obeyed the applicable theoretical relationship (14).

$$\Delta i_{\max} = 0.62 \frac{n^2 F^2}{4RT} A C D^{2/3} \omega^{1/2} \nu^{-1/6} \Delta E \quad (2)$$

where nF denotes the number of coulombs per mole, A ($\approx 0.3 \text{ cm}^2$) the area of the rotated disk electrode, C the bulk concentration of the electroreactive moiety, D the diffusion coefficient, ω the rate of rotation, ν the kinematic viscosity of the solution and ΔE the potential pulse amplitude. Several coal liquefaction product samples were analyzed for BT, but none was detected. On the other hand, appreciable concentrations of DBT were found and determined quantitatively in the specimens identified in Table III. Dibenzothiophene contents are listed in Table IV. Two conclusions are apparent, viz.,

1. Where comparisons are available (21,22,23), the pulse voltammetric method is in excellent agreement with other determinations.
2. In all three coal liquefaction product specimens, the dibenzothiophene content was remarkably invariant and high (i.e., in a range between 0.1% and 0.2%).

Differential pulse voltammetry at rotated glassy carbon disk cathodes proved successful for the accurate determination of inorganic sulfur in the S(IV) oxidation state (i.e., SO_3^- , HSO_3^- or SO_2) in coal conversion process streams (18). The determination was carried out in 1 M aqueous hydrochloric acid, converting all forms of S(IV) to sulfur dioxide. The latter was electroreduced (18,24) via the following multistep process:



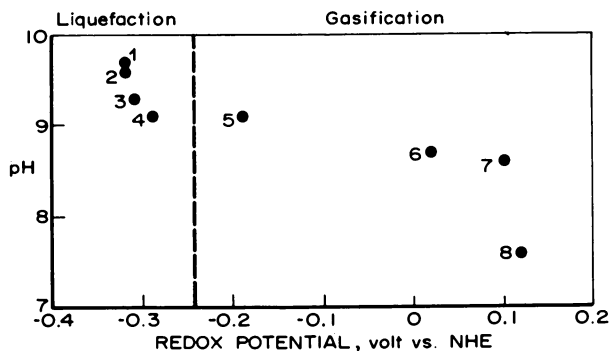


Figure 2. Differentiation between liquefaction and gasification by-product waters by pH and redox potential characteristics: 1 and 2, waste water PETC coal liquefaction development unit, disposable catalyst, runs DCD 13B and DCD 12; 3, waste water, SRC-1 plant; 4, scrubber water, light oil, Blacksville No. 2 coal; 5, waste water, fixed-bed gasifier, METC; 6, waste water, fluidized-bed gasifier, Rosebud coal, PETC; 7, gasifier condensate, 40 atm N_2 , catalyst-impregnated Illinois #6 coal; 8, gasifier condensate, 40 atm He, Montana Rosebud coal.

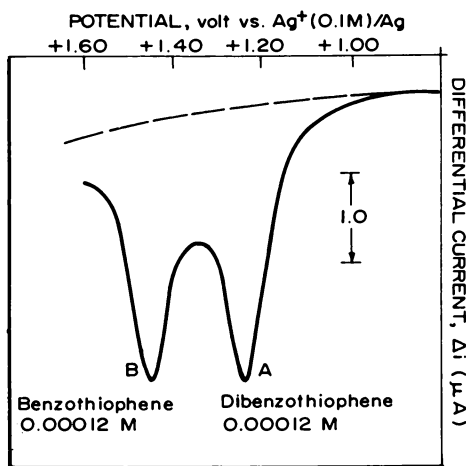


Figure 3. Differential pulse voltammogram of a mixture of dibenzothiophene and benzothiophene in acetonitrile. Supporting electrolyte 0.1M tetraethylammonium perchlorate. Indicator electrode: glassy carbon disk, rotated at 1800 rpm. Linear potential ramp, 0.002 volt/s. Pulse amplitude, $\Delta E = 0.025$ V. Pulse duration, 57 ms. Current sampling time, 17 ms.

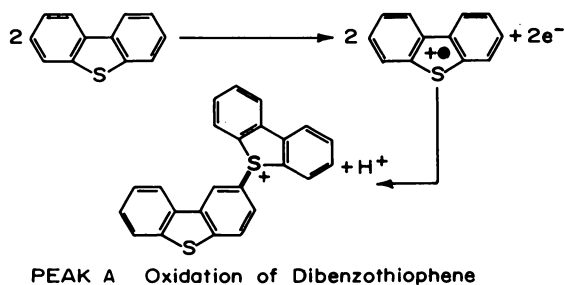
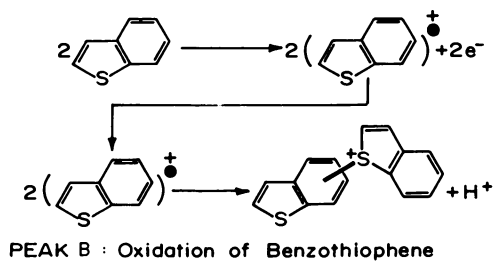


Figure 4. *Electrode reactions yielding the differential peak voltammograms shown in Figure 3*

Table III

Coal Liquefaction Product Specimens Analyzed
for Dibenzothiophene(a)

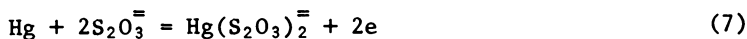
(1)	(2)	(3)
<u>Identification Number (b)</u>	<u>Description</u>	<u>Characteristics</u>
101	Black, viscous synthoil product	0.7% total sulfur (0.6% organic sulfur)
102	SRC II boiler stripper product	2.1% total sulfur
103	DOE surrogate analysis program sample, simu- lating #2 fuel oil	Blend of 40% mid- dle distillate plus 60% heavy distillate

(a) All samples made available by Pittsburgh Energy Technology Center.

(b) Ad-hoc designation, used for convenience in Table IV.

A well defined pulse voltammetric peak signal was obtained (at a potential of -0.48 volt versus the saturated calomel electrode) which was accurately proportional to the sum of the concentrations of the S(IV) moieties in the sample.

Classical anodic depolarization reactions (25) of mercury were successfully used for the determination of sulfides, thio-sulfate and sulfite in coal conversion process streams (18,19). The relevant electrode reactions are



Corresponding well defined pulse polarographic peaks were obtained at the dropping mercury electrode (26) which were strictly proportional to the concentration of the depolarizers S^{\equiv} , $\text{S}_2\text{O}_3^{\equiv}$ and SO_3^{\equiv} . The three were readily determined in each others' presence, because their peaks were sufficiently separated, as shown in Table V.

Differential pulse voltammetric and polarographic methods described in this section represent a significant enhancement of the available instrumental analysis capabilities for the quantitative speciation of sulfide, thiosulfate, sulfite and of hetero-aromatic sulfur moieties in coal conversion process streams and products.

Enthalpimetric Methods

"Enthalpimetry" (27) is a generic designation for methodologies relying on various forms of adiabatic calorimetry for quantitative analysis. The basic principle is that the heat evolved or absorbed in a chemical reaction represents a quantitative measure of the amounts reacted, viz.,

$$\Delta T = \frac{-\Delta H \cdot N}{k} \quad (9)$$

where ΔT is the temperature change under adiabatic conditions, ΔH is the heat of the reaction, N denotes the number of moles reacted and k the heat capacity. It is apparent from Equation 9 that ΔT is proportional to N if k and ΔH are invariant. In dilute aqueous solutions, k can be maintained virtually constant, when volume changes are minimized. Furthermore, at very high dilutions the convenient approximation holds:

$$\Delta H \cong \Delta H^{\circ} = \text{const.} \quad (10)$$

However, the tradeoff is that temperature changes are small (because N is small). This, in turn, requires sensitive

Table IV

Dibenzothiophene (DBT) Content of Specimens
Identified in Table III

<u>Identification</u> <u>Number (a)</u>	<u>% DBT</u>	
	<u>This Work</u>	<u>Other Findings</u>
101	0.2	
102	0.1	
103	0.14	0.11 ^(b) , 0.1 ^(c) , 0.2 ^(d)

(a) See Column 1 of Table III.

(b) Chesler, National Bureau of Standards by gas chromatography (21).

(c) Petersen, Battelle N.W., by phosphorescence (22).

(d) Petersen, Battelle N.W., by fluorescence (23).

Table V

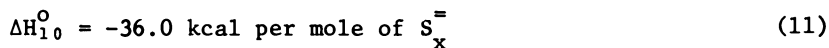
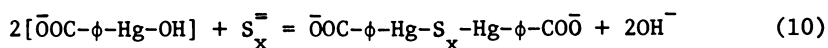
Differential Pulse Polarographic Peak Potentials
at the Dropping Mercury Electrode (18,19)

<u>Depolarizer (a)</u>	<u>Supporting Electrolyte</u>	<u>Peak Potential, V vs SCE</u>
$S^=$	Aqueous 1 M NaOH	-0.80
$S_2O_3^=$	Aqueous 0.1 M K_2HPO_4 + 0.1 M KH_2PO_4 , pH 6.5	-0.15
$SO_3^=$	Aqueous 0.1 M K_2HPO_4 + 0.1 M KH_2PO_4 , pH 6.5	-0.01

(a) Electrode reactions identified in Equations 6,7,8.

temperature detectors. Contemporary enthalpimetric analysis has relied almost exclusively on thermistor circuits which can measure temperature differences as small as a millidegree with the precision of 1%, i.e., with a resolution on the order of 10 micro-degree. The thermistor is typically wired as an arm of a Wheatstone Bridge, whose unbalance potential is proportional to the change in temperature. The signal is on the order of 10 millivolt per degree which is the equivalent of the response of a thousand-junction thermocouple. A circuit diagram is shown in Figure 5 coupled with an appropriate adiabatic cell. Two techniques were used for enthalpimetric analysis in coal conversion process streams, viz., thermometric enthalpy titrations (TET) and direct injection enthalpimetry (DIE). In the TET mode an appropriate reagent was titrated with the aid of a motor-driven buret, yielding an endpoint which corresponded to a well defined stoichiometric equivalence point. In the DIE mode, excess reagent was rapidly injected into the sample solution, yielding an instantaneous temperature increment which was proportional to the concentration of the sample. In either case, the choice of the reagent was crucial: because enthalpy change is a universal property of chemical reactions, specificity depends on the reagent.

Sulfide ($S^=$) and the polysulfides $S_2^=$, $S_3^=$, $S_4^=$ and $S_5^=$ were determined (11,17,18) by titrating coal conversion process stream specimens into 25 to 30 ml of 0.01 M orthohydroxymercurybenzoate (HMB). This is a Lewis acid which reacts as follows with the Lewis bases $S^=$ through $S_5^=$:



A typical thermometric enthalpy titration curve is shown in Figure 6. The well defined endpoint provided a convenient method for quantitating sulfidic sulfur.

Sulfite was converted by acidification to bisulfite and determined as such by DIE (16). Advantage was taken of the heat of the classical adduct formation reaction with formaldehyde:



An example of the resulting readout is illustrated in Figure 7. A linear relationship between the ΔT and sulfite (bisulfite) concentration is predicted by Equation 9. Indeed, substituting

$$k = s \cdot V \quad (14)$$

(where V denotes the volume of the solution and s its specific heat per unit volume) in Equation 9 yields

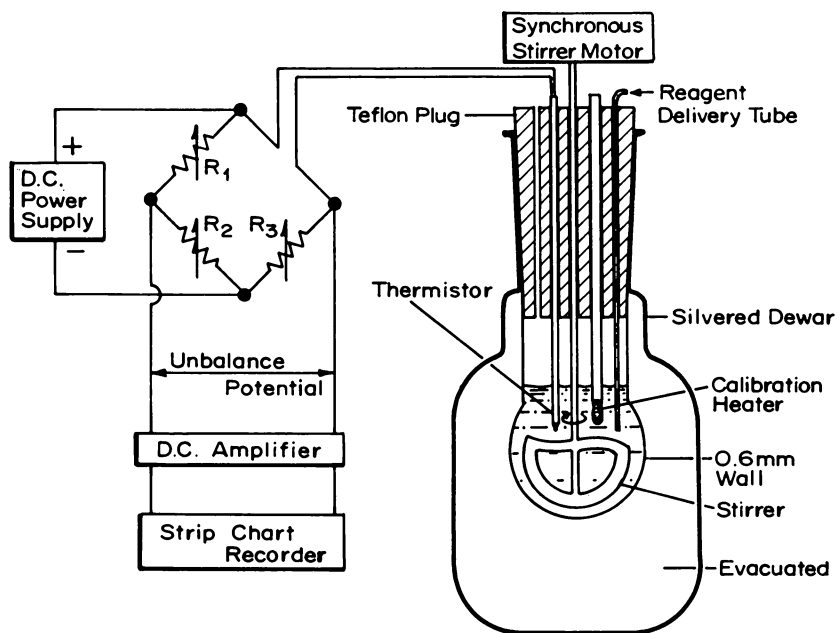


Figure 5. Temperature measuring circuit (thermistor bridge) and adiabatic cell for enthalpimetric analysis

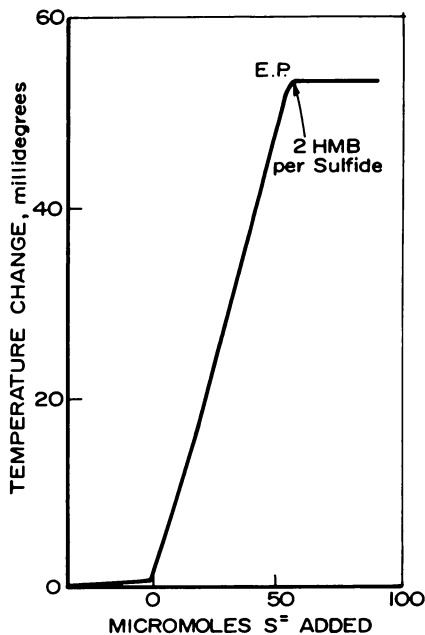


Figure 6. Thermometric enthalpy titration of HMB with sulfide: 27 mL of 3.60mM HMB titrated with 0.123M S^2 ; EP, endpoint. Note: a second poorly defined endpoint (not shown) is apparent at an approximate stoichiometry of 1 HMB per sulfide.

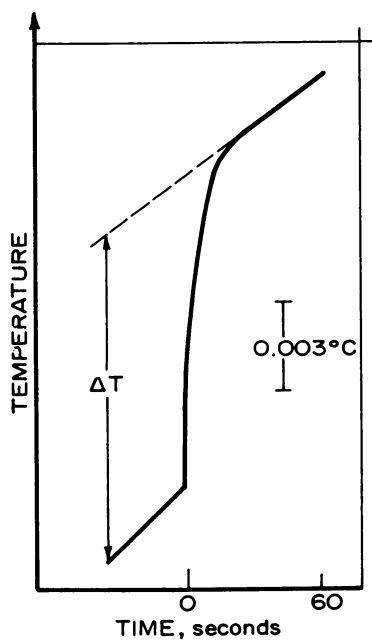


Figure 7. Determination of sulfite by DIE: 500 μL of 2M formaldehyde injected into 27 mL of 0.001M Na_2SO_3 dissolved in acetate buffer of pH 4.76. The concentration of sulfite was evaluated from the measured ΔT via Equation 15.

$$\Delta T = \frac{\Delta H}{s} \cdot \frac{N}{V} = \frac{\Delta H}{s} \cdot C \quad (15)$$

Experimentally, Equation 15 was found to hold in a range of sulfite concentrations between 0.001 M and 0.050 M. The precision and accuracy of the sulfite determination was 2%.

Sulfidic sulfur, $S_x^{=}$, and sulfite are important contaminants in coal conversion process streams. The voltammetric methods described in the preceding section of this paper and the thermochemical techniques based on Equations 9-15 above provide alternative options for the determination of sulfides and of $SO_3^{=}$ in coal conversion process streams. Cross checking of results with the aid of both types of methods must necessarily provide dependable information. The electroanalytical and enthalpimetric methods are conceptually so diverse that they cannot conceivably be subject to similar systematic errors. Their combined use is effectively "fail-safe."

Acknowledgement

The work described in this paper has been supported by the U.S. Department of Energy under Contracts No. EF-77-S-01-2710 and AS01-77ET10482 with The Pennsylvania State University. We thank the Pittsburgh Energy Technology Center (PETC) for specimens and counsel.

Literature Cited

1. See, e.g., the authoritative editorial by Abelson, P.H.; Science 1975, 189, 253.
2. Nickless, G.; "Inorganic Sulphur Chemistry"; Elsevier: New York, 1969.
3. Karchmer, J.H., Ed.; "The Analytical Chemistry of Sulfur and its Compounds"; Wiley Interscience: New York; Part I, 1970; Part II, 1972; Part III, 1971.
4. Szekeres, L.; Talanta 1974, 21, 1-44.
5. Ashworth, M.R.F.; "The Determination of Sulfur-containing Groups"; Academic Press: London; Vol. 1, 1972; Vol. 2, 1976; Vol. 3, 1977.
6. Karr, Clarence, Jr., Ed.; "Analytical Methods for Coal and Coal Products," Vols. I,II,III; Academic Press: New York, 1978.
7. Pourbaix, M.; "Atlas d'Equilibres Electrochimiques"; Gauthiers-Villars: Paris, 1963; English Edition, Pergamon Press: Oxford, 1966.
8. Jordan, J.; FE-2710-2, NTIS: U.S. Department of Energy, 1978.
9. Jordan, J.; FE-2710-3, NTIS: U.S. Department of Energy, 1978.

10. Jordan, J.; FE-2710-6, NTIS: U.S. Department of Energy, 1979.
11. Jordan, J.; FE-2710-10, NTIS: U.S. Department of Energy, 1980.
12. Jordan, J.; FE-2710-11, NTIS: U.S. Department of Energy, 1980.
13. Jordan, J.; FE-2710-12, NTIS: U.S. Department of Energy, 1980.
14. Myers, D.J.; Osteryoung, R.A.; Osteryoung, J.; Anal. Chem. 1974, 46, 2089.
15. Robbat, A.; Thesis, Pennsylvania State University, 1980.
16. Jordan, J.; FE-2710-4, NTIS: U.S. Department of Energy, 1978.
17. Jordan, J.; FE-2710-5, NTIS: U.S. Department of Energy, 1979.
18. Jordan, J.; FE-2710-7, NTIS: U.S. Department of Energy, 1979.
19. Jordan, J.; FE-2710-8, NTIS: U.S. Department of Energy, 1979.
20. Jordan, J.; FE-2710-9, NTIS: U.S. Department of Energy, 1980.
21. Chesler, S.; Private Communication.
22. Petersen, M.; Schmidt, C.; Private Communication.
23. Petersen, M.; Schmidt, C.; Private Communication.
24. Miles, A.; Thesis, Pennsylvania State University, 1977.
25. For a review see: Zhdanov, S.; "Sulfur," Chapter IV-6 in "Encyclopedia of the Electrochemistry of the Elements," Vol. IV; Bard, Ed.,; Marcel Dekker: New York, 1975, pp. 274-360.
26. Noel, D.L.; Tappi 1978, 61(5), 73.
27. Jordan, J.; Stutts, J.D.; Brattlie, W.J.; "Proceedings, The State of the Art of Thermal Analysis"; NBS, Special Publication No. 580: Gaithersburg, 1980, pp. 149-182.

RECEIVED March 9, 1981.

INDEX

A

Acid extraction of coals	403
Acid-II fraction, 600-MHz NMR spectrum of	308f
Alginite(s)	25
¹³ C CP/MAS spectra of	27
Aliphatic hydrogen in coal conversion, role of	67
Aliphatic hydrogen, correlation of tar yield with	68f
Alkali metal/naphthalene/THF system	77
Alkylation of solvent	167
Anodic depolarization reactions of mercury for the determination of sulfides	437
Anodic oxidative coupling reactions ..	333
Anthracites, SAXS curves for	10
Aromatic	
band in PSMC-53	37
clusters	45
of HVL-P fractions	232
compounds, chemical shifts of CH ₃ and CH ₂ proton in	301t
stabilization energy	117
Aromatic-1 fraction, 600-MHz NMR spectrum of	300f, 305f
Aromatization, free radical-induced bond formation and	123
ASTM procedure	402

B

Battelle coal liquefaction experiments, typical time vs. temperature curves for	138f
Belle Ayr coal	154
reaction conditions and product analysis of	164t
SCT liquefaction of	163
Benzenoid carbon with metal and nonmetal halides, interaction of ..	74
Benzenoid character of graphite and PAHs	73
Benzothiophene using <i>iso</i> -butane PCI, comparison of SRC-II 135' MS/MS spectrum with reference spectra of 5-indanol and	279f

Benzothiophene in acetonitrile, differential pulse voltammogram of DBT and	434f
Benzylic hydrocarbon radicals, estimating the stability of	111
BF ₃ , (<i>see</i> Boron trifluoride)	
Bibenzyl, decomposition rate of	109
Bibenzyl, liquid-phase pyrolysis of ...	124
mechanism for formation of major products in	125t
Bitumens, SAXS curves for	8
Bituminous coal: an EPR and NMR study, interaction of naphthalene with	173-190
Bituminous coals as cross-linked macromolecular networks	43
Blacksville coal	369
Blocking of specified equilibria, kinetic Bond	432t
breaking	101
formation and aromatization, free radical-induced	123
homolysis	101
rates of	102
in Tetralin	104t-107t
β -Bond scission	
in coal chemistry, significance of ...	103
coal-related structures susceptible to rapid	108f
radical	102
Boron trifluoride (BF ₃)	74
with PAHs, interaction of	75
<i>n</i> -Butyllithium in <i>n</i> -hexane, Li-7 NMR of	81f

C

C ₁₆ BF ₄	
EPR investigation of	82
ESR absorption of	76f
wide-line fluorine, NMR of	75
C-13 CP/MAS spectra	
of alginite	27
of fusinite	27
of sporinite	27
of vitrinite	27
C-13 CP/MAS study of coal macerals of varying rank	23-42
C-13 NMR correlation chart and PSMC-67, composite of	33f

447

American Chemical
Society Library
1155 16th St. N. W.

Cage effects	98	Coal(s) (<i>continued</i>)	
Calcium data on the residues from acid extractions	411	conversion(s) (<i>continued</i>)	
Cann electrobalance used for measur- ing coal and lignite, schematic of	391f	and reaction severity, relation- ship between	156f
Capacitance current, effect of	340f	role of aliphatic hydrogen in	67
Carbon		role of hydroaromatic hydrogen in	67
catalyzed by K ₂ CO ₃ , steam gasifica- tion of	80	on solvent composition, effect of	161
conversions to various products at 2500 PSI, maximum	215t	technologies, resource develop- ment in the analytical chemistry of sulfur com- pounds for new	427-443
plot of f_a vs. fixed	36f	contribution of mineral matter to the scattering in	16
Carboxylic acids, neutral loss scan detection of	272f	cross-linked structures in	43-59, 46f
Catalysis, homogeneous	325	-derived	224
Catalyst screening	322	liquids (CDL)	224
Catalysts, supported cobalt	326	to coal structure, relationship of	223
CDL (<i>see</i> Coal-derived liquids)		from different processes, char- acteristics of	223-242
Charged-particle activation analysis (CPAA)	87	fractionation of	225
coal oxidation by	87-94	600-MHz proton magnetic resonance study of	289-318
Chronoamperometry, double potential step	340f	produced from Clear Creek bituminous coal, PDMS for heavy	233f
Clean Kentucky coal with sulfur- containing additives	371	research in the electrochem- istry of	331-345
Clear Creek bituminous coal, PDMS for heavy CDL produced from ..	233f	materials, FTIR analysis of	254
Clear Creek coal, proximate and ultimate analysis of	224t	materials by matrix isolation spectroscopy, characteriza- tion of	251-265
Clusters, aromatic	45	products, preparation and frac- tionation of	227f
Coal(s)		desulfurization	403
acid extraction of	403	with diluent, thermal oxidative degradation of untreated and oxydesulfurized Montana Rosebud Seam	420f
with added pyrite	369	effect of solvent composition on the liquefaction behavior of western	153-171
analytical data	132t	electron microprobe analysis on vitrinite level of raw and leached	410t
and its application to metals specia- tion, dialytic extraction of ..	243-249	an EPR and NMR study, interac- tion of naphthalene with bituminous	173-190
before and after oxydesulfurization, analysis of	406t	EPR spectra of	177f
Belle Ayr	154	-naphthalene-d ₈	177f
SCT liquefaction of	163	-naphthalene-h ₈	177f
Blacksville	369	evaluation of the removal of sulfur from	401-414
West Virginia	379	and extracts, analysis of	246f
chemistry, significance of β -bond scission in	103	and its extracts, metals analysis of Ireland Mine	247t
comparison of dialytic extracts with the parent	245		
conversion(s)	153		
effect of solvent composition on a fundamental chemical kinetics approach to	97-129		
interrelationship of graphite intercalation compounds, ions of aromatic hydro- carbons, and	73-86		
Mössbauer study of the trans- formation of iron minerals during	377-387		
to pyridine solubles, MAF	139		

- Coal(s) (*continued*)
- flash hydrogasification of 216f
 - fractions, 600-MHz spectra of 293f
 - g-factors of heated Illinois No. 6 .. 181f
 - heated with naphthalene,
 - g-factors of 180
 - heated with naphthalene-d₈ or naphthalene-h₈, radical concentration in samples of 179f
 - Indiana Minshall Seam
 - comparison of a normal thermal oxidative degradation with an alternate programmed-isothermal treatment for oxydesulfurized 423f
 - with diluent, thermal oxidative degradation of untreated and oxydesulfurized 420f
 - in oxygen and air, comparison of the thermal oxidative degradation of oxydesulfurized 425f
 - with and without a diluent, thermal oxidative degradation of untreated 419f
 - iron-bearing minerals in 378
 - with iron-containing materials 371
 - and lignite 389-400
 - analysis of pyrite in 389-400
 - is analyzed, schematic of weight change observed as pyrite in 393f
 - samples received from the coal research laboratory of the Pennsylvania State University 396t
 - schematic of the Cann electrobalance used for measuring liquefaction 138f
 - apparatus, schematic of 138f
 - applications 360
 - conditions, Fe-S-O-H system under 349-376
 - in continuous reactors, pyrrhotites formed during 362
 - experiments, actual reaction conditions for 136t
 - experiments, typical time vs. temperature curves for
 - Battelle 138f
 - of Monterey bituminous 151
 - product specimens analyzed for .. 436t
 - short-contact-time 131-152
 - MAF conversions to pyridine solubles from 145
 - solvent changes during 169f
 - liquid 291
 - acidic and basic fractions 291
- Coal(s) (*continued*)
- liquid (*continued*)
 - fractions 311t
 - analysis of functional groups in chromatographically separated 311t
 - 600-MHz NMR spectra of 307f
 - NMR structural parameters of saturate fraction, 600-MHz NMR spectrum of 299f
 - saturates, IR spectra of 298f
 - samples, MI spectrometry for identifying PAHs in 256
 - upgrading using metallophthalocyanine catalysts 319-330
 - Louvilia/ISU, Lovilla/ROM, and Illinois No. 6 404
 - low-temperature oxidation of 93
 - macerals of varying rank, C-13 CP/MAS study of 23-42
 - mineral matter catalysis in liquefaction 191-200
 - molecule during thermal decomposition, cracking of hypothetical molecule and thermal decomposition products for PSOC 170 .. 62
 - and naphthalene, exchange of hydrogen between 184
 - nature of cross-links in 45
 - obtained from the scattering curves and from adsorption data, specific surfaces for 14t-15t
 - oxidation by CPAA 87-94
 - oxide layer depths of 90t
 - PDMS for heavy CDL produced from Clear Creek bituminous peak-to-peak linewidths of 183f
 - to produce naphthalene, abstraction of hydrogen from Tetralin by proximate and ultimate analysis of Clear Creek 224t
 - PSOC 3
 - to pyridine solubles, relationship between reaction time, temperature, reaction severity, and conversion of Wyodak 134t
 - pyrolysis, nonisothermal kinetics of gas formation in 416
 - radical concentration in samples of heated 178f
 - raw and treated
 - analysis of 403
 - before and after extraction with nitric acid, nitrogen and iron content in 409t
 - with 2:3 hydrochloric acid and/or 1:7 nitric acid, extraction of 407t

Coal(s) (continued)

reactions of Tetralin in the presence of	193
under reducing conditions, nonisothermal kinetic method for estimation of organic sulfur containing functional groups in	416
-related structures susceptible to rapid β -bond scission	108f
removal of sulfur from	406f
as a route to sulfur functionality, thermal oxidative degradation of	415-426
scattering patterns for various	8
SAXS	11
studies of	4
sample(s)	48f
apparent swelling behavior of	48f
EPR measurements of heated	176
scattering curves for	6f
separation and characterization plus SRC-II and H_2 , Mössbauer spectra at various temperatures for	384f
true swelling behavior of cross-linked structure in	56f
small-angle X-ray investigation of the porosity in	3-22
and solvents	131
-solvent interactions	173
subbituminous	
comparison of experimental data for New Mexico	92f
correlation coefficient, results of the sensitivity analysis for ..	208f
estimated values of various parameters for	206f
flash hydrogenation of	209f-214f
lignite and, kinetics of	201-219
oxydesulfurization of the Montana	418
results, correlation coefficients and standard errors for	208f
in solvents, Wyodak	151
ultimate analysis of lignite and ..	203f
structure	63f
information in a hypothetical coal molecule	63f
parameters	64f
relationship of CDL to	223
and thermal decomposition	61-71
with sulfur-containing additives, clean Kentucky	371
sulfur content in	401
swelling behavior—effect of porous structure, true	51
systems, pathway for polymerization and cross-link formation in	123

Coal(s) (continued)

tar	65
vs. time, uptake of oxygen by selected	91f
transformation of the iron sulfides in an Illinois No. 6	382
volume fraction	
at equilibrium swelling, dependence of apparent	
on the carbon content for American coals	52f, 53f
on the carbon content for Japanese coals	53f
on the oxygen content of coals	54f
at equilibrium swelling in pyridine, dependence of true ..	57f
number average molecular weight between cross-links as a function of the thermodynamic parameter and	55f
Cobalt catalysts, supported	326
Combined rotation and multiple-pulse spectroscopy (CRAMPS)	24
Condensation of alkyl aromatics and phenols, dimerization and	167
Condensed-phase product (CPP)	235
Coupling reactions, anodic oxidative ..	333
CP/MAS (see Cross-polarization and magic-angle spinning)	
CPAA (see Charged-particle activation analysis)	
CPP (condensed-phase product)	235
Cracking of hypothetical coal molecule during thermal decomposition ..	63f
CRAMPS (see Combined rotation and multiple-pulse spectroscopy)	
Cross-polarization and magic-angle spinning (CP/MAS)	24
spectrum(a)	
of fusinite from Westfield mine ..	33f
of PSMC-67	35
of sporinite concentrates	31f
of vitrinite concentrates	32f
of vitrinite samples from the Lower Kittanning Seam	38f
study of coal macerals of varying rank, C-13	23-42
Cross-link(s)	
in coal, nature of	45
determination of the number average molecular weight between	
formation in coal systems pathway for polymerization and	123
as a function of the thermodynamic parameter and the coal volume fraction, number average molecular weight between	55f
number average molecular weight between (M_c)	44

- Cross-link(s) (*continued*)
 number of repeating units between.. 45
 cross-linked macromolecular net-
 works, bituminous coals as .. 43
 Cross-linked structure in coal(s) ..43-59, 46f
 samples, true coal swelling
 behavior of 56t
 Cyclicvoltammogram of atmospheric
 overhead distillate 334f
 of Panasol oil and hydrogenated
 Panasol oil 334f
 of SRC-II fuel oil A 335f
- D**
- daf (dry, ash-free) 404
 DBT (*see* Dibenzothiophene)
 Decalin, product yields from
 Tetralin and 196f
 Decalins, isomerization of 195
 Decomposition, concerted 103
 Decomposition rate of bibenzyl 109
 Decoupling effect on α -CH₂ proton
 signals of indane and its deriva-
 tives 303f
 Decoupling effect on α -CH₂ proton
 signals in Tetralin and its de-
 rivatives 302f
 Desulfurization, coal 403
 Desulfurization experiments 411
 Dialysis apparatus, continuous 246f
 Dialytic extraction of coal and its
 application to metals specia-
 tion 243-249
 Dialytic extracts with the parent coals,
 comparison of 245
 Dibenzothiophene (DBT)
 and benzothiophene in acetonitrile,
 differential pulse voltammo-
 gram of 434f
 coal liquefaction product speci-
 mens analyzed for 436t
 content of specimens 438t
 DIE (*see* Direct injection
 enthalpimetry)
 Differential pulse
 polarographic peak potentials at
 the dropping mercury electrode 438t
 voltammetry 433
 voltammogram of DBT and benzo-
 thiophene in acetonitrile 434f
 9,10-Dihydroanthracene, formation of 332
 Dimerization and condensation of
 alkyl aromatics and phenols 167
 Direct injection enthalpimetry (DIE).. 441f
 Disproportionation 167
 molecular
 formation of free radicals by 121
 rates of 114
 Disproportionation (*continued*)
 molecular (*continued*)
 with Tetralin as H-donor118t-119t
 values, comparison of empirical
 rate constants for H₂ trans-
 fer from hydroaromatics
 with 120t
 radical 115
 from Tetralin 116
 Distillate, cyclicvoltammogram of
 atmospheric overhead 334f
 Distillation products from HVL-P
 and its cyclohexane soluble
 fraction, comparison of 231t
 dmmf (dry mineral matter-free) 404
 Double potential step chrono-
 amperometry 340f
 Dry, ash-free (daf) 404
 Dye laser-induced fluorescence spectra
 in a *n*-heptane matrix at 15 K 258f
 of SRC-I 257f
- E**
- Electrode film formation on the
 voltammetric traces, effect of 335f
 Electrode reactions yielding differen-
 tial peak voltammograms 435f
 Electrochemical rate constants, varia-
 tions of 341t
 Electrochemistry of CDL, research
 in 331-345
 Electron paramagnetic resonance
 (EPR) 174
 investigation of C₁₆BF₄ 82
 measurements of heated coal
 samples 176
 of naphthalene samples, NMR and
 and NMR study, interaction of
 naphthalene with bituminous
 coal 173-190
 spectra of coal 177f
 -naphthalene-d₈ 177f
 -naphthalene-h₈ 177f
 Elovich kinetics 93
 Enthalpies of H-atom addition to
 polyaromatics 113t
 Enthalpimetric analysis, temperature
 measuring circuit adiabatic
 cell for 440f
 Enthalpimetry 437
 EPR (*see* Electron paramagnetic
 resonance)
 Equilibrium(a)
 constant(s) 354t
 for the equilibrium Fe + 1/2
 S₂FeS 354t
 for the equilibrium H₂ + 1/2
 S₂ ⇌ H₂S 355t

Equilibrium(a) (<i>continued</i>)	
constant(s) (<i>continued</i>)	
for polyaromatic equilibria,	
liquid- and gas-phase	99t
solvation effects on	98
kinetic blocking of specified	432t
line, pyrite-pyrrhotite	369
swelling theory	44
ESR absorption of C ₁₀ BF ₄	76f
ESR absorption against microwave	
power for Illinois No. 6 coal	78f
Ethanol extraction products from	
HVL-P, yields and analytical	
data on	230t
Extraction(s) with nitric acid	
with boiling	408
with cold	408
nitrogen and iron content in raw	
and treated coals before and	
after	409t
of raw and treated coals with 2:3	
hydrochloric acid and/or 1:7	407t
F	
f _a (<i>see</i> Fraction of aromatic carbon)	
Fe + 1/2 S ₂ ⇌ FeS, equilibrium	
constant for the equilibrium	354t
Fe-S-O-H system	
at 327°C	352f
at 350°, 400°, 427°, and 527°C	353f
system under coal liquefaction	
conditions	349-376
FeS, high-temperature transforma-	
tion(s) of	380
Fe ₇ S ₈ , Mössbauer spectrum of	383f
FeS at various temperatures, Möss-	
bauer spectra of	381f
FeS ₂ , decomposition of	379
Fe ₇ S ₈ high-temperature transforma-	
tion(s) of	380
Mössbauer spectrum of the FeS	
obtained from	383f
Fe ₇ S ₈ above the magnetic transition	
temperature, Mössbauer spectra	
of	381f
Faraday balance, variation of the satu-	
ration magnetization of 1 mg iron	
metal with temperature as	
recorded by	391f
Flash	
hydrogasification of coal	216f
hydrogenation of lignite and sub-	
bituminous coal, kinetics	
of	201-219
hydrogenation of subbituminous	
coal	209f-214f
Flory-Huggins theory	44
Fluoranthene in SRC using standard	
addition method, quantitation of	286f
Fluorescence spectrum(a)	
in a <i>n</i> -heptane matrix at 15 K, dye	
laser-induced fluorescence	
spectra in	258f
in a nitrogen matrix at 15 K	257f
of SRC I in a <i>n</i> -heptane matrix at	
15 K, dye laser-induced	257f
Fluorine NMR of C ₁₀ BF ₄ , wide-line ..	75
Fourier transform infrared (FTIR)	
analysis of coal-derived materials ..	254
spectra of PAHs, MI	255
spectrometry	254
Fraction of aromatic carbon (f _a)	23-24
values, maceral	24
values, sources of error in measur-	
ing	39
Fractionation of CDL	225
Free radical(s)	
H-atom transfer	121
-induced bond formation and	
aromatization	123
by molecular disproportionation,	
formation of	121
FTIR (<i>see</i> Fourier transform infrared)	
Functional groups in chromatographi-	
cally separated coal liquid frac-	
tions, analysis of	311t
Functional groups, thermal decompo-	
sition of	66
Fusinite(s)	25
spectrum(a) (of)	35
C-13 CP/MAS	27
from Westfield mine, CP/MAS ..	33f
G	
g-factors	175, 180
of coals heated with naphthalene ..	180
Gas	
chromatography (GC)	260
with MI fluorescence spectrome-	
try, interfacing of	263
MI-FTIR	260
phase data to the liquid phase,	
conversion of	97
phase equilibrium constants for	
polyaromatic equilibria, liquid	
and	99t
Gasification by-product waters by pH	
and redox potential characteris-	
tics, differentiation between	
liquefaction and	434f
GC (<i>see</i> Gas chromatography)	
Graphite	
and hydrocarbons, reductive	
alkylation treatment of	77

- Graphite (*continued*)
- intercalation 83*t*
 - compounds, ions of aromatic hydrocarbons, and coal conversion, interrelationship of 73-86
 - and PAHs, benzenoid character of 73
- H**
- H-atom addition to polyaromatics, enthalpies of 113*t*
- H-atom transfer, free-radical 121
- H/C atomic ratio of the SRC 157
- H-donors and yield of methylnaphthalene dimers 169*f*
- ¹H NMR (*see* High-resolution proton NMR)
- H₂ transfer from hydroaromatics with molecular disproportionation values, comparison of empirical rate constants for 120*t*
- H₂ + 1/2 S₂ ⇌ H₂S, equilibrium constant for the equilibrium 355*t*
- Halides, interaction of benzenoid carbon with metal and nonmetal 74
- HDN (*see* Hydrodenitrogenation)
- High-resolution proton nuclear magnetic resonance (H-1 NMR) 289
- temperature transformations of FeS 380
- temperature transformations of Fe₇S₈ 380
- HMB (*see* *o*-Hydroxymercurybenzoate)
- Homogeneous catalysis 325
- HPLC separation of Synthoil, fluorescence spectra after 261*f*
- Heating value recovery 404
- Heavy liquid product (HVL) and HVL-P extraction 225
- n*-Heptane matrix at 15 K, dye laser-induced fluorescence spectra in 258*f*
- of SRC-I 257*f*
- Heteroatoms, distribution of 301*t*
- percent 301*t*
- n*-Hexane, Li-7 NMR of *n*-butyllithium in 81*f*
- HVL (*see* Heavy liquid product)
- HVL-P and its cyclohexane soluble fraction, comparison of distillation products from 231*t*
- extraction, HVL and 226
- and its fractions, analytical data on fraction 232
- aromatic clusters of 232
- HVL-P (*continued*)
- fraction (*continued*)
- possible structural units in 240*f*
 - structural parameters of 234*t*
 - SP-300, and SP-320 fractions 235
 - structural parameters for 232
 - yields and analytical data on ethanol extraction products from 230*t*
- Hydroaromatic hydrogen in coal conversion, role of 67
- Hydroaromatics with molecular disproportionation values, comparison of empirical rate constants for H₂ transfer from 120*t*
- Hydrocarbons
- benzenoid character of graphite and polycyclic aromatic 73
 - interaction of BF₃ with polycyclic aromatic 75
 - reductive alkylation treatment of graphite and 77
- Hydrodenitrogenation (HDN) 319
- with metallophthalocyanines 320
 - of quinoline 319
- Hydrogen
- in coal conversion, role of aliphatic 67
 - in coal conversion, role of hydroaromatic 67
 - between coal and naphthalene, exchange of 184
 - correlation of tar yield with aliphatic 68*f*
 - depleted solvent, liquefaction in 145
 - exchange reactions, chemical mechanism for 186
 - /oxygen/nitrogen/sulfur content vs. reaction severity 165*f*
 - from Tetralin by coal to produce naphthalene, abstraction of 194
 - transfer, rates for 117
- Hydrogenation activity with [M(PC)] 320, 328
- Hydrogenation of quinoline 319
- to 1,2,3,4-tetrahydroquinoline with [Co(PC)]/SiO₂ 326*t*, 327*t*, 328*t*
 - in homogeneous solution at 300°C 325*t*
 - with [M(PC)] supported on Al₂O₃ and SiO₂ · Al₂O₃ at 290°C 324*t*
 - with [M(PC)] supported on SiO₂ at several temperatures 323*t*
- Hydroxyl groups with methyl groups, effects on vapor pressures of replacing 100*t*
- o*-Hydroxymercurybenzoate (HMB) .. 440*f*

I

Illinois No. 6 coal	
ESR absorption against microwave power for	78f
g-factors of heated	181f
Mössbauer spectrum of	383f
and Pittsburgh Seam coal, difference NMR spectrum between SRC-II middle distillates from run with SRC-II and H ₂ , Mössbauer spectrum of the liquefaction residue of	385f
transformation of the iron sulfides in	382
and Western Kentucky 9/14 coal, difference NMR spectrum between SRC middle distillates from	315f
Indane and its derivatives, decoupling effect on α -CH ₂ proton signals of	303f
5-Indanol and benzothiophene using isobutane PCI, comparison of SRC-II 135 ⁺ MS/MS spectrum with reference spectra of	279f
5-Indanol, effects of ion kinetic energy on MS/MS spectrum of	274f
Indiana Minshall Seam coal, oxydesulfurized	
comparison of a normal thermal oxidative degradation with an alternate programmed-isothermal treatment for	423f
with diluent, thermal oxidative degradation of untreated and	420f
in oxygen and air, comparison of thermal oxidative degradation of	425f
Indiana Minshall Seam coal with and without a diluent, thermal oxidative degradation of untreated	419f
Intercalation compound(s)	74
intermediates	80
Intercalation of graphite	83f
Ion kinetic energy on MS/MS spectrum of 5-indanol, effects of	274f
Ionic processes and water formation	123
Ionization in MS/MS, chemical	269
Ireland Mine coal and its extracts, metals analysis of	247t
Iron	
-bearing minerals in coal	378
-containing materials, coal with	371
content in raw and treated coals before and after extraction with nitric acid, nitrogen and	409t
phase diagrams of the stability regions of	355
saturation magnetization of	394

Iron (*continued*)

sulfides in an Illinois No. 6 coal, transformation of	382
Isomerization of Decalins	195

K

K ₂ CO ₃ , steam gasification of carbon catalyzed by	80
Kinetic blocking of specified equilibria	432t
Kratky SAXS system	7

L

LC of Synthoil sample in isopropyl alcohol	259f
Li-naphthalenide in THF, Li-7 NMR of	81f
Li-7 NMR of <i>n</i> -butyllithium in <i>n</i> -hexane	81f
Li-7 NMR of Li-naphthalenide in THF	81f
Lignite	
is analyzed, schematic of weight change observed as pyrite in coal or	393f
coal and	
analysis of pyrite in	389-400
samples received from the coal research laboratory of the Pennsylvania State University	396t
schematic of the Cann electrobalance used for measuring	391f
North Dakota	206t
with diluent, thermal oxidative degradation of untreated and oxydesulfurized	420f
Linewidths, radical	182
Liquefaction	
behavior of western subbituminous coal, effect of solvent composition on	153-171
(of) coal	
experiments, actual reaction conditions for	136t
Monterey bituminous	151
in -019 solvent, elemental analysis of SRC from	146f
in -035 solvent, elemental analysis of SRC from	147f
in -019 and -035 solvents	148f
short-contact-time	131-152
Wyodak, elemental analysis of SRC from in solvent(s)	
-019	141f, 142f
and -035, comparison of	144f

- Liquefaction (continued)**
 (of) coal (continued)
 Wyodak elemental analysis
 of (continued)
 obtained by distillation and
 heptane precipitation
 from 142f
 -035 143f
 Wyodak and Monterey, in -019
 solvent 149f
 Wyodak and Monterey, in -035
 solvent 150f
 coal mineral matter catalysis in 191-200
 and gasification by-product waters
 by pH and redox potential
 characteristics, differentiation
 between 434f
 hydrogen-depleted solvent 145
 residue of the Illinois No. 6 coal
 run with SRC-II and H₂,
 Mössbauer spectrum of 385f
 residue obtained from a run with
 SRC-II + N₂, Mössbauer
 spectrum of 384f
- Liquid phase**
 conversion of gas-phase data to 97
 and gas phase equilibrium con-
 stants for polyaromatic
 equilibria 99f
 pyrolysis of bibenzyl 124
 mechanism for formation of
 major products in 125f
- Lower Kittanning Seam, CP/MAS**
 spectra of vitrinite sample from .. 38f
- M**
- Maceral(s)**
 concentrates, chemical composi-
 tion of 28f
 concentrates, petrographic analysis
 of 26f
 f_n values 24
 ultimate and proximate analysis
 of vitrinite 29f
- Macropores and transition pores,**
 specific surfaces of 17
- MAF**
 coal conversions to pyridine
 solubles 139
 conversions to pyridine solubles
 from short-contact-time coal
 liquefaction 145
 Wyodak coals to pyridine solubles,
 comparison of conversion of .. 141f
- Magnetometry and thermogravimetry**
 Mass
 -analyzed ion kinetic energy spec-
 trometer (MIKES) 273
- Mass (continued)**
 spectrometry/mass spectrometry
 (MS/MS) 267
 analysis scheme 270f
 analysis of syngases 267-288
 chemical ionization in 269
 fragmentation processes, reac-
 tions observed in 268f
 instrumentation, flexibility of 271
 quantitation 269
 spectrum 274f
 of 5-indanol, effects of ion
 kinetic energy on 274f
 of 3-methylindole and 2-
 methylindole, slow scan
 of the charge stripping
 region in 277f
 with reference spectra of 5-
 indanol and benzothio-
 phene using isobutane
 PCI, comparison of
 SRC-II 135* 279f
 with the reference spectrum
 of 3-methylindole, com-
 parison of SRC-II mass
 132 277f
 to syngas characterization,
 applications of 275
 spectrum, chemical noise in 270f
- Matrix isolation (MI)**
 fluorescence spectrometry 253
 characteristics of 253
 disadvantage of 253
 interfacing of GC with 263
 molecular 252
 FTIR spectra of PAHs 255
 FTIR spectrum of one chromato-
 graphic peak system from the
 aromatic extract of SRC-I 262f
 spectrometric characterization of
 real samples 255
 spectrometry for identifying PAHs
 in coal liquid samples 256
 spectroscopy, characterization of
 coal-derived materials by 251-265
- MDC (see Molar distribution**
 coefficients)
- Metallophthalocyanine(s) ([M(PC)])** .. 320
 catalysts, coal liquid upgrading
 using 319-330
 HDN with 320
 hydrogenation activity with 320,328
- Metals**
 analysis of Ireland Mine coal and
 its extracts 274f
 analysis of reactor deposit and
 feed coal from FB-61 243f
 speciation, dialytic extraction of
 coal and its application to . 243-249

Methyl groups, effects on vapor pressures of replacing hydroxyl groups with	100t	Montana Rosebud Seam coal with diluent, thermal oxidative degradation of untreated and oxydesulfurized	420f
1-Methylindan and naphthalene and the ratio of trans/cis Decalin as a function of pyrite concentration, yields of	198f	Montana subbituminous coal, oxydesulfurization of	418
1-Methylindan yield as a function of time in the presence of additives	198f	Monterey coal(s), liquefaction of bituminous	151
2-Methylindole, slow scan of the charge stripping region in the MS/MS spectrum of 3-methylindole and	277f	in -019 and -035 solvents	148f
3-Methylindole, comparison of SRC-II mass 132 MS/MS spectrum with the reference spectrum of	277f	in -019 solvent, elemental analyses of SRC from	146f
3-Methylindole and 2-methylindole, slow scan of the charge stripping region in the MS/MS spectrum of	277f	in -035 solvent, elemental analyses of SRC from	147f
Methylnaphthalene dimers, H-donors and yield of	169f	and Wyodak in -019 solvent	149f
Methylphenanthrenes in CDCL ₃ , 600-MHz NMR spectra of	306f	and Wyodak in -035 solvent	150f
MI (see Matrix isolation)		[M(PC)] (see Metallophthalocyanines)	
MIKES (mass-analyzed ion kinetic energy spectrometer)	273	MS/MS (see Mass spectrometry/mass spectrometry)	
Mineral matter to the scattering in coals, contribution of	16		
MINUIT	202	N	
Mössbauer spectrum(a)		Naphthalene	
of FeS obtained from the high-temperature transformation of Fe ₇ S ₈	383f	abstraction of hydrogen from Tetralin by coal to produce	194
of FeS at various temperatures	381f	with bituminous coal: an EPR and NMR study, interaction of	173-190
of Fe ₇ S ₈ above the magnetic transition temperature	381f	exchange of hydrogen between coal and	184
of Illinois No. 6 coal	383f	g-factors of coals heated with	180
of the liquefaction residue	385f	and the ratio of trans/cis Decalin as a function of pyrite concentration, yields of 1-methylindan and	198f
of the Illinois No. 6 coal + 5% FeS ₂ run	385f	samples, NMR and EPR of	175
of the Illinois No. 6 coal run with SRC-II and H ₂	385f	in THF	79
obtained from a run with SRC-II + N ₂	384f	yield as a function of time in the presence of additives	196f
at various temperatures for a coal samples plus SRC-II and H ₂	384f	Naphthalene-d ₈ , fraction of protium incorporated in the α and β positions of	185f
Mössbauer study of the transformation of iron minerals during coal conversion	377-387	Naphthalene-d ₈ or naphthalene-h ₈ , radical concentration in samples of coal heated with	179f
Molar distribution coefficient (MDC) requirements for estimation of	428	Naphthalene-h ₈ , radical concentration in samples of coal heated with naphthalene-d ₈ or	179f
Molecular		Negative chemical ionization (NCI) MS of SRC	271, 281
disproportionation, rates of	114	Neutral loss scan(s)	278
parameters, definitions and formulae of	228	detection of carboxylic acids	272f
weight between cross-links, number average (\bar{M}_c)	44	and PCI MS of acylated SRC-II	280f
		New Mexico subbituminous coal, comparison of experimental data for	206t
		Nitric acid, nitrogen and iron content in raw and in treated coals before and after extraction with	409t
		Nitrogen	
		adsorption, low-temperature	19

- Nitrogen (*continued*)
 and iron content in raw and treated
 coals before and after extrac-
 tion with nitric acid 409*t*
 matrix at 15 K, fluorescence
 spectrum in 257*f*
- NMR
 and EPR of naphthalene samples .. 175
 spectrum(a)
 600-MHz
 of Acid-II fraction 308*f*
 of Aromatic-I fraction 300*f*, 305*f*
 of coal liquid fractions 307*f*
 saturate 299*f*
 of methylphenanthrenes in
 CDCL₃ 306*f*
 between SRC-II middle distillates
 from Illinois No. 6 and
 Pittsburgh Seam coal dif-
 ference 314*f*
 between SRC-II middle distillates
 from Illinois No. 6 and
 Western Kentucky coal,
 difference 315*f*
 study, interaction of naphthalene
 with bituminous coal: an
 EPR and 173-190
 structural parameters of coal liquid
 fractions 309
 North Dakota lignite 206*t*
 with diluent, thermal oxidative
 degradation of untreated and
 oxydesulfurized 421*f*
- Number average molecular weight
 between cross-links (\bar{M}_c)
 determination of 50
 as a function of the thermody-
 namic parameter and the
 coal volume fraction 55*f*
- O
- Oil, DCD 13 B, irreversible and
 reversible behavior of product 338*f*
 Oxidation of coal, low-temperature .. 93
 Oxidation linear sweep 339
 Oxidative coupling reactions, anodic .. 333
 Oxidative degradation procedure,
 difficulties with 422
 Oxide layer depths of coals 90*t*
 Oxide layer divided by total volume
 of the particle diameter, volume
 of 91*f*
 Oxydesulfurization, analysis of coals
 before and after 406*t*
 Oxydesulfurization of the Montana
 subbituminous coal 418
 Oxygen
 adsorption, labeled 90
- Oxygen (*continued*)
 -containing molecules, uptake of 89
 depth profile 88, 89
 by selected coals vs. time, uptake of 91*f*
- P
- PAHs (*see* Polycyclic aromatic
 hydrocarbons)
 PAR (Princeton Applied Research) .. 332
 Panasol oil and hydrogenated Panasol
 oil, cyclicvoltammograms of 334*f*
 Panasol oil, voltammogram of 333
 PCI (*see* Positive ion chemical
 ionization)
 PDMS (*see* Plasma desorption mass
 spectroscopy)
 Peak
 current with concentration,
 variation of 338*f*
 height and form, effect of initial
 delay time on 337*f*
 -to-peak linewidths of coals 183*f*
 potentials at the dropping mercury
 electrode, differential pulse
 polarographic 438*t*
 signals 433
 voltammograms, electrode reactions
 yielding differential 435*f*
- PETC (*see* Pittsburgh Energy Tech-
 nology Center)
 Petrographic analysis of maceral
 concentrates 26*t*
 Phase diagrams of the stability
 regions of iron 355
 Pittsburgh Energy Technology Center
 (PETC) 243, 333
 voltammogram of product oil from
 the 1000 lb/d pilot plant at .. 337*f*
 Pittsburgh Seam coal, difference NMR
 spectrum between SRC-II middle
 distillates from Illinois No. 6 and 314*f*
 Plasma desorption mass spectros-
 copy (PDMS) 232
 for heavy CDL produced from
 Clear Creek bituminous coal .. 233*f*
 PMR (*see* Proton magnetic resonance)
 Polyaromatic equilibria, liquid and
 gas phase equilibrium constants
 for 99*t*
 Polyaromatics, enthalpies of H-atom
 addition to 113*t*
 Polycyclic aromatic hydrocarbons
 (PAHs) 252
 benzenoid character of graphite and
 in coal liquid samples, MI spec-
 trometry for identifying 256
 MI-FTIR spectra of 255

Polymerization and cross-link formation in coal systems, pathway for	123	Pyrite (<i>continued</i>)	
Pore(s)		with Tetralin, reduction of	197
SAXS	11	transformations of	378
specific surfaces of the macropores and transition	17	Pyrolysis of bibenzyl, liquid-phase mechanism for formation of major products in	125 <i>t</i>
structure	49	Pyrrhotite(s)	
Porosity in coals, small-angle X-ray investigation of	3-22	from autoclaves	373 <i>f</i>
Porous structure, true coal swelling behavior—effect of	51	clean Kentucky coal plus sulfur-containing additives	373 <i>f</i>
Positive ion chemical ionization (PCI) MS of acylated SRC-II, neutral loss scan and	275	coal only	370
Pourbaix diagram, tridimensional	430 <i>f</i>	coal plus H ₂ S	370 <i>f</i>
Pourbaix diagrams and algorithms, thermodynamic predictions and	428	coal plus iron-containing material	373 <i>f</i>
Princeton Applied Research (PAR)	332	coal plus pyrite	372 <i>f</i>
Product isolation	161	and reactors	372 <i>f</i>
Protium, conservation of	187	equilibrium line, pyrite—	369
Protium incorporated in the α and β positions of naphthalene-d ₈ , fraction of	185 <i>f</i>	from reactors	365 <i>f</i>
Proton magnetic resonance (PMR) study of CDL, 600-MHz	226	observed in autoclave runs	366 <i>t</i> –368 <i>t</i>
PSMC-53, aromatic band in	289–318	observed in reactor runs	363 <i>t</i>
PSMC-67, CP/MAS spectrum of	37	product distribution after reaction of fresh Tetralin with	199 <i>f</i>
PSOC coals	35	pyrite vs.	195
Pyridine, dependence of true coal volume fraction at equilibrium swelling in	3	stability field, pyrite—	352 <i>f</i>
Pyridine solubles			
comparison of conversion of MAF Wyodak coals to	57 <i>f</i>		
conversion(s) to	141 <i>f</i>		
MAF coal	159 <i>f</i>		
from short-contact-time coal liquefaction	139		
relationship between reaction time, temperature, reaction severity, and conversion of Wyodak coal to	145		
Pyrite	134 <i>t</i>		
analysis results with those by Pennsylvania State University, comparison of	191		
coal with added	397 <i>t</i>		
in coal and lignite, analysis of	369		
in coal or lignite is analyzed, schematic of weight change observed as	389–400		
concentration, yields of 1-methylindan and naphthalene and the ratio of trans/cis Decalin as a function of	393 <i>f</i>		
vs. pyrrhotite	198 <i>f</i>		
–pyrrhotite equilibrium line	195		
–pyrrhotite stability field	369		
	350, 352 <i>f</i>		
		Q	
		Quinoline	
		HDN of	319
		hydrogenation of	319
		to 1,2,3,4-tetrahydroquinoline, hydrogenation of	
		with [Co(PC)]/SiO ₂	326 <i>t</i> , 327 <i>t</i> , 328 <i>t</i>
		in homogeneous solution at 300°C	325 <i>t</i>
		with [M(PC)] supported on Al ₂ O ₃ and SiO ₂ · Al ₂ O ₃ at 290°C, of	324 <i>t</i>
		with [M(PC)] supported on SiO ₂ at several temperatures	323 <i>t</i>
		R	
		Radical(s)	
		–bond scission	102
		concentration(s)	176
		reduction	180
		in samples of coal heated with naphthalene-d ₈ or naphthalene-h ₈	179 <i>f</i>
		in samples of heated coal	178 <i>f</i>
		disproportionation	115
		linewidths	182
		stabilized	
		classes of resonance	111
		reactions involving highly	114
		thermochemistry of resonance	110
		features of	112

- Reaction severity (R_s) 154
 hydrogen/oxygen/nitrogen/sulfur
 content vs. 165*f*
 parameter to predict conversion,
 application of 158
 relationship between coal con-
 version and 156*f*
 relationship between SRC compo-
 sition and 156*t*
- Reactor(s)
 pyrrhotites formed during coal
 liquefaction in continuous 362
 runs, pyrrhotite observed in 363*t*
 zone 357
 for Fe-S-O-H system
 at 527° and 427°C 359*f*
 at 327°C 361*f*
- Reductive alkylation treatment of
 graphite and hydrocarbons 77
 Regression analysis, results of 205
 Regression technique 202
 Repeating unit size 47
 Repeating units between cross-links,
 number of 45
 Resonance stabilized radicals,
 classes of 111
 Resonance stabilized radicals,
 thermochemistry of 110
 features of 112
- S**
- Saturation magnetization of the iron .. 394
 Saturation magnetization of 1 mg
 iron metal with temperature as
 recorded by Faraday balance,
 variation of 391*f*
 SAXS (*see* Small-angle X-ray scattering)
 Scattered intensity for Washington
 No. 4 Queen high-volatile A
 bituminous coal 7
 Scattering
 in coals, contribution of mineral
 matter to 16
 patterns for various coals 8
 curves for the coal samples 6*f*
 curves, shoulders in 19
 SCT coal liquefaction, solvent
 changes during 169*f*
 SCT liquefaction of Belle Ayr coal 163
 Short-contact-time coal liquefac-
 tion 131-152
 MAF conversions to pyridine
 solubles from 145
 Silkstone sporinite 34
 Small-angle X-ray investigation of
 porosity in coals 3-22
 Small-angle X-ray scattering (SAXS) 3, 4
 coals 11
 studies of 4
- Small-angle X-ray scattering
 (SAXS) (*continued*) 9
 curves 10
 for anthracites 10
 for bitumens 8
 differences between the specific
 surfaces obtained by adsorp-
 tion and 18
 pores 11
 system 6*f*
 Kratky 7
 Solubilization products, structural
 parameters of 238*t*
 Solvation effects on equilibrium
 constants 98
 Solvent(s)
 alkylation of 167
 changes during SCT coal lique-
 faction 169*f*
 and coals 131
 components, structural changes of .. 163
 composition 162, 166*t*
 changes in 162, 166*t*
 effect of coal conversion on 153, 161
 on the liquefaction behavior of
 western subbituminous
 coal, effect of 153-171
 compositional data 133*t*, 155*t*
 liquefaction in hydrogen depleted .. 145
 preheat, gases produced during 165*f*
 structural analysis of the spent 188
- SP-300 and its fractions, structural
 parameters of 236*t*
 SP-300 and SP-320 fractions,
 HVL-P and 235
 SP-320 fractions, HVL-P,
 SP-300, and 235
- Specific surfaces
 for the coals obtained from the
 scattering curves and from
 adsorption data 14*t*-15*t*
 determination of 11
 of the macropores and transition
 pores 17
 obtained by adsorption and SAXS,
 differences between 18
 Sporinite(s) 25
 C-13 CP/MAS spectra of 27
 concentrates, CP/MAS spectra of .. 31*f*
 silkstone 34
- SRC
 composition 140
 and reaction severity, relation-
 ship between 156*t*
 H/C atomic ratio of 157
 from liquefaction, elemental
 analyses of
 of Monterey coal in -019
 solvent 146*f*

SRC (<i>continued</i>)	
of Monterey coal in -035 solvent	147f
of Wyodak coal	
in -019 solvent	141f, 142f
in -035 solvent	143f
in -019 and -035 solvent, comparison of	144f
NCI MS of	283f
using standard addition method, quantitation of fluoranthene in	286f
SRC-I in a <i>n</i> -heptane matrix at 15 K, dye laser-induced fluorescence spectra of	257f
SRC-I MI-FTIR spectrum of one chromatographic peak system from the aromatic extract of	262f
SRC-II	
chromatographic fractionation of ..	292f
elemental analysis, molecular weight and empirical formula of the major fractions of	294t
fuel oil A, cyclic voltammogram of ..	335f
and H ₂ , Mössbauer spectra at various temperatures for a coal sample plus	384f
integrated molecular weight distribution of	276f
mass 132 MS/MS spectrum with the reference spectrum of 3-methylindole, comparison of middle distillates from Illinois No. 6 and Pittsburg Seam coal, difference NMR spectrum between	314f
middle distillates from Illinois No. 6 and Western Kentucky 9/14 coal, difference NMR spectrum between	315f
135 ⁺ MS/MS spectrum with reference spectra of 5-indanol and benzothiophene using isobutane PCI, comparison of	279f
+ N ₂ , Mössbauer spectrum of the liquefaction residue obtained from a run with	384f
neutral loss scan and MS of acylated	280f
properties of	313t
structural parameters for major fractions of	312t
Steam gasification of carbon catalyzed by K ₂ CO ₃	80
Subbituminous, New Mexico	206t
Sulfides, anodic depolarization reactions of mercury for the determination of	437
Sulfidic sulfur	442
Sulfite conversion	439
Sulfite by DIE, determination of	441f
Sulfur	
from coal(s), removal of	406t
evaluation of	401-414
compounds for new coal conversion technologies, resource development in the analytical chemistry of	427-443
-containing additives, clean Kentucky coal with	371
containing functional groups in coal under reducing conditions, nonisothermal kinetic method for estimation of the organic ..	416
contamination, control of	427
content in coal	401
functionality, thermal oxidative degradation of coal as a route to	415-426
moieties for which thermodynamic data are available	429t
Swelling	
behavior	
apparent	50
of coal samples	48t
of cross-linked structure in coal samples, true coal	56t
—effect of porous structure, true coal	51
on the carbon content for American coals, dependence of apparent coal volume fraction at equilibrium	52f
and Japanese coals	53f
on the oxygen content of coals, dependence of apparent coal volume fraction at equilibrium	54f
in pyridine, dependence of true coal volume fraction at equilibrium	57f
Synfuel characterization, applications of MS/MS to	275
Synfuels, MS/MS analysis of	267-288
Synthoil, fluorescence spectra after HPLC separation of	261f
Synthoil sample in isopropyl alcohol, LC of	259f
T	
Tar yield with aliphatic hydrogen, correlation of	68f
Tetrahydrofuran (THF)	77
Li-7 NMR of Li-naphthalenide in ..	81f
naphthalene in	79
1,2,3,4-Tetrahydroquinoline, hydrogenation of quinoline to with [Co(PC)]/SiO ₂	326t, 327t, 328t

- 1,2,3,4-Tetrahydroquinoline, hydro-
 generation of quinoline to (*continued*)
 in homogeneous solution at 300°C 325*t*
 with [M(PC)] supported on Al₂O₃
 and SiO₂ · Al₂O₃ at 290°C 324*t*
 with [M(PC)] supported on SiO₂
 at several temperatures 323*t*
- Tetralin**
 bond homolysis in 104*t*–107*t*
 by coal to produce naphthalene,
 abstraction of hydrogen from .. 194
 and Decalin, product yields from .. 196*f*
 and its derivatives, decoupling
 effect on α -CH₂ proton
 signals in 302*f*
 disproportionation from 116
 as H-donor, molecular dispropor-
 tionation with 118*t*–119*t*
 in the presence of coal, reactions of 193
 with pyrrhotite, product distribu-
 tion after reaction of fresh 199*f*
 reduction of pyrite with 197
- Thermal decomposition**
 coal structure and 61–71
 cracking of hypothetical coal mole-
 cule during 63*f*
 of functional groups 66
 products for PSOC 170, coal
 molecule and 62
- Thermal oxidative degradation**
 with an alternate programmed-iso-
 thermal treatment for oxyde-
 sulfurized Indiana Minshall
 Seam coal, comparison of a
 normal 423*f*
 apparatus 419*f*
 of coal as a route to sulfur
 functionality 415–426
 of oxydesulfurized Indiana Minshall
 Seam coal in oxygen and air,
 comparison of 425*f*
 of sulfur (TODS) 415
 experiments 422
 of untreated Indiana Minshall Seam
 coal with and without a diluent 419*f*
 of untreated and oxydesulfurized
 Indiana Minshall Seam coal with
 diluent 420*f*
 Montana Rosebud Seam coal with
 diluent 420*f*
 North Dakota lignite with
 diluent 421*f*
- Thermochemistry, features of**
 resonance-stabilized radical 112
- Thermochemistry of resonance sta-
 bilized radicals 110**
- Thermogravimetry and magnetometry 389**
- Thermometric enthalpy titration of**
 HMB with sulfide 440*f*
- THF (*see* Tetrahydrofuran)
- TODS (*see* Thermal oxidative degra-
 dation of sulfur)
- Transformation of the iron sulfides in
 an Illinois No. 6 coal 382
- V**
- Vapor-phase compositions involving
 hydrogen, sulfur, or oxygen 356
- Vapor pressures of replacing hydroxyl
 groups with methyl groups,
 effects on 100*t*
- Vitrinite**
 CP/MAS spectra of
 C-13 27
 concentrates 32*f*
 samples from the Lower Kittan-
 ning Seam 38*f*
 macerals, ultimate and proximate
 analysis of 29*t*
 samples 25
 spectral patterns 34
- Voltammetric methods 433**
- Voltammetric traces, effect of elec-
 trode film formation on 335*f***
- Voltammetry, differential pulse 433**
- Voltammogram of product oil from
 the 1000 lb/d pilot plant at
 PETC 337*f***
- Voltammogram of Panasol oil 333**
- W**
- Washington No. 4 Queen high-volatile
 A bituminous coal, scattered
 intensity for 7
- Water formation, ionic processes and 123
- West Virginia Blacksville coal 379
- Western Kentucky 9/14 coal, differ-
 ence NMR spectrum between
 SRC-II middle distillates from
 Illinois No. 6 and 315*f*
- Western subbituminous coal, effect of
 solvent composition on the
 liquefaction behavior of 153–171
- Westfield mine, CP/MAS spectra of
 fusinite from 33*f*
- Wyodak coal(s)**
 liquefaction of
 elemental analysis of SRC from
 in -019 solvent 141*f*, 142*f*
 in -035 solvent 143*f*
 in -019 and -035 solvents,
 comparison of 144*f*
 and Monterey coals in -019
 solvent 149*f*
 and Monterey coals in -035
 solvent 150*f*

Wyodak coal(s) (<i>continued</i>)		Wyodak coal(s) (<i>continued</i>)	
liquefaction of (<i>continued</i>)		to pyridine solubles, relationship	
with -019 solvent, elemental		between reaction time, tem-	
analyses obtained by distil-		perature, reaction severity,	
lation and heptane precipi-		and conversion of	134 <i>t</i>
tation from	142 <i>f</i>	subbituminous in solvents	151
to pyridine solubles, comparison of		Wyodak SRC vs.	
conversion of MAF	141 <i>f</i>	conversion	164 <i>f</i>